

The Isotope Geochemistry and Petrology of Dalradian Metacarbonate Rocks

Christopher Walter Thomas

PhD

University of Edinburgh

1999



Declaration

This dissertation is entirely my own work except where indicated otherwise

Christopher Walter Thomas

Abstract

The distinctive, primary isotope and trace element compositions of carbonate rocks are commonly modified, but rarely completely destroyed by fluid-rock interaction. This partial response to geochemical change renders carbonate rocks useful in studies of metamorphic fluid-rock interaction, but at the same time, permits elucidation of their pre-metamorphic geochemical character.

This thesis presents a detailed petrographic and geochemical study of several Dalradian metacarbonate and calc-silicate rock units from Scotland and Northern Ireland, which were metamorphosed at greenschist to middle amphibolite facies conditions during the Ordovician Grampian Orogeny.

The study aimed:

- a) to determine the extent to which metamorphic fluid-rock interaction has modified original sedimentary/diagenetic chemical signatures,
- b) to relate original signatures to the pre-metamorphic history of the carbonate rocks, and
- c) to elucidate and quantify the nature and mechanisms of metamorphic fluid-rock interaction.

Conventional bulk carbonate $\delta^{18}\text{O}$, $\delta^{13}\text{C}$ and $^{87}\text{Sr}/^{86}\text{Sr}$ ratios were determined at a range of sample scales, including whole-rock samples from outcrops, small-scale samples from within hand specimens, and mini-core samples from a drilled profile. Oxygen isotope and trace element compositions of two metalimestones were studied on grain and subgrain scales by Secondary Ion Mass Spectrometry (SIMS), aided by cathodoluminescence imaging. This work elucidated fluid infiltration pathways and mechanisms, the extent of altered domains, timescales and mechanisms of isotope

exchange, and the true scale of isotope equilibration. The work also aided interpretation of the bulk carbonate data.

Petrographical and microchemical analysis of calc-silicate rocks from Glen Rinnes, NE Grampian Highlands, indicate varied and complex buffering of the fluid phase. The lack of diopside, the presence of plagioclase + calcite and zoisite breakdown textures indicate local buffering of the fluid phase to more X_{CO_2} -rich compositions along univariant equilibria and to invariant points. This implies local buffering of fluid composition by the rock, mitigating against infiltration of very water-rich fluids.

Stable and strontium isotope data show that pervasive metamorphic fluid infiltration of the limestones did not commonly occur and primary/near-primary $\delta^{13}\text{C}$ and $^{87}\text{Sr}/^{86}\text{Sr}$ ratios have been widely preserved. $^{87}\text{Sr}/^{86}\text{Sr}$ ratios of metadolostones are markedly different to those in metalimestones and probably relate to dolomitisation. Although bulk carbonate $\delta^{18}\text{O}$, at $\sim 11 - 25\text{‰}$, varies more widely than $\delta^{13}\text{C}$ and $^{87}\text{Sr}/^{86}\text{Sr}$, primary/near-primary signatures are preserved in several metalimestones, particularly at the grain-scale.

Dalradian metalimestone $^{87}\text{Sr}/^{86}\text{Sr}$ and $\delta^{13}\text{C}$ data are comparable with available data for unmetamorphosed Neoproterozoic carbonate rock sequences from around the world. Appin and Grampian Group metalimestones beneath the Port Askaig Tillite, have carbonate $^{87}\text{Sr}/^{86}\text{Sr}$ of $0.7065 - 0.7075$ and $\delta^{13}\text{C}$ of $3 - 8\text{‰}$. Taken *together*, the metalimestone data suggest strongly that the Dalradian is younger than $\sim 750 - 800\text{ Ma}$, during which time marine $^{87}\text{Sr}/^{86}\text{Sr}$ appears to have risen sharply from ~ 0.7055 to ~ 0.7065 and carbonate $\delta^{13}\text{C}$ values became strongly positive. The uppermost Argyll Group Tayvallich Limestone and equivalents above the Port

Askaig Tillite have $^{87}\text{Sr}/^{86}\text{Sr}$ in excess of 0.7080. The shift in carbonate $^{87}\text{Sr}/^{86}\text{Sr}$ across the Port Askaig Tillite in the Dalradian is consistent with that observed in carbonate successions across ~600 Ma Varangan/Marinoan tillite sequences elsewhere in the world.

Grain-scale oxygen isotope and trace element studies reveal many features found in other similar recent studies of metacarbonate rocks. Spatial $\delta^{18}\text{O}$ and trace element distributions reveal gross chemical heterogeneity within and between calcite and quartz grains, suggesting metamorphism under anhydrous conditions. There is little evidence for *pervasive* infiltration of metamorphic fluid. Fluid infiltration was only locally significant and structurally focussed along short-lived fractures and other non-equilibrium fluid-pathways adjacent to fractures, and grain boundaries, highlighted by cathodoluminescence imaging. Isotopic exchange between limestone and fluid was largely kinetically controlled, resulting in local volume diffusion gradients, and local dissolution and reprecipitation effects. Modelling of grain-scale $\delta^{18}\text{O}$ profiles give estimates of $10^2 - 10^4$ years for the duration of fluid infiltration at ~ 550 – 600°C. $\delta^{18}\text{O}$ values along veinlets in one sample vary inversely with vein width, suggesting local buffering of fluid $\delta^{18}\text{O}$ by the host along the vein.

In summary, many *calcitic* Dalradian metalimestones have been little affected by fluid infiltration during metamorphism, although two metalimestones studied in detail preserve a record of post peak metamorphic, structurally focussed, fluid infiltration of variable extent. Pre-metamorphic, post-diagenetic carbonate $^{87}\text{Sr}/^{86}\text{Sr}$, $\delta^{13}\text{C}$ and (to a lesser extent) $\delta^{18}\text{O}$ signatures are widely preserved. The combined $\delta^{13}\text{C}$ and $^{87}\text{Sr}/^{86}\text{Sr}$ data strongly suggest that the Dalradian is younger than ~750 – 800 Ma.

Except in grooves of streams, armpits of hills,
Here's a bald, bare land, weathered half away.
It pokes its bony blades clean through its skin
And chucks the light up from grey knucklebones,
Tattering the eye, that's teased with flowers and stones.

Something to do with time has all to do
With shape and size. The million shapes of time,
Its millions of appearances are the true
Mountain and moor and tingling water drop
That runs and hangs and shakes time towards a stop.

...

From: 'A Treeless Landscape'

Norman MacCaig

A Common Grace

1960

Acknowledgements

Part-time PhDs are, perforce, drawn-out affairs, so I make no apology for the length of these acknowledgements to those who have helped and supported me along the way.

This thesis would not exist at all but for a generous and opportune letter from Tony Fallick and a subsequent generous offer from Colin Graham, made over the C-O-H fluid geologists know best...beer...naturally.

So, thanks:

To Colin Graham, for all the supervision, help, support and encouragement, for enthusiasm for things carbonate and Dalradian, for good Islay weather, for patient enlightenment, inspiration and incisive commenting, all of which have kept me going over several years.

To John Mendum, my co-supervisor, for firm support within BGS, for encyclopaedic knowledge of Highlands geology, for being my structural geology mentor over many years, for wet Highlands weather, for not fiddling with the english...too much, and for always careful and constructive discussion and comments.

In the Edinburgh Geology Department:

Thanks to Mike Hall for expertly cutting numerous sections of fiddly bits of limestone, thanks to several fellow students and colleagues, for help and discussion, and fun at Grad School Conferences, particularly Alastair Skelton, to whom thanks also for use of his diffusion program, Coleen Cole, and Steph Lewis, who showed me how to use Alastair's program.

Thanks to Stuart Kearns, Simon Burgess and especially Pete Hill, for electron microprobe support, tea and biccies over several years; and thanks to ion-man himself, John Craven, without whom the ion-probe experience wouldn't be *the* ion-probe experience: 4 am finishes, blown electron gun filaments, vacuum gauges, beer, malt, tea, chocolate hob-nobs, liberally-dispensed wit...etc..., Tom Waits cds to liven up the wee small hours (!?)...the best support you could wish for.

at SURRC, East Kilbride:

To Tony Fallick and Rob Ellam, for enthusiastic support and discussion, especially over too much beer at a grad school conference, for access to SURRC facilities and for stable and strontium isotope analyses, and for whom nothing has been too much trouble. Likewise, thanks to Anne and Vinny for instruction, the chance to do some chemistry again and things mass-spec-ish.

At BGS, Edinburgh:

Many thanks to my colleagues Steve Robertson and Martin Smith, for support, interest, endless discussion, enlightenment and enthusiastic acceptance of my limestone stories, and for general companionship and encouragement.

Particular thanks are also due to Ian Penn, Training Section, BGS, Keyworth, who made sure my PhD was always supported financially, and to Doug Fettes, who, with John Mendum, set me off on the limestones in the first place, many moons ago.

and at home:

Thanks to my family – Sally, Ben and Sam: Sally for suffering too long from my obsession with limestones and for patient support, and the boys, for helping me to keep a sense of proportion...most of the time...

and, finally, thanks to Mum and Dad, for positively encouraging my interest in rocks from an early age and much more besides!

Finally, I would like to acknowledge the abiding influence of the late Dr Denis Field and Dr Tony Dickson (now Cambridge University) for their enthusiastic teaching of things metamorphic and carbonate when I was an undergraduate at Nottingham.

Abbreviations & notations used and definitions

General

CL	Cathodoluminescence
ppl	Plane-polarised light
P	Pressure, kilobars
T°C	Temperature, degrees Celsius
T (K)	Temperature, Kelvins
X _{CO₂}	Mole fraction of CO ₂ in fluid phase
D	Diffusivity, m ² s ⁻¹

Interquartile range: non-parametric measure of dispersion between the first and third quartiles of the sample

Mineral abbreviations

alb: albite **am:** amphibole **bi:** biotite **cc:** calcite **clin:** clinocllore **di:** diopside
dol: dolomite **gr:** grossular **hb:** hornblende **hyal:** hyalophane **ksp:** K-feldspar
mu: muscovite **phl:** phlogopite **pl:** plagioclase feldspar **qz:** quartz **ru:** rutile
sph: sphene **ta:** talc **tr:** tremolite **wm:** white mica **zo:** zoisite

Stable isotopes

Fractionation factor, α

$$\alpha_{A-B} = R_A / R_B$$

Difference

$$\Delta_{A-B} \cong 10^3 \ln \alpha_{A-B} \quad \text{valid where } \alpha_{A-B} \text{ is less than } 10$$

The δ value (‰)

$$\delta_A (\text{‰}) = [(R_A - R_{STD}) / R_{STD}] \times 10^3$$

R_{A,B} : isotope ratios of substances in unknown sample

R_{std} : isotope ratio in the standard

$\delta^{18}\text{O}$ (‰) : quoted throughout relative to Vienna Standard Mean Ocean Water

$\delta^{13}\text{C}$ (‰) : quoted relative to Peedee Belemnite

Strontium isotopes

Bulk carbonate Sr isotope compositions are quoted as $^{87}\text{Sr}/^{86}\text{Sr}$ ratios, normalised to

$$^{86}\text{Sr}/^{88}\text{Sr} = 0.1194$$

Contents

Chapter 1

1 Introduction	1
1.1.1 Variations in carbon and strontium isotopes during the Neoproterozoic	2
1.1.2 Fluid infiltration in limestones and dolostones	3
1.1.3 Dalradian carbonate rocks	4
1.2 Aims	5
1.3 Methods	5
1.4 Thesis Layout	7
Part 1: The geology and petrology of Dalradian carbonate rocks	7
Part 2: Strontium, carbon and oxygen isotope geochemistry of Dalradian limestones and dolostones	7
Part 3: Outcrop- and grain-scale spatial variations in stable isotope compositions of calcite and quartz: fluid infiltration mechanisms and timescales	8

Part 1

The geology and petrology of Dalradian carbonate rocks

Chapter 2

Dalradian lithostratigraphy, structure and metamorphism, with special reference to carbonate rocks

2.1 Introduction	9
2.2 Dalradian Supergroup	10
2.2.1 Outline of Dalradian geology	10
2.2.2 Constraints on the age of Dalradian	13
2.3 Lithostratigraphy of Dalradian carbonate and calc-silicate rocks of Scotland	14
2.3.1 Grampian Group limestones	14
2.3.2 Appin Group carbonate rocks	17
The Pitlurg Calcareous Flag Formation, Lochaber Subgroup (1)	18
Kintra Dolostone, Dufftown Limestone, Ballachullish Subgroup (2)	20
Torulian Limestone Member, Ailnack Phyllite and Limestone Formation (3)	21
Limestones of the Blair Atholl Subgroup: Inchrory Limestone Formation (Northeast Grampian Highlands), Storakaig Limestone Member (Ballygrant Formation, Islay) (4,5),	22
Dolostones and tillites in the Islay Subgroup (6)	24
Tayvallich, Torr Head, Dungiven and Boyne Limestones (7)	25
Leny Limestone	27
2.4 Colonsay Group	28
2.4.1 Basement – cover relationships of the Colonsay Group	28
2.4.2 Colonsay Group Lithostratigraphy	30
2.4.3 Age and regional correlation of the Colonsay Group	30
2.5 Dalradian structure	32
2.5.1 Grampian orogenic structures	33
2.6 Dalradian metamorphism	37

Chapter 3

Petrography and whole-rock geochemistry of Dalradian limestones and dolostones

3.1 Introduction	46
3.2 Petrography	48
3.2.1 Kintra Dolostone, Islay	48
3.2.2 Dolostones from the Staosnaig Phyllite Formation, Colonsay	52
3.2.3 Islay Subgroup dolostones, NE Grampian Highlands	52
3.2.4 Torr Head and Dungiven limestones, Northern Ireland	58
3.2.5 Tayvallich Limestone, Port an Sgadain, Tayvallich Peninsula	64
3.2.6 Storakaig Limestone	66
3.2.7 Inchrory Limestone	68
3.2.8 Torulian Limestone	71
3.2.9 Dufftown Limestone	71
3.2.10 Kincaig limestones	73
3.3 Stability of carbonate rock mineral assemblages	73
3.3.1 Dolostones	73
3.3.2 Limestones	77
3.4 Whole-rock geochemistry	81
3.4.1 Limestone geochemistry	81
3.4.2 Dolostone geochemistry	84
3.5 Summary and conclusions	86

Chapter 4

Constraints on metamorphic fluid-rock interaction in calc-silicate-bearing lithologies.

4.1 Introduction	88
------------------	----

4.1.1 Calc-silicate rocks in metamorphic fluid-rock interaction studies	88
Fluid infiltration mechanisms in calc-silicate rocks	91
Layout of Chapter	91
4.2 General petrography	92
4.2.1 Amphibole	94
4.2.2 Zoisite and feldspars	101
4.2.3 Phyllosilicates	101
4.2.4 Summary	102
4.3 Mineral chemistry	102
4.3.1 Amphiboles	107
Summary of amphibole chemistry	112
4.3.2 Phyllosilicates	112
Phlogopite	113
Chlorite	113
White Mica	113
Summary of phyllosilicate chemistry	116
4.3.3 Plagioclase	116
4.4 T-X _{CO₂} modelling of phase relations	116
4.4.1 Composition space and mineral solutions	117
4.4.2 Estimating peak metamorphic temperatures	121
Effect of pressure on T-X _{CO₂} topology	126
4.5 Detailed electron microprobe petrography	128
4.5.1 EDS and BSE petrography	129
HY471	129
HY474	132
Summary of features in HY474	137
HY491	138
HY1001	141
HY1007	142

4.5.2 Limits on T and X_{CO_2} of observed assemblages	142
Stability of zo + cc + tr + qz assemblages	144
The zoisite – calcite – plagioclase assemblage	145
Phlogopite – zoisite assemblage	147
K-feldspar-bearing assemblages	148
The origin of tremolite – rich laminae	150
4.6 Discussion	153
4.6.1 Location of the Pitlurg calc-silicates in T- X_{CO_2} space	153
4.6.2 Peak metamorphic temperature and pressure estimates from the T- X_{CO_2}	154
4.6.3 The origin of the patches	155
4.7 Summary and conclusions	156

Part 2

Strontium, carbon and oxygen isotope geochemistry of Dalradian limestones and dolostones

Chapter 5

Stable and strontium isotopes in carbonate rocks

5.1 Introduction	158
5.2 Applications of stable and strontium isotopes in studies of carbonate rocks	158
5.2.1 Secular variation of $\delta^{13}\text{C}$ and $^{87}\text{Sr}/^{86}\text{Sr}$ in seawater	159
5.2.2 Quantification of the effects of diagenesis on carbonate rock isotope compositions	160
5.2.3 Stable and Sr isotopes in metamorphic fluid-rock interaction studies of carbonate rocks	163
5.3 Controls on the carbon isotope composition of carbonate rocks	164
5.4 Oxygen isotopes in carbonate rocks and fluids	167
5.5 Strontium isotopes in carbonate rocks and seawater	169
5.5.1 Strontium isotopes in seawater	170
5.5.2 Controls on modern seawater Sr isotopic composition	170
5.5.3 The effects of diagenesis on carbonate $^{87}\text{Sr}/^{86}\text{Sr}$	173
5.5.4 Importance of scale of $^{87}\text{Sr}/^{86}\text{Sr}$ heterogeneity and sampling scale	176
5.6 Summary and conclusions	176

Chapter 6

The Strontium element and isotope geochemistry of Dalradian Limestones

6.1 Introduction	179
6.2 Strontium isotope analysis	180
6.2.1 Methods	184
6.2.2 Pilot study: conclusions	187

6.3 Strontium isotope results	187
6.3.1 Limestones	193
6.3.2 Dolostones	193
6.4 Interpretation of $^{87}\text{Sr}/^{86}\text{Sr}$ data	194
6.4.1 Geochemical criteria for determining preservation of initial $^{87}\text{Sr}/^{86}\text{Sr}$ ratios in carbonate rocks	194
6.4.2 Strontium concentration	196
6.4.3 Manganese concentration	197
6.4.4 Oxygen isotopes	198
6.4.5 Rubidium and Aluminium	199
6.4.6 Relationships between $^{87}\text{Sr}/^{86}\text{Sr}$, Sr, Mn, Rb, Al, $\delta^{18}\text{O}$ and $\delta^{13}\text{C}$	201
$^{87}\text{Sr}/^{86}\text{Sr}$ vs Sr	201
$^{87}\text{Sr}/^{86}\text{Sr}$ vs Mn and the relationship between Mn and Sr	201
6.4.7 Discussion	204
6.4.8 $^{87}\text{Sr}/^{86}\text{Sr}$ vs Al_2O_3	206
6.4.9 Variation of $^{87}\text{Sr}/^{86}\text{Sr}$ with $\delta^{18}\text{O}$	207
6.4.10 Discussion	210
6.4.11 Variation of $^{87}\text{Sr}/^{86}\text{Sr}$ with $\delta^{13}\text{C}$	212
6.5 Discussion of Dalradian carbonate rock $^{87}\text{Sr}/^{86}\text{Sr}$ results	214
6.5.1 State of preservation of initial $^{87}\text{Sr}/^{86}\text{Sr}$ ratios in limestones	214
6.5.2 Estimating $^{87}\text{Sr}/^{86}\text{Sr}$ of Dalradian seawater	216
6.6 Comparison of Dalradian limestone $^{87}\text{Sr}/^{86}\text{Sr}$ data with a Neoproterozoic seawater $^{87}\text{Sr}/^{86}\text{Sr}$ curve	218
6.6.1 Secular variation of Neoproterozoic seawater $^{87}\text{Sr}/^{86}\text{Sr}$	218
6.6.2 A Neoproterozoic $^{87}\text{Sr}/^{86}\text{Sr}$ 'seawater' curve	219
6.6.3 The depositional age of the Dalradian	223
6.7 Shifts in Neoproterozoic seawater $^{87}\text{Sr}/^{86}\text{Sr}$, coeval palaeogeography & tectonics	227
6.7.1 Neoproterozoic palaeogeography – the models of Hoffman, Dalziel and co-	

workers	228
6.7.2 Coincidence of the 600 Ma shift in $^{87}\text{Sr}/^{86}\text{Sr}$ with the Pan African Orogeny	234
6.7.3 A tectonic cause for the '800' Ma shift ?	235
6.8 Conclusions	237

Chapter 7

Whole-rock carbon and oxygen isotope compositions of Dalradian limestones and dolostones

7.1 Introduction	238
7.2 Samples and data sets	239
Tayvallich – Loch Tay Limestone data	242
Bonahaven Dolomite	242
'Colonsay Limestone'	243
7.3 'Whole-rock' carbon and oxygen isotope compositions of Dalradian limestones and dolostones	243
7.3.1 Dolostones	243
7.3.2 Limestones	244
Grampian Group limestones	244
Appin Group limestones	244
Argyll Group Limestones	246
The Leny Limestone	247
7.4 Extent of preservation of primary $\delta^{13}\text{C}$ values	247
7.4.1 Organic carbon as a measure of preservation of primary $\delta^{13}\text{C}$, and organic carbon – calcite ^{13}C exchange during metamorphism	248
7.4.2 'Whole-rock' $\delta^{13}\text{C}$ and $\delta^{18}\text{O}$ co-variation	250
7.4.3 Preservation of primary $\delta^{13}\text{C}$ values	256
Limestones	256
Topmost Argyll Group ('Tayvallich') limestones	264
Constant $\delta^{13}\text{C}$ values vs widely varying $\delta^{18}\text{O}$ - identification of primary $\delta^{13}\text{C}$	

values	265
Preservation of carbonate $\delta^{13}\text{C}$ during diagenesis	267
Tayvallich Limestone, Port an Sgadain – the case for hydrothermal alteration by seawater	268
Dolostones	275
7.5 Comparison of Dalradian carbonate $\delta^{13}\text{C}$ data with other Neoproterozoic sequences:	
carbonate $\delta^{13}\text{C}$ constraints on the age of the Appin Group and wider correlations	280
7.5.1 Comparison of $\delta^{13}\text{C}$ with $\delta^{18}\text{O}$ and $^{87}\text{Sr}/^{86}\text{Sr}$	280
7.5.2 Secular variation in $\delta^{13}\text{C}$ during the Neoproterozoic	284
7.5.3 $\delta^{13}\text{C}$ evidence for the duration of the Varangan glaciation	287
7.5.4 Negative carbonate $\delta^{13}\text{C}$ excursions and Neoproterozoic global glaciation	289
7.6 Summary and conclusions	290

Part 3

Outcrop- and grain-scale spatial variations in stable isotope compositions of calcite and quartz: fluid infiltration mechanisms and timescales

Chapter 8

The mechanisms and time-scales of metamorphic fluid infiltration in calcitic limestones

8.1 Introduction	292
8.2 Porosity, permeability and fluid infiltration in metalimestones	293
8.3 Mechanisms of permeability enhancement	295
8.3.1 Reaction-generated permeability	295
8.3.2 Hydrofracturing	296
8.3.3 The effect of deformation on permeability	297
8.3.4 Permeability enhancement in calcite limestones	302
8.3.5 Summary: fluid infiltration mechanisms in metalimestones	302
8.4 Mapping and quantifying fluid-rock interaction on the grain-scale	303
8.4.1 Mapping fluid pathways using cathodoluminescence	304
8.4.2 The identification of diffusion gradients and the significance of volume diffusion: a case study	304
8.4.3 Elucidating time-scales of fluid infiltration	305
8.4.4 Preservation of diffusion gradients: constraints on cooling rates	308
8.4.5 Implications of gross calcite $\delta^{18}\text{O}$ disequilibrium for front advection modelling	309
8.4.6 Summary: fluid pathway mapping and diffusion gradient modelling	311
8.5 Quantification of fluid-rock interaction in this study	312
8.5 Conclusions	312

Chapter 9

Outcrop profile and grain-scale studies of stable isotopes in the Torulian and Inchrory Limestones

9.1 Introduction	314
9.1.1 Sampling	316
Torulian Limestone sample profile	317
Inchrory Limestone: Limeworks Quarry sample profile	317
Partition of deformation in the Inchrory Limestone profile	317
9.2 Outcrop-scale variation in bulk carbonate $\delta^{18}\text{O}$ and $\delta^{13}\text{C}$	321
9.2.1 Bulk carbonate $\delta^{18}\text{O}$ and $\delta^{13}\text{C}$ data	321
Torulian Limestone	325
Inchrory Limestone	325
9.2.2 Outcrop-scale variation in $\delta^{18}\text{O}$ and $\delta^{13}\text{C}$, Torulian Limestone profile, River Avon	327
Oxygen isotope data	327
Carbon isotope data	328
9.2.3 Outcrop-scale variation in $\delta^{18}\text{O}$ and $\delta^{13}\text{C}$ in the Inchrory Limestone profile	330
9.2.4 Summary of bulk carbonate profile data	332
9.3 Cathodoluminescence (CL) imaging	333
9.3.1 Torulian Limestone: River Avon profile sample CT53	333
Summary of CL in CT53	335
9.3.2 Inchrory Limestone: Limeworks Quarry samples	336
LWQ1/25	336
LWQ1/28	340
LWQ1/30	342
Summary of CL in Inchrory Limestone samples	343
9.4 Spatial variation of $\delta^{18}\text{O}$ and $\delta^{13}\text{C}$ at the grain-scale	343
9.4.1 SIMS grain-scale calcite and quartz $\delta^{18}\text{O}$ data	344
Overview of SIMS calcite $\delta^{18}\text{O}$ data	344

Overview of quartz $\delta^{18}\text{O}$	346
SIMS calcite trace element data	347
9.4.2 Grain-scale variations in $\delta^{18}\text{O}$ and trace elements in CT53	347
Reconnaissance analyses	348
Grain-scale profile analyses in CT53	352
Profile A	354
Profile B	357
Profile C	360
Profile D	363
9.4.3 Discussion and Summary of CT53 profile data	364
Correlation of $\delta^{18}\text{O}$ with luminescent vein and grain boundary domain thicknesses	364
Relationship between bulk-rock and CT53 SIMS calcite $\delta^{18}\text{O}$ data	366
9.4.4 Summary of $\delta^{18}\text{O}$ isotope data in CT53	366
9.4.5 Grain-scale variation in calcite and quartz $\delta^{18}\text{O}$ in Inchrory Limestone	367
LWQ1/25	368
LWQ1/28	369
LWQ1/30	376
Nature of feldspar alteration in LWQ1/28 and 1/30	378
Nature of luminescent calcite vein networks and fluid pathways	381
9.4.5 Discussion of LWQ data	381
Extent of oxygen isotopic equilibrium	381
Fluid – rock interaction	382
Covariation of $\delta^{18}\text{O}$ and trace elements	384
Variation of SIMS calcite $\delta^{18}\text{O}$ data in the Inchrory Limestone samples in relation to profile position	385
Summary of SIMS $\delta^{18}\text{O}$ data in LWQ samples, Inchrory Limestone	386
9.5 Conclusions	387
Are primary $\delta^{18}\text{O}$ signatures preserved?	388

What are the implications of the oxygen data for interpretation of bulk carbonate	
$^{87}\text{Sr}/^{86}\text{Sr}$ and $\delta^{13}\text{C}$?	389
What next?	389

Chapter 10

Modelling of oxygen isotope profiles and mineral fractionations

10.1 Introduction	391
10.2 Calcite - dolomite geothermometry: a temperature estimate for fluid-rock interaction in CT53?	392
10.2.1 Calcite - dolomite geothermometry	393
10.3 Diffusion modelling of profiles in sample CT53	395
10.3.1 Quantitative methods	396
10.3.2 Calculating timescales of fluid infiltration	398
10.3.3 Discussion	402
Do the profiles represent true diffusion profiles?	402
Timescales for profile development	404
Preservation of profiles on cooling	405
Two metamorphic fluid infiltration events?	406
Fluid plumbing: lithological controls on metamorphic fluid flow in the Torulian	
Limestone	407
Sources of fluid	408
10.3.4 Summary	408
10.4 Calcite-quartz oxygen isotope fractionation in the Inchrory Limestone	409
10.4.1 Are quartz and calcite in oxygen isotope equilibrium?	411
10.4.2 The influence of grain-size and modal mineralogy on oxygen isotope fractionation in LWQ1/28 and 1/30	417

The role of feldspar	417
Oxygen isotope exchange in calcite and quartz - grain-size and diffusion controls	419
Time-scale of fluid infiltration in the LWQ samples	423
Discussion	425
10.4.3 Summary	426
10.5 Conclusions	427

Chapter 11

Summary, conclusions and suggestions for further work

11.1 Summary and conclusions	428
11.2 Suggestions for further work	435
Strontium isotopes	435
U-Pb and Pb-Pb dating of the limestones	435
The variation in $^{87}\text{Sr}/^{86}\text{Sr}$ across the Port Askaig Tillite	436
Modelling of modal abundance and grain-size controls on oxygen isotope exchange in metamorphic rocks	436

References	438
------------	-----

Appendices

Appendix A	460
A.1 Sampling details	460
Details of sampling for isotope analyses	460
Whole-rock sampling and sample preparation	460
Carbon and Oxygen isotope analysis of bulk carbonate	461

A.2 Details of lithostratigraphical units used to constrain Neoproterozoic seawater $^{87}\text{Sr}/^{86}\text{Sr}$

Canada	
Victoria Island, Canadian Arctic Archipelago, Northern Territories	461
Windermere Supergroup	462
Southern Africa	464
Namibia	464
Svalbard and Greenland	464
Oman	467
Russia	467
Riphean to early Cambrian carbonate rocks from Siberia	467
Upper Riphean Inzer Formation, Southern Urals, Russia	468

A.3 High-resolution (1cm) core sampling in the field for geochemical profiling studies, using a cordless powerdrill: A short report

Introduction	469
Equipment	471
Coring drills	471
Power drill and batteries	472
Water	472
In use	473
Discussion	473
Conclusions	474

Appendix B

Sample preparation, Sr separation and isotope analysis

Reagents	476
----------	-----

Cation exchange equipment	477
Sample preparation	477
Pilot study	477
Experiment 1	477
Experiment 2	478
Experiment 3	478
Leaching procedure details	478
Separation of Sr and Rb	478
⁸⁷ Sr/ ⁸⁶ Sr analysis	479
C.1 – Ion Probe Secondary Ion Mass Spectrometry	479
The ion microprobe, University of Edinburgh	481
$\delta^{18}\text{O}$ analysis	481
Operating conditions	482
Data processing	483
SIMS Trace element analysis	484
Operating conditions	484
Data processing:	485
C.2 Conventional carbon and oxygen isotope analysis	486
Method	486
C.3 Laser ablation stable isotope analyses	486

Appendix D

SIMS oxygen isotope and trace element analyses

Table D.1 Oxygen isotope analyses	487
Table D.2 Trace element analyses	495

Appendix E

Locality-specific details of geology, petrography and sampling procedures

Torulian Limestone and Inchrory Limestone

E1.1	Torulian Limestone in the River Avon, Bridge of Avon, Tomintoul	497
	Torulian Limestone sample profile	498
	Lithostratigraphy and petrography	498
	Structure	500
	Fault deformation	502
E1.2	Inchrory Limestone in Limeworks Quarry, Tomintoul	504
	Limeworks Quarry sample profile	505
	Lithologies	505
	Structure	509
	Partition of deformation	509

Enclosure in back pocket

Figure 9.8

Chapter 1

1 Introduction

Limestones and dolostones have very distinctive geochemical and isotope and trace element compositions compared to generally more abundant siliciclastic rocks. This distinctiveness primarily reflects the aqueous geochemistry and temperature of the environment in which the carbonate sediments formed. Careful determination of carbonate strontium and stable isotope compositions can yield important information about this environment and its secular variation. This approach has been fundamental to the development of secular seawater carbon and strontium isotope curves which now extend back into the Neoproterozoic. The isotope compositions also render carbonate rocks sensitive to modification by fluid-rock interaction during diagenesis and metamorphism. Study of the textural and chemical modifications can yield information on fluid infiltration mechanisms and pathways, the composition of the fluid phase, the fluid flux and time-scales of infiltration events. Thus, as well as their importance in diagenetic studies, carbonate rocks have come to occupy a central role in efforts to understand metamorphic fluid-rock interaction in recent years. In belts of metasedimentary rocks, carbonates thus have the *potential* not only to elucidate the nature of metamorphic fluid-rock interaction, but also to help understand the pre-metamorphic nature of the environment in which they formed.

1.1.1 Variations in carbon and strontium isotopes during the Neoproterozoic

A number of recent studies of largely unmetamorphosed and undeformed Neoproterozoic carbonate rocks have shown that there were very significant shifts in marine $\delta^{13}\text{C}$ and $^{87}\text{Sr}/^{86}\text{Sr}$ in the period leading up to the explosion in metazoan life at the base of the Cambrian (e.g. Asmerom et al., 1991; Bertrand and Mossine, 1983; Brasier et al., 1992; Burns et al., 1994; Derry et al., 1989; Fairchild et al., 1990; Garde, 1979; Gorokhov et al., 1995; Iyer et al., 1995; Karhu and Holland, 1996; Kaufman et al., 1991; Kennedy, 1996; Knoll et al., 1986; Kuznetsov et al., 1997; Melezhik et al., 1997; Misi and Veizer, 1998; Prave, 1999; Tucker, 1986; Veizer et al., 1983). The period from about 800 Ma through to about 600 Ma was characterised by an overall increase in marine $^{87}\text{Sr}/^{86}\text{Sr}$ and by generally high, positive carbonate $\delta^{13}\text{C}$ values; the latter have generally been interpreted to indicate rapid burial of organic material. The positive carbonate $\delta^{13}\text{C}$ pattern is punctuated by apparently short and sharp negative $\delta^{13}\text{C}$ excursions which have been attributed to glaciations of global extent, of which the later Varangan or Marinoan glaciation at ~ 600 Ma apparently reached low latitudes. This has lead to the currently controversial 'snowball' earth hypothesis in which sea-ice extended to low latitudes and drastically reduced in the oceans the sunlight vital for photosynthesis. Organic productivity is considered to have collapsed for at least 5 – 10 million years, yielding the marked negative carbonate $\delta^{13}\text{C}$ excursions.

Carbonate $^{87}\text{Sr}/^{86}\text{Sr}$ values show very dramatic shifts towards more radiogenic values across Varangan /Marinoan glacial deposits world-wide. This indicates a very large increase in the supply of radiogenic Sr to the oceans via weathering and erosion and is probably linked to Pan African Orogeny, possibly enhanced by weathering of

glacial deposits on deglaciation. An important aim of this study was to determine whether such a shift in $^{87}\text{Sr}/^{86}\text{Sr}$ could be recognised in Dalradian limestones and dolostones which occur above and below the Varangan Port Askaig Tillite Formation.

1.1.2 Fluid infiltration in limestones and dolostones

Limestones and impure dolostones are sensitive monitors of metamorphic fluids, either those generated by internal devolatilisation reactions or exotic infiltrating fluids. Metamorphic limestones commonly display local modification of oxygen isotope compositions in boundary layers whilst calc-silicate rocks contain assemblages characteristic of internal or external buffering of the fluid phase.

The sharp change in isotope composition at the boundaries of limestones adjacent to siliciclastic rocks represents a front or step. In many metamorphic terrains, these 'fronts' have been displaced into the limestone beds due to the infiltration of metamorphic fluids (Baker, 1990; Baker et al., 1989; Baker and Spiegelman, 1995; Bickle and Baker, 1990; Bickle and Chapman, 1990; Bickle et al., 1997; Bickle et al., 1995; Rye et al., 1976). The displacement distance and the shape of the isotope front can be used to determine metamorphic fluid flux using a combined advective-diffusive model based on chromatographic transport theory (e.g. Bickle and McKenzie 1987). Application of this model has proved successful in determining realistic estimates of metamorphic fluid flux, consistent with likely crustal fluid budgets. However, chromatographic theory makes several very major assumptions about the mechanisms of fluid infiltration and the state of porosity and permeability in metamorphic rocks (e.g. Graham et al., 1997; Holness and Graham

1995). Recent work testing these assumptions has shown that pure limestones are impermeable under most metamorphic P-T-X conditions and that fluid infiltration must be facilitated by transient, dynamic mechanisms dominated by hydrofracture (Holness and Graham 1995; Graham et al., 1998; Lewis et al., 1998; Lewis 1999). Time scales for fluid infiltration arising from this work are estimated to be of the order of $10^2 - 10^3$ years – very much shorter than the duration of metamorphic events.

1.1.3 Dalradian carbonate rocks

Although dominated by siliciclastic metasedimentary rocks, the Dalradian contains several important limestone, dolostone and calc-silicate units. The limestones, in particular, have wide regional extent and considerable value in lithostratigraphical correlation. Many of the limestone units have distinctive geochemical compositions which have permitted regional correlation (Hickman and Wright 1983; Thomas 1989; Thomas and Aitchison 1998). Their consistent geochemical compositions over wide areas implies that they retain much of their original, pre-metamorphic character. However, little published work exists on their stable and strontium isotope compositions and on variations in limestone and dolostone isotope compositions both across the Dalradian and through the lithostratigraphy. Furthermore, these isotopes have not been widely studied from the point of view of metamorphic fluid-rock interaction. These carbonate rocks therefore have considerable potential not only to further the understanding of Dalradian metamorphic and pre-metamorphic geology, but also to elucidate the controls on stable and strontium isotopes in metamorphosed carbonate rocks in general.

1.2 Aims

This PhD project is a petrographical and geochemical study of several important Dalradian carbonate and calc-silicate rock units. There have been two main themes to the work: the characterisation of the effects of metamorphism and the elucidation of their geochemical characteristics prior to metamorphism.

I have determined the oxygen, carbon and strontium isotope characteristics of several important Dalradian limestone and dolostone rock units, with three broad aims:

- a) to determine the extent to which metamorphic fluid-rock interaction has modified original sedimentary/diagenetic chemical signatures in Dalradian metamorphosed limestones and dolostones,
- b) to elucidate the nature of any such original signatures with regard to the pre-metamorphic history of the carbonate rocks, and
- c) to elucidate and quantify the mechanisms and time-scales of fluid-rock interaction during metamorphism.

I have also undertaken detailed petrographical and microchemical work on calc-silicate rocks, with the aims of determining the degree to which these rocks have been infiltrated by metamorphic fluids, and the composition of these fluids.

1.3 Methods

Work undertaken early in the project was largely petrographical, concentrating on calc-silicate rocks. Part of this work included study of the phase relationships

amongst the calc-silicate assemblages by the application of thermodynamic principles to construct T- X_{CO_2} sections.

An early aim was also to identify possible targets for the study of advected isotope and mineral reaction fronts. Sample profiles were obtained from two likely localities. In one, limestones occur next to siliciclastic rocks, in the other, limestones contain ortho-amphibolite pods. The first was sampled by conventional chip sampling on the metre scale, the latter by a micro-drilling technique in order to obtain a high resolution sample profile over a metre within a limestone boundary layer adjacent to amphibolite.

Bulk carbonate in these samples, together with samples collected widely from within the Dalradian of Scotland and Northern Ireland, was analysed by conventional techniques for strontium, carbon and oxygen isotopes. The method for strontium isotope analysis included application of a refined preparation technique to allow determination of the lowest likely $^{87}\text{Sr}/^{86}\text{Sr}$ ratio in the carbonate fraction. Samples were studied petrographically by standard optical methods and by cathodoluminescence (CL), the latter being used to reveal the likely extent of alteration and possible fluid pathways.

I have made a detailed grain-scale study of the variation of oxygen isotopes in calcite and quartz in four samples, one of which came from the metre-scale profile, the other three from the micro-drilled profile. I was able to use the combined CL imaging and grain-scale isotope data to constrain fluid infiltration pathways and to determine the extent of fluid-rock interaction. I also modelled grain-scale oxygen isotope profiles present in one sample to constrain likely time-scales of infiltration.

1.4 Thesis layout

The thesis is divide into three main parts.

Part 1: The geology and petrology of Dalradian carbonate rocks

In Chapter 2, I review broadly the geology of Dalradian metasedimentary rocks with regard to lithostratigraphy, structure and metamorphism, focussing in particular on carbonate rocks. I also include a section on the geology of locally carbonate-bearing metasedimentary rocks on Colonsay which are presently of undetermined lithostratigraphical affinity.

In Chapters 3 and 4 I discuss the petrography of the limestones, dolostones and calc-silicate rocks and the implications of the petrology for interpretation of the isotope data. I present work on modelling the mineral assemblages in T-X_{CO₂} sections using thermodynamic principles. In Chapter 3, I use these sections to place broad constraints on equilibrium fluid compositions. In Chapter 4, the T-X_{CO₂} sections provide the framework for interpreting complex phase relations, the elucidation of metamorphic fluid composition and the extent of fluid infiltration. I discuss the implications arising from this work with regard to scales of equilibrium.

Part 2: Strontium, carbon and oxygen isotope geochemistry of Dalradian limestones and dolostones

As a precursor to the work on strontium, carbon and oxygen isotopes presented in Chapters 6 and 7, I discuss in Chapter 5 the main controls on isotope geochemistry of the marine environment, the ways in which carbonate sediments

record this geochemistry and the ways in which isotope signatures may be modified, particularly during diagenesis.

Part 3: Outcrop- and grain-scale spatial variations in stable isotope compositions of calcite and quartz: fluid infiltration mechanisms and timescales

In Chapter 8, I review the current state of knowledge on fluid transport mechanisms in metamorphic rocks, with particular reference to limestones. I have concentrated particularly on recent work which has elucidated likely time-scales of infiltration through the study of diffusion profiles.

In Chapter 9, I discuss outcrop and grain-scale oxygen and carbon isotope data for limestones from two localities and the implications of these data for metamorphic fluid rock interaction. I go on to discuss the grain-scale oxygen isotope data for calcite and quartz with regard to fluid-rock interaction processes.

In Chapter 10, I present quantitative and semi-quantitative modelling of the grain-scale oxygen isotope data, particularly diffusion profiles present in one sample and quartz-calcite oxygen isotope fractionation in two others. I determine the likely mechanisms by which fluid infiltrated the limestones and the conditions under which infiltration occurred. I also estimate the likely time-scales over which infiltration occurred.

In Chapter 11, I summarise the work discussed in the thesis, present the main conclusions and consider areas of further research.

Part 1

The geology and petrology of Dalradian carbonate rocks

Chapter 2

Dalradian lithostratigraphy, structure and metamorphism, with special reference to carbonate rocks

In this Chapter:

- ❖ The lithostratigraphy of Dalradian carbonate rocks
- ❖ Summary of Dalradian structure and metamorphism
- ❖ The geology of Colonsay

2.1 Introduction

In this chapter I summarise briefly the geology of the Dalradian Supergroup of mainland Scotland and the islands of the Inner Hebrides. At the end of the chapter I highlight briefly the current controversy over the age of the Dalradian. The implications of carbonate Sr isotope data with regard to this problem are discussed in Chapter 6.

Several recent publications, particularly Harris et al., (1994), Stephenson and Gould (1995), Robertson and Smith (1999) and Smith et al., (1999) have discussed Dalradian lithostratigraphy in considerable detail. Rather than reiterating this published work, this account focusses chiefly on the lithostratigraphy of metacarbonate rocks discussed in this thesis. More specific lithological and petrological details are given in Chapters 3 and 4.

The geology of the enigmatic Colonsay Group on Colonsay (Inner Hebrides) is also briefly discussed. Although rare on Colonsay, the carbonate rocks are potentially important with regard to elucidating possible regional correlatives (see Section 2.4).

2.2 Dalradian Supergroup

2.2.1 Outline of Dalradian geology

Metasedimentary and predominantly mafic metavolcanic rocks assigned to the Dalradian Supergroup crop out from Shetland, through the mainland Scottish Highlands, into Ireland, covering an area of *c.* 48 000 km² (Harris et al., 1994). On the Scottish mainland, the Dalradian is bounded to the northwest by the Great Glen Fault and to the southeast by the Highland Boundary Fault (Figure 2.1). Possible correlation between lowermost Dalradian strata in the Central Highlands of Scotland and uppermost Moine metasedimentary rocks northwest of the Great Glen has been conjectured on the basis of lithological similarity (Soper and England, 1995), but the issue remains unresolved.

The heterolithic sediments of the Dalradian were deposited in ensialic, largely shallow marine basins on the now fragmented eastern margin of Laurentia and its supercontinent predecessor, Rodinia (e.g. Dalziel 1997). Together with the Moine, they are broadly equivalent, in age and tectonic setting, to other great Neoproterozoic clastic sequences that now fringe the North Atlantic. These include the Hecla Hoek (Svalbard), the Eleonore Bay Supergroup (Eastern Greenland), the Hagen Fjord Group (eastern North Greenland) and the Fleurs de Lys (Newfoundland) (Soper, 1994). These

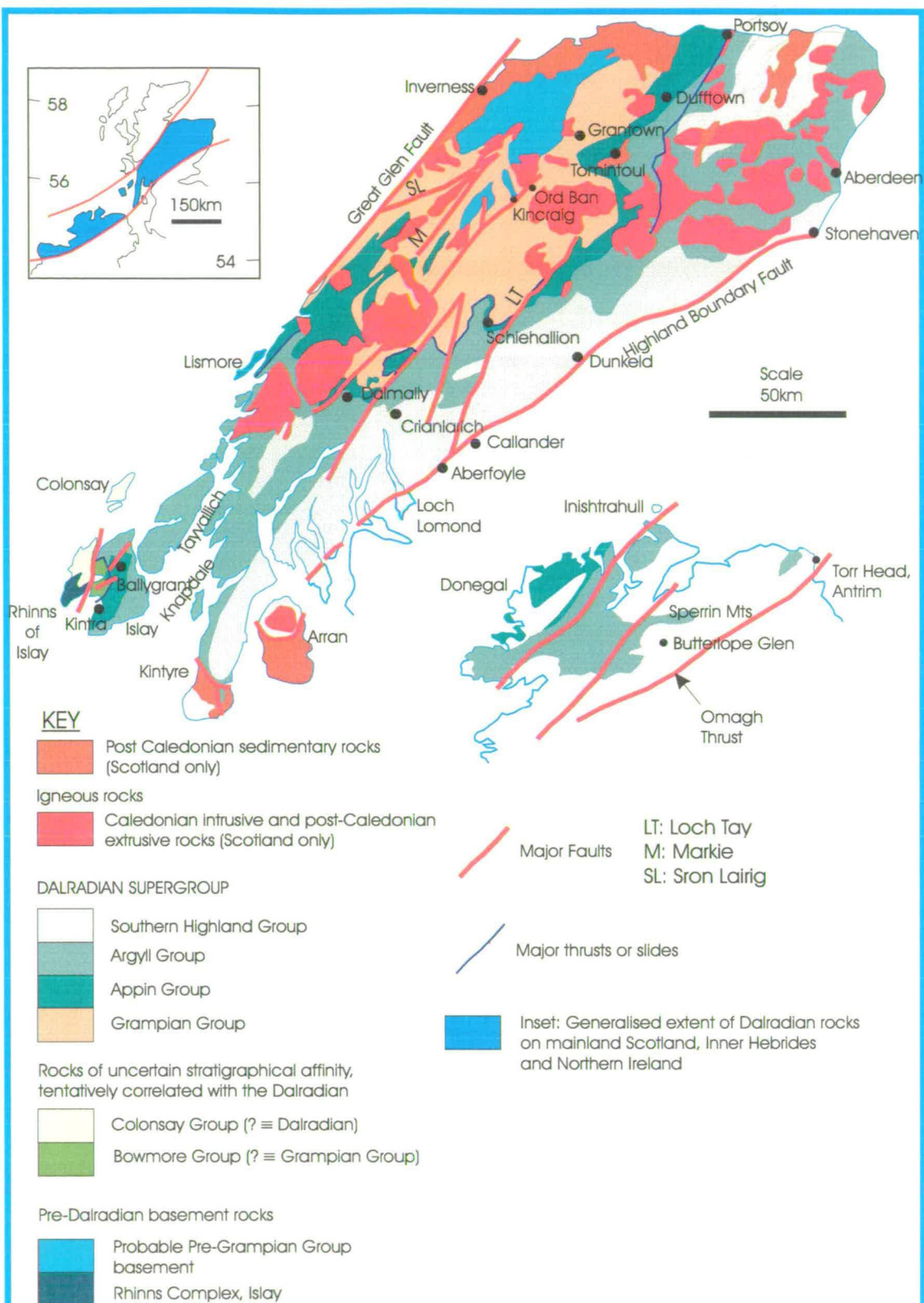


Figure 2.1 Distribution of Dalradian rocks on mainland Scotland, the Inner Hebrides and Northern Ireland (only Dalradian shown in Northern Ireland)

After Harris et al 1994 and Stephenson and Gould, 1995.

‘Atlantic’ Neoproterozoic sequences also have important ‘Pacific’ equivalents on the western margins of the United States and Canada, in the form of the Windermere Supergroup and the Mackenzie Mountains Supergroup (Narbonne and Aitken, 1995; Narbonne et al., 1994) and similar sequences also occur in southeastern Australia (Young, 1992). The *aggregate* thickness of Dalradian sediments is estimated at some 25-28 km (Harris et al., 1994; Soper, 1994), but true sedimentary thicknesses at any one point are probably only ~ 15 km.

Neither the true stratigraphical base nor top of the Dalradian are exposed in Scotland. Gneissose psammites and semipelites in the Central Highlands (Piasecki and Temperley, 1988; Piasecki and Van Breeman, 1979)) are considered to form basement to the Dalradian in the Central Scottish Highlands (Piasecki and Van Breeman, 1979; Robertson and Smith, 1999; Smith et al., 1999), although this interpretation is disputed by others (Highton et al., 1999; Lindsay et al., 1989; Noble et al., 1996). The top of the Dalradian is marked by sheared and faulted contact with Ordovician rocks of the Highland Border Complex in the Highland Boundary Fault Zone. West of Loch Lomond and north and northeast of Blairgowrie, Devonian and Lower Carboniferous rocks rest unconformably upon the Dalradian.

The Dalradian Supergroup is divided into four lithostratigraphical Groups as follows (oldest to youngest): Grampian, Appin, Argyll and Southern Highland (Figure 2.1). Each Group is lithologically distinctive and, despite the structural complications due to the Grampian Orogeny, the Groups ‘young’ outwards from the Central Highlands to the west, south and east. As it does so, the Dalradian sequences change from largely feldspathic psammitic rocks, through the classic Dalradian (*s.l.*) quartzite-carbonate-

pelite bearing successions that locally include volcanic rocks, into turbidites with locally important volcanoclastic units.

2.2.2 Constraints on the age of Dalradian

The Grampian and Appin Groups occur below the basal Argyll Group tillites that are equated with the Varangan tillites of East Svalbard, Spitsbergen (Fairchild and Hambrey, 1995; Hambrey, 1983; Hambrey et al., 1991). The tillites have been dated at approximately 600 Ma (Kaye and Zartman, 1980; Knoll and Walter, 1992; Krogh et al., 1988), but may be older in part (Pringle, 1973). The maximum age of the Grampian Group is currently undefined and remains controversial (see discussion in Section 2.6). Recent arguments are synthesised in a set of thematic conference papers published in the Journal of the Geological Society, volume 156, part 6, November 1999.

The Argyll Group is bracketed by the ~600 Ma Port Askaig Tillite and the Tayvallich volcanics (595 ± 4 Ma; Halliday et al., 1989). The age constraints, if correct, imply the Argyll Group was deposited in a very short period of time (~10 – 20 Ma). This is at least consistent with the stratigraphical evidence for very rapid deposition in extensional, fault-controlled basins coupled with coeval volcanism, particularly in the upper parts of the Group (*e.g.* Anderton 1985; 1988).

The succeeding Southern Highland Group extends into at least the lower Middle Cambrian (*c.* 510-520 Ma), based on the trilobite fauna in the Leny Limestone near Callander (Cowie et al., 1972; Pringle, 1940). Following the recent work of Tanner (1995), the Leny Limestone is now considered on structural and lithostratigraphical evidence to be part of the Dalradian. A recent putative Arenig age for the Macduff Slate of Banffshire is based on a single, poorly preserved specimen of

the acritarch *Veryhachium* cf. *lairdii* (Molyneux, 1998) is considered here to be unreliable and requiring corroboration. I consider the depositional age of the Dalradian further in Chapter 6, where I present and discuss the implications of carbonate $^{87}\text{Sr}/^{86}\text{Sr}$ data.

2.3 Lithostratigraphy of Dalradian carbonate and calc-silicate rocks of Scotland

Dalradian lithostratigraphy is now well-established within the Dalradian outcrop of mainland Scotland (Figures 2.2, 2.3). In the following sections, I concentrate briefly on the lithostratigraphical setting of the carbonate and calc-silicate rocks studied in detail in this thesis. The numbers at the end of headings for each limestone unit refer to those in Figure 2.2.

2.3.1 Grampian Group limestones

Grampian Group successions are dominated typically by feldspathic, psammitic rocks with subordinate semipelitic and pelitic lithologies. Bed-parallel, calc-silicate laminae and lenses occur in a number of the psammitic units, but carbonate rock units themselves are very rare, being restricted to the lowermost Kincaig Formation at the base of the Corrieyairack Subgroup (Figure 2.3).

The limestones are part of an important heterolithic succession which includes kyanite-bearing pelites and amphibolites in the Kincaig Formation. They vary from grey, medium-grained to coarsely crystalline white limestones; they are dominantly calcitic. The limestone – pelite – amphibolite assemblage crops out near Kincaig and at Ord Ban (Figure 2.1), where it forms the local base of the Grampian Group, resting

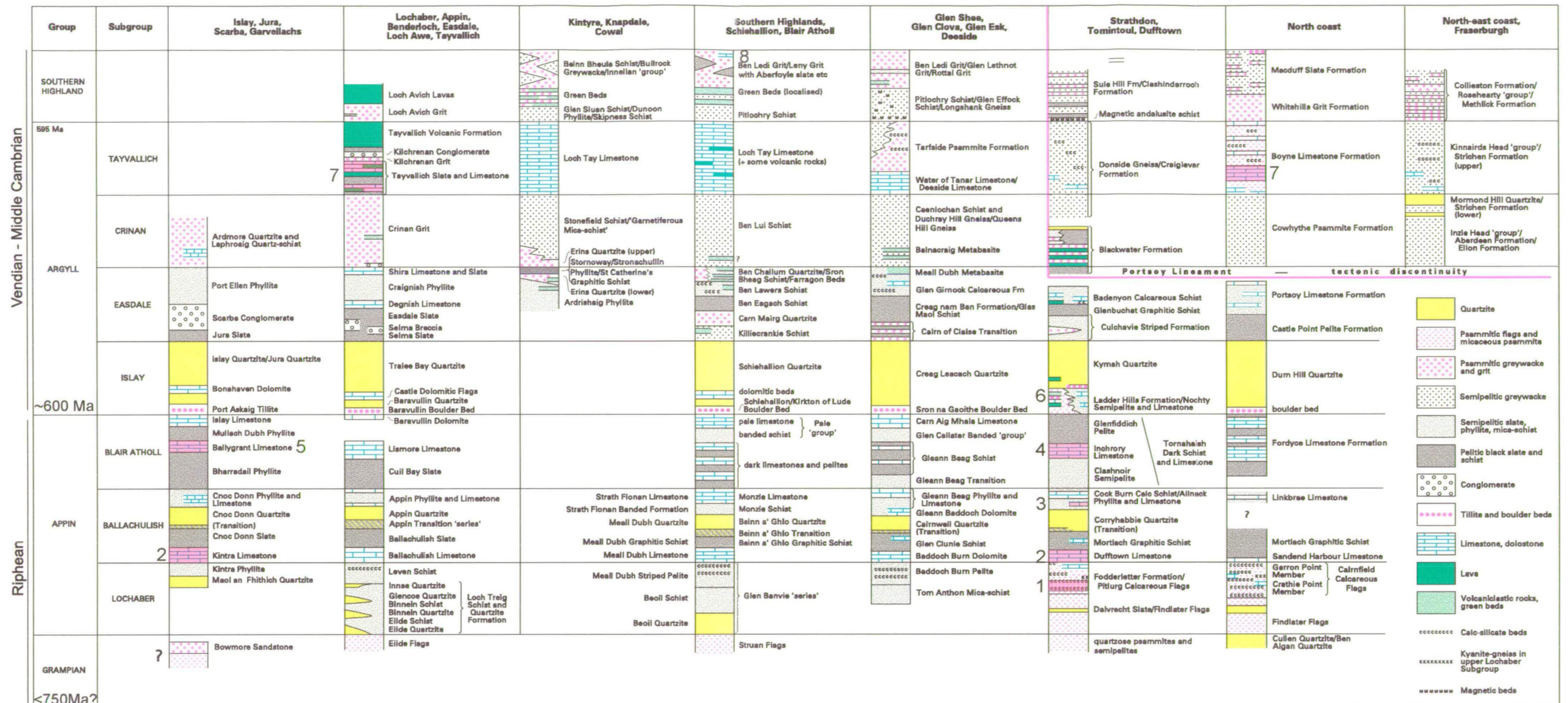


Figure 2.2 Dalradian lithostratigraphy of the Scottish mainland. The numbered, red-shaded limestone units are those discussed specifically in this study.

- 1: Pitlurg Calcareous Flag Formation
- 2: Kintra Dolostone Formation, Islay; Dufftown Limestone Member, Mortlach Graphitic Schist Formation
- 3: Torulian Limestone Member, Ailnack Phyllite and Limestone Formation
- 4: Inchory Limestone Formation
- 5: Storakaig Limestone Member, Ballygrant Limestone Formation, Islay
- 6: Dolostones associated with tillites in the basal Argyll Group, Northeast Grampian Highlands
- 7: Tayvallich Limestone, Tayvallich Slate and Limestone Formation; Boyne Limestone Formation
- 8: Lenny Limestone

Modified from Stephenson and Gould 1995

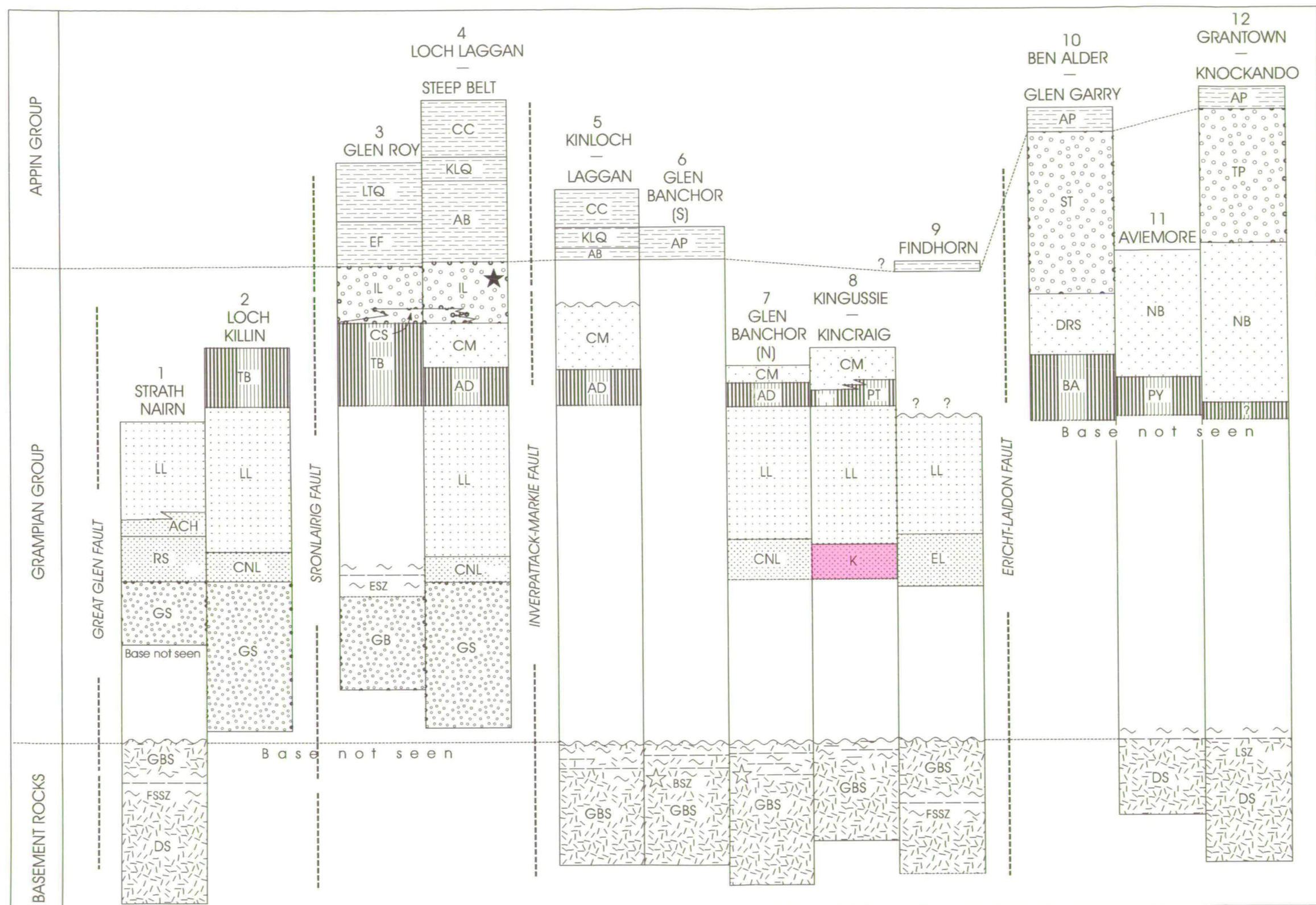


Figure 2.3 The stratigraphy of the Grampian and lowermost Appin Group in the Central Grampian Highlands, showing the relative position of the limestone-bearing Kinraig Formation (K) within the Grampian Group. The limestones in this formation are currently the oldest known in the Dalradian. They crop out principally in the Ord Ban and Kinraig areas (see also Figure 2.1). Other abbreviations are given in Smith, et al., 1999. Modified after Smith et al 1999.

directly on rocks now assigned to the basement succession (Figure 2.3) (Smith et al., 1999).

Originally termed the Ord Ban Subgroup by Winchester and Glover (1988), this limestone-bearing assemblage at the base of the Coireyairack Subgroup was correlated by Stephenson and Gould (1995) with the well-known carbonate-bearing successions in and around Grantown (the 'Grantown Series' of Hinxman and Anderson (1915)) and renamed the Grantown Formation. However, limestones in the Ord Ban and Kincaig outcrops are geochemically distinct from any other Dalradian limestones (Thomas and Aitchison, 1998). Recent lithostratigraphical mapping by the BGS has shown that the limestones at Kincaig and Ord Ban cannot be lithostratigraphically equivalent to the Grantown Formation and they are currently the oldest known Dalradian limestones.

2.3.2 Appin Group carbonate rocks

The Appin Group comprises a strongly heterolithic assemblage of pelites, semipelites, calcitic and dolomitic limestones, dolostones, quartzites and calc-silicate rocks. In contrast to the Grampian Group, carbonate rock units are common and lithostratigraphically important.

The Group is divided into the Lochaber, Ballachulish and Blair Atholl Subgroups, the last-named being the youngest. The sediments comprising the Appin Group are entirely marine and were deposited during an extended phase of thermal subsidence in the upper part of the Riphean, probably between *c.* 700 and *c.* 600 Ma.

The Pitlurg Calcareous Flag Formation, Lochaber Subgroup (1)

The Lochaber Subgroup contains rocks that are transitional between the carbonate-poor Grampian Group and the carbonate-bearing sequences of the Ballachulish and Blair Atholl Subgroups. It becomes calcareous in its uppermost parts in many places along its outcrop, particularly in the Northeast Grampian Highlands (Stephenson and Gould, 1995) and the appearance of carbonate rocks is an important feature of the Lochaber Subgroup (Figure 2.2).

The main parts of the Lochaber Subgroup are dominated by shallow marine mature siliciclastic lithologies, chiefly quartzites and semipelites, which exhibit rapid lateral and vertical facies changes (Figure 2.2). In the Northeast Grampian Highlands three approximately equivalent formations are recognised: the Fodderletter, Formation and the Pitlurg and Cairnfield Calcareous Flag formations. Phyllites, schists with calc-silicate rich rocks, and thin calcitic to dolomitic limestones and dolostones are developed in background psammitic lithologies.

The Pitlurg Calcareous Flags Formation crops out in the Dufftown area [NJ320400] (Figures 2.1, 2.2). To the south and east of Dufftown, the Pitlurg Calcareous Flags lie in the core of a complex regional F_3 fold termed the Ardonald Anticline (see also Figure 4.1). The formation includes calc-schists, calc-silicate rocks and calcitic limestones. They are locally well exposed in stream sections in Glen Rinnes, about 6 km southwest of Dufftown. The lithologies are thinly laminated to thinly bedded with bed thickness ranging up to a few tens of centimetres.

Anderton (1988) considered that the fining upward sequence observed towards the top of the Lochaber Subgroup in the Southwest Scottish Highlands may represent a transition from tidal shelf to deeper water sedimentation. However, as discussed in

Chapter 4, the aluminous, magnesian and potassic character of the mineral assemblages in these rocks, together with the presence of common accessory hyalophane suggests that the protolith to the calc-silicate assemblages was an aluminous and potassic dolostone. One can conjecture that, in the Northeast of Scotland at least, this was a very shallow water deposit, subject, possibly to sub-aerial exposure during which there were periods of desiccation and possibly formation of evaporites, increasing K and Ba concentrations. The aluminous character implies the introduction of Al-rich clay minerals from a deep-weathered hinterland.

The abundance of Mg may have come from primary or early diagenetic dolomite or possibly even primary magnesite, as can occur in some extreme ephemeral lake systems (e.g. Coorong, Southern Australia; Bathurst 1975). Though subject to alteration during metamorphism, the fine-grained lamination in the rock is considered to reflect original sedimentary layering; patch-laminae relationships in some thin sections support this interpretation.

The calc-silicate rocks occur just on top of the Grampian Group quartzites. Grampian Group sedimentation was dominated by clastic fill of rift-bound basins (Robertson and Smith 1999), which became increasingly mature towards the top. Deposition of the calc-silicate protolith can be seen as the culmination of this period of basin fill and a period of quiescence in Dalradian sedimentation. Renewed flooding is marked by the onset of first limestone and then mudstone deposition at the base of the overlying Mortlach Graphitic Schist Formation as Dalradian sedimentation became dominated by cyclic flooding and regression during Appin Group and early Argyll Group times.

Calc-silicate rocks, such as those which occur in the Pitlurg Calcareous Flag Formation, are important in metamorphic fluid-rock interaction studies. In Chapter 4, I present detailed work on the petrography and mineral chemistry of the calc-silicate assemblages aimed at elucidating their fluid-rock interaction history.

Kintra Dolostone, Dufftown Limestone, Ballachulish Subgroup (2)

The increasingly calcareous character of the Lochaber Subgroup culminates in the development of the Ballachulish Limestone and its lithostratigraphical equivalents at the base of the overlying Ballachulish Subgroup (Figure 2.2). The Ballachulish Subgroup comprises two successions containing calcareous and pelitic rocks, separated in many places by the Appin Quartzite and its equivalents.

On Islay, the basal Ballachulish Subgroup ‘limestone’ is represented by the Kintra Dolostone Formation. It is best seen in coast exposures in the type area at Port Alsaig [NR 311 479], near Kintra on the north coast of the Mull of Oa, where it crops out as a rusty-brown weathering, fine grained and massive dolostone.

Equivalent units in the Northeast Grampians include the Blairfindy, Dufftown and Sandend Harbour Limestone Members (Figure 2.2). In this region, these limestones are blue-grey and dominantly calcitic with some finer-grained, grey dolomitic limestone and rare dolostone.

The Dufftown Limestone is reasonably well-exposed in the Dufftown area and along the northwestern side of Glen Rinnes, notably in a disused quarry at Rinaitin [NJ264328]. It can be traced around the southern closure of the Ardonald Anticline at the head of Glen Rinnes (see Figure 4.1), but it dies out rapidly when traced northeast along the southeastern limb on the southeast side of the glen, leaving rocks of the

overlying Mortlach Graphitic Schist (= Ballachulish Slate Formation) in direct contact with rocks of the underlying Pitlurg Calcareous Flag Formation.

Anderton (1988) thought that the Ballachulish Limestone was deposited in relatively deep water in the 'Leven Schist' basin under anoxic conditions, as suggested by the presence of graphitic carbonate in the upper part of the limestone. Paradoxically, he also remarked on the presence of quartz-dolomite-pyrrhotite laths, interpreted by Hall (1982) to be anhydrite pseudomorphs, as 'the first of several indications of evaporative conditions within the Dalradian' (Anderton, 1988, p.415). The regional lithostratigraphical continuity of the basal Ballachulish Subgroup limestones across the Dalradian outcrop indicates that this unit represents a major flooding event succeeded by deposition in deep water of aluminous mudrocks which form the Ballachulish Slate and its equivalents, including, in Northeast Scotland, the Mortlach Graphitic Schist.

Torulian Limestone Member, Ailnack Phyllite and Limestone Formation (3)

Following deposition of the Appin Quartzite, there was a return to shallow water depositional environments dominated by fine-grained siliciclastic and calcareous sediments (Anderton, 1988) but including subordinate psammites and thin quartzites. Successions above the Appin Quartzite and equivalents typically become progressively more calcareous towards their tops and a number of limestone units are present in many places in the upper central and uppermost parts of the Formation. (Figure 2.2).

Distinctive white limestone is commonly developed in the lowermost parts of the Appin Phyllite and Limestone, in places in contact with the underlying quartzites. Although it is laterally very discontinuous, this lithology is known from many

successions at this level in the Scottish mainland outcrop of the Dalradian (Figure 2.2). It may be thick enough to form a mappable member, but it occurs more commonly as a single thin bed. In the Lochaber district it is known as the Onich Limestone. The main equivalent in the Northeast Highlands is the Torulian Limestone Member. This lithology is a coarse-grained white rock consisting almost entirely of calcite, although it is locally sulphidic.

The overall nature of the sediments and the increasingly calcareous character of the 'Phyllite and Limestone' units is strikingly similar to the upper parts of the Lochaber Subgroup. The siliciclastic and calcareous rocks are commonly thinly interbedded or interlaminated. The calcareous rocks in the Appin Phyllite and Limestone are generally calcitic, but dolomitic rocks and dolostones occur locally.

Limestones of the Blair Atholl Subgroup: Inchrory Limestone Formation (Northeast Grampian Highlands), Storakaig Limestone Member (Ballygrant Formation, Islay) (4,5),

Dark grey limestone units dominate the central parts of the Blair Atholl Subgroup, either as thick, individual units, or in dominantly calcareous dark schist and limestone units. These units are considered to have been deposited in relatively deep, anoxic water (Anderton 1988).

On Islay, the Storakaig Limestone Member of the Ballygrant Limestone Formation is a very dark, fine-grained lithology and is very well-bedded in outcrop, e.g. in Ballygrant Quarry, Ballygrant, Islay. The equivalent limestone in the Northeast Grampians is the Inchrory or Fordyce Limestone Formation. This limestone extends northwestwards from the Glen Gairn pluton to Tomintoul, where it is thickened

considerably by folding. It can be traced throughout the Northeast Grampian outcrop to the Banffshire coast.

In the Northeast Grampians, the 'mid Blair Atholl' limestones are characteristically coarsely crystalline with a grey to blue-grey, almost translucent, colour. They are quite commonly banded in appearance, particularly where paler in colour. Beds are marked by thin pelitic laminae; these pelitic interbeds may be more prominent in places and, on a larger scale, there is clearly a continuum from thick, almost pure limestone to more mixed and thinly interbedded sequences. Locally, as in Upper Donside, they contain strings and blebs of cherty silica. Another characteristic feature of these limestone units in the Northeast Grampians and elsewhere is the presence of roughly concordant lenticular pods of amphibolite. These are particularly well-seen in Limeworks Quarry [NJ156194], 1 km west of Tomintoul, where an *en echelon* train of amphibolite pods traverse the rear (northwest) quarry wall (see Figure 9.2).

The various limestone units at this 'mid' level in the Blair Atholl Subgroup have conspicuously similar chemistry (Thomas 1989; Thomas and Aitchison 1998) in the Southern Central and Northeast Grampian Highlands. The characteristic geochemical composition has been of considerable use in aiding lithostratigraphical correlation through poorly-exposed districts.

Limestones also dominate the lithostratigraphy of the uppermost parts of the Blair Atholl Subgroup in Central Southern and Southwestern Highlands and in areas of upper Deeside. Formations include the Lismore Limestone, forming most of Lismore Island, the Lossit Limestone on Islay and the Carn Aig Mhala Pale Limestone in the central districts (Figure 2.2). On Islay, the uppermost Blair Atholl Subgroup Lossit

Limestone is locally unconformable on the pelite-limestone Ballygrant Formation. In the Northeast Grampians, the uppermost parts of the subgroup are more siliciclastic and variable, with only thin limestones, particularly in the ground between Strathdon and Dufftown (J R Mendum in Harris et al., 1994, p.47; Stephenson and Gould 1995).

Upper Blair Atholl limestones in the Southwest Highlands locally become dolomitic towards their tops and contain stromatolites, flake breccias and oöids (Anderton 1988, and references therein). Fairchild (1985) recorded the presence of fibrous cements characteristic of waters of high salinity. These phenomena clearly indicate a return to very shallow water, evaporitic and probably arid conditions during deposition of the uppermost part of the Appin Group in this area (Anderton 1988).

Dolostones and tillites in the Islay Subgroup (6)

The most important feature of the Islay Subgroup is the presence of tillites, the best-known being the Port Askaig Tillite of Islay and the Garvellach Islands (Eyles and Eyles, 1983; Spencer, 1971; Stephenson and Gould, 1995) (Figure 2.2). The tillites become thinner to the northeast and are only locally developed at the base of the Creag Leacach Quartzite (= Islay Quartzite) in the Braemar area (Upton 1986). Similarly, in the Northeast Grampians, tillites are only sporadically developed and, north of Keith, it is inferred from large blocks of tillite-like material adjacent to the Durnhill Quartzite outcrop and very limited exposure on Lurg Hill.

In the Inner Hebrides, the tillites are succeeded by the Bonahaven Dolomite Formation (Fairchild, 1978) before the incoming of the thick, cross-bedded and pebbly Islay and Jura Quartzites. The Bonahaven Dolomite is interpreted as a supra- to sub-tidal, lagoonal facies, dominated by tidal and storm-controlled sedimentation in a

coastal marine environment partially restricted by off-shore shoals (Fairchild, 1980a). Brasier and McIlroy (1998) have recently documented ichnofossils from this unit on Islay. On the mainland of the Southwest Highlands, similar successions occur at Ardmucknish Bay in the Benderloch area (Litherland 1980).

In the Northeast Grampian Highlands, thin dolostones underlie tillites exposed in the Muckle Fergie Burn, south of Tomintoul. Also present here beneath the tillites are thin basic, sometimes pillowed lavas, signalling the beginnings of the volcanic activity characteristic of the upper parts of the Argyll Group. In the Ladder Hills northeast of Tomintoul, dolostones occur with sparse tillites within the Ladder Hills Formation, where there are also some lenses of volcanoclastic lithologies, and in the laterally equivalent Water of Nocht Semipelite Formation.

The association of dolostones with tillites (particularly those of c. 600 Ma Varangan/Marinoan age) is characteristic of many Neoproterozoic successions and the dolostones have been the subject of much debate and study in recent years (e.g. Fairchild, 1980a, 1980b, 1985; Kennedy et al., 1996; Myrow and Kaufman, 1999; Prave, 1999; Williams, 1979). A key feature of many of the dolostones above the tillites is that they have negative $\delta^{13}\text{C}$ signatures (see discussion in Chapter 8).

Tayvallich, Torr Head, Dungiven and Boyne Limestones (7)

The Tayvallich Subgroup is notable for two distinctive lithologies: the Tayvallich Limestone and its equivalents, the Loch Tay, Deeside and Boyne Limestones, and the Tayvallich Volcanic Formation (Figure 2.2). Although locally discontinuous along strike, the limestone is one of the most persistent marker horizons in the Dalradian.

In the Southwest Scotland, the limestone is interbedded with pelites in the Tayvallich Slate and Limestone Formation. Farther east in the Southern Highlands, the limestone represents the whole of the subgroup. However, it thins again to the northeast and is locally absent. In the Angus glens, it is represented by the Water of Tanar Limestone (= Deeside Limestone). In Aberdeenshire, the limestone is only poorly represented in the Donside Gneiss and Craigievar Formation, but is better developed again on the Banffshire coast, where it is known as the Boyne Limestone, well-seen in Boyne Bay.

The Tayvallich Limestone is readily traceable into Northern Ireland, where it is termed the Torr Head Limestone on the Antrim Coast and the Dungiven Limestone in County Tyrone. The Torr Head Limestone is particularly well-seen at Torr Head on the Northeast Antrim coast. Here it forms a unit of black, thin bedded and coarsely crystalline limestone some ten metres or so in thickness (see Chapter 3). Its contact with structurally underlying Southern Highland Group sediments is perfectly exposed and is transitional over a few metres from limestone, through thin bedded marly sediments into thick, hummocky cross-stratified sandstones, which then pass down (structurally) into turbiditic sediments characteristic of the Southern Highland Group.

The age of the Tayvallich Limestone (and equivalents) is well-constrained by the immediately overlying Tayvallich Volcanic Formation, dated at 595 ± 5 Ma (see also Chapter 3). This age constraint renders the limestone particularly important in the interpretation of $^{87}\text{Sr}/^{86}\text{Sr}$ initial ratio data for late Proterozoic seawater and also constrains the age of the tillites at the base of the Argyll Group (Chapter 6).

The limestone marks a sharp change in sedimentation at the end of the Crinan Subgroup. Anderton (1988) notes that although the Tayvallich Limestone locally

contains oöids, mainly in limestone clasts (see also Chapter 3), the original carbonate sediment was deposited by turbidity currents from adjacent shelves and is thus derived. According to Anderton, it commonly occurs as a calcarenite to calcirudite channel fill, or as thinner, fine-grained sheets in outer fan to basinal areas; he ascribes the change to carbonate deposition to a major change in the palaeogeography and tectonic character of the source area.

Leny Limestone

Apart from rare derived turbiditic limestones in the Whitehills Grit Formation of Banffshire, the Southern Highland Group is generally devoid of significant carbonate rocks. The notable and very important exception is the Leny Limestone of Callander, Perthshire. This unit is well-known for its Cambrian *Pagetides* trilobite assemblage (Cowie et al., 1972; Pringle, 1940). Until recently, the limestone and its host pelites and arenites of the Keltie Water Grit Formation (Tanner 1995) were assigned to the Cambro-Ordovician Highland Border Complex, which crops out discontinuously in tectonic slices along the Highland Boundary Fault. However, recent detailed structural and stratigraphical work by Tanner (1995), corroborated by Harris and Fettes (1998), shows conclusively that the Leny Limestone and its host rocks belong to the Dalradian. As discussed above, this implies Dalradian deposition continued at least into the lower Middle Cambrian.

The limestone is very poorly exposed and is best seen in the long-abandoned Leny Quarry, north of Callander. It is a black, lenticular-bedded and thoroughly graphitic limestone occurring within black graphitic and sulphidic pelite. In the Leny Quarry, the outcrop consists of two or three beds with a total thickness of about 1 m.

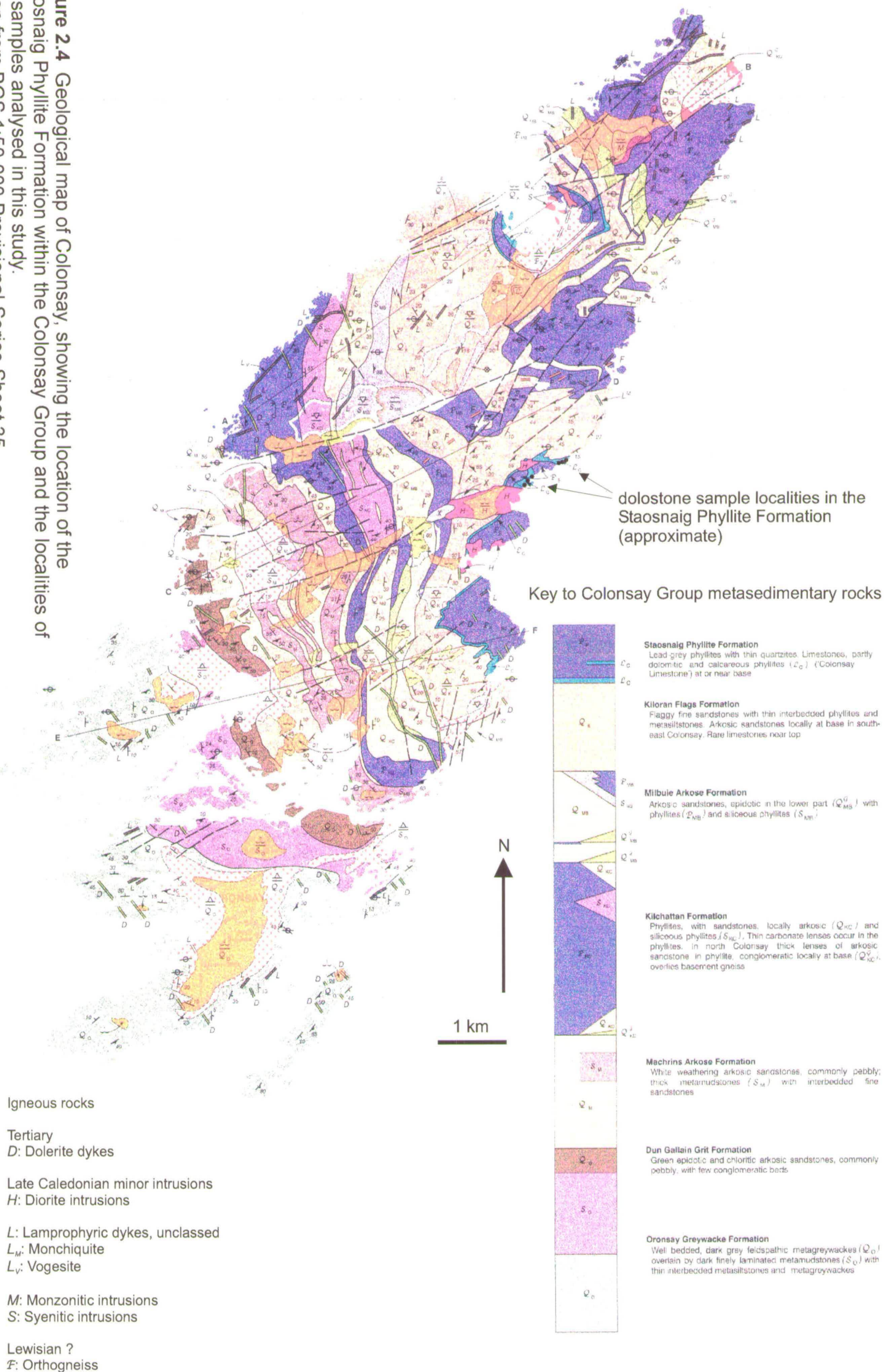
2.4 Colonsay Group

The Colonsay Group consists of about 6 km of predominantly siliciclastic and rare carbonate metasedimentary rocks cropping out on Colonsay, Oronsay and the Rhinns of Islay (Stephenson and Gould, 1995) (Figure 2.4). Their lithostratigraphical relationship with mainland metasedimentary successions remains unclear, and they have been variously ascribed to the Torridonian, the Grampian Group and the Dalradian. I have investigated the geochemical and petrographical characteristics of the rare carbonate rocks on the island in an endeavour to resolve this problem.

2.4.1 Basement – cover relationships of the Colonsay Group

The contact between the Colonsay Group and Rhinns Complex basement on Islay is marked by the Kilchiaran Shear Zone within which basement and cover rocks are tectonically interleaved (Muir et al., 1992). On Colonsay, quartzofeldspathic gneisses at the north end of the island are considered to form basement to the Colonsay Group metasedimentary rocks. The basement-cover contact is marked by mylonites and phyllonites in a high strain zone that Bentley (1988) interpreted as a sheared unconformity. Although the gneisses are currently assigned to the Rhinns Complex, they are lithologically very different to the syenitic and gabbroic basement on Islay. Available lithological and petrological descriptions suggest they have more in common with the Lewisian, to which they were originally assigned (Cunningham-Craig et al., 1911). Although deformed by early shearing and recumbent folding and later upright folding, Colonsay Group sediments have been metamorphosed only under lower

Figure 2.4 Geological map of Colonsay, showing the location of the Staosnaig Phyllite Formation within the Colonsay Group and the localities of the samples analysed in this study.
Taken from BGS 1:50 000 Provisional Series Sheet 35.



greenschist facies conditions and retain much of their sedimentary character (Muir et al., 1994).

2.4.2 Colonsay Group Lithostratigraphy

The siliciclastic succession (Figure 2.4) is dominated by arkosic arenites and wacke sandstones, but also includes phyllites, and it is considered to have been deposited as delta-top sands (Stewart and Hackman, 1973) and muds, and deeper water, delta-slope turbidites which become progressively more distal in character up through the succession (Stewart, 1962). Some of these siliciclastic rocks are rich in volcanogenic detrital phases, including epidote, amphibole, biotite and zircon and were deemed to have been derived from a mafic igneous source by Flett in Cunningham-Craig et al., (1922). Carbonate rocks are rare, but, where they occur in the upper part of the succession, are considered to indicate shallower water conditions (Muir et al., 1994).

Thin carbonate rocks occur in the phyllitic Kilchatten Formation and towards the top of the Kiloran Flags. Carbonate rocks are best developed at the base of the Staosnaig Phyllite Formation, exposed around Loch Staosnaig on the east side of the island, and around Kiloran Bay on the northwest side (Figure 2.4). These comprise grey, impure dolomitic limestones and dolostones and calcareous phyllites.

2.4.3 Age and regional correlation of the Colonsay Group

The Colonsay Group is cut by a series of small appinitic, alkaline monzonitic to syenitic intrusions at Kiloran Bay, nearby Balnahard and Scalasaig which belong to the Caledonian Appinite Suite and which have been dated at 439 ± 8.8 Ma (Muir et al.,

1997). Their field relationships with the Colonsay Group show that they were intruded between early and late phases of deformation (Bentley, 1988). Fitches and Maltman (1984) and Bentley et al. (1988) believe the rocks to have been affected by a major deformation phase apparently not observed on the Scottish mainland. Muir et al., (1997) supported this view, although they considered structures within the intrusions to have been developed during their emplacement. They considered the late structures to correlate with the Islay Anticline, but early structures to correlate with structures seen on the Rhinns of Islay, west of the Loch Gruinart Fault and with no obvious counterpart to the east. Thus, the intrusions are most easily considered as late Caledonian and provide little constraint on the age of the Colonsay Group.

In original work by the Geological Survey of Scotland, it was considered that the basement to the Colonsay Group is Lewisian; the Colonsay Group itself was correlated with the Torridonian (Cunningham-Craig et al., 1911). However, the Torridonian-Colonsay Group correlation has been discounted in recent years. The presence of carbonate rocks has led several authors to suggest that the Colonsay Group should be correlated with Appin Group (Dalradian) (Rock, 1985; Stephenson and Gould, 1995, and references therein). It is noted here that, superficially, at least, the uppermost parts of the succession are similar to those of the upper Lochaber and lowermost Ballachulish Subgroup in the Lochaber district, which are characterised by transition from quartzose to pelitic sedimentation via a phase of commonly dolomitic carbonate deposition (see preceding sections on the Lochaber and Ballachulish Subgroups). This lithological similarity has also been suggested previously by Litherland (as a personal communication in Stewart and Hackman, 1973). However, difficulties remain in reconciling lithologies, such as the epidotic grits, the presence of

supposed volcanic detritus and the nature and timing of deformation events with nearby Dalradian successions (Fitches et al., 1990; Muir et al., 1994). Because of these uncertainties, Anderton and Bowes (1983) have regarded the Colonsay Group as a separate succession. The strontium and carbon isotope geochemistry of the 'Colonsay Limestone' is discussed in Chapters 6 and 7.

2.5 Dalradian structure

The tectonic structure of the Dalradian results in broad terms from four main episodes of orogenic deformation acting on the pre-existing sedimentary basin architecture. Pre-orogenic structures significantly influenced both Dalradian sedimentation and subsequent orogenic phenomena (e.g. Anderton, 1988; Fettes et al., 1986, and references therein). Several putative syndepositional faults are thought to have been reactivated during Grampian orogenesis, resulting in the well-known Dalradian slides and other zones of attenuated lithostratigraphy (Anderton, 1985; 1988; Robertson and Smith, 1999; Soper and Anderton, 1984). Other, trans-Caledonoid structures, such as the Cruachan Lineament (Graham, 1986) and the Deeside Line (Fettes et al., 1986), and the Portsoy-Duchray-Hill Lineament (Stephenson and Gould 1995), have had a profound effect on a wide range of Dalradian features, including the distribution of Dalradian metasedimentary rocks and Caledonian granitic and granitoid intrusions, orogenic structure and metamorphism, and regional geochemical and geophysical characteristics. The Cruachan Lineament also appears to limit the southwesterly extension of the Boundary Slide. The potential of these pre-orogenic structures to affect limestone geochemistry is clearly important and must be considered.

2.5.1 Grampian orogenic structures

Grampian orogenic events resulted from the closure of the Iapetus Ocean and probable continent-arc and/or continental fragment collision along the eastern Laurentian margin during the lower Palaeozoic between about 510 and 425 Ma. The recent acceptance of the Cambrian Leny Limestone and its host Keltie Water Grit Formation as being part of the Dalradian (Harris et al., 1998 ; Tanner, 1995), and the revised interpretation of the 590 ± 2 Ma Ben Vuirich Granite (Rogers et al., 1989) as wholly pre-tectonic (Tanner, 1996) constrains Grampian orogenic deformation to be wholly lower Palaeozoic, concentrated during the middle Ordovician.

Despite wide local and regional variations in the nature and number of discrete deformation events and persistent problems in correlating major structures across the Dalradian (Fettes et al., 1986), evidence for four main phases of deformation can be recognised (Fettes et al., 1986; Stephenson and Gould, 1995). These events and associated notable structures are summarised in Table 2.1; the gross structure of the Scottish Grampian Highlands is shown schematically in Figure 2.5. The events can be characterised as follows:

a) D_1

In the Southern Highlands, the southeast-facing recumbent Tay Nappe dominates the early structure. In the Southwest Highlands, northwest of the Tay Nappe, the southeast facing Ardrishaig Anticline, the upright, composite Loch Awe Syncline and the northwest facing Islay Anticline define a zone of structural divergence. In

Deformation event	Effects	Timing	Notable structures
D ₁	Nappe formation, early cleavages in Southern Highlands	Post-dates Leny Limestone (c. 515 Ma) & predates onset of D ₂ (c. 480 Ma)	Tay Nappe ¹ , Ardrishaig Anticline, Islay Anticline, Beinn a Chuallich Folds, Creag na h'Iolair Anticline, Loch Awe Syncline, Ben Ledi Antiform, Aberfoyle Synform ²
D ₂	Tectonic thickening, refolding of F ₁ folds in Ben Lui Fold complex, deformation of Tay Nappe in Southern Highlands, ductile movement along shear zones and slides	c. 470 Ma, based on intrusion of basic masses in NE Scotland. Just pre- to syn peak of metamorphism	F ₂ folds of the Ben Lui Fold Complex, Stob Bhan Synform, deformation along Boundary Slide, Fort William Slide, Grampian Slide
D ₃	Minor, SE-closing folds and related cleavages in Southern Highlands, ? regional scale folds in central and NE Scotland, movement on Portsoy - Duchray Hill Lineament	c. 460-470 Ma. Syn- to just post peak of metamorphism	? Folds in the Ben Lui Fold Complex, ? Boyndie Syncline
D ₄	Uplift to form steep belts and late folds, followed by compression to form F ₄ folds and cleavages. Associated retrogressive metamorphism and albite porphyroblast in SW Scotland	460 - 440 Ma	Highland Border Downbend, Tarbet Monoform, Ben Lawers Synform
¹ Names of structures taken from Stephenson and Gould 1995, and references therein ² 'Aberfoyle Anticline' in literature; strictly, a synform ³ Regarded as D1 by Treagus and Roberts, 1981)			

Table 2.1 Summary of main features of Dalradian structure

Northeast Scotland, D₁ structures are upright and recumbent nappe structures are considered largely to be absent, except possibly on the Aberdeenshire coast, as at Collieston, north of Aberdeen (Ashcroft et al., 1984; Mendum, 1987).

b) D₂

D₂ is considered to be the main pervasive deformation event of the Grampian Orogeny. Early folds were refolded and it was during D₂ that there occurred the main ductile movements along the well-known Dalradian slides and shear zones, such as the Boundary Slide and the Portsoy-Duchray Hill Lineament (Beddoe-Stephens, 1990). Peak metamorphic conditions are considered to be syn- to post-D₂ in many areas (Section 2.6)

c) D₃

D₃ is generally considered to have been temporally related to D₂ but is much more variable in orientation and intensity. In many areas it is considered to just post-date the peak of metamorphism, although Dempster and Harte (1986) record post-D₃ higher pressure metamorphism effects in the Central Scottish Highlands. Although intensely developed in some areas, such as the Angus Glens (Robertson, 1994), it is absent in others, as, for example, in parts of the Southwest Highlands (Skelton et al., 1995). In Northeast Scotland, the large basic masses of the Buchan area are associated spatially with and disrupted by the major shear zones which were active during D₃ (Ashcroft et al., 1984; Stephenson and Gould, 1995). In the Southern Highlands, D₃ only appears at lower structural levels and is first seen manifest as minor folds just over the axis of the Highland Border Downbend (see below) in the Trossachs area (personal observations).

d) D₄

Events ascribed D₄ are likely to have been complex, protracted and diachronous (Dempster, 1983; Dempster, 1985; Harte et al., 1984). Many structures were probably developed only locally. Post orogenic uplift is considered the main feature of D₄ and is thought to have been associated with extension and normal faulting, but it appears to have been followed by further compression. Localised differential uplift is indicated to have begun early in the Southeastern Highlands (Dempster, 1984; Dempster, 1985). The best-known D₄ structures are the Highland Border Downbend, the Ben Lawers Synform and the Cowal Antiform. The Downbend is thought to have resulted from the draping of Southern Highland Group rocks in the hinge zone of the Tay Nappe over a deep-seated basement step. Harte et al., (1984) consider that this structure formed between 460 and 440 Ma.

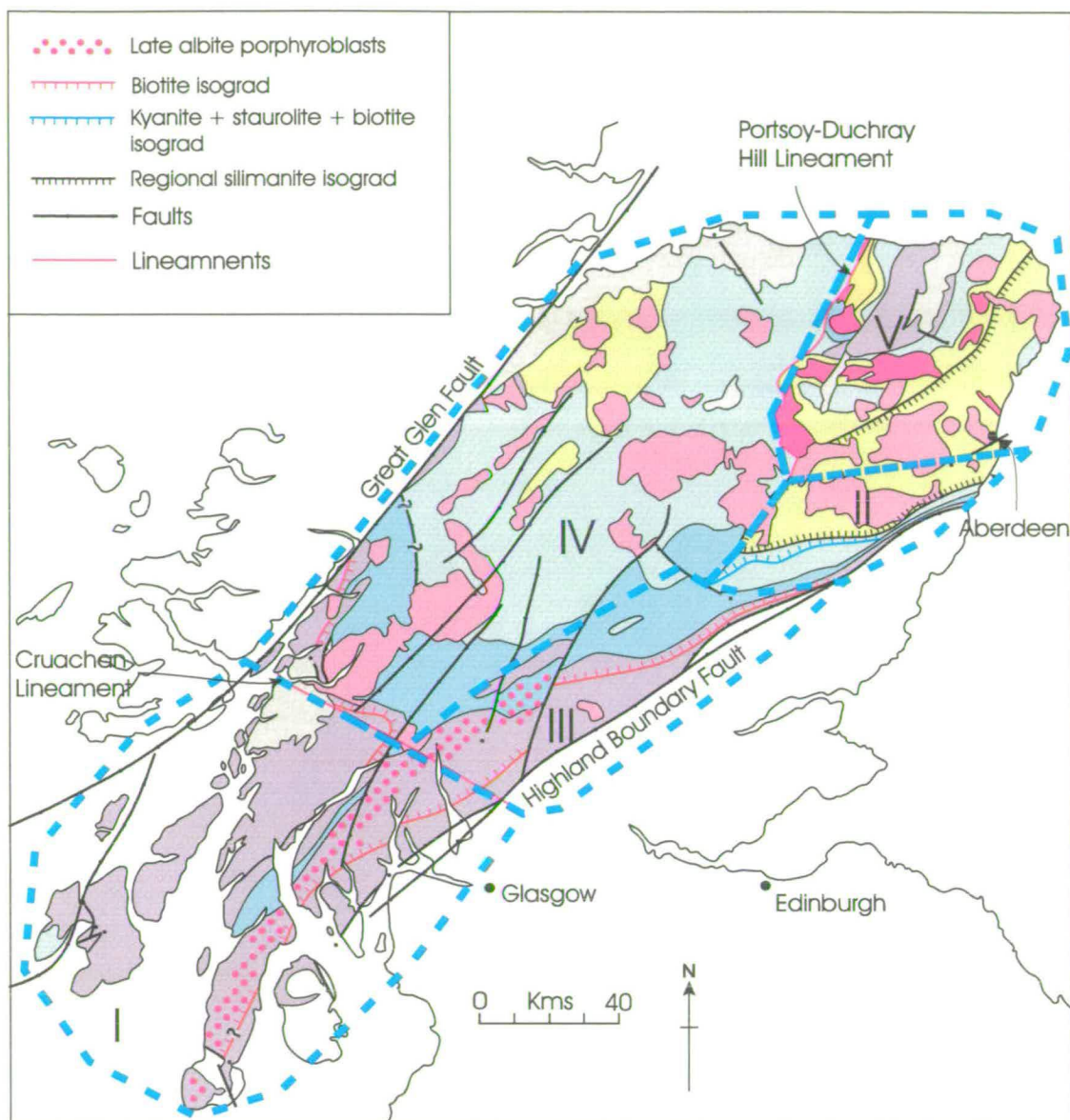
2.6 Dalradian metamorphism

Harte (1988) divided the Dalradian of the Scottish mainland into a series of domains with coherent metamorphic characteristics within fairly distinct geographical areas, commonly defined by tectonic features, notably lineaments and steep belts. These domains remain a useful way of summarising Dalradian metamorphism and are given in Table 2.2, together with summary peak metamorphic temperature conditions; the distribution of metamorphic facies and Harte's domains is shown in Figure 2.6.

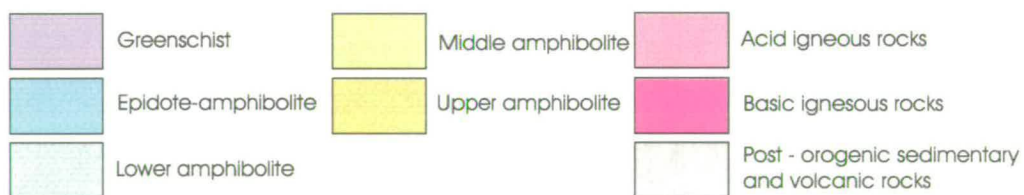
Prograde regional metamorphism accompanied D₂ and D₃ deformation events, followed by a retrograde event which coincided with parts of the complex late

Domain	Metamorphic facies	Peak metamorphic temperatures (°C)	Extent	Relative Timing	Comments
Southwest* (I)	Largely greenschist facies, but with a 'spine' of epidote-amphibolite facies rocks; pressures of 8 - 12 kbars	Greenschists: 410 - 510 ±30 garnet grade rocks: 510 - 540 ±30 <i>Graham et al (1983); Skelton et al (1995) and references therein</i>	Bound to the east by the Cruachan Lineament. The central spine of garnet-grade rocks lie in Knapdale	Post D ₁ -D ₂ deformation	Marked deflection of isograds coincides with the Cruachan Lineament in northwest of the area. The garnet isograd is the incoming of garnet in metabasic rocks.
Southeast (II)	Greenschist to amphibolite in general; local granulite facies rocks around Glen Muick. Pressures of up to 8 kbars	Up to 650 in SE at sillimanite isograd. Upto 800 in Glen Muick area (gnt - cpx) <i>Dempster 1985; Baker 1985</i>	East of the Portsoy - Duchray Hill Lineament, extending south of the sillimanite isograd of Eastern Scotland, to the Highland Boundary Fault	Post D ₂ to syn-D ₃	Characterised by very steep temperature gradients adjacent to the Highland Boundary Fault; the type area for Barrovian metamorphism
Central Southern Highlands (III)	Greenschist to epidote-amphibolite facies; pressures up to about 8 kbars	c. 400 - 520 (Flat Belt) <i>Dempster & Harte 1986</i>	South of the Tummel Steep Belt and east and west, respectively, of the two above domains	Complex. D ₂ -D ₃ to syn D ₃ ; post D ₃ locally	Dempster and Harte (1986) record increased pressure after D ₃ into the Tummel Steep Belt. Beddoe-Stephens (1990) records a pressure increase west of the Portsoy-Duchray Hill Lineament, coeval with thrusting along this structure during D ₂ , D ₃ .
Central** Highlands (IV)	Lower amphibolite facies at 7 to 10 kbars	c. 500 - 650 (Tummel Steep Belt) <i>Dempster & Harte 1986</i> 550 - 700 approx. (Margins, Central Highland Migmatites <i>Phillips et al in press</i> 500 - 650 (West of Portsoy - Duchray Hill Lineament) <i>Beddoe-Stephens 1990</i>	Including and to the north of the Tummel Steep Belt, into the Central Highlands, including Grampian Group and extending westwards to the Portsoy - Duchray Hill Lineament north of the Cairngorms		
Buchan (V)	Greenschist to amphibolite facies, including sillimanite-bearing rocks in SE; markedly lower pressures of 2 - 5 kbars	430 ±15 (cordierite isograd) to 550 ±50 (Upper Staurolite Zone) <i>Hudson 1985</i>	East of the Portsoy-Duchray Hill Lineament and north, approximately, of the putative Deeside Lineament		
<p>Roman numbers after domain name indicate area on Figure 2.6</p> <p>* Includes the Inner Hebrides (Islay, Jura, Colonsay, Arran)</p> <p>** Domain 6 of Harte (1988) can be included here, following more recent work on metamorphic conditions by Phillips et al 1999. This domain includes putative basement rocks which are considered to have undergone a Precambrian metamorphic event at about 800 Ma, also at amphibolite facies.</p>					

Table 2.2 Peak metamorphic domains in the Dalradian of mainland Scotland and the Inner Hebrides. Modified after Harte (1988)



METAMORPHIC FACIES



Approximate limits to Harte's (1988) tectonometamorphic domains (see Table 2.2)

Figure 2.6 The distribution of metamorphic facies in the Grampian Highlands, after Stephenson and Gould 1995 and Harte 1988.

deformation events assigned to D₄. The nature, distribution and timing of metamorphic events are complex (Baker, 1985; Beddoe-Stephens, 1990; Dempster, 1985; Dempster and Harte, 1986; Graham et al., 1983; 1988; Harte and Hudson, 1979; Hudson, 1985; Piasecki and Van Breeman, 1979). As with patterns of sedimentation and structure, the control on metamorphism of long-lived, basement structures is evident (Figure 2.6). Once again, the Cruachan and Portsoy – Duchray Hill lineaments are particularly important, limiting metamorphic phenomena on either side of them (Ashcroft et al., 1984; Beddoe-Stephens, 1990; Fettes et al., 1986; Graham, 1986; Harte, 1988).

Metamorphic facies range in general from greenschist (with a local ‘spine’ of epidote-amphibolite rocks) in the Southwest Highlands, to middle amphibolite at a range of pressures in the Eastern and Central Highlands (Figure 2.6) (Harte, 1988). There is no simple relationship between grade and metamorphic pressure (Harte, 1988). Although only at greenschist facies, metamorphic assemblages in the Southwest Highlands equilibrated under relatively high pressure conditions (Graham et al., 1983) of *c.* 8 – 12 kbars, compared to about 6 to 8 kbars for central areas of the Dalradian. In contrast, metamorphic pressures over most of the Buchan area are indicated to have been only 2-5 kbars, even though peak metamorphic temperatures locally reached *c.* 600°C (Hudson, 1985; Kneller and Leslie, 1984). Immediately south of the Buchan area, pressures of up to about 8 kbars are recorded in the high-grade gneisses of the Glen Muick area (Baker 1985). In both the Central Highlands and to the west of the Portsoy – Duchray Hill Lineament, pressure increases postdating the thermal peak of metamorphism are recorded (Beddoe-Stephens, 1990; Dempster and Harte, 1986). Dempster and Harte (1986) demonstrate that the pressure increase in the Central Highlands was diachronous. The pressure increase occurred before D₃ deformation in

rocks in the southern part of the Tummel Steep Belt, but after D₃ further north in the Tummel Steep Belt (Figure 2.6).

Fluid infiltration events during Grampian metamorphism

Fluids are important during metamorphism as they have the potential to transport matter and heat through a metamorphic pile and may alter the petrology and chemistry of the rocks through which they pass. Several key studies of the petrographical and geochemical effects of metamorphic fluids have been undertaken on Dalradian rocks in the Southwest Highlands of Scotland in recent years (Cole and Graham, 1994, 1997; Fein et al., 1994; Graham et al., 1983; Skelton, 1993, 1995).

Graham et al., (1983) described in detail, prograde metamorphic fluid infiltration phenomena in metabasite sheets and their host calc-phyllites on Islay and in Knapdale. They demonstrated that metamorphic assemblages in the rocks were controlled by infiltration of hydrous fluids. In greenschist facies rocks, calc-phyllites undergoing carbon oxidation reactions produced CO₂-bearing hydrous fluids which infiltrated adjacent metabasic sills, profoundly altering amphibole + epidote + sphene assemblages to assemblages containing chlorite + calcite + epidote, and chlorite + dolomite-ankerite + muscovite + rutile. Graham et al., (*op. cit.*) determined that the degree of fluid-driven alteration observed in the rocks required fluid-rock ratios to have been between 6:1 and 20:1 or more. Because of constraints on fluid sources and volumes, such high ratios implied structurally channelled or lithologically focused fluid infiltration.

The spatial distribution and extent of these assemblages on the margins of thicker metabasite sills were subsequently combined with structural data to constrain 3-

dimensional metamorphic fluid fluxes (Skelton, 1993; Skelton et al., 1995). This work indicated channelled, upward fluid flow focused on the Ardrishaig and Islay anticlines, with fluxes in excess of $10^3 \text{ m}^3 / \text{m}^2$ in the fold hinges. Averaged fluxes of $100 \text{ m}^3 / \text{m}^2$ are considered consistent with fluids having been derived by metamorphic devolatilisation of *c.* 3 km of underlying phyllites. Of importance with regard to driving mechanisms for regional metamorphism, Skelton (1993) showed that the fluid fluxes were too low and/or of too short a duration for the fluid to have been significant heat-transporting agent during Dalradian metamorphism.

During epidote-amphibolite facies metamorphism in the Southwest Highlands, metabasite sheets underwent dehydration, resulting in the generation of garnet-bearing metabasites (Graham et al., 1983). The water generated by this dehydration in the interiors of sills resulted in the removal of carbonate from outer parts of sills. Previous chlorite + calcite \pm rutile assemblages resulting from infiltration of the CO_2 -bearing fluids from the calc-phyllites were converted back to amphibole + epidote + sphene. The effects of infiltration of water into the host metasedimentary phyllites from the devolatilising metabasite sills are highly complex, revealing markedly different fluid-buffering effects on the scale of metres, down to centimetres or less (Graham et al., 1983).

A late retrogressive metamorphic fluid infiltration event at lower greenschist facies is well-documented in the Southwest Highlands, resulting in the development of K-feldspar + chlorite + dolomite-ankerite bearing assemblages in calc-schists (Graham et al., 1983; Skelton, 1993) and in dolomitisation of carbonate rocks (Fein et al., 1994). The distribution of these retrograde assemblages is spatially associated with albite porphyroblast schists (Figure 2.6) and both are considered to have resulted from the

same fluid infiltration event. Textural studies show that the development of these assemblages occurred coeval with the uplift event which formed the Tarbert Monoform in the Southwest Highlands.

2.7 Discussion

Timing of metamorphic events in the Grampian Highlands

The *absolute* timing of Grampian orogenic deformation and metamorphism has long been a matter of debate (e.g. Stephenson and Gould 1995). Although the application of increasingly sophisticated dating techniques, particularly U-Pb systematics in zircon and monazite, have clarified the ages of geological events with markedly increased precision, problems in the interpretation of these ages still remain. Ironically, these problems arise from different interpretations of litho- and tectonostratigraphical field evidence and petrographical textural relationships, which are commonly ambiguous.

The debate about ages of metamorphism and deformation in the Grampian Highlands is currently focussed in the Central Highlands. Here, the relationship between putative basement rocks and the Grampian Group has proved difficult to discern. The problem is confused by ductile shearing and pegmatite formation, and by interpretations of the structural and metamorphic history in terms of an apparent single structural and metamorphic event (Highton et al., 1999; Phillips et al., 1999), as opposed to polyphase events superimposed on putative basement-cover relationships (Piasecki and Van Breeman, 1979; Robertson and Smith, 1999; Smith et al., 1999). It is now known that basement rocks underwent a Precambrian thermal event at *c.* 800 Ma (Highton et al., 1999; Noble et al., 1996; Piasecki and Van Breeman, 1979). Whether this event resulted from orogenesis or from heating during extension is still unclear.

Some workers (e.g. Highton et al., 1999) argue that this event has also affected the Grampian Group and, by implication, the Appin Group. Such an interpretation would make at least these parts of the Dalradian older than ~800 Ma.

Of critical importance in this debate is the currently unconstrained lower age of the Grampian Group. In Chapter 6, I discuss the evidence from carbonate Sr isotopes which strongly suggest that the Dalradian cannot be older than about 750Ma, supporting the hypothesis that the Grampian Group must lie unconformably on mainly migmatitic basement (Piasecki and Van Breeman, 1979; Robertson and Smith, 1999; Smith et al., 1999). The corollary of this is that all the deformation and metamorphism seen in the Grampian Group and upwards results only from the Ordovician Grampian Orogeny.

The Grampian Orogeny itself occurred after the Middle Cambrian (*c.* 515Ma), based on the trilobite age of the Leny Limestone (Section n). The syntectonic (D₂-D₃) Inch basic intrusion of Northeast Scotland was dated at 470 Ma (Rogers et al., 1994); late tectonic intrusions are all younger than this (Stephenson and Gould 1995, table 2, and references therein). Recent high-precision U-Pb dating of earliest and latest intrusive rocks of the mafic Connemara Complex in Ireland by Friedrich et al., (1999) constrains Grampian orogenesis to between 475 and 463 Ma in Connemara. The oldest rocks were intruded during D₂ and remained hot during subsequent D₃ deformation. Given the error on the Rb-Sr age and the possibility of diachroneity in deformation and metamorphism, it is clear that D₂ and subsequent events are younger than *c.* 480 Ma.

Other than being post-Middle Cambrian, the age of D₁ is still poorly constrained. The major phase of rapid uplift and cooling of the Grampian Orogen,

during which D₄ deformation occurred, is constrained to have taken place between c. 460 and 440 Ma, with another phase at between c. 420 – 390 Ma (Dempster, 1985).

Status of the Ben Vuirich Granite

Studies of the foliated Ben Vuirich granite of Perthshire have been particularly important in the recent debate about the age of Grampian orogenesis and its current status requires brief discussion. The U-Pb single zircon age of 590 ± 2 Ma for the Ben Vuirich Granite (Rogers et al., 1989) was initially interpreted as constraining D₂ to be pre-590 Ma and, therefore, Precambrian, because of the apparent presence of regional D₂ fabrics in hornfelses included in the granite. However, this interpretation was irreconcilable with the U-Pb zircon age of 595 ± 4 Ma for formation the Tayvallich lavas (Halliday et al., 1989), which indicated that Dalradian sedimentation continued well after c. 600 Ma. The fabrics in the Ben Vuirich hornfelses have been shown subsequently to be unrelated to regional structures, resulting instead from local deformation during granite intrusion (Tanner, 1996). The age of Ben Vuirich, therefore, offers no constraint on the age of Grampian metamorphism and deformation.

Chapter 3

Petrography and whole-rock geochemistry of Dalradian limestones and dolostones

In this chapter:

- ❖ Petrography of Dalradian limestones and dolostones
- ❖ Constraints on equilibrium fluid compositions and fluid-rock interaction
- ❖ Summary whole-rock geochemistry

3.1 Introduction

In this chapter, I present an overview of the petrography of Dalradian limestones and dolostones whose isotope and mineral chemistry are examined in more detail in the remainder of the thesis. Carbonate mineral textures are important in the interpretation of the stable and strontium isotope data, particularly with regard to the extent to which pre-metamorphic textures are, or are not preserved. Where primary and/or diagenetic textures are recognisable, as indeed they are in some of the Dalradian carbonate rocks studied here, they help elucidate the nature of the original sediments. The petrology, mineral chemistry and abundances of the phases present in the limestones and dolostones also help constrain the composition and flux of fluids

which may have interacted with the limestones. In conjunction with isotope analyses, such data also help elucidate the timing (i.e. pre-metamorphic or metamorphic) and extent of fluid-rock interaction.

I also present summary whole-rock geochemical data for the suites of samples for which isotope data have been obtained. Much of this data comes from a large body of published and documented British Geological Survey work, from which the work presented in this thesis evolved. The relevance of the whole-rock geochemical data lies in the fact that even at the coarse resolution of whole-rock geochemistry, it is possible to distinguish geochemically between various important Dalradian limestones. Although initially used by the British Geological Survey East Grampians Project to aid lithostratigraphical correlation in the poorly exposed Northeast Grampian Highlands (Thomas, 1989), the whole-rock geochemistry indicated that differences between major limestones were of largely primary, sedimentological origin and not the result of metasomatism or metamorphism. This broad geochemical work is the initial investigation from which the detailed isotopic and mineral chemical work presented in Chapters 6,8 and 9 has developed.

The major and trace element characteristics and petrography of each of the limestone units from which isotopic analyses were obtained, is summarised here. Most of the whole-rock samples were not thin-sectioned because of cost limitations on project budgets. The petrography described here is thus based on a limited set of sections. However, considerable care was taken when collecting samples to ensure that they were as homogeneous as possible, free from weathered material, veining and minor, non-carbonate lithologies. It is clear from examination of the many hand-specimens which exist, coupled with consideration of the geochemical data, that the

petrography as described is largely representative of the limestones and dolostones as a whole. Indeed, uniformity in mineral assemblage and textures is a feature of many of the limestones and dolostones from Northeast Scotland, where metamorphism was typically at amphibolite facies. In the Southwest Highlands, where metamorphic grade was lower, limestone petrography is more variable and more illuminating with respect to primary/diagenetic textures and their preservation.

3.2 Petrography

The location and lithostratigraphical details of the limestones and dolostone units described below and in the rest of the thesis are included in Table 3.1. Also included are the sample numbers referred to in the text.

3.2.1 Kintra Dolostone, Islay

Cathodoluminescence (CL) and back scattered electron (BSE) imaging, coupled with reconnaissance energy dispersive (EDS) x-ray analysis, shows that the mineralogy is dominated by non-luminescent, fine grained dolomite spar. Equant, very fine grained polygonal quartz and albite occur in elongate patches and strings. Together with the quartz strings, elongate felts of very fine grained muscovite define a wavy lamination in the rock (Figure 3.1). This lamination may be stromatolitic in origin. The mica felts are weakly deformed and locally boudinaged into lozenges. Clusters of rutile crystals occur in masses adjacent to and amongst the mica felts (Figures 3.1, 3.2). The spatial association of rutile with mica suggests that the former *may* have been derived from TiO_2 released from previously titanium-bearing detrital phyllosilicates, but some is also likely to have been detrital originally. Quartz grains

Sampled unit	Subgroup	Locality	Lithology	NGR	Samples	Sample #
Limestones						
Southern Highland Group						
Leny Limestone		Callander, Stirlingshire	Limestone, black, graphitic	NS 615 098	2	HY1362-64
Uppermost Argyll Group (Tayvallich and equivalents)						
<u>Scotland</u>						
Boyne Limestone	Tayvallich	Boyne Bay, Banffshire coast	Limestone, pale to medium grey, with thin calc-silicate pods and laminae	NJ 616 660	4	HY147-50
<u>Northern Ireland</u> Torr Head Limestone		Torr Head, Co. Antrim	Limestone, grey-black, coarsely-crystalline, well-bedded, beds commonly coarser towards centre	H 232 406**	2	HY1348-9
Dungiven Limestone		Butterlope Glen, Co. Tyrone		C 493 047**	1	HY1350
		Banagher Glen, Co. Tyrone		C 668 047**	1	HY1351
Appin Group						
<u>Islay</u>						
Storakaig Limestone Member	Blair Atholl	Ballygrant Quarry, Islay	Limestone, dark grey, graphitic, fine grained and well-bedded, with thin films and laminae of pelite	NR 395 666	5	HY1333-7
<u>Mainland Scotland</u> Inchrory Limestone		Limeworks Quarry, Tomintoul	Limestone, medium dark grey, fine to medium grained, well-bedded, with thin films of schistose pelite	NJ 151 194	5	HY56-60
Torulian Limestone (Bed)	Ballachulish	Bridge of Avon, River Avon section	Limestone, white/very pale grey, commonly coarsely crystalline, massive	NJ 1496 2019	1	HY43
		Carn Daimh, Glenconglass		NJ 1749 2259	1	HY47
		Glen Suie		NJ 2766 2595	1	HY360
		Tor Elick, Glen Fiddich		NJ 3166 3202	1	HY393
				NJ 3186 3205	1	HY394
Dufftown Limestone Member		Parkmore Quarry, Dufftown	Limestone, pale to medium grey, thinly bedded/foliated, fine to coarse grained	NJ 334 411	5	HY67-71
Grampian Group						
Kincraig Formation	Corrieyairack	Kincraig Quarry	Limestone, medium grey, medium grained crystalline and foliated	NH 8213 0640	2	HY1072-73
		Kincraig Farm, Dunnachton track	Limestone, white, coarse-grained with calc-silicate strings in places	NH 8214 0577	2	SMS446-7
		Allt na Baranachd	Limestone, very pale grey, coarsely crystalline	NH 7959 0586	2	SMS448-9

Table 3.1. Lithostratigraphical, location and sample number details of samples

Sampled unit	Subgroup	Locality	Lithology	NGR	Samples	Sample #
Dolostones						
<i>Islay Subgroup, Argyll Group</i>						
<i>Northeast Scotland</i>						
Nochty Semipelite & Limestone	Islay	Water of Nochty	Dolostone, grey, fine grained, massive	NJ 2933 1622	2	HY85, 86
Ladder Hills Formation		Carn Dulach, Ladder Hills	Dolostone, white/creamy white, massive, fine grained	NJ 2407 1767	1	HY72
Auchnahyle Formation		Muckle Fergie Burn		NJ 1656 1397	1	GX1064
<i>Ballachulish Subgroup, Appin Group</i>						
<i>Islay</i>						
Kintra Dolostone	Ballachulish	Port Alsaig, Kintra, Mull of Oa	Dolostone, very pale grey, tan-weathering, very fine-grained		4	HY1338-41
<i>Uncertain lithostratigraphical status (?Dalradian, possibly Ballachulish Subgroup)</i>						
<i>Colonsay</i>						
Staosnaig Phyllite Formation	Unknown	Rubha an Dobhrain, Scalasaig,	Dolostone, medium grey, very fine grained, locally with micaceous	NR 4045 9482	2	HY1342-43
		Geodha nan Ceann, Scalasaig	films and partings; contains vein quartz strings and pods (avoided in samples)	NR 4030 9475	2	HY1344-45
				NR 3997 9461	2	HY1347-47
Total:					50	

** Irish National 1:10 000 grid coordinates

Table 3.1. Lithostratigraphical, location and sample number details of samples

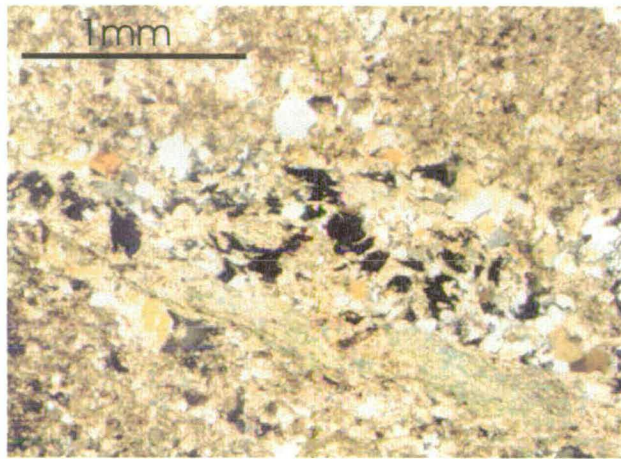


Figure 3.1 Muscovite felts with rutile in the Kintra Dolostone, Islay.



Figure 3.2 Detail of rutile needle cluster in Kintra Dolostone

recrystallised from finer –grained aggregates in places. There is no sign of reaction between the phases in the Kintra Dolostone, showing that dolomite + quartz + white mica is stable (Figures 3.3, 3.4).

3.2.2 Dolostones from the Staosnaig Phyllite Formation, Colonsay

Many of the features observed in the Kintra Dolostone samples are also seen in the dolostones from the Staosnaig Phyllite Formation. However, the latter rocks are slightly coarser grained and appear more strongly deformed locally, defining, in part, a cleavage (compare Figures 3.5, 3.6).

Mica is replaced by later chloritoid and rutile clusters similar to those observed in the Kintra Dolostone are also present. No tremolite or other calc-silicate minerals characteristic of metamorphosed, impure dolostones have been observed optically. The petrological implications of the lack of such phases in these dolostones is discussed further below in Section 3.3.

3.2.3 Islay Subgroup dolostones, NE Grampian Highlands

Dolostones from the Ladder Hills and Auchnahyle formations are creamy white and fine- to medium-grained. HY72 from the Ladder Hills contains scattered, irregular patches of relatively coarser and more evenly grained carbonate in a matrix of finer-grained carbonate; all carbonate crystals have equant polygonal shape. Scattered sparsely throughout are coarse (~0.5 - 1mm), anhedral, poikiloblastic tremolite crystals (Figure 3.7). No quartz or diopside were found, but electron microprobe data

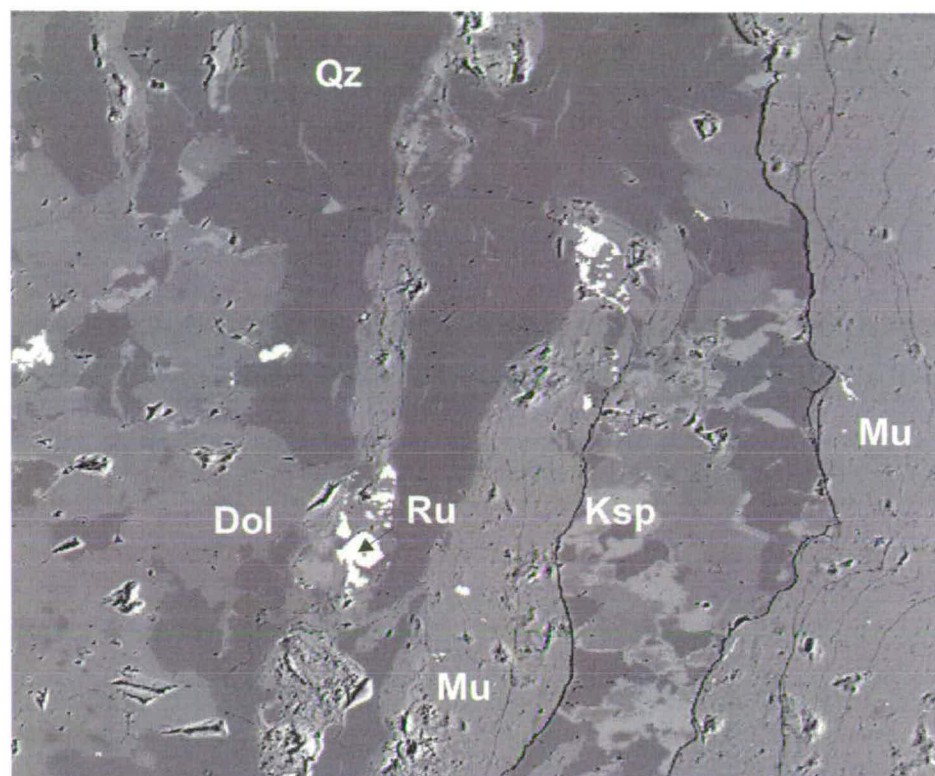


Figure 3.3 Dol + cc + qz + mu + ru assemblage, HY1341, Kintra Dolostone, Islay. BSE image, Field of view ~ 2mm.

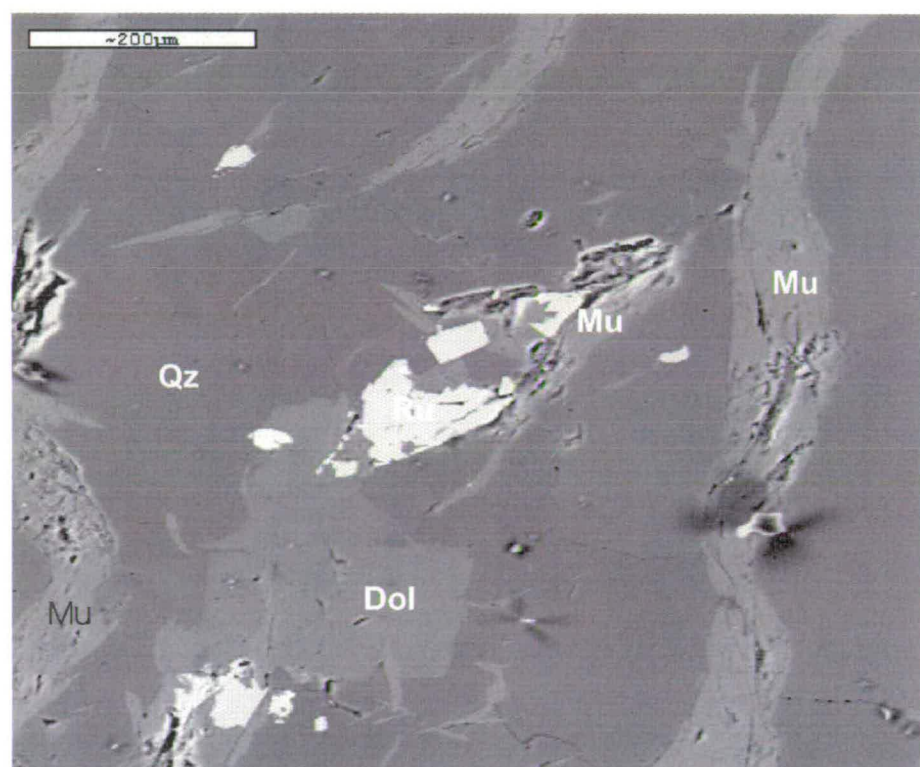


Figure 3.4 Detail of rutile in dol + cc + qz + mu + ru assemblage, HY1341, Kintra Dolostone, Islay. BSE image.



Figure 3.5 Muscovite lamination in dolostone from the Staosnaig Phyllite Formation, Colonsay

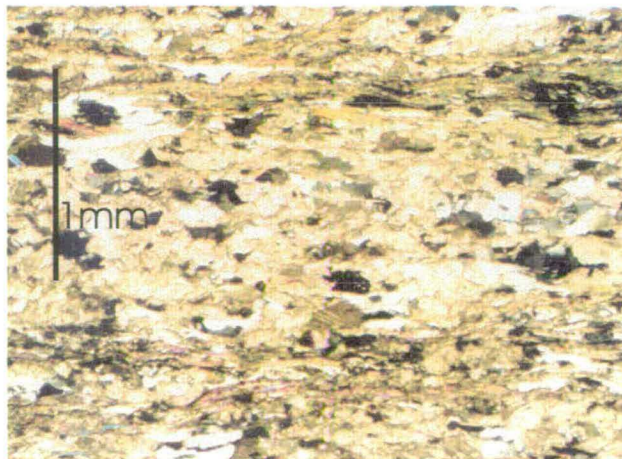


Figure 3.6 More deformed variant of the muscovite lamination shown above; dolostone, Staosnaig Phyllite Formation

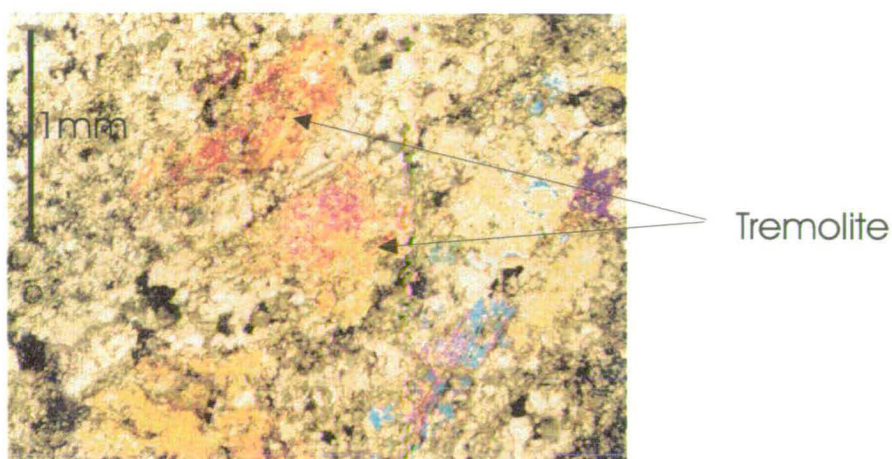


Figure 3.7 Ragged, anhedral tremolite in dolomite, dolostone, HY72, Ladder Hills Formation, Islay Subgroup, North East Grampian Highlands.

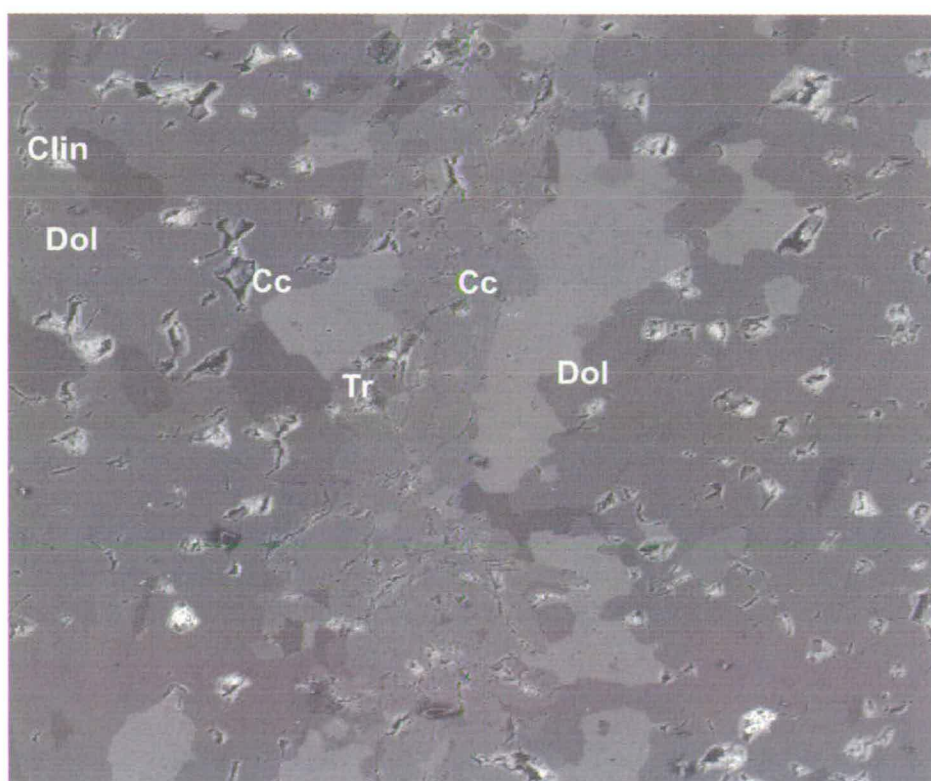


Figure 3.8 The quartz-absent dolomite + clinocllore + tremolite + calcite assemblage in dolostone from the Ladder Hills Formation, Islay Subgroup, Northeast Grampian Highlands, Scotland. Field of view ~ 1 mm.

show that calcite is present and has a close spatial association with tremolite (Figure 3.8). The stability limits of the tremolite + dolomite + calcite assemblage are discussed below in Section 3.3.

Back scattered electron imaging reveals complex geochemical zoning in many dolomite grains in which dark rhombic cores are overgrown by successively more rounded and paler, more calcian dolomite (Figure 3.9). The well-formed polygonal grain boundaries cut across the geochemical zoning, in places right through the core. In places, calcite (bright) is seen edging dark rhombic dolomite within the later, paler dolomite. The relationship between this calcite and the dolomite is more complex in places (Figure 3.10). The rhombic cores, geochemical zoning textures and calcite overgrowths are considered to be principally diagenetic in origin. They are similar to textural and geochemical features in replacive dolomite described by Fairchild (1980b) in dolostones from the Bonahaven Formation, Islay Subgroup, Islay.

The polygonal grain boundary architecture may also be largely diagenetic in origin, but may have been altered to varying degrees during any metamorphic recrystallisation. The polygonal grain boundary network is simpler and straighter between intersections than dolomite mosaics figured by Fairchild (1980a, fig 14; 1980b, fig 6d) suggesting textural equilibration during metamorphism. It is clear, however, that compositional zoning and original rhombic dolomite shape in many grain cores have survived amphibolite facies metamorphism and coeval deformation. It is suggested that the heterogeneity in major element chemistry, revealed by back scattered electron images, may extend to stable and strontium isotopes. The only way of testing this would be by SIMS analysis (cf. Chapter 9).

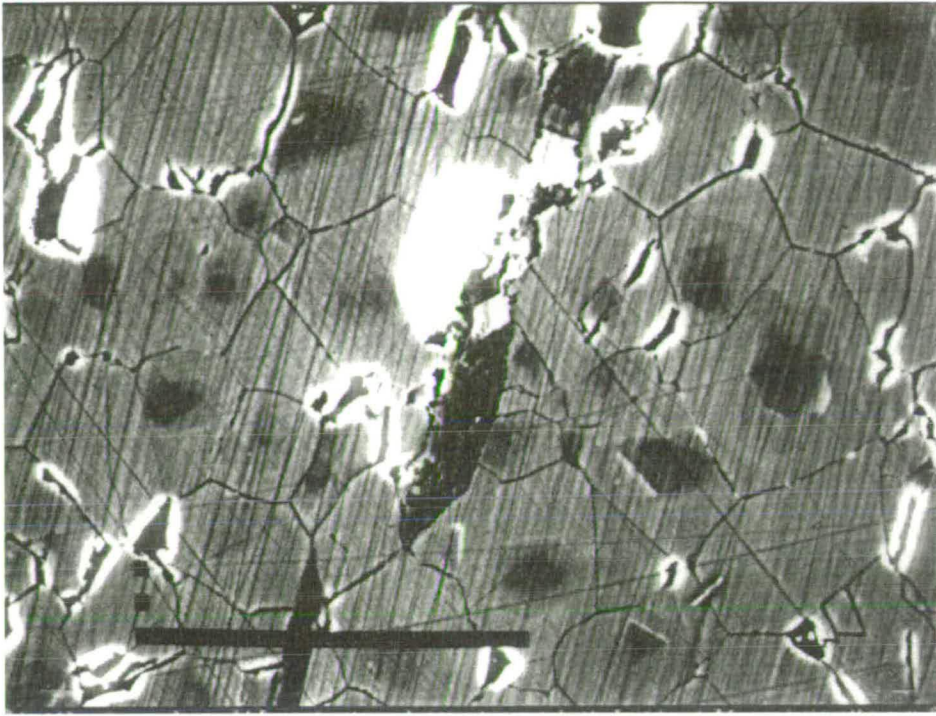


Figure 3.9 Early, diagenetic rhombohedral dolomite forming cores to the later metamorphic grain architecture. Dolostone, Ladder Hills Formation, Islay Subgroup, Northeast Grampian Highlands, Scotland. Scale bar is 200mm.

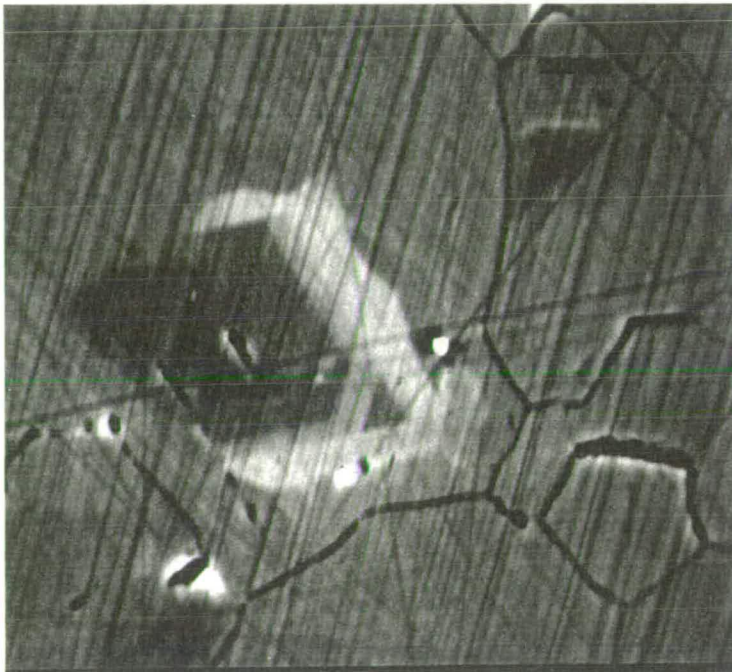


Figure 3.10 Calcite overgrowths on an early dolomite rhomb within dolomite, Islay Subgroup dolostone. The calcite is interpreted to be diagenetic in origin; locality as above.

3.2.4 Torr Head and Dungiven limestones, Northern Ireland

Samples from these two 'Tayvallich' limestones vary considerably in their petrography. Samples from the Torr Head limestone retain relict sedimentary textures. In one section, variably fine-grained calcite microspar hosts coarser round to oval patches of calcite (Figure 3.11). These patches are interpreted as relict ooids/peloids. The wide scatter of these coarser patches indicates they were matrix supported, suggesting reworking of carbonate grains into carbonate mud. Elsewhere, calcite textures and grain sizes vary widely, even on the scale of a thin section. Good polygonal textures with abundant triple-point contacts are commonly observed. Quartz grains commonly appear rounded where isolated, suggesting retention of sedimentary form. Where quartz grains occur in clusters, they generally appear recrystallised, having good, metamorphic polygonal form.

A particular feature of these limestones is the presence of large, single crystals of calcite full of opaque dusty inclusions, probably of graphite; these crystals may reach a centimetre or more in size. These impart the black colour and very coarse crystalline appearance characteristic of these limestones at several localities, most particularly Banagher Glen and Torr Head (Figure 3.12a,b). In both hand specimen and thin section, the coarse crystals can be seen to be polygonal in form and surrounded by clear, white equant calcite mosaics (Figure 3.13a). Some of the crystals have clear, optically continuous overgrowths. Furthermore, the dusty inclusions define a fabric in the crystals which is generally aligned in thin section. Commonly, near-adjacent crystals have matching boundaries and it is clear they were once touching, but are now separated by clear, more luminescent calcite (Figure



Figure 3.11 Relict ooids in variably coarsely crystallised calcite matrix,, Torr Head Limestone, Torr Head, Co. Antrim, Northern Ireland.



Figure 3.12a Coarse, black crystalline limestone, Dungiven Limestone, Banagher Glen, Northern Ireland. Lens cap is 49 mm.



Figure 3.12b Coarse, black, crystalline limestone, Torr Head Limestone, Torr Head, Co. Antrim, Northern Ireland. Hammer is ~40 cm

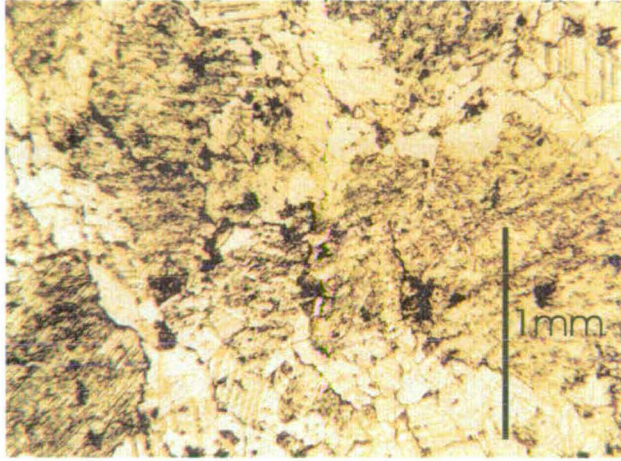


Figure 3.13a Large, optically continuous calcite plates with aligned dusty graphite inclusions, enclosed in clear, polygonal calcite spar

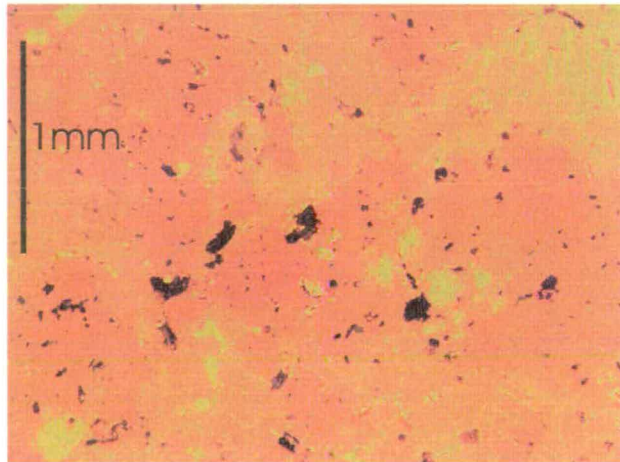


Figure 3.13b Same as above, under cathodoluminescence. Note the slightly stronger luminescence in the sparry calcite and the correspondence of the luminescence with the inclusion-rich calcite plates.

3.13b). The origin of this texture is unclear, but it is formed in rocks which are low in siliciclastic impurities. The lack of significant impurities probably minimised grain-boundary pinning effects, so that the calcite crystals could grow relatively unimpeded. However, it is also clear that the inclusion-rich crystals originally formed a continuous matrix in which the crystal boundaries were replaced by some mechanism with clear calcite spar. The general alignment of the inclusion trails and the adjacency of matching boundaries show that the early inclusion-rich crystals were not significantly rotated during the development of the clear calcite, indicating that the disruption of the original crystal architecture was passive rather than mechanical.

Calc-silicate phases are notable by their absence from most of the limestones in this study. However, in HY1350 (Butterlopie Glen, Co. Tyrone, N Ireland), small equant euhedra of colourless tremolite are developed, along with zoisite, K-feldspar, albite and plates of altered plagioclase and locally developed quartz. These phases are commonly concentrated adjacent to or within diffuse curvilinear domains, most particularly the zoisite (Figure 3.14). Tremolite crystals are also scattered moderately abundantly throughout the matrix, *within* the large platy calcite crystals. Here, they are also moderately aligned with a fabric defined by dusty inclusions and extremely fine grained silicate phases (dominantly amphibole, but including coexisting muscovite and K-feldspar) (Figure 3.15). Quartz is rare in the matrix.

The presence of tremolite, zoisite and K-feldspar, and the alteration of plagioclase in the presence of calcite and quartz, indicates interaction with very hydrous fluid (see Section 3.3.2), consistent with the strongly depleted carbonate $\delta^{18}\text{O}$ signature of this limestone (see Chapter 7).

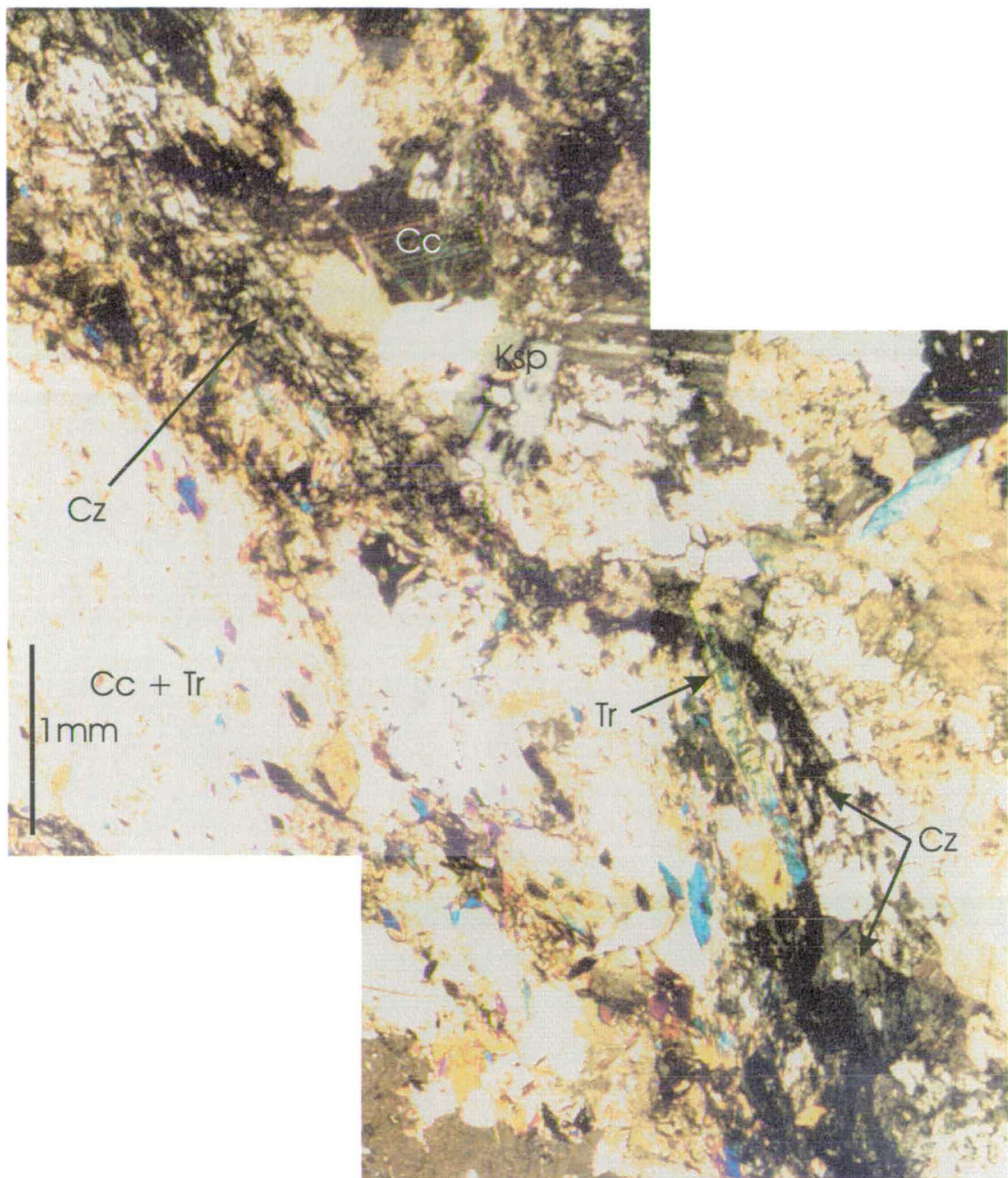


Figure 3.14 Calc-silicate phases in HY350, Dungiven Limestone, Butterlopie Glen, Northern Ireland.

Cc: calcite
 Cz: clinozoisite
 Ksp: K-feldspar
 Tr: tremolite

The diffuse domain with clinozoisite also includes altered plagioclase with albite.

3.2.5 Tayvallich Limestone, Port an Sgadain, Tayvallich Peninsula

Six thin sections corresponding to the samples provided by C Graham (personal communication) for isotopic analysis reveal considerable lithological and textural variation in the Tayvallich Limestone from this locality. The limestone lies between Tayvallich Lavas extruded onto the sediment surface and a metadolerite sill; tongues of lava locally intrude the uppermost limestone (Figure 3.16). Sample T2 comes from immediately beneath the lavas. In thin section, a fine-grained matrix comprising calcite, quartz and ?plagioclase with chlorite and white mica hosts well-rounded to more elongate patches of coarse calcite and scattered sulphide grains. The well-rounded grains are up to 1 mm across and commonly consist of a few or even a single crystal; several have thin rims of opaque material (Figure 3.17). The more elongate patches and clusters of large single crystals are similar in character to the well-rounded grains in all but shape and it is concluded they share the same origin. In places, several crystals in clusters are in optical continuity. In addition, the well-rounded grains, elongate patches and clusters of crystals quite commonly have clear calcite overgrowths in optical continuity with a dustier rounded core. The well-rounded grains are clearly sedimentary and are interpreted as relict ooids. The other coarser calcite patches and crystals are considered to be more thoroughly recrystallised ooids. It is notable that the best-preserved ooids are found in more phyllosilicate-rich domains. The phyllosilicates may well have protected these ooids from recrystallisation during deformation, unlike those in the more pure, carbonate-rich domains where recrystallisation proceeded more readily. Section T3 contains fine-grained calcite hosting large (~ 1 mm) quartz grains and ghosted round to oval



Figure 3.15 Large calcite plate enclosing aligned tremolite euhedra, Dungiven Limestone, Butterlopie Glen, Northern Ireland.



Figure 3.16 Tongue of Tayvallich Lava intruding impure Tayvallich Limestone immediately beneath the Tayvallich lavas, Port an Sgadain, Tayvallich, Argyll, Southwest Highlands, Scotland. Hammer is ~ 40 cm.

patches of coarser calcite. The latter ghosted patches may have been ooids, by analogy with textures seen in T2.

T4 and T6b are silicate-rich, impure limestones containing quartz, plagioclase feldspar and a little white mica. The feldspars commonly have saussuritised cores and clear, optically continuous overgrowths (Figure 3.18). The rounded shape of the cores suggests a sedimentary origin. Saussuritisation is taken to indicate hydrothermal alteration of plagioclase (Deer et al., 1966) and the feldspar overgrowths are probably albite. These petrographic features, along with homogenisation of bulk carbonate $\delta^{18}\text{O}$ values to $\sim 16\text{‰}$ (see Chapter 8) are consistent with fluid infiltration of the limestones, probably during hydrothermal activity associated with the voluminous extrusion and intrusion of mafic magma (Graham, 1976).

Samples T5 and T6a are very fine grained limestones with very fine grained silicate impurity, probably chiefly quartz and plagioclase with some white mica. These rocks carry a weak fabric. This is overgrown by small, randomly orientated laths of white mica with possibly a contact metamorphic origin, given that the two samples are adjacent to the metadolerite sill at the base of the limestone.

3.2.6 Storakaig Limestone

The Storakaig Limestone preserves abundant relict sedimentary textures in thin section, the most obvious of which are relict ooids and peloids, together with clasts

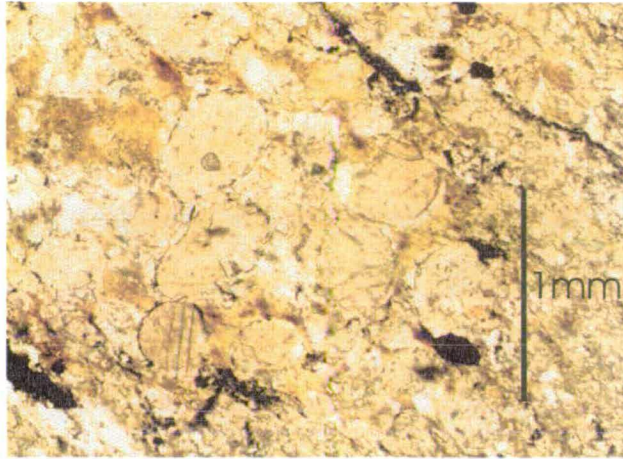


Figure 3.17 Relict oolites, Tayvallich Limestone, Port an Sgadain, Tayvallich, Argyll, Southwest Highlands, Scotland

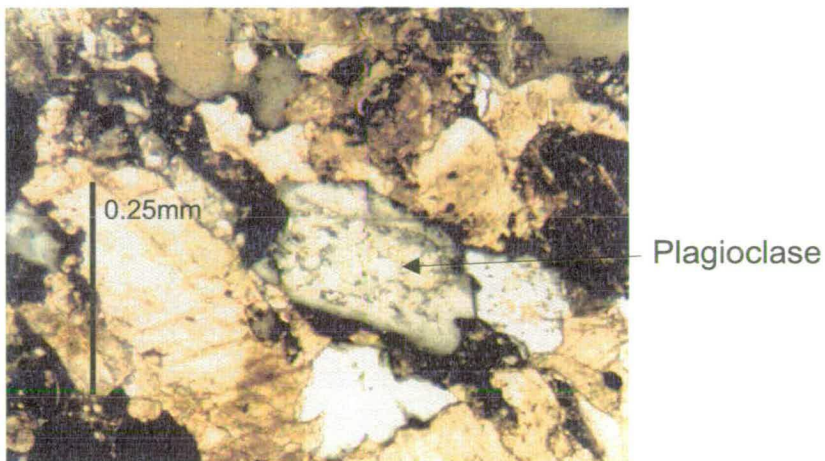


Figure 3.18 Saussuritised plagioclase feldspar with clear albite overgrowths, Tayvallich Limestone, Port an Sgadain.

of oolite. Although ooid interiors are generally replaced by relative coarse sparry calcite, concentric laminae are preserved in places. Black material concentrated in the outer parts of relict ooids is considered to be organic material which once occurred between carbonate laminae (Figure 3.19a). Figure 3.19b, shows the section in 3.19a under cathodoluminescence (CL). The CL shows greater, but speckled luminescence of the fine-grained matrix compared to the carbonate clasts. In other sections, the ooids are represented by recrystallised, weakly deformed, polygonal mosaics of calcite in round to elongate patches coarser than the host calcite matrix (Figure 3.20). These are very like the patches seen in the 'Tayvallich' limestones, reinforcing the interpretation as ooids and/or peloids in the latter. The matrix to the carbonate clasts/grains is a fine- to very fine-grained calcite microspar which may have recrystallised from micritic carbonate mud. As with the Torr Head and Dungiven limestones, the textural evidence suggests that the clasts in the limestones are reworked, rather than in-situ.

3.2.7 Inchrory Limestone

Thin sections of the Inchrory Limestone reveal thoroughly recrystallised metamorphic fabrics. Calcite crystals are equant to elongate and lie in domains bounded by more phyllosilicate –rich lithons consisting of white mica and late chlorite (Figure 3.21). Fine-grained equant quartz and feldspar are scattered throughout and are locally abundant. The carbonate is dusted variably by very fine grained opaque material considered to be graphite. No relict sedimentary textures or grains have been observed. Sphene is present locally, forming scaly masses which are

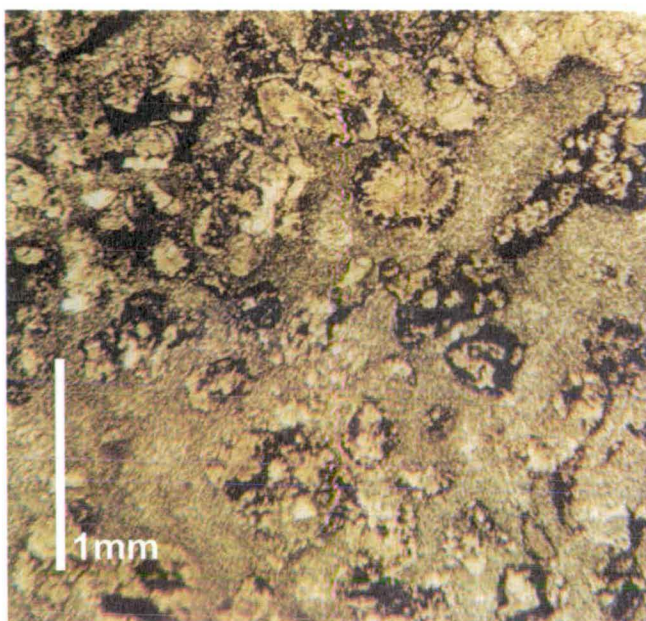


Figure 3.19a Relict ooids in calcite microspar, Storakaig Limestone, Ballygrant Formation, Blair Atholl Subgroup, Ballygrant, Islay. Note the abundance of opaque, organic material associated with and, in places, rimming the oolites.

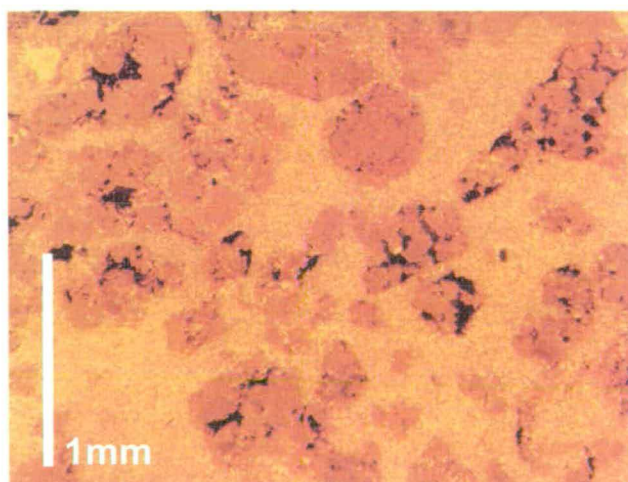


Figure 3.19b The above under cathodoluminescence. Note the correspondence of the oolites with the darker luminescent calcite and the variable, speckled luminescence of the calcite microspar.

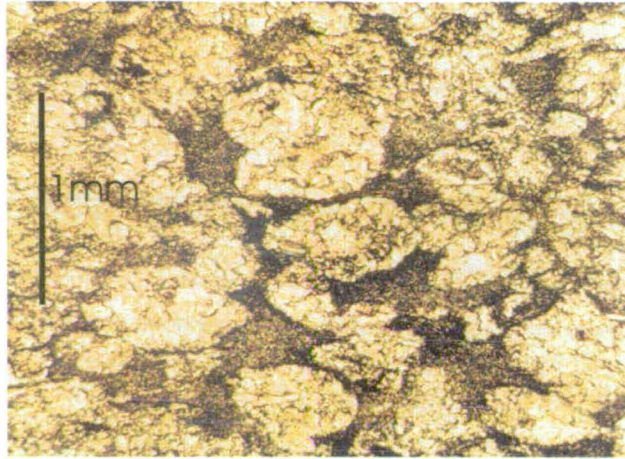


Figure 3.20 Relict, weakly deformed ooids, Storakaig Limestone; same locality as 3.19. Note the poorer, more recrystallised state of preservation compared with the ooids in figure 3.19a.

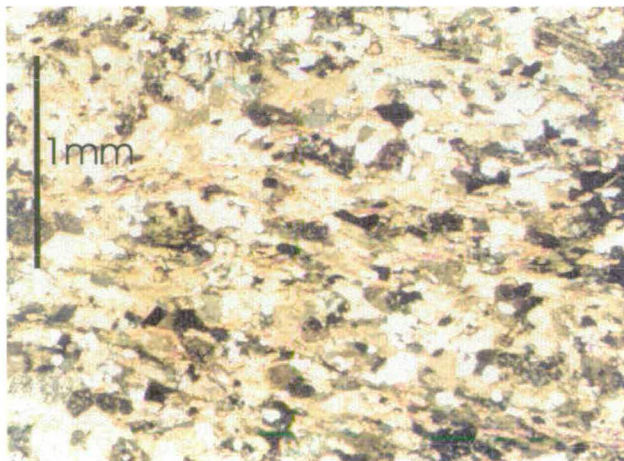


Figure 3.21 Inchrory Limestone thoroughly recrystallised by amphibolite facies metamorphism and coeval deformation. Note the elongate calcite crystals and the aligned muscovite defining the dominant S_2 - S_3 peak metamorphic fabric. The assemblage is calcite + plagioclase (An_{25}) + quartz + muscovite + sphene. Sample from near Tomintoul, Northeast Grampian Highlands, Scotland.

occasionally vaguely lozenge-shaped, similar to better-crystallised sphene (Figure 3.22). Disseminated sulphide grains are locally abundant and both pyrrhotite and pyrite are present; locally at least, the latter is subordinate to pyrrhotite. The petrography of samples of this limestone used for detailed SIMS oxygen isotope analysis is discussed further in Chapter 9.

3.2.8 Torulian Limestone

This limestone is a white crystalline and generally pure calcitic limestone with locally abundant strings of sulphides. It is dominated by coarsely crystalline calcite plates which define a typical polygonal metamorphic texture in some samples. In several sections, however, ragged to sutured grain boundaries and twinning patterns implying high strain are characteristic and the calcite is commonly very dusty in appearance (Figure 3.23). Some of this reflects the density of twin planes, but also results from inclusions. In some samples from the River Avon section near Tomintoul, grain-size reduction is observed and the rocks very locally develop protomylonitic textures.

Quartz, feldspar and sulphides locally form strings defining a weak fabric. The coarseness of the purer limestones is probably a function of the absence of impurities which would have otherwise pinned grain boundaries.

3.2.9 Dufftown Limestone

A thin section of HY67 reveals this to be a relatively pure limestone. Strings and patches of quartz and feldspar are scattered through a more coarsely-grained calcitic

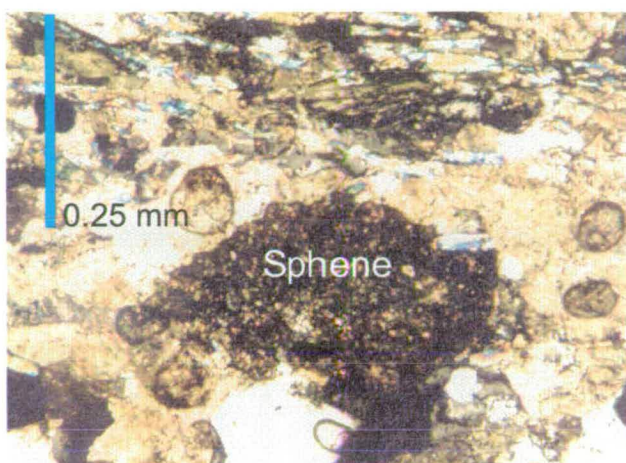


Figure 3.22 Scaly sphene with subhedral form in muscovite-bearing domain, Inchrory Limestone; same locality as figure 3.21.

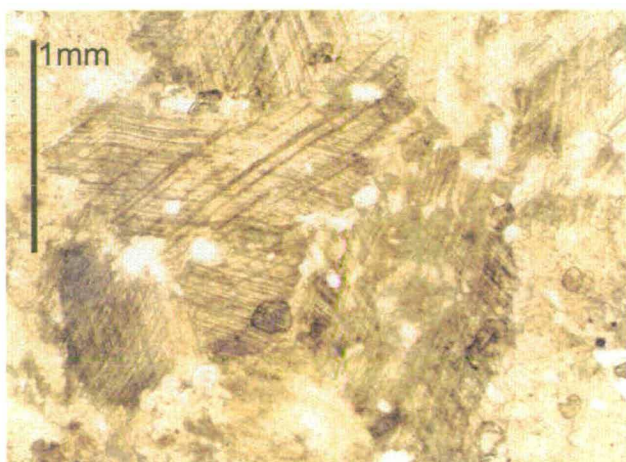


Figure 3.23 Large strain-twinned calcite plates, Torulian Limestone, Ballachulish Subgroup; sample from near Tomintoul, Northeast Grampian Highlands, Scotland.

matrix (Figure 3.24). The calcite is predominantly deformed into elongate crystals which define the metamorphic fabric. Phyllosilicates are rare.

3.2.10 Kincraig limestones

No thin sections of the Kincraig limestones are available. Hand specimens of the samples studied here range from white and coarsely-crystalline limestones, flecked with dark mica of ?phlogopitic composition, to pale grey, coarsely crystalline grained limestones with pelitic films and laminae. Whole-rock analyses show that these limestones have low MgO contents (Table 3.2; Section 3.4) and are calcitic.

3.3 Stability of carbonate rock mineral assemblages

The metamorphic mineral assemblages in the limestones and dolostones can be used to place *broad* limits on their T-X_{CO₂} stability and thereby help in the elucidation of their fluid-rock interaction history. For the following discussion, T-X_{CO₂} sections have been calculated using the Perple-X software suite (Connolly, 1990), and the diagrams produced by the associated thermodynamic diagram plotting software VertexView (Castelli et al., 1997). The thermodynamic data set used in the calculations is that of Powell and Holland (1985), as updated in 1994.

3.3.1 Dolostones

Tremolite and calcite in the Islay Subgroup dolostones from the Ladder Hills formed *via* reaction of dolomite and quartz, *viz*:

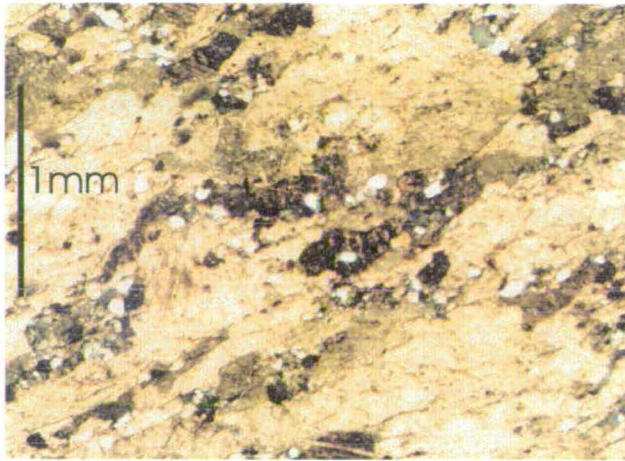


Figure 3.24 Textures in the Dufftown Limestone, basal Ballachulish Subgroup. Note the elongate calcite and the low abundance of silicate impurity (quartz, plagioclase). Parkmore Quarry, Dufftown, Northeast Grampian Highlands, Scotland.

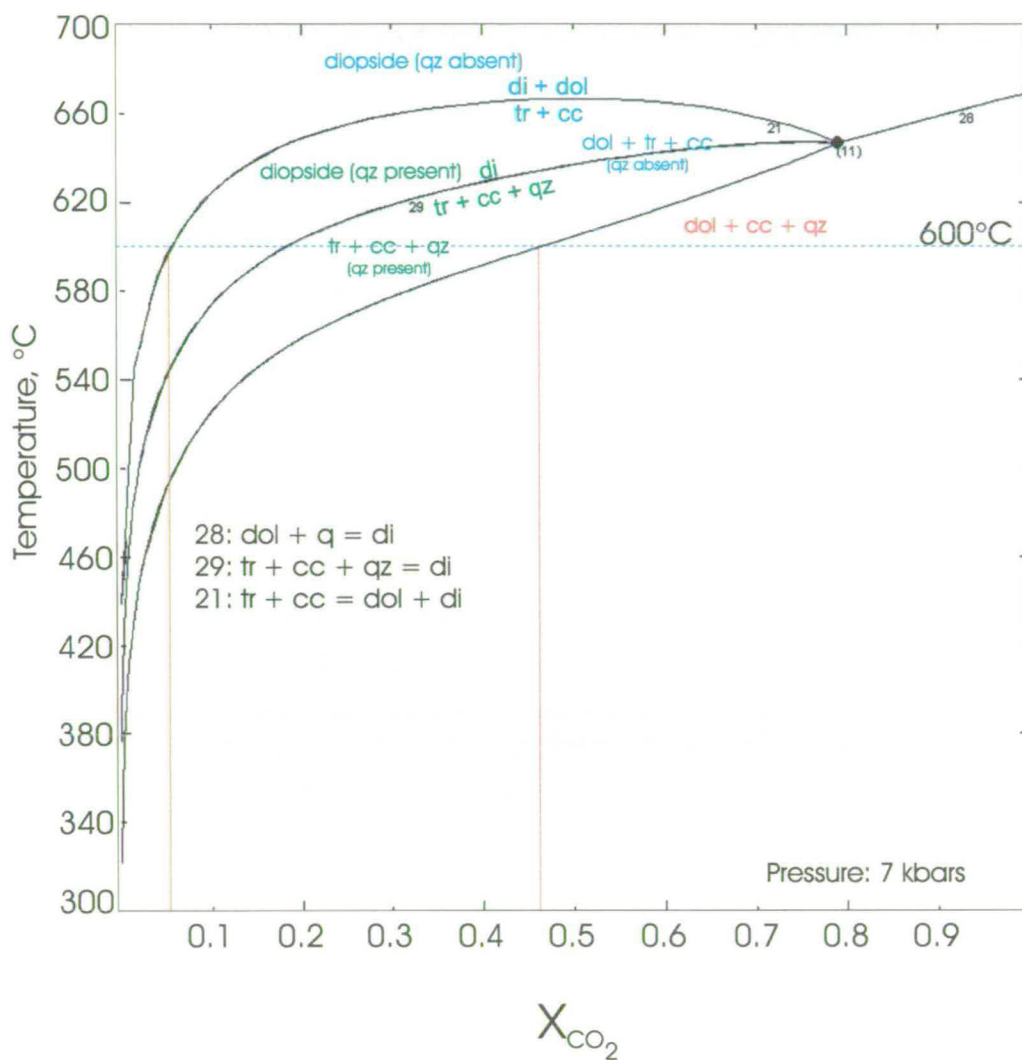
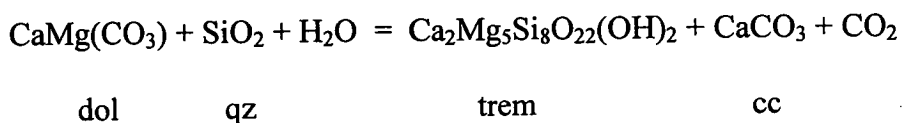


Figure 3.25 The main phase relations for the dolostones. Reactions and assemblages in green are quartz-present, those in blue are quartz-absent. Note that diopside appears at much higher temperatures in quartz-absent assemblages than in quartz-bearing assemblages; see text for discussion.



The absence of quartz indicates that this reaction has gone to completion. The upper temperature stability of the resulting tr + cc + dol assemblage is limited by the quartz-absent diopside-forming reaction between tremolite and calcite:

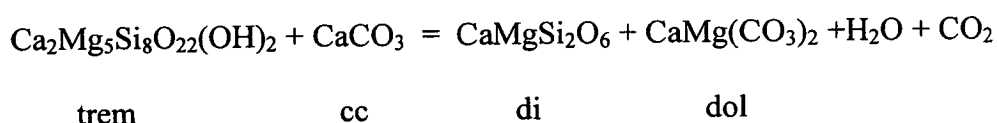


Figure 3.25 shows the position of the relevant reactions in T- X_{CO_2} space, modelled in the composition space CaO-MgO-SiO₂-H₂O-CO₂ (CMSH; end-member modelling is justified here because of the low Al and Fe contents).

The quartz-present diopside-forming reaction between tremolite, calcite and quartz is shown for comparison, highlighting the wider stability of tremolite + calcite in the absence of quartz. At the nominal peak P,T conditions under which these rocks are considered to have been metamorphosed (~600°C, ~7kbars, Beddoe-Stephens, 1990), X_{CO_2} for the assemblage tremolite + calcite + dolomite ranges from ~0.06 to 0.47.

In the Kintra and Staosnaig Phyllite Formation dolostones, the assemblage dolomite + quartz is clearly stable, consistent with the low grade of metamorphism at greenschist facies (Chapter 2).

3.3.2 Limestones

The key petrographic features of the limestones are the presence, in the main, of plagioclase + calcite (rather than zoisite + calcite), the stability of calcite + muscovite and the presence of sphene. With the exception of the Dungiven Limestone sample HY1350, discussed above, tremolite is notable by its absence, reflecting the generally Mg-poor bulk rock compositions of these limestones (Section 3.4.1).

The limit to the stability of calcite + muscovite + plagioclase in T - X_{CO_2} space is shown in Figures 3.26a,b. The diagrams have been calculated using an activity correction for plagioclase with a composition of An_{25} , the approximate composition of plagioclase in the Inchrory Limestone samples from Limeworks Quarry, Tomintoul (see Table 9.5). Although an oversimplification, phyllosilicates are treated as end-members. Activity correction of just one phase in an assemblage is strictly incorrect thermodynamically (Connolly 1990; see also Chapter 4). However, it is useful in semi-quantitative estimation of the effects on the position of equilibria in a phase diagram where the activity of a phase (in this case, anorthite) is less than 1. The equilibria are also calculated at 8 and 10 kbars, to elucidate the effect of pressure on their positions in T - X_{CO_2} .

The very wide T - X_{CO_2} stability range of the assemblage calcite + plagioclase (An_{25}) + quartz extends to very water-rich fluid compositions at the likely temperatures at which these rocks were metamorphosed, thereby limiting the possibility of developing zoisite in these rocks (Figures 3.26a, b). Calcite and white mica (muscovite) appear to be in textural equilibrium in the Inchrory Limestone (Figure 3.21). The thermal stability of calcite + muscovite is a strong function of

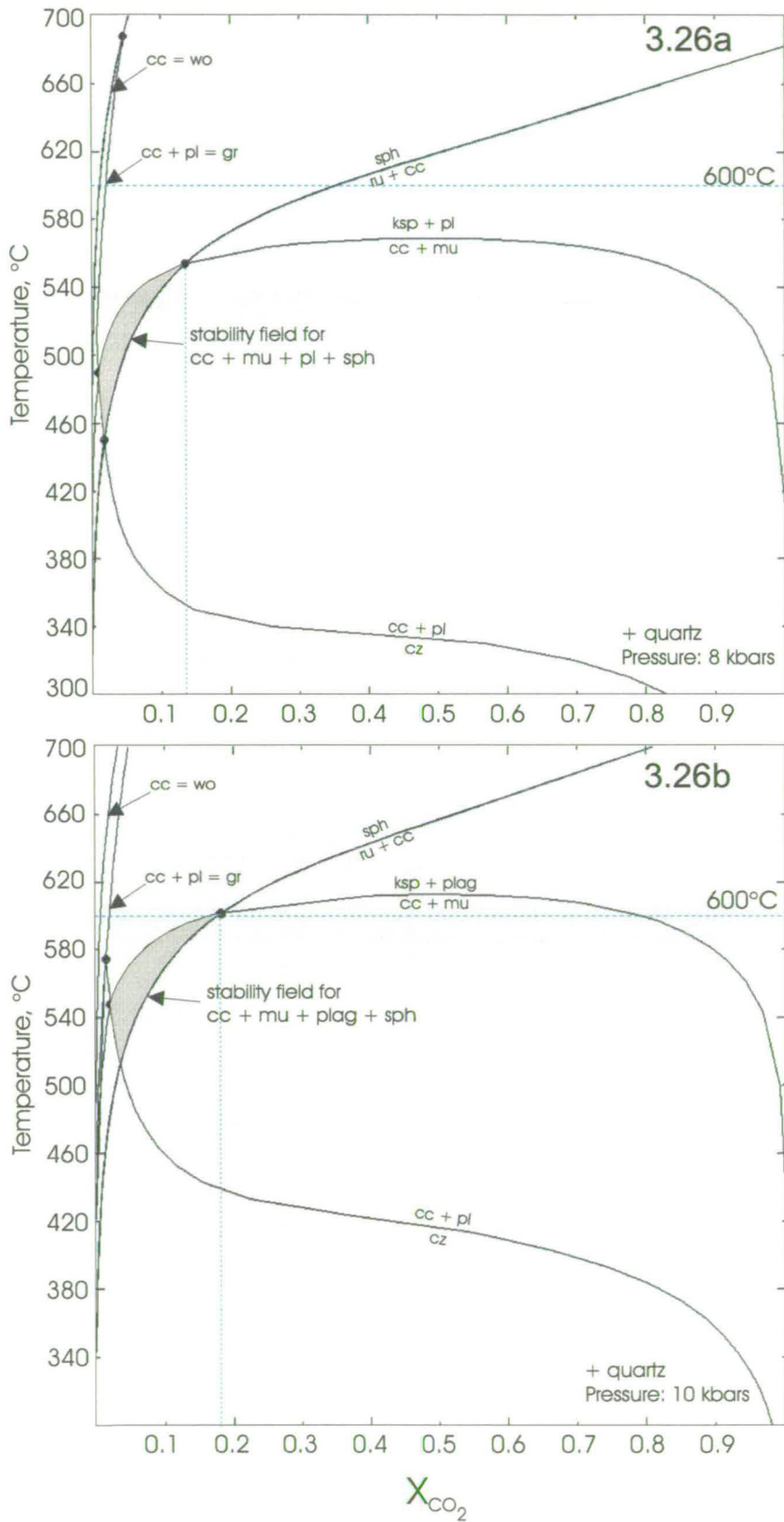
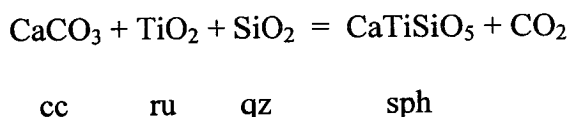


Figure 3.26a, b Significant phase relations in the limestones, calculated at pressures of 8 kbars (3.26a) and 10 kbars (3.26b); see text for discussion.

X_{CO_2} at extremes of fluid composition, but reaches a maximum of about 560°C at $X_{\text{CO}_2} \sim 0.5$ and 8 kbars across a broad plateau between ~ 0.2 and $0.7 X_{\text{CO}_2}$. At 10 kbars (the likely maximum peak pressure), this maximum is markedly higher at $\sim 615^\circ\text{C}$, due to the large volume change associated with this reaction. The phase relations calculated at 10 kbars are consistent with geothermometric calculations made using pelites in the same general area from which the Inchroory Limestone samples were collected (Beddoe-Stephens 1990).

A constraint on likely maximum X_{CO_2} may be provided by the presence of scaly sphene crystals, assuming them to be in equilibrium with calcite (Figure 3.22). The stability field for the equilibrium assemblage calcite + muscovite + plagioclase + sphene is limited to the shaded area in Figures 3.26a,b. The maximum X_{CO_2} for this assemblage is ~ 0.14 at 8 kbars and ~ 0.18 at 10 kbars. The stability of sphene in quartz-saturated, carbonate rocks is defined by the reaction:



The presence of sphene, rather than rutile, indicates that fluid compositions were *relatively* water rich where sphene exists. On the other hand, the stability of the assemblage calcite + muscovite + quartz shows that X_{CO_2} must have exceeded ~ 0.2 at $\sim 600^\circ\text{C}$ in the greater part of the rock. Given that the sphene is associated spatially with the mica, it may be that hydrous fluids with which it may have been in equilibrium were channelled along these more phyllosilicate-rich domains and that fluid compositions were locally different to those in the wider body of the rock dominated by calcite + quartz + plagioclase assemblages. However, the scale of the

phyllosilicate domains is small (Figure 3.21) and it is difficult to envisage partitioned fluid flow on such a scale during peak metamorphism and deformation. The corollary is that any metamorphic fluids were buffered by the assemblage calcite + muscovite + plagioclase + quartz + sphene to occupy the small triangular areas shaded in grey in Figure 3.26a, b.

In contrast to the above conclusion that the bulk of the limestones buffered fluids internally, the abundant calc-silicates in the sample of Dungiven Limestone from Butterlopie Glen (HY1350) (Figure 3.14) indicate that fluids were externally buffered in this limestone sample and that the rocks interacted with a very hydrous fluid phase under amphibolite facies metamorphic conditions. The scattered tremolite shows calc-silicate formation occurred throughout the rock. This reflects a more magnesian composition compared to other samples of 'Tayvallich' limestones (Section 3.4.1; Table 3.2), suggesting that it was originally dolomitic. The occurrence together of K-feldspar and zoisite indicate equilibrium with very water-rich fluids (Figures 3.26a,b), but the concentration of these calc-silicate phases along specific domains (Figure 3.14) also indicates bulk compositional variation on a small scale within the limestone. This locally developed bulk composition is critical to the formation of these phases, but it *may be* that hydrous fluid infiltration was concentrated here in any case via reaction-enhanced transient porosity. However, as already indicated above, calcite $\delta^{18}\text{O}$ is very depleted in these rocks (Chapter 7). This, along with the calcite grain architecture, which appears to postdate the formation of the tremolite fabric, and the scattered tremolite itself indicates that hydrous fluid infiltration was extensive and pervasive.

3.4 Whole-rock geochemistry

Seven major limestone and three dolostone units for which carbon, oxygen and strontium isotope analyses have been obtained, have been analysed for whole-rock major oxide and trace element compositions (Table 3.1). Summaries of the geochemical data for the groups of samples are presented in Table 3.2. Note that the minimum, median and maximum values for each analysed component given in Table 3.2 *do not represent individual analyses*, hence the absence of totals. The median and ranges are preferred to the mean and standard deviation as measures of location and spread, as the latter can be badly affected by the effects of outliers, particularly in small data sets such as these.

Data for the Dufftown, Torulian and Inchrory limestones come from larger data sets for each of these units included in Thomas (1989; bound in) and deposited with the library of the Geological Society, London and the British Library, Boston Spa as Supplementary Publication number Sup 18055 (23 pages). Data for the remaining groups of samples are unpublished.

3.4.1 Limestone geochemistry

Grampian and Appin Group limestones are relatively pure, with silica being the main contaminant. Median concentrations of Al_2O_3 only exceed 2 wt% in the ‘Tayvallich’ limestones; in all the limestones, alumina reflects the plagioclase and mica contents. The Dufftown, Torulian and Storakaig limestones are very pure, as indicated by low silicate-derived oxide concentrations and median CaO concentrations in excess of 50%, but they tend to be a little more magnesian than the Kincaig and Inchrory

	Grampian Group			Appin Group												Argyll Group								
	Corrieyairack Subgroup			Ballachulish Subgroup						Blair Atholl Subgroup						Tayvallich Subgroup						Torr Head and Dungiven		
	Limestones from Kincaig			Dufftown Limestone			Torulian Limestone			Inchrory Limestone			Storakaig Limestone			Boyne Limestone			limestones, N. Ireland					
	Min	Median	Max	Min	Median	Max	Min	Median	Max	Min	Median	Max	Min	Median	Max	Min	Median	Max	Min	Median	Max			
SiO ₂	6.52	8.72	11.12	2.26	4.33	8.52	1.27	4.19	8.16	5.72	7.68	11.91	0.83	1.83	3.95	9.06	20.60	27.09	5.39	8.24	16.55			
TiO ₂	0.08	0.10	0.13	0.02	0.03	0.04	0.00	0.01	0.08	0.04	0.06	0.10	0.01	0.01	0.02	0.06	0.18	0.23	0.07	0.10	0.15			
Al ₂ O ₃	1.57	1.75	1.95	0.27	0.57	0.99	0.01	0.47	1.93	1.05	1.81	2.59	0.16	0.28	0.41	2.05	5.52	7.55	1.58	2.49	3.35			
Fe ₂ O _{3, total}	0.73	0.81	1.03	0.15	0.24	0.39	0.07	0.27	0.70	0.42	0.54	0.89	0.13	0.25	0.71	0.83	1.83	2.30	0.62	0.87	1.39			
MgO	0.54	0.75	0.96	0.32	0.85	0.91	0.23	0.63	1.98	0.26	0.31	0.40	0.50	1.93	3.94	1.13	2.21	3.32	0.42	0.55	4.13			
MnO	0.02	0.51	0.58	0.02	0.03	0.07	0.01	0.02	0.04	0.01	0.02	0.04	0.01	0.04	0.05	0.04	0.08	0.09	0.02	0.02	0.50			
CaO	47.46	49.89	50.48	49.43	52.42	53.07	46.45	52.63	55.84	46.02	49.12	51.17	48.52	52.36	54.63	32.29	37.71	47.29	41.67	49.34	50.80			
Na ₂ O	0.22	0.41	0.51	0.08	0.12	0.17	0.00	0.07	1.04	0.03	0.16	0.30	0.02	0.03	0.07	0.44	0.82	1.08	0.31	0.45	0.84			
K ₂ O	0.13	0.33	0.59	0.06	0.09	0.18	0.00	0.03	0.13	0.19	0.41	0.55	0.04	0.05	0.11	0.51	1.32	1.96	0.14	0.50	0.85			
P ₂ O ₅	0.04	0.05	0.08	0.10	0.30	0.30	0.00	0.01	0.03	0.03	0.06	0.09	0.01	0.02	0.03	0.08	0.09	0.10	0.05	0.11	0.13			
LOI	37.25	37.89	39.46	39.33	41.31	43.00	39.19	41.83	42.28	37.21	39.40	40.76	42.37	43.02	43.71	24.54	28.52	37.79	31.33	37.07	39.82			
Ba	46	51	117	-1	11	27	-1	23	43	16	76	82	22	26	79	37	99	191	27	137	309			
Ce	8	9	13	-1	-1	24	-1	-1	-1	-1	-1	15	-1	10	13	-1	32	42	11	20	27			
Ga	1	2	3	-1	-1	-1	-1	-1	4	-1	2	4	-1	-1	1	2	7	11	2	3	4			
La	5	6	8	-1	-1	5	-1	-1	10	-1	-1	8	7	9	14	9	13	22	-1	11	15			
Nb	2	2	5	-1	1	2	-1	-1	2	1	2	4	1	1	1	3	5	6	3	3	3			
Ni	2	5	10	-1	-1	-1	-1	-1	-1	-1	-1	-1	1	1	1	-1	7	10	3	6	8			
Pb	3	7	14	7	8	10	-1	7	11	7	8	10	2	3	3	13	15	18	6	32	50			
Rb	1	9	16	4	7	12	4	4	9	9	16	21	3	4	6	13	33	52	3	16	26			
Sr	1545	1775	1975	714	1217	1712	593	822	2178	1471	2104	2211	1881	2014	2622	2695	3380	4607	265	1990	2299			
V	4	5	6	4	6	8	-1	3	13	8	8	14	-1	-1	-1	11	21	32	-1	10	16			
Y	1	3	3	3	4	6	-1	2	4	3	4	5	3	6	10	6	11	15	4	7	9			
Zn	7	11	13	4	19	699	-1	4	44	4	6	8	3	4	6	18	27	37	19	48	88			
Zr	10	18	23	12	21	22	13	18	38	20	26	40	37	41	50	29	75	111	20	65	94			
n	6			5			5			5			5			4			4					

-1: below detection

Table 3.2 Summary whole-rock major and trace element geochemistry of the limestones listed in Table 3.1

	Appin Group			Argyll Group			?Dalradian		
	?Ballachulish Subgroup			Islay Subgroup			Staosnaig Phyllite Formation		
	Kintra Dolostone			Islay Subgroup dolostones			Dolostones		
	Min	Median	Max	Min	Median	Max	Min	Median	Max
SiO ₂	37.76	39.04	39.91	8.29	10.58	13.70	25.69	29.90	46.17
TiO ₂	0.29	0.31	0.34	0.06	0.09	0.12	0.16	0.22	0.30
Al ₂ O ₃	5.22	5.38	6.05	1.28	1.42	2.23	3.62	5.15	7.16
Fe ₂ O _{3, total}	2.03	2.14	2.22	1.11	1.30	1.64	1.12	1.94	4.30
MgO	10.17	10.59	10.75	18.04	19.89	21.15	8.78	13.29	15.44
MnO	0.07	0.08	0.08	0.10	0.14	0.21	0.04	0.04	0.20
CaO	15.13	15.49	16.07	25.17	29.03	29.65	12.30	18.17	20.46
Na ₂ O	0.27	0.96	1.23	0.18	0.22	0.96	0.41	0.64	1.10
K ₂ O	1.32	1.67	1.88	0.00	0.00	0.38	0.88	1.26	1.97
P ₂ O ₅	0.05	0.10	0.10	0.00	0.03	0.04	0.07	0.12	0.14
LOI	23.71	24.09	25.26	36.50	38.21	39.40	19.77	28.07	31.93
Ba	244	300	369	-1	-1	46	163	217	273
Ce	29	39	42	-1	-1	13	29	32	33
Ga	6	7	8	1	2	2	4	6	9
La	14	16	18	-1	6	7	12	14	20
Nb	6	7	8	2	2.5	4	3	5	6
Ni	6	7	8	9	14.5	20	6	9	15
Pb	6	10	16	6	9	11	6	9	14
Rb	41	53	62	1	2	16	28	41	60
Sr	234	289	456	162	174	245	135	235	422
V	8	12	18	8	13	18	13	26	36
Y	18	19	21	4	6.5	8	9	12	16
Zn	22	24	27	33	158	694	21	34	45
Zr	188	198	215	26	48.5	56	83	116	146
n	4			4			6		

-1: below detection

Table 3.2 Summary whole-rock major and trace element geochemistry of the limestones listed in Table 3.1

limestones. The 'Tayvallich' limestones are rather more impure overall, but, with the exception of the more Mg-rich HY1350, have essentially the same geochemical character as the other limestones.

Loss on ignition values are approximately equivalent to the amount of CO_2 which would be evolved from CaCO_3 in the rock, assuming the latter to be contained entirely within calcite. This is true even of the Boyne Limestone samples which contain lenses of calc-silicates (avoided during sampling). Decarbonation in most of the limestones has been minimal.

Few limestones have trace elements with median concentrations >10 ppm, the exceptions being Ba, Sr and Zr. Strontium values well in excess of 1000 ppm are typical for low-MgO calcite Dalradian limestones. Such values are notable because they are considered indicative of original carbonate sediment dominated by aragonite (Chapter 5).

3.4.2 Dolostone geochemistry

The Kintra Dolostone and dolostones from the Staosnaig Phyllite Formation have similar chemistry and both contain abundant silica (25 – 46 wt%) and relatively high levels of Al_2O_3 , Fe_2O_3 and alkalis. Al_2O_3 and alkalis reflect the amount of phyllosilicate observed in thin section, whilst SiO_2 reflects the abundance of quartz. The iron most likely occurs in the dolomite spar which dominates the mineralogy, imparting the buff- to tan-coloured weathering typical of these rocks. Although the dominant carbonate phase is dolomite, the proportion of CaO to MgO is such that it

is in slight excess for stoichiometric dolomite, assuming all the MgO to be in dolomite.

Dolostones from the Islay Subgroup rocks of Northeast Scotland are markedly purer than the Kintra and Staosnaig dolostones, although even here SiO₂ reaches nearly 14 wt% (Table 3.2). With the exception of iron and manganese, all other oxides are present at very low concentrations and only alumina exceeds 1 wt%. The abundance of iron relative to other impurities in these dolostones is higher than in the other dolostone sample suites. Manganese is enriched relative to iron; MnO/Fe₂O_{3(total)} ratios range from 0.09 to 0.13 in these samples, whilst they range from 0.02 – 0.04 in the Kintra and Staosnaig dolostones. This reflects the greater abundance of carbonate.

Comparatively high concentrations for several trace elements in the Kintra and Staosnaig dolostones can be attributed to the presence of the phyllosilicates. Ba is notably enriched compared to the limestones, as is Zr and Rb. In contrast, the purity indicated by the major oxides for the Islay Subgroup samples is reflected in lower concentrations for Ba, REE and Y and Zr. Zn is conspicuously enriched and may reflect the presence of sphalerite in the sulphide phase.

Sr concentrations are an order of magnitude less than those in the limestones, ranging from 162 – 456 ppm. However, they are similar for all three suites of samples and are high for dolostones (Note, however, that although Sr concentrations are much the same, there are significant differences in Sr isotope compositions; see Chapter 6). These relatively high Sr concentrations indicate that the primary mineralogy of these dolostones was aragonite (see also Chapter 5).

3.5 Summary and conclusions

- The limestones and dolostones are dominated by assemblages which indicate that fluid buffering was *largely* controlled by the rocks and that, in general, interaction between the carbonate rocks and external fluids was *limited*, except in the Dungiven Limestone.
- Sedimentary textures are commonly preserved in the Southwest Highland and Northern Ireland limestones samples, most particularly ooids and oolitic clasts; in general, these carbonate grains appear to have been reworked into re-deposited carbonate sediments.
- Limestone samples from the Northeast Grampian Highlands, lack any original textures, these having been destroyed by metamorphic recrystallisation and fabric development.
- Although having a polygonal metamorphic grain architecture, dolostones from the Northeast Grampian Highlands preserve grain-scale geochemical zoning reminiscent of dolomite replacement textures observed in dolostones from Islay.
- The key assemblages in the limestones are calcite + muscovite + plagioclase + quartz and sphene + calcite + quartz: whilst sphene indicates that equilibrium fluids were hydrous, the lack of zoisite and K-feldspar shows that they still carried significant X_{CO_2} .
- Tremolite is common in Islay Subgroup dolostones from the Northeast Grampian Highlands, indicating that the reaction $\text{dol} + \text{qz} = \text{tr} + \text{cc}$ has occurred, whilst dolostones from Islay and Colonsay preserve stable $\text{dol} + \text{qz} + \text{mu} + \text{rutile}$

assemblages. These assemblages are consistent with the grades of metamorphism to which the rocks were subjected.

- In the Islay Subgroup dolostones, the stable assemblage is tr + dol + cc with quartz absent; diopside is not developed because a quartz-absent tr + cc assemblage is stable to higher P,T conditions than tr + cc + qz and these are outwith the P,T conditions which affected these rocks.
- Where calc-silicate development is extensive (HY1350, Dungiven Limestone), the petrographic evidence indicates extensive hydrous fluid infiltration, locally facilitated by reaction-enhanced, transient porosity. This is consistent with strongly depleted bulk-rock carbonate $\delta^{18}\text{O}$.

Chapter 4

Constraints on metamorphic fluid-rock interaction in calc-silicate-bearing lithologies.

In this Chapter:

- ❖ Phase relations and mineral chemistry of calc-silicates
- ❖ Limits on stability of assemblages in T- X_{CO_2} space
- ❖ Implications for fluid-rock interaction and fluid buffering

4.1 Introduction

In this chapter, I outline petrographical and mineral chemical work undertaken on calcsilicate assemblages in the Pitlurg Calcareous Flag Formation (Chapter 2, Figure 2.2), with the aim of elucidating their fluid-rock interaction history. Detailed petrography elucidating phase relations, mineral chemistry and T- X_{CO_2} sections have been used to determine the nature of mineral - fluid buffering and to establish the degree to which the rocks have been infiltrated by metamorphic fluid.

4.1.1 Calc-silicate rocks in metamorphic fluid-rock interaction studies

In recent studies of metamorphic fluid-rock interaction, pure limestones have become

very important because their distinctive stable and strontium isotope compositions are systematically modified during fluid infiltration (see chapters 8 – 10). However, they are generally of less value in determining the composition and evolution of infiltrating fluid because their mineralogy is generally relatively simple (principally calcite) and is stable over a wide range of P-T-X conditions.

In contrast, impure dolomitic rocks undergo various mixed-volatile, decarbonation and/or dehydration reactions to produce calc-silicate assemblages (e.g. Greenwood, 1967; Bowen, 1940; Hoschek, 1980; Connolly and Trommsdorff, 1994). Depending upon the fluid volume, such rocks have the capacity to buffer the composition of the fluid phase (*internal buffering*) or, conversely, to undergo reaction driven by external fluid infiltration (*external buffering*). The resulting calc-silicate assemblages and their phase relationships record this fluid-rock interaction, allowing the composition of the fluid phase to be elucidated. Calc-silicate rocks which have been infiltrated extensively by fluid and, therefore, externally buffered, will develop high variance assemblages in which reactions have gone to completion. Rocks in which the fluid has been internally buffered will develop complex assemblages of low variance containing both reactants and products. They may also preserve complex reaction textures as fluid compositions are buffered along univariant equilibria towards invariant points.

In originally marly dolomitic lithologies, calc-silicate phase relations can be highly complex, particularly where internally buffered, because of the complex chemistry of the protolith and the wide range of metamorphic reactions which can occur in such bulk compositions (e.g. Hoschek, 1980). As will be discussed further below, numerous reactions occur close together in P-T-X space for complex bulk

compositions like those of the rocks considered here and determining their relative significance for each particular domain can be difficult.

Impure dolomitic rocks are important in studies of metamorphic fluid rock-interaction and have been used to quantify fluid flux in metamorphic terrain. Ferry (1983, 1984, 1986, 1989, 1992) pioneered use of reaction progress in calc-silicate rocks to calculate both fluid:rock ratios and to determine fluid fluxes. In his gradient flow model (Ferry, 1989), the fluid phase is assumed to have been buffered by univariant equilibria along the fluid flow path, over which there is a temperature gradient. In a different approach, other workers have used chromatographic theory to calculate fluid flux by modelling advective displacement of reaction fronts from lithological boundaries into reactive lithologies like impure dolostones and metabasic rocks (e.g. Bickle et al., 1990; Skelton, 1993; Skelton et al., 1995) (*note that this petrographical approach to quantifying fluid flux is the same, in principle, as that applied to the advection of isotopic fronts, as briefly described in Chapter 8*). Fluid infiltration drives the reaction and displaces the reaction front downstream. In this model, the reaction assemblage is externally buffered by the fluid phase.

The importance of calc-silicate rocks in studies of metamorphic fluid-rock interaction is highlighted by brief discussion of a study from the Southwest Highlands of Scotland with relevance to the calc-silicate rocks described later in this chapter.

Graham et al. (1983) discuss calc-silicate assemblages in impure metacarbonate rocks adjacent to amphibolites within the Tayvallich Limestone at South Bay, near Tarbert, Loch Fyne, North Kintyre. At this locality, they describe the distribution of calc-silicate assemblages in which assemblages with different fluid-

buffering characteristics occur in close proximity (Graham et al. *op. cit.*; figure 6). Although all the assemblages in the metacarbonate rocks indicate infiltration by a hydrous fluid phase, the X_{CO_2} -composition of the fluid phase was variable on the scale of centimetres to metres. Assemblages in equilibrium with extremely hydrous fluids contain grossular and minor diopside and were externally buffered. Assemblages in equilibrium with progressively more CO_2 -rich fluid lose grossular and gain clinozoisite and some of these assemblages buffered the fluid phase by reactions at invariant points. The formation of the calc-silicate assemblages was driven by infiltration of fluid derived from the dehydration of the amphibolite sheets under epidote-amphibolite facies conditions. Graham et al. (1983) also document later regional retrogressive fluid infiltration at greenschist facies, in which dolomite and rutile-bearing assemblages replace the high temperature assemblages.

Fluid infiltration mechanisms in calc-silicate rocks

Fluid infiltration in calc-silicate rocks is likely to be facilitated by somewhat different mechanisms than infiltration into pure limestones (see Chapter 8). This is because porosity and permeability will be generated as the devolatilisation reactions proceed. Hydrofracture (see Chapter 8) is always likely to be important, but its effects may be enhanced by reaction. If infiltration and reaction is accompanied by deformation, then fluid infiltration may be facilitated further, but it will be possible for infiltration to occur without deformation

Layout of Chapter

This chapter is divided into three main sections. In the first, I discuss the general

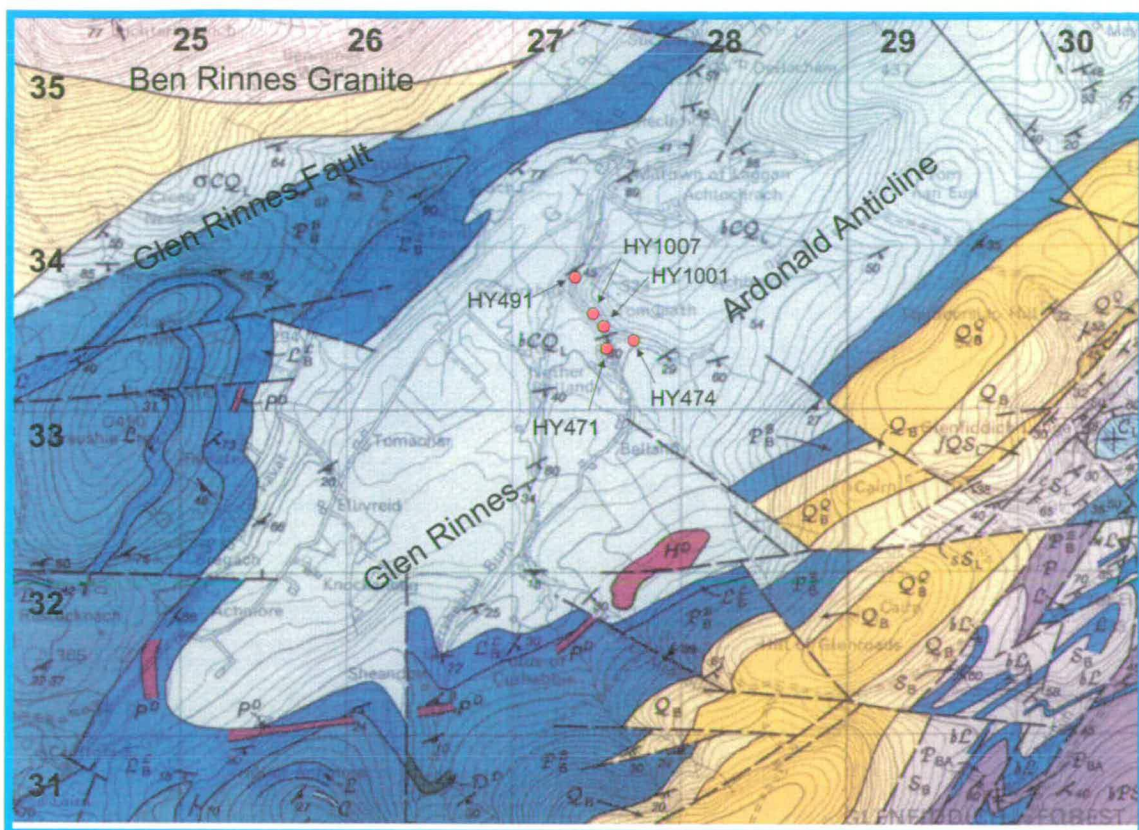
petrology and mineral chemistry of the calc-silicate assemblages. The basic petrological and mineral chemical data are used in the second section to construct T- X_{CO_2} sections. These provide the framework for interpreting the calc-silicate assemblages. In section three, I use the T- X_{CO_2} sections to elucidate the variability of composition of the fluid phase in equilibrium with the assemblages. In particular, I consider the scale of the domains over which particular assemblages exist, their fluid-buffering properties and the implications for fluid-rock interaction in the calc-silicate lithologies.

4.2 General petrography

The general geology of the Pitlurg Calcareous Flag Formation (Lochaber Subgroup, Appin Group) is described Chapter 2, Section 2.3.2. The samples come from exposures in Glen Rinnes, southwest of Dufftown [NJ 324 399], as shown in Figure 4.1. The rocks were metamorphosed at amphibolite facies at peak temperatures estimated to be $\sim 600^\circ\text{C}$ and pressures of the order of 8 kbars (Beddoe-Stephens, 1990).

In Glen Rinnes, the Pitlurg calc-silicate-bearing rocks are thinly bedded to laminated and generally very fine grained (<1 mm), grey to dark brown rocks. They are carbonate poor, though there are some thin limestones near the top of the formation, just below its boundary with the overlying Dufftown Limestone Member (Mortlach Graphitic Schist Formation, basal Ballachulish Subgroup).

In the field, the lamination, together with an aligned early penetrative cleavage, is prominent and is locally crenulated by an upright fabric which is oblique to the limb of the Ardonald Anticline, but which is probably related to later



Gridlines are from National Grid in 100km square NJ

Scale: 1:50 000



Key

P_B^B	Mortlach Graphitic Schist Formation	} Ballachulish Subgroup
L_B^L	Dufftown Limestone Member	
bCQ_L	Pitlurg Calcareous Flag Formation	Lochaber Subgroup

- Sample location and number

Figure 4.1 Location of calc-silicate samples in the Pitlurg Calcareous Flag Formation. Geological map taken from BGS 1:50 000 Sheet 85E, Glenlivet

deformation focussed upon the main fold structure; here this later crenulation is termed S2.

Thin sections of several samples reveal that the strong millimetre-scale lamination in the rocks is punctuated by elongate and commonly irregular patches of different bulk composition (Figures 4.2, 4.3a, b, 4.4). These patches are commonly colourless and generally lie approximately parallel to the late crenulation, indeed, they often appear to be the focus of nucleation of the crenulation. Commonly, their mineralogy is different to that of adjacent laminae, showing that they have different bulk chemistry. They have markedly different textures to the immediate adjacent laminae. Their petrology and possible modes of origin are discussed below in more detail.

The mineralogy is dominated by colourless amphibole, pale brown phlogopite and, in some samples, pale to darker brown biotite. Quartz is usually present in excess, but is locally absent in some assemblages. Although thin calcite-rich laminae occur locally, calcite is not ubiquitous and dolomite is entirely absent. Other phases include zoisite, plagioclase and K-feldspar, albite and hyalophane, sphene, chlorite and muscovite. Diopside and grossular are conspicuously absent. The mineralogy shows that, in addition to being calcareous, the rocks are variably magnesian, aluminous and potassic. The mineral assemblages are listed in Table 4.1, including data from more detailed petrographical work undertaken using the electron microprobe, described in Section 4.5.

4.2.1 Amphibole

Euhedral to anhedral amphibole is abundant in many laminae and is stubby to

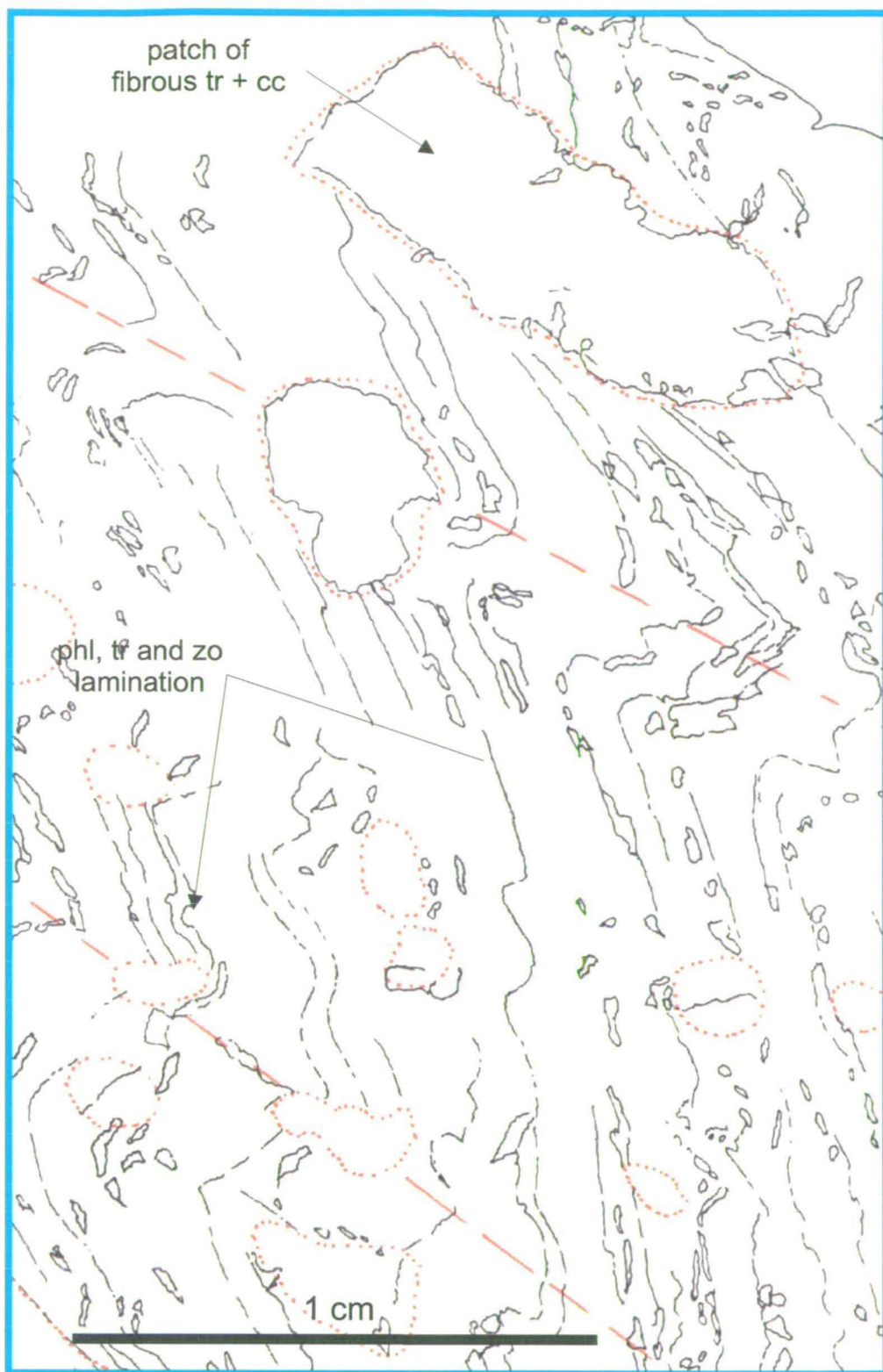


Figure 4.2 Sketch of crenulated lamination and coarse patches (outlined in dotted red) in HY474. The large patch at the top of the sketch is shown in more detail in Figure 4.4. Note the alignment of the elongate patches with the axial plane of the crenulation. See also Figure 4.3a.

Figure 4.3a Elongate patch of differing bulk composition to laminae in HY1001. The assemblage in the patch is am + pl + ksp + qz + cc + sph. Note the nucleation of the crenulation cleavage on the patch (see Section 4.5 for discussion).

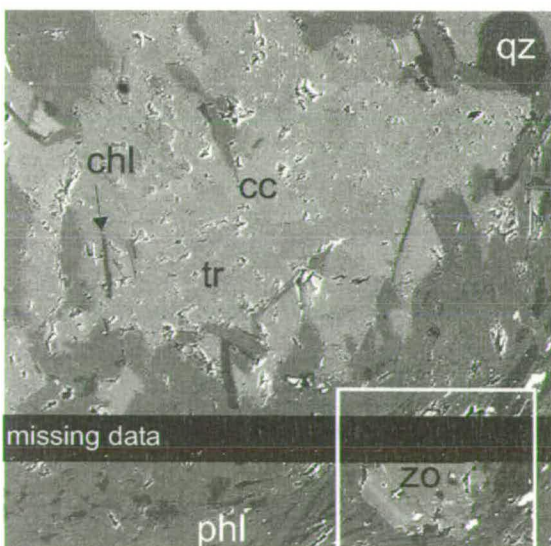
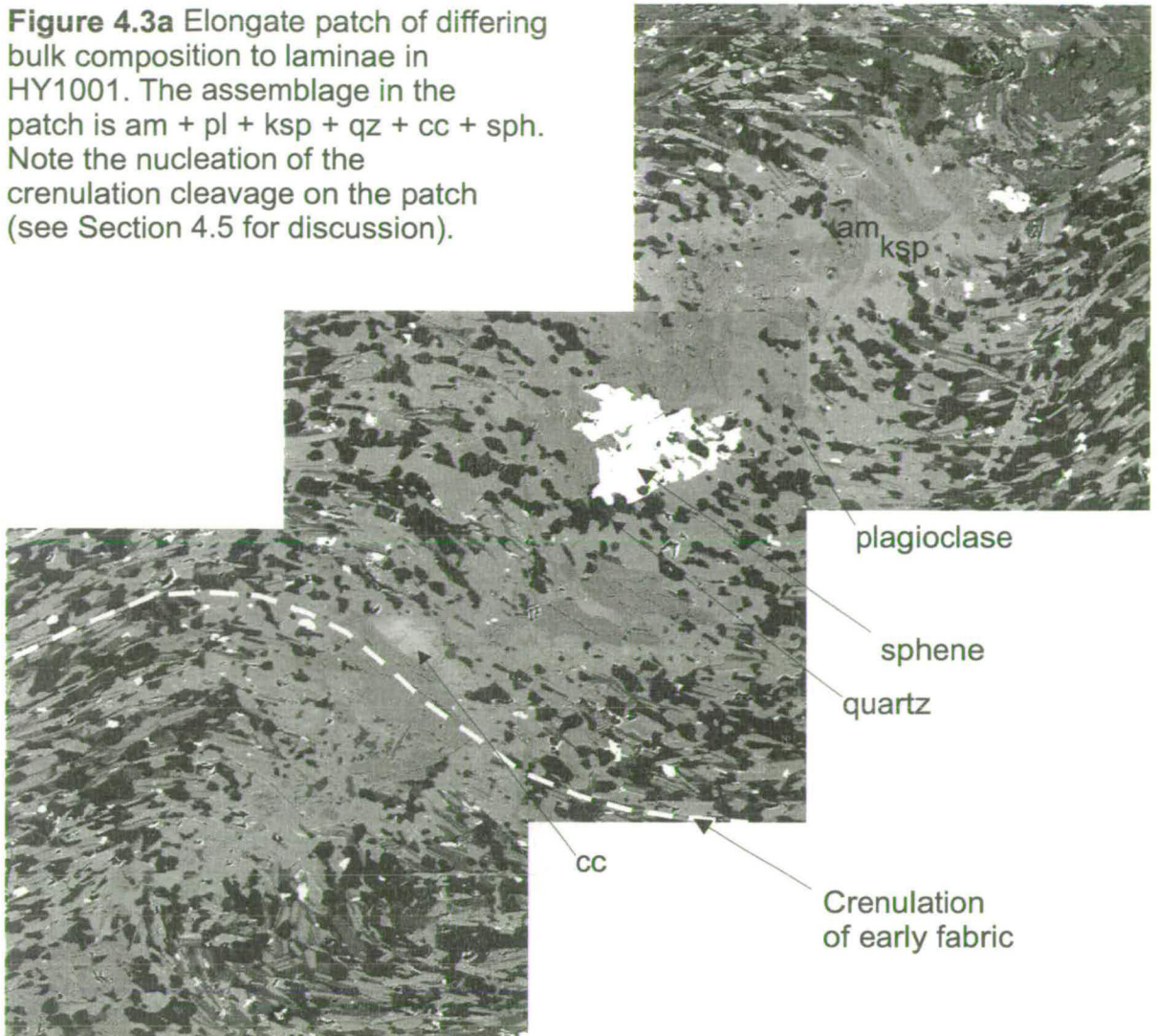


Figure 4.3b Edge of coarse patch in HY474. This patch cuts across the lamination defined by phlogopite-rich domains.

The assemblage is cc + tr + qz with subordinate phl + chl. See Section 4.5 for discussion

Boxed area contains zo-pl-cc and tr-ksp-phl-chl reaction assemblages (Section 4.5, See also Figures 4.20 and 4.21).

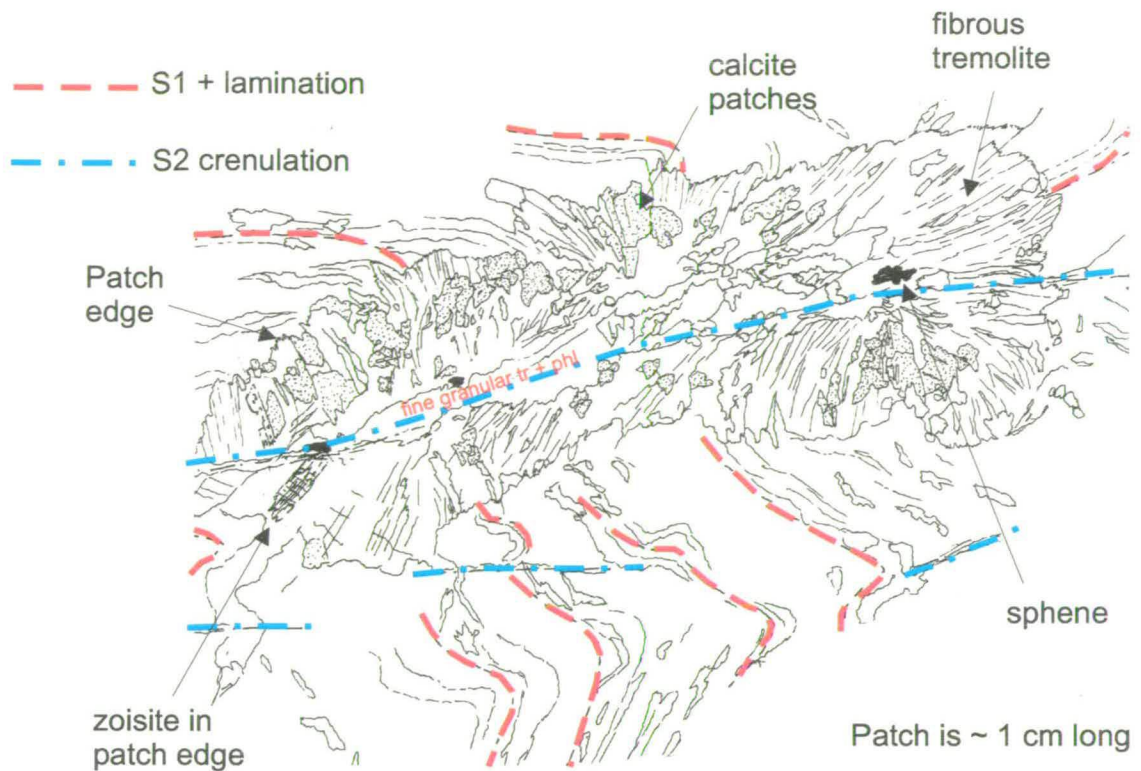


Figure 4.4 Sketch of textures in patch in HY474 (see Figure 4.2)

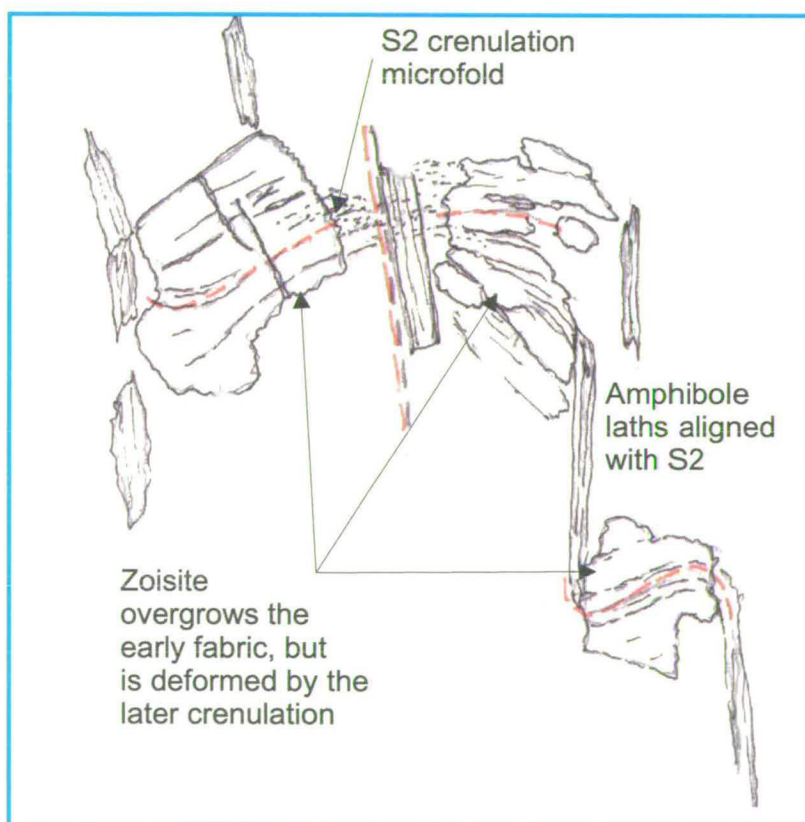


Figure 4.5 Relationship of zoisite to fabrics, showing that it overgrows the early penetrative fabric, but is itself deformed by the later S2 fabric, possibly growing early in the development of S2. Sketch, field of view ~ 1 mm

	Domain			
Sample	Dominant phases	Trace	Absent	Comments
HY471	am, phl/clin, pl, qz	alb, hyal, mu	zo, cc	domains phl-rich or poor; mu armoured by pl
HY474	Area 1			
	<i>Lamina A</i> am, qz, phl	cc, pl	zo, sph, ksp	
	<i>Boundary between A & B</i> zo, ksp, sph, am, phl, clin	qz, cc		am, phl and clin being replaced ksp + zo
	<i>Lamina B</i> am, phl, qz, pl	alb, zo	cc	alb inclusions in pl
	<i>Lamina C</i> am, cc, qz, phl		zo, pl, ksp	
	<i>Lamina D</i> ksp, zo, phl	am, cc	qz, pl	
	<i>Patch</i> cc, am, qz, phl/cli, ksp, zo			
	Area 2			
	<i>Lamina A</i> am	phl, qz, sph	cc	
	<i>Lamina B</i> am, phl/clin, sph	ksp, alb	zo	

Table 4.1 Mineral assemblages in calc-silicate rocks from the Pitlurg Calcareous Flag Formation

Domain				
Sample	Dominant phases	Trace	Absent	Comments
HY491	Lamina C zo, phl, cc, pl, ksp, am, qz			
	Patch am, cc, qz, phl/clin			qz occurs as inclusions in am
	Area 1 Lamina A bi, zo, qz, am, clin, pl	ksp, cc		ksp as inclusions in pl, cc as inclusions in zo
	Lamina B bi, pl, qz,	am, ksp, cc, alb	zo	ksp as inclusions in pl
HY1001	Area 2 bi, zo, am, cc, qz, pl			
	Area 3 bi, qz, am, pl	zo, cc		
	Area 1 Lamina A bi, tr, qz, zo, hyal, pl, clin			
	Lamina B tr, qz, pl, clin, hyal, bi, zo			bi, zo much less abundant than in Lamina A
	Patch tr, ksp, qz,	cc, clin	zo, bi	zo, bi & cc unstable at edge of patch

Table 4.1 Mineral assemblages in calc-silicate rocks from the Pitlurg Calcareous Flag Formation

Domain				
Sample	Dominant phases	Trace	Absent	Comments
	Area 2 <i>Laminae</i> zo, ksp, pl, bi, qz <i>Patch</i> am, pl, ksp, qz, cc	cc, sph	am	Elongate patch across laminae
HY1007	Area 1 am, wm, ksp, cc	phl/clin, zo	qz	ksp grows after wm
	Area 2 Assemblage 1 tr, cc, qz Assemblage 2 tr, wm, qz	sph, ksp		ksp rims wm
HY990	tr, cc, zo, qz, sph		clin, pl	

Table 4.1 Mineral assemblages in calc-silicate rocks from the Pitlurg Calcareous Flag Formation

acicular in form, commonly with typical amphibole terminations. There are probably several phases of amphibole growth (see also Sections 4.3 and 4.5 below). In some phlogopite-rich laminae, it overgrows the mica and contains inclusion trails of fine quartz. This early amphibole commonly defines the early penetrative, lamination-parallel fabric with phlogopite in most samples. In one sample, later amphibole laths are aligned with the open crenulation fabric and in some lithons, the early amphibole is crenulated by the later crenulation fabric.

4.2.2 Zoisite and feldspars

Zoisite may be abundant locally. It overgrows the early fabric, which occurs as inclusion trails of quartz and, more rarely, calcite, in some zoisites. However, it is deformed in part by the later crenulation cleavage (Figure 4.5). It forms ubiquitously anhedral crystals.

K-feldspar and plagioclase are the most abundant of the feldspars, the former particularly so in some laminae. K-feldspar commonly overgrows phlogopite, forming ragged colourless patches within the latter. Hyalophane and albite occur only in very small amounts and their presence was only detected by electron microprobe.

Plagioclase is an important phase in these rocks (Section 4.4) but is very difficult to determine optically because of its small grain size; its composition was determined by electron microprobe (see section 4.4.3 and 4.5).

4.2.3 Phyllosilicates

Phlogopite is the most abundant phyllosilicate and K-bearing phase and gives the rocks their brownish tinge. Along with much of the amphibole, it defines the early

fabric. It forms extensive ragged plates and laths and is moderately to weakly pale brown pleochroic. Many phlogopite-rich laminae also contain abundant zoisite.

Although originally identified optically as chlorite, a colourless, chlorite-like phase is actually an Al-poor clinochlore – serpentine mineral (see Section 4.3). It is nearly always finely intergrown with phlogopite. For convenience, it will be referred to as clinochlore in the rest of the Chapter. Some late chlorite plates occur in places, overgrowing all the fabrics. Such late chlorite is common in most of the rocks in the region and is considered part of a late retrogression which particularly affects pelitic rocks in the region as a whole.

Muscovite is uncommon, but its presence in some samples is important in determining the petrographic evolution of some assemblages.

4.2.4 Summary

- The mineralogy is dominated by amphibole and phlogopite and these are generally early phases.
- Zoisite and K-feldspar are locally abundant and generally post-date the amphibole and phlogopite.
- Textural evidence shows that zoisite begins to form after the formation of the primary fabric and before the onset of the S2 crenulation.

4.3 Mineral chemistry

The results of electron microprobe analysis of phases in the calc-silicates are summarised in Table 4.2. In the following discussion, mineral compositions for amphibole and phyllosilicates are considered in a little more detail, largely in terms

Table 4.2 Summarised representative chemistry of phases in calc-silicate rocks, Pitlurg Formation, Glen Rinnes

Note: most data represent summaries, rather than individual analyses, unless otherwise indicated

Amphibole																		
	HY471 n = 47			HY474 n = 11			HY479 n = 21			HY491 n = 19			HY1007 n = 7			HY990 n = 33		
	Min	Median	Max	Min	Median	Max	Min	Median	Max	Min	Median	Max	Min	Median	Max	Min	Median	Max
SiO ₂	48.59	54.66	56.83	42.38	55.44	56.30	51.97	54.47	56.54	49.89	53.97	56.96	54.30	55.42	56.63	52.49	55.57	56.42
TiO ₂	0.07	0.14	0.31	0.07	0.10	0.17	0.10	0.17	0.25	0.04	0.16	0.30	0.05	0.12	0.19	0.01	0.05	0.16
Al ₂ O ₃	1.87	4.27	11.40	2.12	3.18	4.05	2.30	5.02	7.53	1.18	4.48	9.37	2.20	4.31	6.03	0.91	1.44	4.71
FeO	2.39	3.01	4.07	1.94	2.35	2.78	2.60	2.83	3.31	4.28	5.08	6.06	3.09	3.35	3.59	4.27	4.74	5.49
MnO	0.03	0.06	0.09	0.00	0.01	0.01	0.00	0.01	0.01	0.01	0.01	0.02	0.01	0.01	0.01	0.04	0.06	0.11
MgO	17.71	20.74	21.99	18.16	22.14	22.73	19.72	20.95	21.86	17.09	19.42	21.03	19.10	20.37	21.36	19.27	20.83	21.39
CaO	12.30	13.03	13.50	13.01	13.37	22.60	12.38	13.26	13.45	12.48	12.92	13.22	12.73	13.25	13.48	12.70	13.25	13.52
Na ₂ O	0.20	0.40	1.12	0.11	0.18	0.30	0.18	0.38	0.72	0.10	0.36	0.99	0.22	0.45	0.64	0.08	0.12	0.49
K ₂ O	0.03	0.10	0.33	0.04	0.10	0.46	0.02	0.07	0.91	0.03	0.15	0.28	0.05	0.09	0.28	0.01	0.04	0.36
<i>Cations to 23 O pfu</i>																		
Si	6.89	7.59	7.88	6.74	7.66	7.75	7.26	7.53	7.80	7.08	7.59	7.93	7.55	7.64	7.83	7.49	7.84	7.89
Ti	0.01	0.02	0.03	0.00	0.01	0.02	0.01	0.02	0.03	0.00	0.02	0.03	0.01	0.01	0.02	0.00	0.01	0.02
Al	0.31	0.70	1.91	0.35	0.52	0.67	0.37	0.82	1.24	0.19	0.74	1.57	0.36	0.70	0.97	0.15	0.24	0.79
Fe _{total}	0.28	0.35	0.48	0.26	0.27	0.32	0.30	0.33	0.39	0.50	0.60	0.72	0.36	0.39	0.41	0.50	0.56	0.65
Mg	3.74	4.28	4.64	4.31	4.56	4.69	4.08	4.31	4.52	3.61	4.06	4.39	3.91	4.19	4.40	4.07	4.37	4.48
Ca	1.78	1.94	2.00	1.94	1.99	3.85	1.85	1.97	2.01	1.85	1.95	1.98	1.87	1.97	1.99	1.92	1.99	2.05
Na	0.05	0.11	0.31	0.03	0.05	0.08	0.05	0.10	0.20	0.03	0.10	0.26	0.06	0.12	0.17	0.02	0.03	0.13
K	0.01	0.02	0.06	0.01	0.02	0.09	0.00	0.01	0.16	0.01	0.03	0.05	0.01	0.02	0.05	0.00	0.01	0.06

Very minor amounts of Cr₂O₃, BaO, F and Cl not included

Table 4.2 Summarised representative chemistry of phases in calc-silicate rocks, Pitlurg Formation, Glen Rinnes

Phlogopite												
	HY471 n = 11			HY474 n = 4			HY479 n = 4			HY491 n = 3		
	Min	Median	Max	Min	Median	Max	Min	Median	Max	Min	Median	Max
SiO ₂	38.92	40.41	41.01	39.62	39.78	39.97	39.75	39.79	45.33	39.16	39.21	39.28
TiO ₂	0.56	0.74	0.77	0.68	0.70	0.84	0.56	0.74	0.77	1.07	1.12	1.24
Al ₂ O ₃	16.26	16.98	17.73	17.07	17.26	17.37	12.54	17.35	17.75	17.15	17.17	17.49
FeO	4.28	4.47	4.80	3.82	3.93	4.04	4.08	4.22	4.52	7.62	7.77	8.07
MnO	b.d.	b.d.	0.01	b.d.	b.d.	b.d.	b.d.	b.d.	0.01	0.05	0.08	0.08
MgO	20.74	21.59	22.02	22.13	22.32	22.77	20.74	21.06	21.51	18.61	18.62	18.72
CaO	0.02	0.06	0.13	0.02	0.06	0.08	0.08	0.27	0.52	0.01	0.03	0.08
BaO	0.11	0.19	0.32	0.20	0.30	0.36	b.d.	0.07	0.13	0.21	0.23	0.23
Na ₂ O	0.11	0.20	0.27	0.11	0.13	0.16	0.04	0.06	0.21	0.09	0.09	0.11
K ₂ O	8.61	9.07	9.18	9.08	9.49	9.69	6.02	9.78	9.87	6.96	7.21	7.22
F	0.29	0.44	0.62	0.74	0.74	0.75	0.34	0.41	0.68	0.30	0.47	0.57
<i>Cations to 22 O pfu</i>												
Si	5.69	5.76	5.87	5.64	5.69	5.70	5.68	5.72	6.31	6.27	6.27	6.29
Ti	0.06	0.08	0.08	0.07	0.08	0.09	0.06	0.08	0.08	0.13	0.14	0.15
Al	2.79	2.86	2.98	2.88	2.90	2.91	2.06	2.94	2.99	3.24	3.24	3.30
Fe _{total}	0.51	0.54	0.53	0.46	0.47	0.48	0.48	0.51	0.55	1.02	1.04	1.08
Mn	b.d.	0	0	0	0	0	0	0	0.01	0.01	0.01	0.01
Mg	4.44	4.61	4.69	4.72	4.75	4.83	4.36	4.49	4.57	4.44	4.45	4.47
Ca	0.00	0.01	0.02	0.00	0.01	0.01	0.01	0.04	0.78	0.00	0.01	0.01
Ba	0.01	0.01	0.02	0.01	0.02	0.02	b.d.	b.d.	0.01	0.01	0.01	0.01
Na	0.03	0.06	0.07	0.03	0.04	0.04	0.01	0.02	0.06	0.03	0.03	0.03
K	1.58	1.65	1.70	1.65	1.73	1.77	1.07	1.79	1.81	1.42	1.47	1.48
F	0.13	0.20	0.28	0.33	0.34	0.34	0.15	0.19	0.31	0.15	0.24	0.29

Very minor amounts of Cr₂O₃ and Cl not included

Table 4.2 Summarised representative chemistry of phases in calc-silicate rocks, Pitlurg Formation, Glen Rinnes

Chlorite														Muscovite			
	HY471 n = 2		HY474 n = 6			HY479 n = 4			HY491 n = 1	HY1001 n = 5			HY1007 n = 1		HY1007 n = 4		
	1	2	Min	Median	Max	Min	Median	Max		Min	Median	Max			Min	Median	Max
SiO ₂	30.97	32.00	29.48	30.35	35.97	28.33	30.48	32.06	28.95	27.87	28.08	28.39	32.69	SiO ₂	50.40	51.94	52.83
TiO ₂	0.06	0.08	0.02	0.07	0.09	0.06	0.08	0.08	0.07	0.02	0.03	0.05	0.04	TiO ₂	0.01	0.03	0.04
Al ₂ O ₃	18.32	18.54	17.71	19.73	20.50	20.40	20.45	23.19	20.50	19.50	19.79	20.25	16.22	Al ₂ O ₃	25.94	26.63	29.62
FeO	6.63	6.59	4.52	5.28	6.42	5.01	5.03	5.72	9.80	11.23	11.71	12.43	6.18	FeO	0.83	1.03	1.22
MnO	0.04	0.05	0.02	0.05	0.07	0.02	0.04	0.06	0.10	0.17	0.19	0.27	0.05	MnO	0.03	0.04	0.04
MgO	29.07	29.30	25.91	30.29	31.05	26.71	29.23	29.82	25.96	25.38	25.90	26.08	30.58	MgO	2.83	4.01	4.17
CaO	b.d.	b.d.	0.04	0.08	0.10	0.04	0.11	0.17	0.09	0.02	0.07	0.08	0.27	CaO	0.02	0.04	0.21
BaO	b.d.	b.d.	0.03	0.06	0.09	0.02	0.02	0.02	b.d.	n.d.	n.d.	n.d.	n.d.	Na ₂ O	0.03	0.03	0.04
Na ₂ O	b.d.	b.d.	b.d.	0.01	0.05	0.01	0.02	0.02	0.05	0.00	0.01	0.02	0.02	K ₂ O	10.97	11.07	11.15
K ₂ O	0.30	0.55	0.03	0.08	3.13	0.06	0.22	0.49	0.01	0.02	0.04	0.07	0.06	F	n.d.	n.d.	n.d.
F	0.15	0.25	0.08	0.09	0.11	0.14	0.16	0.22	0.02	0.06	0.13	0.24	n.d.				
Cations to 28 O pfu																	
Si	6.04	6.11	5.70	5.88	6.65	5.45	5.82	6.19	5.74	5.57	5.63	5.67	6.30	Si	6.71	6.93	6.99
Ti	0.01	0.01	0	0.01	0.01	0.01	0.01	0.01	0.01	0.00	0.00	0.01	0.01	Ti	0.00	0.00	0.00
Al	4.21	4.17	4.06	4.39	4.64	4.59	4.65	5.25	4.79	4.61	4.66	4.77	3.69	Al	4.08	4.17	4.65
Fe _{total}	1.08	1.05	0.70	0.85	1.05	0.81	0.81	0.91	1.62	1.88	1.96	2.08	1.00	Fe _{total}	0.09	0.11	0.14
Mn	0.01	0.01	0.00	0.01	0.01	0.003	0.01	0.01	0.02	0.03	0.03	0.05	0.01	Mn	0.00	0.00	0.01
Mg	8.45	8.34	7.14	8.69	9.01	7.69	8.38	8.49	7.66	7.68	7.74	7.85	8.79	Mg	0.56	0.80	0.83
Ca	0	0	0.01	0.02	0.02	0.01	0.02	0.04	0.02	0.00	0.01	0.02	0.06	Ca	0.00	0.01	0.03
Ba	0	0	0	0	0.01	0	0	0	0	n.d.	n.d.	n.d.	0	Na	0.01	0.01	0.01
Na	0	0	0	0	0.02	0	0.01	0.01	0.02	0.00	0.00	0.01	0.01	K	1.86	1.88	1.90
K	0.08	0.14	0.01	0.02	0.74	0.02	0.05	0.12	0	0.01	0.01	0.02	0.01	F	n.d.	n.d.	n.d.
F	0.09	0.15	0.05	0.06	0.06	0.08	0.10	0.14	0.01	0.04	0.08	0.15	0				

Table 4.2 Summarised representative chemistry of phases in calc-silicate rocks, Pitlurg Formation, Glen Rinnes

Plagioclase feldspar							K-feldspar						
	HY471 n = 5			HY474 n = 7			HY491 n = 12			HY1001	HY474 n = 4		
	Min	Median	Max	Min	Median	Max	Min	Median	Max	1	Min	Median	Max
SiO ₂	56.89	57.43	57.70	54.15	55.25	55.69	55.72	57.26	58.52	56.78	61.06	61.70	63.58
Al ₂ O ₃	24.99	25.98	26.58	26.68	26.72	27.88	25.06	26.02	27.16	26.52	18.12	18.33	19.44
CaO	8.03	8.38	8.64	8.76	8.91	10.49	7.62	8.36	9.53	8.91	b.d.	0.82	3.39
BaO	b.d.	0.02	0.12	b.d.	0.09	0.10	b.d.	0.02	0.10	b.d.	0.52	0.55	1.54
Na ₂ O	6.41	6.66	6.98	4.99	6.03	6.32	6.18	6.60	6.80	6.34	0.17	0.20	0.34
K ₂ O	0.05	0.05	0.07	0.17	0.29	0.46	0.07	0.24	0.85	0.15	13.29	14.68	15.82
<i>Cations to 8 O pfu</i>													
Si	2.58	2.60	2.61	2.49	2.54	2.55	2.54	2.59	2.64	2.58	2.89	2.95	2.99
Al	1.35	1.39	1.42	1.44	1.45	1.51	1.33	1.39	1.45	1.42	1.01	1.03	1.08
Ca	0.39	0.41	0.42	0.43	0.44	0.52	0.37	0.41	0.46	0.43	0	0.04	0.17
Ba	0	0	0	0	0	0	0	0	0	0	0.01	0.01	0.03
Na	0.57	0.59	0.61	0.44	0.54	0.56	0.54	0.58	0.60	0.59	0.02	0.02	0.03
K	0	0	0	0.01	0.02	0.03	0	0	0	0.01	0.80	0.89	0.95
An	39	41	43	43	45	54	39	41	46	42			

Albite				Hyalophane	
HY471, HY474		n = 4		HY471	HY1001
Min	Median	Max		1	1
SiO ₂	64.72	66.39	69.49	58.911	62.416
Al ₂ O ₃	18.69	19.02	21.10	17.573	18.827
CaO	0.11	1.08	1.83	0.011	0.076
BaO	-1.00	0.01	0.04	2.236	2.937
Na ₂ O	10.59	11.41	11.88	0.33	0.498
K ₂ O	0.04	0.19	0.66	14.836	14.688
<i>Cations to 8 O pfu</i>					
Si	2.89	2.97	3.01	2.951	2.949
Al	0.97	0.99	1.11	1.037	1.048
Ca	0.01	0.05	0.09	0.001	0.004
Ba	0	0	0	0.044	0.054
Na	0.92	0.99	1.00	0.032	0.046
K	0	0.01	0.04	0.948	0.885
An	1	5	8		

Zoisite				
HY474		n = 10		HY491
Min	Median	Max		1 2
SiO ₂	37.74	39.01	40.58	39.68 39.38
TiO ₂	0.03	0.06	0.08	0.17 0.03
Al ₂ O ₃	30.20	31.76	33.18	32.51 33.10
FeO	0.44	0.55	0.96	1.11 0.93
CaO	23.37	24.19	24.61	24.15 24.21
Si	5.98	6.06	6.19	6.05 6.00
Ti	0.00	0.01	0.01	0.02 0.00
Al	5.63	5.73	6.01	5.84 5.94
Fe _{total}	0.06	0.07	0.13	0.14 0.12
Ca	3.89	3.98	4.16	3.94 3.95

of the main exchange vectors, such as Mg-Tschermaks, $\text{Mg}_{-1}\text{Si}_{-1}\text{AlAl}$.

4.3.1 Amphiboles

Amphiboles range in composition mainly from near pure tremolite to magnesio-hornblende, with nearly 15% Al_2O_3 . Actinolite to hornblende compositions also occur where the Fe/Mg is higher (see below).

The amount of alumina is clearly a function of the bulk rock composition. Tremolites with low Al occur in Al-poor domains containing the classic tr + cc + qz assemblage. Amphiboles in phlogopite-, K-feldspar- and zoisite-rich domains are much more aluminous and commonly display the zoning described above. These amphiboles range from aluminous tremolites through to Mg-hornblendes, the dominant variation in chemistry being via Mg-Tschermaks exchange ($\text{Mg}_{-1}\text{Si}_{-1}\text{AlAl}$), as shown in Figure 4.6. The whole range in amphibole composition can occur in a single amphibole crystal (See Section 4.5).

Commonly, diffusely zoned amphibole cores ranging in composition from aluminous tremolite to tremolitic hornblende are overgrown sharply by Mg-hornblende (Figure 4.7). Furthermore, early amphibole is commonly more Al-poor than that formed later. Partly, this will be a function of the Al-contents of particular minerals in amphibole-forming reactions involving aluminous phases (see Section 4.4), but it may also reflect increased partitioning of Al into amphibole with increased pressure. As discussed in Chapter 2, the region from which the samples come in the Northeast Grampian Highlands experienced a pressure increase late in the metamorphic peak history, with replacement of andalusite by kyanite. However, examination of the whole data set for amphibole analyses ($n = 153$) does not reveal

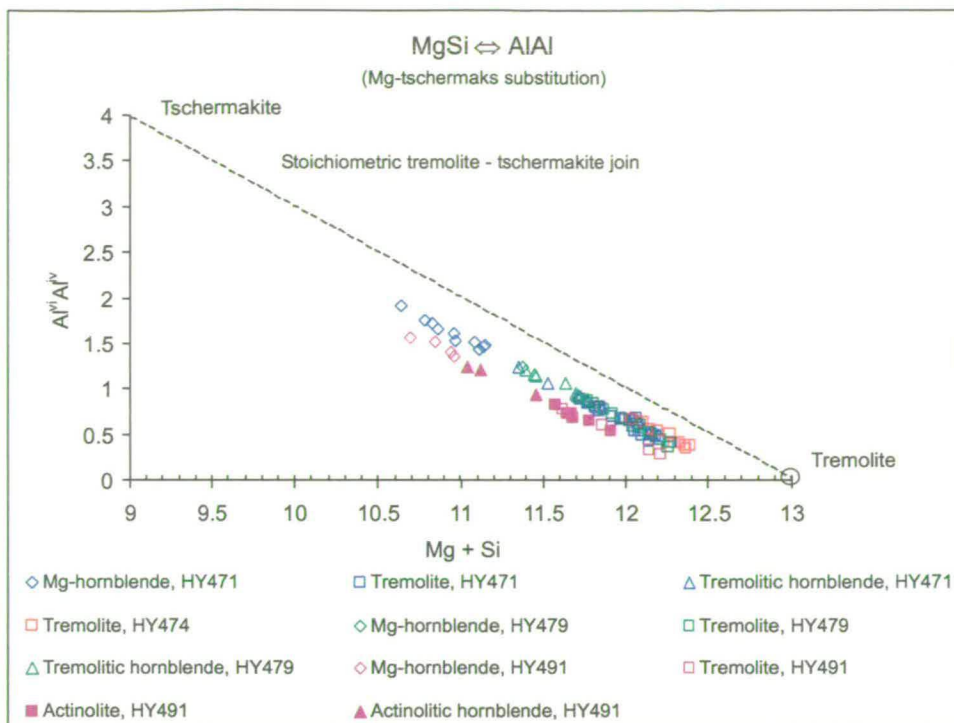


Figure 4.6 The Tschermaks substitution in amphiboles. The dominance of this substitution is indicated by the degree of parallelism with the stoichiometric tremolite - tschermakite join. The displacement is due to Fe substitution, hence the greater displacement of the actinolitic amphiboles.



Figure 4.7 Patchy zoning in amphibole in HY471, showing early rhombic amphibole largely but irregularly over grown by later Mg-hornblende. The matrix is phlogopite, interleaved with chlorite.

any sign of a miscibility gap between tremolite/actinolite and Mg-hornblende/hornblende (Figure 4.6) (cf. Graham, 1974), as reported by some (Jenkins, 1994; Smelik et al., 1991).

Fe-Mg ratios are controlled principally by the bulk-rock composition and $\text{Fe}_{\text{total}} / (\text{Fe}_{\text{total}} + \text{Mg})$ shows two parallel groups of data: amphiboles with higher Fe/Mg have actinolitic – hornblende compositions, occurring in rocks with biotite, rather than phlogopite (Figure 4.8). There is a clear parallel trend towards higher Fe/Mg in both groups. The Fe-Mg data indicate limited change in Fe-Mg partitioning during the development of amphibole. The increase in Fe/Mg in the two groups of amphibole is attributed to increasing Fe^{III} substitution as Al increases in the amphibole.

Although the amphiboles are in distinctly potassic rocks, the alkali substitution is dominated by Na, which shows linear variation with amphibole type from tremolite to Mg-hornblende in HY471 (Figure 4.9). In contrast, K contents increase slightly in tremolites, but then flatten and show no further increase for tremolitic hornblende and Mg-hornblende (Figure 4.9). The decoupling of the alkalis is clearly not a function of bulk composition and must relate to a changing distribution coefficient between minerals as the amphiboles become more aluminous.

Plotting data for the exchange vectors $\text{vac}_{-1}\text{Si}_{-1}\text{NaAl}$ (edenite) and $\text{Ca}_{-1}\text{Mg}_{-1}\text{NaAl}$ ('jadeite' for glaucophane) shows that the amphiboles lie nearly parallel to the respective joins between tremolite and edenite, and tremolite and glaucophane (Figures 4.10, 4.11); the data for all amphiboles lie slightly above the stoichiometric tremolite – edenite join and that the displacement from it increases slightly towards the more hornblendic amphiboles (Figure 4.10). However, the data

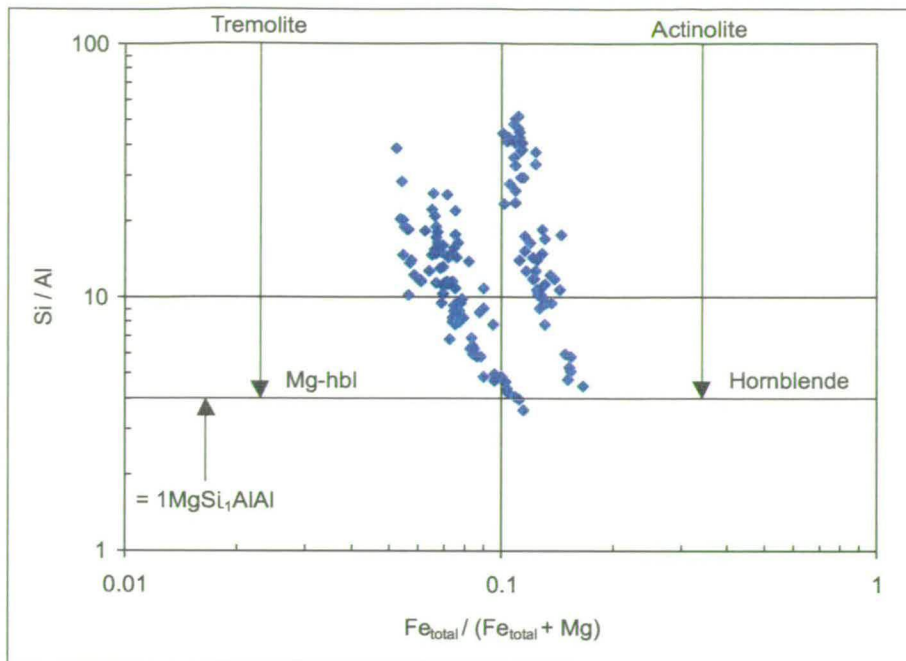


Figure 4.8 Fe/(Fe+Mg) vs Si/Al in all amphiboles (n = 153). Note the apparent lack of a miscibility gap in the Mg-rich amphiboles. The parallel grouping and Fe/Mg trends indicate dominantly bulk compositional control on Fe/Mg.

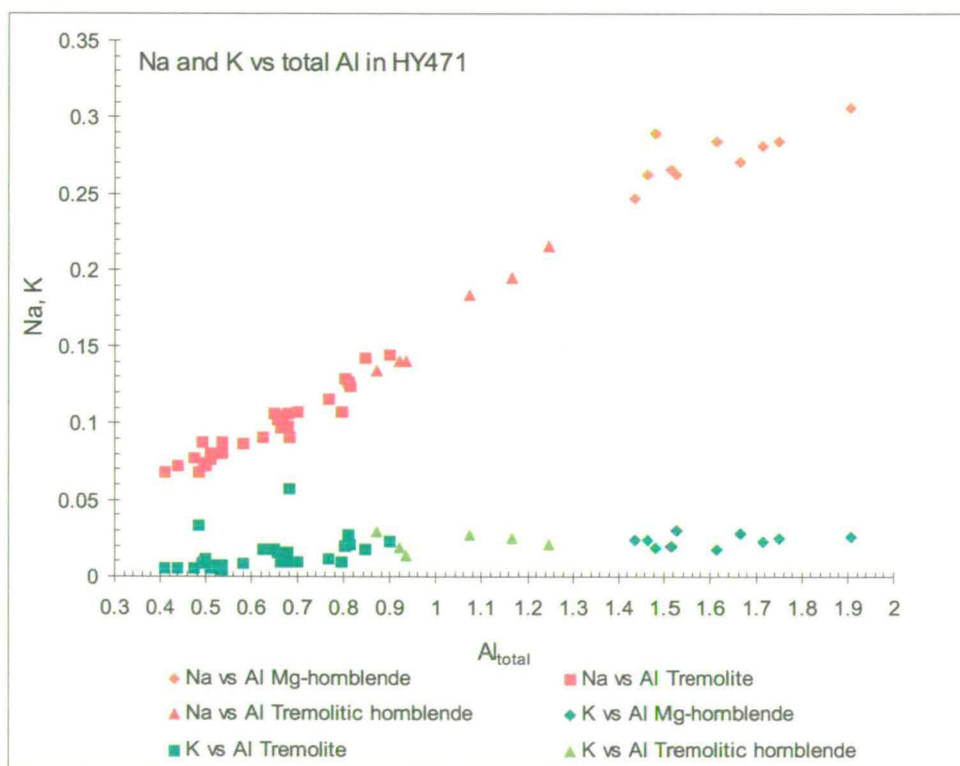


Figure 4.9 Variation in Na and K with total Al in HY471, showing the linear increase in Na through to Mg-hornblende, but increasing K only in tremolites.

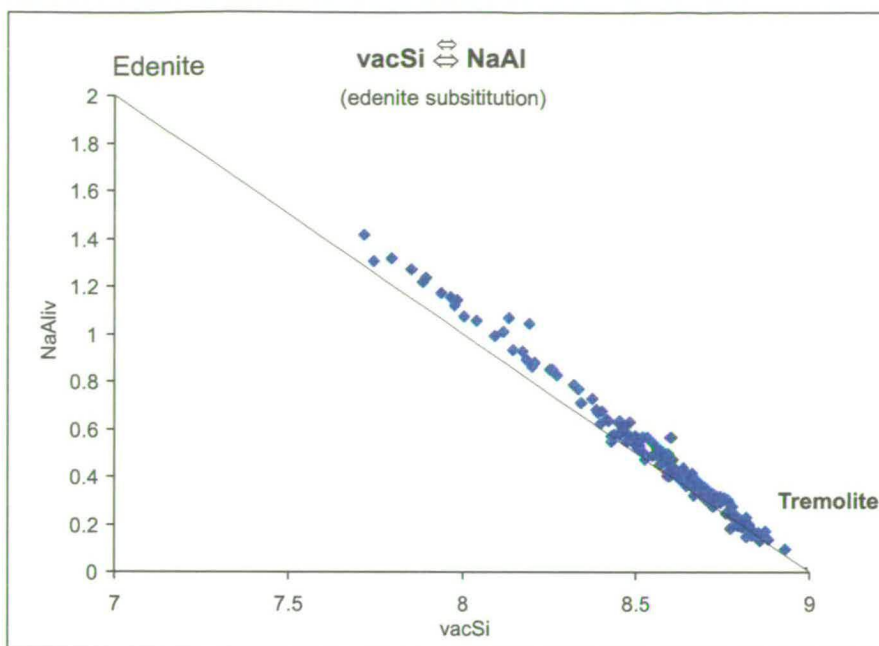


Figure 4.10 $\text{vac}_{-1}\text{Si}_{-1}\text{NaAl}$ substitution in amphiboles, showing it to be slightly in excess of the stoichiometric tremolite - edenite join.

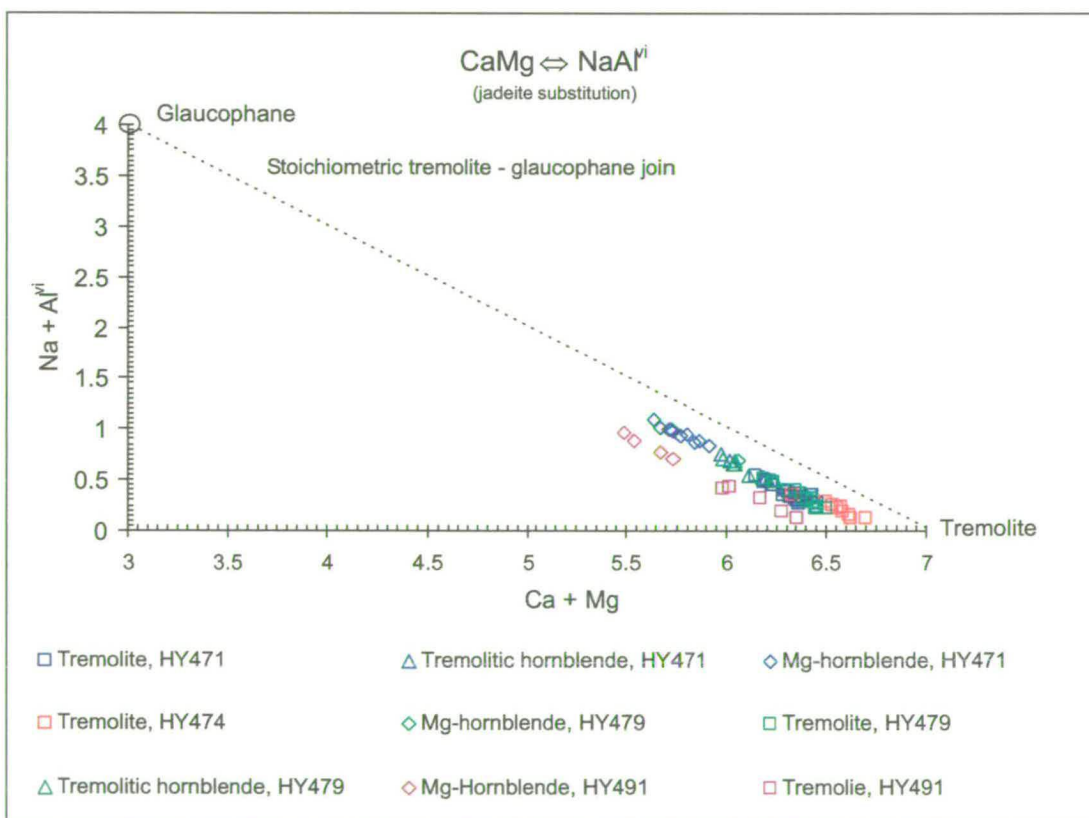


Figure 4.11 The $\text{Ca}_{-1}\text{Mg}_{-1}\text{NaAl}^{\text{vi}}$ exchange in amphiboles, showing the parallelism with the stoichiometric join between tremolite and glaucophane. This is considered to indicate the influence of increasing pressure on the amphibole chemistry. Note the consistent offset from the join shown by the more actinolitic amphiboles.

lie precisely parallel to the glaucophane join. The data suggest the influence of pressure on the amphiboles, increasing the Na content of the amphibole M4 site and octahedral Al in the M2 site (e.g. Jenkins, 1994).

Summary of amphibole chemistry

- Amphiboles range in composition from slightly aluminous tremolite through to Mg-hornblende and, in some more Fe-rich rocks, from actinolite to hornblende.
- There is no good evidence in the data for a solvus between Al-poor and Al-rich amphiboles, either in the tremolite – Mg-hornblende or actinolite – hornblende data.
- Fe increases slightly but consistently as amphiboles become more hornblendic, but the dominant control on Fe-Mg in the amphiboles is the bulk composition.
- The dominant variation in composition is described by Tschermak's exchange of Mg and Si for 2Al. In addition, there is edenitic and 'jadeitic' exchange as Na increases smoothly through the compositional range for the amphiboles.
- The increasing Na and Al contents, particularly Na on the M4 site, suggest the influence of increasing pressure.

4.3.2 Phyllosilicates

In contrast to the amphiboles, the phyllosilicates have very restricted ranges in composition, particularly with regard to variation in Al content. Phlogopite and chlorite are close in composition to their respective Mg end-members, K-phlogopite and clinochlore.

Phlogopite

The dominant deviation from end-member K-phlogopite is due to Mg Tschermaks substitution, leading to more Al-eastonitic compositions (Figure 4.12), but there is also some 'K-edenite' substitution ($\text{vac}_{-1}\text{Si}_{-1}\text{KAl}$), yielding compositions trending towards talc, and some Na – K exchange associated with this, such that the more 'talcose' phlogopites have more Na (Figure 4.13). Fluorine is present in readily detectable amounts and occupies up to about 8% of the volatile component of the mica.

Chlorite

The 'chlorite' lies compositionally between an $\text{Mg}_{11}\text{AlSi}_7$ composition and serpentine ($\text{Mg}_{12}\text{Si}_8$) (Figure 4.14). The analysed chlorite is that intergrown with phlogopite. The more serpentinitic compositions of the 'chlorite' matches the observed tendency in the phlogopite data towards more Mg-rich, Al-poor, talcose compositions. $\text{Fe}/(\text{Fe}+\text{Mg})$ ratios reach 0.2 in one or two more iron-rich samples, but values are generally much less than this.

White Mica

The white mica ranges in composition from near pure muscovite towards phengitic compositions (Figure 4.15). As with the other phyllosilicates, there is a clear tendency towards more siliceous and Mg-rich compositions with reduced Al. Na/K ratios are very low, so that the white micas lie very close to the muscovite – pyrophyllite join.

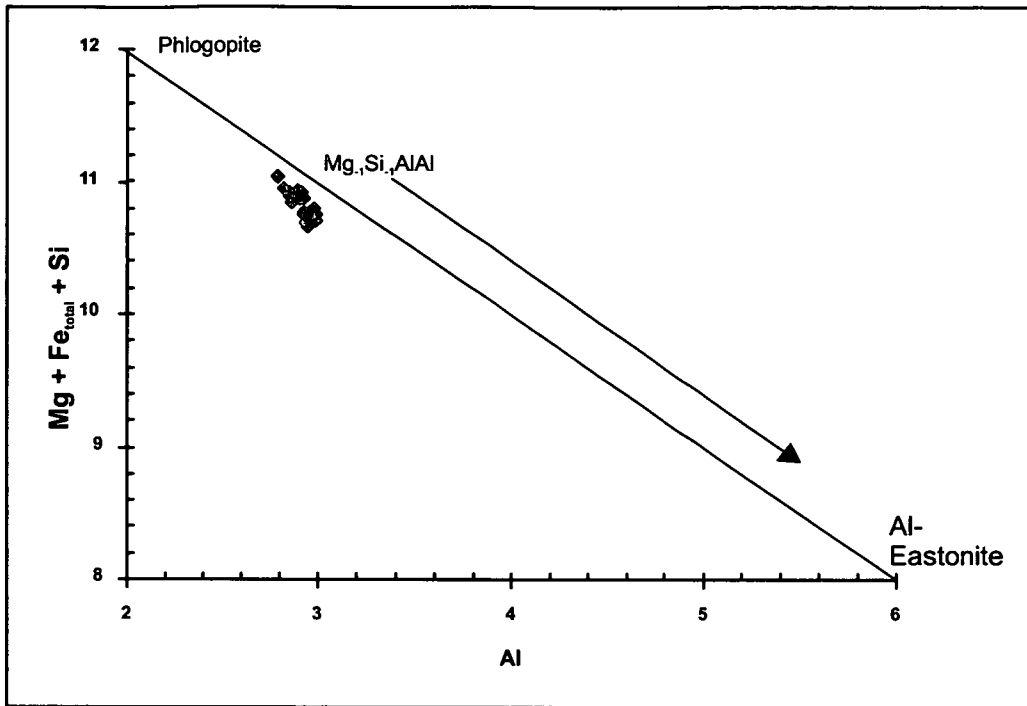


Figure 4.12 Range of Tschermaks exchange in phlogopites

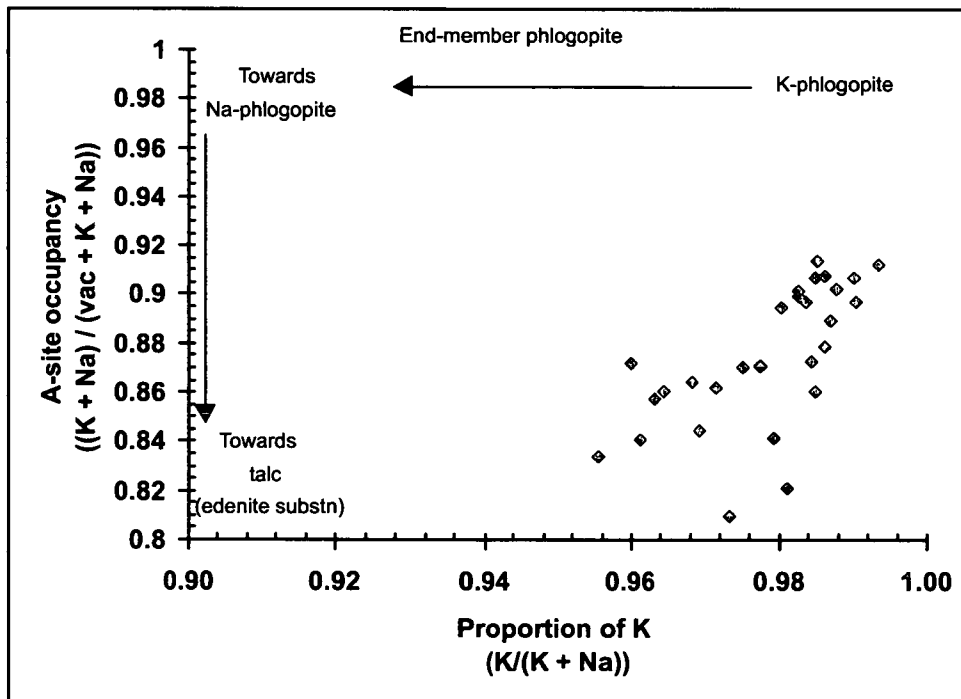


Figure 4.13 Variation in Na and K with the 'K- edenite' substitution in phlogopites

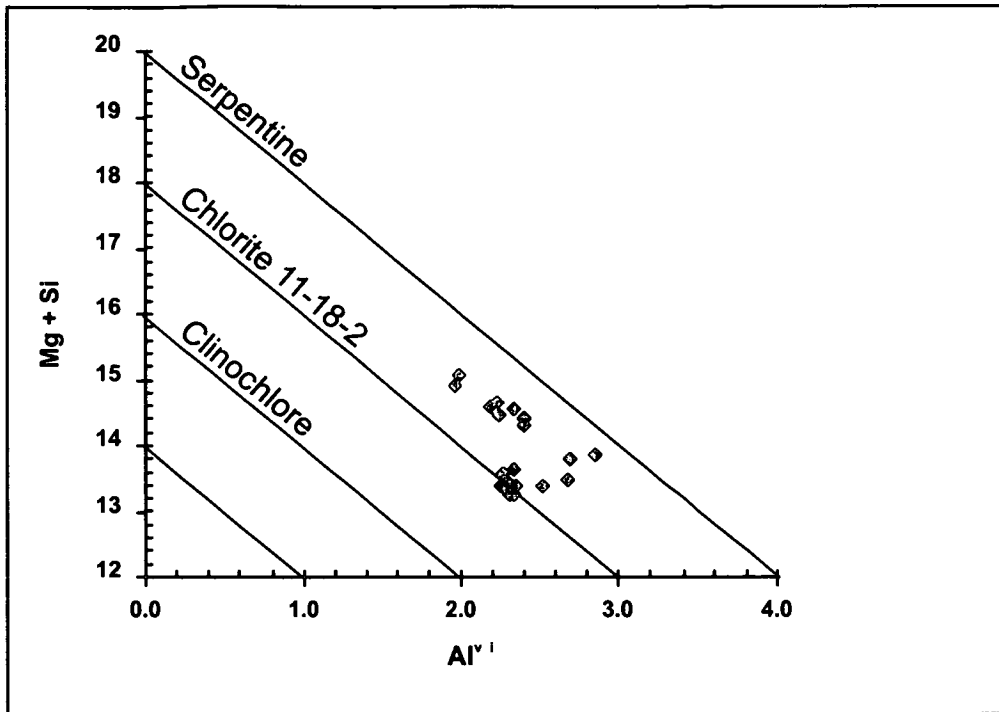


Figure 4.14 Composition of 'chlorite' intergrown with phlogopite. Note that the compositions are actually Al-poor and serpentinitic.

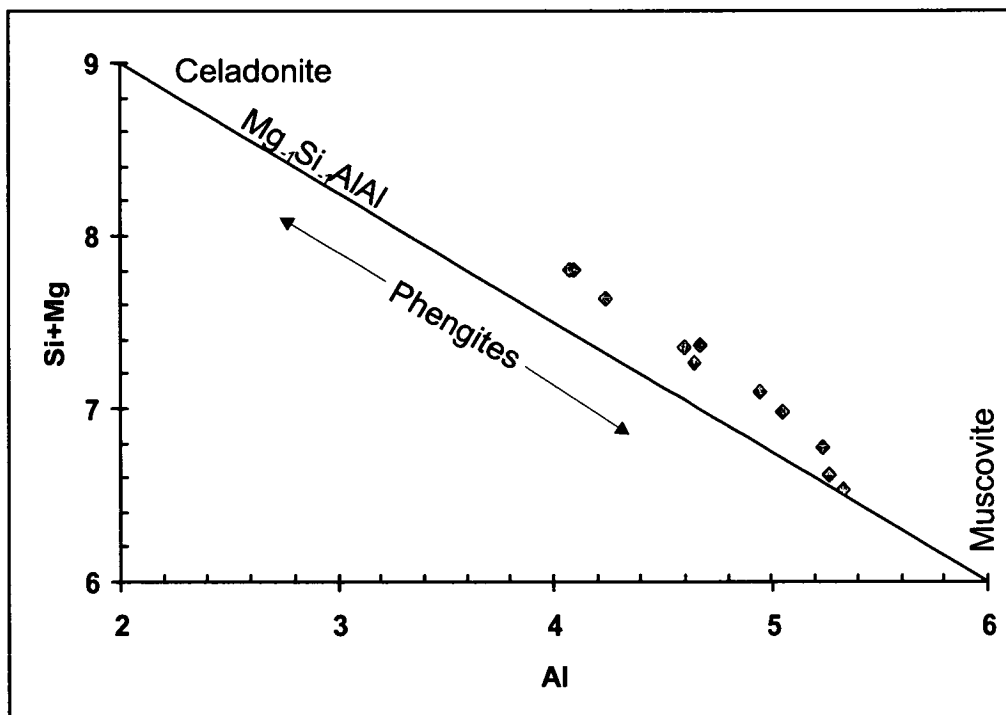


Figure 4.15 Tschermaks substitution in white micas from muscovite to celadonite.

Summary of phyllosilicate chemistry

- The phyllosilicates all show the same trends in composition and are relatively
- enriched in Mg and Si compared to Al.
- Tschermaks substitution is the dominant exchange vector, accompanied by minor 'edenite' exchange towards more siliceous compositions with decreased occupancy of the A site.
- Though minor compared to those observed in the amphibole, variations in phyllosilicate composition are much the same as those observed in the amphiboles. However, it appears that the amphibole is the sink for both Al, (leaving the phyllosilicates depleted in Al, but enriched in Mg and Si) and Na in these rocks.

4.3.3 Plagioclase

Along with Zoisite, plagioclase is an important phase in these rocks because the assemblages pl + cc and zo + cc are strongly a function of X_{CO_2} and mutually exclusive, except at the univariant reaction $\text{zo} = \text{pl} + \text{cc}$ (see Sections 4.4, 4.5). Its variable textural characteristics are described in more detail in Section 4.5 as these are only discernible using back scattered electron imaging. Chemically, the bulk of the plagioclase is andesine, ranging from about An_{39} to about An_{46} , although cores of some plagioclase crystals are labradorite (Table 4.2).

4.4 T- X_{CO_2} modelling of phase relations

As stated in the introduction, the primary objective of this work is to elucidate the

behaviour and composition of the fluid phase in these rocks. In calc-silicate rocks, this is effected most easily by construction and examination of T-X_{CO₂} sections for the phases observed in the rocks.

In Section 4.5, I describe a range of textures, some suggesting textural equilibrium and others indicating complex reaction textures suggesting local buffering of the fluid phase. In several places within thin sections, reaction textures occur on the margins of domains which otherwise look to be in equilibrium. In some domains, the preserved assemblages indicate very low variance, whilst others are almost monomineralic.

In order to provide a framework within which to discuss the textures, the phase relations amongst the assemblages observed in the detailed petrography and their implications for fluid buffering, I outline construction of T-X_{CO₂} sections.

4.4.1 Composition space and mineral solutions

In modelling the assemblages, I have aimed to keep the analysis tractable and have been more concerned about the *relative* fluid buffering constraints of the assemblages, rather than to generate a thermodynamically accurate T-X_{CO₂} net of reactions. Recent developments in modelling phase equilibria in complex calc-silicates indicate more sophisticated means of analysis are available, including equilibria with singular points and modelling mixed volatile equilibria in P-T space (Baker et al., 1991; Connolly and Trommsdorff, 1994). Some of the concepts presented in these studies are almost certainly of application to the assemblages discussed here, but are beyond the scope of this thesis.

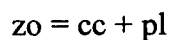
The composition space within which the assemblages have been modelled is

TiO₂ – K₂O – CaO – MgO – Al₂O₃ – SiO₂ – CO₂ – H₂O (TKCMASCH).

Application of this space ignores Fe and Na, but this is deemed justifiable because the minerals have low to very low Fe and Na contents, and because the bulk of the chemical variation is via Mg-Tschermaks exchange.

Modelling mineral solutions has also been considered. Although not documented here due to lack of space, I attempted to model the mineral solutions using methods outlined by James Connolly in his documentation for the PeRple-X program suite (see below). I was satisfied that mineral solutions have limited effect on the positions of key equilibria and make little difference to the conclusions about the nature of fluid buffering in these rocks. Errors on the loci of equilibria in T-X_{CO₂} sections arising from errors on thermodynamic parameters in the data set are likely to be more important than the effects of varying the composition of the mineral phases. Moreover, the phase relations in these rocks suggest that there are perhaps more fundamental problems related to scale of the equilibrium and compositional domains. Thus, I have used end-member compositions for all minerals except plagioclase to model the loci of TKCMASH univariant and invariant equilibria in T-X_{CO₂} space.

Plagioclase has been modelled as an activity-corrected composition of An₄₀, assuming ideal mixing. The reason for treating plagioclase thus is because the X_{CO₂} position of the important, quartz-absent, terminal zoisite breakdown reaction:



is shifted to much more X_{CO₂}-poor positions with decreasing An content. Because of the steep $-dX/dX_{\text{CO}_2}$ slope of this reaction in the critical region of upper greenschist to amphibolite facies conditions (see below), the position of the reaction is critical in

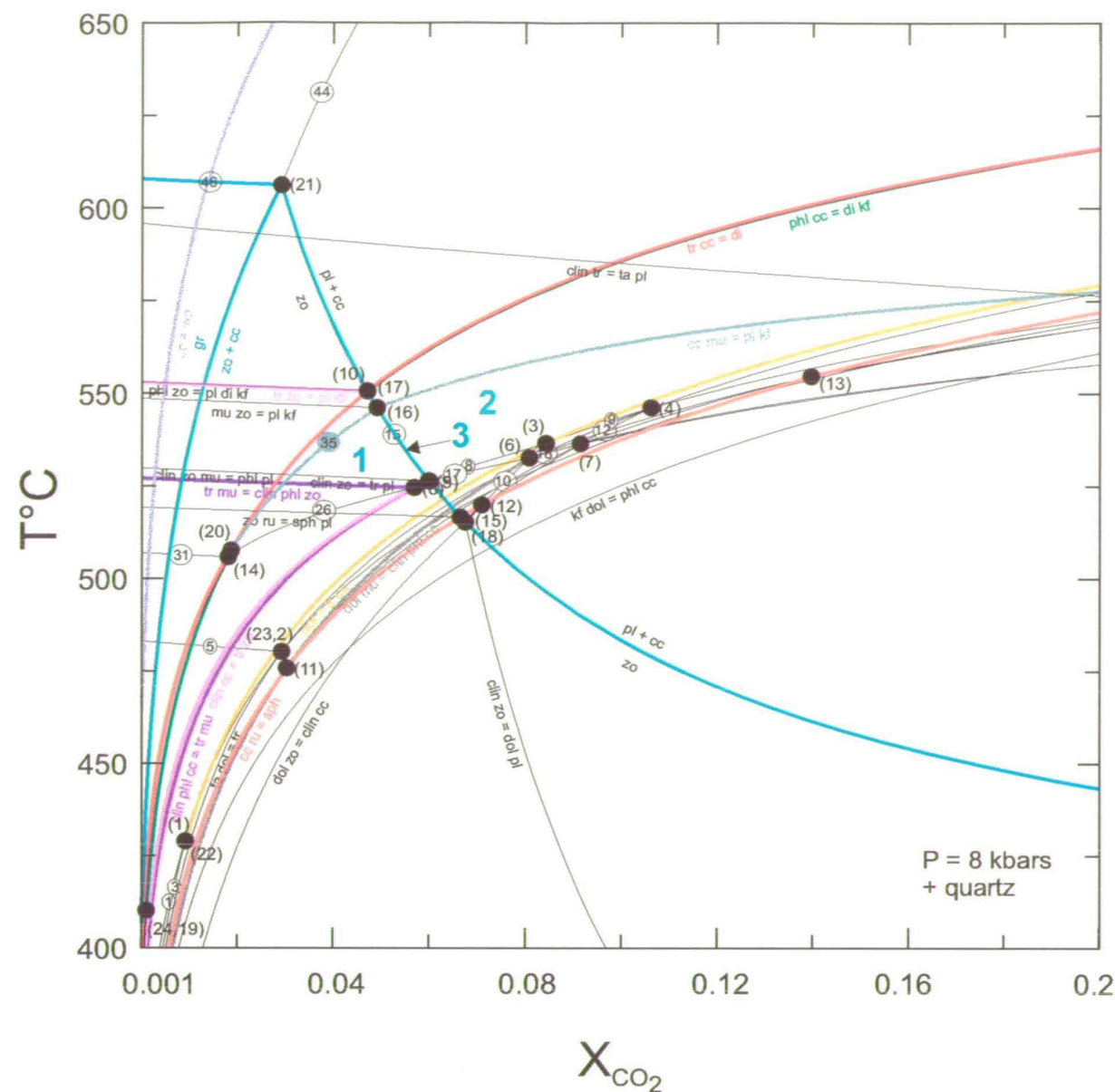
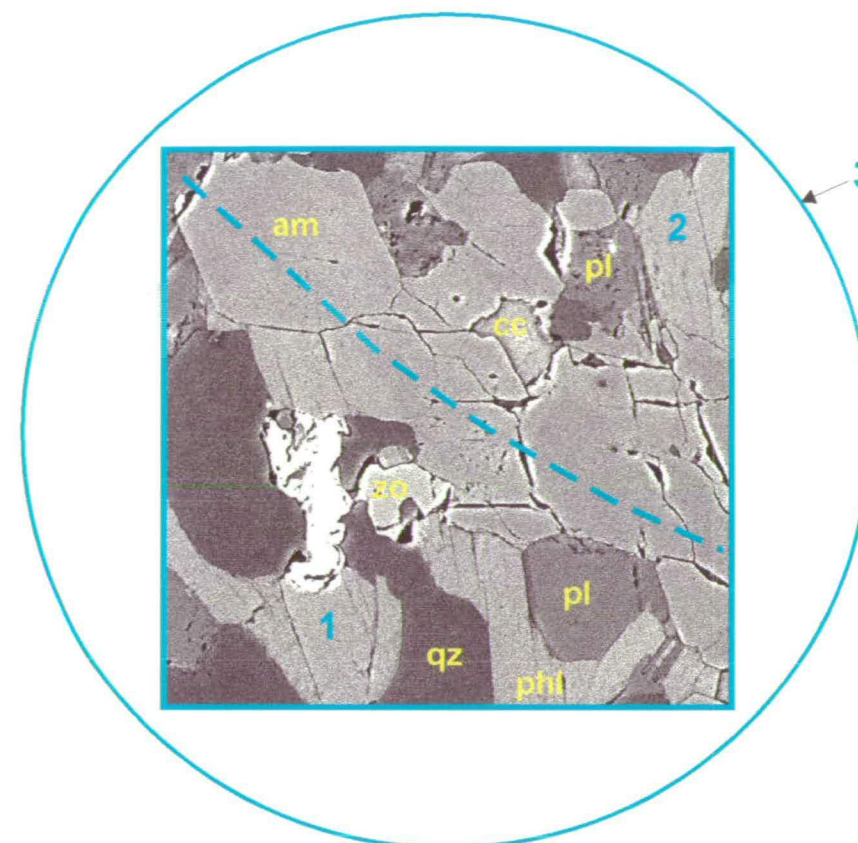


Figure 4.16 T- X_{CO_2} section for calc-silicate assemblages from the Pitlurg Calcareous Flag Formation, Lochaber Subgroup, Glen Rinnes, North East Grampian Highlands.

The composition space is TKCMASCH with quartz in excess. The full set of reactions is given in Table 4.3 with numbers of invariant points and univariant reactions. Phases are end-member compositions, except pl = An_{40} . Several unimportant sph-ru-silicate-carbonate reactions have been omitted for clarity.

(13): invariant point

① univariant reaction



Scales and domains of equilibrium

Various interpretations possible for the location of zo + pl + cc assemblage in Figure 4.25 in T- X_{CO_2} space. Is this an equilibrium zo + pl + cc assemblage or is the fluid buffered to different fluid compositions in domains 1 and 2?

Field of view ~ 1mm

See Section 4.6 for discussion.

- 1: zo + pl without cc: domain stable to left of zo = pl + cc
- 2: pl + cc without zo: domain stable to right of zo = pl + cc
- 3: equilibrium assemblage: zo + pl + cc

Numbers refer to location on the T- X_{CO_2} section in Figure 4.16 adjacent.

Reaction
(1-1) .833 ta 1.00 cc .667 q = .500 tr .333 H2O 1.00 CO2
(2-1) .500 ta 1.00 dol 2.00 q = .500 tr 2.00 CO2
(3-1) 1.00 dol 1.33 q .333 H2O = .333 ta 1.00 cc 1.00 CO2
(4-1) 1.00 dol 1.60 q .200 H2O = .200 tr .600 cc 1.40 CO2
(5-1) .833 ta 1.00 sph = .500 tr 1.00 ru .333 q .333 H2O
(6-1) 1.00 dol 1.00 ru 2.33 q .333 H2O = .333 ta 1.00 sph 2.00 CO2
(7-1) 1.67 dol 1.00 ru 3.67 q .333 H2O = .333 tr 1.00 sph 3.33 CO2
(8-1) 1.00 clin 3.00 cc 7.00 q = 1.00 tr 1.00 pl 3.00 H2O 3.00 CO2
(9-1) 1.00 clin 5.00 dol 15.0 q = 2.00 tr 1.00 pl 2.00 H2O 10.0 CO2
(10-1) 5.00 dol 1.00 pl 1.00 q 4.00 H2O = 1.00 clin 6.00 cc 4.00 CO2
(11-1) 1.00 clin 3.00 sph 4.00 q = 1.00 tr 3.00 ru 1.00 pl 3.00 H2O
(12-1) 5.00 dol 6.00 ru 1.00 pl 7.00 q 4.00 H2O = 1.00 clin 6.00 sph 10.0 CO2
(13-1) 1.50 clin 5.00 cc 10.5 q = 1.50 tr 1.00 zo 4.00 H2O 5.00 CO2
(14-1) .167 clin 1.00 zo 1.17 q = .167 tr 1.67 pl 1.00 H2O
(15-1) 1.00 zo .500 CO2 = .500 cc 1.50 pl .500 H2O
(16-1) 8.00 dol 1.00 mu 3.00 q 4.00 H2O = 1.00 clin 1.00 phl 8.00 cc 8.00 CO2
(17-1) .600 clin 1.60 cc 1.00 mu 1.40 q = 1.00 phl 1.60 pl 2.40 H2O 1.60 CO2
(18-1) .333 clin 1.33 dol 1.00 mu 1.67 q = 1.00 phl 1.33 pl 1.33 H2O 2.67 CO2
(19-1) 3.00 dol 1.00 mu 2.00 q = 1.00 phl 2.00 cc 1.00 pl 4.00 CO2
(20-1) 8.00 dol 8.00 ru 1.00 mu 11.0 q 4.00 H2O = 1.00 clin 1.00 phl 8.00 sph
(21-1) .600 clin 1.60 sph 1.00 mu = 1.00 phl 1.60 ru 1.60 pl .200 q 2.40 H2O
(22-1) 3.00 dol 2.00 ru 1.00 mu 4.00 q .222E-15 H2O = 1.00 phl 2.00 sph 1.00
(23-1) 1.00 clin 1.00 phl 3.20 cc 9.80 q = 1.60 tr 1.00 mu 2.40 H2O 3.20 CO2
(24-1) .640 tr 1.00 mu = .400E-01 clin 1.00 phl .640 zo 3.08 q .160 H2O
(25-1) .600 clin 2.13 cc 1.00 mu 1.40 q = 1.00 phl 1.07 zo 1.87 H2O 2.13 CO2
(26-1) .600 tr .133 cc 1.00 mu = 1.00 phl .667 zo 2.80 q .267 H2O .133 CO2
(27-1) .600 clin 3.20 zo 1.00 mu 1.40 q = 1.00 phl 6.40 pl 4.00 H2O
(28-1) .200 tr .600 cc .400 q = 1.00 di .200 H2O .600 CO2
(29-1) .200 tr 1.20 zo .400 q = 1.80 pl 1.00 di .800 H2O
(30-1) 1.00 cc 1.00 ru 1.00 q = 1.00 sph 1.00 CO2
(31-1) 2.50 tr 4.50 mu 1.00 di = 4.50 phl 3.00 zo 13.0 q 1.00 H2O
(32-1) .333 phl .556 cc .222 zo 1.33 q = .333 mu 1.00 di .111 H2O .556 CO2
(33-1) 2.00 zo 1.00 ru 1.00 q = 1.00 sph 3.00 pl 1.00 H2O
(34-1) 1.00 cc 1.00 mu 2.00 q = 1.00 pl 1.00 kf 1.00 H2O 1.00 CO2
(35-1) 1.33 cc 1.00 mu 2.00 q = .667 zo 1.00 kf .667 H2O 1.33 CO2
(36-1) 1.00 mu 2.00 zo 2.00 q = 4.00 pl 1.00 kf 2.00 H2O
(37-1) 1.00 phl 3.00 cc 6.00 q = 3.00 di 1.00 kf 1.00 H2O 3.00 CO2
(38-1) 1.00 phl 6.00 zo 6.00 q = 9.00 pl 3.00 di 1.00 kf 4.00 H2O
(39-1) 7.50 dol 1.00 zo 1.50 q 5.50 H2O = 1.50 clin 9.50 cc 5.50 CO2
(40-1) .833E-01 clin 1.00 zo .833 CO2 = .417 dol 1.58 pl .833E-01 q .833 H2O
(41-1) 1.00 phl 1.20 cc 4.80 q = .600 tr 1.00 kf .400 H2O 1.20 CO2
(42-1) 1.00 tr 1.00 kf = 1.00 phl 2.00 di 4.00 q
(43-1) 1.80 mu 2.40 di = .800 phl 1.20 zo 1.00 kf 1.20 q .400 H2O
(44-1) 2.00 cc 1.00 pl 1.00 q = 1.00 gr 2.00 CO2
(45-1) 1.67 cc .667 zo 1.00 q = 1.00 gr .333 H2O 1.67 CO2
(46-1) 4.00 zo 1.00 q = 5.00 pl 1.00 gr 2.00 H2O
(47-1) .333 kf 1.00 dol .333 H2O = .333 phl 1.00 cc 1.00 CO2
(48-1) 1.00 clin .500 tr 5.00 q = 2.50 ta 1.00 pl 2.00 H2O
(49-1) 1.00 mu 1.00 sph 1.00 q = 1.00 pl 1.00 ru 1.00 kf 1.00 H2O
(50-1) 1.00 cc 1.00 q = 1.00 wo 1.00 CO2

Table 4.3 TKCMASCH mineral reactions for assemblages in Pitlurg calc-silicate rocks. Reactions in bold are discussed further in the text

discussion of fluid phase composition in this study.

The PeRple-X software suite (Connolly, 1990) was used to generate the T- X_{CO_2} sections for the following phases in the TKCMASCH composition space:

dolomite, calcite, quartz, diopside, tremolite, phlogopite, muscovite, clinocllore, talc, K-feldspar, An₄₀ plagioclase, zoisite, grossular, rutile and sphene, with quartz as the saturated phase. Dolomite, diopside, talc, grossular and rutile and *primary* chlinochlore are conspicuous by their absence, but must be included to generate and place X_{CO_2} limits on the observed assemblages. The T- X_{CO_2} sections were plotted from the PeRple-X graphics file output using VertexView (Castelli et al., 1997).

The T- X_{CO_2} net was calculated for temperatures in the range 400 – 650°C over a range of X_{CO_2} from 0.001 – 0.2 at nominal P = 8 kbars, encompassing the range in temperature and peak pressure calculated from pelites in the area by Beddoe-Stephens (1990) and Baker (1985).

The thermodynamic data set used in the calculations is that of Holland and Powell (Holland and Powell, 1990), as modified in 1994. The equation of state for the fluid phase is the CORK equation of Holland and Powell (1991), because this is internally consistent with their thermodynamic data set. The resulting T- X_{CO_2} section is shown complete in Figure 4.16. The list of univariant TKCMASCH reactions is given in Table 4.3 - the numbers attached to the reactions in the text below refer to the reaction reference numbers in the first column of this table.

4.4.2 Estimating peak metamorphic temperatures

In attempting to determine independently the peak temperatures under which these

Thermometer	Formulation: (T =)	Range (T°C)	Compositional constraints
Edenite - tremolite	$-76.95 + 0.79P + Y_{ab} + 39.4X_{Na}^A + 22.4X_K^A + (41.5-2.89P) \cdot X_{Al}^{Mz}$	400 - 900	<u>Amphibole</u>
	$-0.0650 - R \cdot \ln(B)$		Na^A Al^{vi} Si > 0.02 < 1.8 6.0 - 7.7
	$B = 27 \cdot X_{\square}^A \cdot X_{Si}^{T1} \cdot X_{an}^{plage} / 256 \cdot X_{Na}^A \cdot X_{Al}^{Ti}$ \square = vacancy on A site Where $X_{ab} > 0.5$: $Y_{ab} = 0$ otherwise $Y_{ab} = 12.0(1 - X_{ab})^2 - 3.0$ kJ		<u>Plagioclase (mole fraction)</u> X_{an}^{plag} < 0.9
Edenite - richterite	$-78.44 + Y_{ab-an} - 33.6X_{Na}^{M4} - (66.8 - 2.92P) \cdot X_{Al}^{Mz} + 78.5X_{Al}^{I1} + 9.4X_{Na}^A$	500 - 900	<u>Amphibole</u>
	$-0.0721 - R \cdot \ln(B)$		X_{Na}^{M4} Al^{vi} Si > 0.03 < 1.8 6.0 - 7.7
	$B = 27 \cdot X_{Na}^A \cdot X_{Si}^{T1} \cdot X_{An}^{plage} / 64 \cdot X_{Ca}^{M4} \cdot X_{Al}^{T1} \cdot X_{ab}^{Plage}$ Where $X_{ab} > 0.5$: $Y_{ab-an} = 3.0$ kJ otherwise $Y_{ab-an} = 12.0(2X_{ab} - 1) + 3.0$ kJ		<u>Plagioclase (mole fraction)</u> X_{an}^{plag} $0.1 < X_{an} < 0.9$
R = Gas constant: 0.0083144 kJ K ⁻¹ mol ⁻¹ P = Pressure in kilobars			

Table 4.4 Formulation of the amphibole-plagioclase geothermometers developed by Holland and Blundy (1994). See text for discussion.

Table 4.5 Example calculation for temperature from the amphibole - plagioclase geothermometer

Holland and Blundy Edenite-Tremolite geothermometer

Data: HY474 Mg-hbl (Spot A48) and plagioclase (Spot A51)

Amphibole analysis

Element	Fe ²⁺ = total iron	Element	Adjusted for Fe ³⁺
Si	7.194	Si	7.177
Al	1.436	Al	1.433
Ti	0.027	Ti	0.027
Cr	0.000	Cr	0.000
Fe ²⁺	0.414	Fe ³⁺	0.106
Mn	0.005	Fe ²⁺	0.307
Mg	3.915	Mn	0.005
Ca	1.927	Mg	3.906
Ba	0.000	Ca	1.923
Na	0.248	Ba	0.000
K	0.025	Na	0.247
Total	15.160	K	0.025
		Total	15.156
		Fe ²⁺ /Mg	0.0785

Fe²⁺/Fe³⁺ adjustment factors

f ₁	1.05541	f ₆	0.92700
f ₂	1.11204	f ₇	0.99108
f ₃	1.00759	f ₈	0.99537
f ₄	1.03788	f ₉	0.65865
f ₅	1.00000	f ₁₀	0.99100
Smallest f	1.00000	Largest f	0.99537
f _{average}	0.99769		

Plagioclase analysis

Element	
Si	2.620
Al	1.350
Ti	0.000
Cr	0.000
Fe ²⁺	0.005
Mn	0.000
Mg	0.000
Ca	0.410
Ba	0.000
Na	0.600
K	0.000
Total	5.000

Mole fractions

Albite	0.6
Anorthite	0.41
Sum	1.01

Element mole fractions on sites

(after Powell, 1978)

Site	Element	Mole frac.
T sites		
	T ₁	X _{Si} 0.7943
	T ₂	X _{Al} 0.2057
M sites		
	M _{1,3}	X _{Si} 1.0000
M ₂		
M ₄		
A site		

End-member mole fractions

End-member	mol. fraction	Norm. Constant
Tremolite	0.080128706	0
Edenite	0.041520515	9.48
Cummingtonite	0.086715682	0
Tschermakite	0.023559621	16
Pargasite	0.037998326	64

Cummingtonite substitution

cm 0

Site terms for thermometers

(after Holland and Blundy, 1994)

X _{Si} ^{T1}	0.794336806
X _{Al} ^{T1}	0.205663194
X _{M2}	0.305011574
X _K ^A	0.02494213
X _{Vacancy} ^A	0.805092593
X _{Na} ^A	0.169965278
X _{Na} ^{M4}	0.038730324
X _{Ca} ^{M4}	0.961269676

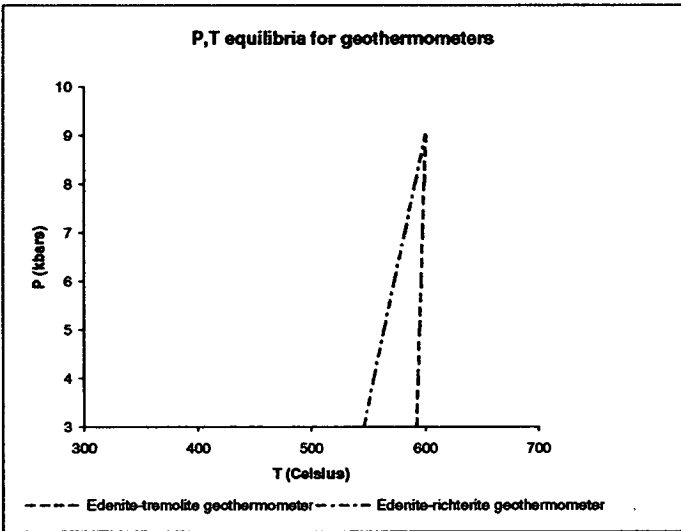
Model temperatures

Edenite-Tremolite geothermometer

T (K)	T° C	P (kbars)
865	592	3
867	594	4
868	595	5
870	597	6
871	598	7
872	599	8
874	601	9

Edenite-Richterite geothermometer

T (K)	T° C	P (kbars)
819	546	3
828	555	4
837	564	5
846	573	6
855	582	7
864	591	8
873	600	9



Geothermometers

Gas constant, R: 0.008314 kJ K⁻¹

Terms of Edenite-Tremolite equation

Numerator (-76.95 + 0.79 P + Y_{ab} + 39.4 X_{Na}^A + 22.4 X_K^A + (41.5 - 2.89 P) X_{Al}^{M2})

Denominator (-0.0650 - R ln(27 X_{Vacancy}^A X_{Si}^{T1} X_{Al}^{T1} X_{Na}^{M4} / 256 X_{Na}^A X_{Al}^{T1}))

Terms of Edenite-Richterite equation

Numerator (-78.44 + Y_{ab-an} - 33.6 X_{Na}^{M4} - (66.8 - 2.92 P) X_{Al}^{M2} + 78.5 X_{Al}^{T1} + 9.4 X_{Na}^A)

Denominator (-0.0721 - R ln(27 X_{Na}^A X_{Si}^{T1} X_{Al}^{T1} X_{Na}^{M4} / 64 X_{Ca}^{M4} X_{Al}^{T1} X_{ab}^{Plage}))

Calculation details

Edenite-tremolite geothermometer

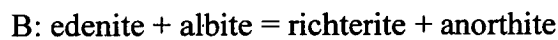
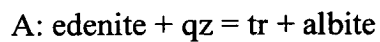
Numerator							Denominator				
Constant	0.79P	Y _{ab}	39.4X _{Na} ^A	22.4X _K ^A	(41.5-2.89P)*X _{Al} ^{M2}	Num. Result	Constant	R	Numerator	Denominator	ln(Num/Den)
-76.95	2.3700	0	6.6966	0.5587	10.0135	-57.3111	-0.0650	0.00831	10.3601	8.9486	0.1465
-76.95	3.1600	0	6.6966	0.5587	9.1320	-57.4026	-0.0650	0.00831	10.3601	8.9486	0.1465
-76.95	3.9500	0	6.6966	0.5587	8.2506	-57.4941	-0.0650	0.00831	10.3601	8.9486	0.1465
-76.95	4.7400	0	6.6966	0.5587	7.3691	-57.5856	-0.0650	0.00831	10.3601	8.9486	0.1465
-76.95	5.5300	0	6.6966	0.5587	6.4876	-57.6771	-0.0650	0.00831	10.3601	8.9486	0.1465
-76.95	6.3200	0	6.6966	0.5587	5.6061	-57.7686	-0.0650	0.00831	10.3601	8.9486	0.1465
-76.95	7.1100	0	6.6966	0.5587	4.7246	-57.8600	-0.0650	0.00831	10.3601	8.9486	0.1465

Edenite-richterite geothermometer

Numerator							Denominator				
Constant	Y _{ab-an}	(-33.6X _{Na} ^{M4})	(-66.8-2.92P)*X _{Al} ^{M2}	78.5X _{Al} ^{T1}	9.4X _{Na} ^A	Num. Result	Constant	R	Numerator	Denominator	ln(Num/Den)
78.44	3	-1.301338889	-17.70287176	16.14456076	1.597673611	80.17802373	0.0721	0.00831	0.3406	7.5916	-3.1042
78.44	3	-1.301338889	-16.81223796	16.14456076	1.597673611	81.06865752	0.0721	0.00831	0.3406	7.5916	-3.1042
78.44	3	-1.301338889	-15.92160417	16.14456076	1.597673611	81.95929132	0.0721	0.00831	0.3406	7.5916	-3.1042
78.44	3	-1.301338889	-15.03097037	16.14456076	1.597673611	82.84992512	0.0721	0.00831	0.3406	7.5916	-3.1042
78.44	3	-1.301338889	-14.14033657	16.14456076	1.597673611	83.74055891	0.0721	0.00831	0.3406	7.5916	-3.1042
78.44	3	-1.301338889	-13.24970278	16.14456076	1.597673611	84.63119271	0.0721	0.00831	0.3406	7.5916	-3.1042
78.44	3	-1.301338889	-12.35906898	16.14456076	1.597673611	85.5218265	0.0721	0.00831	0.3406	7.5916	-3.1042

rocks were metamorphosed, I have applied the amphibole – plagioclase geothermometer (Blundy and Holland, 1990; Holland and Blundy, 1994) to several amphibole – plagioclase pairs in several samples. The form of the geothermometers and an example calculation are set out in Tables 4.4 and 4.5. The results are set out in Table 4.6.

Holland and Blundy (1994), revised an earlier version of their amphibole – plagioclase geothermometer (Blundy and Holland, 1990) to provide two geothermometers based on the following reactions for exchange between amphibole and plagioclase:



The latter is of value in that it can be used for quartz-absent assemblages. They give compositional limits for the amphiboles which can be used with these thermometers (Table 4.4). Also, geothermometer B should give results less than A if the amphibole and plagioclase are in equilibrium, if the Fe^{III} has been ‘correctly’ estimated and if the amphibole is within the compositional range of the calibrant data set (Holland and Blundy, 1994, page 441). Examination of Table 4.6 shows that in all but one example, temperatures from B are higher than those of A and that some temperature estimates are spurious. Only one amphibole-plagioclase pair (HY471, column 3, Table 4.6) gave results in accord with the suggested relative temperature estimates to be expected from A and B (Holland and Blundy, 1994), yielding temperatures of $\sim 600^\circ\text{C}$ from geothermometer A. Whilst this is comparable with the temperature estimates from pelite geothermometry of Beddoe-Stephens (1990), it is much higher than that indicated by the phase relations in the T-X_{CO_2} section (Figure 4.16),

	HY471			HY474		HY491	
A: Edenite-tremolite geothermometer							
P (kbars)	1	2	3				
3	345	581	597	525	537	555	590
4	342	580	598	518	531	557	590
5	338	578	599	512	525	560	589
6	334	577	600	505	519	562	589
7	330	575	601	498	513	565	589
8	326	574	602	492	507	567	589
9	322	572	603	485	501	570	589
B: Edenite-richterite geothermometer							
3	622	579	552	583	587	565	575
4	626	586	561	585	590	576	583
5	630	593	570	587	593	587	591
6	634	601	579	589	596	597	599
7	638	608	588	591	599	608	607
8	642	615	597	593	602	619	615
9	646	623	605	595	604	630	624

1: Tremolite; spot A45

TremoliteTremoliteMg-hblMg-hbl

2: Tremolitic hornblende; spot A49

3: Magnesio-hornblende; spot A48

Plagioclase is Andesine (Ab₆₀An₄₀)

Shaded boxes: temperatures in range of pressure estimates calculated for Glen Rinnes (Beddoe-Stephens, 1990)

Table 4.6 Results of amphibole - plagioclase geothermometry in Pitlurg calc-silicate rocks.

particularly indicated by the restriction of phlogopite + zoisite bearing assemblages to $\sim 550^{\circ}\text{C}$. One possibility is that the pressure estimate is too low, as mentioned with regard to comparison with the pelite geothermobarometry. However, it would require pressures of ~ 10 kbars to bring the equilibria into the 600°C temperature range. Clearly, this geothermometer scheme is difficult to apply with any confidence to these rocks. Assuming the behaviour of the geothermometers to be a reasonable estimate of the degree of equilibration between amphibole and plagioclase, the results suggest that these two phases are not well-equilibrated. Given the complex zoning of the amphiboles, this is perhaps not surprising, but even very closely adjacent analyses gave inconsistent results. It is significant in this regard that work on the thermochemistry of tremolite-edenite amphiboles involved in reaction A, above, suggests that amphibole – plagioclase disequilibrium may be common (Graham and Navrotsky, 1986). Reaction A is characterised by a small ΔG . Graham and Navrotsky (*op. cit.*) suggest that, once formed, possibly by reaction paths other than A, probably large activation energies of edenitic hornblendes arising from coupled substitutions would inhibit equilibration with plagioclase.

Effect of pressure on $T\text{-}X_{\text{CO}_2}$ topology

The $T\text{-}X_{\text{CO}_2}$ section presented in Figure 4.16 has been used to place stability limits on the assemblages as they appear now. However, it cannot be used to elucidate the evolution of the assemblages in the rocks because P is fixed for all T . In order to demonstrate the effect of pressure on the $T\text{-}X_{\text{CO}_2}$ topology, I have used *PerpleX* to calculate 6 $T\text{-}X_{\text{CO}_2}$ sections for pressures from 4 to 9 kbars. The results are shown in

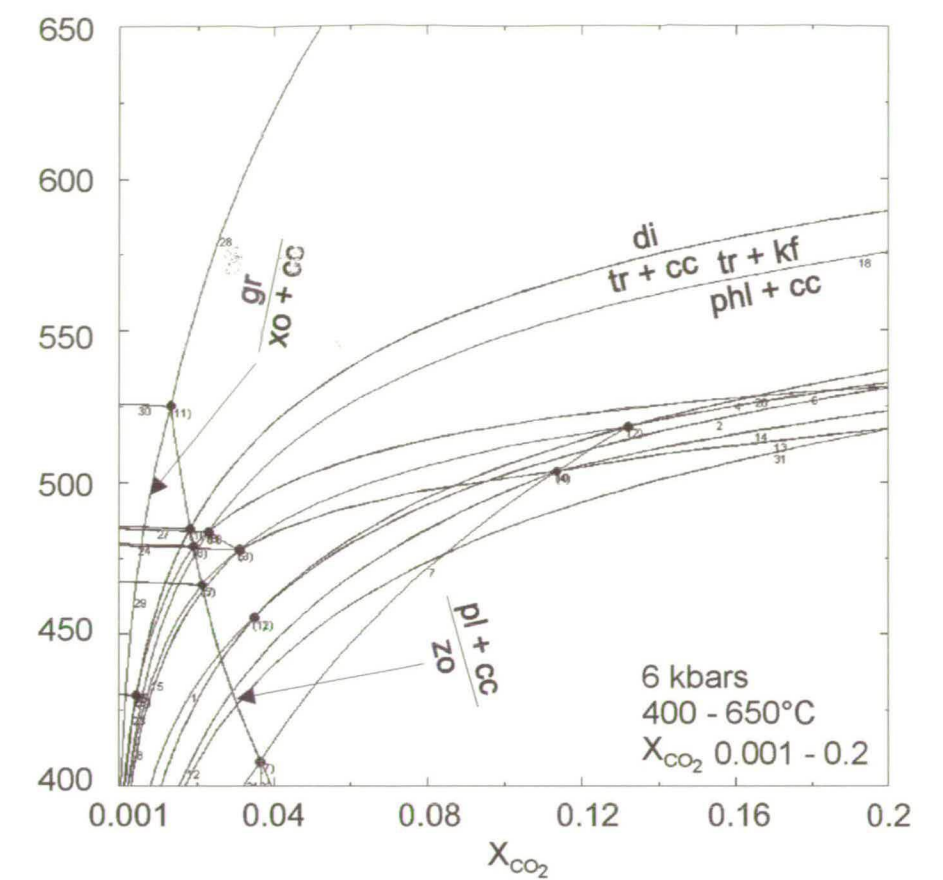
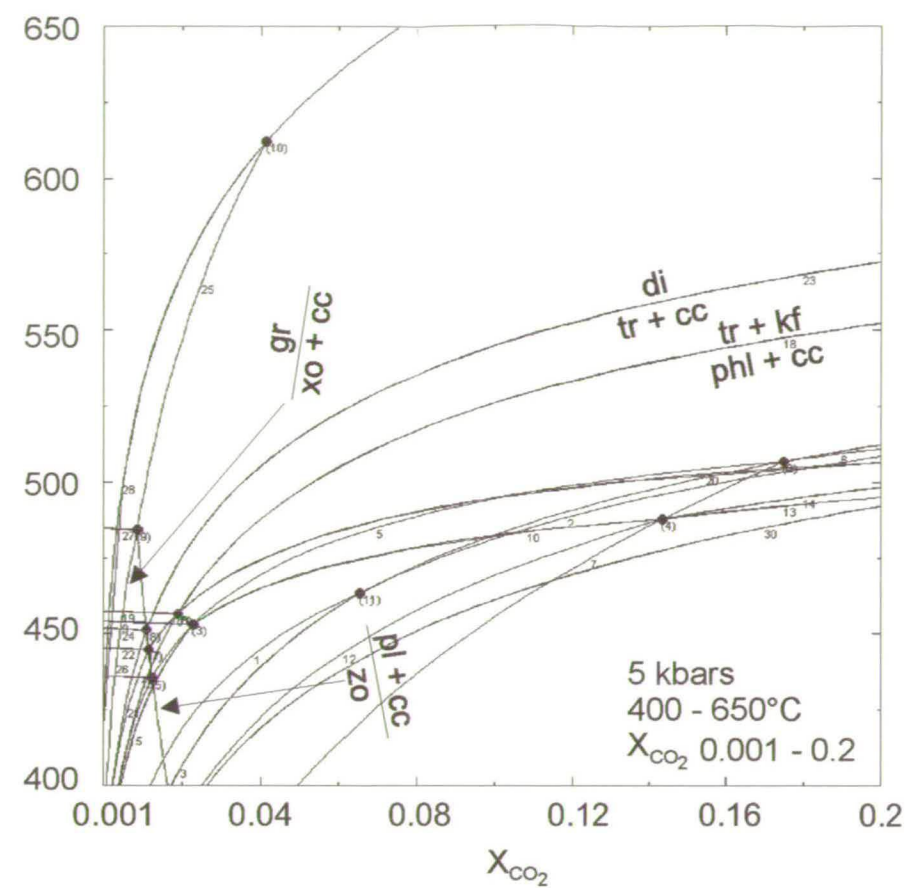
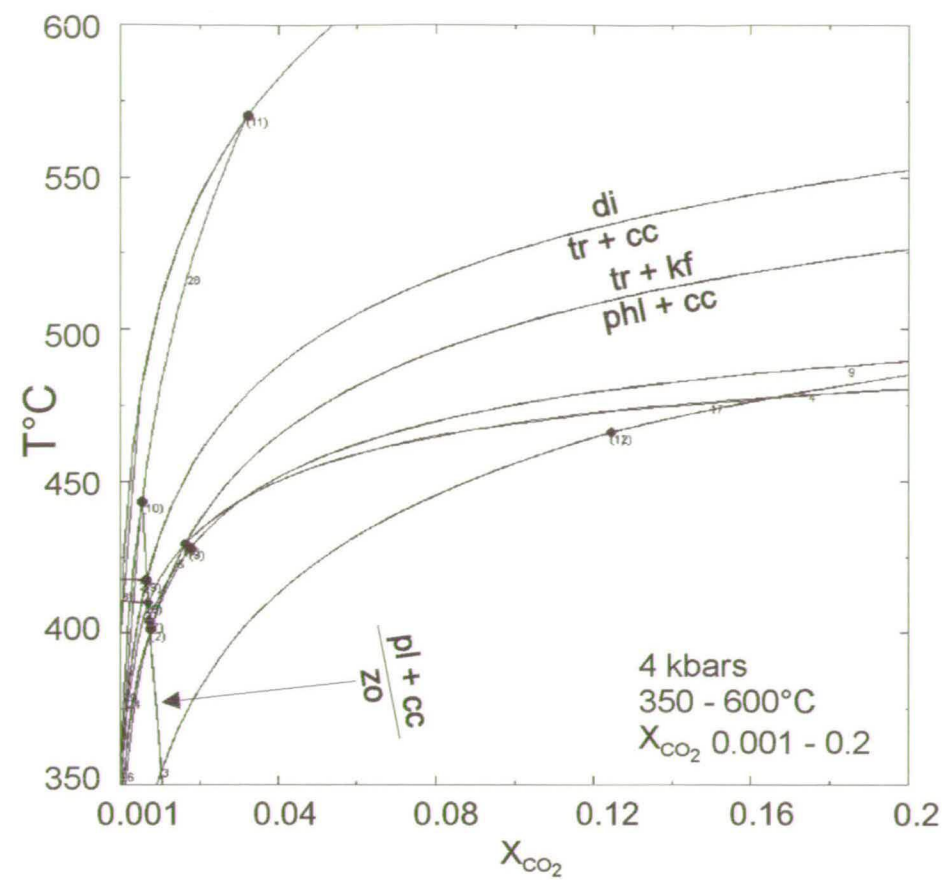


Figure 4.17 The effect of changing pressure on the topology of KCMASCH reactions in T - X_{CO_2} space, highlighting selected important equilibria. Note the appearance and increasing thermal and X_{CO_2} stability of the phlogopite + zoisite stability field (shaded) at pressures above 7 kbars and the change in the products of the $\text{phl} + \text{cc}$ reaction from $\text{tr} + \text{kf}$ to $\text{di} + \text{kf}$ above 8 kbars.

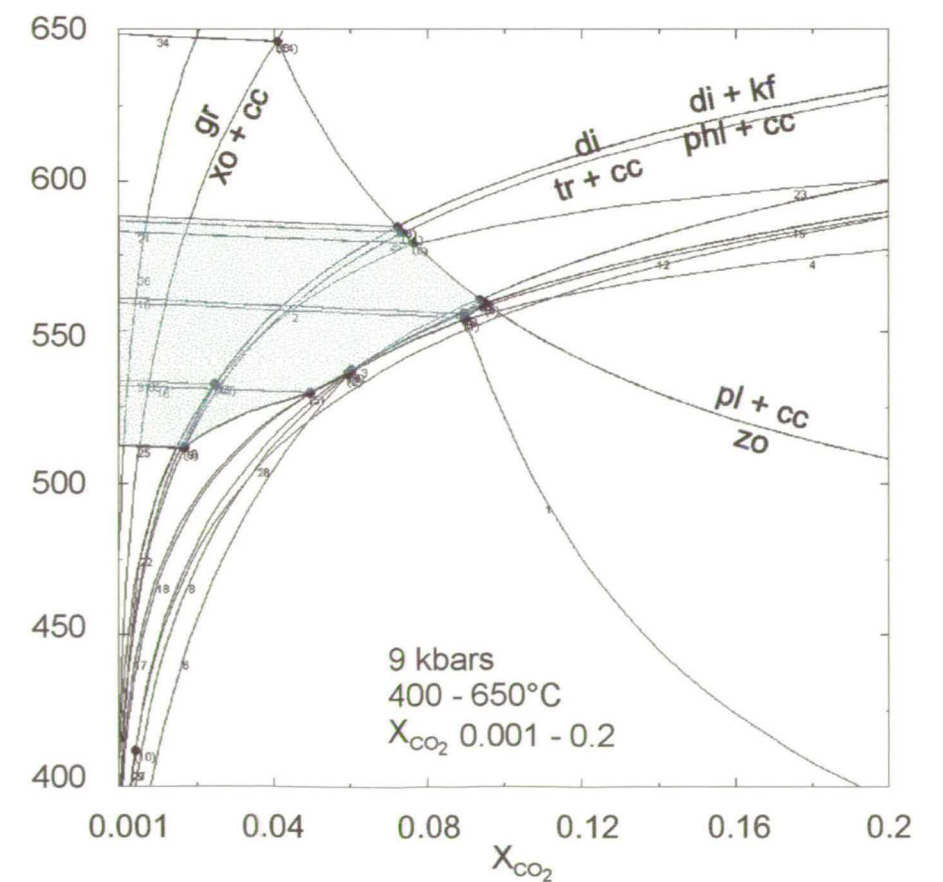
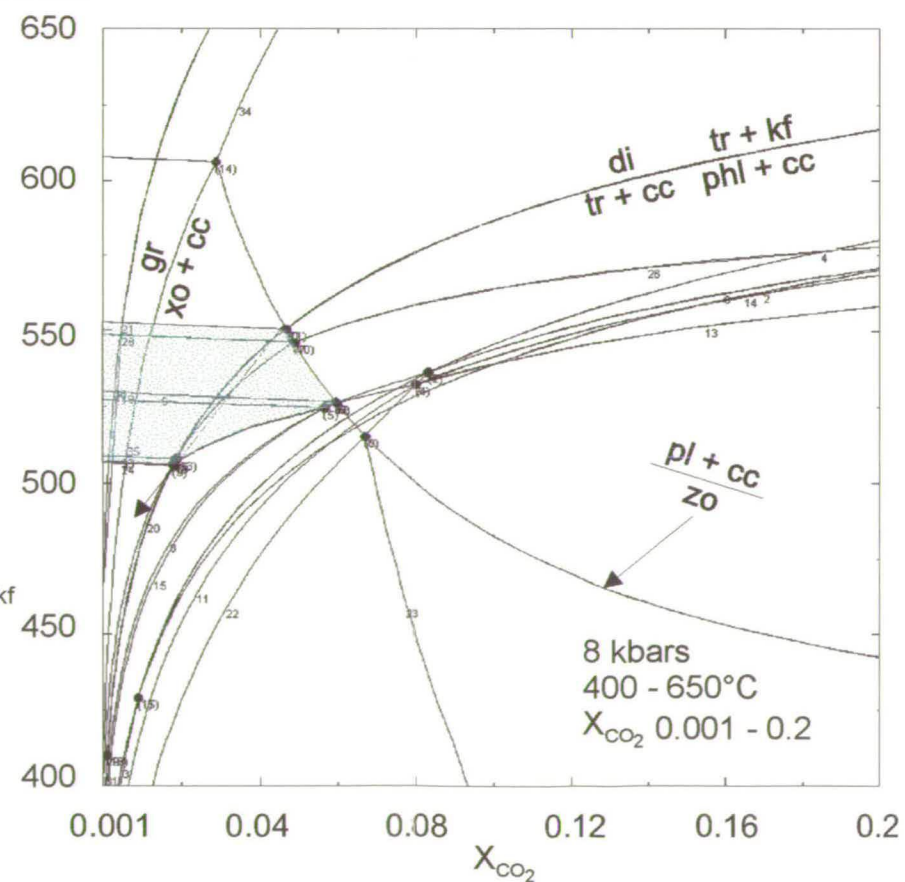
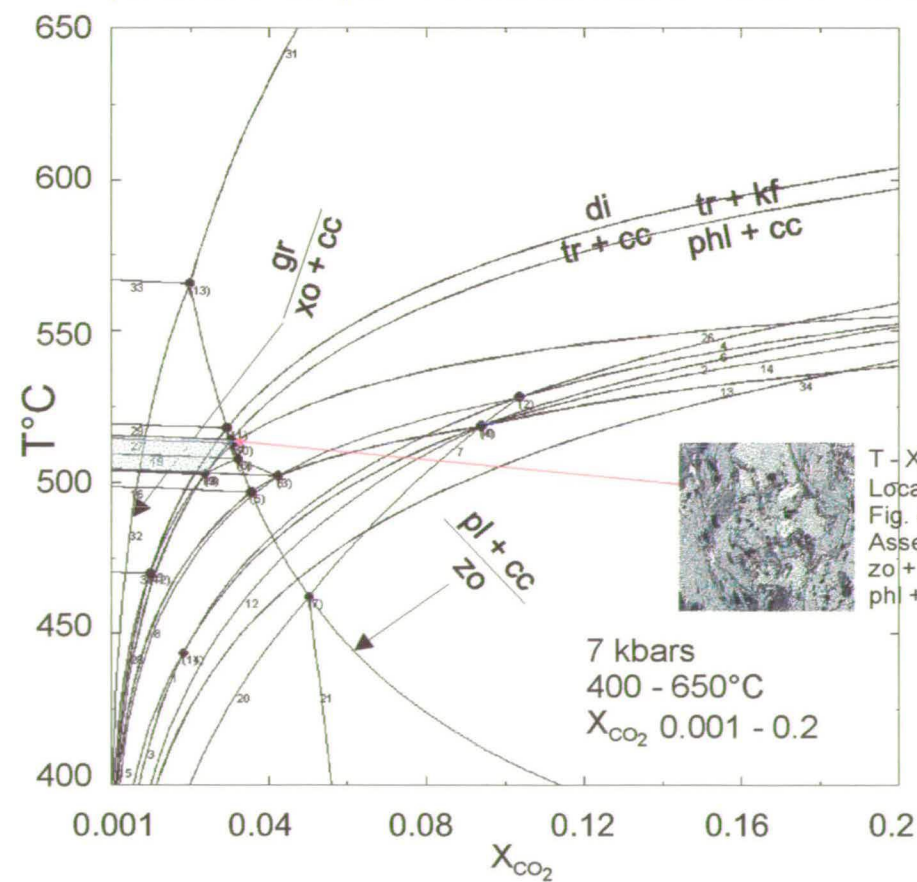


Figure 4.17. The effect on certain key equilibria and the T- X_{CO_2} space they delimit is immediately apparent and marked. With increasing pressure, zo remains stable in increasingly X_{CO_2} – rich fluids. The reaction $\text{phl} + \text{cc} = \text{tr} + \text{kf}$ merges with $\text{tr} + \text{cc} = \text{di}$ at 8 kbars, being forced more rapidly to higher temperatures with increasing P than the latter. Beyond 8 kbars, $\text{phl} + \text{cc}$ yields diopside + kf. The stability field of $\text{phl} + \text{zo}$ assemblages only appears at pressures between 6 and 7 kbars and then increases markedly in T- X_{CO_2} . The limiting reaction $\text{phl} + \text{zo} = \text{kf} + \text{tr} + \text{pl}$ moves from temperatures of $\sim 515^\circ\text{C}$ at 7 kbars to temperatures in excess of 575°C at 9 kbars. Given that errors on geobarometric estimates are commonly quoted to at least ± 1 kbar, a difference of 60°C in the calculated position of the equilibrium between 7 and 9 kbars makes a very considerable difference to the interpretation of the likely fluid composition. In discussion of fluid-rock interaction based on T- X_{CO_2} equilibria, this pressure effect compounds the similar problems arising from errors on temperature estimates remarked upon by Wood and Graham (1986) in discussion of Ferry's reaction progress modelling of fluid-rock ratios (Ferry, 1984) (Chapter 3).

4.5 Detailed electron microprobe petrography

A major problem in understanding the petrography of these rocks arises from their fine grain size and the fine scale of the domains with different assemblages. In order to overcome this, the petrography of several samples has been investigated in detail using back scattered electron imaging on the electron-microprobe. The results reveal considerable petrological complexity. Key textural features are described in the following section.

The key objectives of the petrographical work using the electron microprobe were:

- to constrain the mineral assemblages which define the lithological laminae and coarse patches,
- to elucidate and interpret the petrological differences between the laminae and patches, and
- to characterise textural relationships

The data obtained from this work are combined with the T-X_{CO₂} section to develop an understanding of the petrological evolution of the calc-silicate-bearing lithologies with particular regard to the composition and behaviour of the fluid phase.

4.5.1 EDS and BSE petrography

This section describes the features observed using EDS and BSE imaging; the interpretation of the observed assemblages is discussed in Section 4.6. The assemblages are summarised in Table 4.1.

HY471

HY471 is a strongly and finely laminated calc-silicate-rich rock dominated by amphibole and phlogopite. The mineral assemblage identified in this sample is:

am + phl + clin + pl + qz

Very small amounts of hyalophane (BaO ~ 2.2wt%), albite and muscovite are also present. Zoisite and calcite are conspicuous by their absence.

Two domains are identified in the sample: one is relatively phlogopite-rich and the

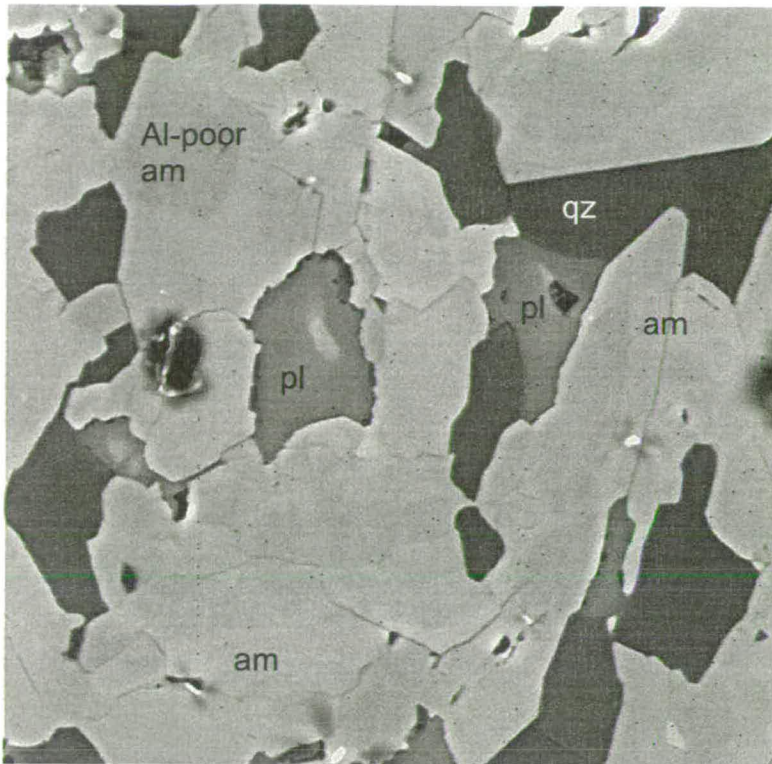


Figure 4.18 Textural relationships in HY471, showing commonly straight grain boundaries in amphibole. Note weak zoning in amphibole and plagioclase. Paler amphibole is richer in Al and the bright cores of the plagioclase are more calcic (see Section 4.3)

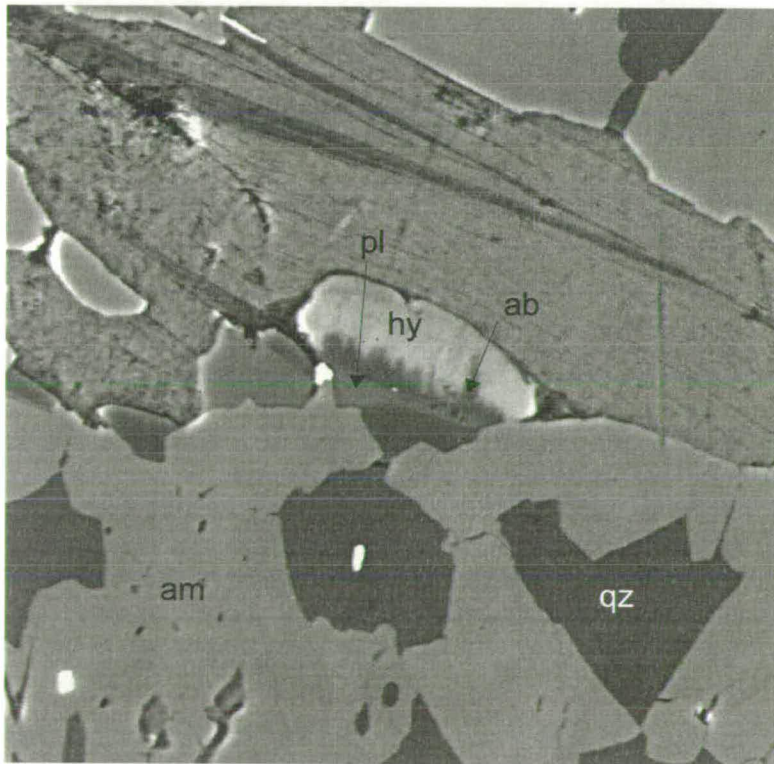


Figure 4.19 Albite and hyalophane on plagioclase in HY471 in a tr + qz + phl + pl assemblage.

other phlogopite-poor. Textures suggesting equilibrium are well-developed in this rock, with good, straight-edged grain-boundaries and many triple point contacts (Figure 4.18). Some amphiboles tend towards the classic truncated rhombic habit, though other phases are generally anhedral in form. Both the amphibole and the plagioclase are commonly zoned (Figure 4.18). The amphiboles have cores of tremolite with Al_2O_3 with rather less than 5wt% (dark on Figure 4.7). The rims are generally, though not always, much more aluminous magnesio-hornblende (Mg-hornblende) with Al_2O_3 often in excess of 10wt%. The zoning in the outer parts of amphibole is commonly discrete where it occurs; sharp internal boundaries are clearly visible in the back-scattered electron images and shows that the earlier, tremolite-dominated cores had good crystal form before they were overgrown by the magnesio-hornblende (Figure 4.7). In the cores of amphibole crystals, slightly more diffuse, irregular, patchy zoning is often observed due to tremolitic hornblende.

Many of the larger plagioclase crystals preserve small, more calcic cores (e.g. Figure 4.18). The rims are andesine with compositions around An_{40} , whilst the cores have An_{55-75} . The plagioclase in this sample is clearly different to that seen in HY474 (see below) and is considered part of the prograde assemblage. It is inclusion-free, has no albite or K-feldspar intergrowths and, where elongate, is aligned with the penetrative fabric.

Clinochlore appears to occur in three forms. There is some discrete early chlorite aligned with the fabric apparently in textural equilibrium with the other phases. However, most of the clinochlore is observed intergrown with phlogopite (Figure

4.7), a feature of chlorite in many samples. There are also late chlorite plates which lie obliquely across the main fabrics.

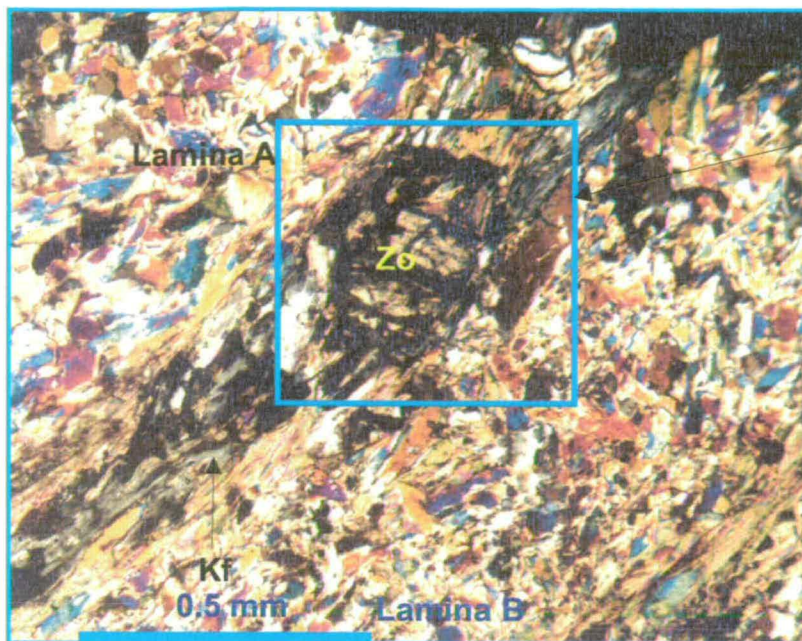
The muscovite is rare and occurs in small pockets armoured by plagioclase and amphibole. Although it could be a late retrogression, its spatial isolation suggests that it is a relict rather than retrogressive phase.

The alkali feldspars commonly occur together, exhibiting a consistent order of overgrowth, with albite nucleating on plagioclase and the hyalophane overgrowing the albite. The albite often has a very irregular, interdigitating contact with the barian feldspar (Figure 4.19).

HY474

Introduction HY474 is a fine sample of very prominently laminated calc-silicate-rich rock in which the laminae are prominently deformed by the later, open to close crenulation microfolds with strongly oblique axial planes (Figure 4.2, 4.20). The laminae are no more than a few millimetres thick and grain size within the laminae is generally less than 0.1 mm.

Laminae Some laminae consists of principally of tremolite, with $\text{Al}_2\text{O}_3 \sim 2\text{-}3\%$, and quartz; phlogopite is only moderately abundant and calcite and plagioclase are present in only trace quantities. Apatite is a common accessory, but no sphene is observed and there is no zoisite. Some of these laminae become almost monomineralic tremolite towards their boundaries. The presence of plagioclase and calcite, albeit in small quantities and the lack of zoisite is significant with regard to



Area of back-scattered electron image in Figure 4.21

Figure 4.20 Zoisite and K-feldspar growing in the boundary between laminae A and B, HY474 (Table 4.3).

Lamina A: am + phl + qz with minor cc + pl and no zo or kf

Lamina B: am + phl + qz + pl with minor zo and no cc

The presence of zo in B indicates lower X_{CO_2} than Lamina A (see text for discussion)

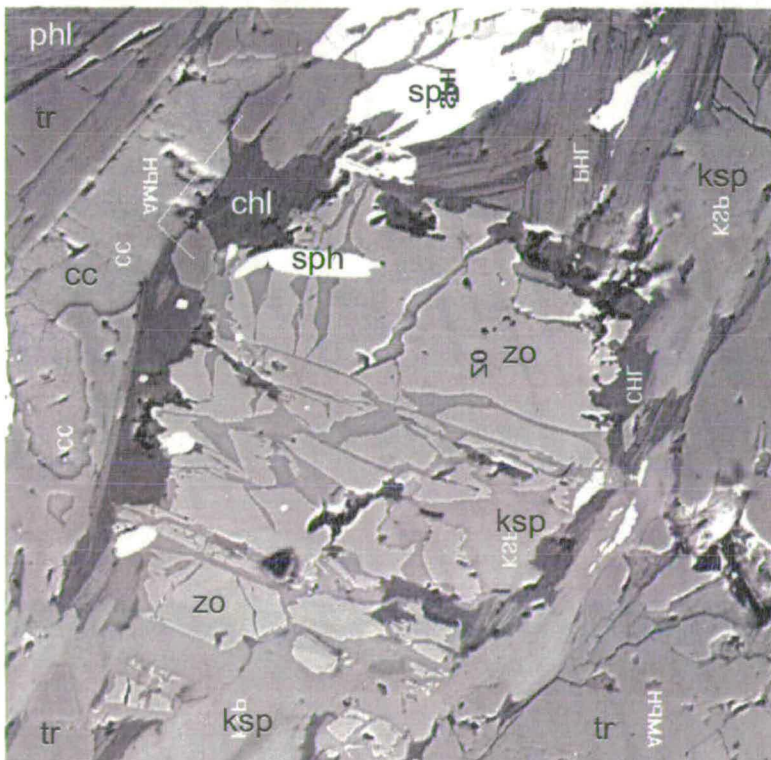


Figure 4.21 Intergrown zoisite and K-Feldspar. Sample HY474. Note also how K-feldspar overgrows phlogopite and new tremolite grows within K-feldspar in the southwest corner of the image.

Field of view ~ 0.5 mm; see also Figure 4.20

X_{CO2} of the fluid phase (Section 4.6).

Other laminae contain small amounts of zoisite and plagioclase in a tremolite + phlogopite (~ An₄₄-An₅₂) + quartz assemblage notably lacking calcite. Phlogopite is finely intergrown with clinocllore and albite rims the plagioclase or occurs as inclusions within the latter.

Some laminae contain K-feldspar in addition to zoisite, phlogopite and scarce tremolite. They also contain calcite but lack plagioclase and quartz. Calcite and tremolite occur only in small amounts and calcite commonly occurs close to zoisite and as small inclusions in tremolite. K-feldspar and zoisite are spectacularly intergrown in one laminae (Figure 4.21), with the feldspar apparently filling 'cracks' in the zoisite crystal; the K-feldspar also has wisps of phlogopite and new tremolite euhedra within it. Spene is quite abundant, contrasting with its general absence in the other laminae.

At the boundary between tremolite-rich and zoisite-phlogopite-rich laminae adjacent to a coarse patch, K-feldspar, zoisite and calcite are rather more abundant than in the laminae and plagioclase appears (Table 4.3, HY474, Area 1, laminae A & B). The phases present are zoisite, calcite, plagioclase, K-feldspar, phlogopite, tremolite, clinocllore, quartz and albite and complex textures are observed between them (Figures 4.3b, 4.22). The plagioclase has a spongy appearance, with fine and irregular intergrowths and overgrowths of albite and K-feldspar in places and patchy albite and K-feldspar inclusions (Figure 4.22). A large zoisite grain in Figure 4.22 is observed intergrown with calcite in a ragged area on its southeastern margin. Along the boundary between the laminae *away* from the patch, plagioclase disappears, as does clinocllore, and albite is associated with zoisite and some calcite. Zoisite and

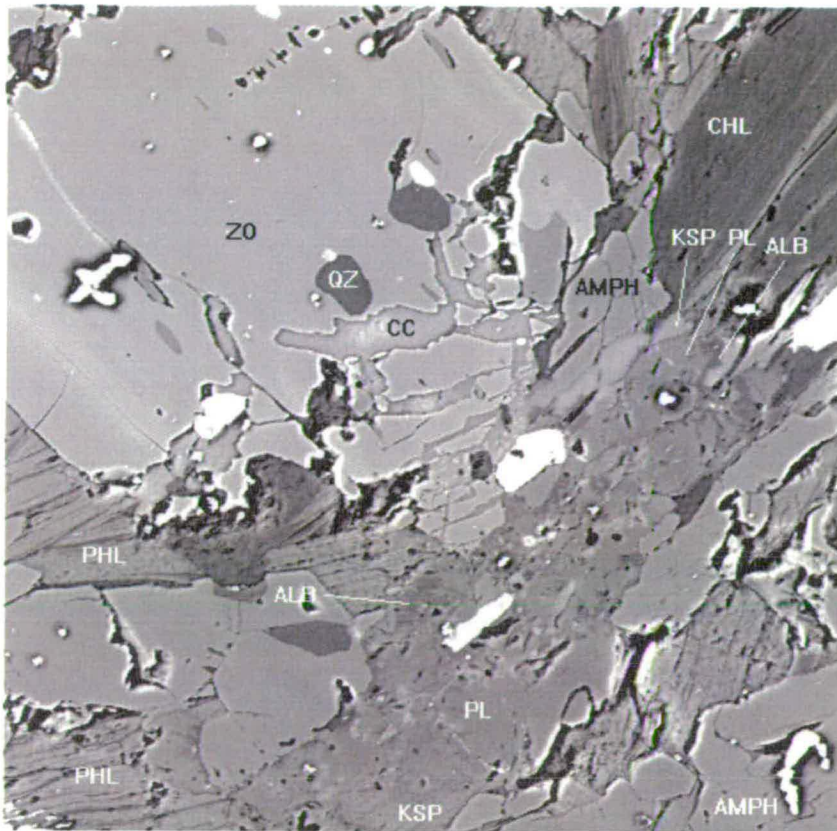
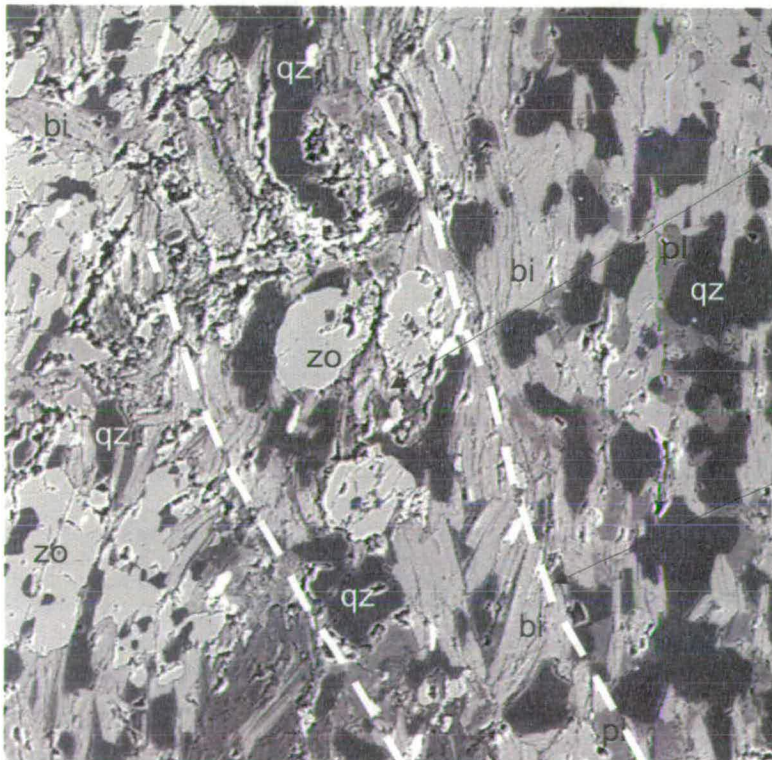


Figure 4.22 Reaction textures at the edge of a zoisite, HY474. The key reaction assemblage here is $zo = pl + cc$.



Sample HY491
zone at boundary
where zo, cc and pl
display reaction
textures, as shown in
Figure 4.24,
below

weak crenulation of
early penetrative fabric

Figure 4.23 Boundary between zo-bi-am lamina (left) and bi-pl-am lamina (right) and the narrow domain of reaction between them (see also Figure 4.24, below)

tremolite are intergrown, with tremolites preserving an early fabric as inclusion trails in the zoisites. The zoisites are weakly zoned, and some tend to have inclusion-rich cores and relatively inclusion-free rims.

Patches The patches contain assemblages similar to the laminae, but are different texturally and generally coarser-grained (e.g. Figure 4.4). The laminae are generally truncated by the patches, though wisps of the laminae are possibly preserved across patches in places. The minerals in the patches are dominated by conspicuously acicular amphibole, which, in the more rounded patches, is disposed radially around the patch centre. In the elongate patches, the amphibole is approximately normal to the patch margins (Figure 4.4).

One studied in detail is mineralogically complex, containing $\text{tr} + \text{cc} + \text{phl} + \text{cli} + \text{qz} + \text{kf} + \text{zo}$. Tremolite dominates, but calcite and quartz are also abundant in places, forming irregular patches in the acicular amphibole mesh. K-feldspar is intergrown with tremolite and zoisite, the zoisite-K-feldspar intergrowth being similar to that observed in boundary layers between tremolite- and phlogopite-rich laminae, as described above.

Other patches are much simpler mineralogically, dominated by $\text{tr} + \text{cc} + \text{qz}$ with some phlogopite/clinochlore. Some are very calcite-rich, but lack feldspar and zoisite. Relatively large subhedral to euhedral sphenes are generally aligned with the patch long axis and are clearly different to the sphene observed elsewhere in the rock, the latter occurring as small rounded masses and aggregates.

Summary of features in HY474

- The mineralogy is dominated by amphibole and phlogopite, with variable amounts of zoisite, plagioclase, K-feldspar, quartz, calcite and clinocllore. Sphene and apatite are common accessories.
- In general, plagioclase and zoisite are mutually exclusive; where they do occur together, they are mutually unstable, showing complex reaction textures containing calcite.
- Tremolite-rich laminae commonly have extremely tremolite-rich margins adjacent to phlogopite-rich laminae.
- Between tremolite- and phlogopite-rich laminae, a thin boundary layer is commonly developed which is rich in K-feldspar and zoisite. Tremolite is rather less abundant than in the laminae whilst K-feldspar may be very abundant in places.
- The patches are dominated by tremolite, calcite, quartz and phlogopite, but may also contain the other phases seen in the laminae; sphene is a notable accessory.
- Variations in modal abundances occur on a scale smaller than the thickness of the laminae

- Phlogopite and clinocllore are nearly always observed intergrown on a fine scale within individual phlogopite crystals.
- Calcite is uncommon or absent within most (but not all), laminae, but may be very abundant in the coarse patches.
- Plagioclase is spongy-looking, being very finely and irregularly intergrown with K-feldspar and albite, and is also inclusion-rich.
- Quartz is very variable in abundance, but there is probably just sufficient for it to be considered to be in excess in general. It is often abundant in the patches.
- Amphibole appears to be texturally stable everywhere.

HY491

Introduction HY491 is a strongly laminated sample in which planar laminae are between 1 and 5mm in thickness, with 2-3mm being the average. The dominant phyllosilicate in this sample is an Fe-poor biotite, rather than phlogopite, due to higher bulk Fe/Mg compared to the other samples discussed here.

Figure 4.23 shows two laminae, one zoisite-bearing, the other zoisite-free. The zoisite-bearing lamina (lefthand side of Figure 4.23) contains bi + zo + qz + am + clin + pl (An₄₁-An₄₆). Spene and K-feldspar occur in small amounts. The larger amphiboles are more aluminous than the smaller crystals which occur wholly within biotite plates. K-feldspar occurs as very small inclusions within the plagioclase.

Calcite occurs as inclusions in the zoisite and where zoisite occurs near the plagioclase, the latter always looks unstable. Zoisite also contains inclusions of biotite and amphibole. Chlorite is most commonly observed intergrown with the biotite, but late plates with their cleavage lying oblique to the dominant fabric are also present.

The immediately adjacent zoisite-free lamina (right hand side of Figure 4.23) contains bi + pl (andesine, An₄₇) + qz + am, with very small amounts of calcite, K-feldspar and albite, but no zoisite. Amphibole is less abundant than in other domains and K-feldspar only occurs as inclusions within plagioclase.

Other domains are rich in biotite and zoisite, with subordinate amphibole, calcite and quartz. Zoisite postdates the early fabric defined by the biotite and amphibole, but partly predates the crenulation. This is consistent with other thin sections which show the zoisite to be later than phlogopite/biotite. In one of the crenulated domains wrapping a zoisite crystal, plagioclase, calcite and K-feldspar and small tremolite grains are present surrounding zoisite and reaction textures between these phases are readily apparent (Figure 4.24).

Finally, some domains contain bi + qz + am + pl with minor amounts of zoisite and calcite. The distribution and abundance of zoisite, calcite and plagioclase are variable. Away from the later crenulation cleavage, zoisite looks fresh and stable, calcite is uncommon and plagioclase absent. However, there are small domains within which zoisite, plagioclase and calcite are in very close proximity and look to be in textural equilibrium (Figure 4.25).

HY491 is exceptional for the range of relationships it shows between zoisite, calcite and plagioclase and these have significance for the T-X_{fluid} relationships in the

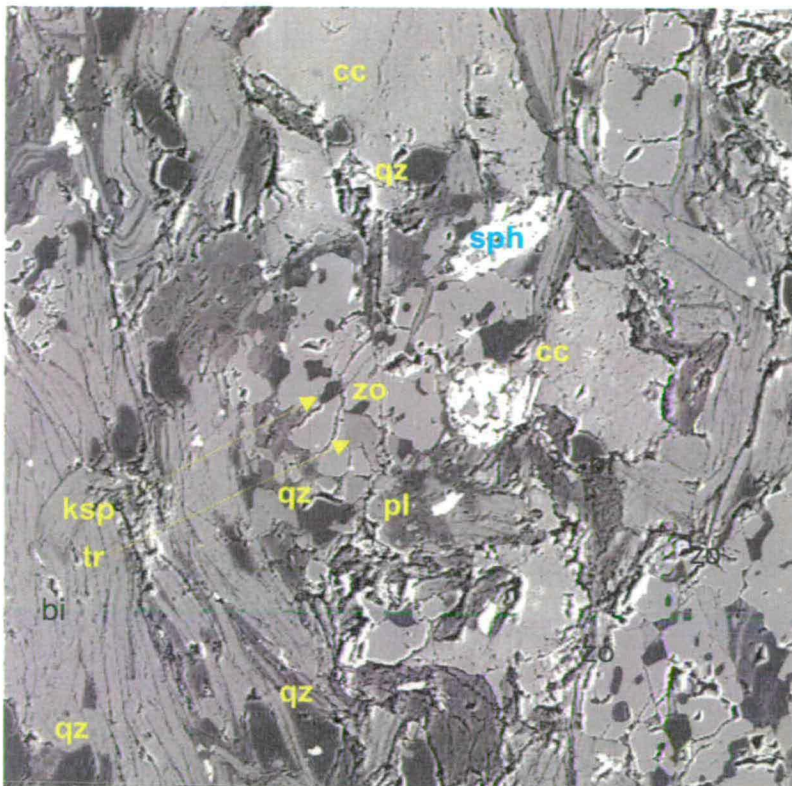


Figure 4.24 Reaction textures between zo, pl and cc in HY491 within a weak crenulation hinge. Zo contains qz inclusions, pl is patchy. Fine grained cc occurs within the mesh of pl and zo and new tr and ksp lie adjacent to the bi southwest of the central zo. The key reactions are:
 $zo = pl + cc$ and $phl + cc = tr + kf$

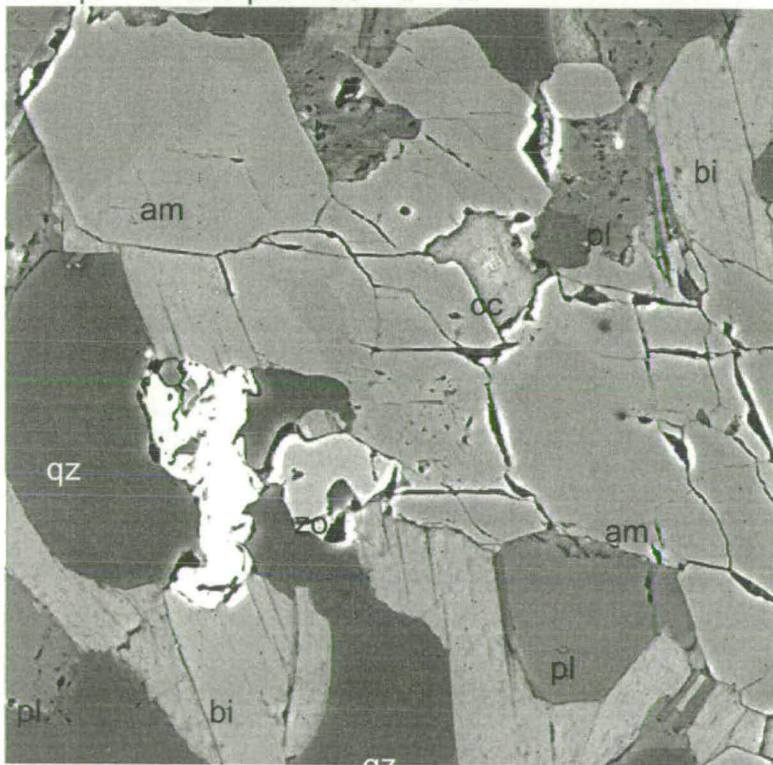


Figure 4.25 Zo + cc + pl in an assemblage dominated by am + bi + qz + pl in HY479. The assemblage zo + cc + pl is univariant, if in equilibrium (cf. zo-cc-pl relationships in Figures 4.23 - 4.25 and see discussion)

rock. This is discussed further below in Section 4.6.

HY1001

This sample is a moderately strongly laminated calc-silicate-bearing rock in which pale wispy elongate patches lie oblique to the lithological foliation.

One domain includes two distinctive laminae and an elongate patch. The darker, biotite-rich lamina contains quartz, tremolite, biotite, zoisite, plagioclase and clinocllore and hyalophane (BaO ~ 3wt%). The hyalophane is abundant and is spatially associated with the biotite and tremolite. The paler lamina contains the same phases, but biotite and zoisite are much less abundant. Calcite is not present. The zoisites have a more bladed habit than observed in other samples and there appears to be good textural equilibrium between the phases.

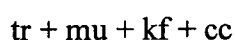
The patch contains tremolite, K-feldspar, quartz, calcite, clinocllore, plagioclase and sphene; zoisite and phlogopite are conspicuous by their absence. The calcite and clinocllore are present in only small amounts, but both look to be in textural equilibrium with the rest of the assemblage. K-feldspar is abundant and forms large areas of the patch comprising anhedral crystals. The plagioclase is andesine. On the margins of the patch, zoisite crystals in the laminae look unstable, as do some adjacent biotite and calcite crystals.

HY1001 also contains elongate patches oblique to the laminae. One example, shown in Figure 4.3a, has a very elongate patch running across a rather uniform lamina rich in biotite and zoisite. The lamina contains biotite, zoisite, quartz, K-feldspar, plagioclase with small amounts of calcite and sphene. Clinocllore is intergrown with the biotite. There is no tremolite or muscovite. K-feldspar, zoisite

and plagioclase are common. The patch contains tremolite, plagioclase, K-feldspar, quartz and calcite and lacks zoisite and biotite. Where zoisite is observed adjacent to the patch, it contains calcite in cracks, adjacent to small amounts of plagioclase, once again suggesting the breakdown of zoisite.

HY1007

This sample is mineralogically and chemically somewhat different to most of the assemblages so far described in that it contains abundant white mica and calcite, but is locally quartz-free. In white mica bearing domains, the assemblage is



with small amounts of phlogopite and intergrown chlorite, and some zoisite; significantly, quartz is absent. K-feldspar is abundant, intergrown with phlogopite and intimately associated with the white mica, which it post-dates. Zoisite is observed very finely intergrown with K-feldspar inside a large white mica felt (Figure 4.26); there is no quartz and the wider assemblage is tremolite, white mica and calcite. Elsewhere, the classic $\text{tr} + \text{cc} + \text{qz}$ assemblage is dominant. However, the presence of quartz-absent assemblages immediately adjacent to quartz-rich assemblages is significant.

4.5.2 Limits on T and X_{CO_2} of observed assemblages

There are several key assemblages and reactions which place general limits on the temperature at which these rocks were metamorphosed and the composition of the equilibrium fluid phase.

Two particular phases are particularly useful. Zoisite stability is of crucial

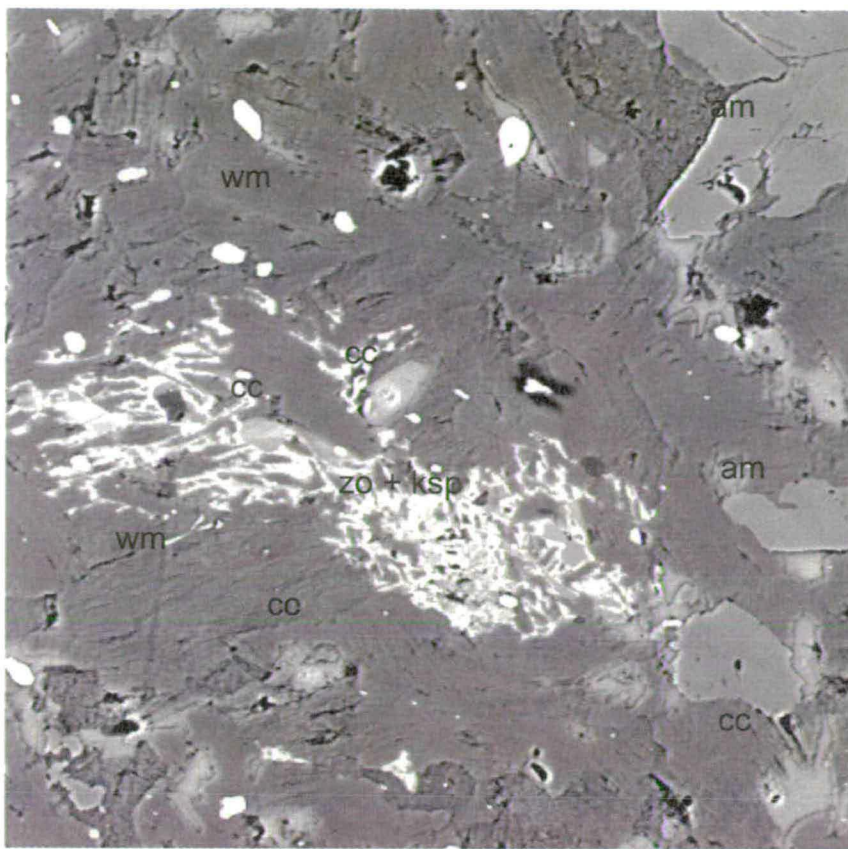


Figure 4.26 The assemblage $zo + ksp + wm + cc$ in a quartz-absent domain in HY1007. This is the divariant assemblage $ksp + zo + cc + mu$ arising from the reaction $mu + cc + qz = zo + ksp$. See also Figure 4.29 for $T-X_{CO_2}$ stability limit.

importance and is discussed further below with regard to zo + cc + pl assemblages and the zo = cc + pl reaction (15-1, Table 4.3); this reaction has the further advantage of being quartz-free and is clearly observed in some assemblages. The stability of sphene also helps place general upper limits on the T-X_{CO₂} domain occupied by the rocks via the reaction ru + cc = sph (30-1, Table 4.3). Reactions 15-1 and 30-1 are included on all T-X_{CO₂} sections for reference.

Stability of zo + cc + tr + qz assemblages

The CMASCH assemblage zo + cc + tr + qz is commonly observed in a number of domains (Table 4.1). The absence of gr, which forms via the reaction zo + cc + qz = gr, limits the stability of the zo + cc + qz assemblages and places a lower limit on X_{CO₂}, whilst the lack of di limits the stability of the common assemblage tr + cc + qz. The absence of both gr and di precludes infiltration of the rock by large amounts of extremely H₂O-rich fluid in domains which contain tr + cc + zo + qz (cf Graham et al., 1983), but restricts X_{CO₂} to be less than that defined by the zoisite terminal breakdown reaction, as shown in Figure 4.16. The thermal stability of tr + cc + zo + qz assemblage is limited by the interception of the reaction:



with reaction (25-1) terminating at invariant point (17), at which di should appear by reaction of tr with either cc or zo. As no di has been recorded in any assemblage, this invariant point has not been reached, nor have di-producing equilibria projecting from it been crossed. Thus thermal stability of tr + zo + cc + qz limits temperatures to be less than ~550°C, with an upper limit on X_{CO₂} of ~0.05 at invariant point (17).

The zoisite – calcite – plagioclase assemblage

The loci of the zoisite terminal breakdown reaction is important in constraining X_{CO_2} because of the steep $-dT/dX_{\text{CO}_2}$ slope of the reaction above $\sim 500^\circ\text{C}$. Higher pressures push this reaction to higher X_{CO_2} as fluid behaviour becomes increasingly non-ideal (see Figure 4.17). This results in extension of the stability fields of all zo-bearing assemblages at higher pressures, such as the one discussed above, since they terminate against this reaction (Figures 4.16, 4.27).

A change in pressure estimate from 7 to 8 kbars more than doubles the X_{CO_2} limit of this reaction from <0.04 to ~ 0.08 at 500°C (Figure 4.17, bottom left and centre). Thus, variation in pressure estimates will have a very significant bearing on the estimate of X_{CO_2} .

Since pressures are generally not very well constrained geobarometrically, having errors of at least ± 0.5 kbars, it is not possible establish the true equilibrium X_{CO_2} of the assemblage. However, because of the locus of the $\text{zo} = \text{pl} + \text{cc}$ reaction, it is possible to use zo stability to place relative constraints on X_{CO_2} for the assemblages in the Pitlurg rocks.

Zoisite – plagioclase – calcite assemblages are observed in several domains, as discussed above (Table 4.1). There are several millimetre-scale domains with $\text{zo} + \text{cc}$ and $\text{pl} + \text{cc}$ assemblages from which either pl or zo are absent, indicating locally different equilibrium fluid compositions (Figure 4.16). However, in some cases zo , cc and pl are observed together. In one or two samples they *appear* to be in equilibrium (e.g. Figure 4.25), but they more commonly display reaction textures

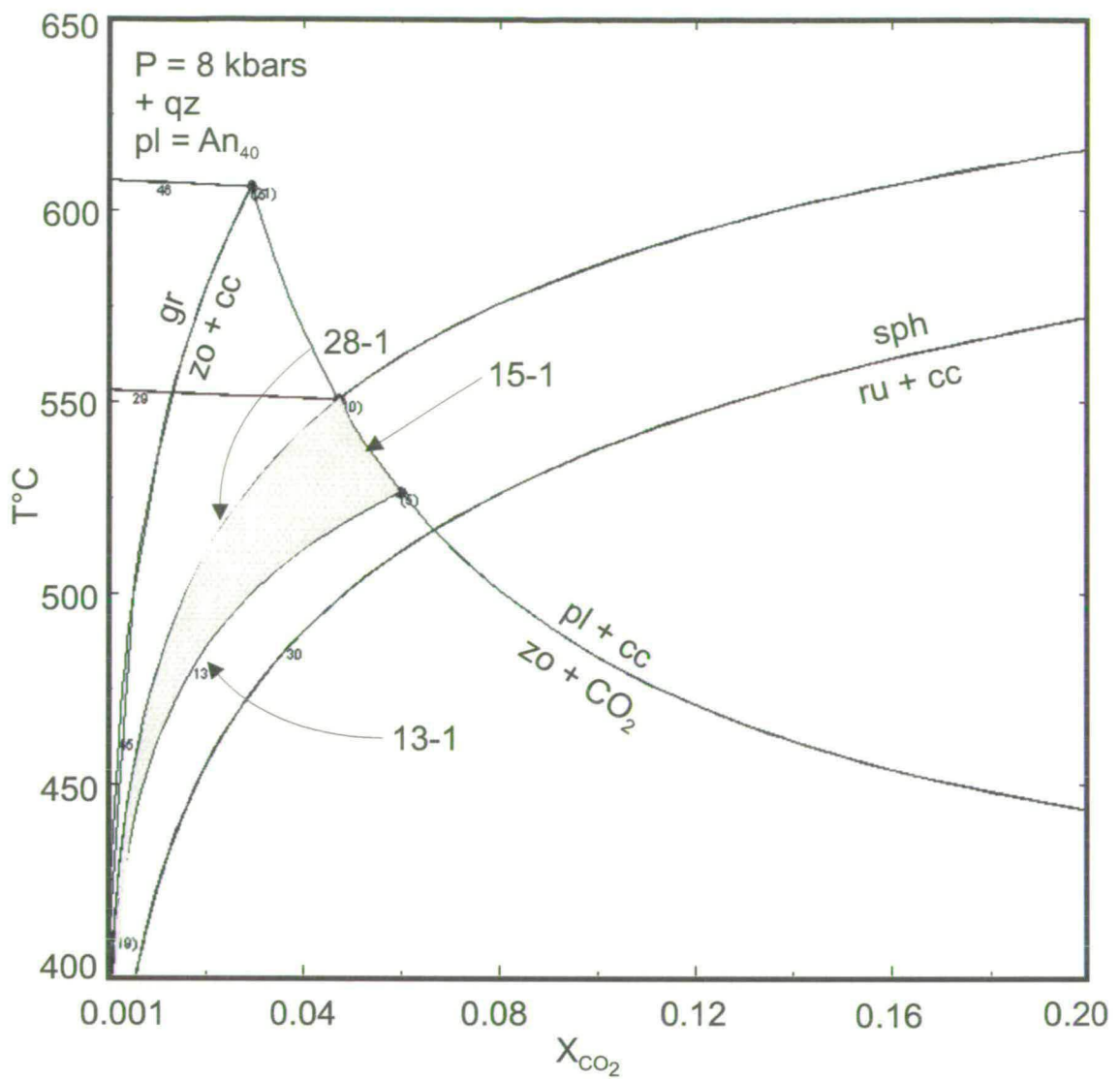
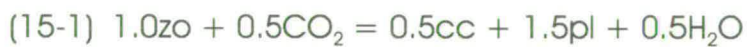
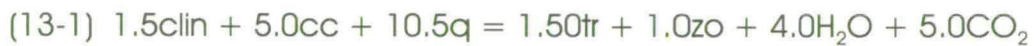


Figure 4.27 Stability limit (shaded) of the assemblage tr + zo + cc + qz in T- X_{CO_2} . The limiting reactions are (Table 4.3):



showing zo breaking down to pl, as shown in Figures 4.22 and 4.23. In domains where reaction is observed, such as those shown in Figures 4.22 and 4.23, the zo, cc and pl lie within a zone of weakly developed crenulation cleavage (Figure 4.22). The occurrence of reaction textures in the crenulation suggests a possible link with the deformation, with the formation of the crenulation providing an opportunity for fluid migration at the boundary between the two laminae. One possible explanation is that formation of the crenulation cleavage has facilitated infiltration of a fluid richer in CO₂ than that which would be in equilibrium with zoisite. The scale of any interaction is clearly very small and does not reflect significant infiltration of external fluid: all the textural features indicate very local buffering of the fluid phase by the assemblage. The assemblage phl + tr + pl + qz is stable over a wide range of T-X_{CO₂} and so would be stable in the presence of a relatively X_{CO₂} – rich fluid. Conversely, zo + cc stability is limited by the zo + cc + qz = gr reaction (Figure 4.27). The lack of grossular shows that the rocks have not been infiltrated by extremely water-rich fluids.

Phlogopite – zoisite assemblage

The phlogopite – zoisite assemblage is commonly observed. The stability of this assemblage is limited in its range of X_{CO₂} by zo = pl + cc and, at 8 kbars, by four reactions producing phl + zo :



(qz in excess) as shown in Figure 4.28.

The phl + zo stability field is pressure dependent and it only appears on the calculated T-X_{CO₂} sections between 6 and 7 kbars at temperatures above 550°C (see also below in discussion on pressure effects on T-X_{CO₂} topology).

Reaction (38-1) defines the upper thermal stability limit for the assemblage at about 550°C with a maximum X_{CO₂} of ~0.048 at invariant point 10. As diopside is universally absent, where phl + zo occurs with tr + cc, then the assemblage tr + phl + zo + cc + qz assemblage lies on the tr + cc of the tr + cc + qz = di reaction, so that the lower T-X_{CO₂} limit is ~510°C at X_{CO₂} ~ 0.02. The stability limit of phl + zo + tr + cc is shown by the darker shaded area on Figure 4.28.

K-feldspar-bearing assemblages

In the absence of diopside, K-feldspar is produced by just three reactions at temperature conditions consistent with the other observed assemblages at 8 kbars and above ~500°C. These are:



(Figure 4.29). Reaction 35-1 intersects the tr + cc = di reaction at invariant point 20 and terminates at the zo = pl + cc reaction at invariant point 16. When combined with the stability fields for other assemblages within which K-feldspar occurs, the loci of these reactions (34-1 to 36-1) constrains the T-X_{CO₂} space within which these assemblages can occur to narrow domains defined by cc + mu and di stability, as

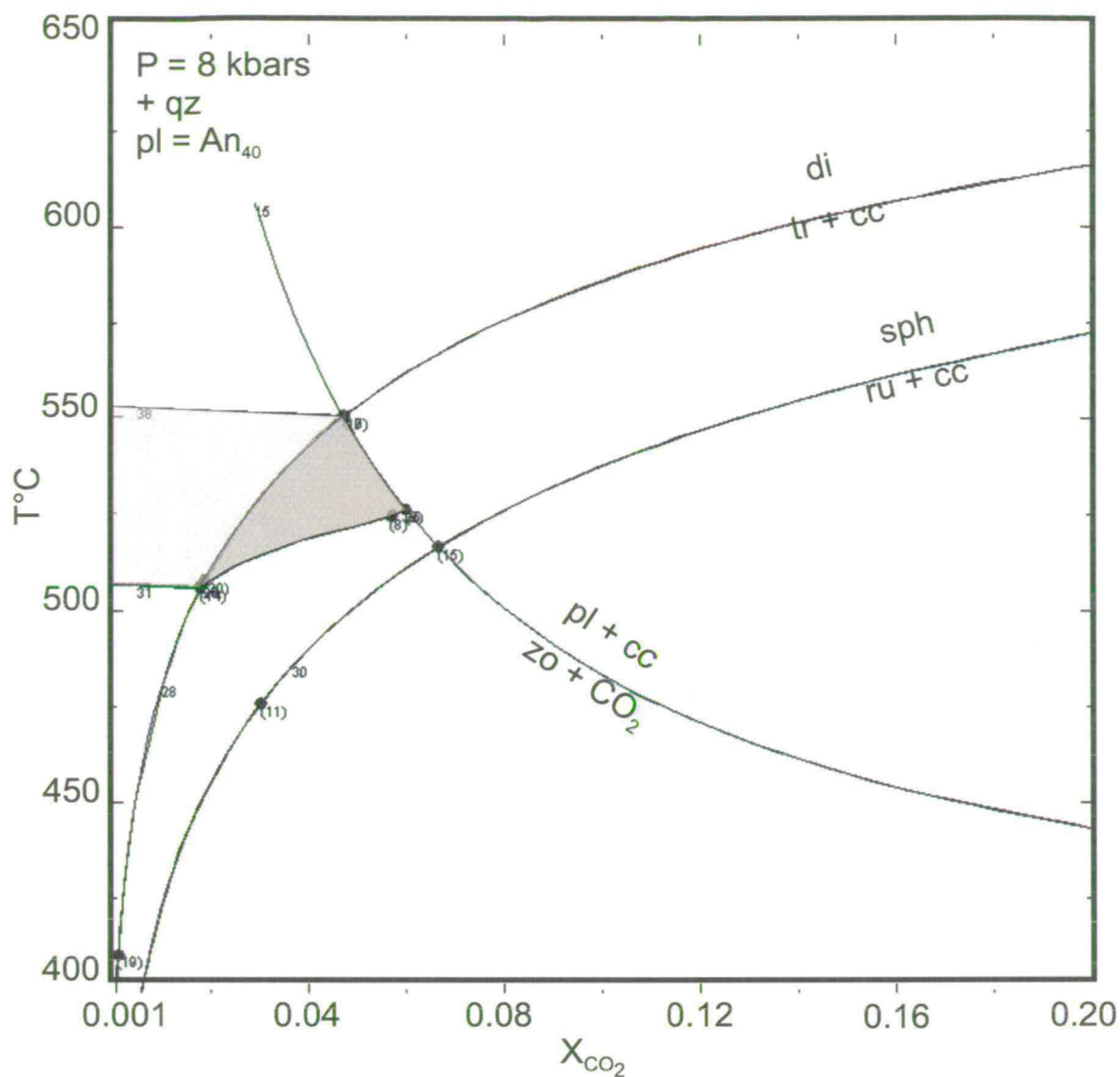
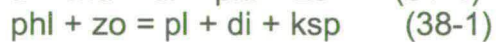
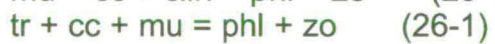


Figure 4.28 Phl + zo stability field (shaded), limited by reactions:



The darker shaded area shows the stability limits of the phl + zo + tr + cc assemblage.

shown in Figure 4.29. Figure 4.26 shows occurrence of reaction 35-1 in HY1007 very well, yielding a mesh of K-feldspar and zoisite in muscovite and calcite in a now quartz-absent domain.

In several small domains (e.g. Figures 4.22, 4.25), small amounts of K-feldspar are seen overgrowing phlogopite and some new, fine-grained amphibole appears. These textural features suggest that tr and kf are forming at the expense of phl + cc via the reaction $\text{phl} + \text{cc} = \text{tr} + \text{kf}$. This reaction does not appear on Figure 4.16 because, at 8 kbars, phl + cc react to form di + kf, coinciding with the $\text{tr} + \text{cc} = \text{di}$. Since no diopside has been recorded, the presence of the phl + cc + tr + kf reaction assemblage implies that the pressure must have been less than 8 kbars. The change in the locus of the $\text{phl} + \text{cc} = \text{tr} + \text{kf}$ reaction is shown on Figure 4.17.

The occurrence together of phl + cc + tr + kf and zo + pl + cc implies reaction at an invariant point on the $\text{zo} = \text{pl} + \text{cc}$ univariant equilibrium (as indicated on Figure 4.17). At 7 kbars, the X_{CO_2} of this invariant point is about 0.03 at a temperature of $\sim 514^\circ\text{C}$.

The origin of tremolite – rich laminae

In the introduction, I discussed the presence of very tremolite-rich laminae which are nearly monomineralic. These contrast with the commonly complex assemblages present in most of the rocks. cursory consideration suggests two possible options for the development of these, both of which may have occurred. Firstly, they may result from dolomite and talc reactions (reactions 1-1 to 3-1, Table 4.3), all of which occur at relatively low grade and at relatively low X_{CO_2} (Figure 4.29). Secondly, tremolite abundance in some laminae may have been increased by Ostwald ripening processes,

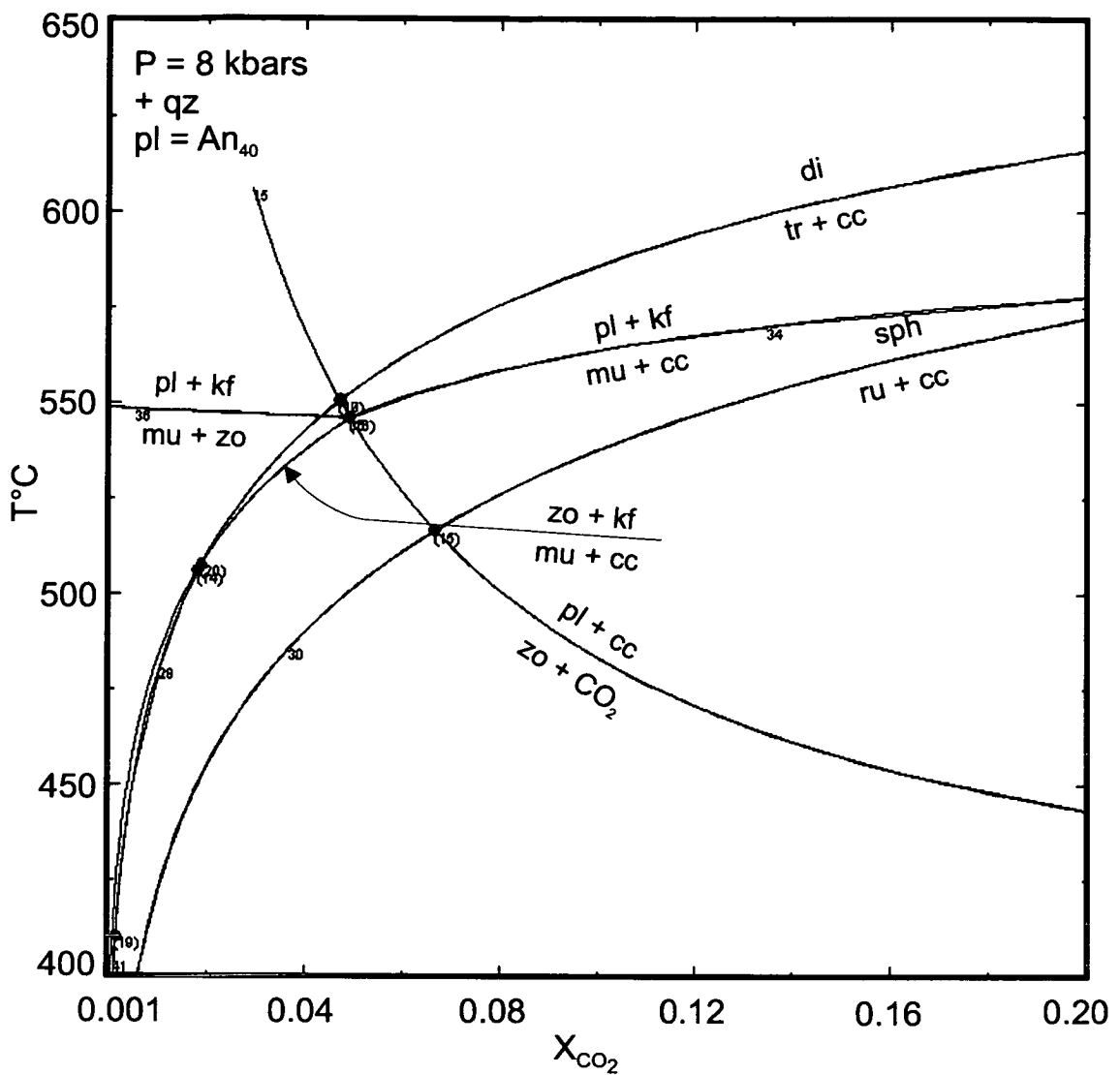
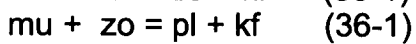
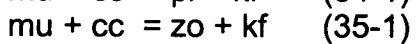
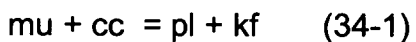


Figure 4.29 Lower K-feldspar stability, limited by reactions:



Where k-feldspar occurs with tr + cc, then the stability domain of the assemblage is limited by the tr + cc + qz = di reaction.

The mu + cc = zo + kf reaction is observed in HY1007, as shown in Figure 4.16.

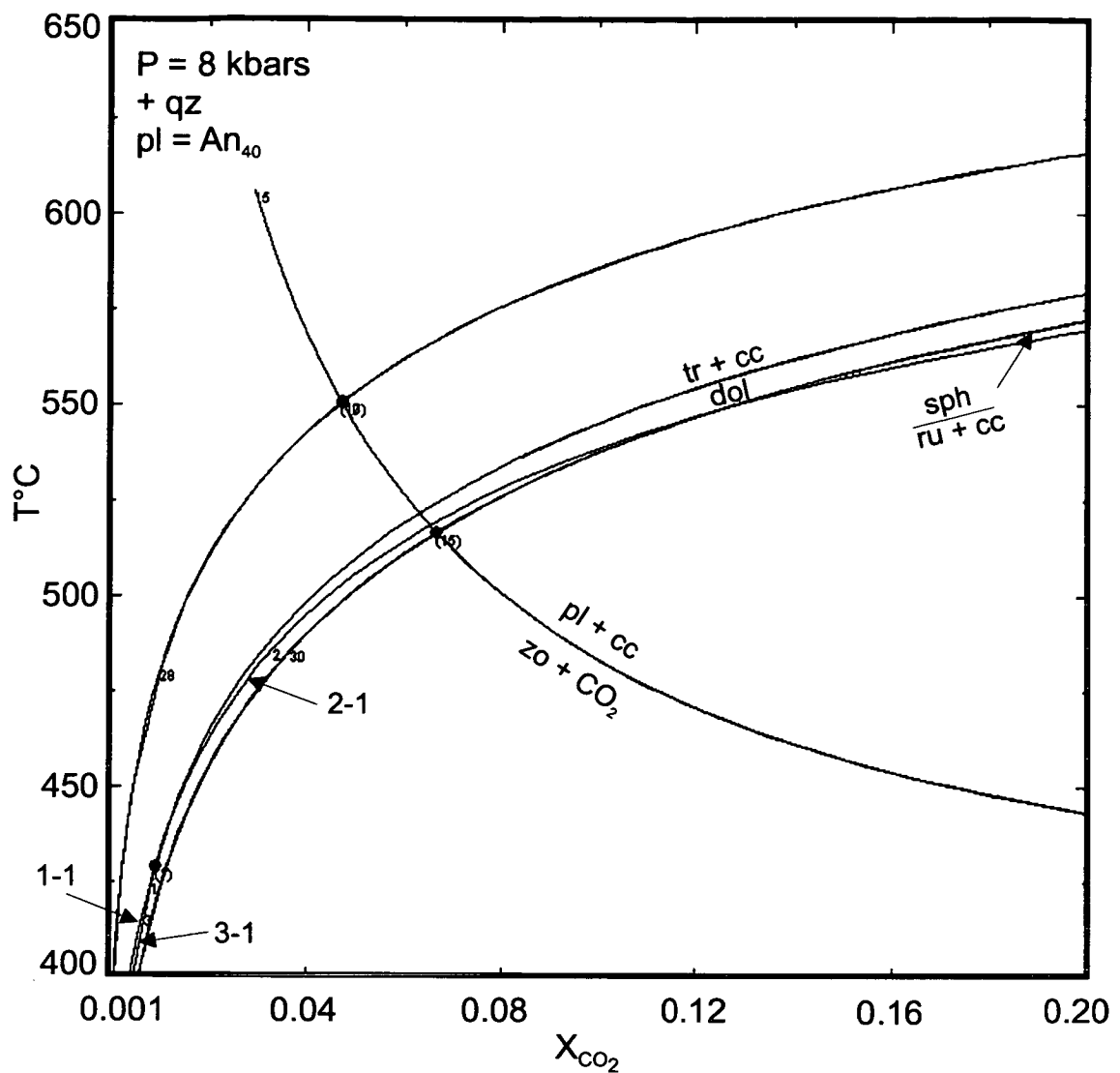
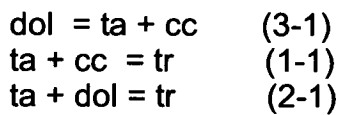


Figure 4.30 Tremolite-forming reactions involving talc and dolomite:



The $\text{dol} + \text{qz} = \text{tr} + \text{cc}$ reaction is shown for reference; this reaction terminates at invariant point 1, beyond which the equivalent reaction is $\text{dol} = \text{ta} + \text{cc}$.

similar to those invoked by Holness (1997) for the development of Liesegang rings in calc-silicates around chert nodules.

4.6 Discussion

4.6.1 Location of the Pitlurg calc-silicates in T - X_{CO_2} space

Inspection of the assemblages in Table 4.1 with regard to the T - X_{CO_2} sections in Figure 4.16 and 4.17 indicates that although the equilibrium fluid composition is H_2O -rich, assemblages in many domains have buffered the fluid phase towards more X_{CO_2} - rich compositions at the presumed temperatures of metamorphism. Thus zo + cc is stable, rather than grossular, and tr + cc is stable, rather than diopside. Fluid in equilibrium with many tr + cc bearing laminae cannot have had X_{CO_2} much less than 0.02 at 8 kbars. The patch in Area 2 of HY491 (Table 4.1) contains tr + cc + pl + kf + qz. This assemblage is stable beyond $X_{\text{CO}_2} \sim 0.05$ at 550°C and 8 kbars. However, if one assumes that peak metamorphic temperature was no greater than 550°C (see below), then X_{CO_2} cannot have been greater than ~ 0.06 , because at $X_{\text{CO}_2} > 0.06$ at 550°C , the stable assemblage is tr + cc + mu. Thus the domain in which the tr + cc + pl + kf assemblage is stable at 550°C is constrained to lie close to the zo breakdown reaction.

Overall, the petrographic and thermodynamic evidence suggests buffering of the fluid phase by many of the assemblages to X_{CO_2} near the locus of the zo = pl + cc reaction, with most lying on the water-rich side. However, it is difficult to be precise about the actual X_{CO_2} because of the significant effect of pressure on the topology of the T - X_{CO_2} section (discussed above) and the poor precision on pressure estimates.

The presence of phl + cc + tr + kf assemblages and the absence of diopside suggest that maximum pressures of metamorphism cannot have been much above 7 kbars.

It is also apparent that there was very local buffering of the fluid phase, as revealed by the presence of zo + cc in some laminae and pl + cc in others (e.g Figure 4.24), particularly since the laminae in the calc-silicate rocks are generally only a very few millimetres thick. Furthermore, zoisite is commonly observed breaking down adjacent to calcite-rich, plagioclase-bearing patches. This suggests that relatively CO₂-rich fluid in equilibrium with the patches is infiltrating the laminae, resulting in zoisite breakdown. These very local scale effects raise questions regarding the scale of equilibrium and the domains which can be interpreted to contain equilibrium assemblages (see below).

The evidence for localised buffering is not consistent with infiltration of significant volumes of external fluid, which would be expected to drive equilibria towards diopside and grossular-bearing assemblages. The assemblages recorded here and their implications for fluid buffering, contrast markedly, for example, with those recorded by Baker et al. (1989) and Lewis (1999), which include diopside, grossular and vesuvianite.

4.6.2 Peak metamorphic temperature and pressure estimates from the T-X_{CO₂}

The reactions phl + zo = pl + di + kf (38-1) and tr + zo = pl + di (29-1) coincide at 8 kbars and, within the context of the T-X_{CO₂} section, limit peak metamorphic temperatures to a little over 550°C. This is lower than peak metamorphic temperature estimates of ~600°C for the Glen Rinnes district (Beddoe-Stephens, 1990).

Increasing P to 9 – 10 kbars places the temperature range of several key assemblages

within the range calculated by Beddoe-Stephens; such an increase in pressure also increases the X_{CO_2} of the fluid in equilibrium with the assemblages (Figure 4.17). However, as discussed above, the presence of the phl + cc + tr + kf assemblage is inconsistent with pressures of 8 kbars or more. The invariant KCMASCH assemblage phl + zo + am + zo + pl + cc + qz, (Figure 4.24) from which the reaction $\text{phl} + \text{zo} = \text{pl} + \text{di} + \text{kf}$ emanates, limits maximum temperatures to $\sim 515^\circ\text{C}$ (*this reaction limits the top of the shaded area in the lower left T- X_{CO_2} section in Figure 4.17*).

Thus, the phase relations in the calc-silicate assemblages apparently indicate significantly *lower* peak metamorphic conditions than do the pelite geothermobarometers used by Beddoe-Stephens (1990). Peak conditions estimated here are $\sim 520^\circ\text{C}$ at ~ 7 kbars. Note that the indicated temperature conditions are also lower than those estimated by amphibole – plagioclase geothermometry (Table 4.6, HY471, column 3; see also earlier discussion on am – pl thermometry).

4.6.3 The origin of the patches

The cross-cutting, elongate patches described in the petrology section are a common feature of these rocks. Their petrology is essentially that of the laminae, though they are commonly richer in calcite. The simplest explanation of these patches is that they were originally dessication or possible synaeresis cracks which became filled with sediment of a different composition to the immediately adjacent laminae. In some thin sections, it is clear that some laminae ‘flame’ into adjacent laminae, producing patch-like structures. Subsequently, they have become the focus for late deformation, acting as sites for the nucleation of microfolds and crenulation. It is not considered

that they are a product of focussed fluid flow which has changed the mineralogy by driving reactions because it is clear that their mineralogy is controlled by bulk compositional constraints and they develop much the same mineralogy as the laminae. Whether they have acted subsequently as *channels* for fluid is uncertain, but it may be possible, given that they traverse laminae (Figure 4.2) and are commonly texturally different (Figure 4.4). In places, zo, in particular, looks unstable on the margins of the patches (Figures 4.3b, 4.21) and the patches are commonly zo-free, but contain K-feldspar and, in places, plagioclase. This may reflect buffering of the fluid phase to higher X_{CO_2} along the K-feldspar + plagioclase producing reaction through the X_{CO_2} stability limit of zoisite.

4.7 Summary and conclusions

- The calc-silicate rocks contain abundant amphibole, phlogopite and zoisite and locally abundant calcite in generally quartz-saturated, aluminous, magnesian and potassic bulk compositions.
- The rocks are strongly laminated with wide, millimetric-scale variation in domain composition, but are cut locally by rounded to elongate patches of differing bulk composition which are interpreted as syn-sedimentary or diagenetic in origin.
- Early phlogopite and Al-poor amphibole define the penetrative, lamination-parallel, primary fabric. This is crenulated by micro-folds and crenulation cleavage in places; the axial planes to this fabric are aligned with the more elongate patches, the latter appearing to have acted as a focus for deformation.
- Amphibole ranges in composition from near pure tremolite to Mg-hornblende. Phyllosilicates show much less range in composition. Plagioclase is $\text{An}_{40}\text{-An}_{50}$

with locally more anorthite-rich cores; locally it is spongy-looking and contains albite patches.

- Modelling the assemblages as end-member minerals in TKCMASCH reveals complex equilibrium relationships. Zoisite-bearing and plagioclase + calcite bearing assemblages constrain X_{CO_2} , indicating differences in X_{CO_2} on the millimetric scale of the compositional domains and very local buffering effects.
- The lack of phases such as grossular, vesuvianite and diopside, together with the local scale of fluid buffering, indicates lack of extensive infiltration of very water-rich fluids.
- The thermal stability of certain assemblages, particularly phl + cc + tr + kf limits the maximum metamorphic temperatures to $\sim 520^\circ\text{C}$, based on the T- X_{CO_2} section at pressures of no more than about 7 kbars. This is inconsistent with the higher temperatures of $\sim 600^\circ\text{C}$ recorded by pelite and some amphibole-plagioclase geothermometry.

Part 2

Strontium, carbon and oxygen isotope geochemistry of
Dalradian limestones and dolostones

Chapter 5

Stable and strontium isotopes in carbonate rocks

In this Chapter:

- ❖ An outline of the primary controls on C, O and Sr isotopes in carbonate rocks and the subsequent alteration of primary isotope signatures

5.1 Introduction

In Parts Two and Three of this thesis, I present and discuss the carbon, oxygen and strontium isotope compositions of the Dalradian carbonate rocks discussed in Chapter 3.

As an introduction to the isotope work in Chapters 6, 7, 9 and 10, I outline briefly below the primary controls on C, O and Sr isotope compositions of carbonate rocks and the ways in which the compositions may be altered subsequently by diagenesis and metamorphism.

5.2 Applications of stable and strontium isotopes in studies of carbonate rocks

Carbonate rocks and minerals are particularly suitable for isotopic studies because their C, O and Sr contents and isotopic compositions are fixed during precipitation of carbonate-bearing phases and depend on the physical and chemical environment in which the carbonate formed.

Primary or near-primary isotope signatures are commonly preserved in carbonate rocks. Even though chemical and mineralogical alteration often occurs during diagenesis and metamorphism, the primary signatures are rarely completely destroyed (e.g. Graham et al 1998; Lewis et al 1998). These signatures and the ways in which they have been altered can therefore be used to elucidate the nature of depositional and diagenetic processes and wider environmental conditions.

With these matters in mind, three areas of research on stable isotopes in carbonate rocks relevant to the work in this thesis are outlined below.

5.2.1 Secular variation of $\delta^{13}\text{C}$ and $^{87}\text{Sr}/^{86}\text{Sr}$ in seawater

Studies of C, O and Sr isotopes and their secular variations in unmetamorphosed Phanerozoic and Precambrian carbonate rocks have been the key to elucidating secular variation in $\delta^{13}\text{C}$ and $^{87}\text{Sr}/^{86}\text{Sr}$ compositions of seawater, the evolution of the hydrosphere, atmosphere and biosphere and the links between these 'spheres' and global tectonics over geological time (e.g. Mackenzie and Piggott, 1981; Tucker and Wright, 1990, and references therein; Wilkinson et al., 1985).

The large volume of recent, wide-ranging work on stable and strontium isotopes in Neoproterozoic (c.1100 – 543Ma) carbonate-rich successions from around the world (Table 5.1) is directly relevant to the work discussed in this thesis. This body of work indicates that some of the largest known shifts in seawater and sedimentary C, O and Sr occurred during this time and were coeval world-wide (Kaufman and Knoll, 1995). As well as being of environmental significance, the accumulated isotopic data are also of great value in efforts to correlate the disparate carbonate sequences both within and between cratonic regions (e.g. Fairchild and

Reference	Unit(s)	Age	Ma	Location	Isotope data	Cation data
Asmerom et al 1991	Shaler Group	Riphean	~770-880	Victoria Island, Canada	O, Sr	Ca, Mg, Mn, Sr
Bartley et al 1998	Platonovskaya Formation	Late Vendian - Lower Cambrian		Turukhansk, Western Siberia	C, O	
Burns et al 1994	Huqf Group	Late Vendian	~560 - 540	Central Oman	C, O, Sr	Mn, Sr
Derry et al 1989	Polarisbreen & Akademikerbreen Groups	Riphean - Vendian	800 - <610	Svalbard & East Greenland	Sr	
Gorokhov et al 1995	Numerous	Riphean - Lower Cambrian	<1100	Olenek, Turukhansk & Ura uplifts Siberia	O, Sr	Ca, Fe, Mg, Mn
Iyer et al 1995	Bambui Group	?Riphean		Sao Francisco Basin Brazil	C, O, Sr	
Knoll et al 1986	Numerous	Riphean - Vendian	<800	East Greenland & Svalbard	C	
Kaufman et al 1991	Nama & Witte Groups	Vendian - basal Cambrian	<610	Kalahari Craton, Southern Namibia	C	
Kennedy 1996	Several	Vendian	~610	Australia	C, O, Sr	Ca, Fe, Mn, Sr
Kimura et al 1997	Kahar & Soltanieh Formations and others	Vendian - Cambrian	<610	Elburz Mountains, North Iran	C	
Kuznetsov et al 1997	Inzer Formation	Upper Riphean	>610	Bashkir Anticlinorium, Southern Urals	Sr	Fe, Mg, Mn, Rb, Sr
Misi and Veizer 1998	Una and Bambui Groups	?Riphean		Ireze & Sao Francisco Basins, Brazil	C, O, S, Sr	Al, Fe, Mn, Sr
Narbonne et al 1994	Windermere Supergroup	Vendian	<610	Yukon Territory, Northwestern Canada	C, O, Sr	
Narbonne and Aitken 1995	Mackenzie Mountains & Windermere Supergroups	Riphean - Vendian	1100 - ?550	Yukon Territory, Northwestern Canada	C, Sr	
Saylor et al 1998	Nama & Witte Groups	Vendian - basal Cambrian	<610	Kalahari Craton, Southern Namibia	C	
Tucker 1986a	Several	Vendian - Lower Cambrian	<610	Morocco	C	
Tucker 1986b	Pahrump Group	?Late Riphean - Vendian		Death Valley, California	C	Ca, Mg, Fe, Mg, Mn, Na, Sr
Yang et al 1999	Sinian System	Vendian - Lower Cambrian	<610	Yangste Region, South China	C, O, Sr	Mn, Sr

Table 5.1 Recent detailed studies of stable and strontium isotopes in late Proterozoic (Riphean - Vendian) carbonate-bearing successions from around the world. Shaded references have been used in the construction of Neoproterozoic carbon and strontium seawater curves in Chapters 6 and 7

Hambrey, 1995; Kaufman and Knoll, 1995; Kennedy, 1996; Misi and Veizer, 1998; Narbonne et al., 1994; Yang et al., 1999).

5.2.2 Quantification of the effects of diagenesis on carbonate rock isotope compositions

In this thesis, I concentrate on elucidating the likely effects of fluid-rock interaction during metamorphism. However, fluid-rock interaction during diagenesis of carbonate sediments is likely to be much more significant than metamorphic fluid-rock interaction and may have significant effects on the isotope chemistry of the original sediment. Large volumes of fluid are generally involved in turning initially highly porous, unlithified carbonate sediment with an unstable mineralogy into a compact, low-magnesium limestone of low-porosity, or into dolostone (e.g. Bathurst 1975). Such large-scale fluid-rock interaction commonly may have a very significant effect on limestone chemistry, particularly during dolomitisation (e.g. Tucker and Wright, 1990). Note that the high porosity of unlithified carbonate sediment contrasts very strongly with the low porosity and permeability of buried limestones prior to metamorphism (see Chapter 8).

The geochemistry of diagenesis is a large and complex field (e.g. Bathurst, 1975; Tucker and Wright, 1990) and more than cursory consideration is beyond the scope of this thesis. However, as an illustration of the likely geochemical effects of diagenesis on the limestones and the likely fluid volumes involved, I very briefly review work by Banner and Hanson (1990), who have quantified the geochemical effects of water-rock interaction in limestones specifically during diagenesis. This is

particularly important with regard to the potential for decoupling Sr, O and C isotope systems from one another.

Banner and Hanson (1990), in recognising the advances made in quantifying fluid-rock interaction in igneous and metamorphic rocks (e.g. Graham et al 1987), have formulated equations in which mass-balance and equilibrium isotope partitioning relationships are used to determine carbonate isotope and elemental concentrations before and after infiltration of and equilibration with a fluid phase.

The results of their modelling are cast in terms of fluid-rock ratios, so are similar in essence to the early attempts to model fluid-rock interaction in metamorphic systems (Graham et al 1987). These are less useful than fluid flux estimates, but at least give an indication of the likely fluid volumes required. The results also highlight the disparate behaviour of O, C and Sr isotopes during diagenesis. Shifts of *c.* 8 ‰ in whole-rock calcite $\delta^{18}\text{O}$ may be achieved by fluid-rock ratios of < 10 , whilst similar shifts in $\delta^{13}\text{C}$ and shifts of 0.012 in $^{87}\text{Sr}/^{86}\text{Sr}$ will require fluid-rock ratios of at least 10^3 to 10^4 where the fluids are seawater or riverwater. The critical point is that orders of magnitude more fluid are required to shift C and Sr isotopes significantly, compared to O, because C and Sr are *usually* at very low concentrations in diagenetic fluids. Furthermore, the fluid-rock ratios are conservative estimates because they are based on fluids which are far from isotopic and chemical equilibrium with carbonate sediment. The effects will be mitigated where the diagenetic fluid is similar to that in which the carbonate sediment was originally precipitated, for example, during marine diagenesis (see also section 5.5). The volumes of fluid estimated to be involved during diagenesis are very large compared to reasonable estimates of volumes of fluid involved in metamorphic fluid-

rock interaction (e.g. Graham et al 1997). The corollary is that where high ($> 20 \text{ ‰}$) $\delta^{18}\text{O}$ values are maintained in metamorphosed carbonate rocks, the likelihood is that the values of $\delta^{13}\text{C}$ and $^{87}\text{Sr}/^{86}\text{Sr}$ are unlikely to have been shifted significantly from their primary values, by either diagenetic or metamorphic fluid-rock interaction.

5.2.3 Stable and Sr isotopes in metamorphic fluid-rock interaction studies of carbonate rocks

Primary isotopic compositions of sedimentary carbonate rocks are markedly different to those of siliciclastic and igneous rocks and the bulk of crustal fluids. Interaction between crustal fluids (whose C, O and Sr isotopic compositions are buffered mainly by silicate-rich rocks), and carbonate rocks, results in modification of isotopic signatures in the latter. Variation of stable and strontium isotopes in carbonate rocks at grain, outcrop and regional scales, have become critically important in efforts to understand and quantify metamorphic fluid fluxes, fluid-rock interaction processes, mechanisms and time-scales (Bickle and Baker, 1990; Blattner and Lassey, 1990; Cole and Graham, 1994; Fein et al., 1994; Graham et al., 1998; Lewis et al., 1998; Rye et al., 1976). The development of models for quantification of metamorphic fluid-rock interaction and their application in this study are discussed further in Chapter 8.

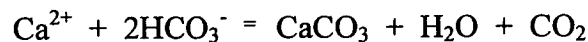
In the following section, I discuss the primary controls on C, O and Sr isotope compositions of carbonates. Discussion of these controls and their implications with regard to the chemical evolution of Dalradian and other Neoproterozoic carbonate rock is given in Chapters 7, 8, 9 and 10.

5.3 Controls on the carbon isotope composition of carbonate rocks

The two main reservoirs for carbon are (Hoefs, 1987; Tucker and Wright, 1990):

- a) organic compounds, such as CH₄, fossil fuels and native carbon (*the reduced reservoir*), and
- b) CO₂, HCO₃⁻ and carbonate minerals (*the oxidised reservoir*).

Each of these reservoirs has very distinct isotopic compositions resulting from very different controlling reaction mechanisms. However, the two reservoirs are linked by atmospheric CO₂, the latter being central to both photosynthesis and abiogenic carbonate precipitation. Kinetic effects dominate in biological processes, such as photosynthesis (Hoefs, 1987), resulting in enrichment of ¹²C in the organic matter and strongly negative δ¹³C values relative to PDB. The δ¹³C of decayed or buried organic matter lies in the range -5 to -35‰ (Hoefs, 1987, p.37, figure 11; Tucker and Wright, 1990). In contrast, the precipitation of carbonate is dominated by thermodynamically controlled chemical exchange between CO₂ and HCO₃⁻ in the following net reaction for carbonate precipitation (Hoefs, 1987, p.35):



This reaction holds for precipitation governed abiotically or by biological consumption of carbon dioxide. The resulting carbonate is strongly enriched in ¹³C relative to organic matter. The largest isotopic fractionation here is between CaCO₃ and CO₂, the latter being depleted in ¹³C by about 8 - 10‰ relative to PDB (Hoefs, 1987). Modern marine carbonates have δ¹³C of around 0‰, as do many ancient

carbonates, whereas the $\delta^{13}\text{C}$ composition of freshwater carbonates varies from around 0‰ to c. -15‰.

The dominant control on the isotopic composition of carbonate sediments is the isotopic composition of Total Dissolved Carbon (TDC) in seawater. TDC itself is a function of the balance between the organic and carbonate carbon reservoirs. Organic matter is generally oxidised rapidly by respiration in oxic environments and is thus rapidly recycled.

This rapid recycling has maintained $\delta^{13}\text{C}$ in marine carbonates at around 0‰ over much of geological time. However, positive and negative excursions in $\delta^{13}\text{C}$ of many ancient marine carbonates indicate that the isotopic composition of TDC has varied significantly at times. Retention of isotopically light carbon in organic matter buried in sediments results in enrichment of ^{13}C in TDC and positive $\delta^{13}\text{C}$ values in carbonates. This is typical during periods of high organic productivity and is also taken to imply high sedimentation rates. Such positive excursions in $\delta^{13}\text{C}$ are known to have occurred at several times in the geological past, notably in the early Proterozoic (Melezhik and Fallick, 1996; Melezhik et al., 1997), the Neoproterozoic (particularly the Riphean) (e.g. Derry et al., 1992), the Precambrian-Cambrian boundary (Tucker, 1986), and during the Permian (e.g. Mackenzie and Piggott, 1981). The direct link between positive carbonate $\delta^{13}\text{C}$ and sedimentation rate is disputed by some (e.g. Derry et al., 1992; Kaufman and Knoll, 1995). These authors argue that the important factor determining high carbonate $\delta^{13}\text{C}$ is not so much high productivity and sedimentation rate as the *fraction* of organic C which is buried. The positive excursion in $\delta^{13}\text{C}$ through much of the Riphean is coupled with relatively low estimates of organic productivity and low $^{87}\text{Sr}/^{86}\text{Sr}$ (see below), suggesting low

sedimentation rates. Conversely, negative excursions in $\delta^{13}\text{C}$ values for carbonates arise during periods of markedly *decreased* organic productivity, when ^{12}C is not taken into the organic reservoir, but retained in TDC.

During the Neoproterozoic, the two main negative excursions are generally considered to be associated with the Varanger (~600 Ma) and Sturtian (~740 Ma) glacial epochs. The former, particularly, is viewed by some as a very major glacial episode, during which the earth was covered in sea-ice to very low latitudes and organic productivity collapsed through lack of sunlight to drive photosynthesis in the oceans – this is the controversial ‘snowball earth’ hypothesis (e.g. Hoffman et al., 1998b). This ‘catastrophic’ view of the Varangan glaciation is disputed by others on both geochemical (Kennedy et al., 1998) and geophysical grounds (Meert and Van der Voo, 1994).

The secular variation of carbonate $\delta^{13}\text{C}$ through the Neoproterozoic has attracted a very great deal of attention in recent years because of the rise in complex metazoa, some of which were becoming skeletalised. There is now a very considerable literature characterising variations in $\delta^{13}\text{C}$ in Neoproterozoic carbonate sequences worldwide and discussing their environmental and biogeochemical significance (e.g.: (Bartley et al., 1998; Brasier et al., 1992; Brasier et al., 1996; Derry et al., 1992; Fairchild et al., 1990; Fairchild and Spiro, 1987; Hoffman et al., 1998a; Kaufman and Knoll, 1995; Kimura et al., 1997; Knoll et al., 1986; Saylor et al., 1998; Tucker, 1986; Yang et al., 1999). Because variations in carbonate $\delta^{13}\text{C}$ are considered to reflect the state of global carbon isotope composition, the secular variations also have considerable correlative value, in a manner similar to $^{87}\text{Sr}/^{86}\text{Sr}$ (see below and Chapter 7).

5.4 Oxygen isotopes in carbonate rocks and fluids

Oxygen is the most abundant element on earth and is ubiquitous in rocks, fluids and natural gases. The range in $\delta^{18}\text{O}$ of natural phases varies from about +40 to -40‰

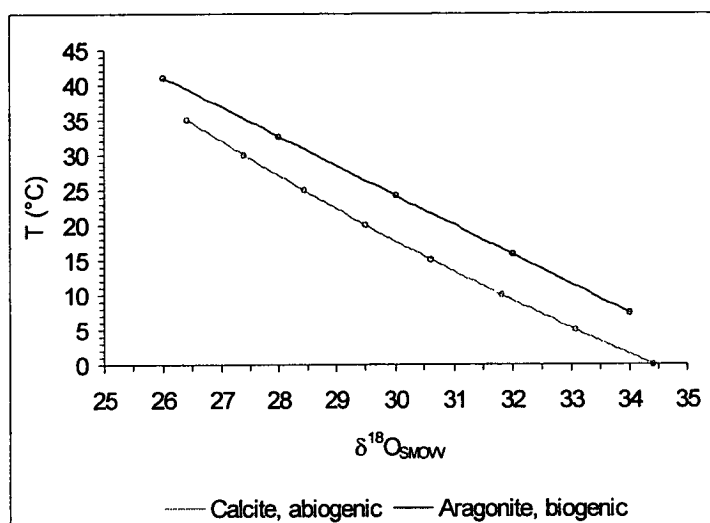


Figure 5.1 $\delta^{18}\text{O}_{\text{SMOW}}$ of calcite- H_2O and aragonite- H_2O as a function of temperature, assuming $\delta^{18}\text{O}_{\text{water}} = 0$.

For calcite: $\alpha = 2.78(10^6 T^{-2}) - 2.89$
(Freidman & O'Neil 1977)

For aragonite: $T(^{\circ}\text{C}) = 20.6 - 4.34(\delta^{18}\text{O}_{\text{PDB}} - \delta^{18}\text{O}_{\text{W}})$
(Grossman & Ku 1986)

(Hoefs, 1987, figure 12).

Modern marine waters vary in $\delta^{18}\text{O}$ by about 1.5‰ around 0‰, although waters from marginal seas and brackish or evaporating lagoons may exhibit greater variation.

Marine carbonates

are conspicuously ^{18}O -rich compared to other abundant sedimentary rocks as ^{18}O is

strongly fractionated into the carbonate phase. For example, for calcite precipitated in equilibrium with water at 25°C, $\Delta^{18}\text{O}_{\text{calcite-water}}$ is 28.4‰, assuming $\delta^{18}\text{O}_{\text{SMOW}}$ of water is 0‰ (Friedman and O'Neil, 1977). The $\delta^{18}\text{O}$ value for primary marine carbonates ranges over about 25-35‰ and is largely a function of temperature (e.g. Bathurst, 1975, Veizer, 1992), as shown for ^{18}O fractionation in calcite and aragonite in Figure 5.1. Although some carbonate sediments deposited from highly evaporated fresh water may have $\delta^{18}\text{O}$ values higher than marine carbonate sediments (Hoefs,

1987), fresh water carbonates minerals generally have lower ^{18}O abundances relative to marine carbonates. Evaporation of seawater results in fractionation of ^{16}O into the water vapour (e.g. Hoefs, 1987, page 179; Veizer, 1992). Resulting meteoric waters are thus depleted in ^{18}O relative to seawater, even though precipitation is slightly enriched in ^{18}O relative to the vapour phase. At low latitudes, where most carbonate sediment is deposited, this depletion is limited to about 5‰ (Veizer, 1992), but is more extreme at higher latitudes.

Most siliciclastic sedimentary and igneous rocks (and their metamorphic equivalents) have $\delta^{18}\text{O}$ values considerably lower than primary carbonate rocks, ranging between about 5 and 15‰ (e.g. Hoefs (1987). Furthermore, fluids evolved by dewatering and devolatilisation of silicate rocks during burial and metamorphism or derived from igneous melts are, therefore, strongly depleted in ^{18}O relative to carbonate rocks.

The primary ^{18}O enrichment of marine carbonate rocks means that they are far from oxygen isotope equilibrium with silicate rocks, their associated fluids and meteoric waters. Any interaction with silicate rocks (and associated fluids) and meteoric waters during diagenesis and metamorphism is likely to reduce the ^{18}O abundance of carbonate rocks over a range of length scales (e.g. Baker et al., 1989; Graham et al., 1998; Lewis et al., 1998; Rye et al., 1976). Studies of length scale variations in the ^{18}O composition of carbonates from metamorphic terrains (such as those cited above) have played a central role in the quantification of fluid-rock interaction in metamorphic rocks (see Chapter 8). Carbonate $\delta^{18}\text{O}$ data have also been used widely to assess the degree of diagenetic and/or metamorphic alteration in limestones and dolostones, thereby helping to elucidate the extent to which primary

signatures of C and Sr isotopes have been preserved. I discuss and make use of this criterion further in Chapters 6 and 7.

Unlike carbon, oxygen isotope fractionation between phases is strongly a function of temperature (Veizer, 1992). This characteristic has led to the development of a range of geothermometers based on oxygen isotope fractionation between phases. These have been used mainly to determine seawater palaeotemperatures in ancient limestones (e.g. Veizer, 1992) and equilibration temperatures in metamorphic rocks (e.g. Valley, 1986). However, oxygen isotope fractionations between phases in high grade metamorphic rocks are now known to be variably reset on slow cooling, where diffusion rates become significant relative to the rate of cooling, particularly in the presence of a fluid phase (e.g. Eiler et al., 1993; Eiler et al., 1995a).

5.5 Strontium isotopes in carbonate rocks and seawater

Although the $Sr_{\text{liquid/solid}}$ partition coefficient varies with carbonate mineralogy and other factors, strontium isotopes are not significantly fractionated when Sr is incorporated into carbonate minerals. Thus, the $^{87}\text{Sr}/^{86}\text{Sr}$ ratio of calcite, aragonite or dolomite reflects that in the fluid from which the carbonate was precipitated.

Furthermore, because Rb is effectively excluded from marine carbonates, there is no addition of ^{87}Sr in the carbonate by radioactive decay of ^{87}Rb following precipitation.

Marine carbonate minerals therefore record the extant seawater Sr isotopic composition at the time of precipitation, making them potentially accurate monitors of the variation of seawater $^{87}\text{Sr}/^{86}\text{Sr}$ with time. However, this initially direct correspondence between seawater and carbonate Sr isotope ratios will be perturbed

by early diagenesis to a greater or lesser extent (Veizer, 1989). Thus, it is necessary to understand the likely extent of such effects before $^{87}\text{Sr}/^{86}\text{Sr}$ ratios of carbonates in rocks can be interpreted in terms of seawater $^{87}\text{Sr}/^{86}\text{Sr}$.

5.5.1 Strontium isotopes in seawater

Although the $^{87}\text{Sr}/^{86}\text{Sr}$ ratio of seawater varies significantly through geological time, this ratio is fixed in the oceans at any instant in time. This constancy arises for several reasons. Seawater is isotopically homogenous with respect to Sr isotopes because Sr residence time in the oceans ($4\text{--}5 \times 10^6$ years) is three orders of magnitude longer than the time oceans take to mix (about 10^3 years) (Elderfield, 1986; Veizer, 1989). Furthermore, because seawater Rb concentration is about $0.1 \mu\text{mol}$ (120ppb) (Elderfield, 1986; Tucker and Wright, 1990) and Sr residence time is four orders of magnitude shorter than the half-life of ^{87}Rb decay (4.99×10^{10} years (Elderfield, 1986; Veizer, 1989), seawater $^{87}\text{Sr}/^{86}\text{Sr}$ ratios are not affected by radioactive decay of dissolved, marine Rb.

5.5.2 Controls on modern seawater Sr isotopic composition

The two main 'endmember' sources of dissolved Sr supplied to the oceans are the continents and the mantle (Figure 5.2). Each of these have had markedly different Sr isotopic compositions since differentiation of the earth's crust resulted in the crust being enriched and the mantle depleted in ^{87}Rb . Subsequently, bulk continental $^{87}\text{Sr}/^{86}\text{Sr}$ has evolved to a value of about 0.716 today (Tucker and Wright, 1990, figure 6.24) whereas present day $^{87}\text{Sr}/^{86}\text{Sr}$ of the mantle and oceanic crust is about 0.703 (Veizer, 1989).

The principal continental sources of Sr are river and groundwater discharge, although the contribution of the latter is estimated at only about 5% of river runoff (Veizer, 1989). The total estimated annual flux of Sr from these sources is estimated at $4.68 \times 10^{12} \text{ g yr}^{-1}$, although the groundwater flux is very poorly constrained and its importance is questioned (Palmer and Edmond, 1989; Veizer, 1989). The estimated

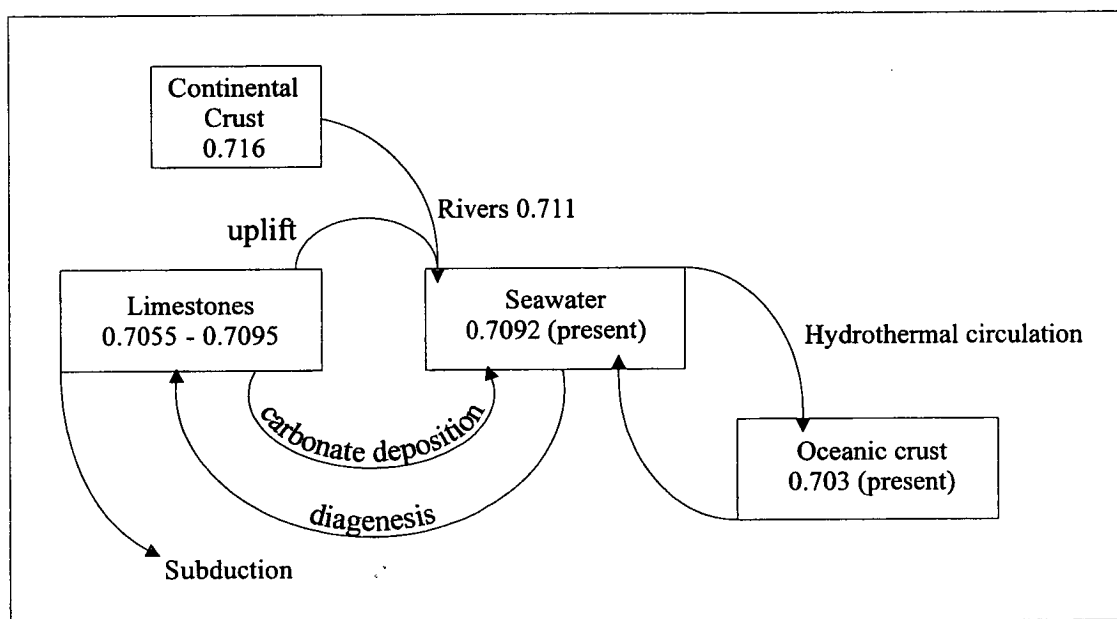


Figure 5.2 Box model illustrating primary controls on carbonate and seawater strontium isotope ratios and the major sources of marine Sr. After Elderfield 1986.

bulk $^{87}\text{Sr}/^{86}\text{Sr}$ ratios for the two continental sources have been estimated at 0.7101 ± 5 (Veizer, 1989, pages 146-147). However, Palmer and Edmond (1989) estimate average $^{87}\text{Sr}/^{86}\text{Sr}$ of the dominant riverine flux to be considerably higher, at ~ 0.7119 .

The mantle source of Sr can also be divided into two components. The primary mantle source arises from hydrothermal fluid-rock interaction at ocean ridge systems. Palmer and Edmond (1989) estimate hydrothermal $^{87}\text{Sr}/^{86}\text{Sr}$ in the range $0.7029 - 0.7047$, encompassing the value of 0.7035 ± 5 quoted by Veizer (1989) and references therein. Elderfield (1986) observes that seawater entering the

hydrothermal system with $^{87}\text{Sr}/^{86}\text{Sr} \sim 0.7092$ leaves as hydrothermal fluid with the $^{87}\text{Sr}/^{86}\text{Sr}$ of ~ 0.703 , the process being one of isotopic exchange without significant mass transfer. Veizer (1989) estimates the primary hydrothermal flux of Sr to be $\sim 0.42 \pm 0.19 \times 10^{12} \text{ g yr}^{-1}$. The second and much less important hydrothermal ocean crustal source is considered to result from low temperature ($< 70 - 100^\circ\text{C}$) submarine weathering processes. These processes principally involve volcanic rocks and result in a $^{87}\text{Sr}/^{86}\text{Sr}$ ratio of 0.7064 for this source (Palmer and Elderfield, 1985). Although difficult to quantify precisely, the estimated flux of Sr from this sources is considered to be an order of magnitude lower than the primary hydrothermal flux (Veizer, 1989).

Veizer (1989), and Palmer and Edmond (1989) also consider the flux of Sr from diagenetic porewaters, predominantly in deep ocean sediments. Veizer (1989) estimates this flux to be $\sim 0.26 \times 10^{12} \text{ g yr}^{-1}$ and quotes $^{87}\text{Sr}/^{86}\text{Sr}$ to be 0.7087, based on the work of Elderfield and Gieskes (1982) and Palmer and Elderfield (1985). Although Veizer's estimate of the diagenetic Sr flux is more than half the primary hydrothermal flux, Palmer and Edmond (1989) consider it relatively minor with regard to the overall seawater Sr budget.

The balance between the fluxes of strontium from continental and mantle sources results in seawater $^{87}\text{Sr}/^{86}\text{Sr}$ ratios intermediate between them. For example, during the Phanerozoic, $^{87}\text{Sr}/^{86}\text{Sr}$ has ranged between ~ 0.7065 and ~ 0.7095 (Burke et al., 1982, figure 1), with variation occurring on a range of timescales. In the Neoproterozoic, $^{87}\text{Sr}/^{86}\text{Sr}$ ratios have varied more widely from ~ 0.7048 to ~ 0.7095 (see Chapters 7 and 8).

The influence of the two main strontium fluxes is buffered by strontium added from carbonate rocks, as they are relatively rich in Sr compared to most other

rocks. Dissolution of limestones on continents will add abundant Sr with lower $^{87}\text{Sr}/^{86}\text{Sr}$ ratios to meteoric waters, thereby significantly lowering the $^{87}\text{Sr}/^{86}\text{Sr}$ ratio of the waters (Tucker and Wright, 1990). Furthermore, carbonate sediments undergoing diagenesis and in diffusive or advective connection with seawater will buffer the seawater $^{87}\text{Sr}/^{86}\text{Sr}$ ratio directly in a similar manner.

The balance between the continental and mantle sources of seawater Sr is largely considered to be a function of the balance between sea floor spreading and continental erosion (*e.g.* Asmerom et al., 1991). Thus, seawater Sr isotope data potentially provide evidence for the nature of large-scale crustal dynamics. The extent to which it is possible to interpret Dalradian carbonate rock Sr isotope compositions in terms of Dalradian seawater chemistry and the tectonic regimes prevailing during sedimentation will be considered in Chapters 6 and 7.

5.5.3 *The effects of diagenesis on carbonate $^{87}\text{Sr}/^{86}\text{Sr}$*

Because the partition coefficient for strontium between calcite and water is < 1 and because diagenesis commonly involves recrystallisation of high-Mg calcite or aragonite to calcite, Sr is partitioned into diagenetic fluids. Analyses of Deep Sea Drilling Project cores reveal a gradual decline in Sr content with age over 100 Myr in low magnesium calcite sediments (Veizer, 1989, figure 5), showing that Sr is gradually stripped out of the carbonate during diagenesis. The decline in carbonate Sr is matched by a 5 to 6 fold increase in Sr in porewaters in the sediment pile (Veizer, 1989, figure 6). In addition, the temporal/depth variation of the Sr isotope signal is smoothed by the mixing of porewaters as diagenetically precipitated carbonate takes on the signal of the ambient porewater (Veizer, 1989). However, diagenetic

perturbation of the Sr isotope signal is probably at a minimum in deep-sea carbonate sediments, since the porewaters will be largely seawater.

Early diagenesis is potentially more likely to affect Sr isotope ratios of shallow water carbonates deposited in marginal seas. In these circumstances, meteoric waters with significantly different Sr isotopic compositions to seawater may be important during diagenesis. In general, such fluids will contain more radiogenic Sr and thus may shift the carbonate Sr ratio to more ^{87}Sr -enriched values during diagenetic dissolution and recrystallisation. Shifts to *lower* $^{87}\text{Sr}/^{86}\text{Sr}$ ratios are possible if meteoric fluids are in contact with young volcanic rocks, but are only rarely observed (Veizer, 1989, page 151). This effect is likely to be more important where carbonate sediments are dominated by metastable high-Mg calcite or unstable aragonite, as these phases readily convert to low-Mg calcite during diagenesis. Dissolution of these phases will also markedly enhance porosity, increasing the porewater volume and, thereby, the potential to shift Sr isotope ratios in the precipitated low-Mg calcite still further. Any shift in Sr isotope ratio will depend on the amount of meteoric water interacting with the carbonate sediments during diagenesis, and its Sr concentration and isotope ratio. The effects may be mitigated by the fact that stabilisation of the sediment mineralogy is usually relatively rapid ($\sim 10^5$ years) and because the Sr concentrations of meteoric waters are usually at parts-per-billion level. Furthermore, during diagenesis, pore fluids will become swamped in carbonate-derived Sr which will buffer the fluid isotopic composition to near original sediment values, despite the fact that the bulk of the Sr would be removed by fluid flow (Veizer, 1989).

The problem of initial marine diagenesis shifting original Sr isotope ratios may be exacerbated further by dolomitisation (Veizer, 1989), deep burial diagenesis and metamorphism; overall, $^{87}\text{Sr}/^{86}\text{Sr}$ in the carbonate will be shifted to higher values. For example, ^{87}Sr may be exchanged between carbonate and silicate impurities in carbonate rocks where such impurities are abundant and contain appreciable ^{87}Rb , such as mica and feldspar. Cements precipitated from infiltrating deep basin fluids are likely to have Sr isotopic compositions rather different to the original marine carbonate rocks (*e.g.* Sullivan et al., 1990). Infiltrating metamorphic fluids are likely to have Sr isotopic ratios similar to pelitic rocks and are likely to contain not only abundant excess radiogenic ^{87}Sr , but also ^{87}Rb . It is clear from at least two studies that Sr isotope ratios of meta-carbonate rocks can be disturbed by metamorphic fluid infiltration (Bickle and Chapman, 1990; Bickle et al., 1995). Both Sr and Rb will be preferentially partitioned into the fluid phase and may be exchanged with either carbonate and silicate phases in the carbonate rocks, potentially adding more excess ^{87}Sr to the carbonate rock. The corollary is that bulk-rock Sr isotope compositions of thoroughly lithified and possibly metamorphosed carbonate rocks potentially *may* bear only a distant relationship to the original carbonate $^{87}\text{Sr}/^{86}\text{Sr}$ ratio and, by analogy, that of seawater.

Despite these diagenetic and metamorphic constraints on the preservation of original Sr isotope ratios in carbonate rocks, it is clear from numerous studies that $^{87}\text{Sr}/^{86}\text{Sr}$ ratios in many ancient carbonate rocks are close to those of coeval seawater. Thus, ancient marine limestones are critically important in revealing variations in the oceanic $^{87}\text{Sr}/^{86}\text{Sr}$ ratio over geological time (*e.g.* Elderfield, 1986; Tucker and Wright, 1990; Veizer, 1989; Veizer and Compston, 1976; Veizer et al., 1983). Sr

isotope ratios of Dalradian carbonate rocks are discussed and interpreted in detail within this context in Chapter 6.

5.5.4 Importance of scale of $^{87}\text{Sr}/^{86}\text{Sr}$ heterogeneity and sampling scale

The scale on which samples have been obtained for isotope analysis has been a very important factor in considering and undertaking the practical work for this study. As discussed elsewhere in this thesis, the case for microsampling and analysis with regard to C and O isotopes in carbonate rocks is now clear from a wide range of studies. The same is also true for Sr isotopes: Kaufman et al (1993) show that luminescent and non-luminescent calcites from a hand specimen have $^{87}\text{Sr}/^{86}\text{Sr}$ ratios different by about 4 in the fourth decimal place (their figure 3). This variation is significantly above the analytical precision and brackets the whole-rock analysis by ± 2 . The value of Sr isotopes in the study of all carbonate rocks is clear but is hampered by sampling scale problems. The facility to be able to analyse Sr ratios in-situ on the scale of a few tens of microns, say by ion probe, is highly desirable. As has happened particularly with oxygen isotope data (e.g. Lewis 1999), microanalytical data would advance considerably our understanding of the spatial distribution of Sr isotopes and improve our understanding of their behaviour during diagenesis and metamorphism.

5.6 Summary and conclusions

- Carbonate rocks are of particular value in elucidating geochemical processes and phenomena because they contain abundant C, O and Sr with very distinctive isotopic compositions

- Carbonate isotope compositions are a function of the aqueous geochemistry of the environment in which they formed; where primary isotope signatures can be determined, they can be used to elucidate these environmental conditions and the way they have changed with time
- In this respect, stable isotope studies have been fundamentally important in advancing understanding of Neoproterozoic geology and geochemistry; carbon, oxygen and strontium isotope data have:
 - a) revealed the Neoproterozoic to be a period of very marked change in global stable and strontium isotope signatures, reflecting significant changes in balances of and fluxes between C, O and Sr reservoirs,
 - b) aided correlation of disparate Neoproterozoic carbonate-bearing sequences from around the world, and
 - c) elucidated the hydrospheric and atmospheric conditions under which metazoan life began to develop and ultimately flourish in the latest Proterozoic and earliest Cambrian
- Because C and O are important elements in biological processes, geochemical and biological phenomena must be causally related and may ultimately be a function of crustal dynamics and tectonics, for which Sr is an important isotopic tracer
- Variations of oxygen and, to a lesser extent, strontium isotope ratios in carbonate rocks have been particularly important in elucidating processes and mechanisms of metamorphic fluid rock interaction

- Studies have ranged from the regional to grain scale. In particular, studies of oxygen isotopes have helped constrain and elucidate:
 - d) the extent of metamorphic isotopic equilibrium and retrograde resetting by diffusion
 - e) temperatures of metamorphism
 - f) metamorphic fluid pathways and their scales and links with deformation
 - g) timing and time-scale of fluid-rock interaction
 - h) the nature, composition and sources of crustal fluids, and
 - i) the relative importance of advection and diffusion as infiltration mechanisms.

The remainder of this thesis focuses on the strontium, carbon, oxygen and isotopic compositions of Dalradian carbonate rocks. In particular, I

- a) document the isotope geochemistry of Dalradian carbonate rocks
- b) elucidate the effects of metamorphism on stable isotope signatures
- c) quantify these effects with regard to metamorphic fluid-rock interaction
- d) determine the extent to which primary isotope signatures have been preserved in carbonate rocks which have undergone mid greenschist to amphibolite facies metamorphism
- e) compare and contrast their stable isotope characteristics with other Neoproterozoic carbonate-bearing sequences, particularly those occurring on the margins of Laurentia.

Chapter 6

The Strontium element and isotope geochemistry of Dalradian Limestones

In this chapter:

- ❖ Strontium isotope sample preparation
- ❖ Evidence for primary $^{87}\text{Sr}/^{86}\text{Sr}$ signatures in Dalradian limestones
- ❖ $^{87}\text{Sr}/^{86}\text{Sr}$ constraints on the age of the Dalradian

6.1 Introduction

In this chapter I present original data on the strontium elemental abundances and isotope compositions of a number of lithostratigraphically important Dalradian limestones and dolostones through the Dalradian, from near the base of the Grampian Group to the Leny Limestone.

I examine the relationships between $^{87}\text{Sr}/^{86}\text{Sr}$ and strontium, manganese and aluminium abundances, and oxygen and carbon isotope data to determine the extent to which primary or near-primary $^{87}\text{Sr}/^{86}\text{Sr}$ compositions have been preserved in the limestones.

The data are used to elucidate the role of diagenesis in controlling the isotope and trace element chemistry of the limestones and dolostones and to estimate $^{87}\text{Sr}/^{86}\text{Sr}$ of the seawater from which the limestones were precipitated.

In the latter part of the chapter, I use the strontium isotope data of the limestones to constrain the lower depositional age of the Dalradian and to corroborate the correlation of the Port Askaig Tillite with Varangan and Marinoan tillites.

Fifty-seven samples for strontium isotope analysis come from nine major limestone and two dolostone units within the Grampian, Appin and Argyll Groups. Dolostones were also sampled from the Staosnaig Phyllite Formation on Colonsay (Chapter 2).

The sampled localities extend across Scotland and Northern Ireland (Figure 6.1); details are given in Table 6.1. A description of sampling details and the lithology and geological setting of the units from which the sample are taken is given in Appendices A.1 and A.2.

6.2 Strontium isotope analysis

This section discusses determination of the $^{87}\text{Sr}/^{86}\text{Sr}$ of the limestones and dolostones. The presumption is that, subject to certain criteria discussed below, $^{87}\text{Sr}/^{86}\text{Sr}$ ratios in the limestones and dolostones are *potentially* interpretable as ‘initial’, with values at or close to $^{87}\text{Sr}/^{86}\text{Sr}$ of the seawater in which the rocks were formed

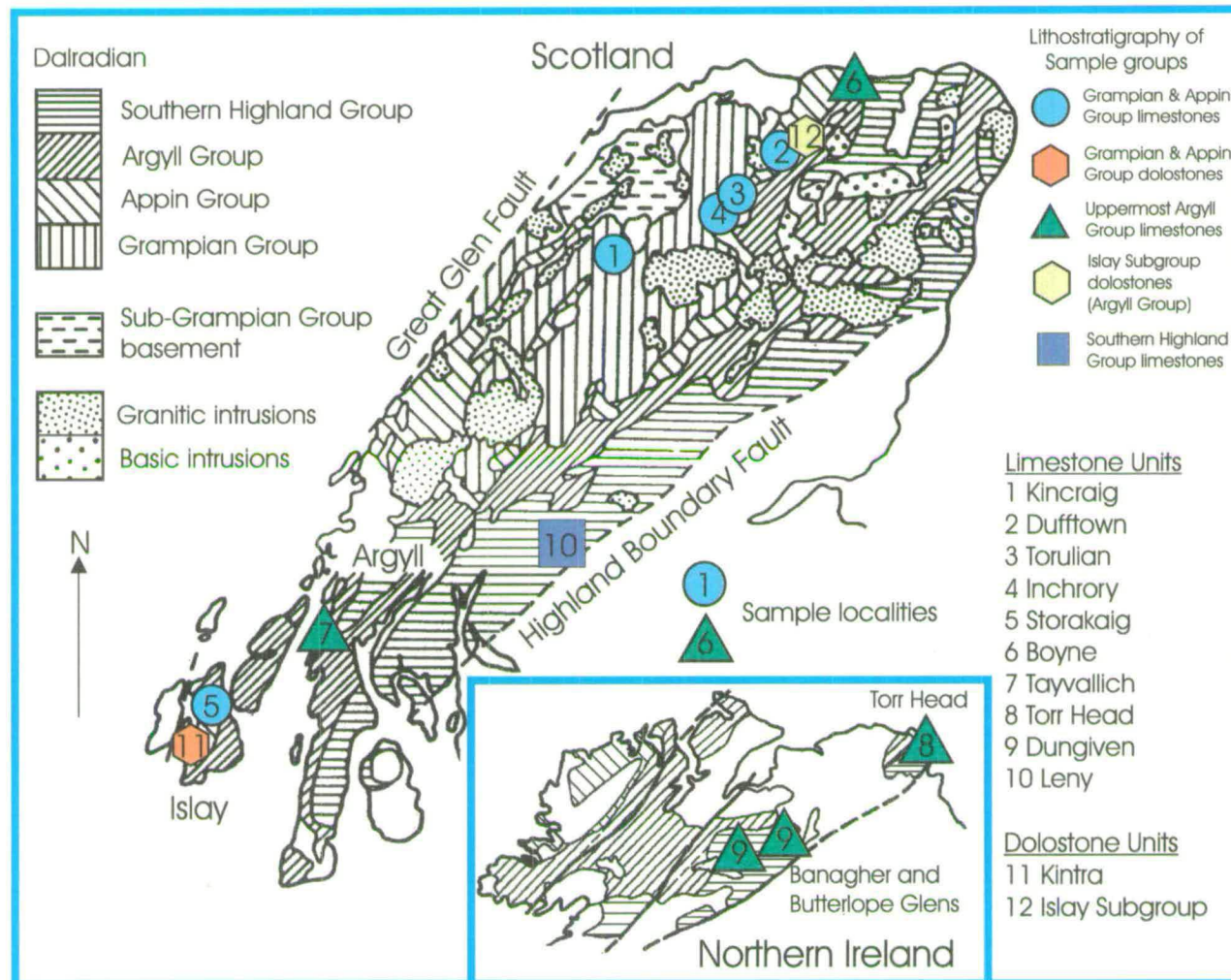


Figure 6.1 Location of samples of Dalradian limestones and dolostones
(See Figure 2. for location of the Staosnaig Phyllite Formation dolostones on Colonsay)

Sampled unit	Subgroup	Locality	NGR	Samples	Sample #	
Limestones						
Southern Highland Group						
Leny Limestone		Leny Quarry, Callander	NN 615 098	2	HY1362, 64	
Uppermost Argyll Group (Tayvallich and equivalents)						
Scotland						
Boyne Limestone	Tayvallich	Boyne Bay, Banffshire coast	NJ 616 660	4	HY147-50	
Tayvallich Limestone		Port an Sgadain, Tayvallich	NR 707 846	7	T1-T6b	
Northern Ireland						
Torr Head Limestone		Torr Head, Co. Antrim	H 232 406	2	HY1348-9	
Dungiven Limestone		Butterlope Glen, Co. Tyrone	C 493 047	1	HY1350	
		Banagher Glen, Co. Tyrone	C 668 047	1	HY1351	
Appin Group						
Islay						
Storakaig Limestone Member	Blair Atholl	Ballygrant Quarry, Islay	NR 395 666	5	HY1333-7	
Mainland Scotland						
Inchrory Limestone		A939 road section, Tomintoul	NJ 151 194	5	HY56-60	
Torulian Limestone (Bed)	Ballachulish	Bridge of Avon, River Avon section	NJ 1496 2019	1	HY43	
		Carn Daimh, Glenconglass	NJ 1749 2259	1	HY47	
		Glen Suie	NJ 2766 2595	1	HY360	
		Tor Elick, Glen Fiddich	NJ 3166 3202	1	HY393	
			NJ 3186 3205	1	HY394	
Dufftown Limestone Member		Parkmore Quarry, Dufftown	NJ 334 411	5	HY67-71	

Table 6.1 Lithostratigraphic and location details of samples selected for Sr isotope analysis (see also Figure 6.1)

Grampian Group						
Coire nan Laogh Semipelite Formation (Kinraig Limestone')	}	Corrieyairack	Kinraig Quarry	NH 8213 0640	2	HY1072-73
			Kinraig Farm, Dunnachton track	NH 8214 0577	2	SMS446-7
			Allt na Baranachd	NH 7959 0586	2	SMS448-9
Dolostones						
Islay Subgroup, Argyll Group						
<u>Northeast Scotland</u>						
Nochty Semipelite & Limestone Ladder Hills Formation Auchnahyle Formation	}	Islay	Water of Nochty	NJ 2933 1622	2	HY85, 86
			Carn Dulach, Ladder Hills	NJ 2407 1767	1	HY72
			Muckle Fergie Burn	NJ 1656 1397	1	GX1064
Ballachulish Subgroup, Appin Group						
<u>Islay</u>						
Kintra Dolostone		Ballachulish	Port Alsaig, Kintra, Mull of Oa		4	HY1338-41
Uncertain lithostratigraphical status (?Dalradian, possibly Ballachulish Subgroup)						
<u>Colonsay</u>						
Staosnaig Phyllite Formation	}	Unknown	Rubha an Dobhrain, Scalasaig,	NR 4045 9482	2	HY1342-43
			Geodha nan Ceann, Scalasaig	NR 4030 9475	2	HY1344-45
				NR 3997 9461	2	HY1347-47
Total:					57	

Table 6.1 Lithostratigraphic and location details of samples selected for Sr isotope analysis (see also Figure 6.1)

6.2.1 Methods

- The chemical method used here to extract Sr from carbonate has been adapted from that of Gorokhov et al. (1995), and references therein. A key part of this method is the treatment of powdered samples with ammonium acetate (NH_4OAc) solution, which is considered to remove readily soluble elements, including Sr, adhering to the surface of crystal lattices (Gao, 1990; Walls et al., 1977). Both limestones and dolostones were treated by this method.
- The following pilot study was carried out to determine the efficacy of this method in yielding the $^{87}\text{Sr}/^{86}\text{Sr}$ value of the carbonate fraction alone. Three separate experiments were undertaken on samples T1 and T2 from the Tayvallich Limestone. Procedural details, reagents and results for standard NBS 987 are given in Appendix B. The results are given in Table 6.2.

Experiment 1 (E1): The 1 M NH_4OAc leach yields Sr significantly more radiogenic than the subsequent acetic acid (HOAc) digestions, indicating that ‘surface’ radiogenic Sr is present and is removed by this procedure.

Digestion in 1 M HOAc yields leachates with $^{87}\text{Sr}/^{86}\text{Sr}$ ratios slightly lower than for digestion in 0.1 M HOAc , but the respective values for the different HOAc concentrations are within error of each other for each of the samples T1 and T2. The values resulting from 1 M HOAc digestion are considered to be the $^{87}\text{Sr}/^{86}\text{Sr}$ ratios of the carbonate component alone and the lowest determinable by these techniques.

Complete digestion of dominantly silicate residues remaining after HOAc digestion of samples T1 and T2 yields Sr with very radiogenic values. Most

Experiment	Sample	Reagent	Conc.	Material	$^{87}\text{Sr}/^{86}\text{Sr}$	$\pm (\times 10^{-6})$	Comments
1	T1	NH ₄ OAc	1	Leachate	0.708954	16	Preliminary leach before digestion in 0.1M acetic acid.
1	T1	HOAc	0.1	Leachate	0.708870	17	Following 1MNH4OAc wash
1	T1	HOAc	1	Leachate	0.708851	20	
1	T1	HF	40% v/v	Residue	0.713218	14	
1	T2	NH ₄ OAc	1	Leachate	0.709451	17	
1	T2	HOAc	0.1	Leachate	0.709263	18	
1	T2	HOAc	1	Leachate	0.709203	20	as above
1	T2	HF	40% v/v	Residue	0.729213	16	
2	T1	HOAc	1	Leachate	0.708866	16	Straight Acetic acid digestion with no preliminary NH ₄ OAc washing.
2	T1	HCl	2.5	Leachate	0.708924	17	Straight digestion
3	T1	NH ₄ OAc	0.15	Leachate	0.709147	16	Wash at 1N (0.15M) strength; cf 1M NH ₄ OAc wash for T1
3	T1	HOAc	1	Leachate	0.708858	20	Digestion after 0.15M NH ₄ OAc wash
3	T2	NH ₄ OAc	0.15	Leachate	0.709604	16	Wash; cf same experiment for T1
3	T2	HOAc	1	Leachate	0.709201	23	Digestion after 0.15M NH ₄ OAc wash

Table 6.2 Results of Sr isotope pilot study undertaken on Tayvallich samples T1 & T2

importantly, these data serve to show that the limestones are extremely heterogeneous with respect to $^{87}\text{Sr}/^{86}\text{Sr}$. Taken with the NH_4OAc and HOAc leachate results, these data show that 'bulk' $^{87}\text{Sr}/^{86}\text{Sr}$ ratios for these rocks would be difficult to interpret correctly.

Experiment 2 (E2): Sample T1 was digested in 1 M HOAc and 2.5 M HCl without pre-treatment in NH_4OAc . These results show that digestion in 1 M HOAc alone yields $^{87}\text{Sr}/^{86}\text{Sr}$ within error but a little higher than for 1 M HOAc digestion after pre-treatment in NH_4OAc in E1. Digestion in 2.5 M HCl yields $^{87}\text{Sr}/^{86}\text{Sr}$ within error of the NH_4OAc leachate in E1. Given the data from the HF digestion in E1, this result is clearly an uninterpretable mixed signal dominated by the carbonate but with a contribution from Sr leached from the silicate component.

Experiment 3 (E3): Gorokhov et al. (1995) appear to have used 1 N NH_4OAc in their work; the equivalent molar concentration is 0.15. As this concentration is only about $1/7^{\text{th}}$ that used in E1, it was important to establish whether leaching in 1 N (0.15 M) NH_4OAc would have the same efficiency in removing surface bound $^{87}\text{Sr}/^{86}\text{Sr}$. The data here show that leaching in 0.15 M NH_4OAc , followed by 1 M HOAc digestion yields $^{87}\text{Sr}/^{86}\text{Sr}$ ratios for the calcite inseparable from those in T1, confirming that 0.15 M NH_4OAc is as equally efficient at removing unwanted Sr as when used at 1M concentration.

6.2.2 Pilot study: conclusions

- 0.15 M NH_4OAc removes a radiogenic Sr component; this treatment, combined with HOAc digestion, yields the $^{87}\text{Sr}/^{86}\text{Sr}$ ratio of Sr of the carbonate fraction alone
- The chances of these $^{87}\text{Sr}/^{86}\text{Sr}$ values being contaminated by Sr from other phases is limited by the abundance of Sr in the carbonate (see below) which will buffer $^{87}\text{Sr}/^{86}\text{Sr}$ to that of the calcite
- Complete digestion of the silicate residue following HOAc dissolution of the calcite in the pilot samples shows the carbonates are very heterogeneous with respect to $^{87}\text{Sr}/^{86}\text{Sr}$.
- The data indicate clearly that Sr isotopes in the limestones have not been homogenised during metamorphism and that radiogenic ^{87}Sr has not been significantly incorporated into carbonate.

On the basis of the results from the pilot study, all the carbonate rock samples were leached in 0.15M NH_4OAc , followed by 1M HOAc digestion of the carbonate fraction.

6.3 Strontium isotope results

The $^{87}\text{Sr}/^{86}\text{Sr}$ ratios for the limestones and dolostones analysed in this study are given in Table 6.3, along with data for elemental abundances of Mn, Sr, Rb and Al and $\delta^{13}\text{C}$ and $\delta^{18}\text{O}$ isotope compositions. The data for the limestones are also summarised graphically in Figure 6.2, along with summary lithostratigraphy.

Sample	$^{87}\text{Sr}/^{86}\text{Sr}$	error	Sr	1/Sr	Mn*	Mn/Sr	Rb	Rb/Sr	Al*	$\delta^{18}\text{O}_{\text{SMOW}}$	$\delta^{13}\text{C}_{\text{PDB}}$
Southern Highland Group											
<i>Leny Limestone</i>											
HY1362	0.711859	0.000030	796	0.00126	n.a.		0.03	0.00004	n.a.	15.7	-4.6
HY1364	0.712781	0.000017	815	0.00123	n.a.		0.04	0.00005	n.a.	18.3	-5.0
Median:	0.712320		806				0.04			17.0	-4.8
Argyll Group											
<i>Boyne Limestone</i>											
HY147	0.709018	0.000016	4607	0.00022	310	0.07	13	0.0028	36998	19.0	1.9
HY148	0.709451	0.000016	2695	0.00037	697	0.26	43	0.0160	21437	19.8	0.5
HY149	0.709305	0.000014	3534	0.00028	697	0.20	23	0.0065	39962	18.2	-1.9
HY150	0.709297	0.000016	3225	0.00031	542	0.17	52	0.0161	13444	18.2	1.2
Median:	0.709301		3380		620		33		29218	18.6	0.9
<i>Tayvallich Limestone</i>											
T1	0.708851	0.000020								20.7	-2.3
T2	0.709203	0.000020								15.4	-0.7
T3	0.708960	0.000017								16.6	1.1
T4	0.709096	0.000018								16.3	1.1
T5	0.709467	0.000020								17.5	1.5
T6a	0.709637	0.000017								17.7	1.6
T6b	0.708969	0.000016								17.3	2.0
Median:	0.709096										
<i>Torr Head Limestone</i>											
HY1348	0.708857	0.000039	1865	0.00054	144	0.08	26	0.0139	16302	14.8	7.4
HY1349	0.708810	0.000032	2115	0.00047	144	0.07	20	0.0095	10480	17.9	7.5
Median:	0.708834		1990		144		23		13391	16.4	7.4

Table 6.3 $^{87}\text{Sr}/^{86}\text{Sr}$, $\delta^{18}\text{O}$ and $\delta^{13}\text{C}$ & Sr, Mn, Rb and Al analyses of selected Dalradian carbonate rocks

Sample	$^{87}\text{Sr}/^{86}\text{Sr}$	error	Sr	1/Sr	Mn*		Rb	Rb/Sr	Al*	$\delta^{18}\text{O}_{\text{SMOW}}$	$\delta^{13}\text{C}_{\text{PDB}}$
<i>Dungiven Limestone</i>											
HY1350	0.708220	0.000033	265	0.00377	3890	14.68	3	0.0113	17732	13.4	7.0
HY1351	0.708745	0.000043	2299	0.00043	216	0.09	12	0.0052	8363	23.4	7.3
Median:	0.708483		1282		2053		8		13048	18.4	7.2
<i>Islay Subgroup Dolostones associated with diamictites</i>											
HY85	0.711169	0.000027	181	0.00552	1626	8.98	2	0.0110	8045	16.3	-0.3
HY86	0.709947	0.000023	162	0.00617	1239	7.65	2	0.0123	6934	19.2	-0.8
HY72	-		167		929	5.56	1	0.0060	6775	16.5	-1.2
GX1064	-		245		774	3.16	16	0.0653	11803	22.1	-0.8
Median:	0.710558		174		1084		2		7490	17.8	-0.8
Appin Group											
<i>Storakaig Limestone, Islay (= Inchrory Limestone)</i>											
HY1333	0.706902	0.000029	2014	0.00050	72	0.04	6	0.0030	2170	23.2	4.1
HY1334	0.706744	0.000041	2622	0.00038	72	0.03	4	0.0015	1429	-	-
HY1335	0.706854	0.000040	2495	0.00040	288	0.12	4	0.0016	1641	23.0	4.4
HY1336	0.706790	0.000019	1937	0.00052	360	0.19	4	0.0021	1482	23.7	3.9
HY1337	0.706651	0.000034	1881	0.00053	360	0.19	3	0.0016	847	25.1	4.1
Median:	0.706790		2014		288		4		1482	23.4	4.1
<i>Inchrory Limestone</i>											
HY56	0.707213	0.000016	1471	0.00068	310	0.21	21	0.0143	13709	22.1	6.6
HY57	0.706923	0.000018	2104	0.00048	77	0.04	12	0.0057	10533	22.2	7.5
HY58	0.706940	0.000016	2135	0.00047	155	0.07	16	0.0075	10798	23.3	7.2
HY59	0.706863	0.000016	2211	0.00045	155	0.07	9	0.0041	5558	23.7	7.7
HY60	0.706974	0.000021	1880	0.00053	77	0.04	18	0.0096	9580	23.5	7.4
Median:	0.706932		2104		155		16		10533	23.3	7.4

Table 6.3 $^{87}\text{Sr}/^{86}\text{Sr}$, $\delta^{18}\text{O}$ and $\delta^{13}\text{C}$ & Sr, Mn, Rb and Al analyses of selected Dalradian carbonate rocks

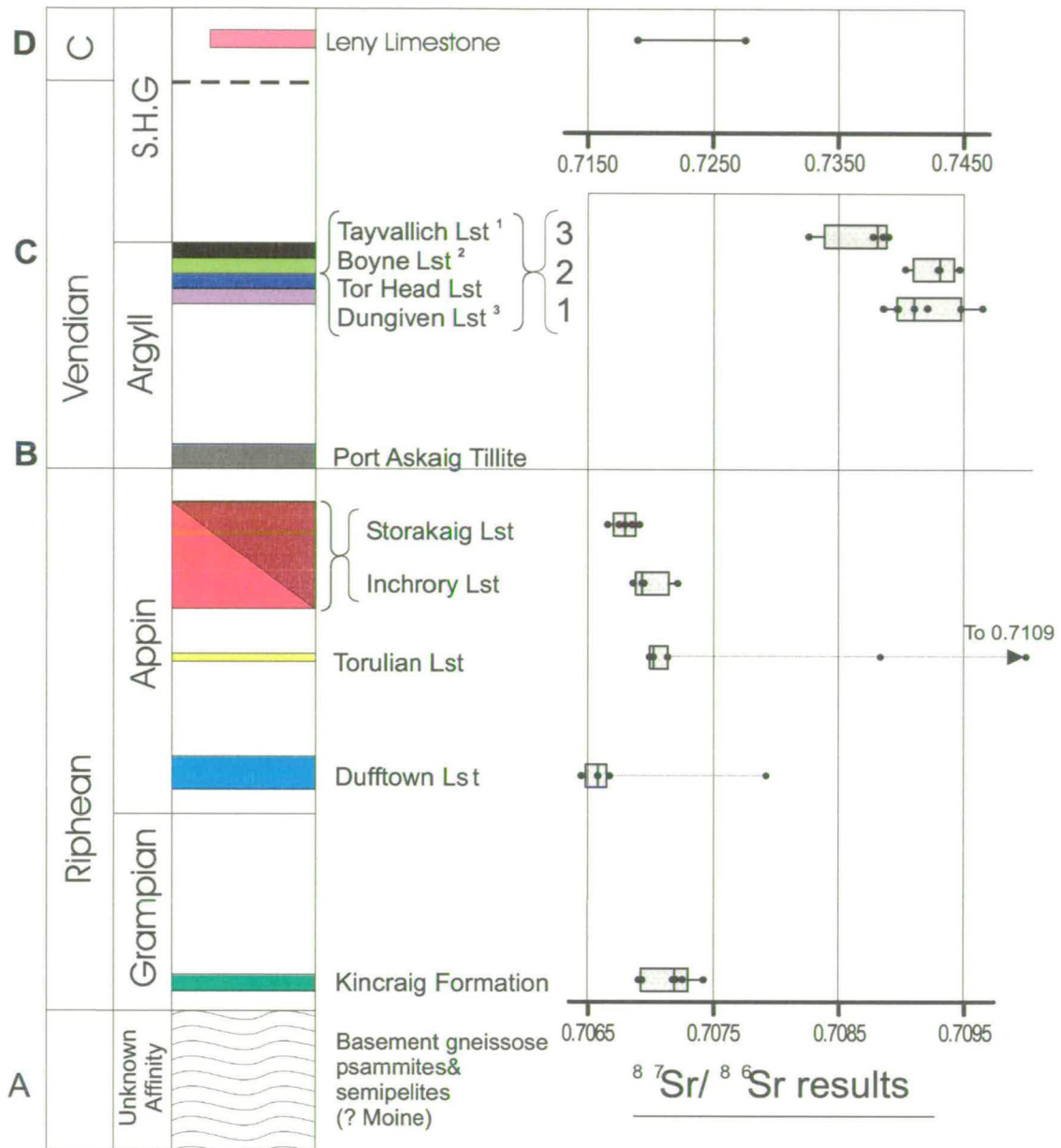
Sample	⁸⁷ Sr/ ⁸⁶ Sr	error	Sr	1/Sr	Mn*		Rb	Rb/Sr	Al*	δ ¹⁸ O _{SMOW}	δ ¹³ C _{PDB}
Torulian Limestone											
HY43	0.710927	0.000018	776	0.00129	310	0.40	9	0.0116	2488	16.2	1.9
HY47	0.708813	0.000017	822	0.00122	232	0.28	4	0.0049	10215	17.4	2.6
HY360	0.707131	0.000017	1316	0.00076	77	0.06	4	0.0030	53	21.1	3.5
HY393	0.706986	0.000016	593	0.00169	155	0.26	6	0.0101	9051	18.5	3.5
HY394	0.707017	0.000016	2178	0.00046	155	0.07	4	0.0018	1588	19.5	4.0
Median :	0.707017		822		155		4		2488	18.5	3.5
Dufftown Limestone											
HY67	0.706667	0.000017	1253	0.00080	310	0.25	12	0.0096	5240	19.3	4.8
HY68	0.706583	0.000017	1217	0.00082	155	0.13	7	0.0058	3017	19.0	4.6
HY69	0.707884	0.000018	714	0.00140	232	0.33	11	0.0154	3123	20.4	3.7
HY70	0.706448	0.000017	1712	0.00058	155	0.09	4	0.0023	1429	19.5	4.7
HY71	0.706576	0.000016	950	0.00105	542	0.57	7	0.0074	2752	18.8	4.7
Median :	0.706583		1217		232		7		3017	19.3	4.7
Kintra Dolostone, Islay											
HY1338	0.720428	0.000036	234	0.00427	648	2.77	51	0.2179	32023	18.4	0.9
HY1339	-		273	0.00366	648	2.37	41	0.1502	27947	17.9	0.6
HY1340	0.721641	0.000028	456	0.00219	576	1.26	62	0.1360	27629	17.8	0.2
HY1341	0.721066	0.000030	304	0.00329	576	1.90	54	0.1776	29006	17.7	0.5
Median :	0.721066		289		612		53		28477	17.8	0.6
Grampian Group											
Kincraig Formation limestones											
HY1072	0.706927	0.000018	1785	0.00056	155	0.09	8	0.0045	9157	17.9	7.8
HY1073	0.706905	0.000016	1764	0.00057	155	0.09	9	0.0051	9136	21.1	8.3
SMS446	0.707203	0.000016	1948	0.00051	432	0.22	2	0.0010	8839	13.4	-1.1
SMS447	0.707177	0.000018	1975	0.00051	360	0.18	1	0.0005	8310	17.0	-3.7
SMS448	0.707414	0.000017	1545	0.00065	576	0.37	12	0.0078	9633	6.3	2.3
SMS449	0.707256	0.000017	1614	0.00062	432	0.27	16	0.0099	10321	10.7	3.8
Median :	0.707190		1775		396		9		9147	15.2	3.0

Table 6.3 $^{87}\text{Sr}/^{86}\text{Sr}$, $\delta^{18}\text{O}$ and $\delta^{13}\text{C}$ & Sr, Mn, Rb and Al analyses of selected Dalradian carbonate rocks

Sample	$^{87}\text{Sr}/^{86}\text{Sr}$	error	Sr	1/Sr	Mn*		Rb	Rb/Sr	Al*	$\delta^{18}\text{O}_{\text{SMOW}}$	$\delta^{13}\text{C}_{\text{PDB}}$
Colonsay (affinity uncertain)											
Staosnaig Phyllite Formation											
HY1342	0.721335	0.000021	243	0.00412	288	1.19	28	0.1152	19161	18.5	-2.3
HY1343	0.722974	0.000025	135	0.00741	288	2.13	55	0.4074	26412	-	-
HY1344	0.720797	0.000031	227	0.00441	288	1.27	28	0.1233	23501	-	-
HY1345	0.720309	0.000034	171	0.00585	360	2.11	35	0.2047	30488	18.0	-1.8
Sample	$^{87}\text{Sr}/^{86}\text{Sr}$	error	Sr	1/Sr	Mn*		Rb	Rb/Sr	Al*	$\delta^{18}\text{O}_{\text{SMOW}}$	$\delta^{13}\text{C}_{\text{PDB}}$
HY1346	0.721194	0.000028	422	0.00237	792	1.88	46	0.1090	28053	20.4	-1.9
HY1347	0.715548	0.000041	366	0.00273	1513	4.13	60	0.1639	40227	16.9	-3.9
Median :	0.720996		235		324		41		27233	18.3	-2.1

Table 6.3 $^{87}\text{Sr}/^{86}\text{Sr}$, $\delta^{18}\text{O}$ and $\delta^{13}\text{C}$ & Sr, Mn, Rb and Al analyses of selected Dalradian carbonate rocks

Lithostratigraphy



S.H.G: Southern Highland Group
C: Cambrian

Age constraints

A: basement gneisses > 800 Ma
B: Port Askaig Tillite c. 600 Ma
C: Tayvallich Volcanics 595 ± 4 Ma
D: Leny Limestone trilobites ~ 515 Ma

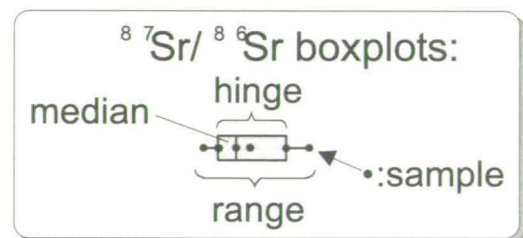


Figure 6.2 Strontium isotope data for Dalradian limestones, plotted with the limestone lithostratigraphy.

Note change of scale for the Leny Limestone

6.3.1 Limestones

The difference in $^{87}\text{Sr}/^{86}\text{Sr}$ between Grampian and Appin Group limestones on the one hand and 'Tayvallich' limestones on the other is striking, as is the consistency *amongst* sample groups above and below the Port Askaig Tillite. The results can be summarised as follows:

- All but three Appin Group samples have similar $^{87}\text{Sr}/^{86}\text{Sr}$ ratios in the range ~0.7064 – 0.7074.
- $^{87}\text{Sr}/^{86}\text{Sr}$ in the 'Tayvallich' limestones is significantly more radiogenic, ranging from ~0.7082 – 0.7096.
- $^{87}\text{Sr}/^{86}\text{Sr}$ in the Leny Limestone is the most radiogenic of any in the limestones..
- The carbonate $^{87}\text{Sr}/^{86}\text{Sr}$ data in the limestones are largely independent of lithology and metamorphism: compare $^{87}\text{Sr}/^{86}\text{Sr}$ values for Inchrory Limestone, metamorphosed at amphibolite facies and the Storakaig Limestone, metamorphosed at greenschist Facies. This independence suggests strongly that the control on carbonate $^{87}\text{Sr}/^{86}\text{Sr}$ is primary.

6.3.2 Dolostones

Carbonate in the dolostones contains much more strongly radiogenic Sr than the limestones (Table 6.3). This is particularly highlighted by comparing the Kintra Dolostone (Ballachulish Subgroup) (~0.7211) with its probable lithostratigraphical equivalent, the Dufftown Limestone (~0.7066). The Kintra dolostones and dolostones from the Staosnaig Phyllite Formation, Colonsay, (0.7210) have very similar $^{87}\text{Sr}/^{86}\text{Sr}$. However, they are both significantly more radiogenic than the Islay

Subgroup dolostones associated with tillites from the NE Grampian Highlands (~0.7106).

6.4 Interpretation of $^{87}\text{Sr}/^{86}\text{Sr}$ data

In the following sections, I discuss the Mn, Sr, Al, ^{18}O and ^{13}C compositions of the limestones and dolostones samples with regard to the interpretation of $^{87}\text{Sr}/^{86}\text{Sr}$. The concentrations of these components in each of the samples are given in Table 6.3.

6.4.1 Geochemical criteria for determining preservation of initial $^{87}\text{Sr}/^{86}\text{Sr}$ ratios in carbonate rocks

- Strontium concentrations and control of original mineralogy
- Mn concentration and its relationship to Sr
- Oxygen isotopes
- Rubidium and Aluminium

Diagenesis and metamorphic fluid rock interaction can introduce exotic Sr with a very different isotopic composition to that in the primary carbonate, thereby disturbing the primary $^{87}\text{Sr}/^{86}\text{Sr}$ signature. High Sr contents and $\delta^{18}\text{O}_{\text{V-SMOW}} (> 23\text{‰})$, Mn/Sr ratios < 1 (Kennedy et al., 1998) and low ($< 700\text{ppm}$) Mn contents (Denison et al., 1994) are considered to be criteria helpful in identifying samples least altered by diagenesis and metamorphism (e.g. Marshall, 1992) and, like many other studies (e.g. as listed in Table 6.4), these criteria have been used here to assess post-depositional alteration. The validity and applicability of these criteria are critically

Authors	Sr	ppm Rb*	Rb/Sr	ppm Mn	Mn/Sr	$\delta^{18}\text{O}_{\text{PDB}}^{\S}$	$\delta^{18}\text{O}_{\text{SMOW}}^{\S}$
Asmerom et al 1991	32 - 520	0.006 - 0.897	≤ 0.01	--	≤ 2	> -8	> 22
Brasier et al 1996	> 500	--	--	--	< 0.6	--	--
Denison et al 1994	> 900	--	--	< 300	< 0.5	--	--
Derry et al 1989	201 - 2474	0.05 - 1.49	$\leq 5 \times 10^{-3} +$	--	--	--	--
Gorokhov et al 1995	--	--	--	--	~ 2	--	--
Kaufman et al 1993	52 - 3705	--	$< 0.001 +$	--	< 1.5	> -11	> 20
Kaufman & Knoll 1995	--	--	--	--	$< 2 - 3$	> -10	> 21
Kennedy et al 1998	> 200	--	--	--	< 1	--	--
Kuznetsov et al 1997	160 - 605	--	--	10 - 50	< 0.5	--	--
Misi and Veizer 1998	$> 250 - 300$	--	--	--	≤ 0.2	> -7.5	> 23
Saylor et al 1998	--	--	--	--	< 2	> -10	> 21
Dalradian rocks in							
this study	ranges:	265 - 4607	1 - 52 ‡	0.0005 - 0.0161	72 - 3890**	0.03 - 14.7	--
	medians:	1881	9	0.010	232	0.15	--

** From XRF wt% data

* Rb in dissolved carbonate fraction

+ as $^{87}\text{Rb}/^{86}\text{Sr}$

‡ in Whole-rock (XRF); cf. Rb in carbonate fraction quoted by Asmerom et al 1991

§ To nearest ‰

Table 6.4 Comparison of geochemistry of Neoproterozoic carbonate rocks and quoted limiting values for Mn/Sr, $\delta^{18}\text{O}$ and $\delta^{13}\text{C}$ identifying 'unaltered' limestones

examined before being used to determine the extent of alteration of $^{87}\text{Sr}/^{86}\text{Sr}$ in Dalradian carbonate rocks.

6.4.2 Strontium concentration

Strontium concentration in carbonate rocks is determined by the primary carbonate mineralogy and the subsequent diagenetic path. In primary carbonate minerals, Sr concentrations decrease in the order: aragonite > high Mg calcite > low Mg calcite > dolomite. Aragonite commonly contains several thousand ppm Sr (Bathurst, 1975); modern oolites are particularly rich in Sr (8-10,000 ppm).

Sr abundances are reduced during fluid-rock interaction because the partition coefficient for Sr between carbonate and fluid is < 1 (e.g. $K_{\text{Sr, calcite}} \sim 0.13$ (Tucker, 1990, page 295, figure 6.10). Thus, conversion of aragonite with several thousand ppm Sr to low Mg calcite reduces Sr concentrations to several hundred to one or two thousand ppm. Diagenesis of primary high and low Mg calcite will yield carbonate rocks with Sr concentrations of a few tens to low hundreds of ppm. Dolomites formed early after aragonitic sediments commonly retain high Sr concentrations of several hundred ppm, whereas those replacing diagenetic calcite will have very low Sr contents, typically of a few tens of ppm (e.g., Tucker and Wright, 1990).

Sr is abundant in nearly all the limestones in this study, generally exceeding 1000 ppm; the Boyne Limestone is particularly rich in Sr. Although dolostones have Sr concentrations an order of magnitude lower than those in the limestones, lying in the range 135 - 456 ppm, they are still high for dolostones (Tucker and Wright, 1990). The high Sr values for both limestones and dolostones suggest strongly that

aragonite was the dominant primary carbonate mineral (e.g., Tucker, 1990), although high Mg-Calcite may have also been present (e.g. Fairchild, et al., 1990). For example, although low in MgO, the Torulian Limestone, which has relatively lower Sr concentrations, contains very small dolomite crystals. Similar dolomite crystals in low-Mg calcites have been considered by Fairchild et al., *op. cit.* to be evidence for a high Mg-calcite primary mineralogy.

If aragonite was the dominant primary mineralogy in the dolostones, then it suggests that dolomitisation was an early phenomenon, because dolomitisation of diagenetic low Mg calcite would yield a dolostone with Sr contents a further order of magnitude lower than those determined here. Although strontium will be concentrated mostly within the carbonate component, it may also occur within phyllosilicates and feldspars, both of which occur in these carbonate rocks, particularly in the limestones. Sr derived from silicate minerals may be significantly enriched in ^{87}Sr due to decay of ^{87}Rb in the source area from which the silicate minerals were derived and may contaminate the Sr in the carbonate component, thereby modifying the carbonate $^{87}\text{Sr}/^{86}\text{Sr}$.

6.4.3 Manganese concentration

Mn is considered an important tracer for diagenetic effects in limestones because, when in reduced form as Mn^{II} , it is preferentially incorporated into calcite and dolomite during recrystallisation in the presence of fluids (e.g. $K_{\text{Mn,cc}} \sim 10$; Tucker and Wright, 1990, figure 6.10). Because Mn is concentrated in meteoric (10^4 ppm) and formation waters (10^3 ppm), but present in exceedingly low concentrations in

seawater (<0.001ppm), marine limestones are strongly depleted in Mn relative to all but marine diagenetic fluids (Tucker and Wright, 1990, figure 6.10). Recrystallisation of calcite during fluid-rock interaction will partition available Mn^{II} into the carbonate, whilst reducing Sr abundance, as discussed above. This indicates that the general effect of diagenesis is to push Sr-Mn relationships towards negative correlation. This effect will be particularly strong during diagenesis involving meteoric or formation waters.

Mn is also important in activating cathodoluminescence (CL) in carbonates, as long as the Fe/Mn ratio is $< \sim 100$ and $FeCO_3 < 2 \text{ wt\%}$ (*cf.* Tucker and Wright, *op. cit.*, page 355). Thus the presence and distribution of calcite relatively enriched in Mn is easily inferred from CL images (see also Chapters 3 and 9).

In the Dalradian carbonate rocks, Mn is generally present at concentrations of a few hundred to a few thousand ppm. Dolostones generally have higher Mn than the limestones, but values vary widely, even within groups of samples from the same unit.

6.4.4 Oxygen isotopes

$\delta^{18}O$ ranges from 6.3‰ to 25.1‰ for bulk calcite in the limestones, but is generally in excess of 18‰. Most Appin Group limestones consistently have the highest values, although two of the limestones from the Kincaig Formation have the lowest recorded in these data.

The Inchrory and Storakaig limestones have values ranging from 22.1 – 25.1‰, although values as high as 27 ‰ were recorded in ion microprobe analysis of

the Inchrory Limestone (Chapter 9). The dolostones have $\delta^{18}\text{O}$ values similar to the limestones, lying in the range 16.3 – 22.2‰.

6.4.5 Rubidium and Aluminium

Rb and Al are sequestered in feldspars and phyllosilicates in the carbonate rocks, so that Al_2O_3 can be used to assess the contents of these phases and the likely effect of any radiogenic Sr they contain from decay of ^{87}Rb on the calcite $^{87}\text{Sr}/^{86}\text{Sr}$. Although Rb occurs in concentrations up to ~65 ppm, the limestones generally have $\text{Rb} < 20$ ppm. The most notable exception is the Boyne Limestone, which has Rb up to 52 ppm. Al_2O_3 is present in Appin Group limestones in small amounts, generally < 2 wt%. Values are higher in the Torr Head and Dungiven limestones (1.58 – 3.35 wt%) and reach 7.55 wt% in the Boyne Limestone. The Kintra Dolostone and Staosnaig Phyllite Formation samples have Al_2O_3 between ~3.6 and 6.2 wt%.

The pilot Sr isotope study discussed above shows that the Tayvallich Limestone, at least, is strongly heterogeneous with respect to $^{87}\text{Sr}/^{86}\text{Sr}$ and that the silicate phases are strongly radiogenic. There is no reason to doubt, given the results for the other limestones, that this is not generally the case. The strong heterogeneity suggests that the effects of radiogenic Sr derived from Rb in silicate phases are limited, as will be discussed further below.

The potential for significant chemical changes during metamorphism is limited by very low porosity and by equilibrium dihedral angle constraints which prohibit the development of interconnecting pore networks (see Chapter 8). Even in metamorphic terrains where high fluxes of fluid rich in ^{87}Sr -enriched Sr can be demonstrated, changes in limestone Sr, O and Mn chemistry are generally only

preserved in boundary layers (Baker and Matthews, 1995; Bickle and Chapman, 1990; Bickle et al., 1997; Bickle et al., 1995). Furthermore, in such boundary layers, systematic changes in Sr isotopes are observed to occur only on scales of <50 cm, compared $10^2 - 10^3$ cm for oxygen (Bickle et al., *op. cit.*).

In carbonate rocks, the most significant shifts in chemistry are likely to occur during diagenesis, when primary and secondary porosity are generally at their highest and the rocks are still in connectivity with, or can be infiltrated by, surface-derived fluids.

Thus calcitic limestones with low Mn, high Sr (and thus low Mn/Sr ratios) and $\delta^{18}\text{O}$ of ~20 - 23‰ are considered least likely to have had their original $^{87}\text{Sr}/^{86}\text{Sr}$ ratios significantly affected during diagenesis. Bounding values for these geochemical criteria suggested by a number of workers are given in Table 6.4, together with summary values for the limestones in this study, included for comparison (see Table 6.3 for full data). Comparison of the Dalradian Mn, Sr, Rb and $\delta^{18}\text{O}$ data with values for criteria in Table 6.4 shows that most limestones lie within quoted limits, particularly with regard to Sr and Mn concentrations and Mn/Sr ratios, whereas the dolostones do not. Oxygen isotope ratios are commonly lower than the 20 - 23‰ value quoted as indicating a 'least altered' state, but, as discussed in more detail below, this may not seriously affect the interpretation of the Sr isotopes in the limestones.

6.4.6 Relationships between $^{87}\text{Sr}/^{86}\text{Sr}$, Sr, Mn, Rb, Al, $\delta^{18}\text{O}$ and $\delta^{13}\text{C}$

$^{87}\text{Sr}/^{86}\text{Sr}$ vs Sr

Figure 6.3a shows that $^{87}\text{Sr}/^{86}\text{Sr}$ increases consistently with *decreasing* Sr in several groups of limestones. This is consistent with alteration of $^{87}\text{Sr}/^{86}\text{Sr}$ during diagenesis in which the rocks suffered Sr loss. Recalling here the very high $^{87}\text{Sr}/^{86}\text{Sr}$ of the silicate component in the leaching experiments described above (Section 6.2.2; Table 6.3), the inverse relationship between $^{87}\text{Sr}/^{86}\text{Sr}$ and Sr content may reflect the influence of radiogenic Sr released from silicates during diagenesis. The limited dolostone data show no clear relationship between $^{87}\text{Sr}/^{86}\text{Sr}$ and Sr (Figure 6.3b).

$^{87}\text{Sr}/^{86}\text{Sr}$ vs Mn and the relationship between Mn and Sr

Mn is considered an important tracer for altered Sr isotopes in carbonate rocks, because Mn is enriched in diagenetic fluids from meteoric or deep basinal sources which have Sr isotope signatures very different to marine carbonates. The nature of the relationship between Mn and Sr and its isotopes is therefore important in determining the degree to which Mn reflects post-depositional alteration of Sr isotopes.

- *Limestones*

$^{87}\text{Sr}/^{86}\text{Sr}$ increases slightly with increasing Mn/Sr for the Boyne and Kincaig limestones, but other limestones show no clear correlation (Figure 6.4a).

Furthermore, even though Dungiven limestone sample HY1350 is the only sample with high Mn/Sr (>14), $^{87}\text{Sr}/^{86}\text{Sr}$ for this sample is significantly lower than the other

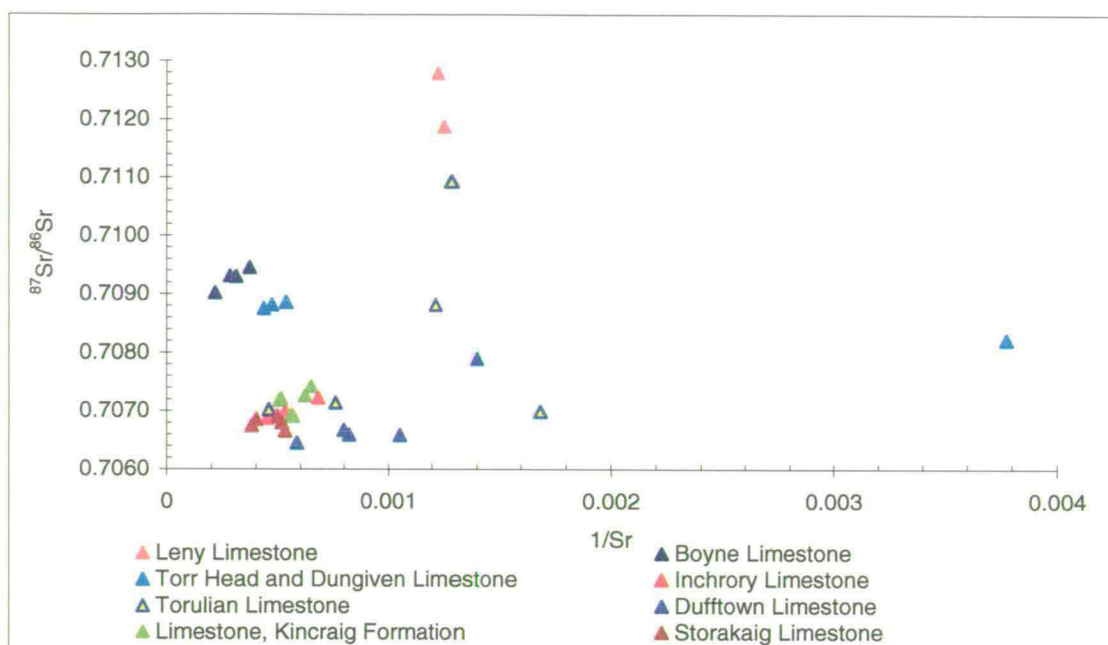


Figure 6.3a Variation of $^{87}\text{Sr}/^{86}\text{Sr}$ with Sr concentration in Dalradian limestones

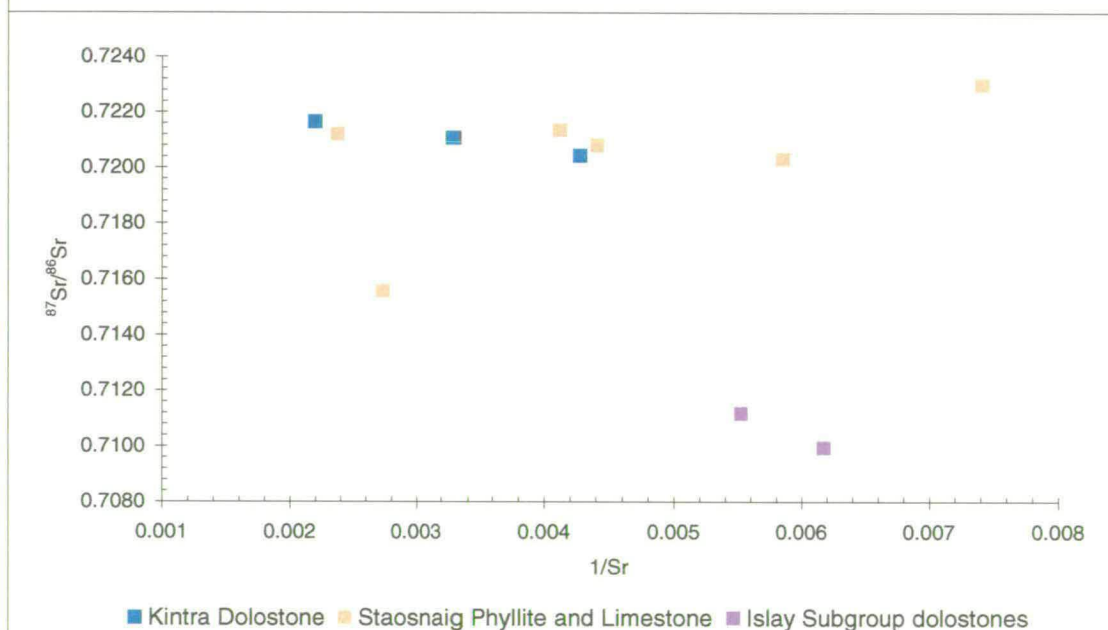


Figure 6.3b Variation of $^{87}\text{Sr}/^{86}\text{Sr}$ with Sr concentration in Dalradian dolostones

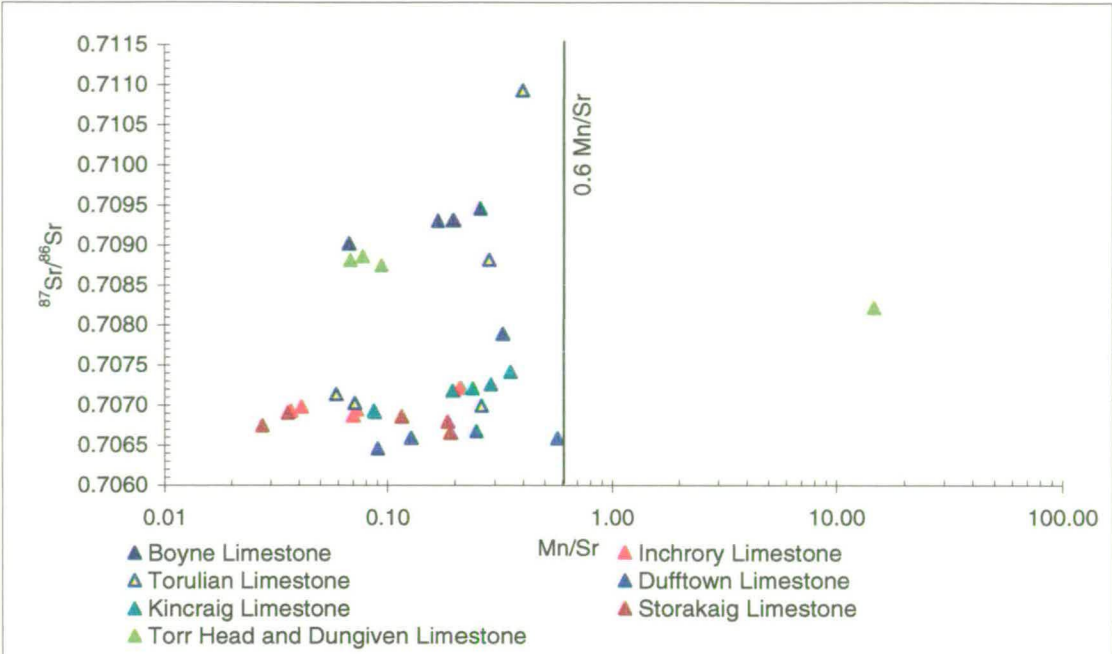


Figure 6.4a Variation of $^{87}\text{Sr}/^{86}\text{Sr}$ with Mn/Sr in Dalradian limestones

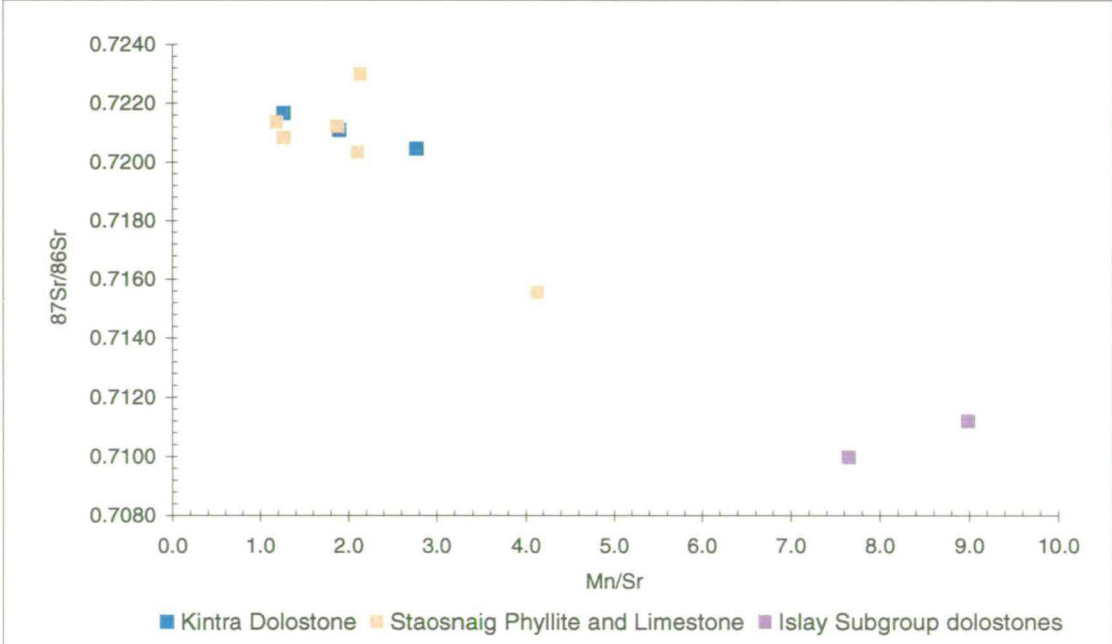


Figure 6.4b Variation of $^{87}\text{Sr}/^{86}\text{Sr}$ with Mn/Sr in Dalradian dolostones

‘Tayvallich’ limestone samples. All other limestones have Mn/Sr <0.6, commonly quoted as the Mn/Sr below which limestones are generally considered ‘unaltered’ (Table 6.4). In these limestones, increasing Mn is not associated with significantly disturbed $^{87}\text{Sr}/^{86}\text{Sr}$.

- *Dolostones*

The dolostone samples show relationships between Mn and Sr similar to those observed in the limestones, albeit at lower Sr concentration. Plotting $^{87}\text{Sr}/^{86}\text{Sr}$ vs Mn/Sr for the dolostones reveals that Mn is actually *lower* relative to Sr in dolostones with higher $^{87}\text{Sr}/^{86}\text{Sr}$ (Figure 6.4b). This suggests that dolomitising fluids were not a source for Mn in the dolostones.

The relationship between Mn and Sr amongst the limestone and dolostone samples is clarified by a plot of (Mn/Al) vs (Sr/Al) in Figure 6.5. The plot shows that, in general, samples with higher Sr also have higher Mn, relative to Al. This relationship is corroborated by ion microprobe Mn and Sr data for the Inchroary and Torulian limestones presented in Chapter 9.

6.4.7 Discussion

- *Evidence for very early incorporation of Mn*

The absence of a negative correlation between Mn and Sr indicates that fluid-rock interaction has not enhanced Mn whilst reducing Sr, as is commonly held to occur during diagenesis. The moderate positive correlation between these two elements in both limestones and dolostones suggests that Mn concentrations are effectively

primary in origin. There has not been significant addition of Mn with concomitant loss of Sr during diagenesis or metamorphic fluid rock interaction.

A complication which has to be taken into account when considering the potential for incorporation of Mn into carbonates is the oxidation state of Mn. Tucker and Wright (1990) state that Mn in open oceanic and meteoric waters is likely to be oxidised (Mn^{3+} , Mn^{4+}), rendering Mn too large to fit into the calcite lattice (it may also be complexed with anionic groups in water (e.g. Sholkovitz and Copeland (1981)). If Mn is to be incorporated into calcite, it must be in the reduced form of Mn^{2+} . Reduction of aqueous Mn probably occurred in reducing pore fluids or anoxic bottom waters by oxidation of sulphide and/or organic carbon. This implies limited circulation and mixing of bottom waters and pore fluids. Under such circumstances, the carbonate sediment would also buffer Sr and $^{87}\text{Sr}/^{86}\text{Sr}$ in the pore fluids towards that in the carbonates. The corollary is that Sr and Mn would show a positive correlation in the stabilised carbonate mineralogy, as seen here.

- In summary, the evidence indicates strongly that Mn abundances in most of the limestones are essentially primary in origin or were established during very early diagenesis.
- There is no good evidence for significant amounts of Mn being introduced during later diagenetic or metamorphic fluid-rock interaction in the limestones.

6.4.8 $^{87}\text{Sr}/^{86}\text{Sr}$ vs Al_2O_3

- *Limestones*

In general, $^{87}\text{Sr}/^{86}\text{Sr}$ increases *slightly, but consistently* with increasing Al_2O_3 (Figure 6.6a). This *implies* a small input of radiogenic ^{87}Sr held in Al-bearing silicates (feldspars, micas). The silicate component, comprising largely feldspars and micas, is very radiogenic in these rocks, compared to the calcite (section 6.2.2). However, although decay of ^{87}Rb will have increased $^{87}\text{Sr}/^{86}\text{Sr}$ in the silicates over time, it is apparent that any radiogenic Sr produced in the silicates has not been significantly incorporated into the carbonate, for three main reasons:

- it will have been limited because Sr is preferentially excluded from calcite during recrystallisation,
- the Sr concentration of the calcite is generally so high that the $^{87}\text{Sr}/^{86}\text{Sr}$ of this Sr would largely buffer any $^{87}\text{Sr}/^{86}\text{Sr}$ resulting from ^{87}Rb decay, and
- temperatures of metamorphism were neither high enough nor maintained long enough to homogenise $^{87}\text{Sr}/^{86}\text{Sr}$ throughout the rocks by diffusional processes (cf. Chapter 10).

Nevertheless, the consistent positive relationship between calcite $^{87}\text{Sr}/^{86}\text{Sr}$ and Al clearly implies some contamination of primary carbonate Sr by radiogenic Sr from silicates. I consider this to result from incorporation of minor radiogenic Sr from silicates, especially clay minerals, during diagenesis. Clay minerals will undergo early diagenetic changes in structure and chemistry, releasing Sr into diagenetic fluids. Being derived largely from crustal rocks with typical ‘continental’ $^{87}\text{Sr}/^{86}\text{Sr}$ values, these detrital phases will bring with them radiogenic Sr which would mix in

pore fluids with the much less radiogenic Sr from the calcite during diagenesis. At least some of this Sr would be included in the calcite recrystallised from primary aragonite. The high Sr values in the limestones suggest that diagenesis occurred under conditions of closed or restricted circulation. The corollary of this is that Sr and Rb would be retained in the system, but the latter could only be included in phyllosilicates and feldspars, since it is almost entirely excluded from carbonates. Once diagenesis had occluded porosity in the limestone and the mineralogy had become diagenetically stable, transfer of Sr between phases would effectively cease and the silicate and carbonate phases would become separate reservoirs for Sr, within which strontium isotope evolution would diverge. ^{87}Rb in the silicates would continue to decay, resulting in the highly radiogenic $^{87}\text{Sr}/^{86}\text{Sr}$ seen in the complete dissolution data for Tayvallich samples T1 and T2, whereas the Sr in the carbonate phase would remain unchanged.

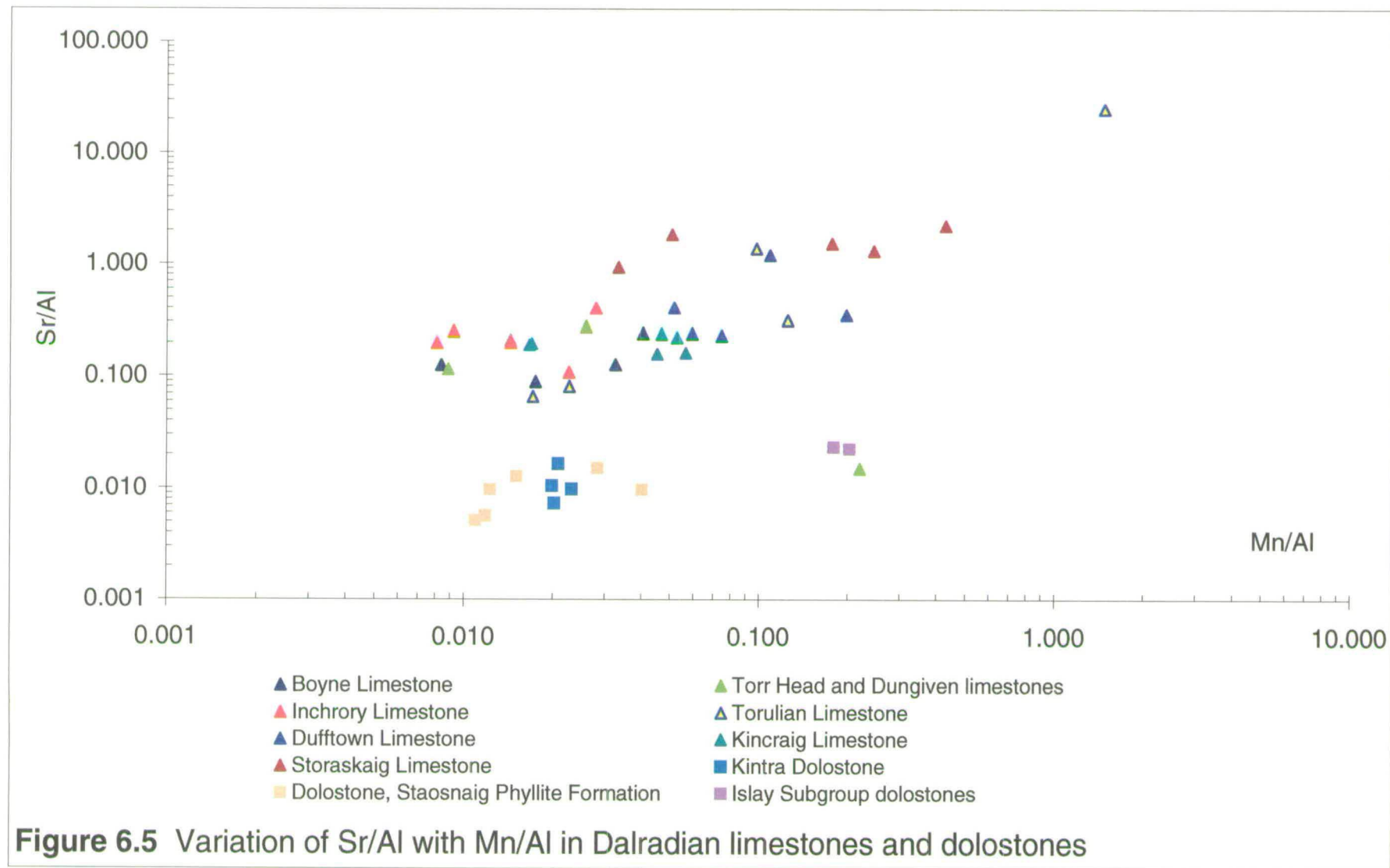
- *Dolostones*

Relationships between $^{87}\text{Sr}/^{86}\text{Sr}$ and aluminium are difficult to discern and there are no clear patterns (Figure 6.6b).

6.4.9 Variation of $^{87}\text{Sr}/^{86}\text{Sr}$ with $\delta^{18}\text{O}$

- *Limestones*

Different relationships between $^{87}\text{Sr}/^{86}\text{Sr}$ and $\delta^{18}\text{O}$ are revealed by the different groups of samples (Figure 6.7).



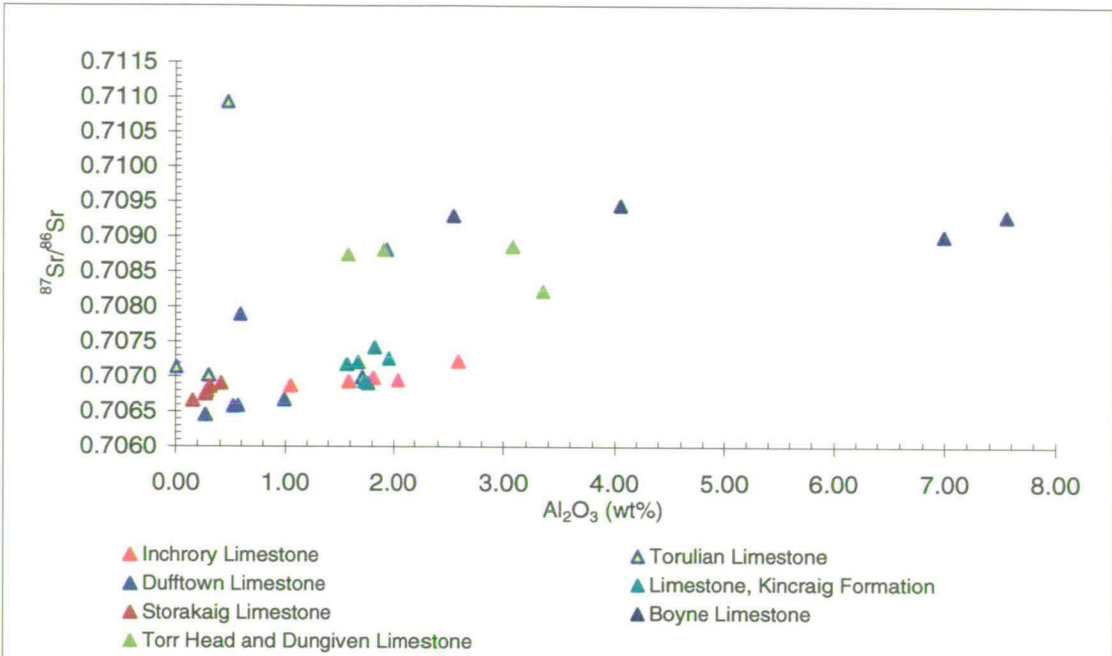


Figure 6.6a Variation of $^{87}\text{Sr}/^{86}\text{Sr}$ with Al_2O_3 in Dalradian limestones

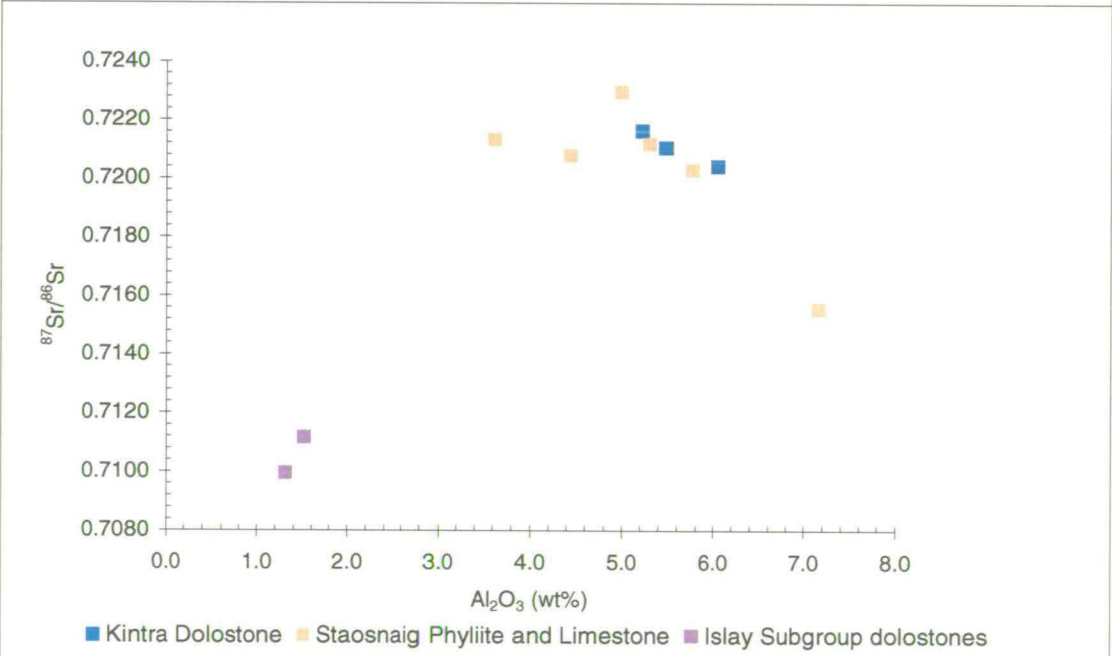


Figure 6.6b Variation of $^{87}\text{Sr}/^{86}\text{Sr}$ with Al_2O_3 in Dalradian dolostones

- The limestones from the Kincaig Formation show a persistent increase in $^{87}\text{Sr}/^{86}\text{Sr}$ with decreasing $\delta^{18}\text{O}$, but alteration is restricted, despite the very strong depletion in $\delta^{18}\text{O}$ in three samples.
- The Storakaig and Inchrory limestones plot in a coherent group with consistent slight negative correlation between $\delta^{18}\text{O}$ and $^{87}\text{Sr}/^{86}\text{Sr}$.
- The Dufftown Limestone samples have no clear relationship between $\delta^{18}\text{O}$ and $^{87}\text{Sr}/^{86}\text{Sr}$.
- The two Torulian Limestone samples with significantly more ^{87}Sr have lower $\delta^{18}\text{O}$ compared to the other three samples, suggesting that $^{87}\text{Sr}/^{86}\text{Sr}$ has been altered in these rocks.
- The 'Tayvallich' limestones display no correlation between $^{87}\text{Sr}/^{86}\text{Sr}$ and $\delta^{18}\text{O}$, either amongst the groups of samples or overall.

Dolostones The Kintra Dolostone and Staosnaig Phyllite Formation samples plot as a loose group, with the exception of one sample with much lower $^{87}\text{Sr}/^{86}\text{Sr}$ and slightly lower $\delta^{18}\text{O}$. The Islay Subgroup dolostone samples indicate markedly reduced $\delta^{18}\text{O}$ with increased $^{87}\text{Sr}/^{86}\text{Sr}$

6.4.10 Discussion

The data indicate that there is no significant relationship between $^{87}\text{Sr}/^{86}\text{Sr}$ and $\delta^{18}\text{O}$, apart from a *small* increase $^{87}\text{Sr}/^{86}\text{Sr}$ with decreasing $\delta^{18}\text{O}$ in Appin and Grampian Groups samples. This is consistent with the different buffering capacities of limestones for O and Sr. Fluids, being so rich in O, can alter carbonate $\delta^{18}\text{O}$

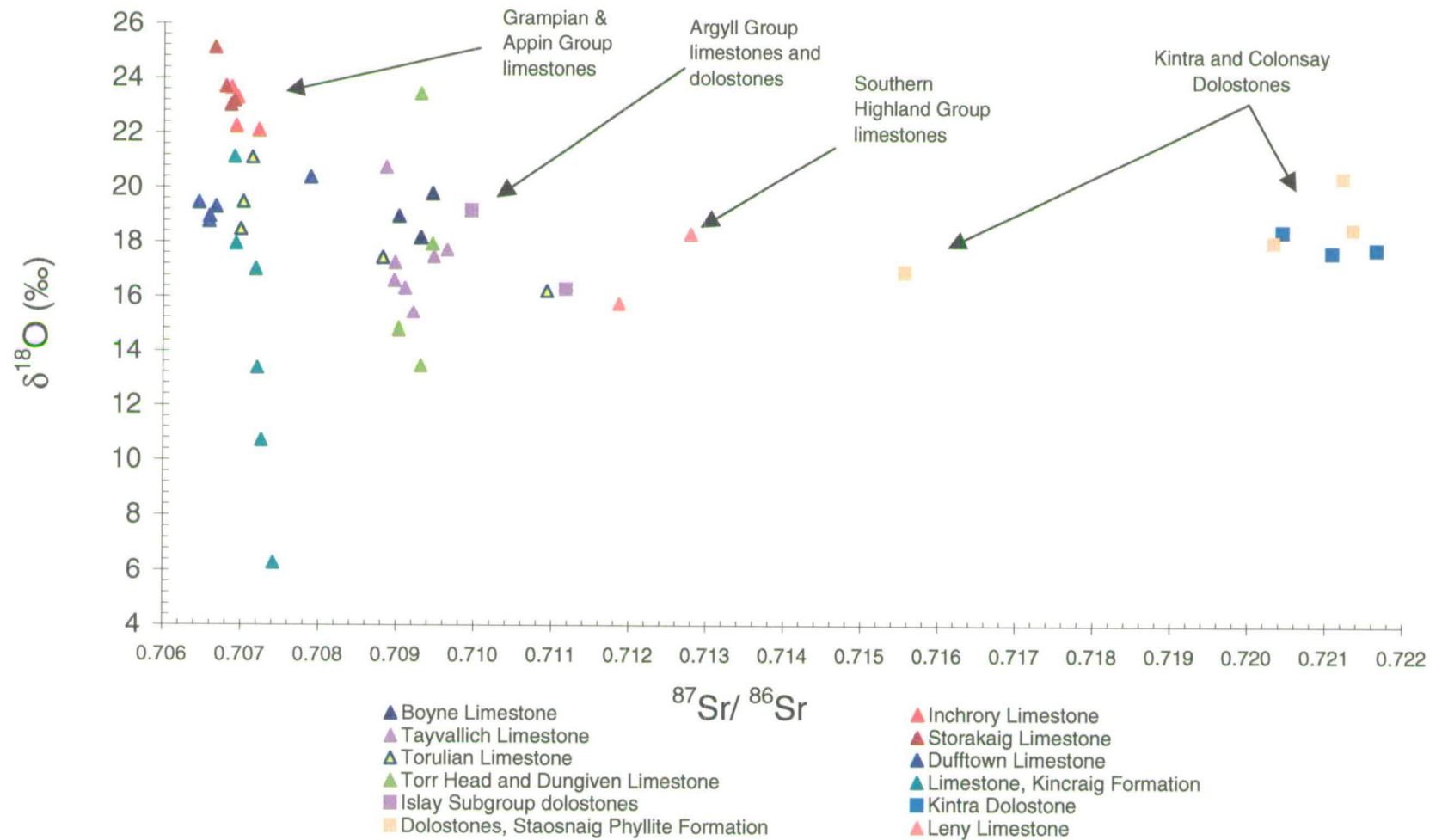


Figure 6.7 $^{87}\text{Sr}/^{86}\text{Sr}$ vs $\delta^{18}\text{O}$ for Dalradian limestones and dolostones

relatively easily. In contrast, diagenetic and metamorphic fluids are generally Sr-poor relative to limestones and this, together with the fact that carbonates other than aragonite exclude Sr from their lattices, limits the extent to which ^{87}Sr from the fluid can be incorporated into diagenetic carbonate.

The data show that the O and Sr isotope systems have been effectively decoupled in the limestones. $\delta^{18}\text{O}$ has been altered strongly in some rocks but $^{87}\text{Sr}/^{86}\text{Sr}$ has been left largely intact.

6.4.11 Variation of $^{87}\text{Sr}/^{86}\text{Sr}$ with $\delta^{13}\text{C}$

Although there is a tendency for rocks with lower $\delta^{13}\text{C}$ to have lower $^{87}\text{Sr}/^{86}\text{Sr}$, there are few significant variations within sample groups (Figure 6.8).

- The very strong depletion in $\delta^{18}\text{O}$ in some of the Kincaig Formation limestones is repeated here in the $\delta^{13}\text{C}$ data, but those samples with high $\delta^{13}\text{C}$ plot together with the Inchroary Limestone samples.
- Four of the Tayvallich Limestone samples show a slight monotonic increase in $^{87}\text{Sr}/^{86}\text{Sr}$ with $\delta^{13}\text{C}$. These four samples (T3 – T6a), come from the central part of the Tayvallich Limestone outcrop where samples at Port an Sgadain (Table 6.1). The remaining three samples show no significant correlation.
- Boyne Limestone samples show no correlation between Sr and C isotopes, despite wide ranging $\delta^{13}\text{C}$ values. Note, however, the very close match in C and Sr isotope values for this and the Tayvallich Limestone.
- The Torr Head and Dungiven Limestone samples show a slight monotonic increase in $^{87}\text{Sr}/^{86}\text{Sr}$ with increasing $\delta^{13}\text{C}$. The slope of this increase is very

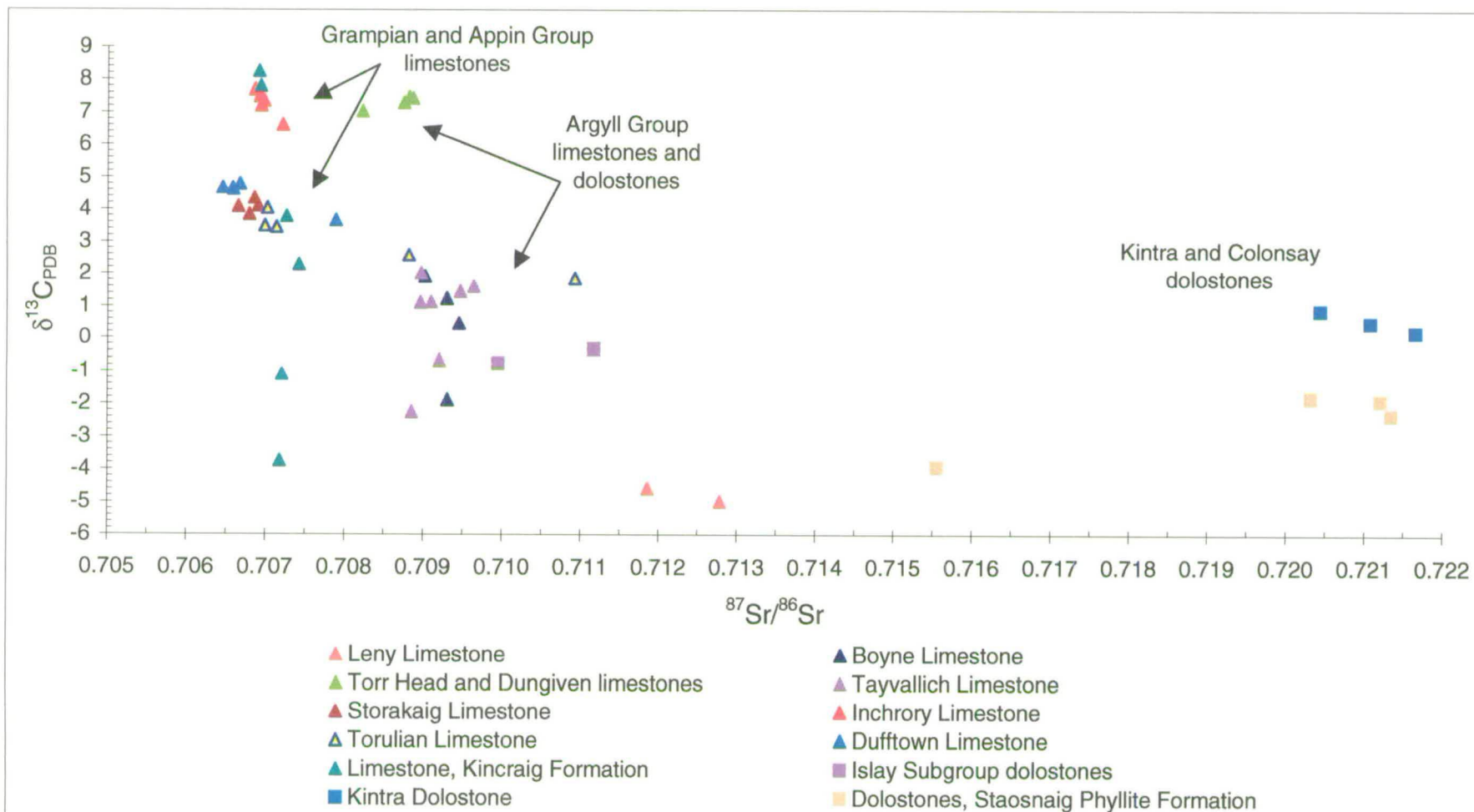


Figure 6.8 $^{87}\text{Sr}/^{86}\text{Sr}$ vs $\delta^{13}\text{C}$ for Dalradian limestones and dolostones

similar to that for the four Tayvallich Limestone samples displaying a similar monotonic relationship.

- No clear relationship between $^{87}\text{Sr}/^{86}\text{Sr}$ and $\delta^{13}\text{C}$ is discernible for any of the dolostone samples.

6.5 Discussion of Dalradian carbonate rock $^{87}\text{Sr}/^{86}\text{Sr}$ results

6.5.1 State of preservation of initial $^{87}\text{Sr}/^{86}\text{Sr}$ ratios in limestones

Comparison of the geochemistry of Dalradian limestones with the values of criteria listed in Table 6.4 considered to indicate a ‘least altered’ state, shows that the limestones lie well within the limits in almost all cases. On this basis alone, the $^{87}\text{Sr}/^{86}\text{Sr}$ data presented here for metamorphosed Dalradian limestones can be compared directly with $^{87}\text{Sr}/^{86}\text{Sr}$ data for *unmetamorphosed* limestones in other studies which have been used to establish secular variation of Neoproterozoic seawater $^{87}\text{Sr}/^{86}\text{Sr}$ (Table 5.1). The bulk of the limestone $^{87}\text{Sr}/^{86}\text{Sr}$ data can be interpreted as being close to that of the seawater from which the carbonate in these rocks was formed. The diversity of lithology and geological setting (metamorphic grade, etc.) of the sampled limestones, as discussed in Chapter 2, indicates the $^{87}\text{Sr}/^{86}\text{Sr}$ are independent these two features.

In most samples, limestone $^{87}\text{Sr}/^{86}\text{Sr}$ values have not been shifted to significantly more radiogenic compositions and that the $^{87}\text{Sr}/^{86}\text{Sr}$ is likely to be *relatively* close to $^{87}\text{Sr}/^{86}\text{Sr}$ of contemporary seawater. *Nevertheless*, co-variation between Sr isotopes and other elements show that there are consistent shifts in $^{87}\text{Sr}/^{86}\text{Sr}$ away from some primary value. Co-variation between $^{87}\text{Sr}/^{86}\text{Sr}$, Sr, Al, Mn

and $\delta^{18}\text{O}$ all indicate that the concentrations of these elements are primary in origin or established by early diagenesis:

- The shift in $^{87}\text{Sr}/^{86}\text{Sr}$ to more radiogenic values in samples with higher Al is attributed to incorporation into calcite of ^{87}Sr released during diagenesis of silicate minerals within the limestone sediments.
- For most of the limestones, the to weakly positive relationships between Sr and Mn suggest that early diagenesis occurred within a pore system with restricted fluid movement in which there was reduction of Mn to Mn^{II} (by sulphide and/or organic material) and buffering of Sr in the pore fluid by the carbonate sediment
- Early diagenesis occurred in a wholly marine regime in most of the limestones.

Two of the five Torulian Limestone samples (HY43, HY47) and one of the Dufftown Limestone samples (HY69) are shifted to much more radiogenic values (Figure 6.2, Table 6.3) compared to other samples in their groups. In Chapter 9, I show that the outcrop from which HY43 was obtained, at Bridge of Avon, near Tomintoul, *has* undergone significant exchange with metamorphic fluids in at least two infiltration events and it is probable that $^{87}\text{Sr}/^{86}\text{Sr}$ was altered during infiltration of the metamorphic fluids. Indeed, the alteration of $^{87}\text{Sr}/^{86}\text{Sr}$ in bulk carbonate to such radiogenic values implies extensive infiltration (cf. Bickle et al., 1990; Bickle et al., 1988).

6.5.2 Estimating $^{87}\text{Sr}/^{86}\text{Sr}$ of Dalradian seawater

I consider that most of the Appin Group limestones have retained $^{87}\text{Sr}/^{86}\text{Sr}$ close to their primary value and, by implication, that of coeval seawater. However, they cannot represent the true value of contemporary Neoproterozoic seawater $^{87}\text{Sr}/^{86}\text{Sr}$ because there is evidence for some probably diagenetic alteration towards more radiogenic values. Thus, even the lowest values are likely to have been altered to some extent. Nevertheless, the covariation of $^{87}\text{Sr}/^{86}\text{Sr}$ with various elements can be used to indicate *approximate* values for $^{87}\text{Sr}/^{86}\text{Sr}$ values of coeval seawater. These trends are most clearly discerned by plotting $^{87}\text{Sr}/^{86}\text{Sr}$ against Al_2O_3 (Figure 6.6a).

- *Grampian and Appin Group limestones*

Intercepts of these trends with $^{87}\text{Sr}/^{86}\text{Sr}$ at $\text{Al}_2\text{O}_3 \sim 0$ indicate minimal values of about ~ 0.7065 for the Inchroary and Storakaig limestones, according well with their presumed lithostratigraphical equivalence in the Blair Atholl Subgroup. With the one obvious exception, the Dufftown Limestone samples lie on a trend with an intercept of ~ 0.7064 . The evidence indicates that Dalradian seawater had $^{87}\text{Sr}/^{86}\text{Sr}$ of $\sim 0.7064 - 0.7065$. The consistency of this estimated seawater $^{87}\text{Sr}/^{86}\text{Sr}$ values with estimates based on data from other Neoproterozoic carbonate successions will be discussed below.

- *Uppermost Argyll Group limestones*

The picture for the Boyne and Torr Head / Dungiven limestones is less clear (Figure 6.6a) (*Note, the Tayvallich limestones cannot be plotted as whole-rock geochemical data are not available*). The least $^{87}\text{Sr}/^{86}\text{Sr}$ -enriched sample is HY1350 from Butterlope Glen ($^{87}\text{Sr}/^{86}\text{Sr} = 0.708220$) and this may be close to $^{87}\text{Sr}/^{86}\text{Sr}$ for upper Argyll Group 'seawater' (ironically, this is by far the most Mn and Al enriched sample of the suite). Although the data again suggest ^{87}Sr has been enriched in these Argyll Group limestones, the covariation between $^{87}\text{Sr}/^{86}\text{Sr}$, Sr, Rb, Mn, Al and $\delta^{18}\text{O}$ data for these limestones are consistent with those amongst Appin and Grampian Group data. It is unlikely, therefore, that the $^{87}\text{Sr}/^{86}\text{Sr}$ values have been shifted significantly more than in the Grampian and Appin Group limestones.

The limestones from the uppermost part of the Argyll Group are thus interpreted to reflect a significantly more radiogenic seawater $^{87}\text{Sr}/^{86}\text{Sr}$, compared to that indicated by the Appin and Grampian Group limestone data. The best estimate for 'Tayvallich' seawater $^{87}\text{Sr}/^{86}\text{Sr}$ is probably ~ 0.708 . As will be shown in Section 6.6, this value is entirely consistent with published data for unmetamorphosed carbonate sequences lying above Varangan tillite sequences elsewhere in the world.

- *Dolostones*

The strongly radiogenic $^{87}\text{Sr}/^{86}\text{Sr}$ in the dolostones are most likely to be related to dolomitisation, given that dolomitisation is generally considered to require some form of mixing of meteoric, formation or other waters with seawater (Tucker and Wright, 1990). Nevertheless, Sr-Mn covariation similar in the dolostones is similar to that in the limestones: although diagenetic fluids must have been considerably

enriched in ^{87}Sr , they were not a significant source of Mn and Sr remained relatively high in the dolomite. In addition, Sr isotopes for the dolostones commonly show relationships with Sr and Mn which are opposite to those observed in the limestones. It is not clear how best to interpret these relationships in the dolostones, but the $^{87}\text{Sr}/^{86}\text{Sr}$ are not interpretable in terms of seawater $^{87}\text{Sr}/^{86}\text{Sr}$.

6.6 Comparison of Dalradian limestone $^{87}\text{Sr}/^{86}\text{Sr}$ data with a Neoproterozoic seawater $^{87}\text{Sr}/^{86}\text{Sr}$ curve

In this next section, I compare the Dalradian $^{87}\text{Sr}/^{86}\text{Sr}$ data with equivalent data for unmetamorphosed Neoproterozoic carbonate rock sequences that have been used to constrain secular variation of seawater $^{87}\text{Sr}/^{86}\text{Sr}$ through the Neoproterozoic into the Cambrian. This enables a *broad*, but nevertheless very significant age constraint to be placed on the lower depositional age of the Dalradian, and, I believe, helps resolve the long-running debate on the status of Proterozoic tectonothermal events in the central Scottish Highlands and their effect, or otherwise, on the Dalradian rocks (as discussed in Chapter 2). I also use the data to substantiate the long-held consensus that the Port Askaig Tillite is a product of the Varangan glacial episode at c. 600 Ma and to consider the lithostratigraphical status of the Staosnaig Phyllite Formation on Colonsay.

6.6.1 Secular variation of Neoproterozoic seawater $^{87}\text{Sr}/^{86}\text{Sr}$

Several key studies of $^{87}\text{Sr}/^{86}\text{Sr}$ in Neoproterozoic carbonate rocks have been used to construct a seawater $^{87}\text{Sr}/^{86}\text{Sr}$ curve for the period from 1100 Ma to the Cambrian –

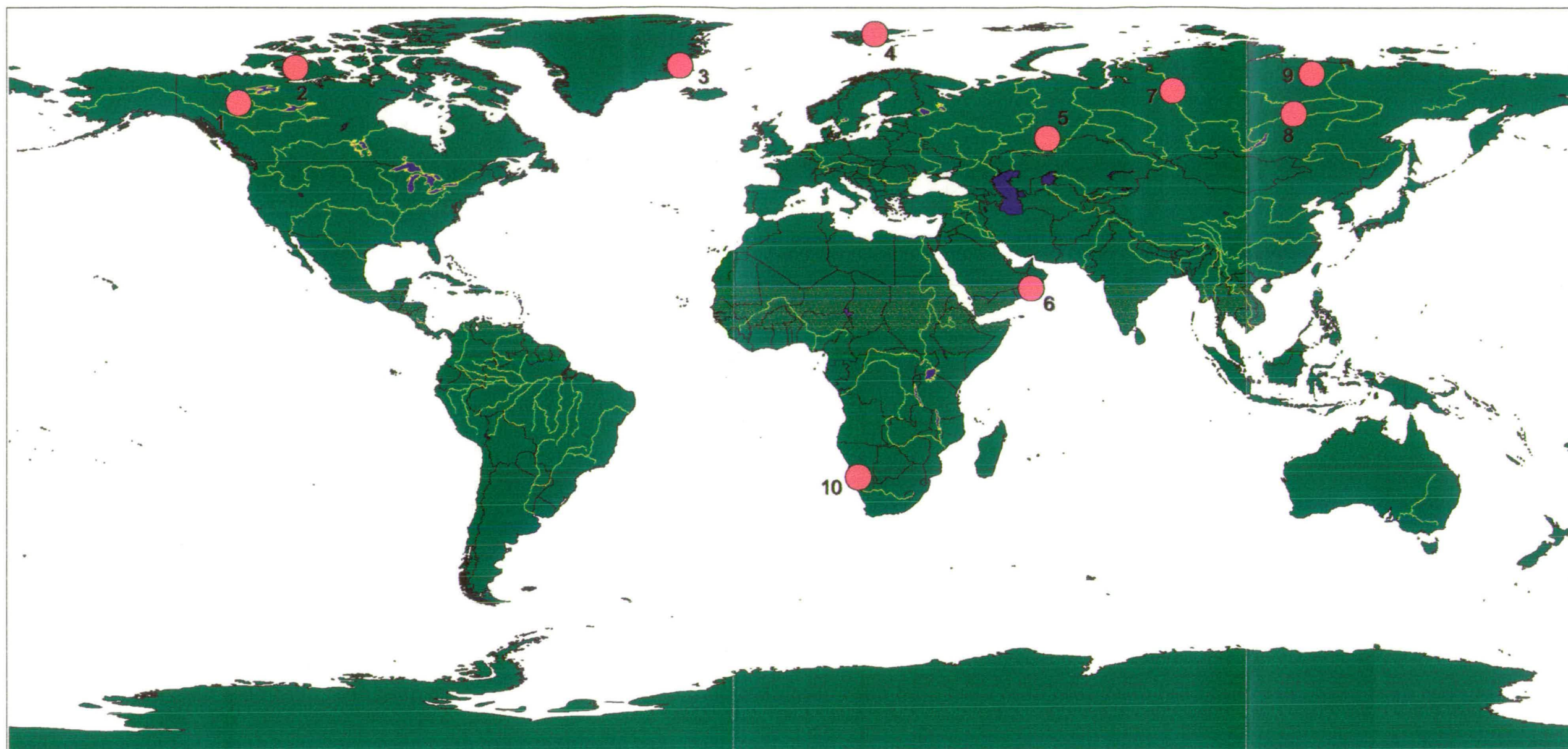
Precambrian boundary at ~ 545 Ma (Asmerom et al., 1991; Burns et al., 1994; Derry et al., 1989; Gorokhov et al., 1995; Kaufman et al., 1993; Kuznetsov et al., 1997) (Table 5.1). Although there are other important studies which record $^{87}\text{Sr}/^{86}\text{Sr}$ in Neoproterozoic carbonate rocks (e.g. Brasier et al., 1996; Kennedy et al., 1998; Narbonne et al., 1994), the studies listed here include estimated specific sample ages in Ma, rather than broad, relative lithostratigraphical age constraints. These data, therefore, provide the best current estimate of the secular variation of seawater $^{87}\text{Sr}/^{86}\text{Sr}$ during the Neoproterozoic.

The sequences from which the $^{87}\text{Sr}/^{86}\text{Sr}$ age data are derived, are distributed globally, coming from cratonic areas in northwest Canada (Kaufman et al., 1993), Victoria Island, northern Canada (Asmerom et al., 1991), Namibia (Kaufman et al., 1993), East Greenland and Svalbard (Derry, et al, 1989; Kaufman et al., 1993), Oman (Burns et al., 1994) the Urals (Kuznetsov et al., 1997) and Siberia (Gorokhov et al., 1995) (Figure 6.9). The successions are described briefly in Appendix A.3 and summarised in Table 5.1.

6.6.2 A Neoproterozoic $^{87}\text{Sr}/^{86}\text{Sr}$ 'seawater' curve

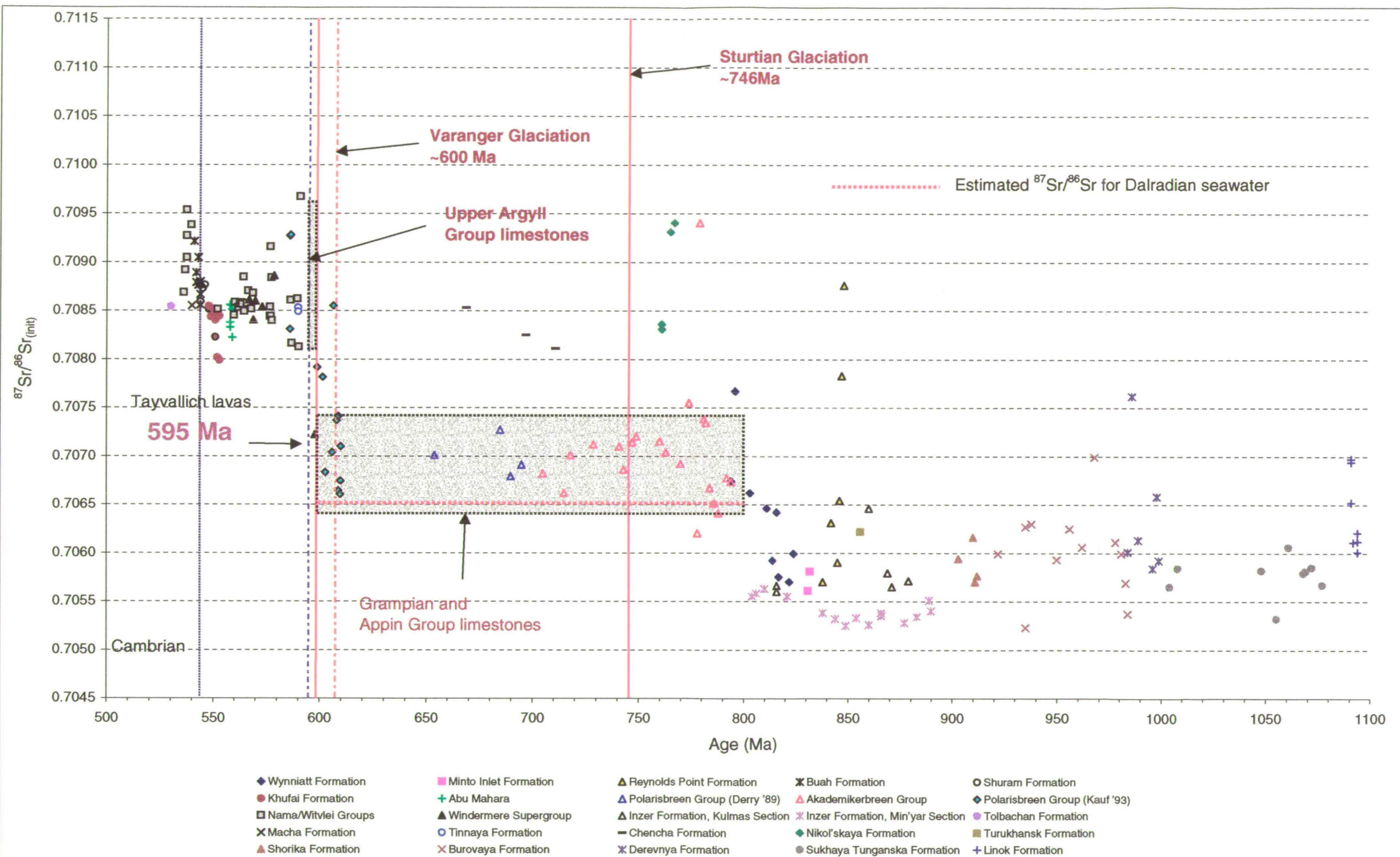
$^{87}\text{Sr}/^{86}\text{Sr}$ data taken from the studies listed in Table 5.1 are shown in Figure 6.10. The shaded boxes represent the Dalradian data.

The most obvious features are the marked, step-like increases in $^{87}\text{Sr}/^{86}\text{Sr}$ at c. 750 - 850 Ma and c. 600 Ma. Marine $^{87}\text{Sr}/^{86}\text{Sr}$ varied from ~ 0.7052 to ~ 0.7064 between about 1100 and 800 Ma. $^{87}\text{Sr}/^{86}\text{Sr}$ values appear to have been at their lowest in the period about 850 Ma, a feature also commented on by Asmerom et al. (1991) with regard to their data, but enhanced here by the data of Gorokhov et al. (1997). In



- 1: Windermere Group, Mackenzie Mountains
- 2: Shaler Group, Victoria Island
- 3: East Greenland
- 4: Polarisbreen and Akademikerbreen Group, Svalbard
- 5: Kulmas and Min'yar sections, Inzer Formation, Urals
- 6: Huqf Group, Oman
- 7: Turukhansk Uplift, Siberia
- 8: Ura Uplift, Siberia
- 9: Olenek Uplift, Siberia
- 10: Nama and Witvlei Groups, Namibia

Figure 6.9 Distribution of limestone-bearing successions used to constrain temporal variation in Neoproterozoic seawater Sr isotope ratio.
See Table 6.5 for references



the period between about 850 and 750 Ma, $^{87}\text{Sr}/^{86}\text{Sr}$ increased to values ranging between 0.7065 and 0.7075. Data for the next 150 – 200 Ma are restricted to those mainly from the North Atlantic Neoproterozoic sequences (Greenland, Spitsbergen, Scotland).

At c. 600 Ma there was another, similar increase in $^{87}\text{Sr}/^{86}\text{Sr}$, apparently over a very short period of time, to values well in excess of 0.7080 which reached a peak in the early Cambrian. This shift in marine $^{87}\text{Sr}/^{86}\text{Sr}$ is of a similar order to that which has occurred during the latter half of the Tertiary, where $^{87}\text{Sr}/^{86}\text{Sr}$ values at 0.7090 are the highest they have been since the Cambrian (Burke et al., 1982). The sharpness of this step may be an artefact of the dating of Polarisbreen samples used by Kaufman et al., (1993), which they assume to be no older than 610 Ma. However, their samples are unlikely to be significantly older than this. Thus, the rise in $^{87}\text{Sr}/^{86}\text{Sr}$ at c. 600 Ma appears to have been a much more rapid event than that between 750 – 850 Ma. For comparison, the sharp rise in seawater $^{87}\text{Sr}/^{86}\text{Sr}$ from the mid-Tertiary to the present day has occurred over ~30 Ma (Burke et al., 1982).

Apparent oscillations in the curve are difficult to interpret because of the imprecision on the absolute ages of the samples on which the curve is based. However, examination of the Phanerozoic seawater $^{87}\text{Sr}/^{86}\text{Sr}$ curve indicates that significant short-lived oscillations are to be expected (Burke et al., 1982). Unfortunately, given the duration of many of the oscillations apparent in the Phanerozoic curve and the poorer resolution of the Neoproterozoic curve, similar oscillations in the Neoproterozoic are not currently resolvable. The apparent periods of long-term stability of $^{87}\text{Sr}/^{86}\text{Sr}$, particularly from 800 – 1100 Ma, could well be an artefact of the data set, rather than reflecting very long term balance between

continental and mantle Sr fluxes (see Chapter 5). Note that the data presented by Gorokhov et al. (1995) and Kuznetsov (1997) are much lower and less variable than data presented by Veizer et al. (1983) for the period 800 – 1000 Ma. The Siberian and Russian data are considered here to be more reliable than the early estimates of seawater $^{87}\text{Sr}/^{86}\text{Sr}$ for 800 - 1000 Ma given in Veizer et al. (op. cit., and references therein).

I assume that the estimated ages of samples used to construct the $^{87}\text{Sr}/^{86}\text{Sr}$ curve are robust enough for a resolution of $\sim \pm 50$ Ma (see Appendix A.3). The shifts reflect periods of major change in the state of global tectonics, apparently separated by periods of relatively minor oscillation. These changes in Neoproterozoic seawater $^{87}\text{Sr}/^{86}\text{Sr}$ are of importance in their own right with regard to Neoproterozoic crustal evolution and their significance of these changes will be discussed further below. However, the nature of these changes and the times at which they occurred are of particular significance for the age of the Dalradian, as discussed in the next section.

6.6.3 The depositional age of the Dalradian

For ease of reference, I recapitulate the main points of the discussion on the age of the Dalradian presented in Chapter 2, Section 2.2., emphasising key areas of controversy for which the limestone $^{87}\text{Sr}/^{86}\text{Sr}$ data have particular relevance.

Present age constraints

- The Dalradian extends at least into the earliest Middle Cambrian (c. 510-520 Ma)

- Peak metamorphism and deformation coincided with the intrusion of metagabbros in Northeast Scotland at *c.* 470 Ma (Rogers et al., 1994); Dalradian strata will not be much younger than *c.* 500 Ma in age.
- The 595 ± 4 Ma age of the Tayvallich Lavas immediately overlying the Tayvallich Limestone (Halliday et al., 1989) limits the age of the latter to *c.* 600 Ma.
- The Port Askaig Tillite is correlated with Varanger Tillites and dated at *c.* 600 Ma by analogy with the Avalonian Gaskiers Tillite (Brasier and McIlroy, 1998; Kaye and Zartman, 1980; Krogh et al., 1988).
- The Appin and Grampian Groups are older than ~ 600 Ma, but the maximum age of deposition of the underlying Appin and Grampian Groups is poorly constrained
- Radiometric and structural evidence is suggested by some to indicate that at least the Appin and Grampian Groups are older than ~ 800 to 850 Ma, but it *is* clear that gneissose rocks beneath the Appin and Grampian Groups did undergo a Neoproterozoic tectonothermal event ~ 850 Ma ago.
- Recent field mapping evidence indicates that the Grampian and Appin Groups are unconformable on successions of gneissose sediments which are interpreted as basement. This evidence indicates that the Appin and Grampian Groups are younger than 800 Ma.

Fairchild and Hambrey (1995, table 1, p.220) suggest correlation of the Appin Group with the Riphean Akademikerbreen Group and the lowermost part of the overlying Vendian Polarisbreen Group of Svalbard (Derry et al., 1989).

$^{87}\text{Sr}/^{86}\text{Sr}$ evidence for the age of the Appin and Grampian groups

The secular variation of marine $^{87}\text{Sr}/^{86}\text{Sr}$ during the late Proterozoic shown in Figure 6.10 places a significant constraint on the lower bounding age of the Appin and Grampian Groups. Appin and Grampian Group limestone $^{87}\text{Sr}/^{86}\text{Sr}$ data lie within the range of data for Polarisbreen and Akademikerbreen Group limestones of NE Svalbard (Derry et al., 1989; Kaufman et al., 1993) (Figure 6.10). Accepting that Appin and Grampian Group limestone $^{87}\text{Sr}/^{86}\text{Sr}$ data reflect closely $^{87}\text{Sr}/^{86}\text{Sr}$ of contemporary seawater, it is clear that the Dalradian as a whole cannot be older than ~ 800 Ma and may well be considerably younger. A considerable period of time would be required to exhume the amphibolite-grade gneissose basement, metamorphosed and deformed at ~850 Ma, before unconformable deposition of the Appin and Grampian Group rocks.

The data presented here corroborate the field lithostratigraphical and structural evidence presented by Robertson and Smith (1999) and Smith et al. (1999) for a major unconformity at the boundary between Grampian and Appin Group rocks and the underlying gneissose rocks.

Global correlation of the Port Askaig tillite: evidence from Sr isotopes

The shift in $^{87}\text{Sr}/^{86}\text{Sr}$ ratios to >0.7080 between Dalradian limestones bracketing the Port Askaig Tillite is comparable to that observed in other studies of limestone sequences bracketing Varangan and southern hemisphere Marinoan tillites (e.g. Derry et al., 1989; Kaufman et al., 1993; Kennedy et al., 1998) (Figure 6.10).

The $^{87}\text{Sr}/^{86}\text{Sr}$ data, the 595 ± 4 Ma age for the overlying Tayvallich Volcanics and the c. 605 Ma age for Harbour Main Group volcanics underlying the putatively

equivalent Gaskiers Tillite of Newfoundland (e.g. Brasier and McIlroy, 1998, fig. 5), tightly constrain the age of the Port Askaig Tillite at *c.* 600 Ma, corroborating its 'Varangan' correlation and supporting the conclusions of Brasier and McIlroy (1998).

The 595 ± 4 Ma age of the Tayvallich Volcanics has implications for the debated correlation of Varangan and Marinoan tillites and the age of the latter (Saylor et al., 1998; Kennedy et al., 1998; Brasier and McIlroy, 1998). Sr isotope data presented here support correlation of the Port Askaig Tillite with southern hemisphere Marinoan tillites. Kennedy et al. (1998) show that $^{87}\text{Sr}/^{86}\text{Sr}$ ratios are shifted by ~ 0.0007 in carbonate rocks immediately above the partly glacigenic Ghaub Formation from the Congo Craton. $^{87}\text{Sr}/^{86}\text{Sr}$ values in platform and slope carbonate rocks immediately below and including the Ghaub Formation range from $\sim 0.7073 - 0.7075$, very similar to the data for the Appin and Grampian Group limestones and those from Svalbard (this similarity extends to the $\delta^{13}\text{C}$ data, as discussed in Chapter 7). Carbonate rocks above the Ghaub Formation have $^{87}\text{Sr}/^{86}\text{Sr} > 0.7079$. Thus the shift in $^{87}\text{Sr}/^{86}\text{Sr}$ in carbonate rocks above and below the Ghaub Formation corresponds to the shift observed in general in carbonate rocks bracketing the Port Askaig Tillite at *c.* 600 Ma (Figure 8.2). The Ghaub Formation has been previously dated indirectly at *c.* 570 Ma by correlation with the Namibian Numees Tillite, the age of which has been estimated by subsidence curves (Grotzinger et al., 1996). It has also been considered as 'Sturtian' (*c.* 760 - 700 Ma), largely on the basis of $\delta^{13}\text{C}$ data (Hoffman et al., 1998). However, the Sr isotope data suggest that the Ghaub Formation and, by inference, other Marinoan tillites, correlate temporally with the Varangan North Atlantic tillites (cf. Kennedy et al., 1998). In this context, the

Tayvallich Lava date of 595 ± 4 Ma becomes very important, as it is the oldest radiometric date for rocks above any of the tillite sequences. Myrow and Kaufman (1999) have recently published on a cap carbonate above the Gaskiers Tillite in Newfoundland in which they quote an upper bounding age of 565 ± 3 Ma for the Gaskiers Tillite, based on work by Benus (1988). If the tillites all correlate, as the Sr chemostratigraphical evidence suggests they do (see also Chapter 7 with regard to C isotope data), then these tillite sequences would appear to reflect one major glaciation event at about 600 Ma. In contrast, Saylor et al. (1998) considered that repeated 'Varangan' glaciation events occurred between *c.* 600 Ma to *c.* 564 Ma on the basis of combined litho- and chemostratigraphic correlation and radiometric dating of Neoproterozoic rocks from southern Namibia. The only possible evidence indicating a later glacial episode in Scotland which might represent part of a putatively younger 'Varangan' glaciation in the manner of Saylor et al. (1998) is that observed by Stoker et al. (1998) in the Macduff Formation of the Banffshire coast. However, the glaciation which caused this event may have occurred at the Cambrian – Precambrian boundary, and so not relate to the Varangan episode at all (Kennedy et al., 1998; Kimura et al., 1997).

6.7 Shifts in Neoproterozoic seawater $^{87}\text{Sr}/^{86}\text{Sr}$, coeval palaeogeography and tectonics

Given the important temporal variation in Neoproterozoic seawater $^{87}\text{Sr}/^{86}\text{Sr}$, it is appropriate to consider the possible tectonic causes. In this next section I discuss briefly the likely coeval tectonic events which were responsible for the observed shifts in the $^{87}\text{Sr}/^{86}\text{Sr}$ curve. I begin with a brief review of current models for

Neoproterozoic palaeogeography and tectonics before considering the links between tectonic events and variations in $^{87}\text{Sr}/^{86}\text{Sr}$.

6.7.1 Neoproterozoic palaeogeography – the models of Hoffman, Dalziel and co-workers

Neoproterozoic palaeogeography has been much debated in recent years and various configurations have been suggested for continental masses between ~ 800 Ma through to the early Cambrian (c. 530 Ma). ‘Traditional’ configurations of Gondwana and Laurentia during the late Neoproterozoic have placed the Appalachian/Caledonian (eastern) margin of Laurentia opposite NW South America and NW Africa (e.g. Torsvik and Trench, 1991) (Figure 6.11). Dalziel (1997) maintains that, whilst *palaeomagnetically* permissible, there is no *geological* evidence for the juxtaposition of Laurentia and the NW African margin of Gondwana. Dalziel further believes that this configuration cannot explain the development of the southern, southeastern and western (Pacific-facing) margins of Laurentia, nor the Pacific margins of South America, Antarctica and Australia. A hitherto enigmatic feature is the presence in the Precordilleran terrane of Northwest Argentina of a Lower Palaeozoic benthic trilobite fauna of Laurentian and **not** Gondwanan affinity. Significantly, this appears to be the only known occurrence of such a fauna outside of Laurentia (Dalziel, 1997).

The SouthWest US – East Antarctica (SWEAT) hypothesis of Moores (1991) began the challenge to the ‘North Atlantic’ view of Neoproterozoic palaeogeography. Moores suggested that striking similarities in the late Archaean and Palaeo- to Mesoproterozoic geology of the western margin of Canadian Laurentia

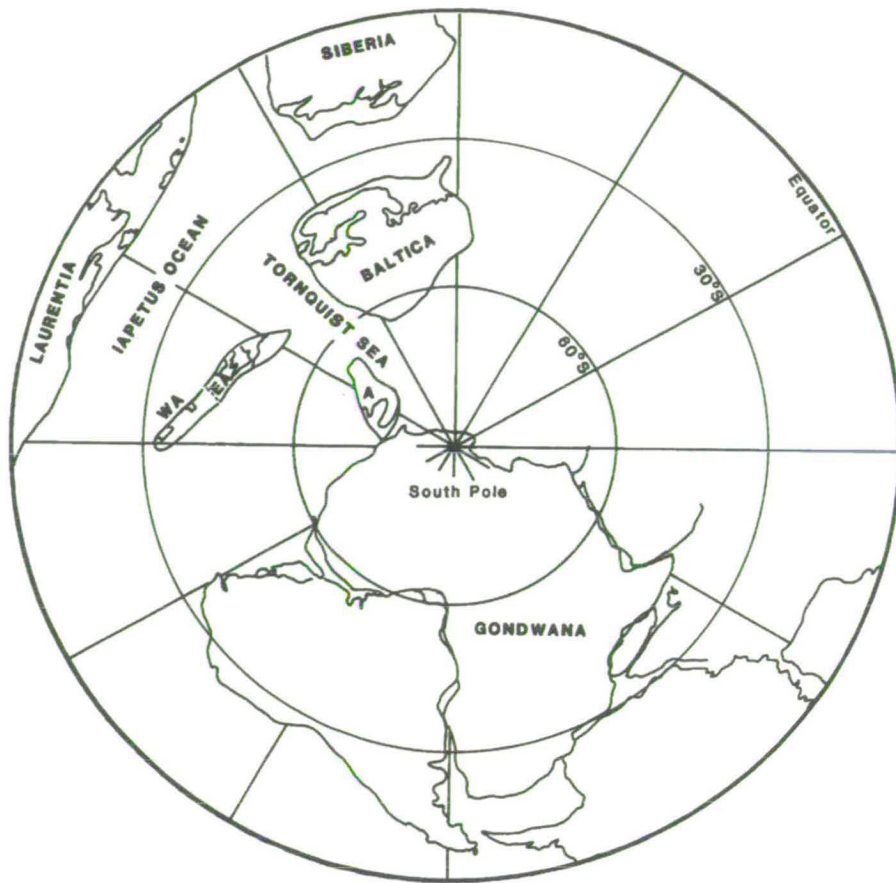


Figure 6.11 Continental reconstruction of Torsvik and Trench (1991) for the mid Ordovician (Llanvirn - Llandeilo), an example of the 'traditional', 'Northwest Africa' view of relationships between Laurentia and Gonwana, as discussed by Dalziel (1997).

and East Australia and Antarctica (as described, for example, in Hoffman, 1994) indicated that these two latter Gondwanan continental elements had been juxtaposed with the Western Cordilleran margin of Laurentia. Remarkable lithostratigraphical similarities also occur in the Neoproterozoic rocks in East Australia and the Western Cordillera, as described by Young (1992). Separation of East Antarctica – Australia (East Gondwana) from Laurentia resulted in the opening of the Pacific sometime around 750 Ma (Dalziel et al., 1994). Hoffman (1994), in noting the distribution of Grenvillian (1.0 – 1.3 Ga) orogenic belts (Figure 6.12), suggested that the eastern Laurentian margin was bordered by Amazonia, Baltica and the Kalahari and Congo cratons of South Africa. This idea has been extended and refined in recent years by Dalziel et al., 1994) and Dalziel (1994, 1997) resulting in a model for the tectonic history of Laurentia from the end of the Grenvillian assembly of the Rodinian supercontinent at ~1.3 – 0.9 Ga through to the diachronous early to middle Ordovician orogenies (including the Caledonian) which affected the eastern margin of Laurentia. Dalziel's view is that the eastern margin of Laurentia was juxtaposed firmly against western South America, with the Scotland promontory of eastern Laurentia docked in the western South American Arica embayment (Figure 6.12) along a Grenvillian orogenic belt. Soper (1994b), whilst accepting the general thrust of the 'South American' model of Dalziel and co-workers, prefers to have the Tornquist margin of Baltica (juxtaposed with NW South America in Figure 6.12) to have been juxtaposed with East Greenland, rather than with the 'traditional' Scandian margin (as shown in Figure 6.11).

Having rifted off Western Laurentia sometime before *c.* 700 Ma, East Gondwana rotated anticlockwise with respect to Laurentia to collide with the African

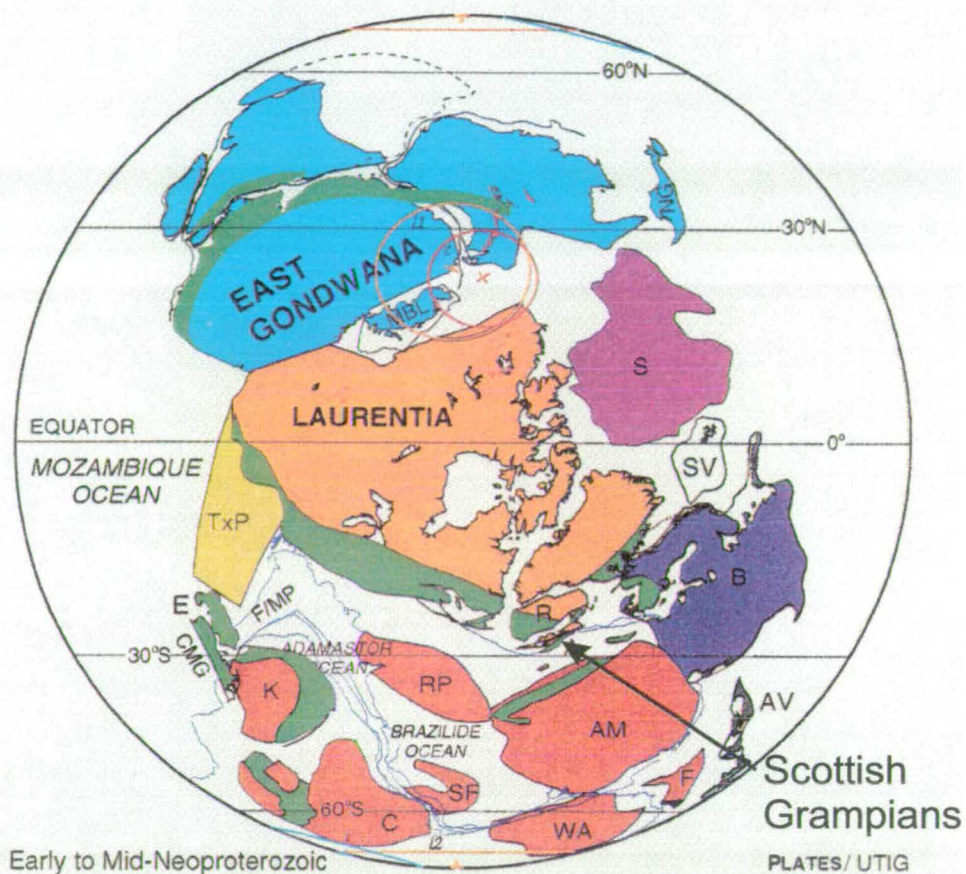


Figure 6.12 Continental reconstruction as proposed by Dalziel (1997) for the relationship between the eastern Laurentian margin and Gondwana within Rodinia, prior to rifting of East Gondwana from the western margin of Laurentia (c. 750 Ma). Taken from Dalziel (1997). Note the position of the Scottish Promontory with respect to South America.

A: Arica Embayment; Am: Amazonian craton; B: Baltica;
C: Congo Craton; K: Kalahari Craton; R: Rockall Plateau;
S: Siberia; SV: Svalbard.

Green shading: Grenville orogens

margin of Gondwana along the Mozambique Belt, during the Pan-African orogeny (Figure 6.13; Dalziel et al., 1994) consider that suturing of East and West Gondwana occurred prior to *c.* 600 Ma. Laurentia began to rift from East Gondwana probably not long after the opening of the Pacific. However, this did not induce continental rupture for another 150 Ma or more as all coeval deposits on the eastern Laurentian margin are continental rift sequences deposited on cratonic basement, with rifting focussed along the line of the Grenville orogen (Figure 6.12). Soper (1994) contends that this rifting was slowed by lack of subduction on Gondwanan and Laurentian Pacific margins, allowing deposition over at least 200 Ma of the very thick Neoproterozoic sequences of Newfoundland, Greenland, Svalbard and, of course, Scotland (Moine, Dalradian), without leading to continental rupture. However, once the Pacific began to subduct beneath the Transantarctic Mountains of Antarctica in the latest Proterozoic, rifting accelerated and became too rapid to be accommodated by extending continental crust; Iapetus opened sometime in the early Cambrian. Presumably, Pacific subduction followed closely on continental collision and assembly of Gondwana along the Mozambique Belt. Hoffman (1994) summarises this Neoproterozoic tectonic activity very graphically: *the cratonic constituents of Gondwana were literally turned inside out by the breakout of Laurentia over a period of some 200 Ma!* Former interior rifts became exterior margins and former margins became landlocked in the Gondwanan cratonic assembly.

How are these tectonic events manifest in the Neoproterozoic seawater $^{87}\text{Sr}/^{86}\text{Sr}$ curve, if at all? In the discussion below, I use the recent 'Laurentia - South American' reconstruction of Neoproterozoic palaeogeography of Dalziel (1997) discussed above, principally because the evidence is cogently argued and the model

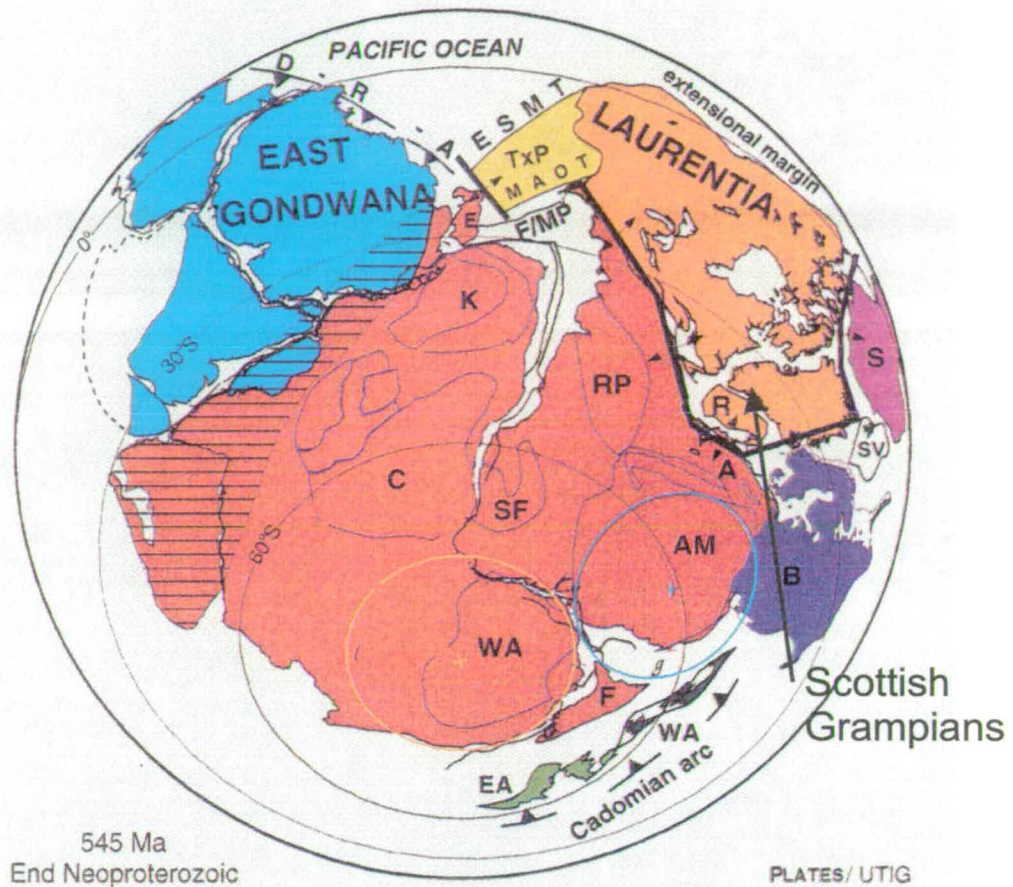


Figure 6.13 Continental reconstruction as proposed by Dalziel (1997) for the relationship between Laurentia and Gondwana after Pan-African assembly of Gondwana and prior to the opening of Iapetus at the end of the Neoproterozoic. Taken from Dalziel (1997).

A: Arica Embayment; Am: Amazonian craton; B: Baltica;
C: Congo Craton; K: Kalahari Craton; R: Rockall Plateau;
S: Siberia; SV: Svalbard.

Thick black line: locus of Iapetus rifting
Barbed line: Pacific ocean subduction

appears coherent and consistent with geological history for the Neoproterozoic. In doing so, however, I note that this model remains controversial and subject to debate (e.g. Dalziel and Dala Salda, 1996; Soper, 1994a, amongst others) and that many recent papers still hold to the 'North Atlantic' Laurentia – Northwest Africa view of the Neoproterozoic, as discussed by Dalziel (1997).

6.7.2 Coincidence of the 600 Ma shift in $^{87}\text{Sr}/^{86}\text{Sr}$ with the Pan African Orogeny

Following the shift in seawater $^{87}\text{Sr}/^{86}\text{Sr}$ from values of ~ 0.7070 to >0.7085 at about 600 Ma, seawater $^{87}\text{Sr}/^{86}\text{Sr}$ values remained well above 0.7085 until the end of the Cambrian (e.g. Burke et al., 1982), whence they declined to ~ 0.7080 towards the end of the Ordovician. The high values persisted for about 100 Ma. Once established, available evidence from estimates of seawater $^{87}\text{Sr}/^{86}\text{Sr}$ indicate the balance of the continental to mantle Sr fluxes to the oceans was maintained in favour of the continental flux. The tectonic event most likely responsible for this shift in seawater $^{87}\text{Sr}/^{86}\text{Sr}$ is the Pan African orogeny, as suggested by Asmerom et al. (1991) and Hoffman (1991).

The Pan African orogenic effect may have been enhanced by continental rupture when Iapetus began to open, resulting in new coastlines across which there would have been an additional flux of continental Sr from West Gondwana and Laurentia. In the Dalradian, transition occurs in the lower part of the Vendian Argyll Group from largely shelf/platform deposition of cyclic quartzite-mudrock-carbonate sequences (similar to those of the Appin Group) to turbidite dominated sequences in the upper part of the Argyll Group and overlying Southern Highland Group (e.g. Anderton, 1988). This change in style of Dalradian sedimentation coincides with the

shift in $^{87}\text{Sr}/^{86}\text{Sr}$ recorded in Dalradian limestones either side of the base of the Argyll Group. Note that continental rupture results in two new coastlines, equivalent in length to the ocean ridge between them. New, active sedimentation on the passive conjugate margins of Gondwanan and Laurentian must have had an effect on the flux of Sr to the oceans and, therefore, on seawater $^{87}\text{Sr}/^{86}\text{Sr}$, possibly increasing the latter, despite the presence of a new source of mantle Sr at the ocean ridge system between them. As noted above in the discussion on Neoproterozoic palaeogeography, prior to rupture, there was active, long-lived sedimentation onto slowly rifting continental crust at the incipient margins of Laurentia and West Gondwana (e.g. Soper 1994) following the opening of the Pacific Ocean. How is it that this rift sedimentation is not obviously reflected in the seawater $^{87}\text{Sr}/^{86}\text{Sr}$ curve between 750 and 600 Ma? This may partly reflect the lack of resolution the seawater $^{87}\text{Sr}/^{86}\text{Sr}$ curve. However, it may also reflect the sedimentation patterns. Although the early phase of sedimentation was dominantly siliciclastic, including turbiditic rocks such as the Rivieradal Sandstones of NE Greenland and the Laggan Psammite Formation in the Grampian Group, carbonate sedimentation was significant or dominant in the later history of these intracontinental rifts. This implies that the continental Sr flux was much reduced. Thus, seawater $^{87}\text{Sr}/^{86}\text{Sr}$ would be buffered towards mantle, rather than continental values.

6.7.3 A tectonic cause for the '800' Ma shift ?

As discussed above, there is good evidence for a major shift in seawater $^{87}\text{Sr}/^{86}\text{Sr}$ beginning at about 850 Ma and continuing until about 750 Ma (Figure 6.10). Discerning a cause for this shift is more problematical than that at 600 Ma. The

obvious major late Proterozoic tectonic event prior to the Pan African is the Grenville orogenic assembly of Rodinia at ~ 1.0 Ga, but this is *c.* 150 – 200 Ma too early for the observed rise at 850 – 750 Ma. Another possibility is that the rise from 850 Ma reflects incipient rifting of Rodinia before breakup at *c.* 750 Ma; deposition of the oldest of the thick, post-Grenville siliciclastic sequences during this time could have caused a marked increase in continental Sr flux. Examples of such sequences include the Moine, the Mackenzie Mountains Supergroup, Canada, most of which is older than 780 Ma (Narbonne and Aitken 1995), the >723 Ma Shaler Group of Northern Canada (Asmerom, et al., 1991), and the Warina Supergroup of Australia, the upper part of which is correlated with the Mackenzie Mountains Supergroup (Young, 1992). Deposition of these sequences would have introduced a considerable Sr flux into the oceans and this may be manifest in the rise in seawater $^{87}\text{Sr}/^{86}\text{Sr}$ between 850 and 750 Ma indicated by the current data.

Finally, there is just the slightest hint in the $^{87}\text{Sr}/^{86}\text{Sr}$ curve of a decline in minimum $^{87}\text{Sr}/^{86}\text{Sr}$ values between 750 and 600 Ma. One is tempted to speculate and see this reflecting the increasing importance of carbonates in late Proterozoic successions up to 600 Ma. Although more marked, the data of Gorokhov et al., (1997) indicates a similar, but more clearly defined decline from about 950 Ma to 850 Ma, a period when carbonates were dominant on the Siberian craton. More work on the $^{87}\text{Sr}/^{86}\text{Sr}$ compositions of younger Appin Group limestones on Islay and the mainland may help establish the existence of gradual decline in $^{87}\text{Sr}/^{86}\text{Sr}$ between 750 and 600 Ma, as carbonate sedimentation came to dominate in the upper part of the Blair Atholl Subgroup.

6.8 Conclusions

- Various geochemical data for Dalradian limestones indicate that $^{87}\text{Sr}/^{86}\text{Sr}$ ratios have been little altered since the limestones were formed and that the ratios can be interpreted as being close to their primary (marine) values.
- Neoproterozoic seawater $^{87}\text{Sr}/^{86}\text{Sr}$, as determined by proxy from $^{87}\text{Sr}/^{86}\text{Sr}$ initial ratios in limestones, displays marked secular variation, with significant shifts at ~800 Ma and ~600 Ma; the latter is particularly well-constrained.
- Comparison of Appin and Grampian Group limestone $^{87}\text{Sr}/^{86}\text{Sr}$ data show that the Dalradian is very unlikely to be older than ~750 – 800 Ma.
- The Appin and Grampian Group limestone $^{87}\text{Sr}/^{86}\text{Sr}$ data strongly supports emerging field evidence for a major unconformity within the Central Scottish Highlands between gneissose and migmatitic rocks and Dalradian metasedimentary rocks.
- The Tayvallich Lava date, coupled with $^{87}\text{Sr}/^{86}\text{Sr}$ data on limestones bracketing tillite deposits assigned to the Varanger/Marinoan ice-ages, suggest that there was only one major late Proterozoic glacial episode and that this was of similar duration to recent Quaternary glacial episodes
- Before 600 Ma, Dalradian seawater had a $^{87}\text{Sr}/^{86}\text{Sr}$ ratio estimated at about 0.7064 – 0.7065. This rose to > 0.7080 after 600 Ma. The data accord well with shifts in seawater $^{87}\text{Sr}/^{86}\text{Sr}$ recorded in other sequences which bracket Varanger/Marinoan tillites.

Chapter 7

Whole-rock carbon and oxygen isotope compositions of Dalradian limestones and dolostones

In this Chapter:

- ❖ Carbon and oxygen isotope compositions of Dalradian limestones and dolostones
- ❖ Preservation of primary $\delta^{13}\text{C}$ compositions
- ❖ Comparison of Dalradian limestone and dolostone $\delta^{13}\text{C}$ data with $\delta^{13}\text{C}$ data from other Neoproterozoic carbonate rock sequences

7.1 Introduction

In this chapter, I present carbon and oxygen isotope data determined on whole-rock samples from Dalradian limestones and dolostones. This chapter follows on from the discussion of carbonate $^{87}\text{Sr}/^{86}\text{Sr}$ data I presented in the last chapter and has broadly the same aims.

Here, I consider:

- the extent to which primary sedimentary C and O isotope signatures have survived alteration during diagenesis and metamorphism

- plausible models for modification of ‘bulk-carbonate’ $\delta^{13}\text{C}$ and $\delta^{18}\text{O}$
- the lithostratigraphical variation of $\delta^{13}\text{C}$ in Dalradian limestones and dolostones, and
- the extent to which Dalradian carbonate rock $\delta^{13}\text{C}$ data can be compared with $\delta^{13}\text{C}$ data for other, unmetamorphosed carbonate rock sequences from the Neoproterozoic (most of the latter data are from the same studies from which I obtained $^{87}\text{Sr}/^{86}\text{Sr}$ data in Chapter 6).

As with the Sr data in the previous chapter, the oxygen isotope data are critical in assessing the preservation of primary carbon isotope values. For this reason, available ‘bulk carbonate’ $\delta^{18}\text{O}$ data are also considered here. *However, this chapter concentrates primarily on the carbon data and their interpretation.* The significance of bulk oxygen data will be discussed in more depth in Chapter 9, where the data are compared with grain-scale $\delta^{18}\text{O}$ variation and scales of isotopic equilibrium elucidated by Secondary Ion Microprobe Spectrometry (SIMS) are considered in detail.

7.2 Samples and data sets

The set of samples used for the carbon and oxygen isotope analysis comprises the samples used for the $^{87}\text{Sr}/^{86}\text{Sr}$ study, together with additional data supplied by C M Graham and A Fallick, published data from Fein et al. (1994) and unpublished data from Greig (1984) (Table 7.1a). Additional data from two detailed sample profiles in the Inchroory and Torulian limestones (Chapter 9) are also included in Table 7.1b.

Sample	$\delta^{13}\text{C}_{\text{pdb}}$	$\delta^{18}\text{O}_{\text{smow}}$	Sample	$\delta^{13}\text{C}_{\text{pdb}}$	$\delta^{18}\text{O}_{\text{smow}}$	Sample	$\delta^{13}\text{C}_{\text{pdb}}$	$\delta^{18}\text{O}_{\text{smow}}$	Sample	$\delta^{13}\text{C}_{\text{pdb}}$	$\delta^{18}\text{O}_{\text{smow}}$	Sample	$\delta^{13}\text{C}_{\text{pdb}}$	$\delta^{18}\text{O}_{\text{smow}}$
Southern Highland Group			Danna			Additional Loch Tay Limestone calcite data			Appin Group			Grampian Group		
Leny Limestone			D5			South Bay, Tarbert			Storaskaig Limestone, Islay			Kincraig Formation limestones		
HY1362	-4.6	15.7				(from Greig, 1984 & Fein et al., 1994)			(~ equivalent of the Inchroy Limestone)			HY1072	7.8	17.9
HY1364	-5.0	18.3				South Bay, Tarbert			HY1333	4.1	23.2	HY1073	8.3	21.1
Argyll Group			Loch Leathan			CA95	0.6	15.9	HY1334	Did not run		SMS446	-1.1	13.4
Boyne Limestone			CE5			Ag-9	0.3	13.8	HY1335	4.4	23.0	SMS447	-3.7	17.0
HY147	1.9	19.0	Tayvallich Limestone			CA58	4.0	17.5	HY1336	3.9	23.7	SMS448	2.3	6.3
HY148	0.5	19.8	Epidote-amphibolite facies			X19	2.9	13.4	HY1337	4.1	25.1	SMS449	3.8	10.7
HY149	-1.9	18.2	Loch na Craige			Z14	2.9	14.2	HY1335	4.4	23.0	<i>Limestones of uncertain lithostratigraphical affinity, Isle of Colonsay, Inner Hebrides</i>		
HY150	1.2	18.2	7765			CA80	2.1	13.8	HY1336	3.9	23.7			
Tayvallich Limestone			70-98			Z14	1.6	12.2	HY1337	4.1	25.1			
T1	-3.8	17.0	CA124			Z12	1.4	15.2	Inchroy Limestone			Staosnaig Phyllite and Limestone		
T2	-0.7	15.4	Loch Fuar Bheinne			CA90	1.3	13.6	HY56	6.6	22.1	HY1342	-2.3	18.5
T3	1.1	16.6	86-02A			X16	1.0	24.8	HY57	7.5	22.2	HY1343	Did not run	
T4	1.1	16.3	86-02B			X1	-3.4	11.1	HY58	7.2	23.3	HY1344	Did not run	
T5	1.5	17.5	86-03			80H	0.0	20.7	HY59	7.7	23.7	HY1345	-1.8	18.0
T6a	1.6	17.7	86-04A			94D	-0.6	19.2	HY60	7.4	23.5	HY1346	-1.9	20.4
T6b	2.0	17.3	86-04B			167G	0.3	18.6	Torulan Limestone			HY1347	-3.9	16.9
Additional limestone data			86-05			167H	0.6	15.5	HY43	3.5	21.1	Colonsay Limestone data (CMG)		
C M Graham, personal communication			Loch Tay Limestone			167I	1.6	16.4	HY47	3.5	18.5	43161	2.3	26.9
Tayvallich Limestone (greenschist facies)			Epidote-amphibolite facies			53D	1.0	16.6	HY360	4.0	19.5	43165	2.5	26.3
Port an Sgadin			Glendaruel			63D	0.6	18.5	HY393	1.9	16.2			
T2	-0.8	15.4	79-04			82D	0.5	15.5	HY394	2.6	17.4			
T3	1.1	16.2	Kennacraig			Torr Head Limestone			Dufftown Limestone					
T4	1.2	16.3	80-14			HY1348	7.4	14.8	HY67	4.8	19.3			
T5	1.2	16.2	CA2			HY1349	7.5	17.9	HY68	4.6	19.0			
T6a	1.3	16.8	CA9			Dungiven Limestone			HY69	3.7	20.4			
T6b	1.4	16.7	Rhu			HY1350	7.0	13.4	HY70	4.7	19.5			
Kilchrenan			CE3			HY1351	7.3	23.4	HY71	4.7	18.8			
85-03	1.1	14.4	CE			Islay Subgroup Dolostones associated with diamictites			Kintra Dolostone, Islay					
85-04	1.5	15.3				HY85	-0.3	16.3	HY1338	0.9	18.4			
85-05	0.8	12.5				HY86	-0.8	19.2	HY1339	0.6	17.9			
Keills						HY72	-1.2	16.5	HY1340	0.2	17.8			
K1	6.1	15.8				GX1064	-0.8	22.1	HY1341	0.5	17.7			
K6	3.8	15.1				Bonahaven Formation?, Margadale, Islay								
						C Graham, personal communication								
						86-15								
						86-16								

Table 7.1a $\delta^{13}\text{C}$ and $\delta^{18}\text{O}$ analyses of bulk carbonate in Dalradian limestones and dolostones

Inchrory Limestone, Limeworks Quarry profile samples

Samples: 7 mm minicores, bulk whole-rock

Conventional analyses			LASSIE analyses	
Sample	$\delta^{13}\text{C}_{\text{pdb}}$	$\delta^{18}\text{O}_{\text{smow}}$	$\delta^{13}\text{C}_{\text{pdb}}$	$\delta^{18}\text{O}_{\text{smow}}$
LWQ 1/23	-	-	2.3	19.3
LWQ 1/23	-	-	3.4	18.4
LWQ 1/25	-	-	6.6	30.7
LWQ 1/25	-	-	6.7	29.4
LWQ 1/25	-	-	6.6	30.9
LWQ 1/25	-	-	6.6	28.9
LWQ 1/26	6.6	22.0	5.5	17.2
LWQ 1/26	-	-	5.5	16.7
LWQ 1/28	-	-	7.7	30.3
LWQ 1/28	-	-	7.2	31.0
LWQ 1/30	-	-	7.5	32.0
LWQ 1/30	-	-	7.1	33.3
LWQ 1/31	7.0	22.5	6.0	17.3
LWQ 1/31	-	-	5.8	16.8
LWQ 1/32	6.9	22.6	4.9	18.8
LWQ 1/32	-	-	6.8	19.4
LWQ 1/33	6.9	22.9	4.6	14.9
LWQ 1/33	-	-	4.6	13.9
LWQ 1/34	6.8	20.7	4.1	10.2
LWQ 1/34	-	-	3.9	12.1
LWQ 1/34	-	-	5.1	13.0
LWQ 1/35	6.8	22.5	4.5	13.5
LWQ 1/35	-	-	4.0	9.8
LWQ 1/36	6.8	22.2	6.0	18.3
LWQ 1/36	-	-	6.1	18.1
LWQ 1/37	6.8	22.4	5.5	16.0
LWQ 1/37	-	-	5.5	18.3
LWQ 1/39	6.8	22.9	4.9	23.4
LWQ 1/39	-	-	6.2	21.2
LWQ 1/41	7.0	22.7	5.8	17.3
LWQ 1/41	-	-	5.9	17.8
LWQ 1/42	6.4	22.6	5.5	17.5
LWQ 1/42	-	-	4.8	17.6
LWQ 1/43	6.7	22.8	4.9	15.7
LWQ 1/43	-	-	4.8	16.6
LWQ 1/44	6.8	23.0	5.4	17.0
LWQ 1/44	-	-	5.2	16.7
LWQ 1/45	6.4	21.6	4.7	16.9
LWQ 1/45	-	-	5.1	17.3
LWQ 1/46	6.2	22.3	3.5	14.5
LWQ 1/46	-	-	4.8	17.0

Summaries			
	Max	Min	Median
Conventional			
$\delta^{13}\text{C}_{\text{pdb}}$			
Range:	7.0	6.2	
$\delta^{18}\text{O}_{\text{smow}}$			
Range:	23.0	20.7	
LASSIE			
$\delta^{13}\text{C}_{\text{pdb}}$			
Range:	7.7	2.3	5.5
$\delta^{18}\text{O}_{\text{smow}}$			
Range:	33.3	9.8	17.3

Summary Inchrory data from Table 8.1a

$\delta^{13}\text{C}_{\text{pdb}}$			
Range:	7.7	6.6	7.4
$\delta^{18}\text{O}_{\text{smow}}$			
Range:	23.7	22.1	23.3

Torulian Limestone, River Avon section

Samples: LASSIE data from hand specimen chips, conventional data from micro-drilled powders

Sample	$\delta^{13}\text{C}_{\text{pdb}}$	$\delta^{18}\text{O}_{\text{smow}}$
CT49	1.5	33.7
CT49	1.2	35.9
CT49	0.6	13.4
CT49	0.5	13.4
CT50	1.0	24.7
CT50	0.8	24.9
CT50	0.9	15.4
CT50	0.8	14.7
CT52	-4.4	19.5
CT52	-4.9	19.0
CT52	-1.0	14.0
CT52	-1.1	14.4
CT53	4.3	22.5
CT53	3.8	23.9
CT53	5.0	38.1
CT53	3.7	37.3
CT53	2.8	17.4
CT53	2.9	17.7
CT54	0.7	15.3
CT54/1	0.2	12.1
CT54/2	1.2	12.4
CT54/3	0.0	13.2
CT54/4	0.2	11.4
CT54/5	0.6	12.5
CT54/6	0.9	13.2
CT55	1.5	16.2
CT55/1	1.5	13.8
CT55/2	1.5	15.6
CT55/3	0.8	15.2
CT57	0.6	7.8
CT57/1	1.7	16.6
CT57/2	1.7	16.6
CT58	1.7	18.1
CT58/1	2.5	19.3
CT58/2	2.2	16.7
CT59	0.6	14.4
CT59/1	0.8	19.7
CT59/2	1.7	19.7
CT60	1.8	14.3
CT60	1.7	14.3
CT60/1	1.2	15.9
CT60/2	2.1	16.0
CT60/3	1.0	14.3
CT61	2.8	15.9
CT61/1	3.0	20.2
CT61/2	3.0	19.9
CT61/3	3.0	20.0
CT61/4	2.9	19.8
CT62	2.6	21.4
CT62	2.6	18.9
CT62/1	2.9	22.3
CT63	1.3	14.2
CT63/1	2.4	18.8
CT63/2	2.0	19.5
CT65/1	-1.1	18.1

Summaries			
	Max	Min	Median
Conventional			
$\delta^{13}\text{C}_{\text{pdb}}$			
Range:	3.0	-1.1	1.6
$\delta^{18}\text{O}_{\text{smow}}$			
Range:	22.3	11.4	16.6
LASSIE			
$\delta^{13}\text{C}_{\text{pdb}}$			
Range:	5.0	-4.9	1.2
$\delta^{18}\text{O}_{\text{smow}}$			
Range:	38.1	7.8	17.4

Summary Torulian data from Table 8.1a

$\delta^{13}\text{C}_{\text{pdb}}$			
Range:	4.0	1.9	3.5
$\delta^{18}\text{O}_{\text{smow}}$			
Range:	21.1	16.2	18.5

Table 7.1b Additional $\delta^{13}\text{C}$ and $\delta^{18}\text{O}$ analyses of bulk carbonate for the Inchrory and Torulian Limestones (see Chapter 9)

The location of the main sample sets is shown in Figure 6.1. In all, the data set includes 89 carbon and oxygen isotope analyses of limestones and 12 of dolostones have been made. Of these, 46 have been made on samples of crushed whole-rock samples, 41 on 7 mm mini-cores or micro-drilled from whole-rock samples.

Tayvallich – Loch Tay Limestone data

Included in the discussion are previously unpublished C and O isotope analyses of calcite in the Tayvallich and Loch Tay limestones, and of limestone within the Erins Quartzite, from a number of localities in the Tayvallich-Knapdale area, (C Graham and A Fallick, personal communication; Greig 1984); some of which are plotted in Fein et al. (1994). Inclusion of these data permit wider consideration of the variability of $\delta^{13}\text{C}$ and $\delta^{18}\text{O}$ in this important limestone, particularly with regard to variation with grade and fuller comparison with samples of equivalent limestones from Northern Ireland.

Bonahaven Dolomite

$\delta^{13}\text{C}$ and $\delta^{18}\text{O}$ data on two samples from dolomitic rocks within the Bonahaven Formation have been provided by C M Graham (personal communication). The samples come from Margadale, north Islay. These data are included because they provide important information on carbonate $\delta^{13}\text{C}$ in rocks immediately overlying the Port Askaig Tillite. Elsewhere in the world, dolomitic rocks overlying Neoproterozoic tillites record negative excursions in $\delta^{13}\text{C}$, making such rocks

important markers in the determination of secular variation in carbonate and, by proxy, marine TDC $\delta^{13}\text{C}$.

'Colonsay Limestone'

Two unlocated samples from the Colonsay Limestone on Colonsay (C Graham, personal communication) are included because they yield near-sedimentary $\delta^{18}\text{O}$, making their $\delta^{13}\text{C}$ potentially interpretable as primary. They contrast strongly with the data presented here from dolostones of the Staosnaig Phyllite Formation.

7.3 'Whole-rock' carbon and oxygen isotope compositions of Dalradian limestones and dolostones

In the next section I describe the 'whole-rock', bulk carbonate $\delta^{13}\text{C}$ and $\delta^{18}\text{O}$ compositions of the carbonate rocks in the data set in relation to lithostratigraphy.

7.3.1 Dolostones

Dolostone samples are characterised by near-zero to moderately negative $\delta^{13}\text{C}$ values. Samples from the Staosnaig Phyllite Formation have the lowest $\delta^{13}\text{C}$, with a minimum of -3.9‰ . Kintra Dolostone samples are weakly positive ($\delta^{13}\text{C}$ $0.2 - 0.9\text{‰}$) and Islay Subgroup samples weakly negative (-0.3 to -1.2‰). The differences in $\delta^{13}\text{C}$ between the three groups of dolostone sample analyses are significantly outwith the analytical error of $\pm 0.1\text{‰}$, although within-group variation is of the same order as the between group variation. The Kintra Dolostone samples have low $\delta^{18}\text{O}$ values, but they are tightly grouped ($17.7 - 18.4\text{‰}$). The Staosnaig Phyllite

Formation and Islay Subgroup dolostones have more wide ranging $\delta^{18}\text{O}$ values (16.3 – 22.1‰).

7.3.2 Limestones

Limestone samples are dominated by positive $\delta^{13}\text{C}$ values, though there are some notable exceptions. The $\delta^{13}\text{C}$ and $\delta^{18}\text{O}$ data are described in relation to lithostratigraphy in the following section.

Grampian Group limestones

Limestones from the Kincaig Formation have very wide ranging $\delta^{13}\text{C}$ (-3.7 – +8.3 ‰) and $\delta^{18}\text{O}$ (6.3 – 21.1 ‰). The lowest values come from pale, coarsely-crystalline limestones which contain graphite flakes (M. Smith, personal communication, December 1999). The two limestones with the highest values come from Kincaig Quarry and are very different lithologically, being pale grey and medium grained limestones.

Appin Group limestones

Samples from the Storakaig Limestone have limited range in $\delta^{13}\text{C}$ values (3.9 – 4.4‰). This tightness in $\delta^{13}\text{C}$ is reflected in the narrow ranges of $\delta^{18}\text{O}$ (23.0 – 25.1) and $^{87}\text{Sr}/^{86}\text{Sr}$ (0.706651 – 0.706902) (Chapter 6). The $\delta^{13}\text{C}$ data for the Inchrory Limestone are similarly tightly constrained, although the values are significantly higher (6.6 – 7.7), whilst the $\delta^{18}\text{O}$ data are very similar (22.1 – 23.7). Additional data from mini-cores indicate slightly lower $\delta^{13}\text{C}$ and $\delta^{18}\text{O}$ values (Table 7.1, Figure 7.1; see also Chapter 9) (SIMS data on three of the mini core samples reveal considerable

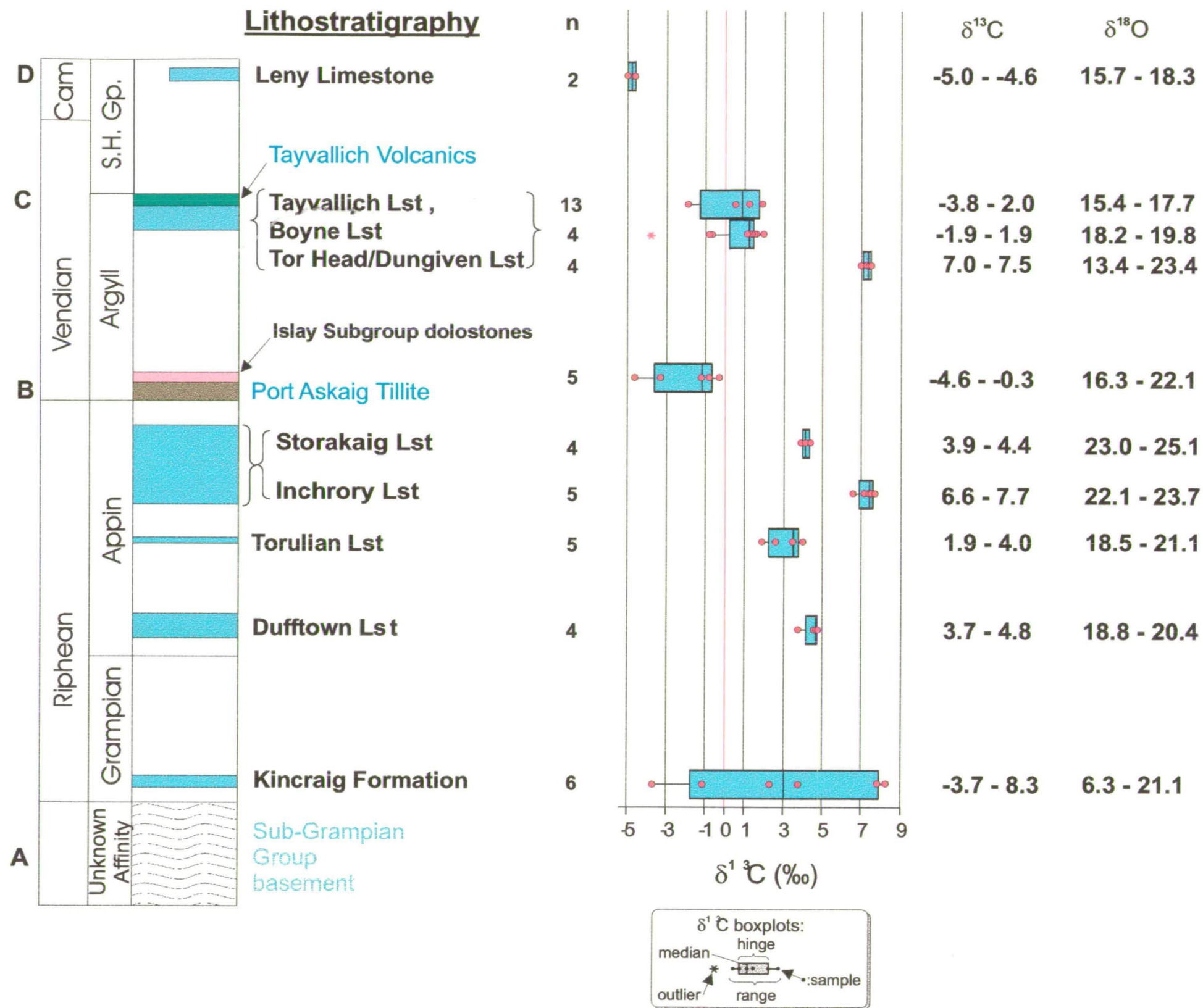


Figure 7.1 Lithostratigraphical variation of $\delta^{13}\text{C}$ in Dalradian limestones and dolostones. Age constraints A-D are as on Figure 6.2.

heterogeneity in $\delta^{18}\text{O}$ on the grain-scale, with values ranging from 15.7 to 27.2‰ on millimetric to sub-millimetric scales – see Chapter 9).

The Torulian Limestone has whole-rock bulk carbonate $\delta^{13}\text{C}$ values ranging from 1.9 to 4.0‰, the higher values being similar to those of the Dufftown Limestone (see below) and the Storakaig Limestone. Additional Torulian Limestone data from samples from the River Avon section, Tomintoul, have $\delta^{13}\text{C}$ values ranging from 3.0 to -1.1 ‰ (Table 9.1) and are thus slightly lower than the whole-rock data (Table 7.1). Furthermore, although the whole-rock $\delta^{18}\text{O}$ values from the Torulian Limestone range from 16.2 – 21.1‰, additional $\delta^{18}\text{O}$ from the River Avon samples indicate more widely ranging $\delta^{18}\text{O}$, with bulk ‘whole-rock’ values from 22.3 to 11.4‰ and a minimum SIMS value of 9.3‰ (Table 7.1 and Table 9.1).

The Dufftown Limestone preserves $\delta^{13}\text{C}$ values closely similar to those from the Storakaig Limestone, ranging from 3.7 to 4.8‰ (figure 7.1), although $\delta^{18}\text{O}$ values are rather lower (18.8 – 20.4).

Argyll Group Limestones

Within error, $\delta^{13}\text{C}$ values for the Tayvallich and Boyne Limestone samples form a group, matching the similarity in their $^{87}\text{Sr}/^{86}\text{Sr}$ ratios (Chapter 6), $\delta^{13}\text{C}$ values ranging from -2.3 to $+2.0$ ‰. However, with one exception, $\delta^{18}\text{O}$ values for the Tayvallich Limestone are rather lower (15.4 – 17.7‰) than those for the Boyne Limestone (18.2 – 19.8‰).

The Northern Irish Torr Head and Dungiven Limestone samples are markedly different to their lithostratigraphical equivalents in Scotland with respect to $\delta^{13}\text{C}$.

Values ranging from 7.0 – 7.5‰ are comparable to those observed for the Inchroy Limestone (see below).

The high and consistently similar $\delta^{13}\text{C}$ values for the Torr Head and Dungiven Limestones contrast sharply with their wide ranging $\delta^{18}\text{O}$ values (13.4 – 23.4‰). The occurrence of the lowest $\delta^{18}\text{O}$ values with high $\delta^{13}\text{C}$ is particularly striking when compared to the lithostratigraphically equivalent Tayvallich and Boyne Limestone data, where higher $\delta^{13}\text{C}$ values generally occur with higher $\delta^{18}\text{O}$ (Table 7.1a, Figure 7.1). In noting the high $\delta^{13}\text{C}$ values of the Irish samples, it is worth reiterating that these limestones also preserve the lowest $^{87}\text{Sr}/^{86}\text{Sr}$ ratios amongst these uppermost Argyll Group limestones (see Table 6.4, Figure 6.2).

The Leny Limestone

The Leny Limestone contains the lightest carbonate of any rock in this study (-4.6 to -5.0 ‰). This limestone and its host pelitic rocks in the Keltie Water Grit Formation are extremely graphitic; the carbonate $\delta^{13}\text{C}$ data clearly reflect exchange with this large source of ^{12}C . The $\delta^{18}\text{O}$ data range from 15.7 – 18.3 ‰, indicating exchange with hydrous fluids in equilibrium with siliciclastic rocks.

7.4 Extent of preservation of primary $\delta^{13}\text{C}$ values

As with carbonate $^{87}\text{Sr}/^{86}\text{Sr}$ ratios, secular variations in $\delta^{13}\text{C}$ during the Neoproterozoic have proved to be of considerable value in aiding lithostratigraphical correlation both within and between cratonic areas (e.g. Brasier, et al., 1996; Kaufman and Knoll, 1995) and in elucidating the environmental geochemical evolution of the earth during this time. Like the interpretation of the $^{87}\text{Sr}/^{86}\text{Sr}$ ratios,

the central tenet of such studies is that primary/near primary $\delta^{13}\text{C}$ signatures have been preserved in the limestones and dolostones and can be recognised as such. Because carbonate rocks have a large buffer capacity for C relative to most crustal fluids, most of the arguments and geochemical evidence pertaining to the recognition of ‘unaltered’ $^{87}\text{Sr}/^{86}\text{Sr}$ ratios in ancient carbonate rocks, as discussed in Chapter 6, apply equally to $\delta^{13}\text{C}$ data. As with the Sr data, the implication is that primary and/or early diagenetic $\delta^{13}\text{C}$ values may also have been preserved and will be discernible. To reiterate from Chapter 6, geochemical criteria for determining state of alteration include, *inter alia*, preservation of high $\delta^{18}\text{O}$, high Sr and low Mn. As a general rule, high carbonate $\delta^{13}\text{C}$ values are likely to be at or close to primary values because alteration will reduce $\delta^{13}\text{C}$. Whilst this means that high $\delta^{13}\text{C}$ values are more easily interpretable as primary, establishing lower carbonate $\delta^{13}\text{C}$ values as primary is more difficult without supporting $\delta^{18}\text{O}$, $^{87}\text{Sr}/^{86}\text{Sr}$ and trace element data because they *may* have been reduced from higher values. The detailed variation of $\delta^{13}\text{C}$ values on the outcrop and hand-specimen scale in the Torulian and Inchrory Limestones is discussed further in Chapter 9.

7.4.1 Organic carbon as a measure of preservation of primary $\delta^{13}\text{C}$, and organic carbon – calcite ^{13}C exchange during metamorphism

Covariation of organic and carbonate $\delta^{13}\text{C}$ in the same sample is considered a powerful means of constraining the degree of ^{13}C alteration in carbonate rocks because there appear to be no processes by which both organic and carbonate $\delta^{13}\text{C}$ can be shifted by the same amount and at the same rate (Knoll et al., 1986). Analysis and comparison of organic and carbonate ^{13}C has, for example, been undertaken

successfully on the Neoproterozoic carbonates of Svalbard by Knoll et al., *op. cit.*, who showed that organic and carbonate ^{13}C co-vary in these rocks as would be expected if primary ^{13}C compositions are preserved. In contrast, Kaufman et al., (1991) found that organic $\delta^{13}\text{C}$ had been variably altered in Namibian Neoproterozoic carbonate rocks. However, such alteration had not seriously affected $\delta^{13}\text{C}$ in the carbonate phase. In consequence, in both studies, the secular variation of the data provided useful constraints on basin-wide lithostratigraphical correlation. In Dalradian rocks, however, greenschist to amphibolite facies metamorphism will have at least partially transformed organic carbon chemically and structurally from complex organic molecules to graphite, altering the isotopic composition (e.g. Kitchen and Valley, 1995). Indeed, ^{13}C exchange between graphite and calcite forms the basis of a useful geothermometer in medium and high-grade metalimestones (Kitchen and Valley, *op. cit.*, and references therein) as increased temperature facilitates ^{13}C exchange between graphite and calcite in a closed system. The effect of this exchange is to increase $\delta^{13}\text{C}$ in the graphite and decrease $\delta^{13}\text{C}$ in the calcite, so that the difference between organic and carbonate $\delta^{13}\text{C}$ decreases with increasing grade. The difference between $\delta^{13}\text{C}$ of organic material and calcite in unmetamorphosed rocks is $\sim 28\text{‰}$ (e.g. Knoll et al., 1986), reducing to $\sim 12\text{‰}$ in greenschist facies rocks and $\sim 4\text{‰}$ in amphibolite facies rocks (Kitchen and Valley 1995, figure 1). Although graphite may only be a minor component in limestones, it contains, weight for weight, more than 8 times as much carbon as calcite. Thus even a small amount of graphite has the potential to reduce the $\delta^{13}\text{C}$ of host carbonate by a significant amount, particularly at elevated temperatures above 500°C . Kitchen and Valley (1995) calculated that graphite – calcite ^{13}C exchange in a limestone with a

$C_{\text{graphite}}/C_{\text{rock}}$ ratio of 0.1 would result in a *c.* 3‰ reduction in $\delta^{13}\text{C}$ of the host calcite. The possibility of reduction in calcite $\delta^{13}\text{C}$ by organic carbon – carbonate carbon ^{13}C exchange during metamorphism must be considered when interpreting the $\delta^{13}\text{C}$ data, bearing in mind that the difference in $\delta^{13}\text{C}$ between several Appin Group limestones is of the order of 3‰.

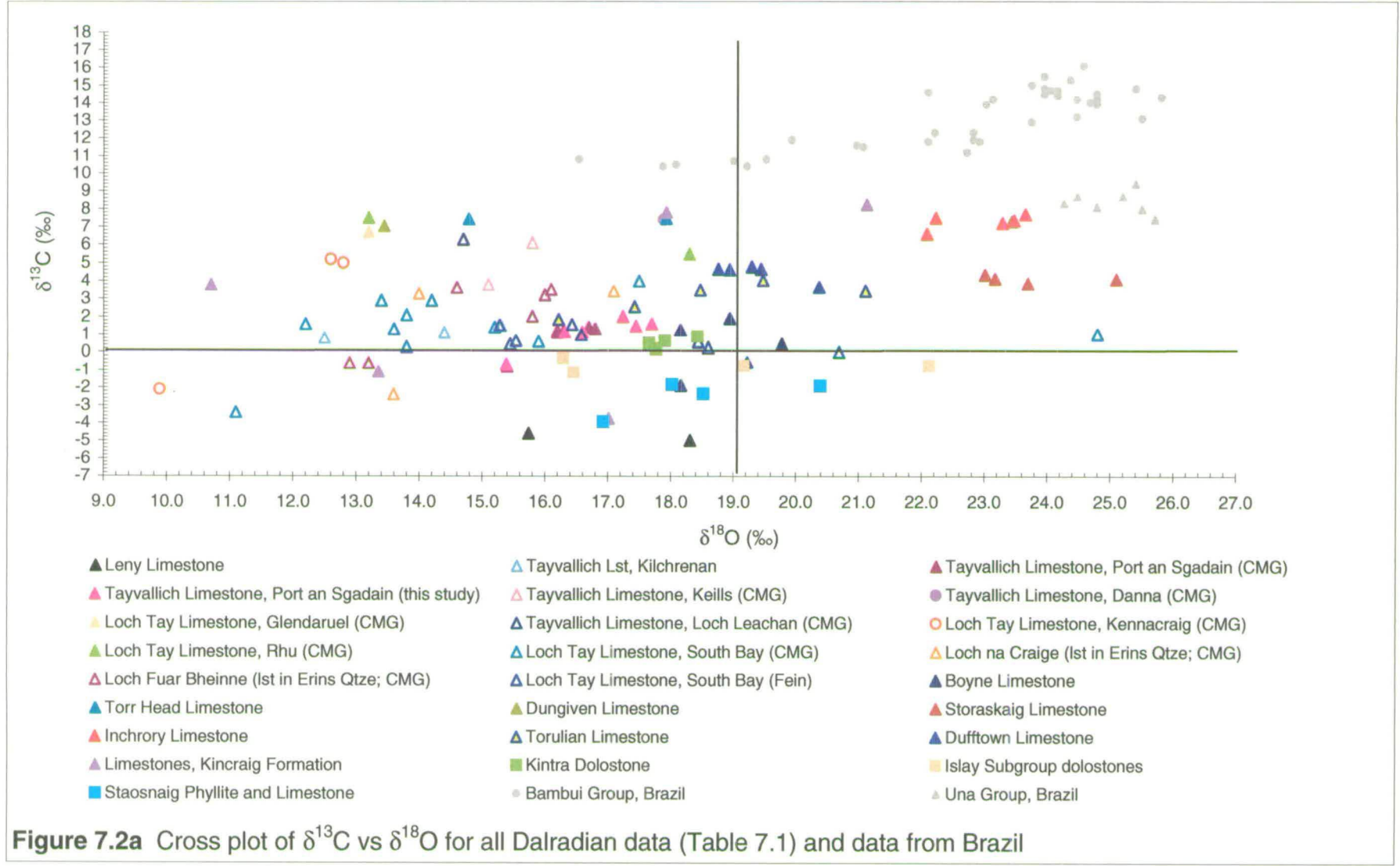
In summary, the $\delta^{13}\text{C}$ of organic carbon now preserved as graphite in metamorphosed carbonate rocks *will* have been altered and may have altered the $\delta^{13}\text{C}$ of the carbonate, depending on the (unknown) abundance of organic material. Coupled low differences between organic and carbonate $\delta^{13}\text{C}$ and low $\delta^{13}\text{C}$ in the carbonate would be strong evidence for significant exchange during metamorphism and the alteration of primary carbonate $\delta^{13}\text{C}$ values. However, although amongst the limestone samples studied in this thesis there are probably several which are suitable for the study of organic carbon $\delta^{13}\text{C}$ and its relationship to carbonate $\delta^{13}\text{C}$ (e.g. Storakaig Limestone, Torr Head Limestone, Leny Limestone), such work has not been undertaken because of time constraints. Thus, assessment of alteration of carbonate $\delta^{13}\text{C}$ relies here on examination of the covariation of $\delta^{13}\text{C}$ and $\delta^{18}\text{O}$, and of these isotope δ -values with respect to whole-rock Mn/Sr data, building on the analysis presented in Chapter 6.

7.4.2 'Whole-rock' $\delta^{13}\text{C}$ and $\delta^{18}\text{O}$ co-variation

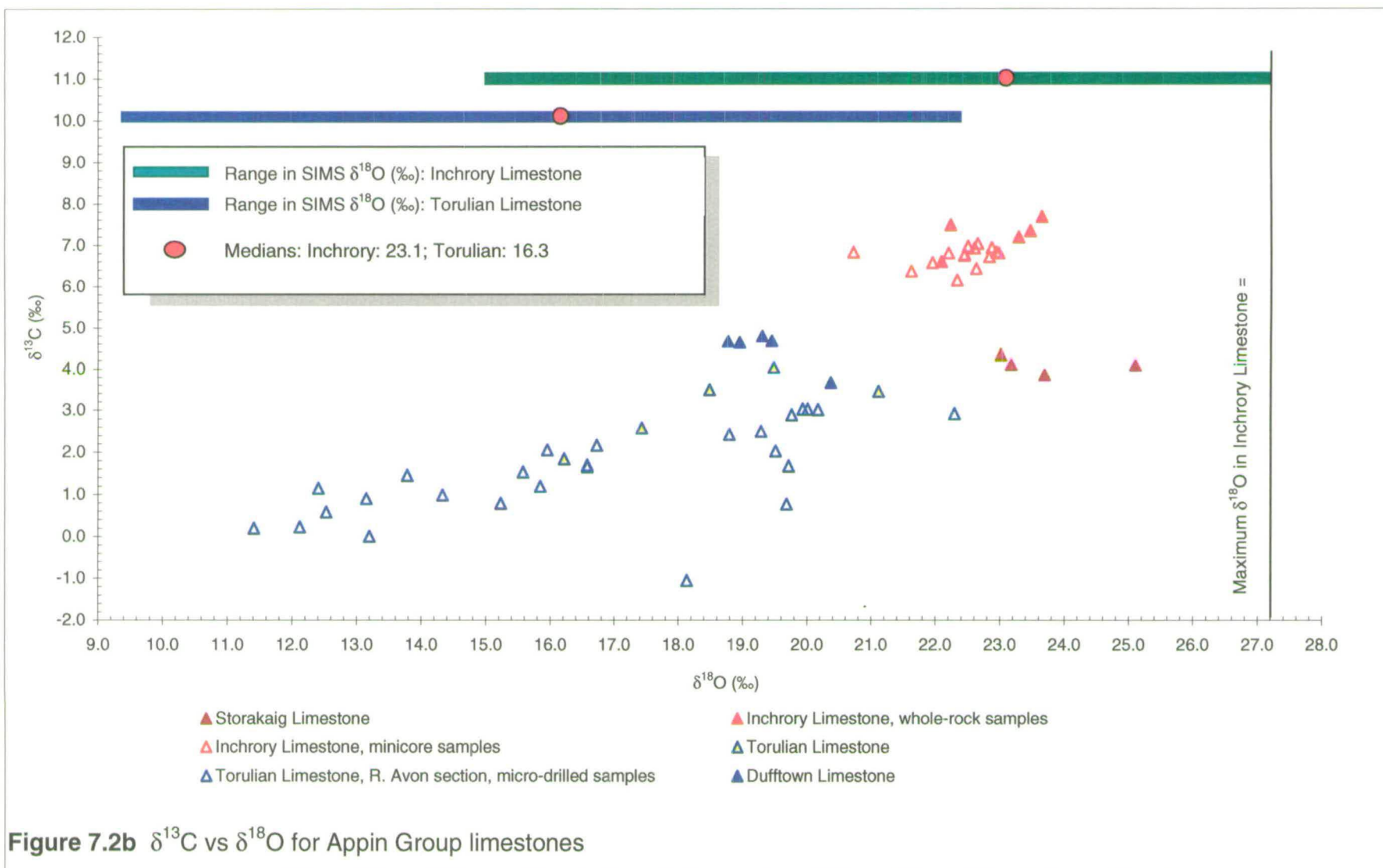
Positive covariation between $\delta^{13}\text{C}$ and $\delta^{18}\text{O}$ is considered indicative of modification by fluid-rock interaction as carbonate $\delta^{13}\text{C}$ is, *as a general rule*, lowered from high primary marine values by interaction with diagenetic and metamorphic fluids containing isotopically light carbon (e.g. as CO_2).

The covariation of $\delta^{13}\text{C}$ and $\delta^{18}\text{O}$ amongst Dalradian limestone and dolostone whole-rock samples is shown in Figures 7.2a-d. All the data are shown together on Figure 7.2a. There are several interesting features:

- 1) The Inchrory Limestone ‘whole-rock’ data show consistent covariation between $\delta^{13}\text{C}$ and $\delta^{18}\text{O}$. In addition, the Inchrory Limestone minicore samples from the Limeworks Quarry profile (see Chapter 9) are slightly depleted in both ^{13}C and ^{18}O relative to the whole rock samples and lie on the same trend (see Figure 7.2b). The overall range is about 2‰ in $\delta^{13}\text{C}$ and 3‰ in $\delta^{18}\text{O}$. The covariation is not monotonic, a number of minicore samples having equivalent $\delta^{13}\text{C}$ have lower $\delta^{18}\text{O}$ values. Notably, amongst these samples there is a tendency for samples in the inner part of the profile to have lower $\delta^{18}\text{O}$ values than samples in the outer part (Chapter 9), though they lie on parallel trends.
- 2) The Storakaig and Dufftown limestones and three of the Torulian Limestone samples show no clear ‘within group’ covariation between $\delta^{13}\text{C}$ and $\delta^{18}\text{O}$ (Figure 7.2b).
- 3) Although lower in $\delta^{13}\text{C}$ than the lithostratigraphically equivalent Inchrory Limestone, the Storakaig Limestone samples, being relatively lower in ^{13}C , are clearly not on the ‘trend’ extending from the Inchrory Limestone sample group through the Torulian Limestone samples (See also Figure 7.2b).



- 4) The Dufftown Limestone samples plot in a position which could be deemed to lie on the 'Inchrory Limestone-Torulian Limestone' 'trend'. However, $\delta^{13}\text{C} - \delta^{18}\text{O}$ covariation parallel to this trend is not observed *within* the sample group.
- 5) Several 'Tayvallich' equivalent limestones show no covariation between $\delta^{13}\text{C}$ and $\delta^{18}\text{O}$, having high $\delta^{13}\text{C}$ values across their range in $\delta^{18}\text{O}$ (see also Figure 7.2c). These include the Torr Head and Dungiven limestones and samples of the Loch Tay and Tayvallich Limestones from the Scottish mainland, including Danna, Rhu, Glendaruel, Keills and Loch Leathan. Glendaruel, Rhu and Dungiven limestones are amphibolite grade, the remainder are greenschist facies.
- 6) With the exception of several limestones with high $\delta^{13}\text{C}$, 'Tayvallich' limestones with $\delta^{18}\text{O} < \sim 18.5\%$ display wide-ranging covariation between $\delta^{18}\text{O}$ and $\delta^{13}\text{C}$. Most limestone sample groups with $\delta^{18}\text{O} > \sim 18.5$ show no clear covariation with $\delta^{13}\text{C}$; the Inchrory Limestone is a notable exception.
- 7) The Boyne Limestone data are ambiguous, with no clear $\delta^{13}\text{C} - \delta^{18}\text{O}$ relationship indicated.
- 8) Several groups of Tayvallich and Loch Tay samples define trends of $\delta^{13}\text{C} - \delta^{18}\text{O}$ covariation parallel to the Inchrory-Torulian 'trend'.



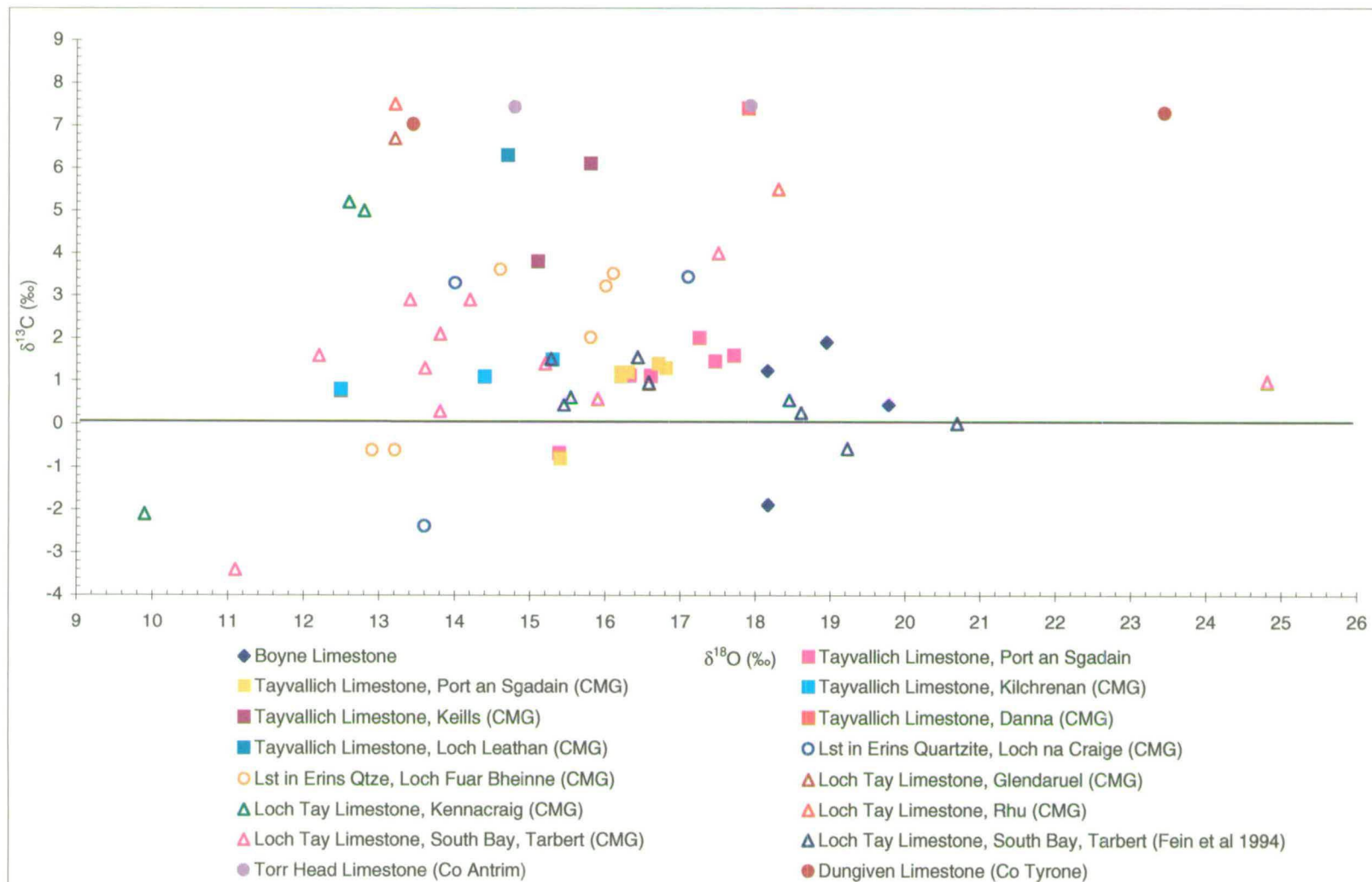


Figure 7.2c Cross plot of $\delta^{13}\text{C}$ vs $\delta^{18}\text{O}$ for Tayvallich and equivalent limestones

- 9) Dolostones with $\delta^{18}\text{O} > \sim 18.5\text{‰}$ show no obvious depletion of $\delta^{13}\text{C}$ (Figure 7.2d). Islay Subgroup dolostones behave in a similar manner to the Torr Head and Dungiven limestones, lacking depletion in $\delta^{13}\text{C}$ at $\delta^{18}\text{O}$ values less than $\sim 18.5\text{‰}$.
- 10) The Kintra Dolostone samples lie parallel to the Inchrory-Torulian 'trend', as do the three Staosnaig Phyllite Formation samples with $\delta^{18}\text{O}$ below 18.5‰ .

7.4.3 Preservation of primary $\delta^{13}\text{C}$ values

The features of Figures 7.2a-d reveal complex, varying and, in some cases, apparently paradoxical behaviour amongst the groups of samples. These are discussed in this next section, in which I establish which of the limestones and dolostones have preserved primary/near-primary $\delta^{13}\text{C}$ values and which have not, and suggest models to explain the observed types of covariation for different groups of limestone and dolostone samples.

Limestones

Difference in carbonate $\delta^{13}\text{C}$ between Inchrory and Storakaig Limestones The Inchrory and Storakaig limestones have very similar $\delta^{18}\text{O}$, overlapping $^{87}\text{Sr}/^{86}\text{Sr}$ values (Chapter 6, Figure 6.2), but very different $\delta^{13}\text{C}$ values (Table 7.1a, Figure 7.2b). These two limestones are considered to be lithostratigraphically equivalent, the *implication* being that they were deposited at *broadly* the same time. If they are coeval, then they *might* reasonably be expected to have closely similar $\delta^{13}\text{C}$ values, especially given their similarity in $^{87}\text{Sr}/^{86}\text{Sr}$ and $\delta^{18}\text{O}$ and assuming that their whole-rock carbon isotope composition is a function of that of marine total dissolved

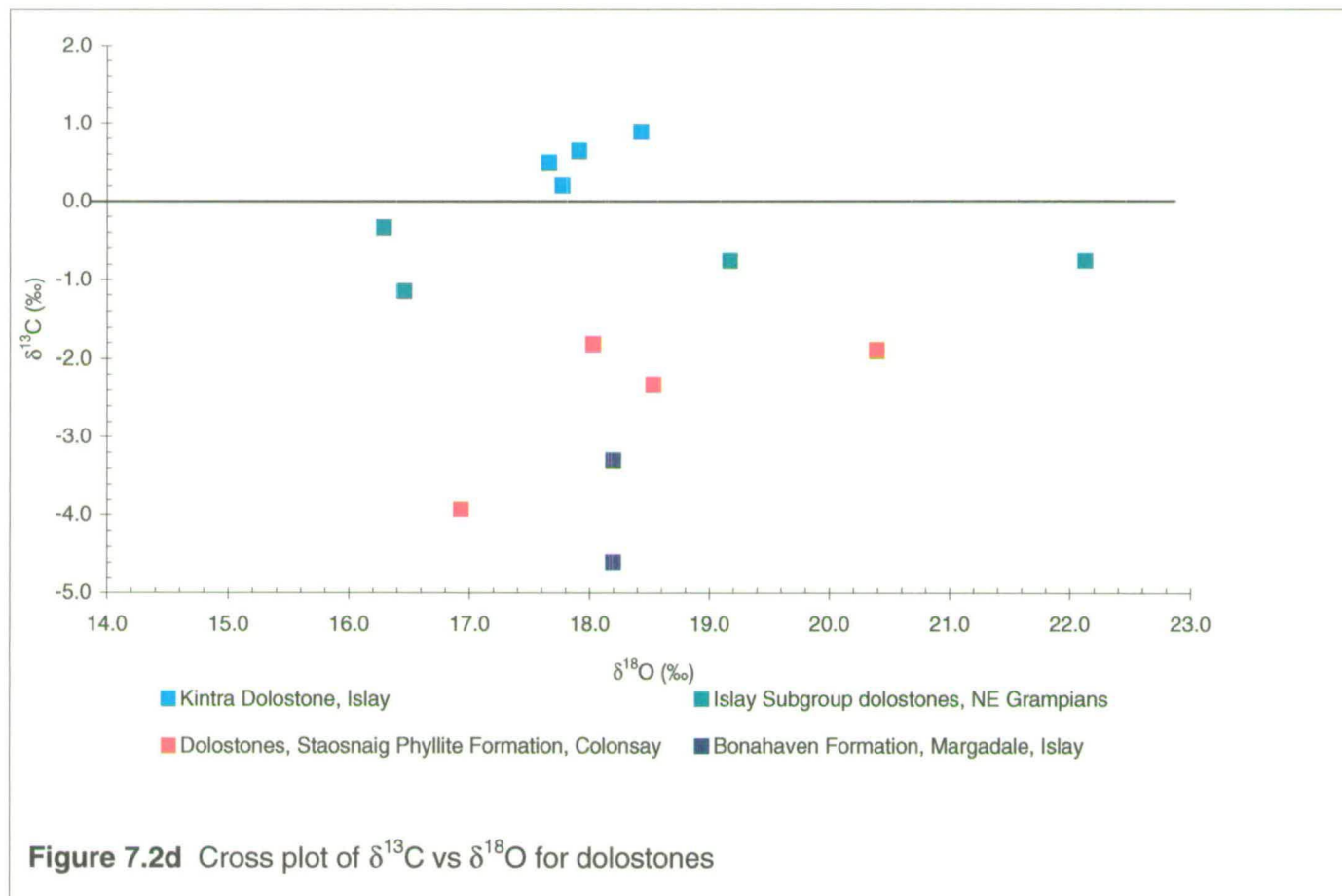


Figure 7.2d Cross plot of $\delta^{13}\text{C}$ vs $\delta^{18}\text{O}$ for dolostones

carbonate (TDC) at their time of deposition. The question then is how to account for the difference in $\delta^{13}\text{C}$ between these two limestones. Is the difference primary, due either to global secular isotopic variation in TDC or local environmental conditions in basins with restricted connectivity to the open oceans (note that the former implies the two limestones are not the same age), or are the differences due to exchange of carbonate in the Storakaig Limestone with a lower $\delta^{13}\text{C}$ source, either in a closed system during metamorphism or during open exchange with an exotic diagenetic or metamorphic fluid?

The high $\delta^{18}\text{O}$ values indicate that exchange with an external diagenetic or metamorphic fluid did not occur in either of these limestones (cf. arguments in Chapter 6 with regard to $^{87}\text{Sr}/^{86}\text{Sr}$ data).

Cathodoluminescence images of oolite-bearing sediments in the Storakaig Limestone reveal that calcite microspar matrix is more luminescent overall than the coarser spar replacing former aragonitic oololiths and ooclasts (Chapter 3; Figure 3.19a,b). However, the correspondence of luminescence with original carbonate grain boundaries indicates that the differences in luminescence have more to do with preserved *primary* chemical differences than alteration during later diagenesis or metamorphism. If the sparry calcite pseudomorphing oololiths is correctly interpreted as replacing original aragonite (Chapter 3), then it appears that this transformation from aragonite to calcite has not masked chemical differences between the oololiths and the matrix.

Petrographical differences between the Inchrory and Storakaig limestones are considerable, reflecting, in the main, different degrees of recrystallisation suffered during metamorphism (Chapter 3). Although pressures are estimated to have reached

~10 kbars in southeastern Islay (Chapter 2; Table 2.4), metamorphic grade reached no more than moderate greenschist facies (400 °C) in the area within which the Storakaig Limestone crops out, and the limestone clearly preserves many primary and diagenetic pre-metamorphic features, the ooliths being the most notable (Figures 3.19a,b). In contrast, the Inchrory Limestone is medium to coarse grained grey limestone with fully metamorphic, commonly elongate polygonal fabrics which, along with phyllosilicates, are aligned to the local, peak metamorphic S_2 cleavage (Chapter 3; Figure 3.21). Metamorphic grade reached well into amphibolite facies, with temperatures near 600° C locally (Chapter 2; Table 2.4). In both rocks, organic material/graphite is present locally in the limestones, where it imparts a dark grey colour, but it is not apparently as abundant in the Inchrory Limestone as in the Storakaig Limestone. In the former it occurs as disseminated 'dust' within the calcite, whereas in the latter it occurs largely in the interstices between relict ooids, but is notably absent from the microspar matrix.

In the absence of evidence for significant infiltration of a metamorphic fluid phase, I conclude that exchange of ^{13}C between organic carbon and carbonate during metamorphism did not occur significantly in the Storakaig Limestone, for the following reasons:

- a) The lower peak metamorphic temperatures experienced by the Storakaig Limestone will have inhibited carbon mobility during low-grade metamorphism; equilibration of ^{13}C between organic material/graphite and carbonate is very sluggish below amphibolite facies (Kitchen and Valley, 1995).

- b) Preservation of diagenetic fabrics, particularly relict ooids, demonstrates the lack of pervasive metamorphic recrystallisation, preventing extensive exchange of ^{13}C between carbonate and organic material, and, linked to this,
- c) organic material is concentrated only locally within the Storakaig Limestone, severely limiting the possibility of exchange with the wider carbonate ^{13}C reservoir in the matrix.

If the organic material in the Storakaig Limestone was oxidised during diagenesis, it is possible that isotopically light carbon could have been released from organic material and incorporated in carbonate. However, the presence of abundant organic matter indicates that much or all of it has been preserved and it is still very locally distributed, so that light carbon has remained locked up in this material. It is very likely that the diagenetic fluid in these rocks was coeval seawater which, additionally, might have been oxygen-depleted if these rocks represent carbonate reworked into deeper water (Chapter 3). Seawater would have had limited potential to oxidise the organic material, once it became pore fluid in buried sediment with restricted connectivity to marine bottom waters. The very uniformity of whole-rock carbonate $\delta^{13}\text{C}$ in the Storakaig Limestone and lack of covariation with $\delta^{18}\text{O}$, suggests that it has been largely undisturbed during both metamorphism and diagenesis.

In contrast, one would expect metamorphic re-equilibration of $\delta^{13}\text{C}$ between organic material and carbonate to have occurred in the Inchroary Limestone, given the grade at which these rocks were metamorphosed. Yet, recorded $\delta^{13}\text{C}$ values are high

(at least 2.2 ‰ higher than in the Storakaig Limestone; Table 7.1, Figure 7.2b), and are tightly grouped.

Although there is covariation between $\delta^{13}\text{C}$ and $\delta^{18}\text{O}$, this is limited and both $\delta^{13}\text{C}$ and $\delta^{18}\text{O}$ values remain high. The combined data indicate that whole-rock carbonate $\delta^{13}\text{C}$ has not been *significantly* affected by ^{13}C exchange with organic material or graphite, or with an external ^{13}C -depleted fluid, during metamorphism. As far as it goes, all the whole-rock isotope data suggests that the Inchrory Limestone has retained primary/near-primary carbonate $\delta^{13}\text{C}$ values and, as will be discussed below, the Inchrory Limestone carbonate $\delta^{13}\text{C}$ values, though high, are entirely consistent with $\delta^{13}\text{C}$ data from unmetamorphosed Neoproterozoic limestones of Riphean age. Nevertheless, peak $\delta^{18}\text{O}$ values of $\sim 27\text{‰}$ are recorded in the three samples of Inchrory Limestone analysed by SIMS (Chapter 9; see SIMS range on Figure 7.2b).

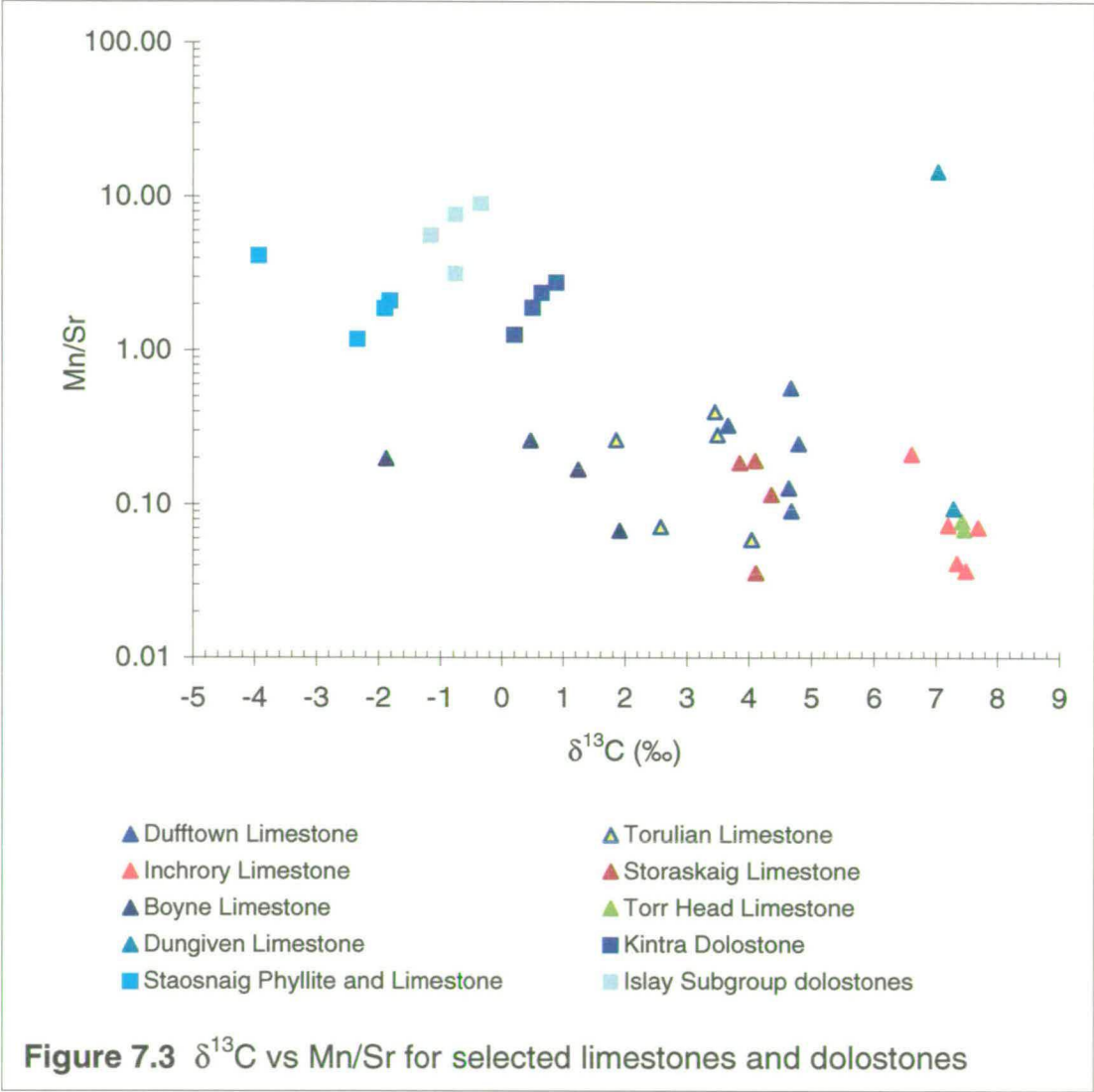
In the light of these sedimentary carbonate $\delta^{18}\text{O}$ values, it is very tempting to speculate, given the $\delta^{13}\text{C}$ - $\delta^{18}\text{O}$ covariation observed in Figure 7.2b, that primary carbonate $\delta^{13}\text{C}$ values might have been even higher than those recorded by whole-rock analyses (SIMS analysis of ^{13}C was not undertaken due to technical difficulties). Very high carbonate $\delta^{13}\text{C}$ values of $\sim 11\text{‰}$ or more are recorded in Neoproterozoic carbonate rocks from Mongolia (Brasier et al., 1996) and Brazil (Iyer et al., 1995; Misi and Veizer, 1998); the Brazilian rocks are of particular interest because various lines of evidence suggests that they are about the same age as the Inchrory Limestone samples. A simple comparison of Inchrory C and O isotope data with the equivalent data for very positive $\delta^{13}\text{C}$ calcites from Brazil (Figure 7.1a; data from Misi and Veizer 1998 and Iyer et al., 1995) shows that it is entirely possible for the Inchrory

Limestone to have had primary carbonate $\delta^{13}\text{C}$ values in excess of 10‰; the data from the Una Group of Brazil (Misi and Veizer 1998) are particularly close.

- Thus, I conclude that the difference in carbonate $\delta^{13}\text{C}$ between the Inchrory and Storakaig limestones is largely a primary phenomenon and has not resulted from significant modification during diagenesis or metamorphism. The implications of this conclusion will be discussed further below.

Dufftown Limestone With one exception, the $\delta^{13}\text{C}$ values for this group of samples are identical (Table 7.1a, Figure 7.2b). The exception, despite having higher $\delta^{18}\text{O}$ than the rest, has significantly higher $^{87}\text{Sr}/^{86}\text{Sr}$ and lower $\delta^{13}\text{C}$. Comparison with other data in Figure 7.2b, including the Brazilian data shows that this is not an isolated phenomenon. The remaining samples cluster tightly with respect to Sr, carbon and oxygen isotopes and, as a group in themselves, show no relationship between $\delta^{13}\text{C}$ and $\delta^{18}\text{O}$. Figure 7.3 shows that there is also no relationship between $\delta^{13}\text{C}$ and Mn/Sr. Consequently, although they lie on a $\delta^{13}\text{C}$ - $\delta^{18}\text{O}$ trajectory from the Inchrory Limestone towards samples deemed to be altered (see below), and although $\delta^{18}\text{O}$ values are depleted relative to sedimentary values, the $\delta^{13}\text{C}$ values are considered to be primary/near primary.

Torulian Limestone – local preservation of primary $\delta^{13}\text{C}$ Geochemical data for the whole-rock samples from this limestone indicate that the three samples with relatively high $\delta^{18}\text{O}$ (>18.5 ‰) are considered to have maintained their $\delta^{13}\text{C}$ values at or near primary levels (Figure 7.2b). However, four of the five samples lie on a very



linear trend in Figure 7.2b and samples with higher $\delta^{13}\text{C}$ have lower Mn/Sr (Figure 7.3). These relationships suggest that there has been some reduction in $\delta^{13}\text{C}$ due to fluid-rock interaction, either during diagenesis or metamorphism. One of these samples (HY47) comes from the section through the Torulian Limestone in the River Avon, near Tomintoul, where additional carbon and oxygen isotope data indicate a protracted history of alteration during metamorphic fluid infiltration events (see Chapter 9 for full discussion).

Topmost Argyll Group ('Tayvallich') limestones

This next section discusses the C and O isotope and trace element geochemistry of the Tayvallich Limestone and its equivalents, the Loch Tay, Torr Head and Dungiven limestones which occur at the top of the Argyll Group (Chapter 2). Included here are unpublished stable isotope data for the Tayvallich and Loch Tay limestones (C M Graham and A E Fallick, unpublished data; Greig (1984); data in Figure 2 of Fein et al., 1994). The geochemical history of the Tayvallich and Loch Tay limestones is complicated and characterised by considerable post-depositional and metamorphic alteration by fluid-rock interaction, specifically:

- a) Hydrothermal alteration and extensive carbonation of mafic rocks occurred coeval with intrusion and extrusion the Tayvallich Lavas and associated rocks (Graham 1976).
- b) Major regional metamorphic fluid flow, focused principally on the axis of the Ardrishaig Anticline (Cole and Graham, 1994; Cole, 1997; Graham et al., 1983; Skelton, 1993; Skelton et al., 1995), in which there was extensive alteration of

the isotope chemistry and mineralogy of metabasic and metasedimentary rocks (see Chapter 6), and

- c) late, fracture-controlled infiltration of retrograde fluid of obscure origin resulted in dolomitisation of limestones and the formation of $\delta^{18}\text{O}$ -enriched dolomite (Fein et al., 1994).

However, high (>5‰) carbonate $\delta^{13}\text{C}$ values are preserved in several limestone samples and these are likely to be near-primary. In addition, the data also help elucidate, in the qualitative overview presented here, the main causes of alteration arising from key fluid-rock interaction phenomena which have affected the Southwest Highlands, as listed above.

The ‘Tayvallich’ limestone samples discussed herein come from widely distributed outcrops in peninsular Argyll, and Northern Ireland (see Figure 6.1). They vary widely in lithology and are locally impure, being interbedded with siliciclastic rocks. Calc-silicate assemblages are developed extensively (e.g. South Bay, near Tarbert (Greig, 1984; Graham et al., 1983) and Perthshire (Cole, 1997)). In addition, vein-controlled late dolomitisation is a common feature of the Loch Tay Limestone (Fein et al., 1994). Metamorphic grade ranges from lower greenschist to amphibolite facies. As a whole, the sample suite exhibits wide-ranging stable isotope characteristics. These isotopic characteristics can be interpreted in terms of processes known to have affected the rocks in specific localities.

Constant $\delta^{13}\text{C}$ values vs widely varying $\delta^{18}\text{O}$ - identification of primary $\delta^{13}\text{C}$ values

Figure 7.2c shows that samples of Tayvallich, Loch Tay and related limestones from several localities contain elevated $\delta^{13}\text{C}$ values between 6 and 8 ‰. These include the

Torr Head and Dungiven Limestone samples and several samples from Scottish mainland localities (Rhu, Keills, Danna, Glendaruel and Loch Leachan). These samples stand out because the available data indicate maintenance of $\delta^{13}\text{C}$, whilst being variably depleted in ^{18}O (range 13.2 – 23.4). This 10 ‰ range in $\delta^{18}\text{O}$ values, the range in Mn/Sr for the Irish samples (Figure 7.3) and the extensive development of calc-silicate minerals (e.g. grossular; see also Chapter 4) consistent with infiltration of H_2O -rich fluid Graham et al. (1983), suggest variably open fluid-rock interaction, which might be expected to induce covariation between carbon and oxygen isotopes. The large black crystals characteristic of the Torr Head and Dungiven limestones (and also found in some outcrops of Tayvallich Limestone in the Southwest Scottish Highlands) contain abundant, finely disseminated opaque material which is probably now graphite, suggesting potential for metamorphic re-equilibration of ^{13}C between organic material and carbonate during metamorphism, as described above. However, the strongly positive and uniform $\delta^{13}\text{C}$ for these samples indicates that equilibration of ^{13}C between the two carbon-bearing phases has not happened during metamorphism, even though graphitic material appears abundant in the large black crystals. This lack of correlation between $\delta^{13}\text{C}$ and grade in these samples is clear from Figure 7.2c. High $\delta^{13}\text{C}$ values are preserved across the range in metamorphic grade (closed symbols: greenschist facies; open symbols: amphibolite facies). In these rocks, at least, exchange of ^{13}C with either an internal or external source of isotopically light carbon did not occur, even in rocks where fluid infiltration is indicated by strongly depleted $\delta^{18}\text{O}$ (e.g. as in samples from Glendaruel, Rhu and Dungiven; Figure 7.3c). The data are taken to indicate that the primary $\delta^{13}\text{C}$ value of the ‘Tayvallich’ limestones was around 7‰.

Preservation of carbonate $\delta^{13}\text{C}$ during diagenesis

Although perhaps surprising, the lack of covariation between $\delta^{13}\text{C}$ and $\delta^{18}\text{O}$ shown by the samples discussed above is not unreasonable. Work by Banner et al., (1990) on the Mississippian Burlington-Keokuk Formation showed that later, second-generation, dolomite had similar $\delta^{13}\text{C}$ values to precursor dolomite, whilst $\delta^{18}\text{O}$ and $^{87}\text{Sr}/^{86}\text{Sr}$ differed. By developing quantitative models for isotope and trace element variations during diagenetic fluid-rock interaction, they were able to show that $\delta^{13}\text{C}$ (and REE also) could be maintained whilst $\delta^{18}\text{O}$ and, to a lesser extent, $^{87}\text{Sr}/^{86}\text{Sr}$ were altered. The main control on this decoupling of isotopic systems are the chemical and isotopic composition of the fluids with which the carbonate rocks interact. This is entirely analogous to the decoupling of $\delta^{18}\text{O}$ and $^{87}\text{Sr}/^{86}\text{Sr}$ observed in metamorphic rocks (Chapter 6; Bickle and Chapman 1990). Carbonate rocks will tend to buffer their $\delta^{13}\text{C}$ compositions to a large extent because fluids tend to be poor in these components relative to rocks. The fact that most fluids will be almost 90% O by weight, compared to 50% for a pure calcite limestone, means that the buffer capacity of carbonates for oxygen isotopes is much more limited relative to C and Sr. Banner and Hanson (1990) indicate the magnitude of this difference by noting that carbonate rocks will equilibrate with fluid $\delta^{18}\text{O}$ values at water:rock ratios three orders of magnitude lower than those required for equilibration with fluid $\delta^{13}\text{C}$.

In light of the modelling results presented by Banner and Hanson *op. cit.*, the simplest interpretation of the $\delta^{13}\text{C}$ data for the Torr Head/Dungiven limestones and the Islay Subgroup dolostones is that they preserve primary $\delta^{13}\text{C}$ values, even though there is clear evidence for oxygen isotope exchange via infiltration of H_2O -rich fluid.

Tayvallich Limestone, Port an Sgadain – the case for hydrothermal alteration by seawater

With the exception of one sample with low $\delta^{13}\text{C}$, samples of the Tayvallich Limestone from Port an Sgadain (Tayvallich Peninsula) have similar carbonate $\delta^{13}\text{C}$ and $\delta^{18}\text{O}$ (~16 - 17‰). (*as Mn and Sr data are not available for these samples, the extent of $\delta^{13}\text{C}$ – Mn/Sr covariation cannot be established*). Figure 7.2 includes previous analyses of C and O isotopes in the Port an Sgadain samples determined by C. Graham (listed as ‘CMG’ in legend); the old and new analyses are effectively the same.

It is clear the from petrographic (Chapter 4) and $\delta^{18}\text{O}$ data (Table 7.1a) that these samples have undergone extensive alteration of oxygen isotope compositions, with carbonate $\delta^{18}\text{O}$ values being reduced to ~16 - 17‰ during isotopic exchange with hydrothermal fluid. In contrast, Graham et al. (1983) concluded that carbon isotopes were buffered by the limestones and remained at near-sedimentary values, since the hydrothermal fluid is likely to have been C-poor. However, Port an Sgadain carbonate $\delta^{13}\text{C}$ values are ~5-6‰ lower than other Tayvallich limestones having consistently high $\delta^{13}\text{C}$ values of ~ 7‰. If the high values reflect the original marine $\delta^{13}\text{C}$ of the Tayvallich limestones in general, $\delta^{13}\text{C}$ in the Port an Sgadain samples have been significantly depleted by ~ 5 – 6 ‰, relative to primary values and homogenised like the $\delta^{18}\text{O}$. Such shifts in carbon isotope values will be a complex function principally of the $\delta^{13}\text{C}$ of the fluid phase, the fluid flux and the length of time over which the fluid has interacted with the rock. Nevertheless, the relative magnitudes of the shifts of $\delta^{13}\text{C}$ and $\delta^{18}\text{O}$ in the Port an Sgadain samples compared with the Irish samples, suggests strongly that the fluid with which the former

interacted was strongly depleted in $\delta^{13}\text{C}$. The fact that both C and O isotopes appear de-coupled with $^{87}\text{Sr}/^{86}\text{Sr}$ in the limestone at Port an Sgadain constrains plausible sources for fluids.

It is possible to reconcile the shifts and covariation in $\delta^{13}\text{C}$ and $\delta^{18}\text{O}$ with the 'stationary' $^{87}\text{Sr}/^{86}\text{Sr}$ data which, taken in isolation, indicate little isotopic alteration. The Tayvallich Limestone at Port an Sgadain is overlain and intruded by Tayvallich lavas. Figure 3.16 shows clearly that the lavas intruded wet, unlithified, impure carbonate sediment at Port an Sgadain. The limestones are bound beneath by a mafic intrusive sheet (C. Graham, personal communication). Examination of the limestone outcrop at Port an Sgadain shows that limestones are locally impure and include greenish-grey calc-phyllites studded with large (2-5mm) black, isolated calcite crystals, similar to those observed in the Torr Head and other 'Tayvallich' limestones.

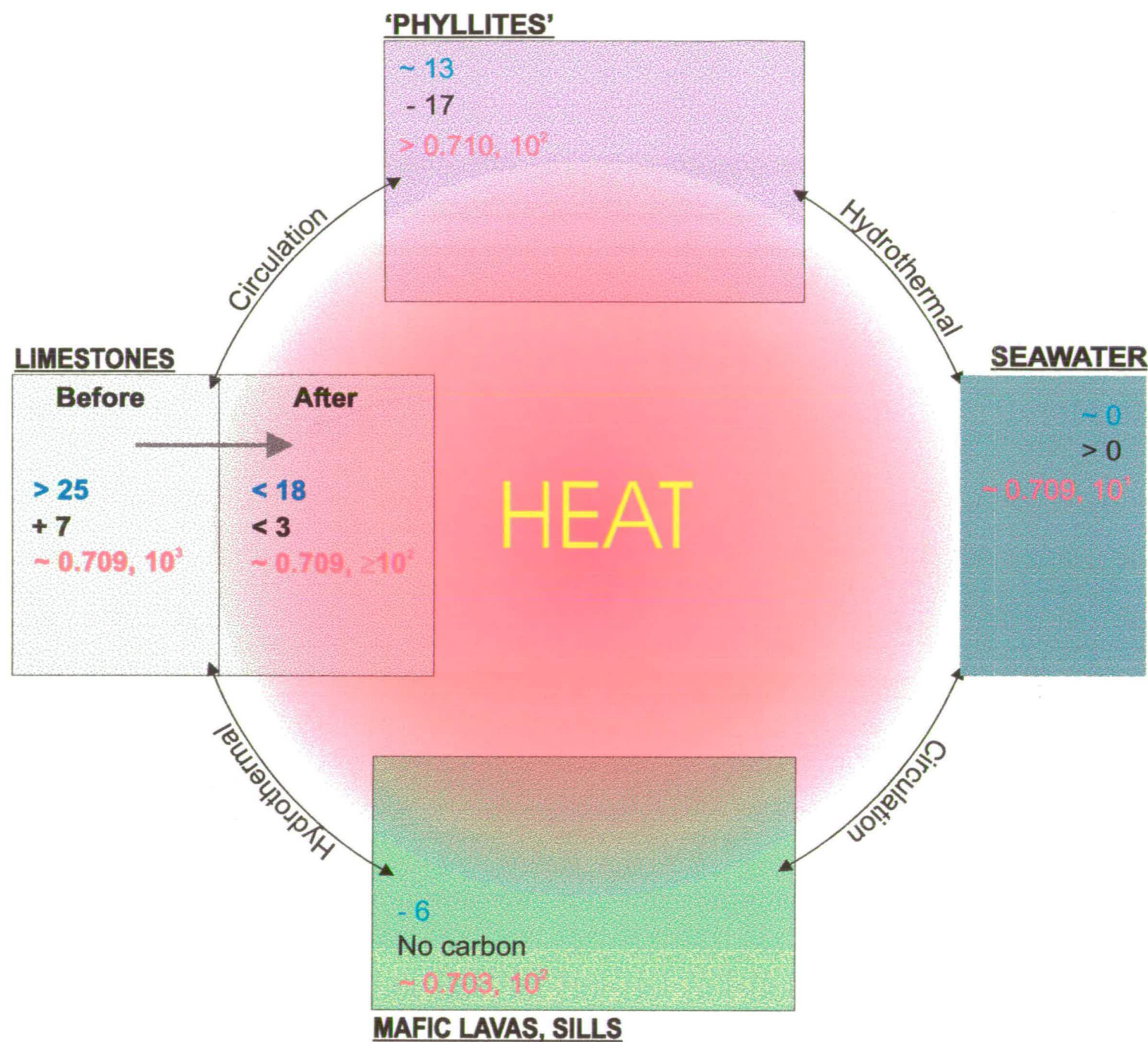
Hydrothermal activity coeval with the extrusion of the lavas and voluminous intrusion of the metabasite sheets in the Southwest Highlands is manifest in well-documented spilitisation of the mafic rocks (Graham, 1976). Thus, I consider it possible that the alteration of C and O isotopes in the Tayvallich Limestone at Port an Sgadain resulted from hydrothermally-driven exchange in an open system during early diagenesis when the limestones and interbedded siliciclastic rocks were still porous and were probably stabilising mineralogically from aragonitic rocks (by analogy, high Sr values in the Torr Head, Dungiven and Boyne limestones suggest an aragonite-dominated primary mineralogy).

The primary fluid was likely to have been dominantly marine: this is suggested by the spilitisation of the mafic rocks. The controls on the isotope and

trace element chemistry of this fluid would have been complex, since it would have interacted with the limestones and intercalated phyllosilicate-rich, siliciclastic lithologies, and the mafic rocks. I have attempted to summarise this hydrothermal model is summarised graphically in Figure 7.4.

Being predominantly derived from coeval seawater, $^{87}\text{Sr}/^{86}\text{Sr}$ in the hydrothermal fluids would have been buffered by the seawater and the limestones to near-seawater $^{87}\text{Sr}/^{86}\text{Sr}$ values. Furthermore, the net effect of fluid interacting with mafic rocks ($^{87}\text{Sr}/^{86}\text{Sr} \sim 0.703$) and siliciclastic rocks ($^{87}\text{Sr}/^{86}\text{Sr} > 0.713$) on carbonate $^{87}\text{Sr}/^{86}\text{Sr}$ would have been limited as their opposite influences on fluid $^{87}\text{Sr}/^{86}\text{Sr}$ would tend to cancel and both rock types have rather lower Sr concentrations than the limestones (Figure 7.4). Note that Tayvallich limestone $^{87}\text{Sr}/^{86}\text{Sr}$ (~ 0.709) is very approximately an average between $^{87}\text{Sr}/^{86}\text{Sr}$ for mafic and siliciclastic rocks. The actual value would have depended on complex mass-balance factors including fluid flux, time, temperature, relative volumes of phyllite, mafic rock and limestone in the hydrothermal cell, and their isotopic compositions. In effect, the $^{87}\text{Sr}/^{86}\text{Sr}$ of the hydrothermal fluid would have been buffered in a fashion analogous to the buffering of $^{87}\text{Sr}/^{86}\text{Sr}$ in seawater by continental and mantle Sr fluxes (Chapter 5).

The limestones would not have had the capacity to buffer oxygen isotope compositions during interaction with a fluid likely to have been depleted in ^{18}O through reaction with mafic and siliciclastic rocks. Estimates of primary $\delta^{18}\text{O}$ compositions of unaltered mafics are $\sim -6\text{‰}$ (C M Graham, personal communication) and of the order of 13‰ for phyllitic material (Graham et al., 1983); both are strongly to very strongly depleted in ^{18}O relative to primary limestone values ($\sim 25\text{‰}$). The $\delta^{18}\text{O}$ compositions of these lithologies would have reinforced to produce a



A simple box model to show sources of C, O and Sr and their isotopic composition for hydrothermal alteration of the Tayvallich Limestone at Port an Sgadain, Tayvallich. See text for sources of values.

KEY

> 25: carbonate $\delta^{18}\text{O}_{\text{SMOW}}$

+ 7: carbonate $\delta^{13}\text{C}_{\text{PDB}}$

~ 0.709, 10³: carbonate $^{87}\text{Sr}/^{86}\text{Sr}$,
magnitude of Sr
concentration in ppm

Sources of isotopes and net effects
on limestone isotope chemistry:

Low $\delta^{18}\text{O}$ from mafics and phyllites: marked
reduction in limestone $\delta^{18}\text{O}$

Very low $\delta^{13}\text{C}$ from organic matter in
phyllites: marked reduction in limestone $\delta^{13}\text{C}$

Phyllites and mafics counter each other in
 $^{87}\text{Sr}/^{86}\text{Sr}$: limestone $^{87}\text{Sr}/^{86}\text{Sr}$ left relatively
unaltered

Figure 7.4 A schematic hydrothermal box model to explain the alteration of C and O isotopes in the Tayvallich Limestone at Port an Sgadain, Tayvallich (see text for discussion).

hydrothermal fluid strongly depleted in ^{18}O during fluid-rock interaction. The *degree* of ^{18}O depletion of the fluid and the magnitude of its effect on ^{18}O in the limestones would have depended again on the complex interplay of a number of factors, but the overall *direction* of alteration during interaction would be one of ^{18}O depletion in the limestones.

Finally, the hydrothermal fluid may also have been $\delta^{13}\text{C}$ depleted by reaction with organic-rich phyllites similar to those from the Ardrishaig Phyllites, which are known to contain organic material with $\delta^{13}\text{C}$ values of *c.* -17‰ (Graham et al., 1983). As mentioned above, the outcrops of Tayvallich Limestone at Port an Sgadain contain abundant pale greenish grey phyllite near the top of the limestones. These interbedded phyllites probably contained organic material. Furthermore, it is likely that the limestones at Port an Sgadain also contained organic material, as it is abundant in other 'Tayvallich' limestones in the Southwest Highlands and Ireland. Thermal alteration of organic matter, involving oxidation, would have released ^{13}C -depleted carbon, lowering the $\delta^{13}\text{C}$ of carbonate in the limestones when they interacted with the fluid.

In summary, both $\delta^{13}\text{C}$ and $\delta^{18}\text{O}$ in the Tayvallich Limestone from Port an Sgadain were altered by interaction with a hydrothermal fluid generated by coeval igneous activity. Sources of ^{13}C - and ^{18}O -depleted materials were locally common, generating a ^{13}C - and ^{18}O -depleted fluid which systematically lowered carbonate $\delta^{13}\text{C}$ and $\delta^{18}\text{O}$ in the limestones. Paradoxically, carbonate $^{87}\text{Sr}/^{86}\text{Sr}$ ratios were relatively unmodified because of the counterbalancing effects of low and high ^{87}Sr sources in the mafic rocks and phyllites respectively. Once again, it is worth emphasising the point that porosities in the sediments would have been high prior to

complete lithification and mineralogical stabilisation, sufficient to permit open-system fluid-rock interaction. Hydrothermal fluid-rock interaction at this early diagenetic stage represents the best opportunity for extensive, nearly homogeneous alteration of limestone isotope chemistry.

The effects of metamorphic reactions and grade on $\delta^{13}\text{C}$ Also shown on Figure 7.2c are previously determined but unpublished $\delta^{13}\text{C}$ and $\delta^{18}\text{O}$ compositions of the Tayvallich and Loch Tay limestones (C M Graham and A Fallick, unpublished data; Greig, 1984; Fein et al., 1994). *Note the difference symbols representing difference in metamorphic grade of the samples: **open symbols** - epidote-amphibolite facies; **filled symbols** – greenschist facies.*

Several features are of note. Firstly, and of significance given the supposed lithostratigraphical equivalence of the Loch Tay, Tayvallich, Torr Head and Dungiven Limestones (Chapter 2), several samples contain high $\delta^{13}\text{C}$ values ($>6\text{‰}$) matching those seen in the Irish samples, despite the depletion of $\delta^{18}\text{O}$ to the low 'teens'. These high $\delta^{13}\text{C}$ samples are from both the greenschist and epidote-amphibolite facies terrains in the Southwest Scottish Highlands.

Secondly, many epidote-amphibolite facies limestones show considerable scatter between $\delta^{13}\text{C}$ and $\delta^{18}\text{O}$, making it difficult to discern any single causal factor for their obvious alteration. This feature is exemplified by the data from South Bay, Barmore, near Tarbert (Greig 1984). The samples from this locality contain a range of calc-silicate minerals including clinozoisite and grossular. The presence of such phases indicates infiltration by very hydrous fluids with trivial CO_2 contents, and different degrees of fluid buffering during metamorphism (Graham et al., 1983;

figure 6; their conclusions about fluid compositions which had reacted with the Loch Tay Limestone at South Bay, based on detailed petrography and Schreinemaker's analysis, are presented in Table 7.2).

The scatter in the isotope data for the epidote-amphibolite facies rocks from South Bay is in marked contrast to the consistent $\delta^{13}\text{C}$ - $\delta^{18}\text{O}$ covariation in the

Fluid composition	Assemblage	Fluid buffering (X_{CO_2} at 530°C)
Extremely H_2O -rich	gr + cc + qz + sph ± di ± ksp ± hy'gr	Unbuffered ($X_{\text{CO}_2} < 0.001$)
	qz + gr + cc + cz ± di ± ksp ± sph	Buffered ($X_{\text{CO}_2} \sim 0.004$)
H_2O -rich	Cc-bearing qz + ksp + cc + am + cz + sph ± ab	Unbuffered
	Cc-free qz + ksp + mu + cz + am + ± ab ± bi ± sph	($0.004 < X_{\text{CO}_2} < \sim 0.007$)
	qz + ksp + ab + mu + bi + cz/ep + cc + am +	Buffered ($X_{\text{CO}_2} \sim 0.005$)

Table 7.2 Buffering constraints of calc-silicate assemblages from South Bay, Tarbert, North Kintyre (after Graham et al 1983)

greenschist-facies Port an Sgadain limestones, but is consistent with the complexity of the phase relationships. Decarbonation driven by fluid infiltration will be a function of the bulk composition and the assemblage.

The situation is complicated further by the fact that buffered and unbuffered calc-silicate assemblages can occur in adjacent domains on the thin-section scale (Graham et al., 1983) (cf. Chapter 4). The presence of buffered and unbuffered assemblages indicates different degrees of reaction progress and thus different degrees of fluid-rock interaction. The isotopic composition of carbonate in domains with such assemblages will not only be a function of that of the infiltrating fluid and the primary carbonate composition, but also fractionation during decarbonation

reactions, the latter affecting $\delta^{13}\text{C}$ considerably more than $\delta^{18}\text{O}$ (Valley, 1986). From the available data it is clear that the rocks are not isotopically homogeneous at the scale of the outcrop at South Bay. This is not the same as saying that the rocks are in a state of isotopic disequilibrium. Given the local complexity in phase relations and the buffering characteristics of the mineral assemblages in the South Bay rocks, isotopic compositions are likely to have been controlled very locally, so it is fundamentally important to understand the scale over which isotopic compositions are homogeneous.

In summary, $\delta^{13}\text{C}$ and $\delta^{18}\text{O}$ have been considerably and variably altered in epidote-amphibolite facies limestones at South Bay which contain abundant calc-silicates developed in response to metamorphic fluid-rock interaction. Alteration of $\delta^{13}\text{C}$ and $\delta^{18}\text{O}$ was a complex function and interplay of fluid infiltration and coupled metamorphic reaction and both $\delta^{13}\text{C}$ and $\delta^{18}\text{O}$ have been disturbed significantly. This is in marked contrast to limestones at both greenschist and epidote-amphibolite facies elsewhere in the region which preserve high and consistent $\delta^{13}\text{C}$ over a wide range of $\delta^{18}\text{O}$ and which are reasonably assumed to be primary/near-primary.

Dolostones

Carbon isotope signatures in dolostones can be difficult to interpret. The data and conclusions presented in many studies of Neoproterozoic carbonate rocks reveal that dolomite $\delta^{13}\text{C}$ is significantly altered from primary values, rendering dolostones unreliable as monitors of secular marine isotopic variations. Other dolostones, however, (particularly fine-grained dolomicrospars), can retain $\delta^{13}\text{C}$ and *may* retain $^{87}\text{Sr}/^{86}\text{Sr}$ of adjacent interbedded limestones (e.g. Derry et al., 1992; Fairchild and

Spiro, 1987; Kennedy, 1996; Yang et al., 1999). Nevertheless, the albeit limited $\delta^{13}\text{C}$ data of two of the three dolostone units sampled for isotopic analysis as part of this study suggest they can be interpreted as near-primary and within the context of known Neoproterozoic variations in $\delta^{13}\text{C}$.

Islay Subgroup dolostones from the Northeast Grampians The reason for undertaking carbon and oxygen isotope analyses of these rocks is because of:

- a) their association with diamictic, tillite-like lithologies in the Dalradian of the Northeast Grampian Highlands which are correlated with the Port Askaig Tillite Formation, and
- b) the possibility that the dolostones may contain low $\delta^{13}\text{C}$ values often found in carbonate rock sequences associated with, or just above, Neoproterozoic tillite sequences worldwide (e.g. Prave, 1999; Kennedy 1996; Narbonne et al., 1994; Saylor et al., 1998, amongst others).

Islay Subgroup dolostones maintain carbonate $\delta^{13}\text{C}$ values in the range -0.3 to -1.3 across a ~ 6 ‰ range in $\delta^{18}\text{O}$ ($16.3 - 22.1$ ‰) (Figure 7.2d) and show no clear relationship between $\delta^{13}\text{C}$ and Mn/Sr (Figure 7.3). Although the $\delta^{13}\text{C}$ analyses are reconnaissance in nature, it is suggested that they can be interpreted as primary or near-primary carbonate $\delta^{13}\text{C}$ values using the same arguments as applied to interpretation of the ‘Tayvallich’ limestones with high and uniform $\delta^{13}\text{C}$. The best evidence here is provided by the lack of covariation with $\delta^{18}\text{O}$, discussed further below, and Mn/Sr. This lack of covariation between $\delta^{13}\text{C}$ and $\delta^{18}\text{O}$ (and, indeed

$^{87}\text{Sr}/^{86}\text{Sr}$) in dolostones has been noted by Kennedy (1996) in his work on the extensive Australian Marinoan cap-carbonates.

Additional supporting evidence for the preservation of $\delta^{13}\text{C}$ values in these dolostones comes from their fine-grained character, commonly held to be indicative of least altered state by others working in this field (e.g. Saylor et al., 1998) and the preservation of diagenetic rhombic dolomite textures within the polygonal metamorphic grain-boundary architecture (see Chapter 3, Figures 3.9, 3.10). Also included here are two dolostone samples from the Bonahaven Formation, Margadale, Islay (C M Graham and A Fallick, unpublished data). (Figures 7.1, 7.2d), which sits above the Port Askaig Tillite Formation.

If interpretation of the $\delta^{13}\text{C}$ data as primary is correct, then their negative values are at least *consistent* with the lithostratigraphical position of the dolostone samples close to tillite lithologies. More detailed work is in hand to elucidate variation in carbonate $\delta^{13}\text{C}$ across the Port Askaig Tillite and adjacent lithostratigraphic units (particular the dolostone-bearing Bonahaven Formation) and to establish the existence or otherwise of a negative excursion.

Kintra Dolostone Although the four samples from the Kintra Dolostone lie within a narrow range of <1‰ for both isotopes and the data are tightly grouped relative to most other groups of samples (Figures 7.2d, a), the isotopic composition probably results from early pervasive dolomitisation of originally aragonitic sediment (Sr 234 – 456ppm), when Sr isotopes were also shifted to continental values ($^{87}\text{Sr}/^{86}\text{Sr}$: 0.7204 – 0.7216). They are now very fine grained and massive, lacking calc-silicates.

Currently, the Kintra Dolostone is correlated lithostratigraphically with the Ballachulish and Dufftown limestones and placed at the base of the Ballachulish Subgroup. Comparison with the Dufftown Limestone shows that the Kintra Dolostone is lower in $\delta^{18}\text{O}$ by $\sim 1\text{--}2\text{‰}$ and in $\delta^{13}\text{C}$ by $\sim 3.5\text{--}4.5\text{‰}$. It was argued above that primary or near-primary $\delta^{13}\text{C}$ had been preserved in the Dufftown Limestone. Without implying any genetic relationship, it is noted that the shift in $\delta^{13}\text{C}$ between the two units is consistent with the scale of shifts in $\delta^{13}\text{C}$ arising from the diagenetic chemical modelling calculations of Banner and Hanson (1990). However, there is no clear geochemical evidence for correlation of these two units.

Staosnaig Phyllite Formation The possibility of correlation of the Staosnaig Phyllite Formation on Colonsay with the Dalradian has been discussed in Chapter 2. Samples were collected from the outcrops on the eastern side of Colonsay in order to characterise their geochemistry, including their $^{87}\text{Sr}/^{86}\text{Sr}$, $\delta^{13}\text{C}$ and $\delta^{18}\text{O}$ compositions and in the hope that the data may aid correlation. Previous unpublished stable isotope analyses of 'Colonsay Limestone' (C M Graham and A Fallick, unpublished data) gave $\delta^{18}\text{O}$ in the range $26\text{--}27\text{‰}$ and $\delta^{13}\text{C} \sim 2.5\text{‰}$ (Table 7.1a). The high $\delta^{18}\text{O}$ values indicate preservation of sedimentary $\delta^{18}\text{O}$ and, by implication, $\delta^{13}\text{C}$ values. Unfortunately, the precise location of these samples is not known.

The samples collected as part of this study are impure dolostones (Chapter 3), although Sr remains relatively high for dolomitic rocks (Chapter 6), suggesting an aragonite precursor. Carbonate $\delta^{13}\text{C}$ for these samples ranges from -3.9 to -1.8 and $\delta^{18}\text{O}$ ranges from 16.9 to 10.4 . The three samples with higher $\delta^{18}\text{O}$ indicate no $\delta^{13}\text{C}$ -

$\delta^{18}\text{O}$ covariation, whilst the relatively $\delta^{18}\text{O}$ -depleted sample also has the lowest $\delta^{13}\text{C}$ value.

The stable isotope data, together with the very radiogenic Sr data, are unique amongst the data presented here and very different to the data for the two previously analysed 'Colonsay Limestone' samples (Table 7.1). Very limited though the data are, arguments used above with regard to other sample groups concerning preservation of $\delta^{13}\text{C}$ suggest that the $\delta^{13}\text{C}$ values for the samples with highest $\delta^{18}\text{O}$ are near-primary. If so, they represent a marked negative excursion in carbonate $\delta^{13}\text{C}$. This could be taken as evidence for correlation with the Bonahaven Formation of Northeast Islay, given their reasonably close *geographical* proximity and assuming that the Bonahaven Formation also has strongly negative $\delta^{13}\text{C}$ (Figure 7.2d; C M Graham, personal communication), in the manner of other late Proterozoic dolomitic 'cap-carbonate' sequences. Such a correlation would have major implications for the age of the siliciclastic, wacke-dominated rocks in the remaining, Colonsay Group metasedimentary rocks underlying the Staosnaig Phyllite Formation. As discussed in Chapter 2, these rocks have no obvious lithological/lithostratigraphical equivalents in the Dalradian. If they were of Dalradian 'age', particularly Appin or Grampian Group, they would represent a distinctive succession. Although they share similar negative $\delta^{13}\text{C}$ with the Islay Subgroup dolostones from the Northeast Grampian Highlands, they have rather more radiogenic $^{87}\text{Sr}/^{86}\text{Sr}$. On the other hand, although they have similar $^{87}\text{Sr}/^{86}\text{Sr}$, they are markedly different in their $\delta^{13}\text{C}$ and petrographical character to the Kintra Dolostone. Thus, the geochemical evidence for inclusion of the Staosnaig Phyllite Formation in the Dalradian is inconclusive. Additional geochemical, petrographical and lithostratigraphical work is required

before possible correlation of the Staosnaig Phyllite Formation with the Dalradian can be clarified.

7.5 Comparison of Dalradian carbonate $\delta^{13}\text{C}$ data with other Neoproterozoic sequences: carbonate $\delta^{13}\text{C}$ constraints on the age of the Appin Group and wider correlations

I showed in Chapter 6 that carbonate $^{87}\text{Sr}/^{86}\text{Sr}$ data strongly indicate that the age of the Appin and Grampian Groups is less than 750 Ma. In this section, Dalradian carbonate $\delta^{13}\text{C}$ data taken to represent primary or near-primary marine $\delta^{13}\text{C}$ values (highlighted in Table 7.1) are compared to equivalent data from the major Neoproterozoic carbonate rock sequences from around the world with respect to $\delta^{18}\text{O}$, $^{87}\text{Sr}/^{86}\text{Sr}$ and age. These sequences have already been described in Chapter 6 and Appendix A.3, to which the reader is referred for details.

7.5.1 Comparison of $\delta^{13}\text{C}$ with $\delta^{18}\text{O}$ and $^{87}\text{Sr}/^{86}\text{Sr}$

Figure 7.5 compares Dalradian $\delta^{13}\text{C}$ and $\delta^{18}\text{O}$ data with other carbon and oxygen data for Neoproterozoic carbonate rocks. The dominantly positive character of $\delta^{13}\text{C}$ throughout much of the Riphean and ‘lower’ Vendian is clear from these data, serving to highlight further the significance of the negative data which do occur. It is immediately apparent that the Appin Group limestones (Storakaig, Inchrory, Torulian, Dufftown) share $\delta^{13}\text{C}$ within the range of most other Neoproterozoic sequences, most particularly those from Svalbard (Polarisbreen and Akademikerbreen group formations) with which they have previously been correlated (Fairchild and Hambrey, 1995) and with which they share similar $^{87}\text{Sr}/^{86}\text{Sr}$ values.

Furthermore, they commonly show less *covariation* between $\delta^{13}\text{C}$ and $\delta^{18}\text{O}$ than do other sample groups over similar *ranges* in $\delta^{18}\text{O}$, despite the generally lower $\delta^{18}\text{O}$. The consistency in $\delta^{13}\text{C}$ between Appin and other groups from the North Atlantic at least lends support to the interpretation of the selected carbonate $\delta^{13}\text{C}$ values as near-primary or primary. Equally, if correctly interpreted, the $\delta^{13}\text{C}$ data are consistent with the suggested temporal correlation of the Appin Group with the lowermost E1 member of the Elbobreen Formation (Polarisbreen Group) and at least the uppermost Backlundtoppen Formation (Akademikerbreen Group) (Fairchild and Hambrey, 1984, figure 2). The high $\delta^{13}\text{C}$ relative to low $\delta^{18}\text{O}$ in the ‘Tayvallich’ limestones is brought out very strongly on Figure 7.5; once again, the lack of covariation with $\delta^{18}\text{O}$ is clear. The rocks nearest in age to the Tayvallich rocks in this figure are the Nama and Witvlei carbonates (e.g. Derry et al., 1992); of these, only the Nama rocks have $\delta^{13}\text{C}$ approaching anything like the high values observed in the ‘Tayvallich’ limestones.

Dolomitic rocks from the Dalradian and the Colonsay Group (Staosnaig Phyllite Formation) are also plotted on Figure 7.5. Their negative $\delta^{13}\text{C}$ values are similar to those carbonate rocks from the Vendian Nama, Witvlei, Polarisbreen groups and the Riphean Akademikerbreen Group which also have negative $\delta^{13}\text{C}$. As discussed above, the negative values in Vendian rocks are recorded in units which occur above tillites or horizons representing glacial episodes. For example, the negative Polarisbreen data come from member D1 of the Dracöisen Formation, which lies above the Varangan tillites of the Wilsonbreen Formation (Knoll et al., 1986; Fairchild and Spiro, 1987). Similarly, the dolostone samples from the Bonahaven Dolomite lie above the Port Askaig Tillite Formation on Islay, whilst the

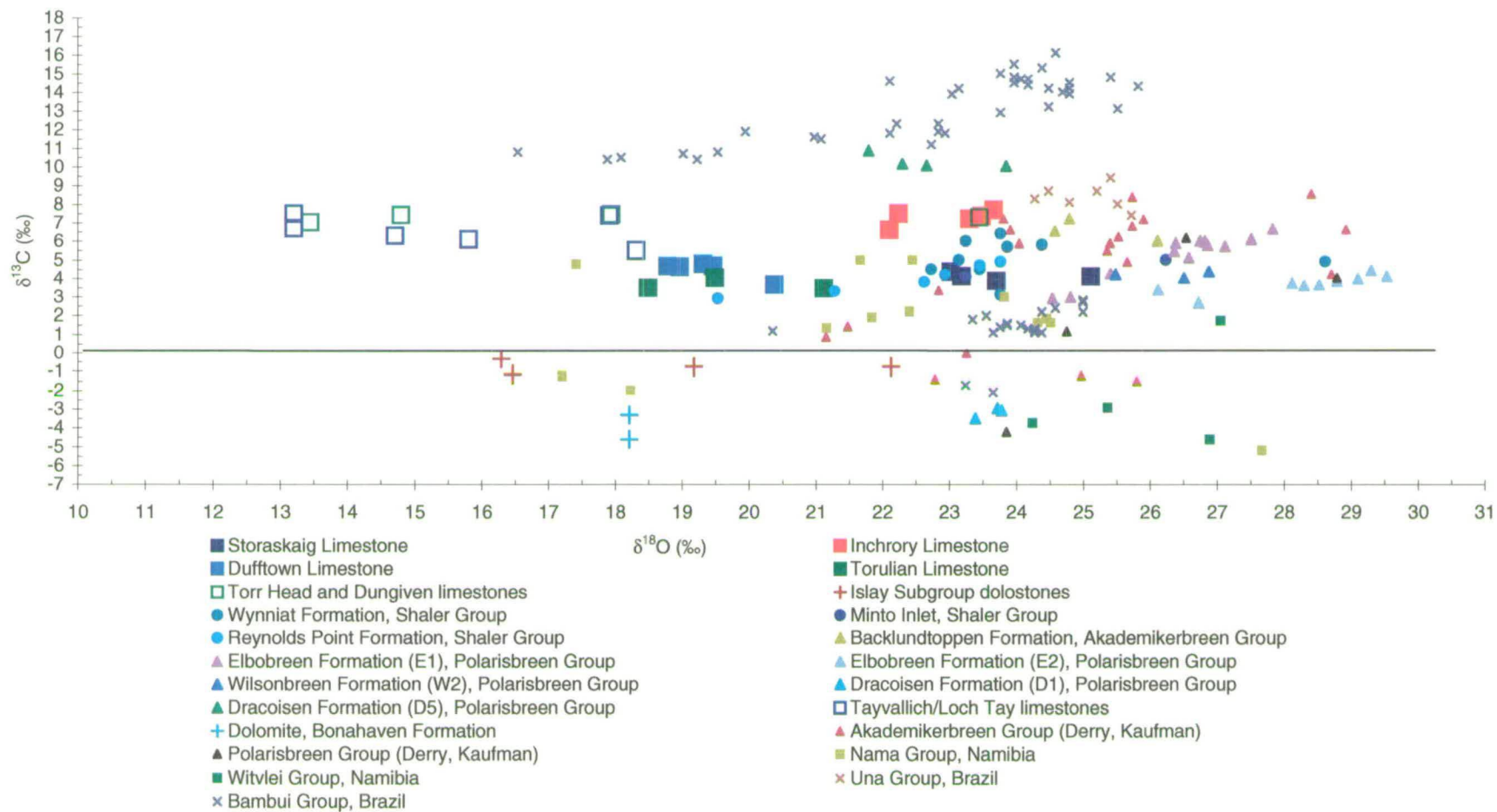


Figure 7.5 $\delta^{13}\text{C}$ vs $\delta^{18}\text{O}$ for Dalradian Limestones and dolostones compared to Neoproterozoic carbonate successions used to constrain secular variation in $\delta^{13}\text{C}$ and $^{87}\text{Sr}/^{86}\text{Sr}$. See Table 5.1 for data sources

Islay Subgroup samples from Northeast Scotland are associated with tillites. It is reasonable to conclude that the Scottish samples are recording the same negative excursion in $\delta^{13}\text{C}$ as seen in the Svalbard successions.

The negative $\delta^{13}\text{C}$ signature recorded in the Staosnaig Phyllite Formation dolostones together with the *relatively* low $\delta^{13}\text{C}$ recorded in the unlocated limestone samples with high $\delta^{18}\text{O}$ (26.3 – 26.9‰) from Colonsay (Table 7.1), remain tantalising in their possible implications for correlation of the Colonsay Group. The possibility of correlation of the carbonate rocks with the Bonahaven Formation has already been discussed above. A further possibility is a ‘Sturtian’ (~ 750 Ma Hoffman et al., 1996) correlation as the rocks have similar $\delta^{13}\text{C}$ values to those from the lower part of the Akademikerbreen Group which are considered by Derry et al. (1992) and Kaufman and Knoll (1995) to define the $\delta^{13}\text{C}$ excursion associated with the ‘Sturtian’ glacial episode (see also Figure 7.7). In addition, the $\delta^{13}\text{C}$ values of the limestones are significantly lower than those of Appin Group limestones. The corollary of a *c.* 750 Ma ‘Sturtian’ age for the Colonsay carbonate rocks is that the underlying siliciclastic succession could then represent an early Grampian Group succession not seen on the Scottish mainland (as noted in Chapter 2, the base of the lowermost Grampian Group rocks in the Glen Shirra succession is not seen). Such an age for the Colonsay Group, however, would be purely speculative and not one I would support.

Perhaps the best opportunity in resolving the Colonsay Group correlation problem is to find and resample carefully the locality from which the high $\delta^{18}\text{O}$ limestones were collected and undertake $^{87}\text{Sr}/^{86}\text{Sr}$ analyses in addition to reviewing the lithostratigraphy as a whole in the light of the recent lithostratigraphical work in

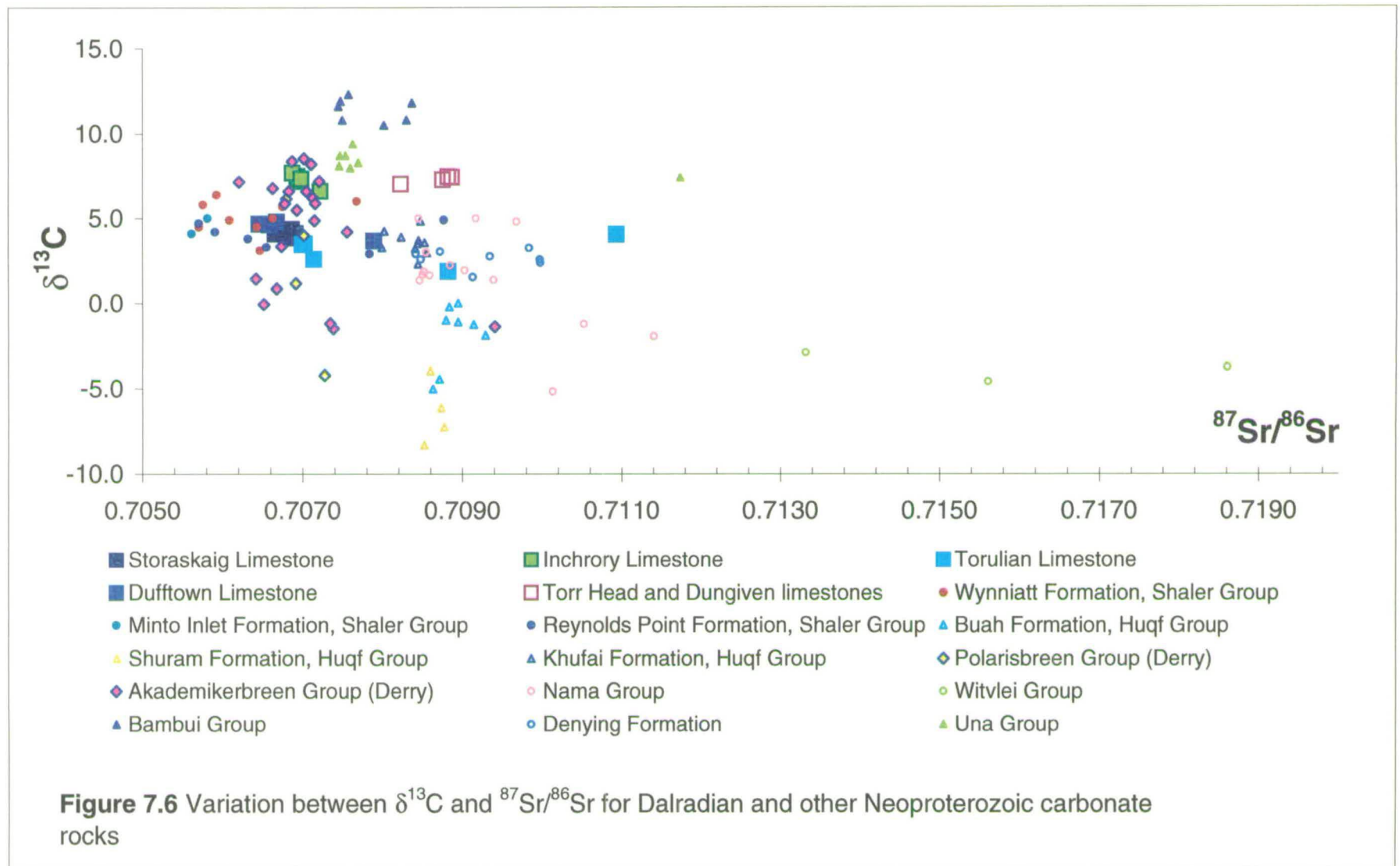
the Central Highlands (Smith et al., 1999). Assuming initial ratios could be identified, a carbonate $^{87}\text{Sr}/^{86}\text{Sr}$ ratio of $\sim 0.706 - 0.707$ would strongly indicate a Riphean age for the Colonsay Group. Anything over 0.708 would suggest a Vendian correlation.

The covariation in $\delta^{13}\text{C}$ and $^{87}\text{Sr}/^{86}\text{Sr}$ in Dalradian and other Neoproterozoic carbonate sequences for which both data exist and can be considered as primary or initial values, is shown in Figure 7.6. (*Dalradian dolostones are not shown because of their ambiguous $^{87}\text{Sr}/^{86}\text{Sr}$ data*).

Although there is scatter, Riphean carbonate rocks (solid symbols) have generally more positive $\delta^{13}\text{C}$ than Vendian rocks (open symbols), but less radiogenic $^{87}\text{Sr}/^{86}\text{Sr}$ (Chapter 6). The overall progression towards lower positive $\delta^{13}\text{C}$ with age (as implied by the increase in initial $^{87}\text{Sr}/^{86}\text{Sr}$) is also clear. The lower positive to negative values shown by the Akademikerbreen Group (magenta diamonds) and Polarisbreen Group (yellow diamonds) are considered to coincide with the major Neoproterozoic Sturtian and Varangan glacial episodes. Notice, however, that the samples from these two groups with lowest $\delta^{13}\text{C}$ are systematically shifted towards higher $^{87}\text{Sr}/^{86}\text{Sr}$, suggesting that these more ^{13}C -depleted samples might not be as 'primary' as interpreted.

7.5.2 Secular variation in $\delta^{13}\text{C}$ during the Neoproterozoic

As with the strontium isotope data (Chapter 6), it is possible to plot $\delta^{13}\text{C}$ against age for a number of the Neoproterozoic data sets. This has resulted in the publication of Neoproterozoic age curves for $\delta^{13}\text{C}$ (e.g. Derry et al., 1992; Kaufman and Knoll, 1995). Appropriate Dalradian carbonate $\delta^{13}\text{C}$ data are combined with published



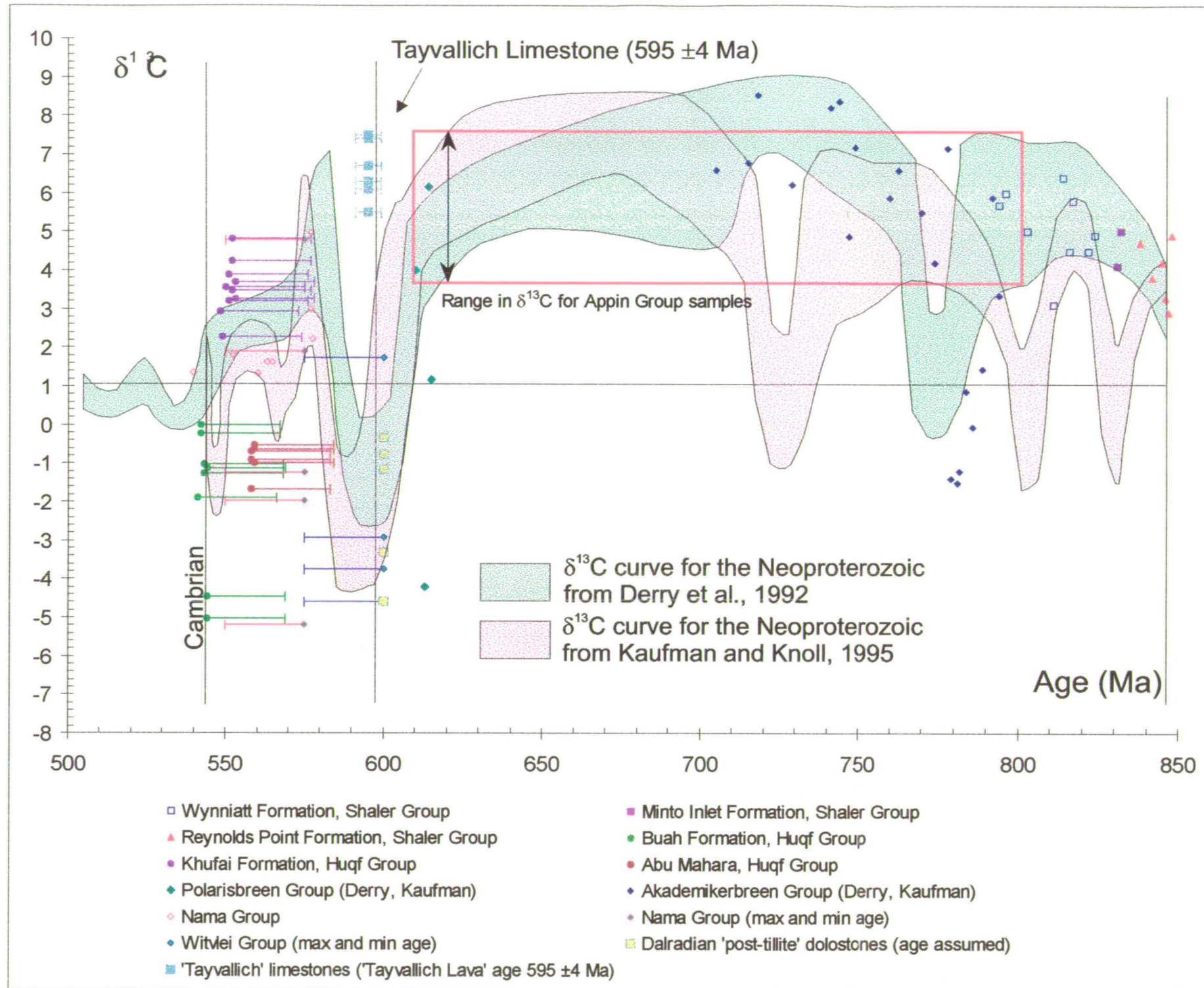


Figure 7.7 Secular variation of $\delta^{13}\text{C}$ through the Neoproterozoic and the range of 'least altered' $\delta^{13}\text{C}$ in Dalradian limestones and dolostones (see text for discussion)

carbonate $\delta^{13}\text{C}$ data for which age estimates exist and shown in Figure 7.7, in similar fashion to Figure 6.10, with which it may be compared. In many cases, the age estimates for data plotted in Figure 7.7 are the same as those used for the $^{87}\text{Sr}/^{86}\text{Sr}$ vs age curve shown in Figure 6.10. The $\delta^{13}\text{C}$ curves on Figure 7.9 are derived from the literature. The blue-shaded curve is from figure 3 of Derry et al. (1992), which shows more data points for the Polarisbreen and Nama and Witvlei groups, but which are not tabulated in the text. The pale pink curve is derived from figure 6 of Kaufman and Knoll (1995; data only shown graphically in figures).

The two comparative curves use essentially the same data, but with obvious adjustments of age estimates for the older Riphean successions. Presentation of both curves serves two purposes: although it highlights the fact that secular variation of $\delta^{13}\text{C}$ around and beyond the putative ‘Sturtian’ negative excursion is still poorly constrained, it emphasises the strongly positive character of carbonate $\delta^{13}\text{C}$ between ~610 and 700 Ma. It is this section of the curve which is of particular interest with regard to the Dalradian. The correspondence of high $\delta^{13}\text{C}$ between the Dalradian and other Riphean carbonate rocks is clear. When coupled with the $^{87}\text{Sr}/^{86}\text{Sr}$ data (Figure 6.10), the $\delta^{13}\text{C}$ data confirm the conclusion reached from the $^{87}\text{Sr}/^{86}\text{Sr}$ data that the age of the Appin Group is younger than (a conservative) 800 Ma (cf. Chapter 6). If the ‘Sturtian’ negative excursion in $\delta^{13}\text{C}$ is correctly ‘dated’ on the curve of Kaufman and Knoll, then the Appin Group is probably much younger.

7.5.3 $\delta^{13}\text{C}$ evidence for the duration of the Varangan glaciation

Along with the Margadale samples from the Bonahaven Formation (Table 7.1), the Islay Subgroup samples from Northeast Scotland have been assigned a *nominal* age

of 600 Ma, based on their 'tillite' association. As discussed in Chapter 6, the current best estimate of the maximum age of the Port Askaig Tillite comes from the ~605 Ma age for the New Main volcanics underlying the Gaskiers Tillite of Newfoundland. The importance of the Tayvallich Lava date (595 ± 4 Ma) is manifest in its utility as an upper age limit for the Port Askaig Tillite, and its constraint on the timing and duration of the shift in $^{87}\text{Sr}/^{86}\text{Sr}$ from ~0.707 in the late Riphean to >0.708 in the Vendian (Chapter 6). This date also has important implications for the interpretation of the $\delta^{13}\text{C}$ data.

The secular $\delta^{13}\text{C}$ curves given by Derry et al. (1992) and Kaufman and Knoll (1995) (Figure 7.9) both indicate a post-Varanger peak in $\delta^{13}\text{C}$ at c. 575-580 Ma. Assuming that this strongly positive peak in $\delta^{13}\text{C}$ is a global phenomenon at this time and that it is also recorded by the 'Tayvallich' limestones, then the Tayvallich limestones, constrained as they are to be coeval with the Tayvallich Lavas, show that this post-Varangan $\delta^{13}\text{C}$ peak actually occurred at least 10 Ma earlier than estimated by Derry et al., *op. cit.* and Kaufman and Knoll *op. cit.*, who both more or less agree on this part of the curve. It is suggested that the data presented here may provide a more accurate estimate of this $\delta^{13}\text{C}$ shift than that provided by the Namibian data on which this portion of the curve is largely based. In the wider scheme of things, an adjustment of ~10 Ma is very little in Neoproterozoic terms and well within the error of most of the current age estimates (e.g. Kaufman et al. 1993). However, the age and duration of the Varangan glacial episode and the now clearly very rapid changes in $\delta^{13}\text{C}$ and $^{87}\text{Sr}/^{86}\text{Sr}$ which occurred during this time are of intense interest to workers studying not only the geochemical evolution of the physical environment, but also the effects on the evolution of metazoans which occurred soon after. Any tightening of

constraints on its age is important if the rates of change of the geochemical and biological phenomena are to be determined and their underlying processes understood. The youngest age for the Tayvallich Lavas/limestones is ~590 Ma. The suggested maximum age for the Port Askaig Tillite is ~610 Ma. In the 20 Ma between these two intervals, the Port Askaig Tillite *and* the whole of the Argyll Group have to be deposited. Assuming that the current radiometric age constraints are correct, it appears that the Varangan glaciation was a short lived (maximum 2-3 Myr) event, similar in duration to Phanerozoic glacial episodes.

7.5.4 Negative carbonate $\delta^{13}\text{C}$ excursions and Neoproterozoic global glaciation

Of relevance to this study are negative $\delta^{13}\text{C}$ excursions which are temporally correlated with the Neoproterozoic Sturtian/Rapitan (*c.* 740 Ma) and Varangan/Marinoan (*c.* 600 Ma) glaciations (e.g. Derry et al., 1992; Kaufman and Knoll 1995; Kennedy et al., 1998). The strongly negative excursions in carbonate $\delta^{13}\text{C}$ recorded in 'cap' carbonates just above Vendian (Varangan/Marinoan) glacial sequences, coupled with sequence stratigraphical and subsidence rate estimates evidence for persistent (*c.* 10 Myr) glaciation (Hoffman et al., 1998a; Saylor et al., 1998) and palaeomagnetic evidence for glaciation at low latitudes (e.g. Schmidt et al., 1991), have led a number of workers to advocate a 'snowball' Earth hypothesis (Hoffman et al., 1998a; Hoffman et al., 1998b; Kirschvink, 1992). This hypothesis proposes that organic production collapsed as sunlight was blocked out by oceans almost completely covered by ice. This collapse in primary production resulted in the strongly negative carbonate $\delta^{13}\text{C}$ excursions as ^{12}C was retained in TDC, rather than being sequestered in buried in sediments. The hypothesis, however, is controversial.

Kennedy et al., 1998) counter the hypothesis with arguments based, amongst other things, on contrary (positive) $\delta^{13}\text{C}$ data from the same sequences from which Hoffman et al. (1998a) apparently recorded negative $\delta^{13}\text{C}$ excursions and coeval secular variation in carbonate $^{87}\text{Sr}/^{86}\text{Sr}$. The data and conclusions of Kennedy et al. *op. cit.* are supported by the data presented in this thesis which suggest a single, short-lived episode of glaciation and the return to strongly positive $\delta^{13}\text{C}$ in successions above the tillites. Furthermore, Meert and Van der Voo (1994) present palaeomagnetic data which indicate that glaciations never reached the low latitudes envisaged by Hoffman et al. *op. cit.*

7.6 Summary and conclusions

- Dalradian limestones are dominated by positive $\delta^{13}\text{C}$ values, ranging up to nearly +8‰. Analysed dolostones have $\delta^{13}\text{C}$ values just above or below 0‰.
- Persistent covariation between $\delta^{13}\text{C}$ and $\delta^{18}\text{O}$ is significant below $\delta^{18}\text{O} < \sim 18\text{‰}$. Samples with $\delta^{18}\text{O} > \sim 18\text{‰}$ appear to preserve primary or near primary $\delta^{13}\text{C}$; this applies to limestones and dolostones.
- ‘Tayvallich’ limestones show wide ranging variation in carbonate $\delta^{13}\text{C}$. Within the data, primary/near primary ‘Tayvallich’ carbonate $\delta^{13}\text{C}$ had values of $\sim 7\text{‰}$. In suites of ‘Tayvallich’ limestone sample showing alteration of $\delta^{13}\text{C}$, alteration can be attributed to hydrothermal effects associated with intrusion/extrusion of the Tayvallich lavas, or to metamorphic fluid infiltration and reaction.
- Appin Group limestones preserve high positive $\delta^{13}\text{C}$ of up to nearly 8‰. The data corroborate the Riphean age of the Appin Group and, when combined with the

$^{87}\text{Sr}/^{86}\text{Sr}$ data, indicate that this group cannot be older than 750 - 800Ma. 700-720

Ma is suggested as a reasonable estimate for the base of the Appin Group.

- Dolostones from the Bonahaven Formation, Margadale (Islay) and dolostones associated with tillites from North East Grampian Highlands preserve near – primary, negative $\delta^{13}\text{C}$ values. The negative values are considered to be part of the negative excursion in $\delta^{13}\text{C}$ observed in other dolomite-bearing units overlying tillites from elsewhere in the world.

Part 3

Outcrop- and grain-scale spatial variations in stable
isotope compositions of calcite and quartz: fluid infiltration
mechanisms and timescales

Chapter 8

The mechanisms and time-scales of metamorphic fluid infiltration in calcitic metalimestones

In this Chapter:

- ❖ the nature of porosity and permeability in metalimestones
- ❖ grain-scale mechanisms of permeability enhancement during metamorphism
- ❖ elucidation of fluid pathways and timing of fluid infiltration
- ❖ modelling of oxygen isotope diffusion gradients and time-scales of fluid infiltration

8.1 Introduction

A central objective of this thesis is to elucidate the extent to which isotope compositions of Dalradian metacarbonate rocks, particularly calcitic limestones, have been modified by metamorphic fluid-rock interaction. As part of this endeavour, I have also aimed to determine:

- a) the mechanisms and pathways by which fluid infiltrated the rocks and exchanged isotope species with the host, and
- b) the time-scales over which such interaction occurred.

In this chapter, I outline likely grain-scale mechanisms which generate or

destroy porosity and permeability in metamorphic rocks. I then review recent research elucidating metamorphic fluid infiltration mechanisms at the grain-scale in calcitic limestones, and the likely time-scales over which infiltration has occurred, as a precursor to detailed oxygen isotope work on samples of the Inchrory and Torulian Limestones discussed in Chapters 9 and 10. Although not directly relevant to the work in this thesis, it is important to note that much of the recent work undertaken to elucidate the timing and mechanisms of fluid infiltration, and the time-scales over which fluid infiltration can occur, has grown out of major research aimed at elucidating metamorphic fluid fluxes, as reviewed recently in Graham et al. (1997).

8.2 Porosity, permeability and fluid infiltration in metalimestones

Prior to metamorphism, deeply buried, compacted limestones have very low porosities and, more significantly for fluid flow, very low permeabilities; the latter, typically in the range $10^{-14} - 10^{-22} \text{ m}^2$, are amongst the lowest of any rocks (e.g. Holness, 1997; Zhang, 1994a). Moreover, under static conditions, texturally equilibrated calcitic limestones are impermeable to most metamorphic fluids under all but very restricted P-T-X conditions (Hays and Evans, 1988; Holness and Graham, 1991; Holness and Graham, 1995), because the solid-solid-fluid dihedral angle in calcitic matrices is greater than 60° . This high dihedral angle isolates pores at crystal triple-point contacts, precluding the development of an interconnected, permeable pore network.

The properties of porosity and permeability of compacted limestones have major implications for fluid infiltration mechanisms and fluid-flux calculations based on chromatographic front transport models of infiltration of fluid into rocks (e.g. Bickle and McKenzie, 1987; Bickle and Baker, 1990; Skelton et al., 1995). Application of this

fluid transport model to isotope profiles observed in metalimestone boundary layers has been successful in yielding *plausible* 1-dimensional fluid fluxes (e.g. Graham et al., 1997, table 8.3). These fluxes are consistent with likely crustal fluid budgets (e.g. Walther and Orville, 1982; Wood and Walther, 1986), but at variance with the porosity and permeability properties of metalimestones outlined above. In order to make use of the chromatographic transport equations, it is necessary to make some major simplifying assumptions about fluid infiltration mechanisms and geochemical exchange between fluid and rock:

- a) fluid flow is assumed to be pervasive in a medium of constant porosity and permeability, implying, in practice, a mechanically static state,
- b) fluid reaches chemical equilibrium with the rock on a timescale short compared to the infiltration event (e.g. Graham et al, 1997).
- c) temperature and pressure remain constant during the fluid infiltration event.

Given the porosity and permeability constraints, these assumptions are unlikely or even untenable, yet boundary layers of metalimestones are clearly infiltrated by fluids. Thus, permeability in metalimestones must be enhanced by deformation during infiltration (Holness and Graham, 1995). Recent work on metalimestones combining cathodoluminescence imaging and oxygen isotope analysis by Secondary Ion Mass Spectrometry (SIMS) at the grain-scale, has aimed to elucidate the mechanisms by which fluid infiltrates metalimestone, the timing of infiltration and the time-scales over which it occurs. The work has successfully revealed the nature of fluid pathways and delineated domains within which volume diffusive exchange has occurred between the rock and fluid and the time-scales of fluid-rock infiltration (Graham et al., 1998; Lewis, 1999; Lewis et al., 1998), as discussed below. The results show that fluid flow is not

pervasive, but channelled along cracks, grain boundaries and twin planes, and that fluid in the pathways did not attain equilibrium with the rock. Moreover, quantitative analysis of diffusion gradients indicates very short time-scales of fluid-rock interaction, typically $< 10^4$ years (Graham et al., 1998; Lewis, 1999); these time-scales are insufficient for attainment of isotopic equilibrium. The nature of the fluid pathways indicates that permeability has been enhanced by mechanisms operating at the grain-scale, including reaction, hydrofracturing and deformation. Such dynamic events must be short-lived and the porosity and permeability they generate will be transient. The grain-scale evidence is for fluid infiltration in a highly dynamic environment, rather than advection through a passively porous medium.

Given the evidence for such short fluid infiltration events, relative to typical time-scales for metamorphism on the order of 10^6 years, what are the likely mechanisms by which permeability may be generated and maintained in calcitic limestones? I summarise these briefly in the next section, following Lewis' (1999) extensive review of the ways in which permeability may be enhanced in metamorphic rocks.

8.3 Mechanisms of permeability enhancement

8.3.1 Reaction-generated permeability

Devolatilisation is a feature of prograde metamorphism and has the potential to produce large volumes of metamorphic fluid: for example, heating pelitic rocks to amphibolite facies will typically produce ~10 – 12% by volume of a largely H₂O-CO₂ fluid phase at ~ 500°C and 5 kbars (Walther and Orville 1982). Devolatilisation reactions, however driven, result in an increase in porosity, whilst the production of

volatiles and the concomitant increase in their volume, increases the pore fluid pressures. As a notable example, the reaction calcite + quartz = wollastonite + CO₂ yields a ~33% reduction in solid volume (Ferry, 1994). Where pore fluid pressures become sufficiently high (> minimum principal stress + tensile strength of rock; see below), they will induce hydrofracturing, weakening the rock and facilitating collapse of the unstable, reaction-generated pore structure by compaction as the fluid escapes via transient permeability (Graham et al., 1997). Fluid escape from a devolatilising rock body is driven by density differences between solid and fluid phases, but the actual flow path will be complex in metamorphic rocks for several reasons (Graham et al., 1997). Metamorphic rocks usually have inhomogeneous and anisotropic permeability structure because of complex lithological layering and tectonic fabrics. In addition to movement of fluid in interconnected pore networks, fluid may be channelled in brittle fractures. Moreover, tectonically imposed deformation will dynamically alter the permeability of a rock. Grain-scale processes induced by deformation may either increase or decrease permeability (e.g. Lewis 1999). The petrological evolution of a rock body during metamorphism will also influence significantly the porosity and permeability (and their relationship) and the rheological response of the rock to deformation.

8.3.2 Hydrofracturing

Hydrofracturing occurs when pore fluid pressures exceed the sum of the minimum principal stress and the tensile strength of the rock (Jaeger and Cook, 1979); it is considered to be the main mechanism facilitating fluid transport through a rock mass (Ferry, 1994). Propagation of fluid-filled cracks generated by hydrofracture is generally

driven by pore fluid pressure, but may also occur because of fluid buoyancy (Nakashima, 1995). As discussed above, high pore fluid pressures sufficient to cause hydrofracturing will be a consequence of devolatilisation reactions, but may also be generated by the differential expansion of minerals and fluids during prograde metamorphism and by deformation (see also below).

Hydrofracturing is a general process and will arise in regional and contact metamorphic settings. However, it is a short – lived, highly dynamic phenomenon ($<10^3$ years; e.g. Niyashima, 1989; Dutrow and Norton, 1995), and the permeability it generates will be transient because cracks will seal quickly once the fluid has escaped. Hydrofracture is enhanced in rocks of low permeabilities and at low rates of strain, but crack propagation rate depends not only on pressure, temperature and the volatile production rate, but also on the fluid composition, the crack geometry and the microstructure of the rock (Atkinson, 1984; Brennan, 1991; Niyashima, 1989).

Cole and Graham (1994) and Cole (1997) document the importance of micro-veining facilitated by hydrofracturing of the host rocks as the dominant fluid transport mechanism in the axial region of the Ardrishaig Anticline of the Southwest Scottish Highlands. The increasing density of calcite-quartz micro-veining in infiltrated metabasite and phyllitic units coincides with a logarithmic increase in fluid flux towards the Ardrishaig Anticline axial surface (Skelton et al., 1995).

8.3.3 The effect of deformation on permeability

Deformation almost certainly facilitates fluid flow in metamorphic rocks, but the relationship is very complex in detail and the mechanisms by which deformation facilitates or drives fluid flow are still poorly understood (Graham et al., 1997).

Moreover, deformation may occur because fluid produced within a rock mass by devolatilisation will weaken the rock itself if pore fluid pressures become sufficiently high. Thus the possible causal relationship between deformation and fluid infiltration is ambiguous. Faults and shear zones are well-documented as loci of fluid flow (McCaig, 1997) and fluid flow may be associated with deformation on a regional scale. Recent work in the Scottish Highlands has shown that the sheared axis of the Ardrishaig Anticline is a zone of high fluid flux (Cole, 1997; Skelton, 1993; Skelton et al., 1995). However, the extent to which varying permeabilities arising from pre-existing, heterogeneous, lithological layering, rather than deformation, control fluid flow in fold structures is unclear (Graham et al., 1997). Understanding the relative timing of fluid production/infiltration in relation to metamorphism and deformation is, therefore, a critical problem; this has only recently begun to be addressed at the critical level of the grain-scale by the application of sophisticated imaging and grain-scale isotope analysis (Valley and Graham, 1996; Graham 1998; Lewis et al., 1998).

Rocks respond to deformation by a range of grain-scale mechanisms, some of which enhance permeability and others which reduce it (Table 8.1). Many factors govern the predominant deformation mechanisms and the balance between those which will generate, and those which will destroy, porosity and permeability. Temperature, pressure and differential stress will affect fluid pressure, the strain rate and the rheological properties of the rock. Controls arising from lithology include mineralogy, grain size, the orientation of crystal lattices, and the porosity, permeability and fluid composition (e.g. Fein et al., 1994; Gerdes and Valley, 1994;

Deformation mechanisms	Increasing T°	Decreasing strain rate	Regime/conditions	Effects
<i>Increasing permeability</i>				
Fracturing and cataclastic flow			Upper crust/low grade metamorphism	Transient interconnected fractures during crack/seal cycles
Plastic intracrystalline deformation			Middle to lower crust	Enhanced fluid P may propagate fractures, increasing permeability
Twinning			Low to high temperature	Preferential fluid flow in along twin planes
Dynamic recrystallisation			High temperature	Fluid redistribution in films, infiltration
Grain boundary sliding (super plasticity)			High temperature, very-fine grained rocks	Dilation due to high fluid pressures?
<i>Reducing permeability</i>				
Pressure solution			Diagenesis/low grade metamorphism	Porosity reduction
Recovery			High temperature	Internal energy minimisation and grain coarsening
Solid-state diffusion creep			Very high temperatures (sub-melting)	Internal crystal lattice vacancy migration
Grain boundary area reduction			High temperature	Internal energy minimisation and grain coarsening
Static recrystallisation			High temperature, or water films along boundaries	Internal energy minimisation and grain coarsening

Table 8.1 Deformation mechanisms and their effect on permeability, in order of increasing temperature and decreasing strain rate, and the regimes and effects with regard to fluid infiltration (After Lewis, 1999, figure 3.2, and discussion therein)

Graham et al., 1997; Holness and Graham, 1995).

Mechanisms which accommodate strain and potentially enhance porosity and permeability will tend to increase the internal energy of the system. Such mechanisms will be countered by mechanisms which reduce that energy by eliminating the strained state. Deformation may be focussed in shear zones or at the boundaries of rock units with different rheological properties, or it may be homogeneous; that which occurs will be a function of strain and strain rate, temperature and the effective pressure (Lewis 1999).

Fracturing and cataclastic flow are characteristic of deformation over large parts of the upper crust. Cataclastic flow involves sliding and rotation of fragments; it is associated with periods of high strain and is facilitated by high fluid pressures. These mechanisms give way to plastic flow with depth, but there is overlap where both brittle and ductile deformation occur together (Knipe, 1989). Fluid will flow through a fractured rock when the fracture density is sufficiently high to generate an interconnected fracture network, but will only continue if the network is maintained (Odling, 1997). Crack sealing and healing will occlude the fracture network, reducing or preventing further fluid flow, and it is likely that the development of permeability by fracturing will be cyclic (Knipe and McCaig, 1994). High fluid pressures may reduce the effectiveness of crack healing by hydrofracturing, producing microcracks. However, continued tectonic deformation will be needed to maintain interconnected fracture networks (Lewis 1999). In this study, faulting has probably been significant in a major part of the fluid infiltration history of the Torulian Limestone at the one locality where its oxygen isotope geochemistry was studied in detail (Chapter 9).

The link between grain-scale deformation mechanisms and fluid flow at higher

temperatures is less obvious, but plastic intracrystalline deformation, twinning, dynamic recrystallisation and grain boundary sliding are considered to be mechanisms mainly facilitating the development of permeability. Intracrystalline deformation work-hardens the rock by stacking up dislocations until the rock becomes brittle and fails. Pressure in fluid-filled pores will increase and if it exceeds the confining pressure, hydrofracturing may occur, producing a transient permeability. This effect will be countered by mechanisms reducing permeability, such as creep, which permit ductile deformation to continue (Lewis 1999).

Recent grain-scale oxygen isotope analysis and CL imaging has shown that twin planes are a focus for fluid infiltration in calcite (Cole, 1997; Graham et al., 1998; Lewis, 1999). However, it is not clear at present whether twinning and fluid infiltration occurred together in response to deformation, or whether the former was a passive conduit along which fluid flowed following deformation. Twinning develops in response to deformation and recent work by Rowe and Rutter (1990) indicates that this can be used to estimate palaeostress. If a link between twinning and fluid infiltration could be established, it might be possible to assess the stress conditions which accompanied infiltration.

Mechanisms which reduce the internal energy of the system, such as static recrystallisation, recovery and grain boundary area reduction all lead to reduction in permeabilities (Lewis 1999). These work dynamically against those grain-scale mechanisms by which deformation is accommodated, so that the development of permeability is likely to be compromised in most rocks at high temperatures as strain-rate decreases. This will increase further the transient nature of any permeability.

In summary, it is clear that deep crustal fluid flow is not a *passively pervasive*

phenomena, but one characterised by highly dynamic transient events. Though individual fluid infiltration events may be short-lived themselves, they may, when integrated over time, give rise to large fluid fluxes in which shearing deformation and the fluid itself play a key role (e.g. Graham et al., 1997).

8.3.4 Permeability enhancement in calcite limestones

Experimental work summarised in Lewis (1999) shows that cataclastic flow and dilatancy are important mechanisms for deformation in limestones up to about 400°C, beyond which plastic, intracrystalline deformation becomes important, with a concomitant reduction in dilatancy. Microcracking, accompanied by increased dilatancy, can occur at temperatures of up to 600°C during deformation (Fischer and Paterson, 1989). However, increasing temperature also has the effect of reducing permeability in calcite matrices, presumably because those mechanisms which work to reduce deformation-enhanced permeability are more readily activated at higher temperatures.

Experimental data on crack and grain boundary healing in calcite indicates that very thin (<60 µm) cracks can heal extremely quickly (on the order of hours), whilst thicker cracks (~700µm) did not heal during heat treatments lasting up to ~1300 hours (Hickman and Evans, 1987).

8.3.5 Summary: fluid infiltration mechanisms in metalimestones

- Prior to metamorphism, compacted limestones have very low porosities and extremely low permeabilities, precluding passive infiltration by metamorphic

fluids.

- Thus, critical assumptions about fluid infiltration mechanisms and fluid-rock equilibration in 1-d chromatographic fluid transport models are unlikely to be valid in metalimestones.
- Porosity and permeability in limestones must, therefore, be enhanced by high pore fluid pressures arising from compaction devolatilisation reactions and deformation and resulting in hydrocracking.
- Any permeability thus generated will be transient and will disappear once fluid has been removed; its development will also be countered by mechanisms which reduce the internal energy of the rock.
- Deformation-produced permeability and porosity will heal quickly in limestones unless maintained by continuing deformation, reaction and high fluid pressures.

8.4 Mapping and quantifying fluid-rock interaction on the grain-scale

As mentioned above, it has, in recent years, become possible to elucidate fluid pathways petrographically using cathodoluminescence (CL) imaging (e.g. Cole and Graham, 1994; Cole, 1997). Very recently, this CL imaging has been coupled with examination of isotopic compositions at the grain-scale using Secondary Ion Mass Spectrometry (SIMS). (Graham et al., 1996; Graham et al., 1998; Lewis et al., 1998; Valley et al., 1998). This has enabled the assumptions about fluid infiltration inherent in the chromatographic transport models to be tested for the first time, constraining the nature, timing and time-scales of fluid infiltration. In this next section, I review the work to date, with particular regard to the quantitative modelling of diffusion data. This has particular relevance to the work discussed in Chapters 9 and 10.

8.4.1 Mapping fluid pathways using cathodoluminescence

Cathodoluminescence (CL) imaging of calcite in metalimestones commonly reveals grains with relatively low luminescence characteristics and bright orange or yellow calcite extending along grain boundaries, cleavage planes and fractures, and forming patches extending into grain interiors from grain boundaries (Cole, 1997; Lewis et al., 1998; Graham et al., 1998). The brightly luminescent calcite is interpreted to result from interaction of the metalimestone with an advected fluid enriched in Mn (hence the enhanced CL response), but generally depleted in ^{18}O and Sr relative to the host. The corollary is that the bright yellow calcite maps out the pathways of the advected fluid. The presence of luminescent calcite along cleavage planes indicates that interaction between the interiors of grains and grain-boundary fluid may be facilitated by the short-circuiting effect of cleavages and other internal, crystal-scale, structural defects. Away from such short-circuiting discontinuities, grains will interact with the fluid by volume diffusion (Valley and Graham, 1996). If the temperature is sufficiently high and there is sufficient time for the rock and the fluid to interact relative to the (water-present) diffusion coefficient for oxygen in calcite (see below), then diffusion gradients may be sufficiently large ($\sim 10^2 \mu\text{m}$) to be detectable by SIMS analysis.

8.4.2 The identification of diffusion gradients and the significance of volume diffusion: a case study

If grain-scale diffusion gradients can be identified in rocks, it is possible to elucidate the timescale(s) over which fluid infiltration occurred (Valley and Graham 1996).

Pioneering work by Wada (1988) and Arita and Wada (1990) revealed for the first time

the extent of oxygen isotopic disequilibrium at the grain-scale in coarse, granulite facies, calcite-marbles, retrogressively metamorphosed at amphibolite facies. Using a 1 mm x 25 μm microtome serial sampling technique, they identified steep gradients in $\delta^{18}\text{O}$ of $\sim 8\text{‰}$ over 200 – 300 μm , with depletion from grain interiors towards grain boundaries. These authors interpreted the depletion to result from interaction between grain-boundary fluid and the calcite grain interiors.

Subsequent work on the same sample by Graham et al. (1998), using SIMS analysis targeted by CL imaging, has considerably refined knowledge of the oxygen isotope characteristics of the Wada limestone. At the same time, the work has elucidated in detail the nature and duration of amphibolite-grade fluid-rock interaction. Their analysis confirms the gross state of isotopic disequilibrium in the rocks and maps out the pathways taken by the fluid responsible for partially resetting the oxygen isotope composition of the rock.

8.4:3 Elucidating time-scales of fluid infiltration

There are two principal features in the data set of Graham et al. (1998):

- a) low $\delta^{18}\text{O}$ fluid was advected along grain boundaries, cleavage planes, fractures and in patches, where dissolution – reprecipitation processes have facilitated greatest chemical exchange on a local scale between rock and fluid, and
- b) away from areas of short-circuiting discontinuities, diffusional gradients developed by volume diffusion from grain boundaries in to grain interiors over 200 – 300 μm .

The diffusion gradients are particularly significant as they yield vital information on the mechanisms of fluid-rock interaction, place limits on plausible temperatures and time scales under which infiltration occurred *and* constrain the nature

of the cooling history following infiltration.

Graham et al. (*op. cit.*) modelled the diffusion gradients using:

$$\text{erf}[x/(4Dt)^{1/2}] = (C_x - C_{rim}) / (C_{core} - C_{rim}) \quad 8.1$$

(Crank, 1975) for ‘transport ($\delta^{18}\text{O}$) into a semi-infinite medium with a planar surface from a fluid phase of (locally) constant composition’, where:

D is the diffusivity of oxygen in calcite in the presence of water,

erf is the error function (or standard normal distribution function),

t is time,

x is distance,

C is the ^{18}O concentration of the calcite grain at the rim, core and at x , expressed as $\delta^{18}\text{O}$ ‰.

If the $\delta^{18}\text{O}$ gradients are due to diffusion alone, they will fit equation 8.1.

Both core and rim values are imprecise. The best estimates of core $\delta^{18}\text{O}$ are taken to be the highest determined values. C_{rim} , the $\delta^{18}\text{O}$ of calcite at the edge of the grain boundary, is taken to be in equilibrium with the infiltrating fluid under amphibolite facies conditions and will be close to the composition of the fluid (Graham et al, *op. cit.*). Since this grain edge calcite is very difficult to analyse for directly, because of problems of locating SIMS ion probe beams very precisely and because the width of grain boundaries is rather less than the ion beam width ($\sim 30 - 40 \mu\text{m}$), C_{rim} is estimated, along with Dt , by fitting equation 8.1 to the isotope profiles using non-linear, least squares regression. If the fit is poor, as estimated by χ^2 , then the gradient is unlikely to result from diffusion alone. Wada’s (1988) original $\delta^{18}\text{O}$ profile data (included in Graham et al., 1998) has a poor χ^2 fit to the diffusion equation and so could not be generated by diffusion alone. Graham et al. (1998) considered that the

poor fit reflected the inclusion of short-circuited domains within the microtome sample. This is likely because the microtome sample, despite its thinness, is actually 2-dimensional (1mm x 25 μm) and, therefore, large enough to include luminescent short circuited domains of low $\delta^{18}\text{O}$. Such domains can be avoided by careful targetting of the ion beam during SIMS analysis, so that SIMS profiles are effectively 1-dimensional.

Because the diffusion of O in calcite is known over a range of temperature and pressure *in the presence of water* (Farver, 1994), D can be calculated for a range of

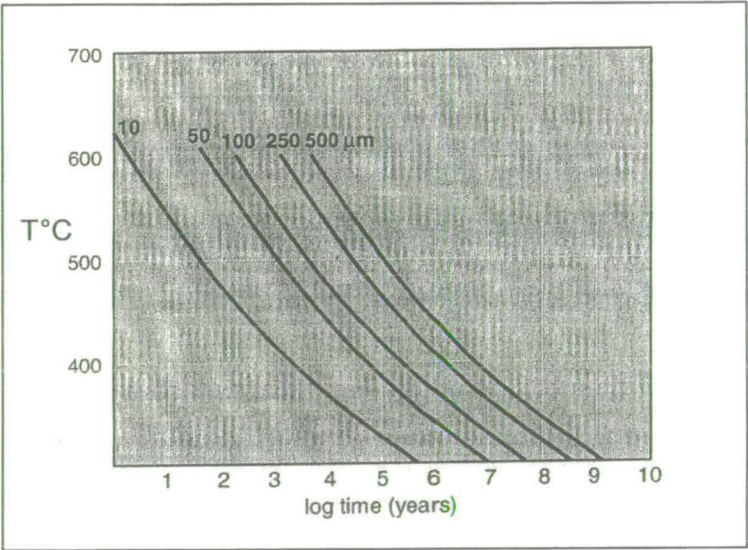


Figure 8.1 Approximate time required for oxygen diffusion distances of 10 – 500 μm in calcite in the presence of water, for temperatures between 300 to 600°C, calculated from the experimental data of Farver 1994; from Graham et al. (1998)

temperatures, thereby permitting estimation of time, t . Graham et al. (1998) estimate that fluid infiltration responsible for the yellow calcite and the diffusion gradients occurred over time scales of $< 10^3$ years at 600°C to $\sim 2 \times 10^4$ years at 500°C. As the authors point out, such time-scales are

several orders of magnitude lower than the estimated time spans of metamorphic events ($10^6 - 10^7$ years) and interpret the short time-scales to reflect short periods when rock permeabilities were much higher than the values of $\sim 10^{-16} - 10^{-20} \text{ m}^2$ calculated in several studies. They attribute the development of such transient permeability to

transiently high fluid pressures which overcome the strength of the rock and maintain open grain boundaries and micro-fractures, enhancing permeability.

Although the time-scales are short, they are realistic and comparable in magnitude to other estimates of fluid infiltration time-scales based on stable isotope metalimestones and other lithologies (Graham et al., 1998). Furthermore, infiltration has to occur at high temperatures ($> 500^{\circ}\text{C}$) for the observed typical $\sim 200\text{ }\mu\text{m}$ length-scale of diffusion gradients to be developed by fluid infiltration in transient permeability. Diffusion at temperatures much lower than this require unrealistically long time-scales under conditions where transient permeability is created by highly dynamic, short-lived mechanisms (Figure 8.1).

8.4.4 Preservation of diffusion gradients: constraints on cooling rates

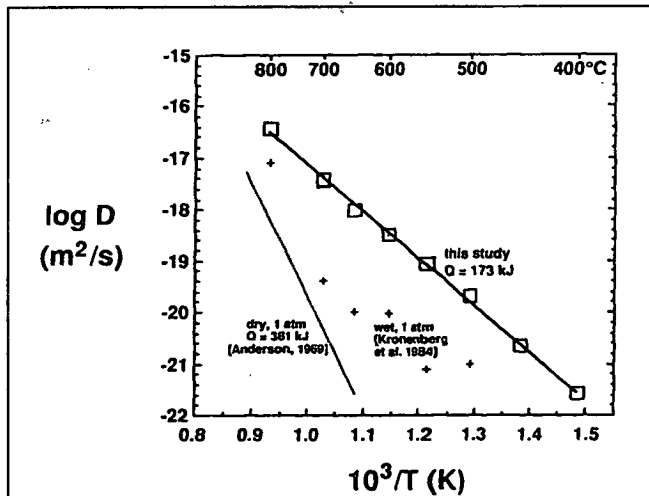


Figure 8.2 The difference in diffusion rate of O in calcite in the presence and absence of water. (From Farver, 1994)

As mentioned above, the corollary of the development of diffusion gradients is that the rocks must have cooled quickly enough for the rocks to preserve the gradients as seen. Graham et al. (1998) model the relaxation of an isotope step at a grain boundary by diffusion on slow cooling, using the Fast Grain

Boundary Model of Eiler et al. (1992) and the *water-present* oxygen isotope diffusion data of Farver (1994). They conclude that cooling must have been *anhydrous* because,

if water had been present, unrealistically high cooling rates would be required to preserve the observed diffusion gradients. Under anhydrous conditions, any cooling rate $> 1^{\circ}\text{C} / \text{million years}$ from an initial temperature $< 600^{\circ}\text{C}$ would leave the gradients intact because the diffusion rate under such conditions is several orders of magnitude less than when water is present (Farver, 1994) and is effectively insignificant over appropriate geological time-scales (Figure 8.2). There is a corollary to this. It is generally assumed that different mineral grains will approach isotopic equilibrium with one another at metamorphic temperatures – this is the basis for oxygen isotope thermometry (e.g. Valley (1986). However, if limestones effectively become dry during prograde metamorphism, losing any pore fluids by compaction and hydrofracturing, etc., and are not infiltrated, then, under anhydrous conditions, diffusion coefficients for minerals like calcite and quartz are so low that they will not equilibrate under normal crustal metamorphic conditions over typical time-scales. This implies that pre-metamorphic $\delta^{18}\text{O}$ signatures *could* be preserved in calcitic limestones where fluid-rock interaction was negligible. Preservation of $\delta^{18}\text{O}$ disequilibrium also implies that even if fluid infiltration events occur during regional metamorphism they must be very short.

8.4.5 Implications of gross calcite $\delta^{18}\text{O}$ disequilibrium for front advection modelling

Studies of metamorphic fluid-rock interaction based on front advection modelling have provided estimates of fluid flux and its localisation which appear to be entirely reasonable with regard to likely fluid budgets in the crust (Baker, 1990; Bickle and Chapman, 1990; Bickle et al., 1997; Bickle et al., 1995; Skelton et al., 1995).

However, the work of Graham et al. (1998) and Lewis et al. (1998) on the grain-scale distribution of $\delta^{18}\text{O}$ in calcite shows clearly that gross isotopic disequilibrium may be typical of limestones metamorphosed up to at least amphibolite facies. The corollary is that whole-rock calcite $\delta^{18}\text{O}$ data used in the modelling of advected fronts, coupled with their diffusional broadening, do not reflect the true character and distribution of isotopes of the rocks in boundary layers. Lewis et al. (1998) determined this by elucidating variation in calcite rim and core $\delta^{18}\text{O}$ values using SIMS analysis in boundary layers in schist-hosted marble in which an advected fluid profile had been determined from bulk carbonate analyses by Baker et al. (1989). Their data showed that the bulk carbonate data represent an average of the rim and core values and that the rim values effectively control the form of the profile based on bulk rock data (Figure 8.3). Moreover, the SIMS data in Figure 8.3 show that the bulk carbonate values at the

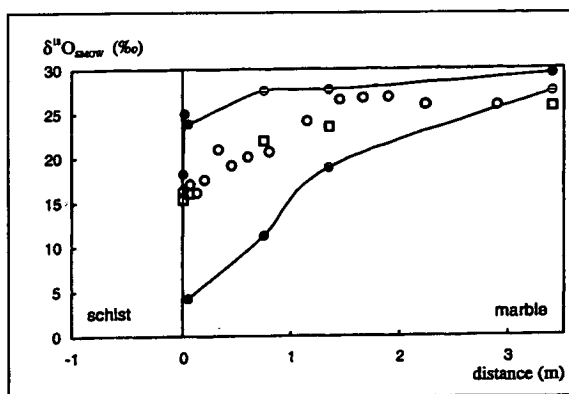


Figure 8.3 Showing the difference between calcite rim and core $\delta^{18}\text{O}$ values and the equivalent average bulk carbonate values from a boundary layer sample profile, Naxos; from Lewis et al. (1998). Filled symbols with high and low $\delta^{18}\text{O}$ values are core and rim calcite analyses, respectively. Open symbols are 'bulk' carbonate $\delta^{18}\text{O}$ analyses from Baker, et al., (1989.) Note how the decreasing rim $\delta^{18}\text{O}$ values pull down the bulk average value and their much lower $\delta^{18}\text{O}$.

schist-pelite boundary cannot be used to give realistic estimate of the $\delta^{18}\text{O}$ composition of the fluid phase.

Quite clearly, oxygen isotope equilibrium between limestones and infiltrating fluids is not easily attained.

Lack of oxygen isotope equilibrium also implies lack of attainment of fluid-rock equilibration of C and Sr isotopes, which are likely to be internally buffered by the limestone. This deduction has major implications for the

interpretation of the isotopes of C and Sr in metamorphosed limestones in which preservation of post-diagenetic or even near-primary isotope values of elements like C and Sr might be common. Moreover, any variation seen in such elements is more likely to result from diagenesis when porosity and permeability would have been much higher than during metamorphism. This will be discussed further in Chapters 5 and 7 – 10.

8.4.6 Summary: fluid pathway mapping and diffusion gradient modelling

- CL imaging reveals fluid pathways in calcite concentrated along fractures and twin planes, which short-circuit fluid transport into grain interiors, grain boundaries and in areas of solution-reprecipitation
- away from short-circuiting pathways, diffusion gradients can be developed by volume diffusion into grain interiors; these can be modelled to give estimates of the duration of fluid infiltration
- time-scales of fluid infiltration are short (10^4 years or less at realistic temperatures), and much shorter than the likely time-scales of metamorphism ($10^6 - 10^7$ years)
- preservation of diffusion gradients indicates that the rocks must have been dry following the infiltration event
- the grain-scale imaging and isotope data show that fluid infiltration is non-pervasive, but fracture controlled and channelled, and that fluid and rock do not reach isotopic equilibrium
- Permeability in metalimestones is enhanced dynamically and is transient
- Under dry conditions, oxygen isotope diffusion coefficients for calcite and quartz are too low for them to exchange isotopically; if metamorphism occurred in the absence of infiltrating fluid, then pre-metamorphic oxygen isotope distributions are

likely to be preserved

8.5 Quantification of fluid-rock interaction in this study

Variation of oxygen and carbon isotopes at the outcrop and grain-scale have been studied in two limestones in this study to elucidate the likely extent of metamorphic fluid-rock interaction (Chapters 9 – 10). However, detailed analysis using the approaches discussed above has been focused mainly on variations at the grain-scale, determined by CL imaging and SIMS (Chapter 9). The data are used not only to elucidate metamorphic fluid-rock interaction which might have occurred in Dalradian limestones, but also to inform interpretation of C and Sr isotopes in Chapters 7 and 8, particularly the extent to which primary or near primary signatures have been preserved

8.6 Conclusions

- Prior to metamorphism, compacted limestones have very low porosities and permeabilities
- Where in textural equilibrium in the absence of deformation, calcitic metalimestones are impermeable under most P-T-X conditions
- Although metalimestones clearly undergo fluid infiltration, 1-dimensional fluid transport equations based on chromatographic theory carry untenable assumptions about the nature of porosity, permeability and fluid-rock chemical equilibration with regard to the infiltration of fluid
- Mapping of fluid pathways using CL imaging and diffusion gradients in oxygen isotope concentrations away from fractures, grain boundaries and twin planes permits modelling of the nature of fluid infiltration mechanisms and the time

over which fluid infiltration occurred

- Fluid infiltration is facilitated by the formation of transient permeability by a range of grain-scale mechanisms dominated by hydrofracturing; time-scales for fluid infiltration events are of the order of 10^4 years or less at realistic temperatures and are much shorter than time-scales of metamorphic events
- Preservation of diffusion gradients requires cooling to occur under water-absent conditions.

Chapter 9

Outcrop profile and grain-scale studies of stable isotopes in the Torulian and Inchrory Limestones

In this chapter:

- ❖ Variation of oxygen and carbon isotope compositions of bulk carbonate in metre- and centimetre-scale outcrop profiles
- ❖ Elucidation of fluid infiltration pathways by cathodoluminescence imaging
- ❖ Variations in calcite and quartz $\delta^{18}\text{O}$ at the grain-scale

9.1 Introduction

The variation and state of alteration Sr and C isotope compositions has been assessed, in large part, with reference to variation in bulk carbonate $\delta^{18}\text{O}$ (Chapters 6, 7). I have shown that $^{18}\text{O}/^{16}\text{O}$ ratios in Dalradian limestones can often be very extensively altered by interaction with fluids with low $\delta^{18}\text{O}$, independently of $^{87}\text{Sr}/^{86}\text{Sr}$ and $\delta^{13}\text{C}$ (e.g. Kincaig, Dungiven and Tayvallich Limestones, Chapter 6). On the other hand, it is also clear that some limestones preserve carbonate $\delta^{18}\text{O}$

values in excess of 20 ‰, at or near sedimentary values (Inchrory and Storakaig Limestones).

The sensitivity of limestones to alteration of carbonate $\delta^{18}\text{O}$ during fluid-rock interaction is well known and has been used widely to elucidate diagenetic and metamorphic fluid-rock interaction histories in limestones (Chapter 5, 8).

In this chapter, I discuss detailed work undertaken to elucidate more clearly the nature of variation in calcite $\delta^{18}\text{O}$ in suites of samples from the Inchrory and Torulian limestones in order to:

- constrain and interpret the spatial variation in bulk carbonate $\delta^{18}\text{O}$ at outcrop scale with respect to boundaries between limestones and contrasting lithologies
- constrain and interpret the spatial relationship between $\delta^{18}\text{O}$, texture and trace element variation at the grain-scale in calcite and quartz
- constrain the scale of carbonate and quartz isotope homogeneity at the grain- and hand-specimen scale, and
- identify the extent of ^{18}O equilibrium between calcite and quartz.

The overall aim is to establish, on the one hand, the extent of preservation of primary calcite $\delta^{18}\text{O}$ values and, on the other the extent to which, and mechanism(s) by which, they have been subsequently altered.

In Chapter 10, I extend this work with discussions of modelling of diffusion gradients and quartz-calcite fractionation, followed by an overall discussion of the implications for interpretation of limestone $\delta^{18}\text{O}$ arising from the outcrop and grain-scale isotope data.

To realise the aims outline above, I have integrated analytical work with detailed petrological work by making extensive use of cathodoluminescence (CL), back-scattered electron (BSE) and scanning electron microscope (SEM) imaging to identify analytical targets, to reveal the textural character of altered domains and to quantify distances between analytical points and grain-sizes.

Oxygen and carbon isotope analyses for outcrop-scale samples were obtained by conventional techniques and are thus bulk carbonate averages; systematic variation in these average values is, nonetheless, significant. Following reconnaissance analysis of $\delta^{18}\text{O}$ and $\delta^{13}\text{C}$ using laser-ablation isotope extraction (LASSIE), variation in carbonate and (in the Inchrory Limestone) quartz $\delta^{18}\text{O}$ at the grain-scale was studied by Secondary Ion Mass Spectrometric (SIMS) analysis of $^{18}\text{O}/^{16}\text{O}$, targetted by CL imaging. I also obtained grain-scale SIMS analyses of selected trace elements. Electron microprobe data were also obtained for feldspars. There are several complementary data sets:

- a) 'bulk' calcite $\delta^{18}\text{O}$ and $\delta^{13}\text{C}$ data obtained by conventional techniques for outcrop-scale samples
- b) grain-scale calcite and quartz $\delta^{18}\text{O}$ data obtained by SIMS analysis
- c) grain-scale calcite trace element data obtained by SIMS
- d) grain-scale calcite, dolomite and feldspar major oxide data obtained by electron microprobe

9.1.1 Sampling

The samples used in the work described below come from sampling profiles of outcrops of the Torulian and Inchrory Limestones near Tomintoul, Northeast

Grampian Highlands (Figure 9.1). Geological details of the two localities are given in Appendix E, to which the reader is referred.

Torulian Limestone sample profile

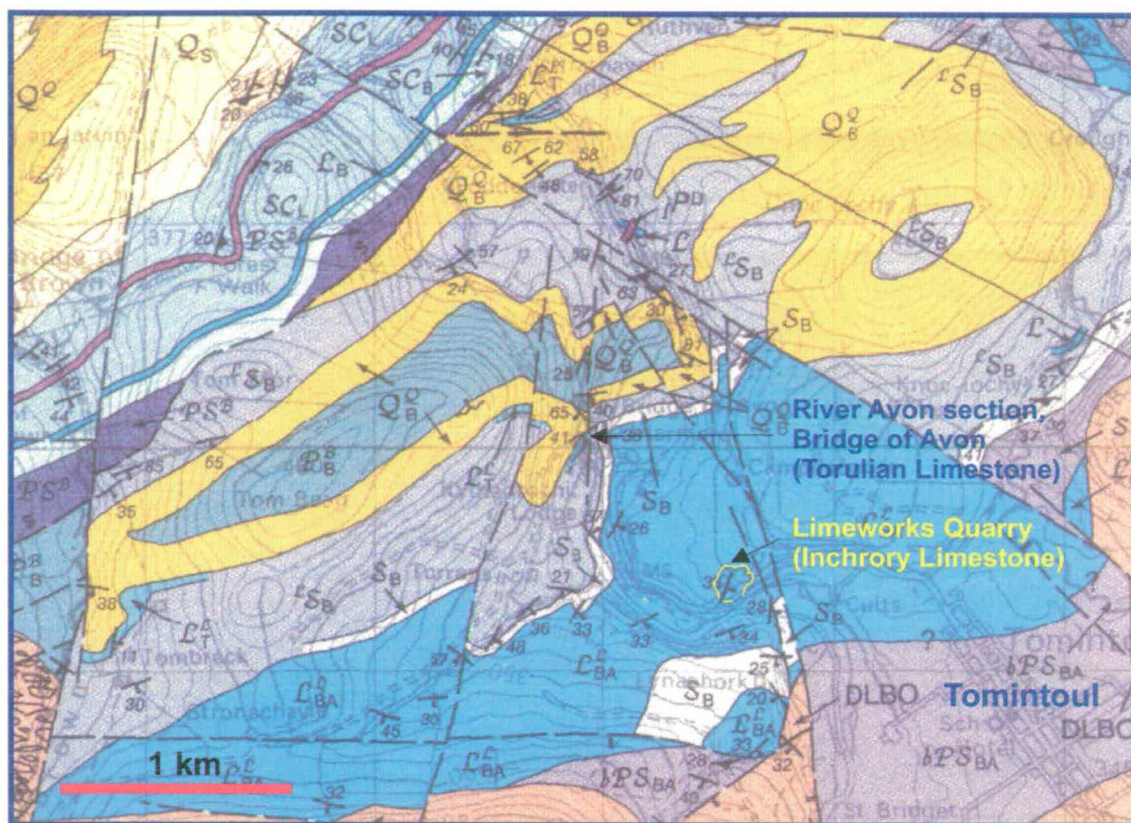
The detailed stable isotope geochemistry of this limestone has been studied via hand-specimen size samples obtained from a metre-scale profile across near-continuous bank-side exposure in the north-south course of the River Avon, immediately north of Bridge of Avon [NJ 150 201] (Figure 9.1). The basic geology of the profile is included in Figure 9.7.

Inchrory Limestone: Limeworks Quarry sample profile

The north wall of Limeworks Quarry provides excellent exposure of contacts between limestone and amphibolite (Figure 9.2). One such contact (Figure 9.3) was sampled in detail over ~ 0.5 m using a high-resolution mini-coring technique, detailed in Appendix A.3. The profile was drilled from the centre of the amphibolite pod out into the limestone. The total profile length was 1m, 0.43 m of which was drilled in the limestone. 22 samples of 7 mm diameter minicore were obtained (LWQ1/25 – 46). Sampling spacing varied from ~1.25 cm at the amphibolite-limestone contact, to 5 cm in the outer part of the profile.

Partition of deformation in the Inchrory Limestone profile

In Appendix E, I describe features of the petrography which shows that deformation increases *away* from the amphibolite – limestone contact over about 10 – 12 cm (Figure E.2a-d). This increase in deformation is potentially important in the fluid-



DLBO Delnabo Conglomerate Formation (Old Red Sandstone)

L_{BA}^c Inchrory Limestone Formation, Blair Atholl Subgroup

L_{SB}^c Ailnack Phyllite and Limestone Formation

L_T^c Torulian Limestone Member

Q^Q Appin Quartzite

} Ballachulish
Subgroup,
Appin Group

Figure 9.1 Geology of the Tomintoul district, showing the location of the sites from which the Inchrory and Torulian Limestones were sampled in detailed profiles. Geology map taken from British Geological Survey 1:50 000 Series map Sheet 75W (Solid) Glenlivet (published 1996). Only the units named in detailed discussion are named in the key. See also Chapter 2.



Figure 9.2 Amphibolite pods in Inchrory Limestone, Limeworks Quarry, near Tomintoul, showing the location of the LWQ sample profile. The hammer is 61 cm long. Note also the white rind developed at the margins of the pods.

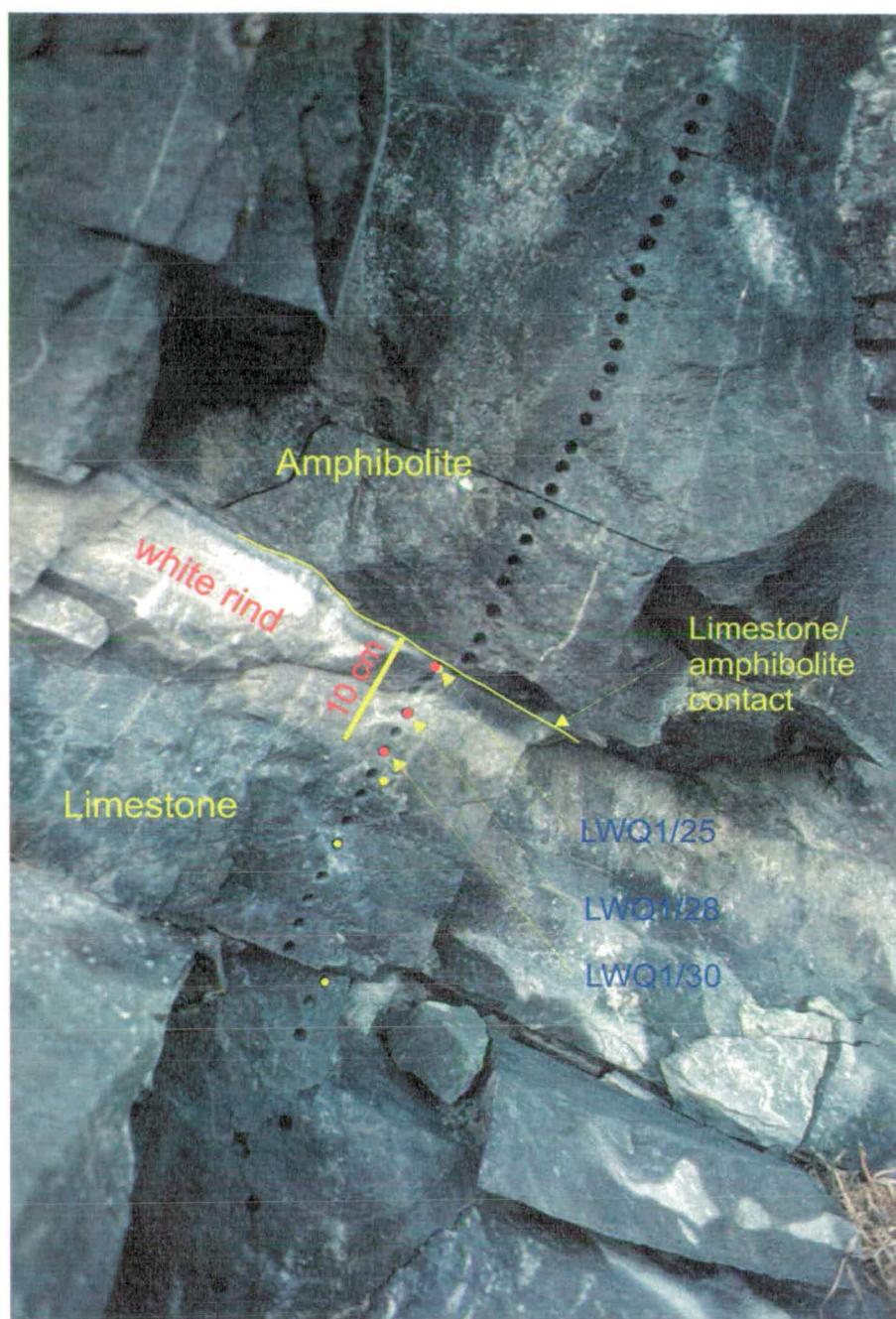


Figure 9.3 Detail of the LWQ sample profile in the Inchrory Limestone, Limeworks Quarry, Tomintoul (cf. Figure 9.2). The three highlighted samples are those study in detail using SIMS. Overall profile length is 1m. Yellow discs are the location of the samples shown in Appendix Figures A.n.2a-d.

rock interaction history of the limestone because of the influence of deformation on permeability. Its possible role in fluid-rock interaction will be discussed in Section 9.4.5 towards the end of the Chapter, following discussion of the stable isotope and CL characteristics of the limestone at this locality.

9.2 Outcrop-scale variation in bulk carbonate $\delta^{18}\text{O}$ and $\delta^{13}\text{C}$

In this section, I describe and discuss the outcrop-scale variation in bulk carbonate $\delta^{18}\text{O}$ and $\delta^{13}\text{C}$ data from the two sample profiles. The isotope data are given in Tables 9.1 (Torulian Limestone) and 9.2 (Inchrory Limestone).

9.2.1 Bulk carbonate $\delta^{18}\text{O}$ and $\delta^{13}\text{C}$ data

Initial reconnaissance analysis of stable isotopes was undertaken using a laser ablation system (LASSIE) at SURRC, East Kilbride; the technical details are given in Appendix C.3. The results contained some extremely high $\delta^{18}\text{O}$ values ($> 28\text{‰}$) in several samples (Figures 9.4a, 9.6a). These required corroboration. Subsequent stable isotope analysis undertaken by conventional and Secondary Ion Mass spectrometry (SIMS) (Section 9.4) revealed that, although the LASSIE data are significantly in error in many cases, the limestones are characterised by gross stable isotope heterogeneity at both grain and outcrop scale.

The LASSIE data are presented for completeness alone; only the conventional and SIMS data are used in geological interpretation in this Chapter.

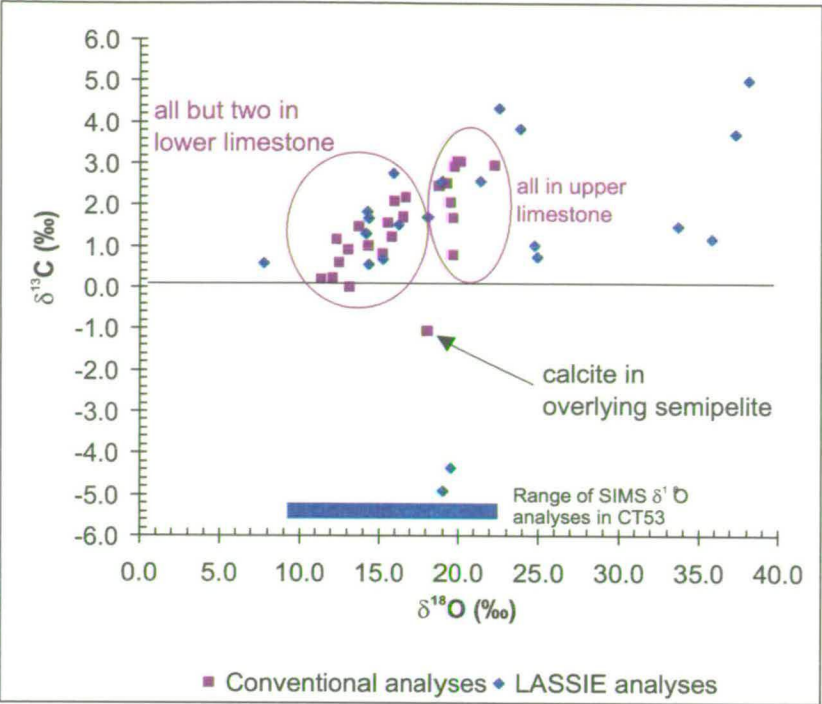
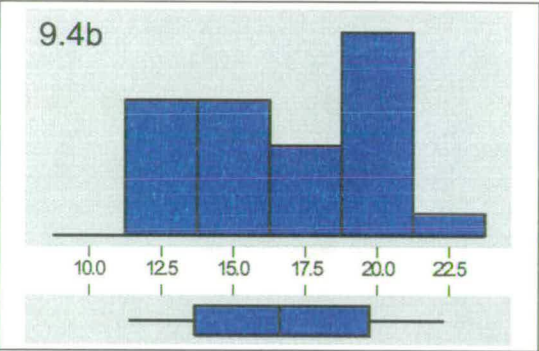
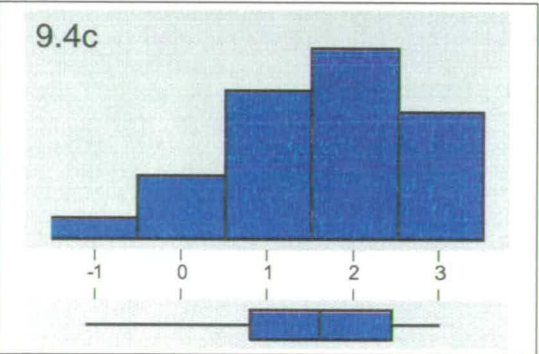


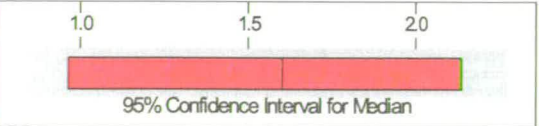
Figure 9.4a
Cross-plot of $\delta^{18}\text{O}$ vs $\delta^{13}\text{C}$ for the Torulian Limestone sample, CT53. Includes the range in SIMS analyses for comparison.



$\delta^{18}\text{O}$ (‰)	
n	26
Minimum	11.4
1st Quartile	13.7
Median	16.6
3rd Quartile	19.7
Maximum	22.3
95% Confidence Interval for Median	
	14.8 19.3



$\delta^{13}\text{C}$ (‰)	
n	26
Minimum	-1.1
1st Quartile	0.8
Median	1.6
3rd Quartile	2.4
Maximum	3.0
95% Confidence Interval for Median	
	0.9 2.1



Figures 9.4b, c Summary statistics for conventional whole-rock carbon and oxygen isotope data, Torulian Limestone, River Avon Profile

Conventional data					LASSIE data			
Sample	Profile Distance	$\delta^{18}\text{O}_{\text{snow}}$	$\delta^{13}\text{C}_{\text{pdb}}$	Comments	Sample	Distance	$\delta^{18}\text{O}_{\text{snow}}$	$\delta^{13}\text{C}_{\text{pdb}}$
CT49	28.8	13.4	0.6		CT49	28.8	33.7	1.5
CT49	28.8	13.4	0.5		CT49	28.8	35.9	1.2
CT50	29.0	15.4	0.9		CT50	29.0	24.7	1.0
CT50	29.0	14.7	0.8		CT50	29.0	24.9	0.8
CT52	29.4	14.0	-1.0		CT52	29.4	19.5	-4.4
CT52	29.4	14.4	-1.1		CT52	29.4	19.0	-4.9
CT53	29.8	17.4	2.8		CT53	29.8	22.5	4.3
CT53	29.8	17.7	2.9		CT53	29.8	23.9	3.8
CT54/1	30.3	12.1	0.2		CT53	29.8	38.1	5.0
CT54/2	30.3	12.4	1.2		CT53	29.8	37.3	3.7
CT54/3	30.3	13.2	0.0	Diffuse calcite 'vein'	CT54	30.3	15.3	0.7
CT54/4	30.3	11.4	0.2		CT55	30.7	16.2	1.5
CT54/5	30.3	12.5	0.6		CT57	31.3	7.8	0.6
CT54/6	30.3	13.2	0.9	Calcite vein	CT58	31.8	18.1	1.7
CT55/1	30.7	13.8	1.5	Calcite in darker laminae	CT59	32.5	14.4	0.6
CT55/2	30.7	15.6	1.5	Calcite in paler laminae	CT60	33.0	14.3	1.8
CT55/3	30.7	15.2	0.8		CT60	33.0	14.3	1.7
CT57/1	31.3	16.6	1.7	Calcite, grey	CT61	33.6	15.9	2.8
CT57/2	31.3	16.6	1.7	Calcite, white	CT62	34.3	21.4	2.6
CT58/1	31.8	19.3	2.5	Calcite, very pale grey	CT62	34.3	18.9	2.6
CT58/2	31.8	16.7	2.2		CT63	34.9	14.2	1.3
CT59/1	32.5	19.7	0.8					
CT59/2	32.5	19.7	1.7					
CT60/1	33.0	15.9	1.2					
CT60/2	33.0	16.0	2.1					
CT60/3	33.0	14.3	1.0	Calcite, grey				
CT61/1	33.6	20.2	3.0	Calcite, white				
CT61/2	33.6	19.9	3.0	Calcite, very pale grey				
CT61/3	33.6	20.0	3.0	Calcite, very pale grey				
CT61/4	33.6	19.8	2.9	Calcite, white				
CT62/1	34.3	22.3	2.9					
CT63/1	34.9	18.8	2.4					
CT63/2	34.9	19.5	2.0					
CT65/1	35.3	18.1	-1.1					

Table 9.1 Oxygen and carbon isotope data for CT samples from the Torulian Limestone, R. Avon

Sample	Prof. Dist. (cm)	Conventional data		SIMS $\delta^{18}\text{O}$ (range)	LASSIE data	
		$\delta^{13}\text{C}$	$\delta^{18}\text{O}$		$\delta^{13}\text{C}_{\text{pdb}}$	$\delta^{18}\text{O}_{\text{smow}}$
LWQ 1/23	44.25				2.3	19.3
LWQ 1/23	44.25				3.4	18.4
LWQ 1/25	47.50			22.4 - 27.2	6.6	30.7
LWQ 1/25	47.50				6.7	29.4
LWQ 1/25	47.50				6.6	30.9
LWQ 1/25	47.50				6.6	28.9
LWQ 1/26	48.75	6.6	22.0		5.5	17.2
LWQ 1/26	48.75				5.5	16.7
LWQ 1/28	51.50				7.7	30.3
LWQ 1/28	51.50			18.4 - 27.0	7.2	31.0
LWQ 1/30	55.50			17.6 - 27.0	7.5	32.0
LWQ 1/30	55.50				7.1	33.3
LWQ 1/31	57.25	7.0	22.5		6.0	17.3
LWQ 1/31	57.25				5.8	16.8
LWQ 1/32	59.00	6.9	22.6		4.9	18.8
LWQ 1/32	59.00				6.8	19.4
LWQ 1/33	61.25	6.9	22.9		4.6	14.9
LWQ 1/33	61.25				4.6	13.9
LWQ 1/34	63.25	6.8	20.7		4.1	10.2
LWQ 1/34	63.25				3.9	12.1
LWQ 1/34	63.25				5.1	13.0
LWQ 1/35	65.75	6.8	22.5		4.5	13.5
LWQ 1/35	65.75				4.0	9.8
LWQ 1/36	68.00	6.8	22.2		6.0	18.3
LWQ 1/36	68.00				6.1	18.1
LWQ 1/37	70.00	6.8	22.4		5.5	16.0
LWQ 1/37	70.00				5.5	18.3
LWQ 1/39	73.50	6.8	22.9		4.9	23.4
LWQ 1/39	73.50				6.2	21.2
LWQ 1/41	77.00				5.8	17.3
LWQ 1/41	77.00	7.0	22.7		5.9	17.8
LWQ 1/42	82.25	6.4	22.6		5.5	17.5
LWQ 1/42	82.25				4.8	17.6
LWQ 1/43	87.50	6.7	22.8		4.9	15.7
LWQ 1/43	87.50				4.8	16.6
LWQ 1/44	92.50	6.8	23.0		5.4	17.0
LWQ 1/44	92.50				5.2	16.7
LWQ 1/45	97.50	6.4	21.6		4.7	16.9
LWQ 1/45	97.50				5.1	17.3
LWQ 1/46	100.00	6.2	22.3		3.5	14.5
LWQ 1/46	100.00				4.8	17.0
Comparative conventional analyses on whole-rock samples, Tomintoul Quarry						
HY56		6.6	22.1			
HY57		7.5	22.2			
HY58		7.2	23.3			
HY59		7.7	23.7			
HY60		7.4	23.5			

Table 9.2 Carbon and oxygen analyses of minicores, Inchrory Limestone, Limeworks Quarry

Torulian Limestone

In most cases, several analyses were made on micro-drilled sub-samples of each of the hand-specimens from the profile. The sub-samples were obtained to establish the scale of isotopic heterogeneity of bulk carbonate within each specimen. Summary statistics for bulk carbonate $\delta^{18}\text{O}$ and $\delta^{13}\text{C}$ data are given in Figures 9.4b and 9.4c, respectively.

$\delta^{18}\text{O}$ data range widely from 11.4 – 22.3‰. Basic statistical analysis of the data shows that whole-rock $\delta^{18}\text{O}$ is bimodal (Figure 9.4a). The class interval for $\delta^{18}\text{O} = 20 \pm 1.25$ ‰ constitutes the mode, with two secondary modes occupying the two class intervals between 11.25 – 16.25 ‰.

With the exception of an analysis of CT65 ($\delta^{13}\text{C} = -1.1$ ‰), which comes from semipelite at the top of the profile, all $\delta^{13}\text{C}$ values range from 0 – 3.0 ‰ (Figures 9.4a, c).

Inchrory Limestone

Bulk carbonate $\delta^{18}\text{O}$ and $\delta^{13}\text{C}$ data are much more tightly grouped in the Inchrory Limestone samples than in those from the Torulian Limestone. $\delta^{18}\text{O}$ ranges from only 20.7 – 23.0 ‰ whilst $\delta^{13}\text{C}$ ranges only from 6.2 to 7.0 ‰ (Figure 9.5a-c). The $\delta^{18}\text{O}$ and $\delta^{13}\text{C}$ data for whole-rock samples from Limeworks Quarry (from which the Sr isotope data were obtained) are also included here for comparison; though slightly higher in $\delta^{18}\text{O}$ and $\delta^{13}\text{C}$ than the conventional analyses of the mini-core data from the profile, they are closely consistent.

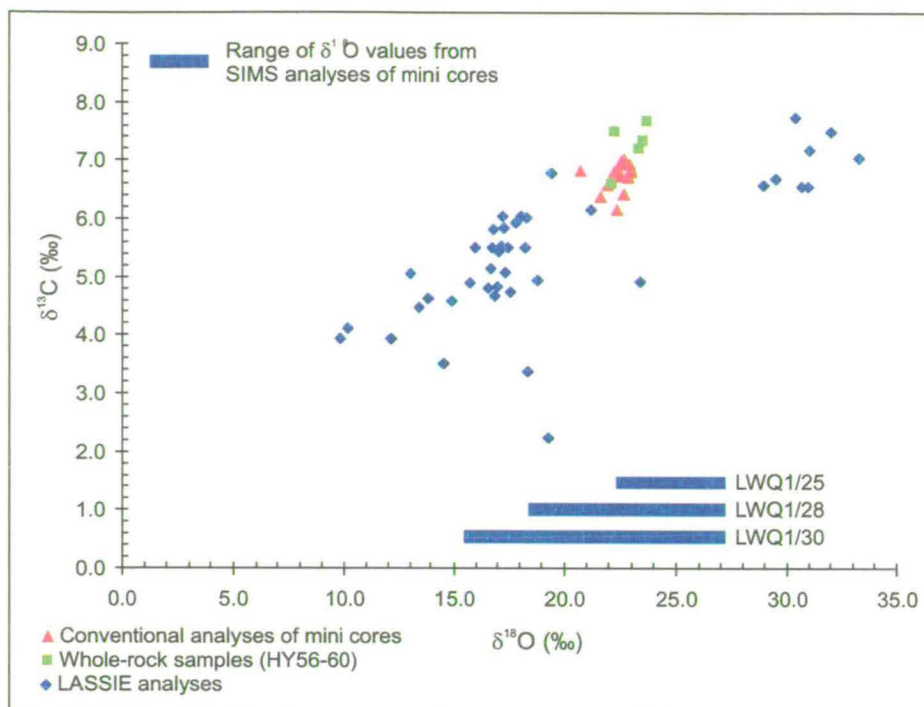
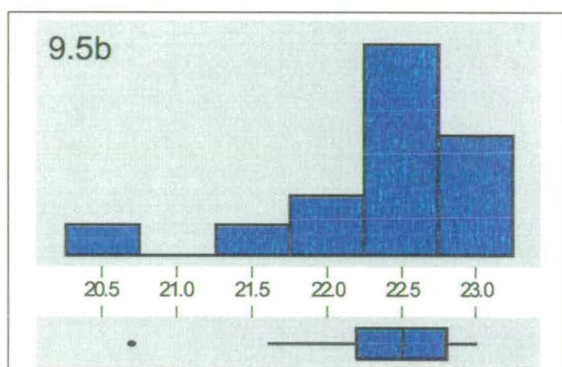
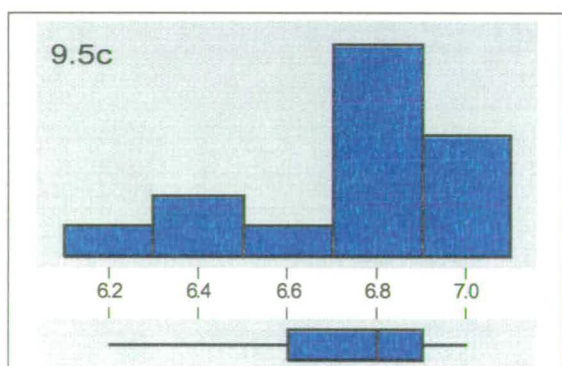
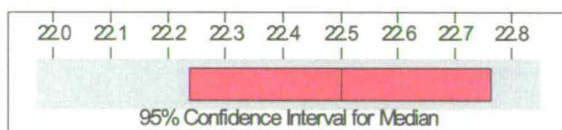


Figure 9.5a
Cross-plot of $\delta^{18}\text{O}$ vs $\delta^{13}\text{C}$ for Inchrory Limestone samples. Includes the range in SIMS analyses for comparison.

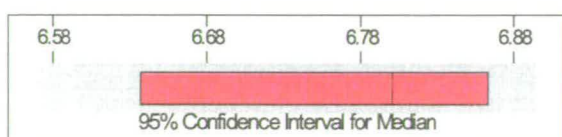


$\delta^{18}\text{O}$ (‰)	
n	15
Minimum	20.7
1st Quartile	22.2
Median	22.5
3rd Quartile	22.8
Maximum	23.0
95% Confidence Interval for Median	
22.2	22.7



Figures 9.5b, c Summary statistics for conventional whole-rock oxygen and carbon isotope data, Inchrory Limestone, Limeworks Quarry Profile

$\delta^{13}\text{C}$ (‰)	
n	15
Minimum	6.2
1st Quartile	6.6
Median	6.8
3rd Quartile	6.9
Maximum	7.0
95% Confidence Interval for Median	
6.6	6.9



9.2.2 Outcrop-scale variation in $\delta^{18}\text{O}$ and $\delta^{13}\text{C}$, Torulian Limestone profile, River Avon

The variation of $\delta^{18}\text{O}$ and $\delta^{13}\text{C}$ calcite in relation lithology in the River Avon section through the Torulian Limestone is shown in Figures 9.6a, b.

Oxygen isotope data

$\delta^{18}\text{O}$ values are variable in the lowermost part of the limestone either side of the thin semipelite unit, with values ranging from 11.4 to 17.7 ‰. Thereafter, $\delta^{18}\text{O}$ values rise steadily from the middle of the lower limestone unit at 30.3 m, to reach a maximum of 22.3 ‰ at 34.3 m 0.6m below the top of the thicker, upper limestone. $\delta^{18}\text{O}$ then declines to 18.8 - 19.5 ‰ at the boundary with the overlying semipelite and 18.1 ‰ 0.4 m into it.

With the exception of the sample at 33.0 m, in which drilled samples record $\delta^{18}\text{O}$ at 14.3 and 16.0 ‰, this cross-profile variation from the middle of the lower limestone unit to the top of the uppermost unit is smooth. The thin semipelite unit at 29.9 – 33.3 m does not, *on the scale of the sampling*, affect the increase in $\delta^{18}\text{O}$ through into the upper limestone, as seen from the value of 16.6 ‰ for $\delta^{18}\text{O}$ at the top boundary of this semipelite unit. The shape of the profile is similar to those recorded over similar scales in other studies of isotope variation in limestone boundary layers (e.g. Bickle and Baker, 1990; Bickle et al., 1995; Rye et al., 1976).

A key feature of the whole-rock oxygen isotope data is the distribution of the values relative to sample position (Figure 9.6a). The lower $\delta^{18}\text{O}$ values all occur in the lower limestone. Only one value below the median $\delta^{18}\text{O}$ value (16.6 ‰) occurs in the upper limestone unit. This spatial distribution shows quite clearly that the lower

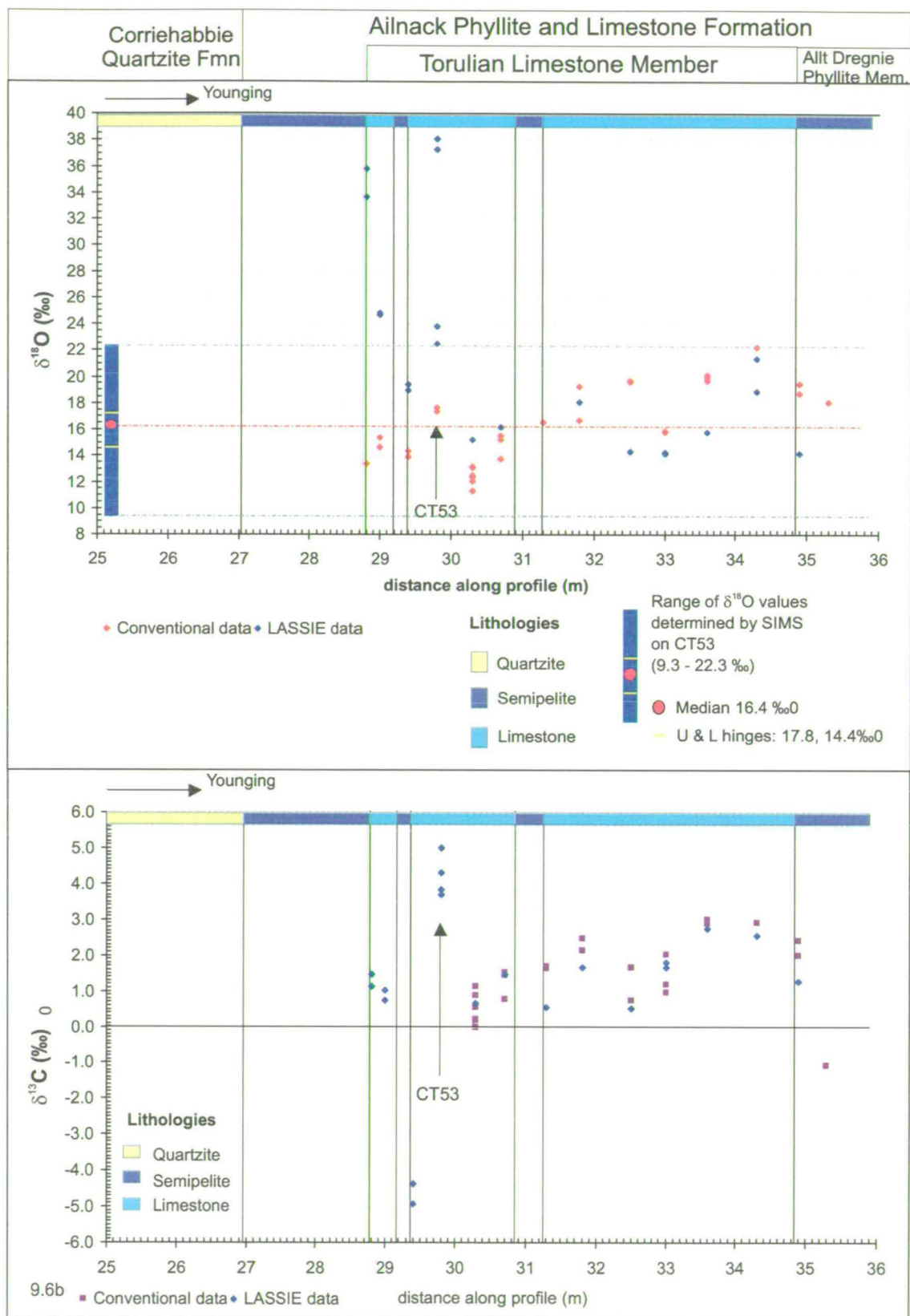


Figure 9.6a, b Variation of conventional and LASSIE $\delta^{18}\text{O}$ and $\delta^{13}\text{C}$ data with distance across the River Avon section through the Torulian Limestone. The section lithostratigraphy is given at the top of 9.4a.

limestone unit has undergone more significant interaction with low $\delta^{18}\text{O}$ fluid than the upper limestone unit. However, smooth variation in the profile does not coincide with the limestone – pelite boundaries, as observed in other studies (e.g. Bickle and Baker 1990; Rye et al., 1976). I consider the implications for this spatial variation for fluid infiltration in this limestone further in Chapter 10.

The whole-rock oxygen isotope data suggest possibly two stages of alteration from primary $\delta^{18}\text{O}$ values likely to have been in the mid-20s ‰. The first resulted in reduction of $\delta^{18}\text{O}$ to values of $\sim 18 - 20$ ‰. The second resulted in reduction to lower $\delta^{18}\text{O}$ values of c. $14 - 15$ ‰. As will be discussed later, the alteration of $\delta^{18}\text{O}$ probably resulted from metamorphic fluid rock interaction. These data are discussed in more detail along with the SIMS data below and in Chapter 10.

The significance of the low $\delta^{18}\text{O}$ data in the limestone at this locality is reinforced by the much more radiogenic composition of the $^{87}\text{Sr}/^{86}\text{Sr}$ recorded in a whole-rock sample from this locality (HY43, see Chapter 6).

Carbon isotope data

Variation in bulk calcite $\delta^{13}\text{C}$ in the River Avon profile is shown in Figure 9.6b. The pattern of variation along the profile is very similar to that shown by $\delta^{18}\text{O}$, but with some exceptions:

In contrast to the bimodal character of the $\delta^{18}\text{O}$ data discussed above, the distribution of the $\delta^{13}\text{C}$ data is smooth and negatively skewed (Figure 9.4b). The mode is in the class 2 ± 0.5 ‰ and contains the median (1.6 ‰). A further distinction between the carbon and oxygen data is that the upper and lower limestones have samples with broadly similar $\delta^{13}\text{C}$ values, although only the upper limestone has

values in excess of 2 ‰. Taken in isolation, the carbon isotope data suggest only a single stage of alteration of $\delta^{13}\text{C}$ from high primary values by interaction with a low $\delta^{13}\text{C}$ source (maximum recorded for the Torulian Limestone is ~ 4 ‰; see Chapter 8).

Examination of the $\delta^{18}\text{O}$ - $\delta^{13}\text{C}$ cross-plot in Figure 9.4a shows slightly different relationships between the two isotope systems in different parts of the plot. Values of $\delta^{18}\text{O}$ clustering about 19 ‰ are associated with a range in $\delta^{13}\text{C}$ values from 0.8 – 3.0 ‰. In contrast, $\delta^{13}\text{C}$ in samples with $\delta^{18}\text{O}$ below 16.7 ‰ shows reasonably good covariation with $\delta^{18}\text{O}$.

9.2.3 Outcrop-scale variation in $\delta^{18}\text{O}$ and $\delta^{13}\text{C}$ in the Inchrory Limestone profile

Conventional, bulk carbonate analyses show that there is little variation in average $\delta^{18}\text{O}$ across the profile, the only exceptions being samples LWQ1/34 ($\delta^{18}\text{O} = 20.7$) and LWQ1/45 ($\delta^{18}\text{O} = 21.6$ ‰); the range for all the data is just 2.3 ‰ (Figure 9.5a). Notably, the median bulk calcite $\delta^{18}\text{O}$ for this profile is, at 22.5 ‰, within error of the maximum bulk $\delta^{18}\text{O}$ value for the Torulian Limestone ($\delta^{18}\text{O} = 22.3$ ‰) (*Note that high bulk carbonate $\delta^{18}\text{O}$ values are considered indicative of 'unaltered' limestones* (e.g. Rye et al., 1976; Derry et al., 1989; Kaufman et al., 1993)). There is even less variation shown by the carbon data ($\delta^{13}\text{C} = 6.2$ to 7.0 ‰; Figure 9.5b).

There is no systematic variation in bulk calcite $\delta^{18}\text{O}$ and $\delta^{13}\text{C}$ in relation to distance from the amphibolite pod (Figure 9.7a, b). Neither is there a clear change in bulk calcite $\delta^{18}\text{O}$ with increasing deformation in the outer part of the profile. The bulk-carbonate data, together with the petrographic evidence for increasing strain

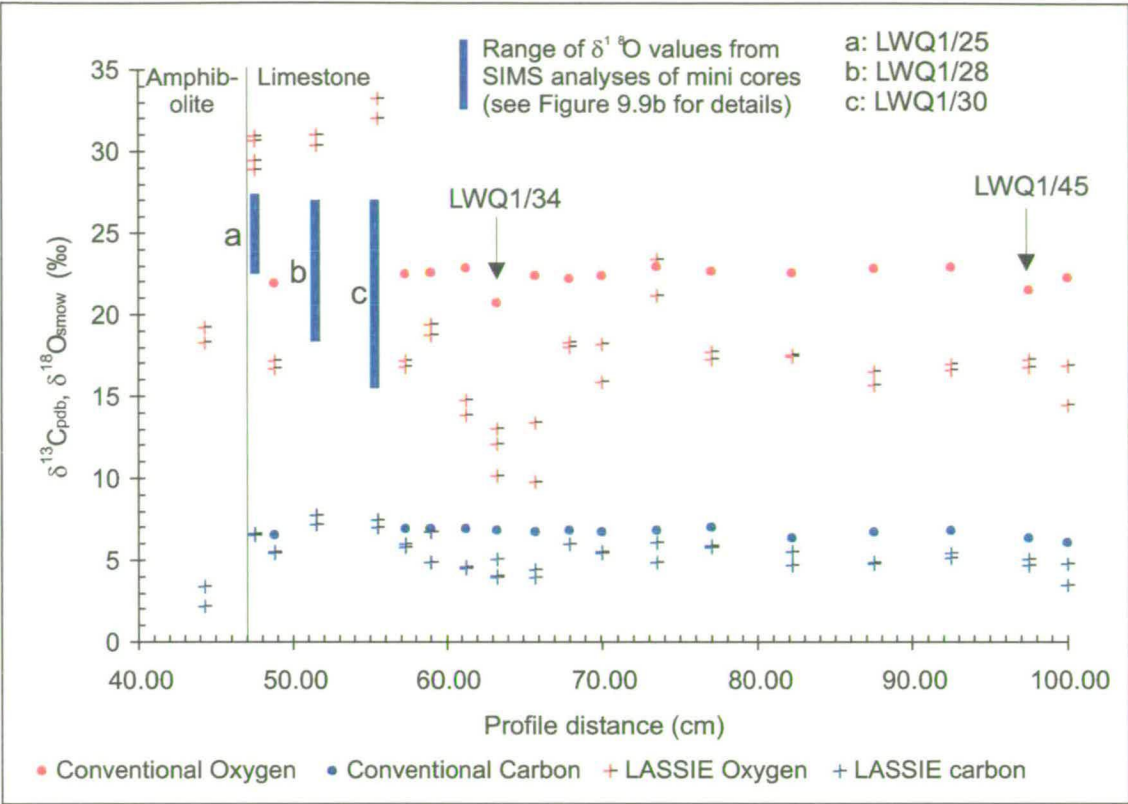


Figure 9.7a Variation in $\delta^{18}\text{O}$ and $\delta^{13}\text{C}$ against distance for the Inchroy Limestone sample profile, Limeworks Quarry, Tomintoul.

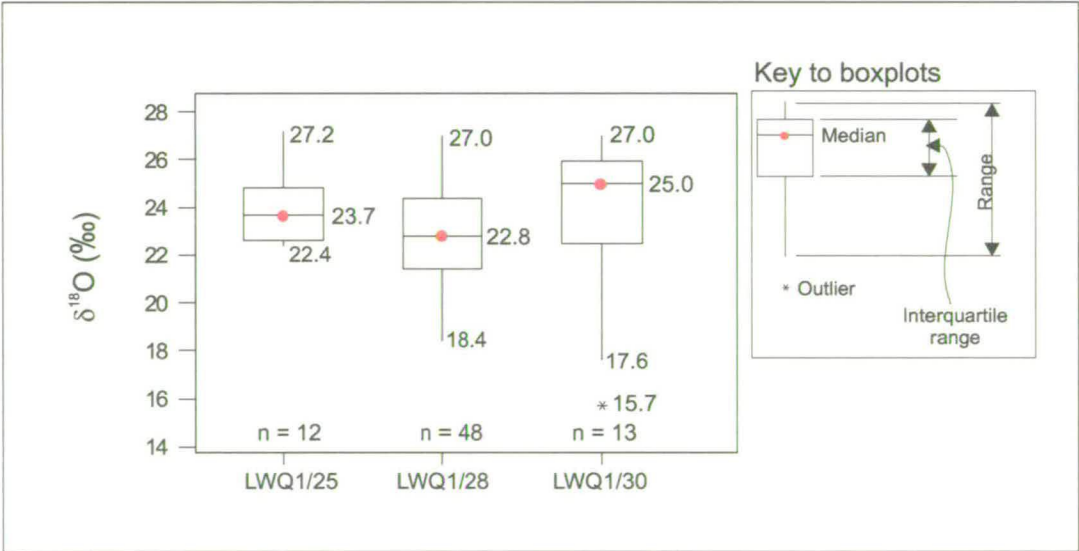


Figure 9.7b Summary of SIMS analyses shown as bars in Figure 9.9a. See also Table 9.3.

away from the amphibolite pod margin (Chapter 3 and Appendix D), indicate that there was no significant interaction with external metamorphic fluid facilitated by increased deformation. Nor has there been any significant isotopic exchange between the limestone and the amphibolite.

The evidence from the bulk carbonate isotope data suggest that there has been no significant metamorphic fluid-rock interaction in this limestone. The veracity of this conclusion based on the bulk carbonate data is examined further when grain-scale data are presented and discussed in Section 9.4.4.

9.2.4 Summary of bulk carbonate profile data

- The Torulian Limestone has a very wide range in bulk carbonate $\delta^{18}\text{O}$ from 11.4 to 22.3 ‰ and a range in $\delta^{13}\text{C}$ values from -1.1 to 3.0 ‰.
- $\delta^{18}\text{O}$ values in the Torulian Limestone vary smoothly from the middle of the lower limestone unit to the top of the upper limestone unit
- The form of the outcrop variation is similar to that observed in limestone boundary layers in other studies, except that in this study, the lowermost values in the profile do not coincide with the limestone pelite boundary
- Low $\delta^{18}\text{O}$ values in the lowermost limestone unit indicate that this part of the limestone has undergone extensive exchange with low $\delta^{18}\text{O}$ fluid
- In contrast to the Torulian Limestone profile data, there is no significant outcrop-scale variation in bulk carbonate $\delta^{18}\text{O}$ and $\delta^{13}\text{C}$ the Inchrory Limestone sample profile

- High bulk carbonate $\delta^{18}\text{O}$ and $\delta^{13}\text{C}$ values are preserved throughout this profile and there is no indication of the variation suggested by the LASSIE data.
- The data imply no significant metamorphic fluid-rock interaction.

9.3 Cathodoluminescence (CL) imaging

I have used CL imaging to elucidate spatial variations in calcite chemistry and to plan SIMS analysis of grain-scale variations in calcite and quartz $\delta^{18}\text{O}$. In this next section, I describe and discuss the images obtained for the four samples analysed in the SIMS study, prior to discussion of the SIMS analytical work in Section 9.4). The samples included in this work are CT53 from the Torulian Limestone and LWQ1/25, 28 and 30 from the Inchrory Limestone.

9.3.1 Torulian Limestone: River Avon profile sample CT53

In the CL image of sample CT53, calcite luminescence ranges from dark orange brown to bright yellow (Figure 9.8; folded in pocket). Some of the very small weakly luminescent brown spots turn out, on subsequent analysis by electron microprobe, to be tiny grains of dolomite (see Chapter 10) (*the presence of dolomite was not anticipated prior to the SIMS work because of the low MgO contents of these rocks; see Table 4.2*)

The complexity of the CL image of sample CT53 in Figure 9.8 is immediately apparent, as is the lack of silicate. A significant aspect of this image is the fact that although *physical* grain boundaries are still visible optically in this sample, their *geochemical* expression, as revealed by CL, is commonly destroyed (*compare this with Figures 9.9 – 9.11 for the Inchrory Limestone samples*). Only in

the left hand end of the image is there any semblance of a polygonal, metamorphic, grain boundary network, picked out by dark orange-brown (**dob**) and dark orange (**do**) luminescent calcite. Elsewhere, the only hint of polygonal grain architecture is given by rather less luminescent calcite patches with ghosted outlines preserved in the upper part of the image. The right-hand part of the image indicates that the original polygonal metamorphic fabric is barely preserved; this region is more generally luminescent and contains more extensive networks of brightly yellow to orange (**byo**) luminescent calcite veins.

Discrete to more diffuse veining is picked out by sharp linear to more patchy diffuse bright yellow luminescent calcite. Grain boundaries in the area preserving the metamorphic polygonal fabric are picked out by thin networks of yellow luminescent calcite. More orange and yellow luminescent calcite can be seen extending from grain boundaries along calcite cleavage planes in the left-hand end of the image. The luminescence 'textures' in this image reveal extensive and complex alteration involving fracturing and fluid-rock interaction.

As well as the bright orange and yellow luminescent calcite in this sample, an irregular patchy to linear and paler orange-brown luminescent calcite is also developed in the interiors of dark orange brown grains in a zone leading diagonally NE across the left-central part of the image in Figure 9.8. This luminescent calcite clearly predates the later bright calcite as the latter cuts the former in several places. However, it is notable that the pale orange-brown calcite lies approximately parallel to the main linear domain of bright calcite in this part of the section. The pattern of the CL of this earlier, more weakly luminescent calcite suggests fracture control, since it cuts across grains, a feature particularly well-seen at the NE-end of the

section. This is interpreted as clear evidence for a fluid infiltration event which predates the bright luminescent calcite. However, it may not have occurred much earlier, as the later bright luminescent calcite clearly re-uses some of the pathways.

The CL image of CT53 reveals a complex, polyphase fluid-rock interaction history in this rock, dominated by fracturing, but including significant alteration along grain boundaries.

Because of the very high $\delta^{18}\text{O}$ values recorded by LASSIE analysis in this sample, CT53 was analysed extensively by SIMS (83 analyses), concentrating particularly on profiles across variably luminescent domains with sharp to diffuse boundaries. Relict cores of darkly luminescent calcite and their commonly more orange luminescent diffuse margins, such as those seen in the central left hand area of Figure 9.8, were also analysed.

Summary of CL in CT53

- The CL image of CT53 reveals extensive and very complex, polyphase alteration of calcite chemistry resulting from fluid infiltration
- Evidence for an early phase of infiltration is preserved in the darker orange and orange brown luminescence in larger grains
- There has been extensive infiltration along fractures and twin planes, effectively short-circuiting fluid infiltration into grain interiors
- Locally extensive patches of recrystallisation are developed and the original metamorphic grain texture is poorly preserved in most of the sample

- The CL evidence for alteration of calcite chemistry is consistent with bulk carbonate $\delta^{18}\text{O}$ data suggesting extensive fluid infiltration in the lowermost limestone unit from which CT53 was collected

9.3.2 Inchrory Limestone: Limeworks Quarry samples

Figure 9.9-11 show CL images of samples LWQ1/25, 28 and 30 respectively. The textural and petrographical differences between the three samples are immediately apparent. Calcite luminescence varies from **dob**, through to **byo** and quartz is black. Although luminescence colour is variable due to slight differences in photographic colour printing, feldspar is generally pale, with a 'duck-egg' blue colour. A particular feature of the feldspar luminescence important in later discussion is that it becomes brownish and mottled in the areas straddling the domains of bright yellow veinlet calcite in LWQ1/28 and 30. This marks a sharp change from oligoclase to albite. Randomly orientated, bladed, non-luminescent crystals on the east side of LWQ1/25 are biotite. The inverse relationship between grain size and the amount of silicate impurity is well-displayed by the three LWQ samples, reflecting reduction in the effect of grain-boundary pinning in restricting calcite grain growth in the purer samples: note the progressive decrease in calcite grain-size from LWQ1/25 to 1/30, whilst silicate grain size remains substantially the same in all three.

LWQ1/25

LWQ1/25 consists chiefly of calcite. Oligoclase is only moderately abundant at about 10 – 15 % and quartz is rare. Calcite in LWQ1/25 is variably luminescent with diffuse patches of more orange luminescent material transecting the polygonal grain

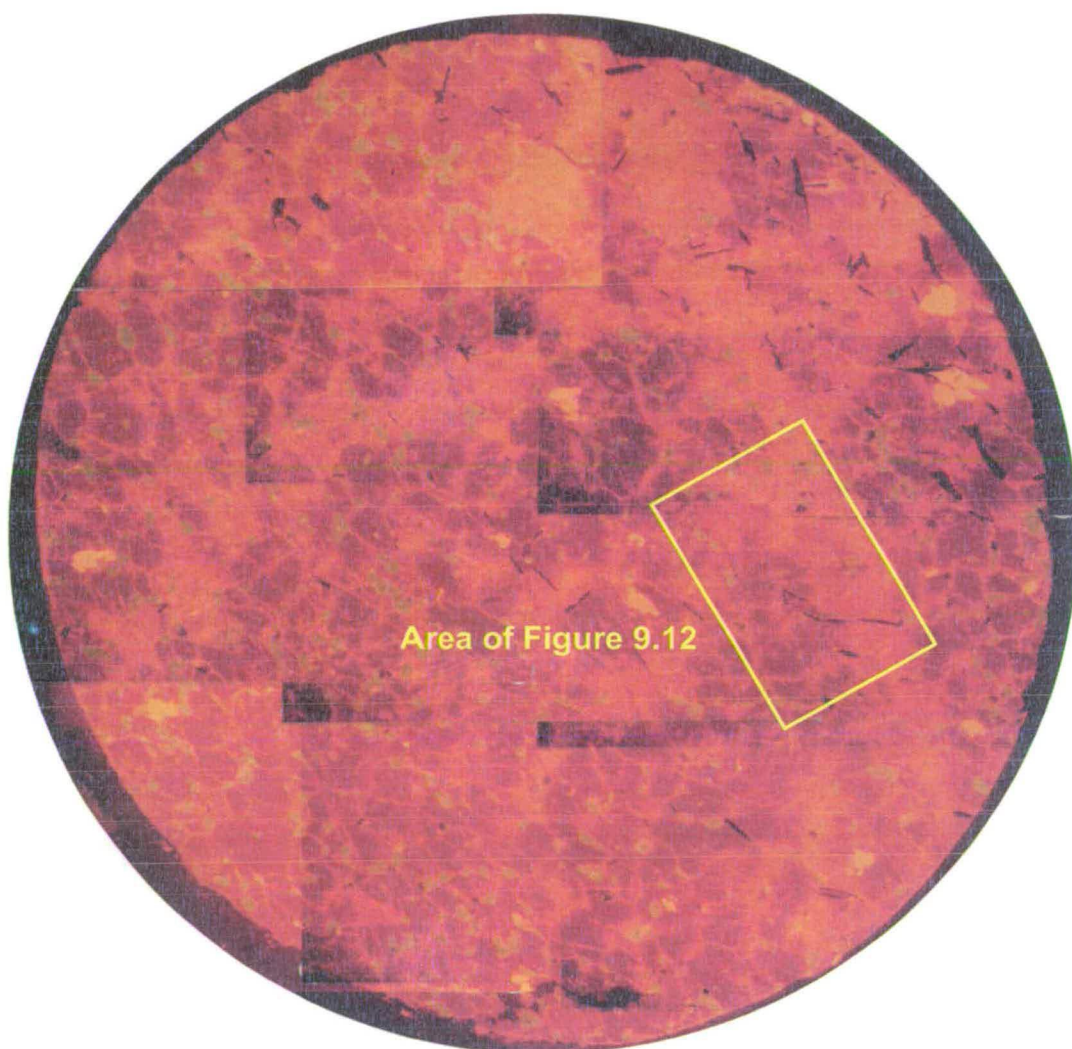


Figure 9.9 CL image of LWQ1/25, showing the location of Figure 9.12. The disc is 7 mm across.

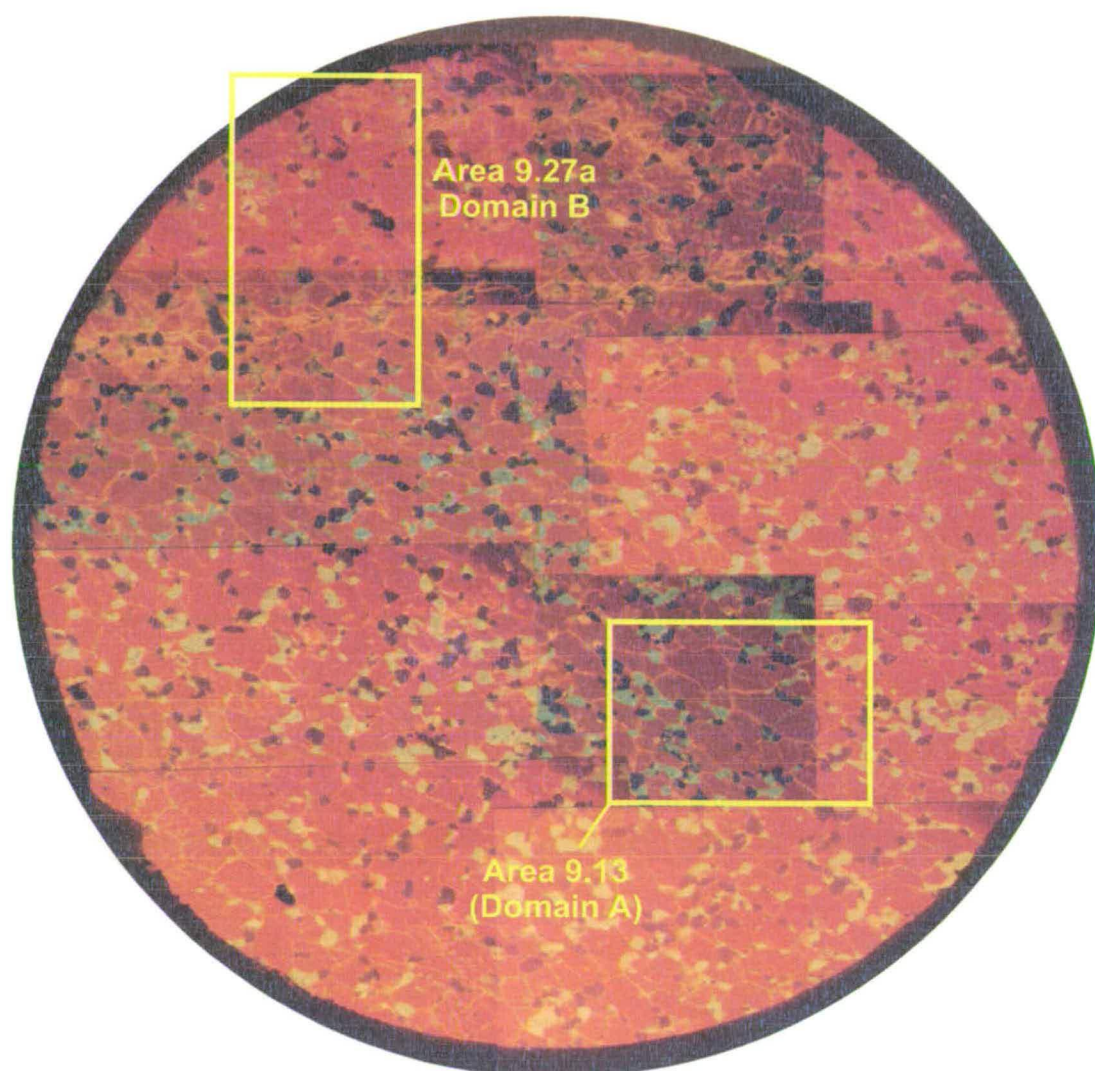


Figure 9.10 CL image of LWQ1/28, showing areas of detailed SIMS analysis shown in Figures 9.13, 9.26 and 9.27. The luminescent micro-vein straddled by Domain B has a halo of altered feldspar (see text for discussion).

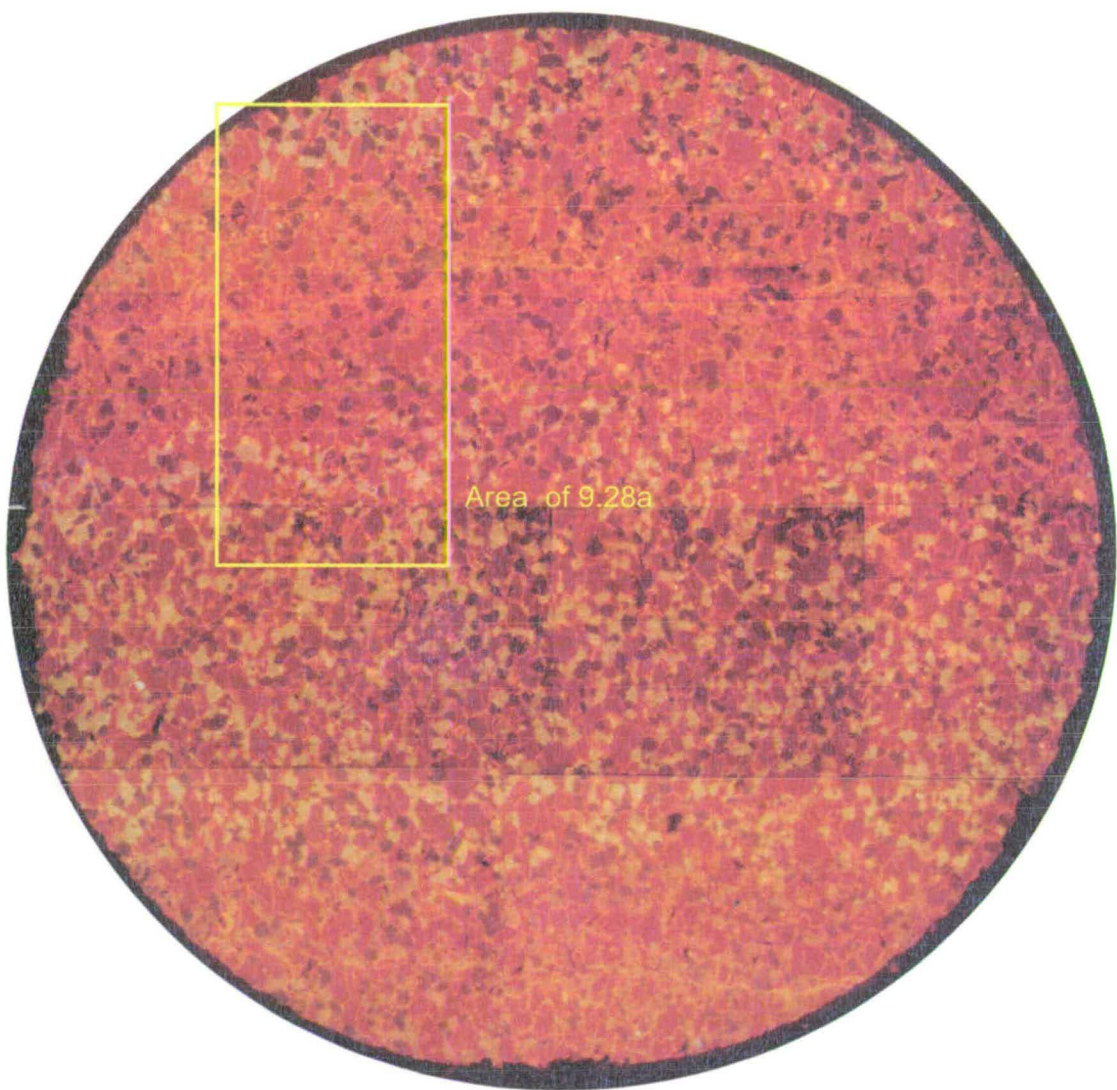


Figure 9.11 CL image of LWQ1/30, showing the location of Figure 9.28a across the luminescent veinlet and altered feldspar halo.

fabric and ghosting it. This is shown in more detail in Figure 9.12 for part of the eastern quadrant. Here the earlier, less luminescent, metamorphic polygonal fabric can be seen being replaced by more luminescent calcite in zones extending principally along cleavage planes from grain boundaries. Other areas, most particularly the northwestern part of the image, preserve the earlier polygonal fabric much more clearly. Optical examination of the more luminescent domains under ppl reveals that the more luminescent calcite is subtly more turbid and ‘dusty’ looking than clearer adjacent calcite. SIMS analyses were undertaken in areas where the polygonal, low-luminescent calcite fabric is better preserved, and in areas where the brighter luminescent calcite is extensively replacing the former.

LWQ1/28

In LWQ1/28, large, well-formed single plates of calcite with straight grain boundaries dominate the mineralogy. Feldspar and quartz are much more abundant than in LWQ1/25 and are in approximately equal proportions (Figure 9.10). Overall, the silicates are well-dispersed throughout the calcite matrix, generally being concentrated along grain boundaries and at triple junctions, rather than clustered. However, there are one or two small domains which are silicate-poor and where calcite grains are relatively large. One such domain lies in the southeast quadrant of LWQ1/28, halfway from the centre to the margin. This area, detailed in Figure 9.13 (Domain A), was the target for detailed SIMS analysis of both calcite and quartz, with supporting trace element analyses (see also Figure 9.24). These analyses were undertaken to test the degree of $\delta^{18}\text{O}$ homogeneity of the calcite grains themselves



Figure 9.12 Detail of area outlined in Figure 9.9, showing diffuse CL 'ghosting' the grain boundaries. See text for discussion.

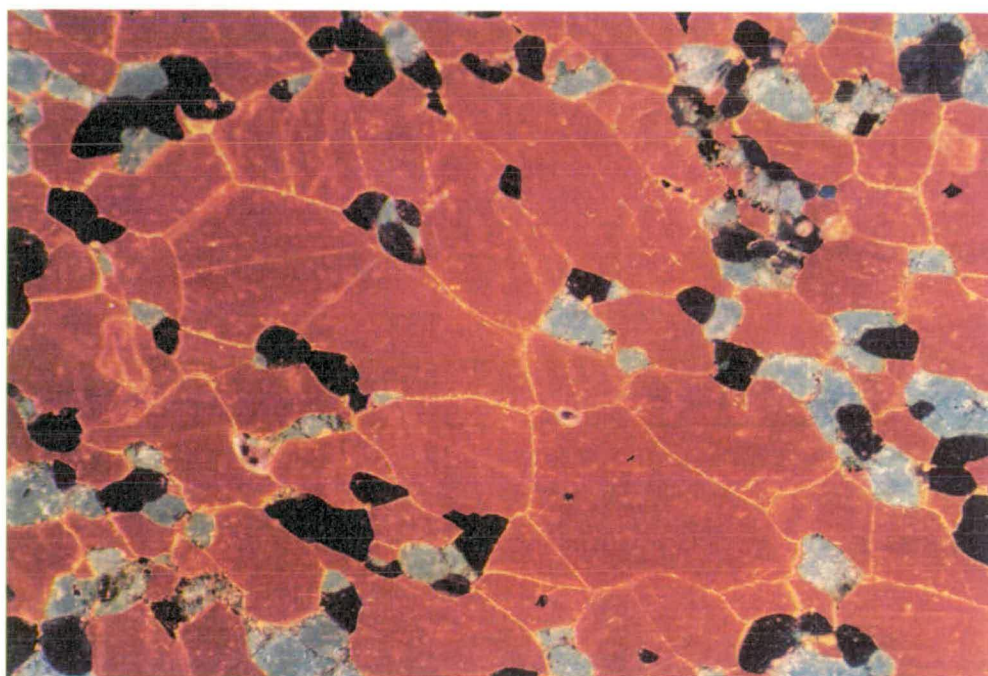


Figure 9.13 Detail of Domain A outlined in Figure 9.10, showing texturally well-equilibrated calcite, quartz (black) and oligoclase (blue). See also Figure 9.26 detailing SIMS analysis sites, and quartz and calcite $d^{18}O$ and trace element results.

and to test the degree to which $^{18}\text{O}/^{16}\text{O}$ is equilibrated between the calcite and the quartz.

Bright yellow luminescent calcite is ubiquitous along grain boundaries in LWQ1/28. However, a narrow, vein network of bright yellow luminescent calcite is conspicuous in the top part of Figure 9.10; associated with it is a halo of the albitised oligoclase mentioned above. Calcite and quartz were analysed by SIMS in a profile extending from the orange luminescent coarse calcite plates at the top-left of the sample into the luminescent veinlet. The aim was to test the extent to which the orange-luminescent calcite and the quartz grains had exchanged with the fluid deemed responsible for the bright yellow calcite in the vein network. The halo of albitised feldspar is clear petrological evidence for metasomatism which extended into the wall-rock of the vein network.

LWQ1/30

LWQ1/30 is the finest grained of the three LWQ samples analysed by SIMS and the most silicate rich (Figure 9.11). Calcite grains are much smaller than in LWQ1/28, generally being of the same size as the feldspar and quartz. Clusters of calcite grains relatively free from siliciclastic impurity are absent in this sample. Two thin vein networks similar to that observed in LWQ1/28 are present, cutting across the top and bottom of the disc. The associated haloes of albitised oligoclase (see below) are conspicuous and in this sample, can be seen to be symmetrical across the lower, longer veinlet; half-widths of the two domains are approximately equal at about 0.85 mm. SIMS analysis was concentrated across this altered domain in the upper southeast quadrant of the sample (Figure 9.11). A few SIMS analyses were also

made of calcite grains well away from the domain to try and establish the likely maximum calcite $\delta^{18}\text{O}$ in this sample.

Summary of CL in Inchrory Limestone samples

- Calcite in LWQ1/25 from the Inchrory Limestone is more luminescent than either of the other samples (LWQ1/28, 1/30) and its luminescence is more patchy
- Calcite in LWQ1/28 and 1/30 is uniformly orange brown luminescent
- All three samples have variably luminescent grain boundaries
- LWQ1/28 and 1/30 have veinlets of luminescent calcite which cut across the calcite fabrics and run along grain boundaries
- These micro-veins have symmetrical halos of altered feldspar which have sharp boundaries and are ~ 0.5 to 0.85 mm across
- The micro-veins and altered feldspar haloes record infiltration of $\delta^{18}\text{O}$ -poor fluid in a fracture network
- In all three samples, grey-brown luminescence highlights the extent of the domains of oligoclase feldspar altered to albite
- The luminescence of the calcite grains within the altered feldspar domains is unchanged

9.4 Spatial variation of $\delta^{18}\text{O}$ and $\delta^{13}\text{C}$ at the grain-scale

In the remaining part of this chapter, I discuss the spatial variation of the oxygen isotope and associated geochemical data on the grain scale in the samples from the Torulian and Inchrory Limestones.

The main aims of this work are to

- constrain the spatial relationship between $\delta^{18}\text{O}$, texture and trace element variation at the grain-scale in calcite and quartz
- determine whether diffusion-controlled isotope gradients are present which could be used in quantitative modelling
- constrain the scale of carbonate and quartz isotope homogeneity at the grain-scale, and
- identify the extent of ^{18}O equilibrium between calcite and quartz

9.4.1 SIMS grain-scale calcite and quartz $\delta^{18}\text{O}$ data

The spatial variation in calcite of oxygen isotopes and trace elements at the grain-scale were investigated by Secondary Ion Mass Spectrometry (Appendix C), allied to the CL imaging described above. Oxygen isotope data were also obtained for quartz in Inchrory Limestone samples LWQ1/28 and LWQ1/30. The results are summarised in Table 9.3; the complete data are given in Appendix D. The data are also shown graphically on Figures 9.4, 9.5, 9.6, 9.7 for comparison with the LASSIE and conventional data.

Overview of SIMS calcite $\delta^{18}\text{O}$ data

The SIMS results reveal considerable and extensive grain-scale heterogeneity in calcite $\delta^{18}\text{O}$, with values widely straddling the $\delta^{18}\text{O}$ results from conventional oxygen isotope analysis (Figures 9.4, 9.5a, 9.6, 9.7).

Sample	Mineral	n	median	maximum	minimum
LWQ1/25	Calcite	12	23.7	27.2	22.4
	± error		1.0	1.3	1.0
LWQ1/28	Calcite	48	22.8	27.0	18.4
	± error		1.1	1.5	0.8
	Quartz	13	23.5	26.1	14.3
	± error		1.5	1.6	1.3
LWQ1/30	Calcite	13	25.0	27.0	15.7
	± error		1.1	1.1	0.9
	Quartz	11	23.6	27.6	19.6
	± error		1.6	1.9	1.4
CT53	Calcite	83	16.4	22.3	9.3
	± error		1.0	1.3	0.8

Table 9.3 Summary of SIMS $\delta^{18}\text{O}$ data for calcite and quartz

Sample		Mg	Si	Fe	Mn	Sr	Sr/Mn	Fe/Mn
LWQ1/25	n = 12							
	median	7062	3	11810	2824	2304	0.8	4.4
	maximum	9923	5204	19830	3749	2661	0.9	6.2
	minimum	4624	1	9014	2464	2089	0.7	3.3
LWQ1/28	n = 7							
	median	3027	18	6801	580	1952	3.4	11.7
	maximum	3055	92540	7189	590	1970	3.4	17.2
	minimum	2050	3	6753	419	1280	3.1	11.5
LWQ1/30	n = 5							
	median	3803	39	7932	418	1978	4.9	18.8
	maximum	3956	712	10570	422	2047	5.0	25.3
	minimum	2263	6	5150	360	1815	4.7	14.3
CT53	n = 20							
	median	3062	54	774	116	849	7.3	7.1
	maximum	25870	92	1591	761	1026	12.5	18.9
	minimum	597	11	559	81	609	1.1	0.8

Table 9.4 Summary of SIMS trace element data (ppm) for Inchrory (LWQ) and Torulian Limestone (CT) samples

In the one Torulian Limestone sample alone (CT53), the SIMS data reveal a *within-sample* range (9.3 – 22.3 ‰) which is *greater* than the range shown by the conventional data for all the other samples in the profile (11.4 – 22.3 ‰) (see Figure 9.5a). However, there are clearly no values remotely close to the >30‰ values indicated by the LASSIE data for CT53 (Table 9.1). The established range in $\delta^{18}\text{O}$ in CT53 is 13 ‰ (*Note: the data given in Tables 9.1 and 9.2 are the same as those in Table 7.1b – they are given again here for ease of reference*)

The SIMS data for the three Inchrory Limestone minicore samples (LWQ1/25, 28, 30) reveal ranges in $\delta^{18}\text{O}$ which vary systematically with distance along the profile (Figure 9.7a). Within error, all samples have maximum $\delta^{18}\text{O}$ values of 27 ‰, showing that primary carbonate $\delta^{18}\text{O}$ signatures have been locally preserved. Minimum values are 22.4 ‰ for LWQ1/25, 18.4 ‰ for LWQ1/28 and 15.7 ‰ for LWQ1/30, the last two being just within error ($\sim \pm 1$ ‰; see Table 9.3). This variation is discussed further below.

Overview of quartz $\delta^{18}\text{O}$

Only samples LWQ1/28 and LWQ1/30 have quartz of sufficient abundance and size for $\delta^{18}\text{O}$ to be analysed by SIMS. Results reveal variations in quartz $\delta^{18}\text{O}$ similar to those observed in the calcite. Maximum quartz $\delta^{18}\text{O}$ values are 26.1 ± 1.9 ‰ in LWQ1/28 and 27.0 ± 1.6 ‰ in LWQ1/30. Quartz $\delta^{18}\text{O}$ in LWQ1/28 shows greatest variation, with a range from 14.3 to 23.5‰, whilst the range in LWQ1/30 is much less at just 4‰ (19.6 – 23.6‰).

SIMS calcite trace element data

Mg, Si, Fe, Mn and Sr in calcite were analysed by SIMS in all four samples (CT53, LWQ1/25, 28, 30). The results are summarised in Table 9.4 and the full data are given in Appendix D. The data for Fe, Mg and Mn in calcite are very closely similar, in ppm terms, to the whole-rock data (Table 4.2), confirming that these elements are partitioned in the carbonate phase. Sr/Mn ratios for calcite are in excess of 1 for all except LWQ1/25, which has relatively high Mn. Fe/Mn ratios are >10 in LWQ1/28 and 1/30, but much less than 10 in LWQ1/25 and commonly <10 in CT53 (Appendix D). The lower Fe/Mn ratios in the latter samples reflect their greater cathodoluminescence response (e.g. Figures 9.8, 9.9). The relatively higher Mg, Fe and Mn in LWQ1/25 most likely results from exchange in these elements between the limestone and the amphibolite, given that LWQ1/25 is only 0.5 cm from the amphibolite – limestone contact. Note, however, that Sr is also significantly higher in LWQ1/25 than the other two LWQ samples, indicating that if there was exchange of Fe and Mn between the limestone and the amphibolite, it did not affect the Sr (LWQ1/28 is 4.5 cm and LWQ1/30 7.5 cm, respectively, from the limestone-amphibolite contact).

9.4.2 Grain-scale variations in $\delta^{18}\text{O}$ and trace elements in CT53

Variation of calcite $\delta^{18}\text{O}$ in Torulian Limestone sample CT53 was investigated by SIMS in two ways:

- a) scattered reconnaissance analyses targeted on differing domains, particularly grain cores and bright yellow luminescent calcite, to establish the likely maximum range in $\delta^{18}\text{O}$ within the sample, and

- b) four detailed profile studies across domains with different luminescence properties to elucidate the degree to which different domains are in isotopic equilibrium and to search for gradients which indicate diffusional isotopic exchange.

Reconnaissance analyses

Analyses CT53-1 to 5 are from the darkly luminescent area 'underlain' by bright yellow calcite in the lower left part of the section (Figure 9.14). The CL image shows three generally distinguishable intensities of luminescent calcite: darkest orange-brown corresponding to grain cores, paler 'smoother' looking dark orange forming irregular patches, generally between grain cores, and rims and bright orange to yellow luminescent calcite forming sharply bound, commonly cross-cutting, veinlets to more diffuse domains at grain boundaries and along cleavage planes. The SIMS analyses shown on Figure 9.14 show that in the two darker forms of luminescence, calcite $\delta^{18}\text{O}$ is the same (16.2 – 17.3 ‰), within error, and therefore, appears to be homogenised within this domain. However, $\delta^{18}\text{O}$ in the brightly luminescent calcite is lower at 13.2 ‰.

Several analyses (CT53-13 to 18) were obtained from the top margin of CT53, where a conspicuously bright orange luminescent curved vein cuts more darkly luminescent calcite (Figure 9.15). Patches of dark orange-brown luminescent calcite have diffuse, ragged margins fringed by dark to paler orange luminescent calcite. The vein curving across the CL image has generally sharp margins at its lefthand end, but these are more diffuse in the central and righthand areas, suggesting interaction with the wall-rock. Calcite $\delta^{18}\text{O}$ values (14.3 – 15.2) of the darker

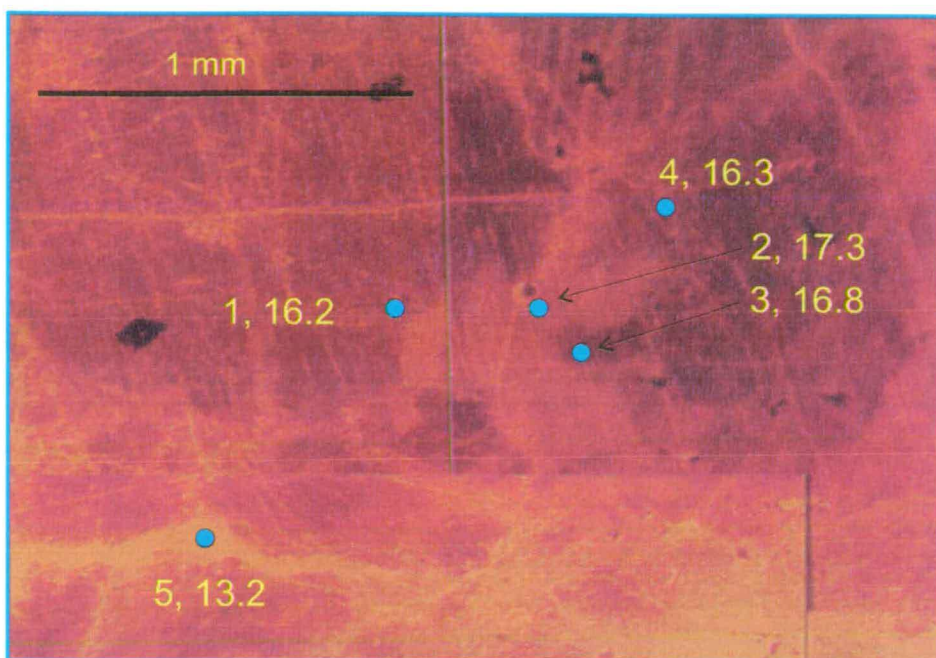


Figure 9.14. Detail of cathodoluminescence and location of SIMS analyses 1 to 5 in CT53, River Avon section, nr Tomintoul. Dark orange brown luminescent calcite is rimmed by dark orange calcite and cut by bright orange to yellow vein network calcite. Blue spots are SIMS analysis locations (size is schematic; analytical domain is $\sim 30 - 40\mu\text{m}$). 1, 16.2: analysis number and $\delta^{18}\text{O}$ value (‰). See text for discussion.

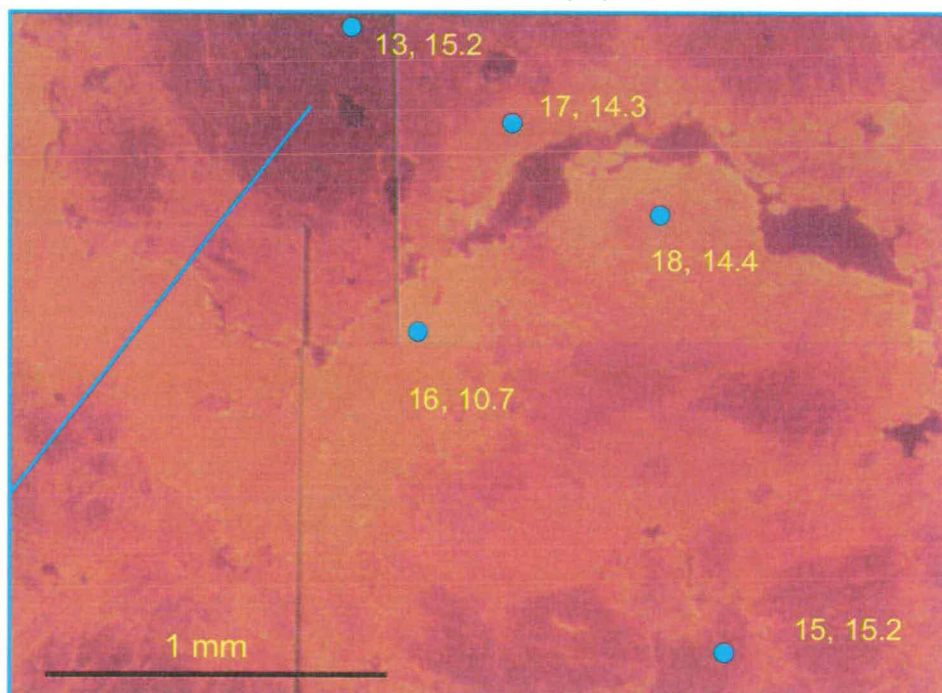


Figure 9.15. Detail of cathodoluminescence and location of SIMS analyses 13, 15 -18 in CT53. The bright luminescent calcite vein cuts darker luminescent calcite similar to that in Figure 9.16, above. The margins of the vein become more diffuse to the right, penetrating the wall-rock, suggesting interaction. Note that although $\delta^{18}\text{O}$ values decline towards the vein, all the wall-rock values are within error of each other. The blue line shows part of the track of CT53 Profile A. See text for discussion.

luminescent calcite are lower than those in Figure 9.16, decreasing slightly, but *very* consistently towards the veinlet (*Note, though, that they are the same within error*). The luminescent calcite in the veinlet has very low $\delta^{18}\text{O}$ at 10.7 ‰

Dark orange-brown luminescent calcite grain cores locally preserve $\delta^{18}\text{O}$ values into the low 20's. Figure 9.16 shows CL texture in the area of the slide about 4mm 'east-southeast' of the domain shown in Figure 9.14. As in other domains, the dark orange-brown luminescent calcite is rimmed by dark orange calcite with similar $\delta^{18}\text{O}$ values (cf. CT53-8 and CT53-9 in Figure 9.16).

The reconnaissance analyses indicate profound isotopic disequilibrium on the sub-millimetre scale in CT53, with large gradients and/or steps in $\delta^{18}\text{O}$. In order to understand the cause(s) of the isotopic heterogeneity, it is necessary to establish whether there are smooth spatial variations (ie gradients) in isotopic composition or sharp steps (fronts), and where these changes occur in relation to textures. The presence of systematic grain-scale gradients would indicate fluid-rock interaction in which oxygen isotope exchange was dominated by diffusional processes. The presence of sharp fronts at grain boundaries between grains and against veinlets indicates no oxygen isotope exchange between adjacent domains.

The CL imaging, coupled with the reconnaissance SIMS $\delta^{18}\text{O}$ analyses indicate that CT53 has undergone extensive, but *not complete* exchange with one or more sources of low $\delta^{18}\text{O}$ fluid. Basic statistical analysis of *all* the SIMS calcite $\delta^{18}\text{O}$ data for CT53 ($n = 83$; including profile data - see below) indicates that there is a smooth, negatively skewed distribution of $\delta^{18}\text{O}$ values throughout the sample (Figure 9.17). This smoothness in the data distribution is highlighted when the $\delta^{18}\text{O}$ data are broken down into type of luminescence, as shown by the boxplots in Figure 9.18.

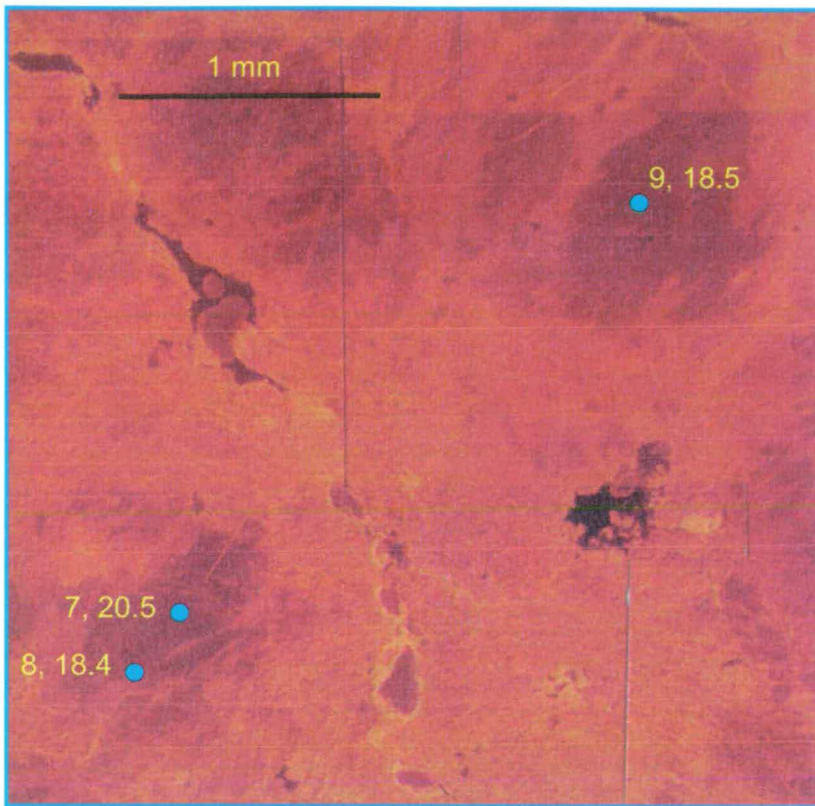


Figure 9.16 Detail of cathodoluminescence and location of SIMS analyses 7 - 9 in CT53. Dark orange brown luminescent calcite is preserved in relict grain cores and rimmed by dark orange calcite. Bright orange to yellow luminescent calcite occurs in a continuation of the vein in Figure 9.15. The $\delta^{18}\text{O}$ of the dark calcite analysed here is amongst the highest in CT53. 1, 16.2: analysis number and $\delta^{18}\text{O}$ value (‰). See text for discussion.

The $\delta^{18}\text{O}$ data for each of the luminescent types overlap within their interquartile ranges. The characteristics of the data *suggest* that there has been isotopic exchange between the darker luminescent calcite and the bright orange/yellow luminescent calcite in the veinlets, patches and cleavage traces. The other feature of these data is the dominance of typically metamorphic values ($\delta^{18}\text{O}$ c. 15 - 17‰) and the fact that these values generally occur in the darker luminescent calcite (*note the overlap between **dob** and **do** luminescent types in Figure 9.18*) and the rarity of values above about 18 ‰.

Grain-scale profile analyses in CT53

In this next section I discuss the results of SIMS analysis examining the nature of spatial variation in $\delta^{18}\text{O}$ across brightly luminescent domains into grain interiors. The aim here is to determine whether gradients in $\delta^{18}\text{O}$ which may have resulted from diffusion-controlled exchange are present.

The grain-scale $\delta^{18}\text{O}$ data were obtained from four profiles across domains with differing textural characteristics. The luminescence characteristics, together with the SIMS sample locations and the calcite $\delta^{18}\text{O}$ results along each profile are shown in Figures 9.21a, 9.23 – 9.25. Distances between pit centres are in microns (μm) and were measured by scanning electron microscope. The size and shape of the SIMS pits (in blue) are shown at the same scale as the CL image. For Profile A, SIMS trace element data were also obtained (Figure 9.19b, 9.22).

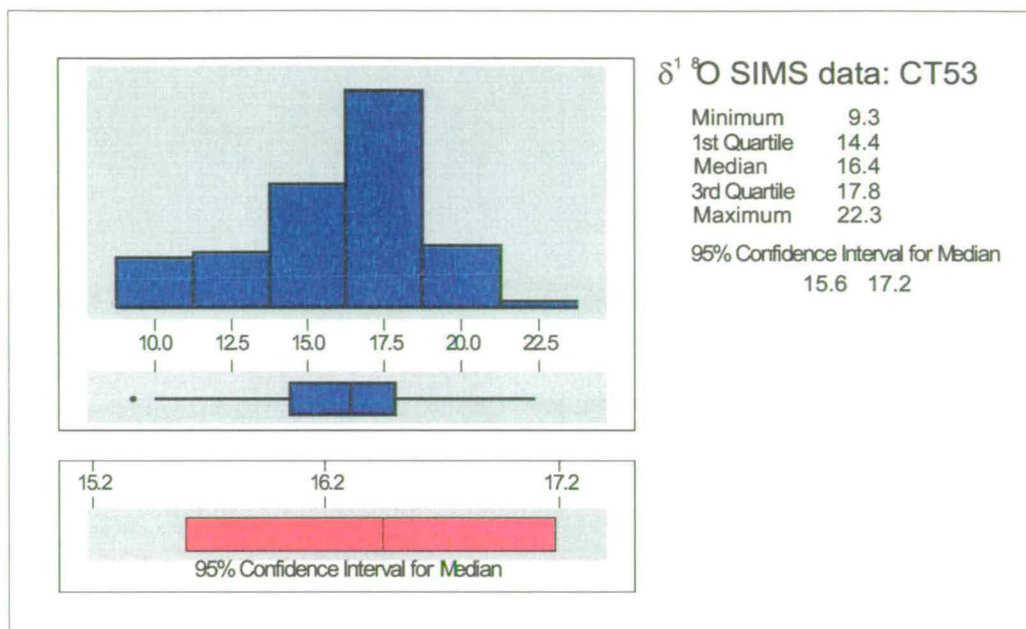


Figure 9.17 Summary statistics for all SIMS calcite $\delta^{18}\text{O}$ data in CT53 ($n = 83$). Note the smooth, but negatively skewed shape of the frequency distribution. The lack of a polymodal distribution suggests there is a continuum between the lowest and highest values. See text for discussion.

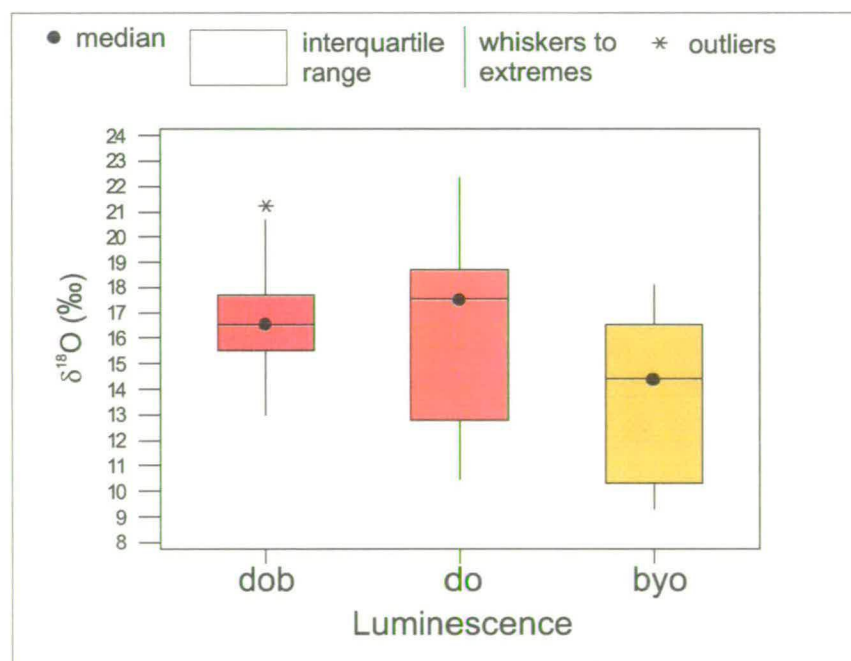


Figure 9.18 Boxplots of $\delta^{18}\text{O}$ against type of luminescence for all SIMS calcite data from CT53, highlighting the smooth variation in calcite $\delta^{18}\text{O}$ composition in this sample (cf. Figure 9.17, above). Luminescence types: dob: dark orange-brown; do: dark orange; byo: bright yellow/orange

Profile A

This profile is located in the top part of CT53, extending from the dark grain 'northeast' of the relatively thick, brightly luminescent calcite veinlet, across the vein and into more patchily luminescent calcite on its 'southwest' side (see also Figures 9.8 and 9.15).

Oxygen isotope results In the grain to the lefthandside of the veinlet, there is a near monotonic gradient in $\delta^{18}\text{O}$ from 10.1 to 16.9 ‰ over $\sim 200\ \mu\text{m}$. This gradient is similar in scale and $\delta^{18}\text{O}$ magnitude to those observed by Graham et al. (1998) in coarse calcite marble and suggests volume diffusional control on isotope exchange. The vein has homogenous $\delta^{18}\text{O}$ composition from contact to contact (10.1 – 10.3 ‰). Given the presence of a diffusion-like profile to the left of the veinlet, the homogeneity of $\delta^{18}\text{O}$ in the veinlet suggests that the $\delta^{18}\text{O}$ composition was pinned at the vein boundary by the fluid in the vein and there was no exchange between the wall-rock and the vein fluid, broadening the change in isotope composition across the vein boundary. This implies that sufficient low $\delta^{18}\text{O}$ fluid was flushed along this fracture to maintain a constant boundary fluid composition, that is, the vein fluid composition was externally buffered.

In the grain to the right of the veinlet, the increase from 10.2 ‰ at the vein edge to 17.5 ‰ in the darker luminescent calcite of the wall-rock is less smooth than that to the left, but the increase still suggests a diffusion-like profile. The ambiguity is caused largely by the $\delta^{18}\text{O}$ value of 17.5‰ at the grain boundary.

The variable nature of the profile in the wall-rock left and right of the vein, highlights the short-circuiting effects of cleavages and micro-fractures in the large

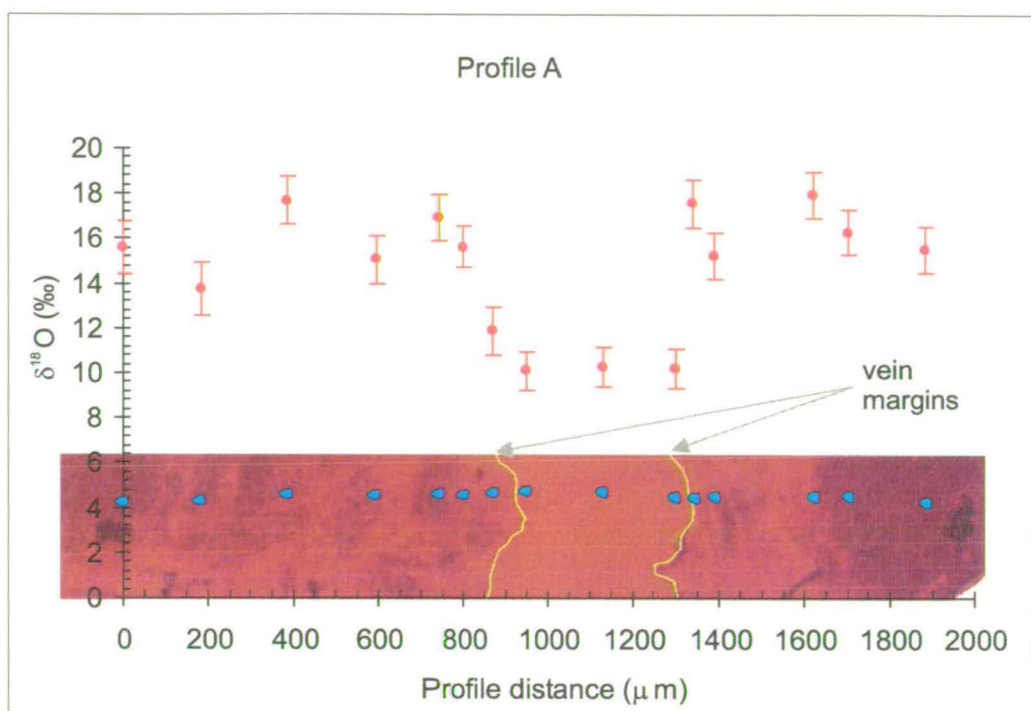


Figure 9.19a SIMS Profile A, CT53. Note the difference in the sharpness in luminescence of the vein margin on its right hand side and the corresponding sharpness in the shift in $\delta^{18}\text{O}$; contrast this with the left-hand margin of the vein. See text for discussion.

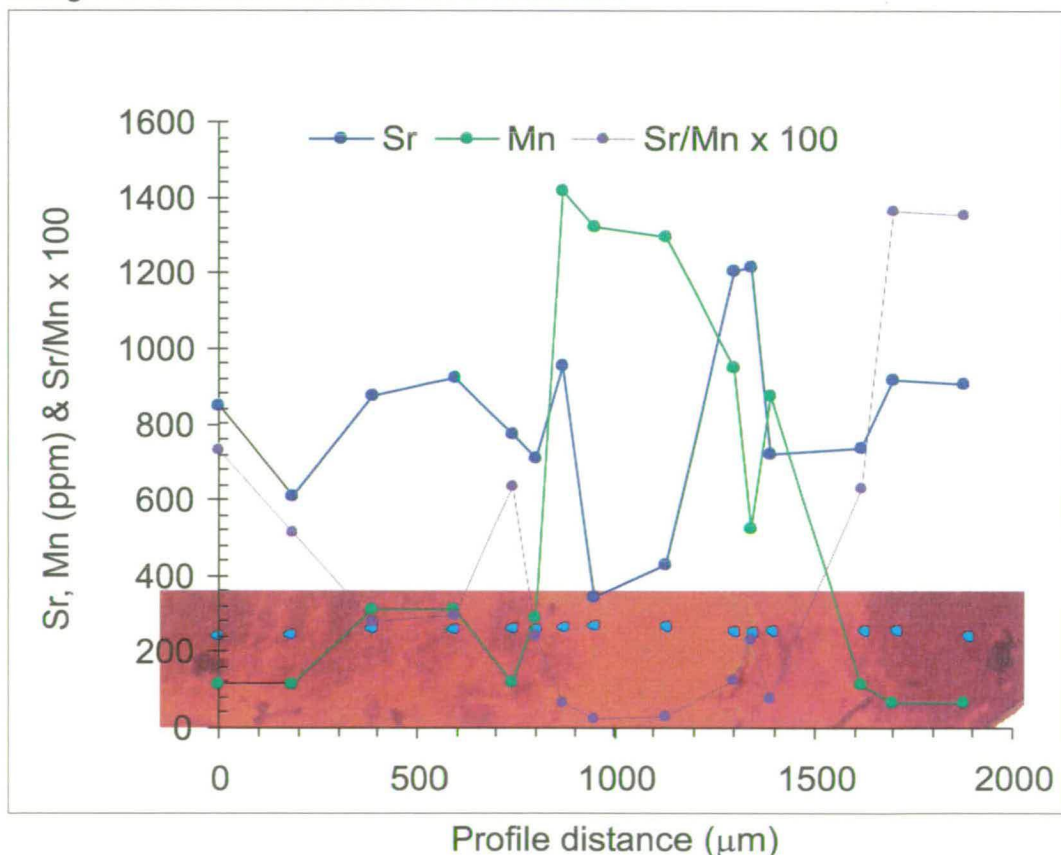


Figure 9.19b SIMS Sr and Mn analyses, Profile A, CT53. See text for discussion.

relict calcite grain. Note that the darker luminescent calcite does not always represent calcite with higher $\delta^{18}\text{O}$, indicating that it too has exchanged ^{18}O with a low $\delta^{18}\text{O}$ fluid.

Trace element results Because of their value in elucidating metasomatic exchange between carbonate-bearing fluids and rocks, strontium and manganese were also determined by SIMS at a number of the SIMS oxygen isotope sites along Profile A (Figure 9.19b). The trace element profile has several features:

- a) in the left hand part of the profile, Sr and Mn co-vary positively, a feature which has also been noted in the whole-rock data for a number of limestones (Chapter 7). This relationship between Mn and Sr is different to that observed in the wall-rock boundary layers close to the vein (see below). Note also that higher Sr and Mn occur with higher $\delta^{18}\text{O}$ in the lefthand grain.
- b) Mn increases and Sr declines towards the boundary between the lefthand grain and the veinlet, although the variation is not as smooth as the decline in $\delta^{18}\text{O}$ data over the same section of the profile.
- c) In the grain to the right of the vein, away from the contact, Sr and Mn values are *similar* to those in the left hand wall-rock.
- d) The ambiguity in the variation in $\delta^{18}\text{O}$ at the righthand vein margin is also shown by the trace elements, which show very sharp changes across the veinlet – grain boundary.

The variation in Sr and Mn data across the profile is, on the whole, *consistent* with the variation in $\delta^{18}\text{O}$ data. In the grain boundary layer adjacent to the left hand

vein contact, Sr/Mn shows a smooth non-linear progression from ~ 6 down to values of ~ 0.3 over the same section of profile which shows a smooth and systematic decrease in $\delta^{18}\text{O}$ (Figures 9.19a, b; *note $\times 100$ scaling of Sr/Mn to fit on diagram*). Moreover, when $\delta^{18}\text{O}$ and Sr/Mn for this section of profile are plotted against one another (shaded inset, Figure 9.20), there is a clear logarithmic relationship between them, supporting the $\delta^{18}\text{O}$ evidence for diffusional exchange between fluid and rock at this boundary. In the righthand grain, Mn increases with decreasing $\delta^{18}\text{O}$ on a trend between grain and veinlet $\delta^{18}\text{O}$ and Mn compositions.

The $\delta^{18}\text{O}$ and trace element data for Profile A provide evidence for bulk diffusional exchange between a fluid from which the vein calcite precipitated and the host rock. This interaction was systematic at the left hand vein – wall-rock contact and appears to have been dominated by diffusion. The evidence for a diffusion gradient at the righthand contact is more ambiguous, but nonetheless consistent with the variation observed in the lefthand grain.

Profile B

Profile B is located near the lower central edge of CT53 (Figures 9.8). It tracks from the centre of a dark orange-brown luminescent grain out into bright orange luminescent calcite which becomes more bright yellow luminescent. This domain lies at the southern end of the extensive, diffusely luminescent region which occupies the centre of the section, extending from the vein of Profile A (Figure 9.8).

Profile B is a half-profile in that it examines geochemical variations across one grain boundary only. The results are shown graphically in Figure 9.21. The extreme left hand end of the profile is located in a complex zone of bright orange

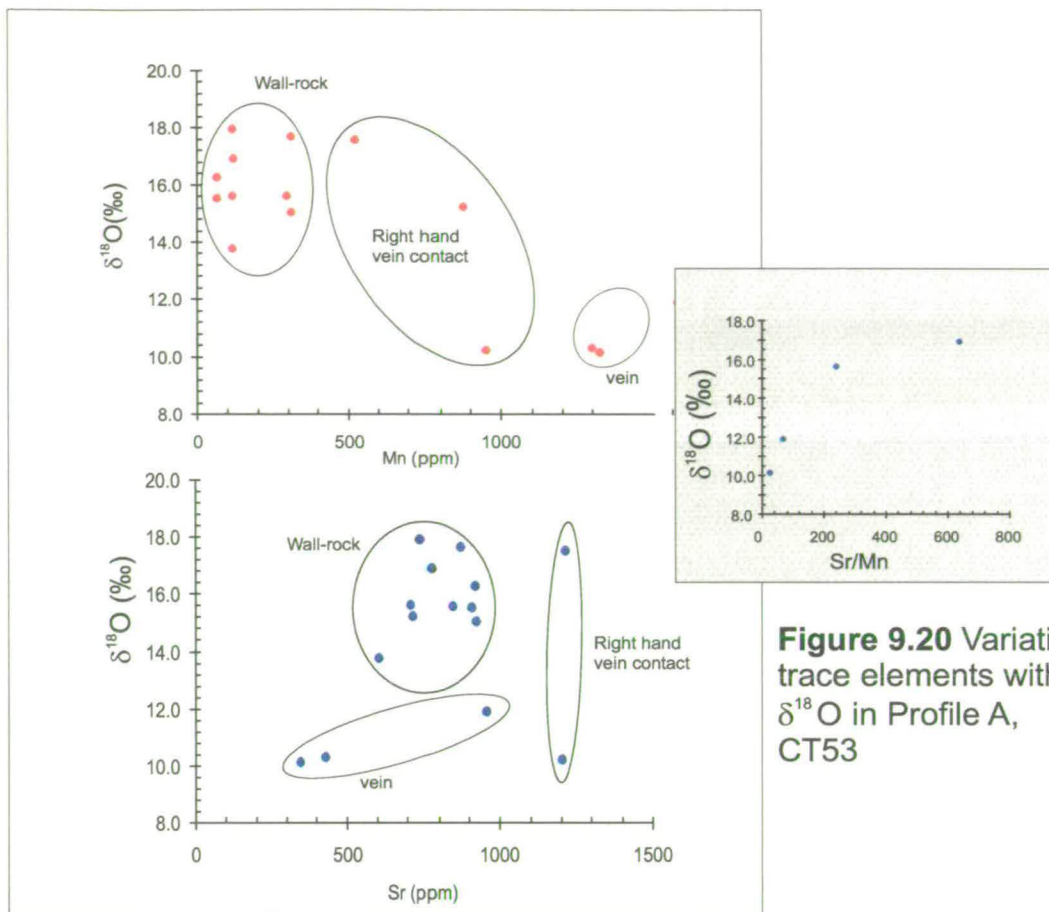


Figure 9.20 Variation in trace elements with $\delta^{18}\text{O}$ in Profile A, CT53

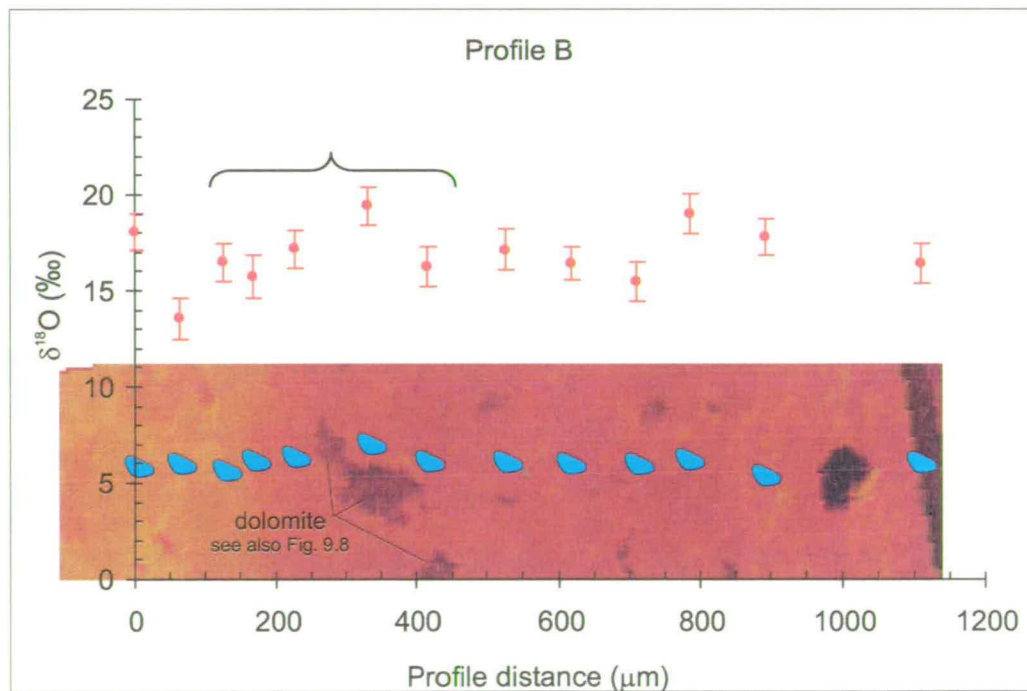


Figure 9.21 Profile B, CT53

luminescent calcite immediately right of a small dark orange luminescent patch. This has $\delta^{18}\text{O}$ of 18.1 ‰ – the highest value recorded for this type of highly luminescent calcite. The profile continues across the zone of orange luminescent calcite with a thin irregular veining of bright yellow calcite in its axial region, into the dark orange luminescent calcite of a large grain. Calcite $\delta^{18}\text{O}$ in the axial region of the brightly luminescent calcite has $\delta^{18}\text{O}$ of 13.6 ‰, the lowest in this profile. $\delta^{18}\text{O}$ values rise progressively (though not quite monotonically) to a high of 19.4‰, representing a shift of 5.8 ‰ over a distance of 268 μm . Once again, this shift is similar in magnitude and scale to those recorded by Graham et al. (1998). The central part of the profile is characterised by a sharp drop to $\delta^{18}\text{O}$ values between 15.5 and 17.2 ‰, before rising as sharply to 19.1 ‰. Thereafter, the two remaining analyses record a decline to 16.5 ‰ over 324 μm .

The rise in $\delta^{18}\text{O}$ in the left hand section of the profile could be due to volume diffusional exchange between the fluid responsible for the luminescent calcite and the darker luminescent grain. However, the drop to lower values in the central portion is not consistent with what might be expected if there was purely diffusional control over the whole domain. Three additional analyses, obtained as a group a few tens of microns to the south of the profile, indicate that even within the consistently dark orange-brown luminescent core, there is gross oxygen isotope disequilibrium at the tens of microns scale (CT53-6: 22.3 ‰ - highest in CT53, CT53-33: 16.6 ‰, and CT53-34: 17.3 ‰). The decline in $\delta^{18}\text{O}$ at the right hand end of the profile *could* be related to exchange at the right hand edge of the grain, where luminescent calcite occupies a patchy linear zone.

The $\delta^{18}\text{O}$ values of 15.5 – 17.2 ‰ in the middle part of the profile are thought to be more typical of the grain as a whole, but it is clear that high values of 19 – 22 ‰ are preserved very locally. Thus, it might be more reasonable and conservative to exclude the $\delta^{18}\text{O}$ of 19.4 ‰ (analysis CT53-28) from any quantitative analysis of the profile, in which case, the profile becomes more curvilinear, with a shift in $\delta^{18}\text{O}$ of 3.6 ‰ over 164 μm . A possible complication with regard to the status of analysis CT53-28 is the fact that it lies in an embayment of a cluster of dolomite grains (Figure 9.21; see also on calcite –dolomite geothermometry in Chapter 10); this close association may have affected the calcite $\delta^{18}\text{O}$ in this region, possibly by the dolomite ‘sheltering’ the calcite from the vein. However, two other analyses lie equally close to the dolomite, but have $\delta^{18}\text{O}$ typical of much of the rest of the grain.

Interpretation of the $\delta^{18}\text{O}$ data in Profile B is clearly difficult, but it is thought that there is sufficient evidence to suggest the development of a diffusional gradient at the left hand end of the profile.

Profile C

This is the longest of the four profiles (~ 2800 μm) and is located in the upper left part of CT53 within a domain of dark orange-brown luminescent grains, bound by brightly luminescent calcite along grain boundaries. Closer examination of the domain shows that locally-developed patchy luminescent calcite extends into grain interiors from grain boundaries, generally along cleavage planes (Figure 9.22), indicating structurally complex alteration of calcite. This complex domain nevertheless reveals systematic gradients in $\delta^{18}\text{O}$, although they are not located where one might expect! Paradoxically, the lowest $\delta^{18}\text{O}$ values nowhere coincide

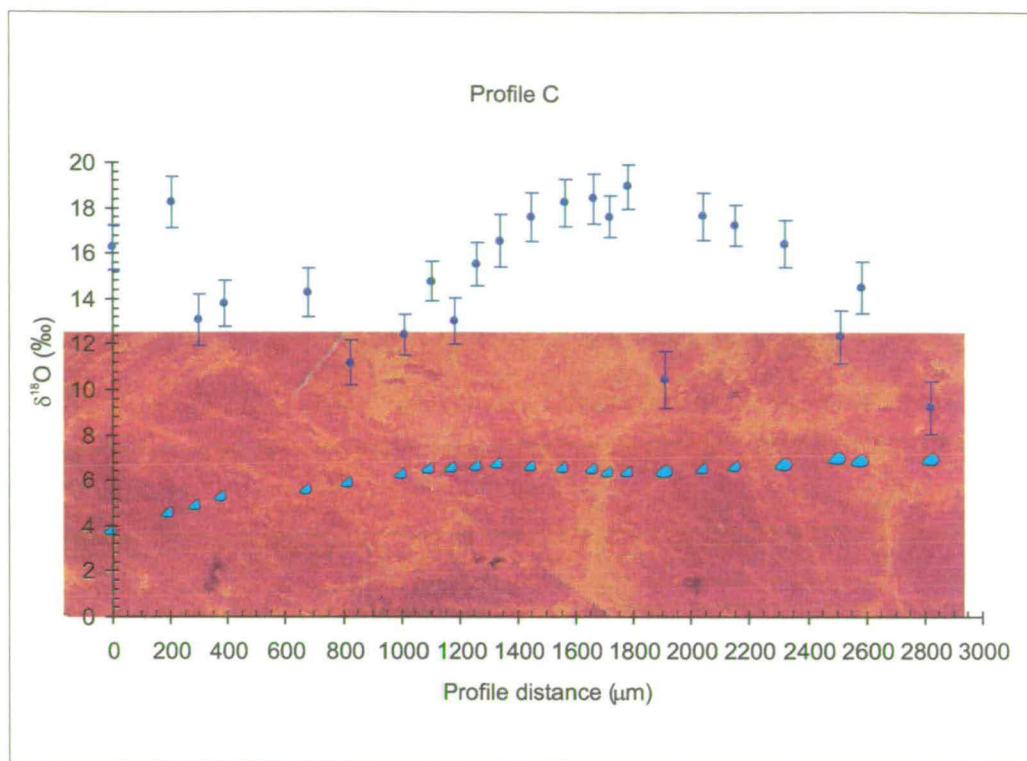


Figure 9.22 Profile C, CT53

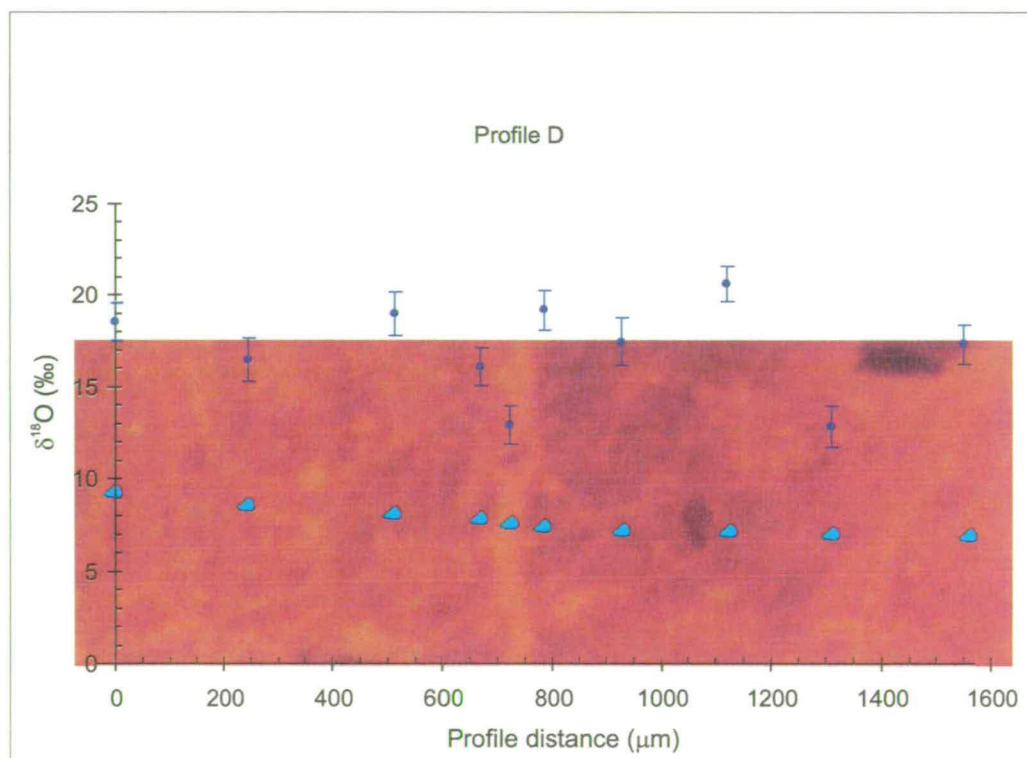


Figure 9.23 Profile D, CT53

with the brightest luminescent calcite. Indeed, the lowest $\delta^{18}\text{O}$ value of 9.3 ‰ lies at the right hand end of the profile in patchy dark orange and orange mottled luminescent calcite. Moreover, analysis CT53-61, located in the middle of the conspicuous bright yellow luminescent calcite grain boundary veinlet near the centre of the profile, has $\delta^{18}\text{O}$ of 17.6 ‰. This is only slightly lower than the two adjacent analyses (18.4 and 19.6 ‰ respectively). The main areas of low $\delta^{18}\text{O}$ are between 700 and 1000 μm and at the right hand end of the profile. Between these two areas, there is, with the exception of two or three points, a remarkably smooth curvilinear increase and then decrease in $\delta^{18}\text{O}$, the values peaking either side of the conspicuous narrow veinlet. Values on the left hand side of this 'arch' of $\delta^{18}\text{O}$ values increase from 11.2 to 19.0 ‰ over a distance of 954 μm , a shift of 7.8 ‰. On the right hand side, the values range even more widely, from 9.3 to 19 ‰ (9.3 ‰ difference) over 1020 μm . The degree of curvature in the profile is very similar on both sides. The three values in the profile markedly lower than their neighbours can be attributed to slightly more luminescent calcite locally developed in short circuiting pathways (cleavages, fractures). The few values at the left hand end of the profile in the generally more darkly luminescent calcite display more random variation.

The results of Profile C indicate extensive alteration of $\delta^{18}\text{O}$ in domains of patchily bright luminescent calcite. The bright luminescent vein/grain boundary records only slight lowering of $\delta^{18}\text{O}$ relative to the wall-rocks. Elsewhere in the sample, larger domains of such luminescent calcite (0.4 mm vein in Profile A, ~ 100 μm in Figure 9.15) have much low $\delta^{18}\text{O}$ (~ 10 ‰, 13.2 ‰ respectively). The vein in Profile C is only ~ 40 μm across, ten times smaller than that the vein in Profile A and little more than the size of the SIMS ablation pit. This suggests that there has been

local buffering of the fluid $\delta^{18}\text{O}$ along the grain boundary by the adjacent calcite grains.

Despite the lack of clear correlation between bright luminescence and $\delta^{18}\text{O}$ in Profile C, the systematic nature of the gradients suggests they can be attributed largely to diffusional processes. However, there was local short circuiting of the diffusional profile and also, paradoxically, some local buffering of fluid $\delta^{18}\text{O}$ along grain boundaries.

Profile D

This profile is located in the right hand side of CT53, amongst the complex patchy luminescence cut by thin brightly luminescent calcite veinlets, towards the top of the sample (Figures 9.8, 9.23). Here the contact between the righthand-most veinlet and the wall-rock is sharp and this is clearly a calcite-filled micro-fracture. As the image in Figure 9.23 shows, the luminescence in this domain is highly complex, with abundant evidence of short-circuiting of fluid pathways along cleavages and micro-fractures and patchy 'replacive' luminescence, particularly on the left hand side of the image. This detailed complexity in CL is reflected in the $\delta^{18}\text{O}$ analyses, which vary from 12.9 to 20.7 ‰. Once again, high values (for this sample) are preserved locally, despite nearby alteration to lower, more 'metamorphic' values. The $\sim 60\ \mu\text{m}$ wide veinlet has $\delta^{18}\text{O}$ of 13.0 ‰. Adjacent values in the wall-rock are 16.2 ‰ on the left hand side and 19.3 ‰ on the right, 55 and 62 μm from the vein respectively. On the left hand side of the veinlet, there is a semblance of a curvilinear gradient over $\sim 200\ \mu\text{m}$. The picture is more ambiguous on the right hand side and there is no evidence for a diffusional profile. Apart from the results of the two analyses on the

extreme right of Profile D, $\delta^{18}\text{O}$ values immediately right of the veinlet are slightly higher than those to the left, consistent with the darker and more even luminescence.

9.4.3 Discussion and Summary of CT53 profile data

Profiles A, B and C contain within them evidence for volume diffusion having taken place during the infiltration by exchange with a $\delta^{18}\text{O}$ -depleted fluid, although form of the diffusion profiles is disturbed by local, very fine-scale short circuiting fluid pathways. The positions of gradients within the profiles coincide with marginal parts of grain boundaries, wall-rock adjacent to veins and extensive areas of patchy luminescence. There is no good evidence for diffusional exchange in Profile D.

The data from profiles A, B and C are modelled as diffusion gradients and the results discussed in Chapter 10.

Correlation of $\delta^{18}\text{O}$ with luminescent vein and grain boundary domain thicknesses

Many of the fluid pathways along grain boundaries and in veinlets picked out by very bright orange to yellow luminescent calcite are of varying width and $\delta^{18}\text{O}$ composition. Available data from five such domains in CT53 reveal a systematic link between luminescent domain width, measured from scaled CL images, and $\delta^{18}\text{O}$. These data are plotted in Figure 9.24. I have included a nominal error to account for variation in vein orientation of up to 45° to the section surface.

With the exception of analysis CT53-82, from the centre of Profile D, the data lie close to a straight line in log domain width vs $\delta^{18}\text{O}$. Assuming, for the moment, that the fluid in these luminescent domains had approximately the same initial $\delta^{18}\text{O}$ composition (nominally $\sim 10\text{‰}$), and fluid-flux, time and diffusion rate

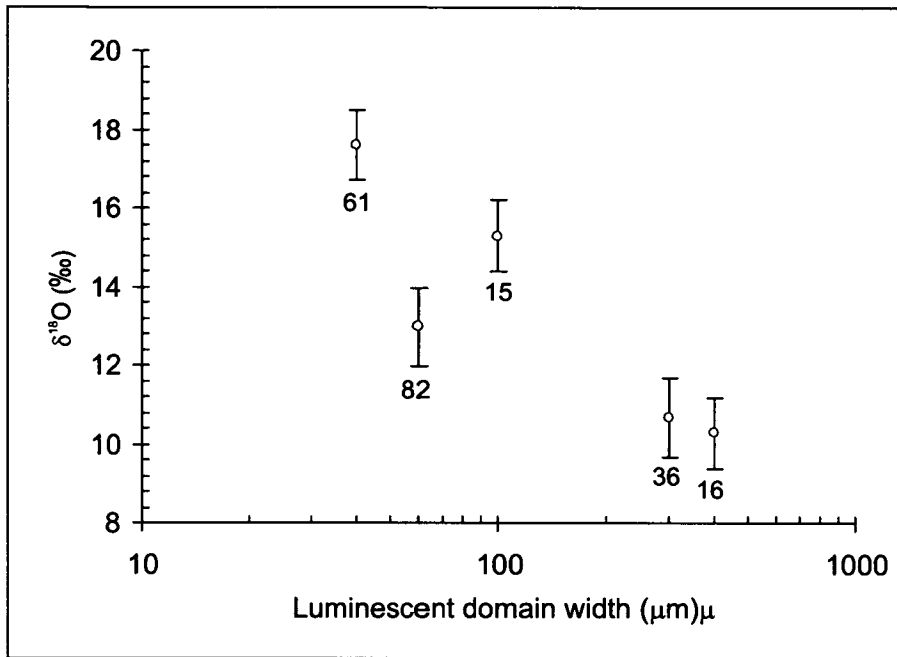


Figure 9.24 Relationship between $\delta^{18}\text{O}$ and log width of bright luminescent domains. The correspondence between width and $\delta^{18}\text{O}$ suggests internal buffering control on the fluid $\delta^{18}\text{O}$ by the host rock. See text for discussion.

constraints notwithstanding, the data *suggest* that the fluid in the narrower domains has been buffered by the host rock. As with the putative volume diffusion gradients, local buffering of the fluid by the host rock has implications for the temperature at which these processes took place. These matters are discussed further in Chapter 10.

Relationship between bulk-rock and CT53 SIMS calcite $\delta^{18}\text{O}$ data

The significance of the $\delta^{18}\text{O}$ variation between the conventional analyses of bulk-rock samples in the profile, and the extent, or otherwise, of isotope homogenisation within them, is informed by the SIMS data from CT53. This is shown by the blue bar in Figure 9.6a. The range of $\delta^{18}\text{O}$ *within* in CT53 (9.8 – 22.3 ‰) is a little greater than the range for the bulk samples, although the maximum values are the same (cf LWQ SIMS data in section 9.4.5, below).

CT53 is characterised by extensive domains of *gross* disequilibrium with regard to $\delta^{18}\text{O}$ and trace elements, reflecting the lack of chemical equilibrium apparent in the CL image (Figure 9.8). These data indicate that although there is apparent consistent variation in bulk calcite $\delta^{18}\text{O}$ across the outcrop profile, considerable care is required in the interpretation of the variation with regard to fluid-rock interaction; I will discuss this matter further in Chapter 10.

9.4.4 Summary of $\delta^{18}\text{O}$ isotope data in CT53

- CT53 is characterised by profound oxygen isotope disequilibrium at the grain-scale
- Although near-primary $\delta^{18}\text{O}$ values are preserved in places in grain interiors, $\delta^{18}\text{O}$ typically lies in the range ~ 15 – 17 ‰

- Values as low as $\sim 10\text{‰}$ commonly occur in domains affected by short-circuit fluid pathways and in bright orange and yellow luminescent calcite in veins and patches
- The CL image shows that fluid infiltration was facilitated along fracture networks, grain boundaries and twin planes
- Although grain interiors are extensively affected by short-circuiting fluid pathways, $\delta^{18}\text{O}$ gradients in grain rims indicate diffusional exchange; this offers the opportunity to model fluid infiltration timescales in this limestone
- The oxygen isotope data and the complex CL image record extensive isotopic and chemical exchange between the rock and a low $\delta^{18}\text{O}$ fluid.

9.4.5 Grain-scale variation in calcite and quartz $\delta^{18}\text{O}$ in Inchrory Limestone

To reiterate from the introduction, SIMS analysis has been used to investigate grain-scale variation of $\delta^{18}\text{O}$ and trace elements in the Inchrory Limestone to:

- a) determine the scale of grain-scale variation
- b) to establish the links or otherwise between grain-scale variation and texture, petrography and cathodoluminescence characteristics
- c) to establish the degree to which calcite and quartz are in oxygen isotope equilibrium and to estimate the temperature at which that equilibration may have occurred.

Results are summarised in Table 9.3 and given in full in Appendix D.

Oxygen isotopes Twelve SIMS oxygen isotope analyses of calcite were obtained from two areas within LWQ1/25, outlined in Figure 9.9:

- a) a small area of dark orange-brown luminescent grains with good polygonal texture in the central part of the 'southwest' quadrant away from more brightly luminescent calcite, and
- b) in the 'eastern' part of the section where the broad diffuse zone of more orange-brown to yellow luminescent calcite cuts across dark orange-brown luminescent calcite with good polygonal texture and relatively abundant phyllosilicate (dark on Figure 9.9).

Analyses LWQ1/25-1 to 6 show that the calcite in the first area has $\delta^{18}\text{O}$ in the range 22.4 – 23.7 ‰. These data show that oxygen isotopes in this domain are effectively homogeneous within instrumental error and are very similar to the bulk carbonate value for adjacent sample LWQ1/26 (22.0 ‰). Analysis LWQ1/25-6 was located in more luminescent calcite at the boundary between two grains. This shows there is no link between the luminescence and oxygen isotope composition in this part of LWQ1/25.

Analyses LWQ1/25-7 to 12 were located in the second area. Overall, the $\delta^{18}\text{O}$ values of this domain are higher than those in the first and have greater range (23.7 – 27.2‰), but, as with the first, there is no link between the values and the luminescence.

These data show that there is significant grain-scale heterogeneity in oxygen isotope composition within this sample, but that this heterogeneity does not

correspond to the luminescence in the manner elucidated by other studies (e.g. Graham et al, 1998; Lewis et al, 1998).

Trace elements SIMS trace element analyses of LWQ1/25, obtained immediately adjacent to the sites of oxygen isotope analysis, show that this sample is considerably richer in Mg, Fe and, significantly, Sr and Mn compared to the other two LWQ samples (see below and Figure 9.25). Of particular note are the Mn concentrations, which are an order of magnitude higher than those in the other samples, whereas Mg, Fe and Sr concentrations are, at very most, only a factor of 2 or 3 higher. Sr ranges from 2139 to 2661 ppm, whilst Mn ranges from 2464 to 3749 ppm.

The relationships between the trace element and $\delta^{18}\text{O}$ data from LWQ1/25 are shown in Figure 9.25a-d. Sr, Fe and Mg correlate positively between themselves and with $\delta^{18}\text{O}$. The positive correlation between Sr, Mn and $\delta^{18}\text{O}$ in this sample is of particular note because the other two samples display different behaviour in this regard (see below and Figures 9.25a – c). However, the relationships between Sr, Fe and Mg appear to be part of a continuum in all three samples (Figure 9.25d).

LWQ1/28

Oxygen isotopes Oxygen isotopes were studied more extensively in LWQ1/28 compared to LWQ1/25 and 30, largely because of the good development of polygonal grain texture and relatively large calcite crystals, veinlet alteration and relatively abundant quartz. There were three particular matters of interest studied in this sample:

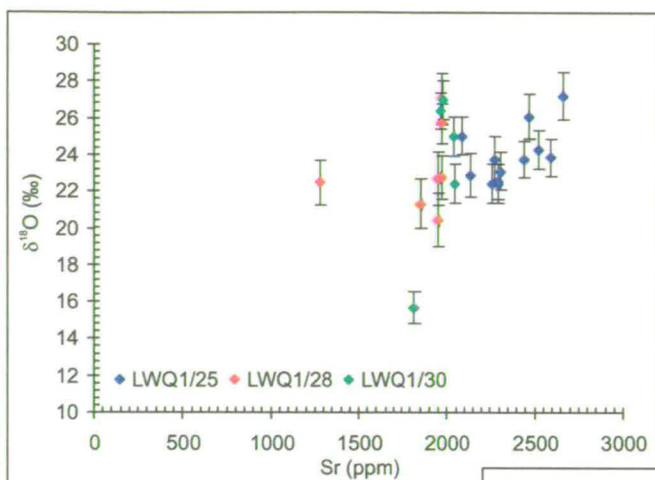


Figure 9.25a Variation between Sr and $\delta^{18}\text{O}$ in LWQ samples 1/25 - 30. Note the generally positive correlation in LWQ1/25 only.

Figure 9.25b Variation between Mn and $\delta^{18}\text{O}$. Note again that positive correlation between Mn and $\delta^{18}\text{O}$ is only recorded in LWQ1/25 (cf. 9.29a) and that Mn is very strongly enriched in LWQ1/25

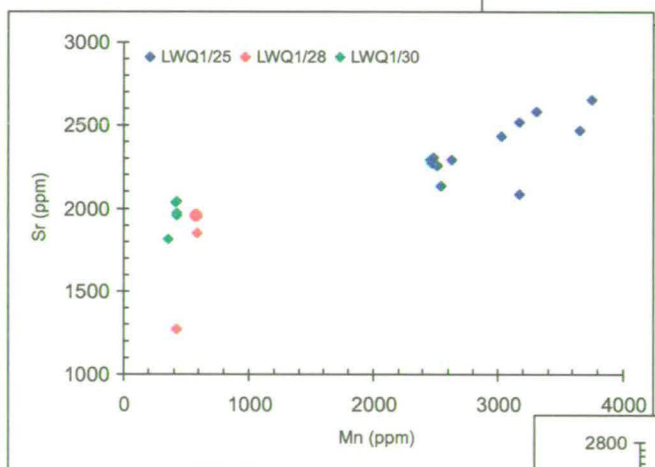
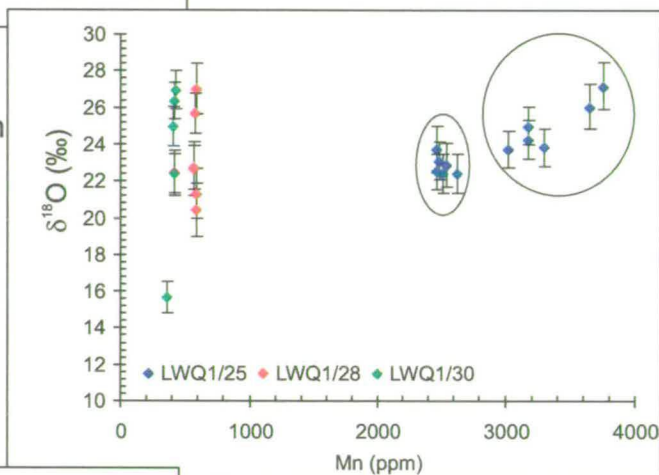
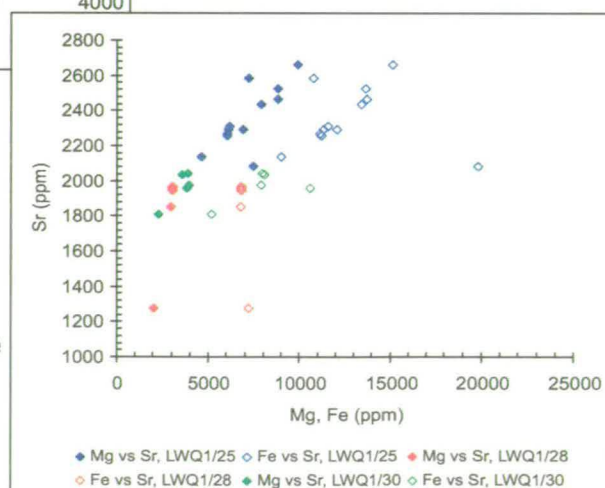


Figure 9.25c Variation between Mn and Sr in LWQ samples. The positive covariation between Sr and Mn in LWQ1/25 suggests it is primary in origin

Figure 9.25d Covariation between Sr, Fe and Mg in LWQ samples. Note that the data from all three samples form, with one or two exceptions, a continuous trend, suggesting that the covariations are primary features.



- a) the development or otherwise of systematic grain-scale variation which might be diffusion controlled,
- b) the development of systematic variation in calcite and quartz $\delta^{18}\text{O}$ across narrow veinlet systems picked out by luminescent calcite haloed by altered feldspar, and
- c) the equilibration of quartz and calcite in texturally well-equilibrated domains and across the veinlet network.

Domain A: oxygen isotopes The possibility of systematic grain-scale variation was investigated in a domain of relatively large polygonal, dark orange-brown luminescent calcite crystals in which quartz and feldspar are relatively poorly concentrated (shown as Domain A in Figure 9.9, see also Figure 9.26).

Bright luminescent calcite in this domain is limited to the grain boundaries, with some luminescent calcite along cleavage planes; this calcite occupies domains too narrow to be analysed discretely by SIMS.

As data in Figure 9.26 show, the dark orange-brown luminescent calcite shows significant variation in $\delta^{18}\text{O}$, ranging from 20.5 to 27.0 ‰. The profile over the large calcite crystal (analyses LWQ1/28-5, 6, 9 – 11) shows that there are ~ 5 ‰ variations *within* individual grains over scales of a few tens of microns. In this particular crystal, the core has higher $\delta^{18}\text{O}$ than the rim, but this is not the case everywhere in this domain. Quartz in this domain shows much less variation in $\delta^{18}\text{O}$, ranging from 23.5 to 26.1 ‰. Adjacent calcite and quartz $\delta^{18}\text{O}$ values vary, but several quartz and calcite $\delta^{18}\text{O}$ analyses in adjacent grains are *consistent* with equilibrium fractionation (see Figure 10.4a and discussion in Chapter 10). Overall,

Key

SIMS analysis pits

○ Trace elements

① Quartz grains

③ Calcite grains

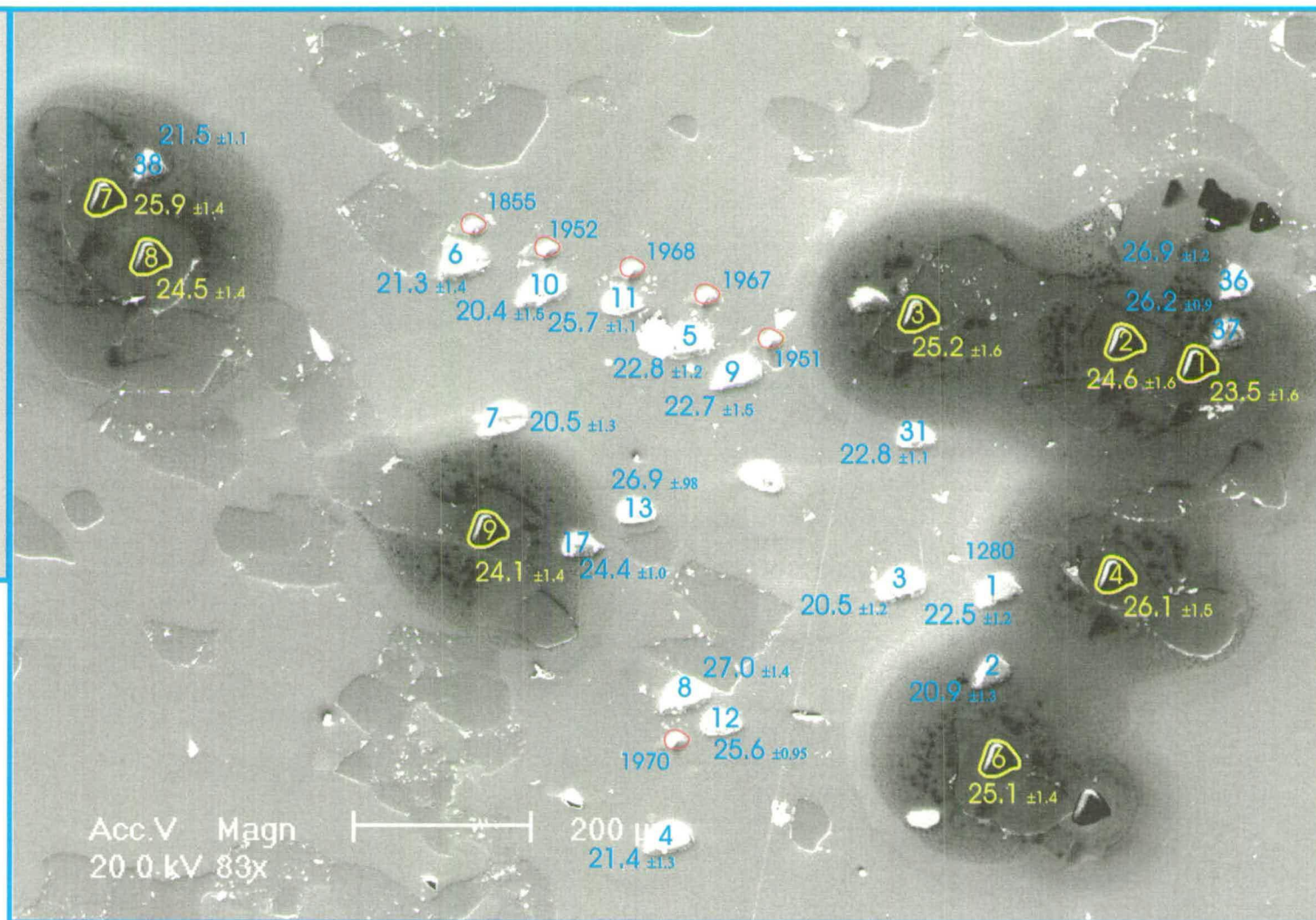
Numbers in pits are analysis numbers

23.5 ±1.6 $\delta^{18}\text{O}$ (‰)

1855 Sr ppm

Figure 9.26

SIMS oxygen isotope and Sr trace element analyses in texturally equilibrated, low-luminescence domain, LWQ 28



however, the calcite and quartz $\delta^{18}\text{O}$ data show that this domain is characterised by isotopic disequilibrium.

Domain A: Trace elements Trace element concentrations were only determined in Domain A in LWQ1/28. Sr in calcite generally co-varies positively with $\delta^{18}\text{O}$ across this crystal, but the range in Sr is only ~ 100 ppm (1855 – 1970 ppm). Mn also shows little variation (419 – 588 ppm) and there is no consistent covariation between Mn, and Sr and $\delta^{18}\text{O}$.

Domain B: oxygen isotopes Domain B occupies the northwest quadrant of LWQ1/28 in Figure 9.10 and includes the obvious filigree vein network of luminescent vein calcite. This network has a clear central portion, where bright yellow luminescent calcite occurs along grain boundaries and extends partially into calcite grains along cleavages. Extending away from the axial region of this network is a halo of oligoclase altered to albite. Associated with this is luminescent calcite extending both along grain boundaries (as elsewhere in the sample) and extensively along cleavage traces into grain interiors. These features are shown in detail in Figure 9.27a. Variation in oxygen isotopes in quartz and calcite across Domain B is shown in Figure 9.27a and b. In 9.27b, the data are shown projected onto the line of section in 9.27a. To simplify matters, I have assumed, on the basis of the halo of altered feldspar, that geochemical effects associated with the vein network are more or less the same *along* the vein network.

These data display some significant features:

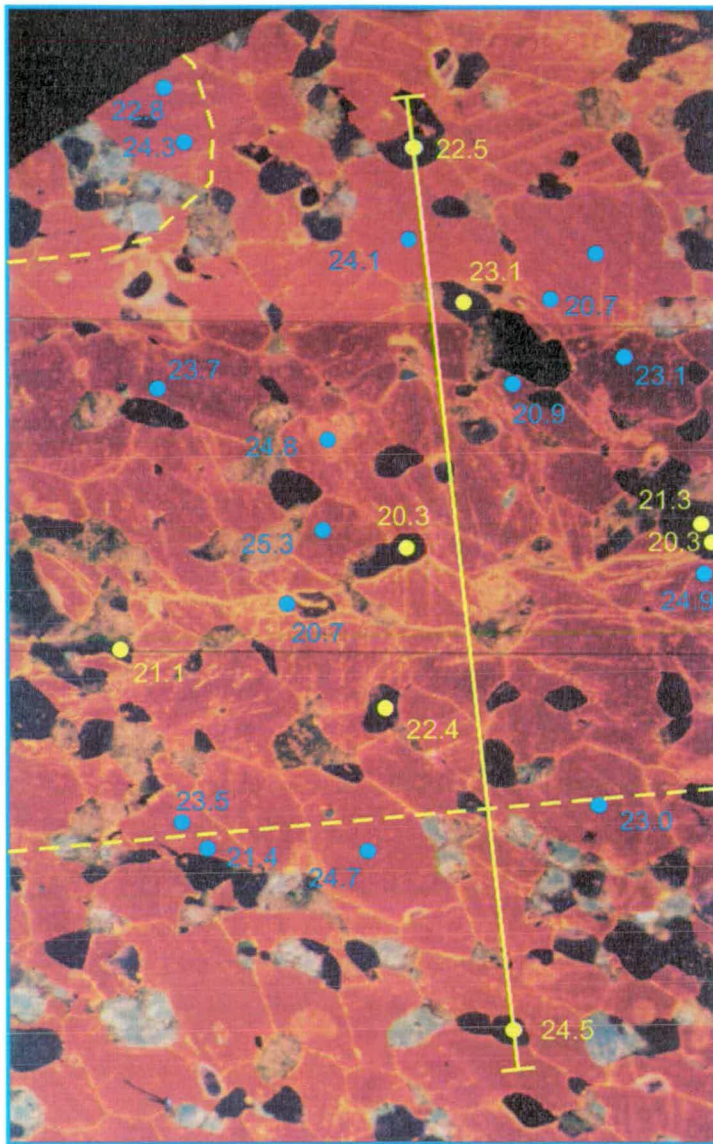


Figure 9.27a Domain B in LWQ1/28, showing the location of SIMS calcite and quartz $\delta^{18}\text{O}$ analyses, the limit of albitisation of oligoclase and the line of profile shown in Figure 9.31b, below.

● Calcite analysis

● Quartz analysis

--- Limit of albitisation of oligoclase

Albitised oligoclase has patchy dark grey to buff luminescence, whereas relatively fresh oligoclase is blue with white patches.

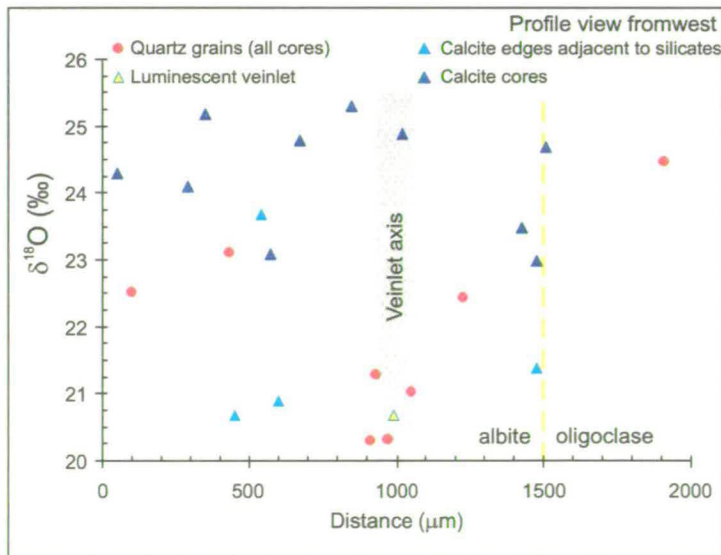


Figure 9.27b Quartz and calcite $\delta^{18}\text{O}$ data projected onto the profile section shown in Figure 9.27a. Note the high core calcite values maintained across the profile, the relatively low calcite edge values and the low quartz values in the axial region. Errors on $\delta^{18}\text{O}$ values are omitted for clarity, but are ~ 1 ‰.

- a) calcite core $\delta^{18}\text{O}$ values are maintained at primary or near primary values across the vein network and halo, even in the axial region,
- b) the calcite edge values are significantly lower in $\delta^{18}\text{O}$ than the cores in all but one case,
- c) the lowest calcite $\delta^{18}\text{O}$ value is in the luminescent material in the vein axis,
- d) quartz core $\delta^{18}\text{O}$ values are significantly lower than the core calcite values,
- e) the quartz $\delta^{18}\text{O}$ values in the axial region are significantly lower than those in the halo, whilst the single quartz analysis outside the halo is significantly higher than the other quartz analyses, and
- f) no clear, quantifiable profiles are developed.

The altered feldspar halo provides clear petrographical evidence for infiltration of a sodic, metasomatising fluid with low $\delta^{18}\text{O}$, concentrated along grain boundaries. Quartz has interacted with this fluid to a significant degree, most particularly in the axial region, where $\delta^{18}\text{O}$ values match those of the vein calcite, within error. Core calcite values show that calcite has interacted with this fluid rather less extensively; $\delta^{18}\text{O}$ values are similar to those in domain A. Calcite near grain boundaries has $\delta^{18}\text{O}$ approaching that of the luminescent calcite in the vein axis. To the 'south' of the lower limit of altered feldspar (Figure 9.27a), the single quartz analysis shows that this grain has not interacted with the fluid, having a $\delta^{18}\text{O}$ value of 24.5 ‰, essentially the same as those in domain A (Figure 9.26). Domain B, like domain A, is characterised by extensive isotopic heterogeneity with a systematic spatial distribution.

Oxygen isotopes and trace elements In this sample, attention was focused on the domain with the axial vein network of luminescent calcite and its attendant halo of albitised oligoclase (Figure 9.28a, b). Note that this halo is similar to that in LWQ1/28 (Figure 9.27), but is symmetrical about the vein network of luminescent calcite. As with the example in LWQ1/28, the $\delta^{18}\text{O}$ data for calcite and quartz have been projected on to a line of section (Figure 9.28a), although in this sample, the data lie closer to the line than do those in LWQ1/28.

Once again, there are several features of note:

- a) $\delta^{18}\text{O}$ in both calcite and quartz varies markedly across the domain,
- b) highest calcite $\delta^{18}\text{O}$ values occur *within* and to the 'south' of the luminescent vein network; two values to the 'north' are consistently lower,
- c) luminescent calcite is characterised by $\delta^{18}\text{O}$ values down to $\sim 15 - 17 \text{ ‰}$, at least 5 ‰ lower than values in the dark orange-brown luminescent calcite
- d) quartz $\delta^{18}\text{O}$ is lower within and adjacent to the network axis, but values may exceed 25 ‰ elsewhere in this domain,
- e) towards the 'northern' limit of the altered halo, quartz $\delta^{18}\text{O}$ values decline to $\sim 22 \text{ ‰}$,
- f) in having quartz $\delta^{18}\text{O}$ greater than calcite $\delta^{18}\text{O}$, the few analyses of adjacent quartz and calcite grains suggest these grains may be, or have been, in isotopic equilibrium,
- g) unlike domain B in LWQ1/28, there is no clear correspondence between grain-size and $\delta^{18}\text{O}$ value for either calcite or quartz data, and
- h) no clear, grain-scale profiles are developed.

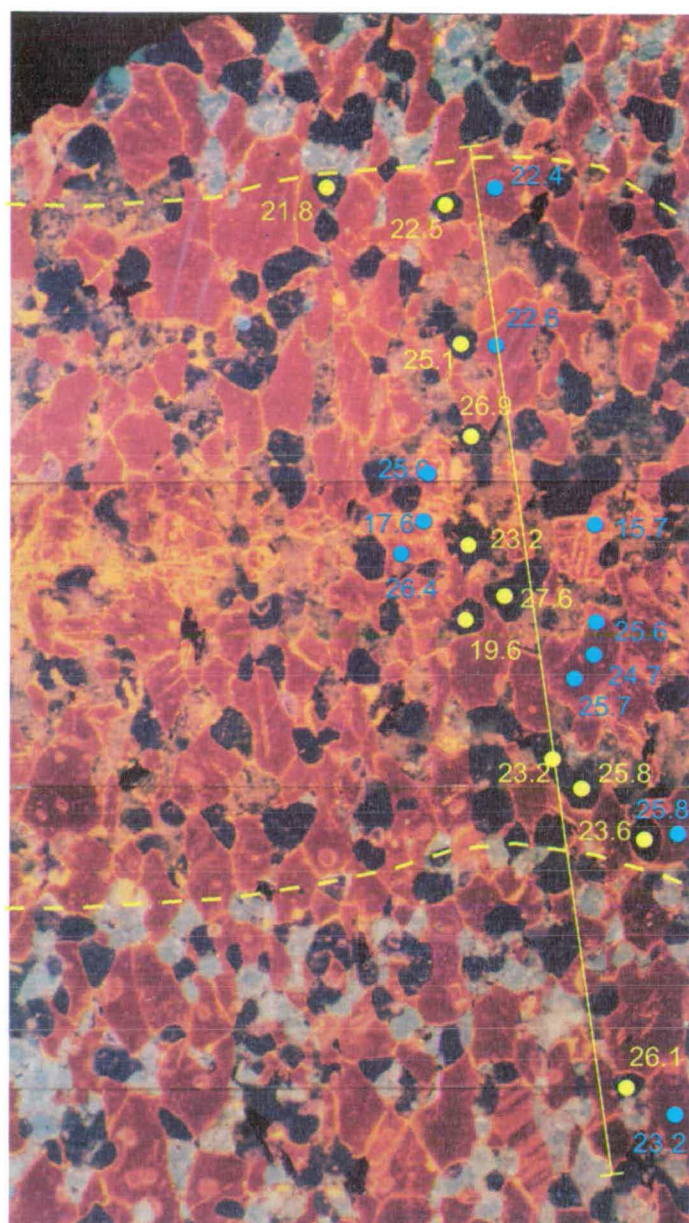


Figure 9.28a The domain in LWQ1/30 with axial luminescent calcite and a halo of albitised oligoclase. $\delta^{18}\text{O}$ data for calcite and quartz have been projected on to the profile section as shown in 9.28b below (cf. Figure 9.27a, b).

Note the symmetrical nature of the halo either side of the luminescent axis and note the corresponding curvature in the halo limit. The halo is about 1.7 mm wide.

- Calcite analysis
- Quartz analysis
- Limit of albitisation of oligoclase

Albitised oligoclase has patchy dark grey to buff luminescence, whereas relatively fresh oligoclase is blue with white patches.

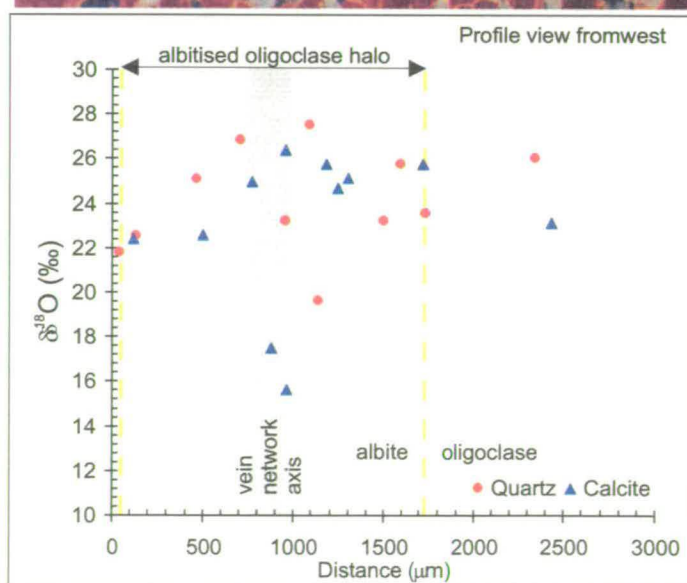


Figure 9.28b Calcite and quartz data projected on to the profile shown in 9.28a. Compare with 9.27b. Here, calcite $\delta^{18}\text{O}$ values are generally less than those of nearby quartz grains. $\delta^{18}\text{O}$ in calcite and quartz is reduced in part within the vein network axis, although some grains maintain high $\delta^{18}\text{O}$ across this domain.

- i) the few trace element analyses made in LWQ1/30 (Table 9.4) show that calcite in the axis of luminescent network (Figure 9.28a) is locally depleted slightly in Sr and Mn (50 – 100ppm), whereas $\delta^{18}\text{O}$ is markedly reduced.

It is clear that the fluid which infiltrated LWQ1/28 also infiltrated LWQ1/30 – this is to be expected, given that LWQ1/28 and 1/30 are just 4 cm apart. In the latter sample, the albite halo around the axial luminescent domain is ~ 1.7 mm across and is symmetrical. Like the data for LWQ1/28, the data for LWQ1/30 indicate considerable isotopic heterogeneity: calcite $\delta^{18}\text{O}$ can vary by up to ~ 11 ‰ within a few tens of microns.

Nature of feldspar alteration in LWQ1/28 and 1/30

Electron microprobe analysis of the feldspar in LWQ1/28 and 1/30 shows that oligoclase is altered to albite within the halo surrounding the luminescent calcite vein networks. The electron microprobe data are summarised in Table 9.5 and shown graphically in Figure 9.29a. This alteration is commonly incomplete, leaving complex peristerite-like intergrowths of albite and oligoclase, best revealed by back scattered electron imaging. An example from LWQ1/28 is shown in Figure 9.29b, where a core of relict oligoclase is surrounded by spongy and porous albite generally intergrown with the oligoclase (the spread in oligoclase analyses (Figure 9.29a) is explained by the ‘averaging’ effect of analysing the feldspars using a 10 μm rastered beam).

Analysis	Oxides, wt%						Cations pfu		Approximate Plagioclase composition
	Na ₂ O	Al ₂ O ₃	SiO ₂	K ₂ O	CaO	BaO	Na	Ca	
LWQ1/25 PLAGE ADJ SIMS 4,5,6	8.86	23.03	61.57	0.10	4.70	0.10	3.09	0.91	An ₂₃
LWQ1/25 PLAGE AT TOP MAP 1	9.08	22.55	61.88	0.12	4.22	-1	3.18	0.82	An ₂₀
LWQ1/25 PL W OF #29	9.00	22.93	61.47	0.10	4.47	0.23	3.15	0.86	An ₂₂
LWQ1/25 PL ADJ SIMS 6 MAP 1	8.68	23.22	61.00	0.10	5.11	-1	3.04	0.99	An ₂₅
LWQ1/25 DK PL ADJ SIMS 6 MAP 1	10.51	20.88	65.34	0.19	1.49	0.21	3.63	0.28	An ₇
LWQ1/25 PL IN DIFF Y LUM DOM.	8.95	23.21	61.93	0.10	4.69	0.22	3.11	0.90	An ₂₂
LWQ1/28 PL CENT LGE GR	8.67	23.45	61.37	0.13	4.91	-1	3.02	0.95	An ₂₄
LWQ1/28 PL, AT TOP LGE GR #40	9.02	22.82	62.04	0.14	4.25	0.20	3.15	0.82	An ₂₀
LWQ1/28 PL SE SIMS 13 MAP 2	8.73	22.25	57.91	0.10	5.34	0.11	3.20	1.08	An ₂₇
LWQ1/28 REPEAT OF ABOVE IN FOCUS	8.46	23.66	60.84	0.09	5.46	0.08	3.00	1.05	An ₂₆
LWQ1/28 ?ALB IN PL #44	11.63	19.58	67.13	0.03	0.64	-1	3.99	0.12	An ₃
LWQ1/28 PL CENT IN QZ GRP	8.70	23.41	61.34	0.08	5.03	-1	3.03	0.97	An ₂₄
LWQ1/28 PL CNTR S SIDE FELDS4	9.38	22.77	62.65	0.09	4.19	0.22	3.25	0.80	An ₂₀
LWQ1/28 PL CNTR PALE CORE	9.75	21.97	63.48	0.11	3.16	-1	3.39	0.61	An ₁₅
LWQ1/28 ?ALB EDGE OF GR OF #49	11.63	19.78	68.08	0.07	0.33	-1	3.95	0.06	An ₂
LWQ1/28 PL INB'RD OF #50	11.51	19.64	67.57	0.02	0.28	0.26	3.93	0.05	An ₁
LWQ1/28 REPEAT OF ABOVE	9.24	22.20	62.90	0.22	3.78	-1	3.22	0.73	An ₁₈
LWQ1/28 PL SW END OF GR #52,53	10.78	19.85	66.11	0.51	0.46	-1	3.74	0.09	An ₂
LWQ1/30 PL CNTR AS ABOVE IN FOCUS	8.60	23.44	61.12	0.17	5.11	0.10	3.00	0.99	An ₂₅
LWQ1/30 PL CNTR SMALL GR S SIMS 1	11.57	19.25	67.66	0.02	0.26	-1	3.97	0.05	An ₁
LWQ1/30 ALB ADJ SIMS 3 MAP 1	11.50	19.35	67.53	0.05	0.29	-1	3.95	0.05	An ₁
LWQ1/30 PL ADJ SIMS 2 SE EDGE	9.06	22.99	61.98	0.09	4.54	-1	3.15	0.87	An ₂₂
LWQ1/30 PL NR EDGE ALB ZONE	9.12	22.68	62.68	0.15	4.26	-1	3.16	0.82	An ₂₀
LWQ1/30 ALB ADJ YELL LUM CC W OF SIM	11.25	19.43	67.13	0.18	0.28	-1	3.88	0.05	An ₁
LWQ1/30 ALB NE SIMS 3	11.67	19.19	67.81	0.04	0.21	-1	4.00	0.04	An ₁

Table 9.5 Feldspar compositions determined by electron microprobe in the minicore samples LWQ1/28, 1/30 from the Inchroory Limestone, Limeworks Quarry, near Tomintoul. -1: below detection

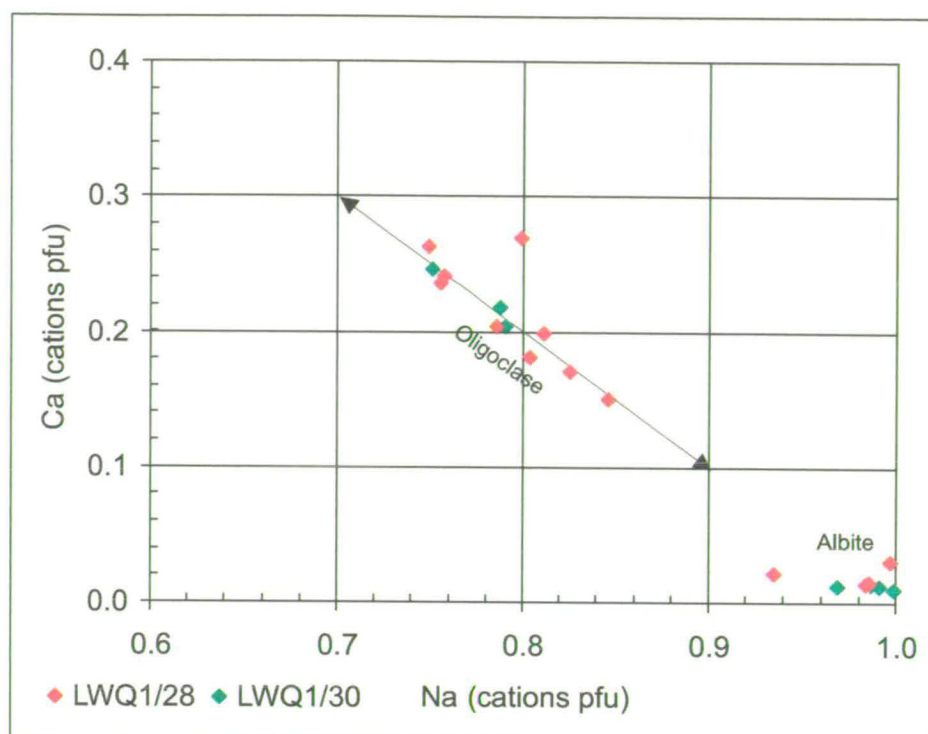


Figure 9.29a Feldspar compositions in LWQ1/28 and LWQ1/30, showing the alteration from oligoclase to albite

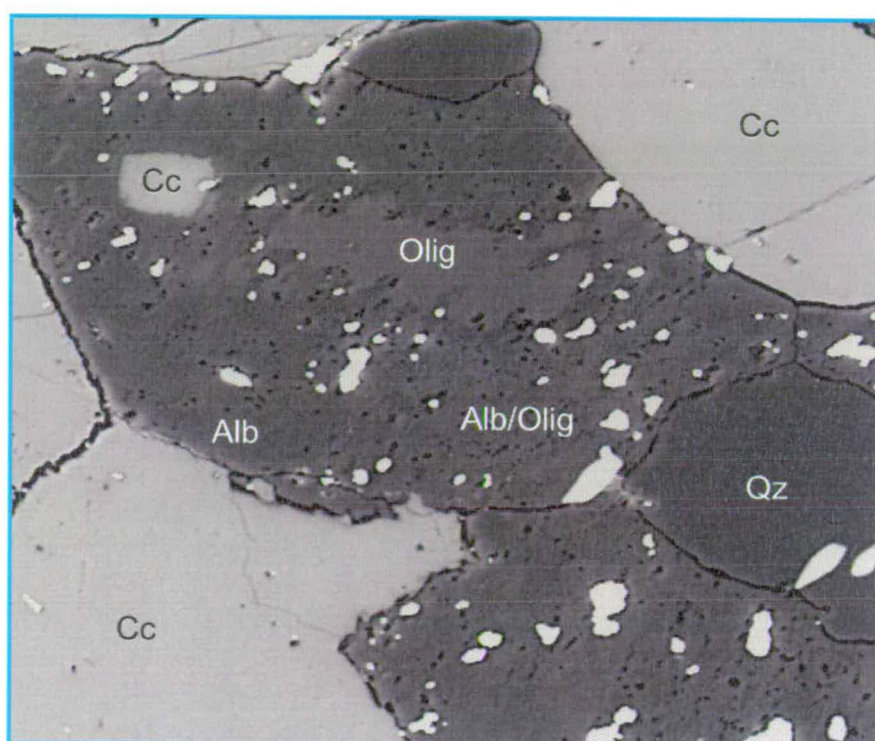


Figure 9.29b Replacement textures in oligoclase altering to albite. Note the spongy albite replacement and the local patchy intergrowth of the two feldspars. Cc: calcite; Qz: quartz; Alb: albite; Olig: oligoclase. White patches are the remains of gold coat for SIMS analysis.

Nature of luminescent calcite vein networks and fluid pathways

The vein networks of bright luminescent calcite clearly cross-cut the weak fabrics in LWQ1/28 and 1/30, defined by the weak elongation of calcite (Figures 9.27a, 9.28a). In LWQ1/28, the network is oblique to the calcite fabric, whilst in LWQ1/30, it is almost normal. The luminescent calcite occupies a fracture network developed generally along grain boundaries, but locally cutting across grains. This indicates that infiltration of the fluid which resulted in the alteration of feldspar and modification of calcite and quartz $\delta^{18}\text{O}$ was facilitated by microcracking most likely resulting from hydrofracture (see Chapter 8). The fact that grain boundaries are almost universally picked out by bright yellow luminescent calcite in these samples indicates that the fluid has pervasively infiltrated grain boundaries throughout the rock.

9.4.5 Discussion of LWQ data

Extent of oxygen isotopic equilibrium

Despite the apparent homogeneity in $\delta^{18}\text{O}$ indicated by bulk carbonate samples from the minicores of the Inchrory Limestone, it is clear from the SIMS data that the rock is not in isotopic equilibrium at the grain scale. Moreover, not all the alteration of $\delta^{18}\text{O}$ from the highest primary values of $\sim 27\text{‰}$ can be attributed to the fluid which infiltrated the samples along the metamorphic grain-boundary network. The lack of simple core to rim variations in $\delta^{18}\text{O}$ suggest that spatial variation in oxygen isotope composition may predate the development of the metamorphic polygonal boundary network and may be primary/diagenetic in origin.

If pre-metamorphic oxygen isotope signatures are preserved, their presence implies that the rock was effectively dry during metamorphism at amphibolite facies,

since the presence of any fluid along grain boundaries would facilitate diffusional re-equilibration. Fluid certainly has infiltrated the rock *very locally* along the fracture networks and has had local effects on the isotopic composition of the limestone, but these effects are *very* limited on the wider scale.

The apparent fractionation of $\delta^{18}\text{O}$ between calcite and quartz is widely inconsistent (see Chapter 10). There is evidence for possible local equilibrium fractionation (where $\delta^{18}\text{O}$ of quartz is significantly higher than that of the adjacent calcite) in Domain A of LWQ1/28, but other quartz – calcite pairs from the same domain show reversals in fractionation, indicating significant *disequilibrium*. The inconsistency thus renders interpretation of the *apparent* equilibrium quartz – calcite data very difficult and it is not at all clear that there is equilibrium between these phases at all, at least not in their present state. This is discussed further in Chapter 10.

Fluid – rock interaction

Although LWQ samples 1/28 and 1/30 have been infiltrated by a low $\delta^{18}\text{O}$ fluid, the extent of significant interaction between this fluid and the host rock is limited to the domains occupied by albitised oligoclase. Even in these domains, the interaction is not pervasive, as revealed by the projected profile data. In LWQ1/28 there appears to be local interaction between the relatively small quartz grains and the fluid, but the interiors of the larger calcite grains appear, on the whole, not to have been affected. In LWQ1/30, the projected data indicate less extensive interaction between quartz, calcite and infiltrating fluid. The lack of systematic correspondence between the two profiles reinforces an interpretation of very localised interaction with limited isotopic

exchange between vein and wall-rock. Away from the altered feldspar domains, there is little evidence that the fluid which infiltrated along grain boundaries and fractures, depositing the yellow luminescent calcite, has exchanged chemically with the host to any significant degree. Amount of fluid, its composition, the infiltration time-scale, temperature and the buffering effect of the host rock will all be factors which will affect the extent of interaction. Infiltration of this fluid clearly post-dates the metamorphic grain fabric in these rocks and is clearly fracture-controlled.

The predominance of calcite $\delta^{18}\text{O}$ values in excess of $\sim 22\text{‰}$ indicates the preservation of primary and near-primary values, though at least some of the lower values must be due to diagenetic fluid – rock interaction during stabilisation of the dominant primary aragonite to low-Mg calcite. However, I do not believe that the rocks were infiltrated significantly during peak metamorphism. $\delta^{18}\text{O}$ values typical of calcite resulting from metamorphic fluid infiltration are absent from texturally equilibrated areas and only found amongst the luminescent vein networks and patches. The last traceable fluid – rock interaction event occurred when the rocks were fractured and grain boundaries were *mechanically* opened up, permitting infiltration of the fluid which altered the feldspar and the bright luminescent calcite vein networks (Chapter 8). During this event, calcite-calcite grain boundaries were not subject to the dihedral angle constraints which render such boundaries impermeable under isostatic conditions during metamorphism (Holness and Graham, 1991; Holness and Graham, 1995). I discuss these matters further in Chapter 10.

Covariation of $\delta^{18}\text{O}$ and trace elements

In discussion of the whole-rock Sr and C isotope data (Chapters 7, 8), investigation of the relationships between $\delta^{18}\text{O}$, Sr and Mn showed these to be indifferent or weakly positively correlated. As with the $\delta^{18}\text{O}$ data, the relationship between the Sr and Mn data in LWQ1/25 show that, at the grain-scale, there is no clear correspondence between bright luminescence and high Mn, and that $\delta^{18}\text{O}$, Sr and Mn are all positively correlated (Figures 9.25a, b, c). This contrasts with findings of Graham et al, (1998) and Lewis et al. (1998), whose data revealed *increased* Mn and *reduced* Sr in luminescent calcite at grain boundaries. The data for LWQ1/28 and 1/30 show that variation in $\delta^{18}\text{O}$ occurs without significant change in Sr or Mn. This corresponds with the lack of covariation shown between $\delta^{18}\text{O}$ and $^{87}\text{Sr}/^{86}\text{Sr}$ in the whole-rock samples (Chapter 7). Taken together, these grain-scale data reinforce the interpretation made of the whole-rock data that there has been little significant *reduction* of Sr and *increase* in Mn by infiltrating fluids. This is reinforced further by the consistent, positive covariation between Sr, Mg and Fe across all three samples (LWQ1/25 – 1/30; Figure 9.25d). The significance of this is that the high Sr and Mn values are most easily interpreted as primary characteristics of the limestones. It could be that the Mn in the limestone in LWQ1/25 was derived from the amphibolite by local fluid-facilitated interaction between it and the limestone. However, it is difficult to envisage how Mn could be increased by an order of magnitude in LWQ1/25 without at the same time significantly disturbing the oxygen isotope and strontium compositions, both of which should show significant signs of depletion, but, in fact, show the opposite (Figure 9.25c).

Variation of SIMS calcite $\delta^{18}\text{O}$ data in the Inchrory Limestone samples in relation to profile position

Variations in SIMS $\delta^{18}\text{O}$ data for LWQ1/25, 28 and 30 with respect to distance from the amphibolite are shown in Figure 9.7a, b.

There are several features of note:

- a) the median values of SIMS data for each sample are similar to the bulk carbonate values for adjacent samples, although, at 25.0 %, the median $\delta^{18}\text{O}$ value for LWQ1/30 is a little higher than adjacent conventional samples,
- b) the range in the SIMS calcite $\delta^{18}\text{O}$ data is much greater than that shown by the conventional $\delta^{18}\text{O}$ data,
- c) peak $\delta^{18}\text{O}$ values reach 27.0 – 27.2 in all three samples, but minimum values consistently decline *away* from the amphibolite – limestone contact from 22.4 in LWQ1/25 to 15.7 in LWQ1/30,
- d) interquartile ranges (Figure 9.7b) are similar for all three samples,
- e) high $\delta^{18}\text{O}$ values are preserved right up to the amphibolite contact, reinforcing the lack of evidence for $\delta^{18}\text{O}$ exchange between amphibolite and limestone in the bulk-carbonate data.

In contrast to the bulk carbonate data, the SIMS data show that there *has* been interaction between the limestones in this profile and a low $\delta^{18}\text{O}$ fluid. However, the extent of this interaction is clearly very limited. If it were much more extensive, there would be clear evidence in the bulk carbonate data, as discussed above. The only sample which hints at this possibility is LWQ1/34 ($\delta^{18}\text{O} = 20.7$) at 63.25 cm along the profile, some 16 cm from the amphibolite.

In the introduction and in Appendix E, I outline the way in which penetrative deformation is partitioned into the outer part of the profile, some 12 cm away from the amphibolite – limestone contact. It is clear from the foregoing that this increase in deformation has nothing to do with the fluid infiltration which can be traced in these rocks as the latter occurs in micro-fractures oblique to the metamorphic fabric.

The point is that the bulk rock carbonate $\delta^{18}\text{O}$ analyses imply that the rock is isotopically homogeneous and equilibrated, with $\delta^{18}\text{O} \sim 23 \text{ ‰}$. The SIMS data show that this is not the case: the LWQ samples are *all* in a state of significant isotopic *disequilibrium*. This extends to the SIMS quartz data. The bulk isotope data mask this disequilibrium completely. Interpretations based on the bulk carbonate isotope data alone would reach quite different conclusions about the isotopic state of the rock and how this state was achieved.

Summary of SIMS $\delta^{18}\text{O}$ data in LWQ samples, Inchrory Limestone

- The LWQ samples analysed by SIMS show that the Inchrory Limestone is, like the Tourulian Limestone sample, in a state of isotopic disequilibrium
- Quartz – calcite oxygen isotope fractionations are only locally consistent with being in equilibrium, but generally reveal a state of isotopic disequilibrium between the two phases
- Fluid infiltration during metamorphism was insignificant, apart from very local, fracture-facilitated infiltration which postdates the main metamorphic fabric in the rocks

- Preservation of metamorphic textures across domains of altered feldspar show that recrystallisation did not accompany fluid infiltration; this implies that alteration of $\delta^{18}\text{O}$ in quartz and feldspar occurred by diffusional exchange
- In addition to time-scale and temperature of fluid infiltration, fluid flux and composition and buffering effects by the host rock, grain-size will also have influenced the extent to which the calcite and quartz could equilibrate with infiltrating fluid in the altered feldspar domains

9.5 Conclusions

- a) In all the samples studied at the grains-scale, there is extensive heterogeneity in $\delta^{18}\text{O}$. This is true even of the Inchrory Limestone samples from the Limeworks profile, which have homogenous bulk carbonate $\delta^{18}\text{O}$.
- b) In CT53, fluid – rock interaction accompanied extensive fluid infiltration, probably facilitated largely by hydrofracturing.
- c) In CT53, profiles across domains of variable luminescence reveal isotopic gradients of a scale and magnitude similar to gradients in other studies which have been shown to been formed by volume diffusion.
- d) In CT53, $\delta^{18}\text{O}$ of the calcite in veinlets appears to be a function of grain width, suggesting buffering of vein fluid $\delta^{18}\text{O}$ by the host limestone, which has a large buffer capacity.
- e) In CT53, there is evidence for infiltration of and interaction with a metamorphic fluid which reduced $\delta^{18}\text{O}$ in the limestone from near primary values to values typical of infiltrated metamorphosed limestones of c. 16 – 17 ‰. This was

followed by further infiltration of low $\delta^{18}\text{O}$ fluid, possibly with a magmatic component, which resulted in reduction of $\delta^{18}\text{O}$ values to c. 10 ‰.

- f) In the LWQ samples, very high, primary $\delta^{18}\text{O}$ values of 27 ‰ are preserved in all three samples (c. 4 ‰ greater than median).
- g) In the Inchrory Limestone sample profile, there is no link between increase in intensity of deformation away from the margin of the limestone and $\delta^{18}\text{O}$ in the bulk carbonate samples, neither is there any clear sign of exchange of isotopes with the amphibolite pod.
- h) In the LWQ samples, the dominant, traceable fluid infiltration event was fracture controlled and very limited in extent; only along the main microfractures was there significant fluid – rock interaction, marked by albitisation of feldspar.
- i) The grain-scale spatial distribution of $\delta^{18}\text{O}$ compositions in LWQ samples does not correspond to the current grain boundary architecture in domains with limited infiltration of external fluid, implying that the spatial variation in $\delta^{18}\text{O}$ in calcite may predate the metamorphism.

Are primary $\delta^{18}\text{O}$ signatures preserved?

Primary oxygen isotope signatures *are* preserved in the Inchrory Limestone, but only locally and their presence is only revealed by SIMS analysis. Over most of the rock, $\delta^{18}\text{O}$ signatures better considered as ‘near-primary’ predominate and are altered from the high primary values to a certain degree. I consider that this alteration probably occurred during diagenesis because of the limited, mappable evidence for alteration during metamorphism. In the Torulian Limestone, the highest $\delta^{18}\text{O}$ values, at ~ 22 ‰ are probably all the result of diagenetic alteration. The low bulk carbonate $\delta^{18}\text{O}$

values and the evidence for very extensive fluid-rock interaction explains why the $^{87}\text{Sr}/^{86}\text{Sr}$ ratio in the limestone from the Bridge of Avon locality is so radiogenic (Chapter 6).

What are the implications of the oxygen data for interpretation of bulk carbonate $^{87}\text{Sr}/^{86}\text{Sr}$ and $\delta^{13}\text{C}$?

Carbonate rocks with $\delta^{18}\text{O} > \sim 20\text{‰}$ are often considered to be ‘unaltered’. As I have shown, even rocks with bulk carbonate of $\sim 23\text{‰}$ can be isotopically very heterogeneous and I have argued that some of the spatial variation in $\delta^{18}\text{O}$ in the Inchrory Limestone could be pre-metamorphic in origin, at least in part. I believe, on the basis of arguments and data presented in Chapters 6, 7 and this chapter, that the bulk of the $^{87}\text{Sr}/^{86}\text{Sr}$ and $\delta^{13}\text{C}$ data can, with care, be interpreted from the point of view of primary seawater signatures. However, oxygen is more easily altered than either $^{87}\text{Sr}/^{86}\text{Sr}$ or $\delta^{13}\text{C}$ and the bulk carbonate $^{87}\text{Sr}/^{86}\text{Sr}$ and $\delta^{13}\text{C}$ data represent averages. Given the observed grain-scale variation in $\delta^{18}\text{O}$, it would be very interesting to know if such variation extended to Sr and C isotopes: Just *how much* variation in Sr and C isotopes is masked by the bulk carbonate values?

What next?

In Chapter 10, I consider further the fluid-rock interaction in these two limestones by quantifying several of the features of the isotope data and their spatial variation. In particular I consider the following:

- Modelling of diffusion profiles in CT53 – estimating fluid-infiltration timescales and temperatures

- Lack of ^{18}O equilibration between calcite, quartz and fluid in LWQ1/28 and 1/30
 - diffusion, buffering and the effects of grain-size and mineral modes.

Chapter 10

Modelling of oxygen isotope profiles and mineral fractionations

In this chapter:

- ❖ Modelling $\delta^{18}\text{O}$ profiles in the Torulian Limestone
- ❖ The role of mode and grain-size in isotopic exchange in the Inchrory Limestone
- ❖ Estimation of fluid infiltration time-scales

10.1 Introduction

In Chapter 9, I showed that, in sample CT53 from the Torulian Limestone, there are gradients in $\delta^{18}\text{O}$ in calcite grains consistent with similar gradients in other studies which have been interpreted as resulting from diffusion (Graham et al., 1998; Lewis, 1999; Wada, 1988) (the grain-scale ^{18}O profile in calcite determined by Wada (1988) is shown here for comparison in Figure 10.1d). The grain-scale profiles are considered to relate to extensive metamorphic fluid infiltration revealed by complex and highly variable CL images (Figure 9.8).

In the Inchrory Limestone samples LWQ1/25, 1/28 and 1/30, I showed that the rocks are in a state of isotopic disequilibrium, even though they appear texturally well-equilibrated. In addition, I showed that two of these limestones have been infiltrated by external fluid along micro-fractures. Whilst this infiltration had the

same macroscopic effect in both samples, resulting in haloes of altered feldspar and the development of luminescent calcite in fractures and along grain boundaries, the effect on the oxygen isotopes in the two samples was different.

In this chapter, I present the results of modelling of the $\delta^{18}\text{O}$ gradients in the Torulian Limestone as diffusion profiles and estimate the time-scales and likely temperatures of fluid infiltration.

For the Inchroary Limestone samples LWQ1/28, and 1/30, I elucidate the mineralogical, compositional and kinetic controls on the modification of $\delta^{18}\text{O}$ in quartz and calcite, highlighting the likely roles of feldspar, grain-size and grain-size contrasts and mineral modes.

10.2 Calcite – dolomite geothermometry: a temperature estimate for fluid-rock interaction in CT53?

Sample CT53 underwent very extensive fluid-rock interaction, during which grain-scale gradients in $\delta^{18}\text{O}$ were developed in calcite. These gradients appear to have resulted from diffusional infiltration by analogy with similar gradients elucidated in other studies (e.g. Graham et al., 1998). If they do result from diffusion, then, bearing in mind arguments about the transient nature of permeability in metamorphic rocks discussed in Chapter 8, they place constraints on the temperature of fluid infiltration: for such diffusion profiles to develop on the likely times-scales for the maintenance of a transient permeability, the rocks must have been at moderate to high metamorphic temperatures (cf. Graham et al., 1998; Lewis, 1999).

Ideally, an independent estimate of temperature is needed to constrain the diffusion modelling. The presence of coexisting calcite and dolomite offers the *possibility* of estimating the temperature of fluid-rock interaction.

Dolomite grains of the order of 100 – 200 μm in size occur locally, although much finer ($<20\ \mu\text{m}$) dolomite is scattered throughout the calcite (dark grains in Figure 9.8). The dolomite is thought to be diagenetic in origin. The dolomite analysed below lies in a domain of even luminescence $\sim 100\ \mu\text{m}$ from bright orange luminescent calcite in Profile B (Figure 9.21 and see Section 10.3). The dolomite is un-zoned and calcian. Moreover, it is also generally very low in Fe (Table 9.5). The adjacent calcite has low to very low Mg and Fe; SIMS trace element analysis for calcite in Profile B shows that Fe rarely exceeds 1500 ppm.

10.2.1 Calcite – dolomite geothermometry

The calcite-dolomite geothermometer of Anovitz and Essene (1987) has been used to calculate calcite – dolomite equilibration temperatures. The analyses and the results of the geothermometric calculations are given in Table 10.1. Note that calcite – dolomite pairs 5 and 6 are outwith the domain shown in Figure 9.28. Calculated temperatures lie in the range 223 – 386°C, with most lying in the range 309 – 356°C. The latter are within a nominal $\pm 40^\circ\text{C}$ error. Median $X_{\text{Mg,dol}}$ vs median $T^\circ\text{C}$ (large point in inset graphic 2, Table 10.1) gives an estimate of the ‘median’ equilibration temperature of 334°C.

The limited data presented here suggest that equilibrium between dolomite and calcite has been achieved locally, but that it has also been reset in places. If calcite and dolomite have maintained chemical equilibrium, $X_{\text{Mg,cc}}$ and $X_{\text{Mg,dol}}$ should

Calcite and dolomite analyses				Cations			Mole fractions in calcite or dolomite			
Analysis #	Comment	Phase	Pairs	Ca	Mg	Fe	x_{Ca}	x_{Mg}	x_{Fe}	Sum
67	Edge	Calcite	1	2.950	0.041	0.001	0.983	0.014	0.000	0.997
68	Edge	Dolomite	1	3.044	2.896	0.060	0.507	0.483	0.010	1.000
69	Edge	Calcite	2	2.945	0.049	0.004	0.982	0.016	0.001	0.999
70	Edge	Dolomite	2	3.032	2.887	0.070	0.505	0.481	0.012	0.998
71	Edge	Calcite	3	2.952	0.041	0.003	0.984	0.014	0.001	0.999
72	Edge	Dolomite	3	3.068	2.859	0.069	0.511	0.477	0.012	0.999
73	Edge	Calcite	4	2.953	0.034	0.008	0.984	0.011	0.003	0.998
74	Edge	Dolomite	4	3.039	2.896	0.060	0.507	0.483	0.010	0.999
75	Edge	Calcite	5	2.958	0.033	0.006	0.986	0.011	0.002	0.999
76	Edge	Dolomite	5	3.059	2.874	0.063	0.510	0.479	0.011	0.999
77	Centre	Dolomite		3.052	2.878	0.063	0.509	0.480	0.011	0.999
78	Edge	Calcite	6	2.953	0.046	0.001	0.984	0.015	0.000	1.000
79	Edge	Calcite	6	2.929	0.061	0.005	0.976	0.020	0.002	0.998
80	Edge	Dolomite	6	3.034	2.899	0.059	0.506	0.483	0.010	0.999
81	Edge	Calcite	7	2.984	0.013	0.002	0.995	0.004	0.001	1.000
82	Edge	Dolomite	7	3.091	2.835	0.065	0.515	0.473	0.011	0.999

Analyses for calcite-dolomite pairs 5 and 6 in different part of CT53. The rest are from the domain in Profile B (see Figures 9.23, 9.28). The two Cc analyses for pair 6 are either side of a small dolomite grain

Calibration:

Calcite-dolomite Mg-exchange geothermometer of Anovitz and Essene, 1987

Basic 'temperature' (A)

$$T(K) = A(x_{Mg,cc}) + B(x_{Mg,cc})^2 + C(x_{Mg,cc})^3 + D(x_{Mg,cc})^{0.5} + E$$

Correction for iron in calcite (B):

$$T^{FeMg}(K) = T_{(A)} + a(x_{Fe,cc}) + b(x_{Fe,cc})^2 + c(x_{Fe,cc}/x_{Mg,cc}) + d(x_{Fe,cc} \cdot x_{Mg,cc}) + e(x_{Fe,cc}/x_{Mg,cc})^2 + f(x_{Fe,cc} \cdot x_{Mg,cc})^2$$

Coefficients

A	-2360.0
B	-0.01345
C	2620.0
D	2608.0
E	334.0
a	1718.0
b	-10610.0
c	22.49
d	-26260.0
e	1.3330
f	3.28E+06

Results

Pair	$x_{Mg,cc}$	$x_{Mg,dol}$	$x_{Fe,cc}$	A	B	Δ_{A-B}
1	0.014	0.483	0.00	334	335	1
2	0.016	0.481	0.00	356	360	4
3	0.014	0.477	0.00	334	337	3
4	0.011	0.483	0.00	312	321	9
5	0.011	0.479	0.00	309	316	7
6	0.015	0.480	0.00	348	349	1
6	0.020	0.483	0.00	386	390	4
7	0.004	0.473	0.00	223	227	5
Median				0.480	334	

Iron correction is negligible

Note: Temperatures given in °C.

Insets

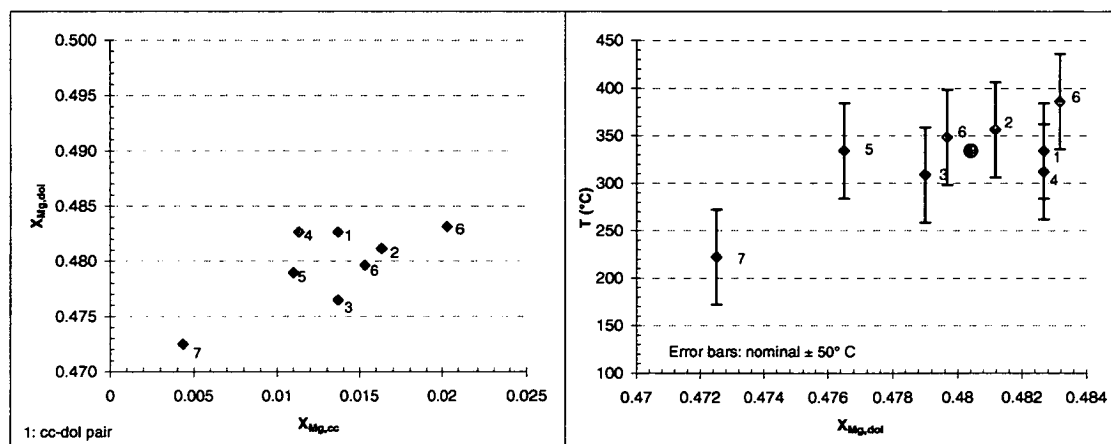


Table 10.1 CT53 Calcite-Dolomite temperatures. See text for discussion

co-vary. Inset 1 in Table 9.5 shows that $X_{\text{Mg,cc}}$ and $X_{\text{Mg,dol}}$ for several pairs (2, 5, 6, 7) lie close to a common trend, suggesting equilibrium, where as pairs 1, 3 and 4 lie off it. However, Pair 7 gives a temperature $\sim 100^\circ\text{C}$ lower than the other data, due to low Mg in calcite, whilst one of the pair 6 calcite analyses gives a significantly higher temperature due to the significantly more magnesian calcite; this may be due to the presence of dolomite inclusions in the calcite caught in the $10\ \mu\text{m}$ raster beam. The cluster of values between 309° and 356°C (Inset 2, Table 9.5) are considered the best estimate of the temperature of equilibration between calcite and dolomite, with a median value of 334°C .

The problem remains as to the interpretation of the calcite - dolomite temperatures. They are some 250°C below the metamorphic peak values for this region of the Dalradian ($\sim 600^\circ\text{C}$; Beddoe-Stephens, 1990). The complex and extensive chemical alteration textures observed by CL in CT53 indicate extensive interaction with a hot fluid of low $\delta^{18}\text{O}$ composition. As will become apparent below, it is unlikely that the calcite – dolomite temperatures record the temperature of the fluid – rock interaction event because they are too low to allow the observed, apparently diffusion-controlled, oxygen isotope profiles to develop over a reasonable time scale. The significance of the temperatures is therefore uncertain. They may reflect cooling from the metamorphic thermal peak, but they place no significant constraint on the temperature of the fluid infiltration event.

10.3 Diffusion modelling of profiles in sample CT53

In this section, I present quantitative modelling of the grain-scale $\delta^{18}\text{O}$ profiles recorded in calcite by SIMS analysis in CT53 from the Torulian Limestone in the

River Avon, near Tomintoul (Chapter 9). The aim in doing so is to establish if they can be modelled as being formed by diffusion and to estimate the likely time-scales required to form the profiles. Determining the time scale of infiltration also places constraints on the nature of the fluid infiltration process. Although the temperature at which infiltration occurred cannot be quantified directly, the results of diffusion modelling provide estimates of the likely temperature because of the short time-scales over which permeability can be maintained (e.g. Lewis, 1999).

10.3.1 Quantitative methods

I have fitted the data from profiles A, B and C to the diffusion equation (10.1), following the methods of Graham et al. (1998) and Lewis (1999) and outlined in Chapter 3 in order to a) establish whether the profiles are consistent with having been formed by diffusion and b) estimate Dt and, therefore, t , the time-scale of infiltration. I describe the modelling in more detail here.

To recapitulate from Chapter 8, if diffusion has been the sole mechanism of transport of ^{18}O into the interiors of calcite grains in regions away from short-circuiting fluid pathways, then the profiles in CT53 should fit the diffusion equation (Crank, 1975):

$$\text{erf}[x/(4Dt)^{1/2}] = (C_x - C_{\text{rim}})/(C_{\text{core}} - C_{\text{rim}}) \quad (10.1)$$

where:

erf is the error function,

x is distance along the measured profile,

D is the diffusivity ($\text{m}^2 \text{s}^{-1}$), in this case of oxygen in calcite ,

t is time (seconds),

C is the concentration of oxygen at the rim, core and at x along the profile respectively, in units of ‰ $\delta^{18}\text{O}$.

The boundary conditions for this equation are that diffusion takes place into a semi-infinite medium from a boundary with the same composition as the fluid phase and maintained at constant composition during the duration of the diffusion event.

Several assumptions are made in applying this equation. Firstly, the temperature and the fluid composition are assumed to be constant during the formation of the isotope profile. Secondly, the rim of the grain is assumed to be in equilibrium with the fluid. These two assumptions *imply* external buffering of the fluid phase because the rock would begin to buffer $\delta^{18}\text{O}$ in the fluid phase if the latter was static. *The corollary is that there was sufficient fluid flow to prevent buffering (cf. possible evidence for buffering of fluid in veins described in Chapter 9, Section 9.4.3).* Thirdly, the equation is 1-dimensional, diffusion is assumed to be isotropic in the calcite (Farver 1994), and the length of the profile is assumed here to be the true diffusion distance, normal to the grain edges. Note that Graham et al. (1998) and Lewis (1999) estimated or measured the orientation of the grain boundary relative to the plane of the analytical surface. This has not been done in this case because the relatively poor grain boundary structure in this sample would make it difficult to determine orientations. Although Graham et al. (*op. cit.*) corrected one of their profiles for geometry, Lewis (1999) found that such corrections made insignificant difference to her modelling results. Finally, for a smooth diffusion profile to develop, the grain must be isotopically homogeneous *before* infiltration, particularly within the critical region up to 300 μm from the grain boundary.

Values of Dt and C_{core} and their 1σ errors were determined by fitting equation (10.1) to the profile data by non-linear, least-squares minimisation, using the program DIFF, written by Alasdair Skelton. I fixed the value of C_{rim} based on the SIMS analyses. The distance, x , of an analysis along a profile from the grain boundary were measured by scanning electron microscope. The errors on the $\delta^{18}\text{O}$ analyses are incorporated into the model. Errors on the distance are ignored.

The results of the modelling are shown in Table 10.2 and the best fit lines to each of the profile data sets are shown in Figures 10.1a – c. The fit of the data to the equation is determined by calculating the χ^2 value for the degrees of freedom. The calculated value of χ^2 is then compared with tabulated value of χ^2 at the 95% level of significance for the number of degrees of freedom. In this case, because two parameters are being fit, the degrees of freedom is $n - 2$, where n is the number of points in the profile. Table 10.2 shows that all the profiles can be accepted as fits to the diffusion equation and the Dt values are closely similar (cf. Graham et al., 1998).

10.3.2 Calculating timescales of fluid infiltration

Dividing Dt by the diffusivity, D , for a specific temperature, T , gives the time for the diffusion profile to form and, by implication, the timescale of the fluid infiltration event. I have used the data for the diffusion of O in calcite *in the presence of water* from Farver (1994) to calculate D for the temperature range 300 – 700°C, using the Arrhenius rate equation:

$$D = D_0 e^{(-Q/RT)} \quad (10.2)$$

with:

$$D_0 = 7.0 \times 10^{-9} \text{ m}^2 \text{ s}^{-1},$$

Profile	points	Parameters			Statistics		
		Fixed	Calculated		degrees of freedom	Goodness-of-fit	
		C_1 (‰)	C_0 (‰)	$Dt \times 10^{-8} \text{ m}^2$	(n - 2)	χ^2_{critical}	$\chi^2_{\text{calculated}}$
A right hand side	5	10.2	16.6 ± 1.2	0.253 ± 0.42	3	7.81	3.01
A left hand side	8	10.1	15.8 ± 1.0	0.505 ± 0.67	6	12.59	10.34
B	12	13.6	17.3 ± 0.7	0.27 ± 0.51	10	18.31	14.28
C	7	13.0	18.5 ± 1.2	1.242 ± 1.75	5	11.07	0.74

C_0 is the $\delta^{18}\text{O}$ value at the grain core

C_1 is the $\delta^{18}\text{O}$ value at the grain rim

Chi-square critical value is for the 95% confidence limit

Table 10.2 Results of diffusion modelling of $\delta^{18}\text{O}$ profiles in sample CT53

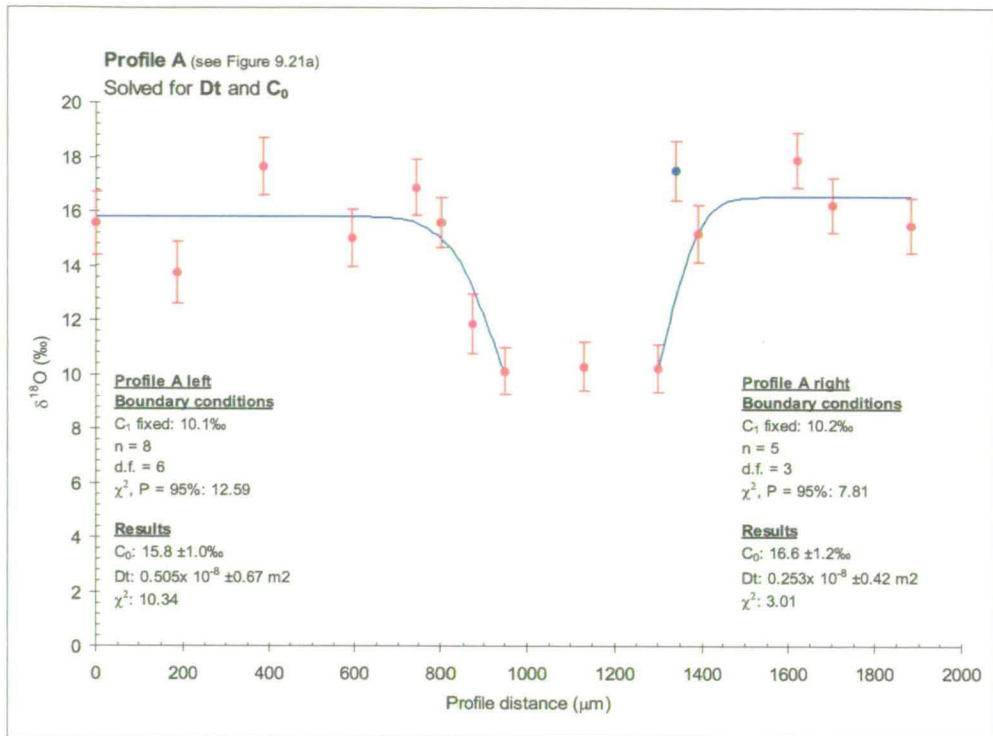


Figure 10.1a Non-linear fit of the diffusion equation (10.1) to the SIMS data for profile A in CT53 to the right and left of the calcite vein. Point shown in dark blue is in luminescent calcite and not used.

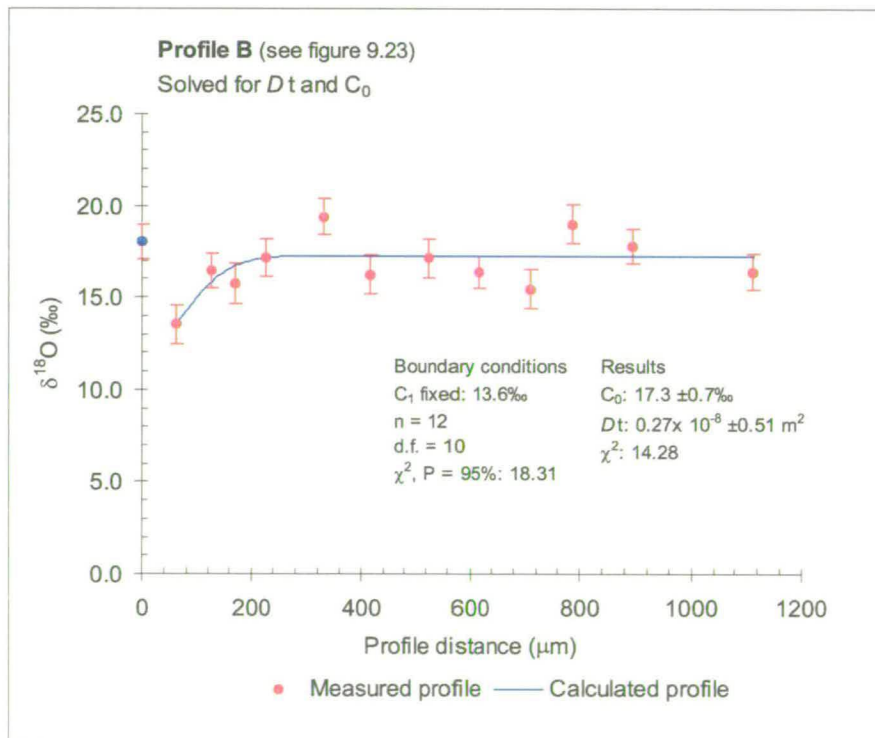


Figure 10.1b Non-linear fit of the diffusion equation (10.1) to the SIMS data for profile B in CT53. Data point in dark blue is outwith the profile.

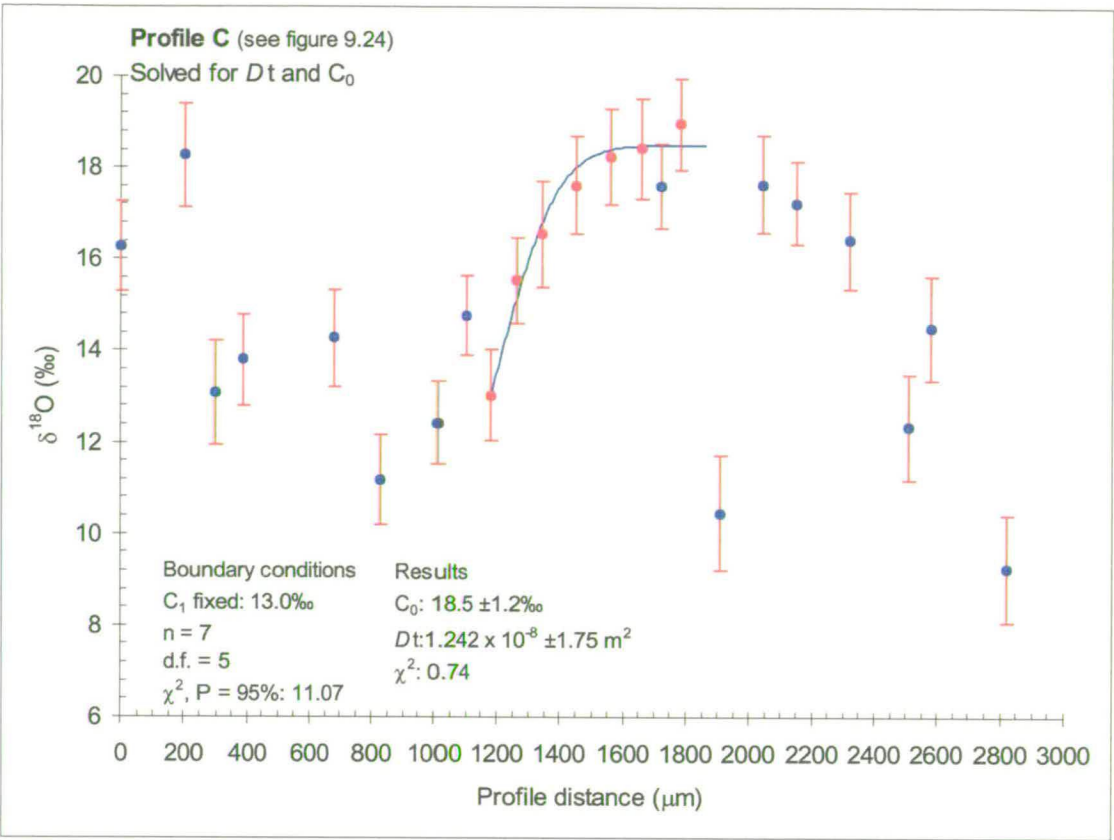


Figure 10.1c Non-linear fit of the diffusion equation (10.1) to the SIMS data for profile C in CT53. Data points in dark blue are either outwith the profile or in short-circuit fluid pathways and are not used.

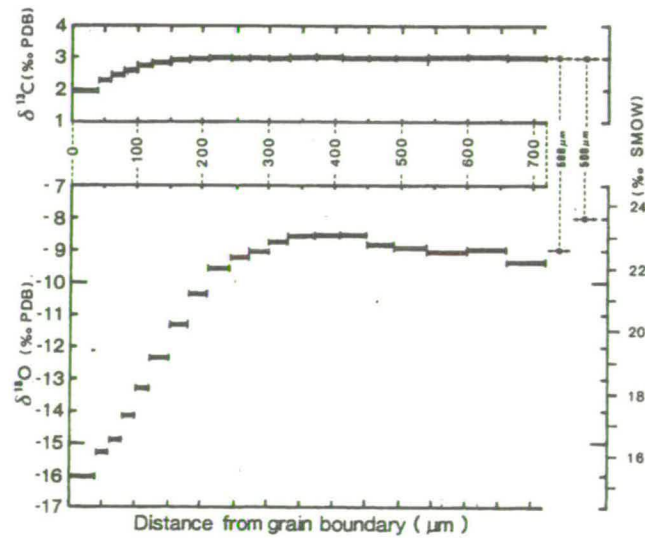


Figure 10.1d The $\delta^{18}\text{O}$ profile in calcite determined by Wada (1988). Although this looks like a diffusion profile, the χ^2 for the fit to the diffusion equation is very large and the profile cannot be modelled by diffusion.

$Q = 173 \text{ kJ mol}^{-1}$, and

$R = 8.314 \text{ J mol}^{-1}$;

T = temperature in Kelvins.

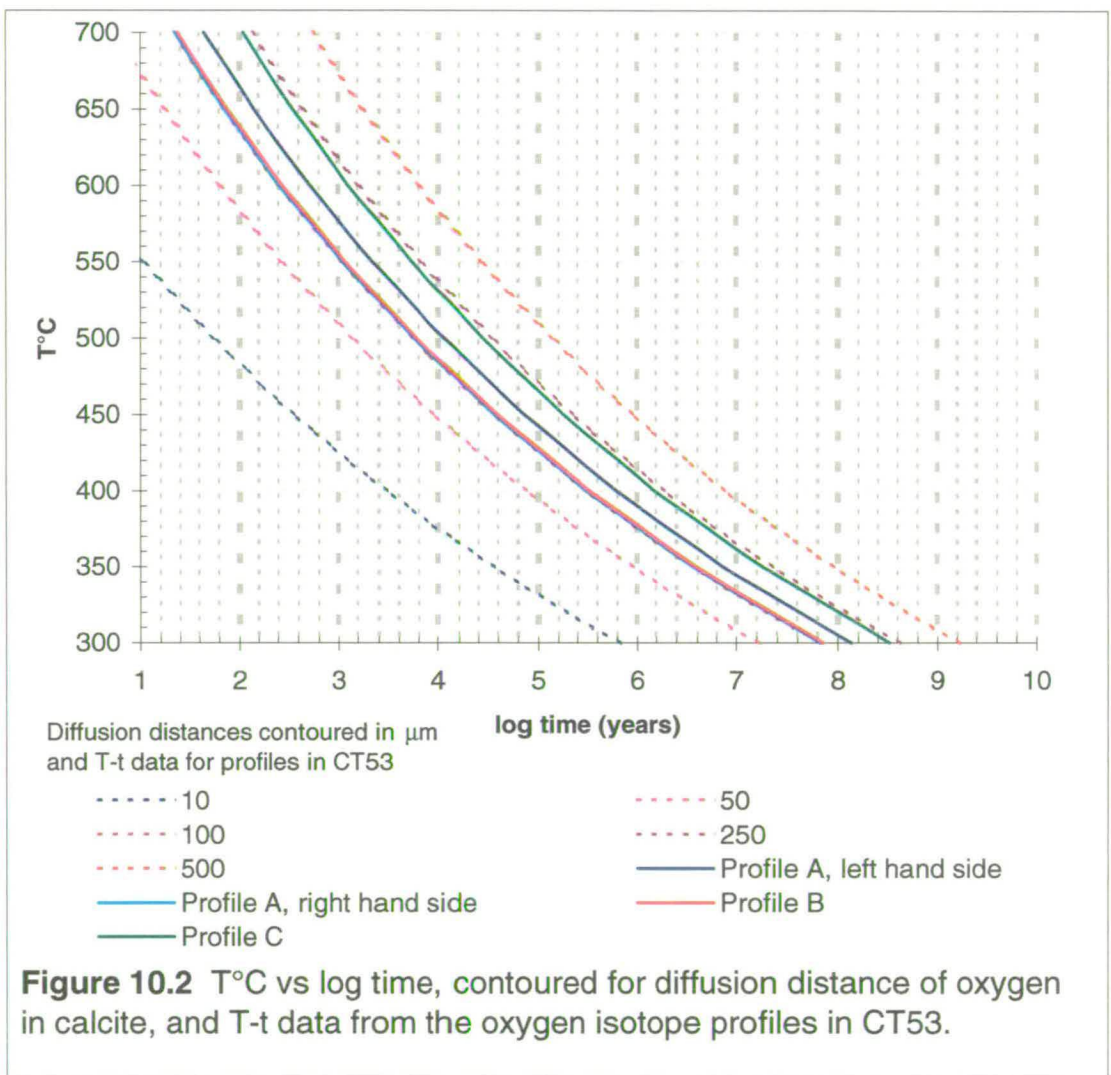
The *characteristic* time taken for diffusion to occur over a specific distance, x , at a temperature, T , can be determined from a re-arrangement of the relationship in the left hand side of (10.1) (Farver and Yund, 1991, page 67):

$$t = x^2/4D \quad (10.3)$$

Substituting various values of x into (10.3) gives values for t which can be plotted against temperature, T , contoured in x (cf. Graham et al., 1998), thus showing the amount of time taken for oxygen to diffuse a specific distance into calcite. This I have done in Figure 10.2. Because Dt/D yields t at a particular temperature, I have also plotted the values of t at various T , calculated from the profile Dt values on Figure 10.2. This shows graphically the characteristic diffusion distance ($x = (4Dt)^{1/2}$ cf. equation 10.3) for each profile, allowing the time over which the profiles developed to be estimated for any particular T .

10.3.3 Discussion

Do the profiles represent true diffusion profiles? Although the calculated χ^2 values are less than the critical values of χ^2 at the 95% level of significance, indicating that the profiles are consistent with diffusion, the scatter on the SIMS analyses and their individual errors have resulted in large errors on the Dt values, such that they are of the same order of magnitude as the Dt values themselves (Table 10.2). Thus the Dt values are poorly constrained in terms of their regression errors. However, given that CT53 is isotopically heterogeneous at the grain scale, the scatter in the Dt values is



unsurprising and reflects the isotopic heterogeneity, which will arise from short-circuit fluid pathways and, *possible*, pre-metamorphic spatial variations superimposed on the diffusion profile. The scale of heterogeneity might well be less than the diameter of the ion beam (typically 20 – 40 μm) or the ion beam might have clipped an edge between two domains with differing $\delta^{18}\text{O}$ during analysis. Comparison with the CL images for marble studied by in Graham et al., (1998) and Wada (1988), shows that CT53 has a much more complex fluid infiltration history and much more extensive development of short-circuit pathways. Thus, the opportunity to find domains which preserve *purely* volume diffusional exchange with a boundary fluid is more limited in this rock. *Nevertheless*, the χ^2 values are well within the critical values and all the profiles show increases in the critical boundary layers close to grain boundaries. Furthermore, *despite* the errors, the *consistency* of the Dt results from one small area of rock (CT53 is $\sim 2 \text{ cm}^2$) indicates that the results can be interpreted quite readily as diffusion profiles and used to provide information on the time scale of fluid infiltration in this rock.

Timescales for profile development

The Dt values for the two A profiles and profile B are similar and give t values of 514, 258 and 244 years at 600°C, and 2190, 1100 and 1170 years at 550°C respectively. For profile C, t estimates are rather larger, being 1260 years at 600°C and 5380 years at 550°C. The results for t in these profiles are comparable in magnitude to those calculated by Graham et al., (1998) for the marble from the Hida metamorphic belt (Wada, 1988) and similar, though slightly longer than, most of those calculated by Lewis (1999) for marbles from Naxos. As Figure 10.2 shows, the

time required to generate the diffusion profiles increases logarithmically with decreasing temperature. Thus, the profiles are unlikely to develop at temperatures much below 500°C, where times in excess of ~ 80 000 years would be required, given that any permeability is likely to be highly transient in this very pure limestone (see Chapter 3). This necessity for high temperatures sufficient to form the profiles over likely time-scales is the key feature of the results of this study and those of Graham et al. (1998) and Lewis (1999). The results show that the calcite – dolomite temperatures (~ 330°C) calculated above cannot represent the likely temperature of fluid infiltration. Furthermore, the time-scales for infiltration are consistent, within an order of magnitude, with theoretical estimates of the duration of hydrofracture veining in the absence of deformation (Niyashima, 1989).

Preservation of profiles on cooling

The short timescale required to produce the diffusion profiles suggests that, over the likely timescale of a metamorphic event ($10^6 - 10^7$) years, the profiles should decay by diffusional resetting on cooling (Eiler et al., 1992), particularly if fluid is present. Graham et al. (1998) have estimated that preservation of profiles similar in scale to those observed here would require unrealistically rapid cooling rates of 100 – 600°C myr⁻¹ in the presence of water at grain boundaries. Thus they argue that cooling must have occurred under anhydrous conditions, wherein oxygen diffusion rates in ‘dry’ calcite (Anderson, 1969, see Figure 8.2) are too slow to permit significant relaxation of the profiles at cooling rates > 1°C myr⁻¹ from initial temperatures of ~ 600°C or less.

Two metamorphic fluid infiltration events?

Taken together, the stable isotope and CL imaging evidence discussed in Chapter 9 indicate that the diffusion profiles resulted from a short-lived, but extensive fluid infiltration event which occurred during or near peak-metamorphic conditions, recorded by the bright orange luminescent calcite. In discussion of the luminescence characteristics of CT53 in Chapter 9, I discussed the nature of pale orange brown luminescence within the large calcite grains and pointed out that it is largely parallel to, but pre-dates the later bright orange luminescent vein network in the central part of the slide (Figure 9.8). I have also suggested in Chapter 9 that there is evidence in the stable isotope data for two fluid infiltration events which have reset the oxygen isotope characteristics of the Torulian Limestone (Chapter 9). The first lowered $\delta^{18}\text{O}$ values from at least 22 ‰ to ~17 ‰, affecting in particular the lower of the two limestone units (Chapter 9, Figure 9.6a). This event is recorded by the pale orange brown luminescent calcite which occupies the relict fracture network in Figure 9.8. The second event resulted in reduction of $\delta^{18}\text{O}$ of ~17‰ to 10 – 13 ‰. This second event may have been more localised, but, as with the first, it appears to have had more effect in the lower limestone (Figure 9.6a). I consider that *both* these events record high temperature metamorphic fluid infiltration at or near the peak of metamorphism, but that they occurred separately. If the estimates of time for fluid infiltration are correct, then these events would have been very short-lived compared to the metamorphic event. Indeed, it is quite possible that the Torulian Limestone at this locality may have undergone several infiltration events during metamorphism.

Limestone

It is notable that the lower limestone is sandwiched between semipelite units, the lowermost of which is approximately 2 m thick. Moreover, the lower semipelite sits on the thick, pure Appin Quartzite. During deformation, the quartzite is likely to have acted as a highly competent body against which the semipelite would have deformed, thereby creating transient permeability in a strongly anisotropic lithology. In addition, because of the purity of the quartzite, dihedral angle constraints (Holness, 1995) indicate that it should be impermeable where undeformed – a likely scenario within the thick quartzite, away from its boundary with the semipelite. Thus it is also likely to have acted as an aquetard. It is quite reasonable to argue, therefore, for a high, layer-parallel fluid flux of low $\delta^{18}\text{O}$ fluid being focussed in the semipelite during prograde metamorphism and D_2 deformation and that this fluid affected the lower limestone much more than the thicker, upper limestone. The limestone sits structurally as well as stratigraphically above the semipelite. Assuming that the limestone has remained structurally above of the semipelite and obliquely orientated to the vertical for the larger part of its orogenic history, then it can be argued that the lower limestone would have seen more of the fluid because buoyancy forces acting on escaping fluid would have resulted in an element of cross-structure flow. This would give rise to asymmetric infiltration profiles similar to those observed in metabasite sheets across the Ardrishaig Anticline in the Southwest Scottish Highlands (cf. Graham et al., 1997; Skelton et al., 1995).

Infiltration into the limestone is likely to have been facilitated by hydrofracturing and by deformation (see Chapter 3). The steady decline in $\delta^{18}\text{O}$ from

the top of the thicker limestone unit towards the base of the lower limestone (Figure 9.7a) indicates that this infiltration was progressively limited across the limestone as a whole. Indeed, it could be argued that the semipelite unit which separates the upper and lower limestones acted as a short circuit fluid pathway, preventing the fluid which had infiltrated the lower limestone penetrating the upper limestone.

Source of fluid(s) The evidence for two fluid infiltration events *implies* that there were two separate fluid sources. In the first event, $\delta^{18}\text{O}$ of the fluid is estimated to have been about 13-15 ‰, based on SIMS analyses of the paler orange brown luminescent calcite in the relict fracture networks. This fluid interacted extensively with the rock. The fluid which infiltrated during the second event appears to have had a rather lower $\delta^{18}\text{O}$ of approximately 9 – 10 ‰, as indicated by SIMS analyses of the bright luminescent veins and patches. Overall, the low $\delta^{18}\text{O}$ values suggest a thoroughly metamorphic fluid source, probably derived largely from devolatilisation of the locally abundant pelitic and semipelitic rocks (cf. data in Rye et al., 1976). However, the second fluid with $\delta^{18}\text{O}$ of 9 – 10 ‰ may have had a magmatic component.

10.3.4 Summary

- Modelling of the grain-scale oxygen isotope profiles in CT53 indicates that they are consistent with having been formed by volume diffusion of oxygen, based on fits to the diffusion equation
- Dt values occupy a narrow range in values from 2.53×10^{-9} to 1.24×10^{-8}

- Estimates of time derived from Dt indicate infiltration time-scales are of the order of 10^2 to 10^4 years at temperatures in the range 550 – 600°C, the likely possible maximum metamorphic temperatures for the Tomintoul area
- There is evidence for two main infiltration events; evidence for both comes from CL images and $\delta^{18}\text{O}$ analyses, but only the latter has left recognisable diffusion profiles
- Fluid infiltration was not facilitated by local faulting
- Consideration of the likely physical properties of quartzite, semipelite and limestone and structure at the locality, suggests that fluid flow would have been focussed in the semipelite and largely layer parallel, but that there was a cross-layer component of fluid infiltration into the limestone facilitated by hydrofracture and deformation.
- Following infiltration, fluid must have escaped rapidly to allow the profiles to be preserved at normal orogenic cooling rates.

10.4 Calcite-quartz oxygen isotope fractionation in the Inchrory Limestone

In this final section, I discuss the fractionation of oxygen isotopes between calcite and quartz in Inchrory Limestone samples LWQ1/28 and LWQ1/30. These two samples are just four centimetres apart in the sample profile from Limeworks Quarry (Chapter 9) and yet display significant differences in their quartz – calcite $\delta^{18}\text{O}$ fractionation. The analysis is largely qualitative, but I aim to show that both the grain-size and the mineral mode have been important in the evolution of the oxygen isotope evolution of the two samples. I have summarised the salient data for the two samples in Table 10.3.

Sample	Phase	Approx. Mode (%)	Grainsize (μm)	Range in $\delta^{18}\text{O}$ (‰)			Altered fsp domain half-width
				Unaltered fsp domain		Altered fsp domain	
LWQ1/28	Calcite	~70	~ 300 - 500	20.4 - 26.9	core rim/axis	23.0 - 25.3 20.7 - 23.7	500 μm
	Quartz	10 - 15	up to ~100	23.5 - 26.1	off axis axis	22.4 - 23.1 20.3 - 21.3	
	Feldspar	15 - 20	up to ~100				
LWQ1/30	Calcite	~40	~100 - 200	23.2 - 27.0	off-axis axis	22.4 - 26.4 15.7 - 17.6	850 μm
	Quartz	25	~100		off-axis axis	21.8 - 26.9 19.6 - 27.6	
	Feldspar	35	~100				

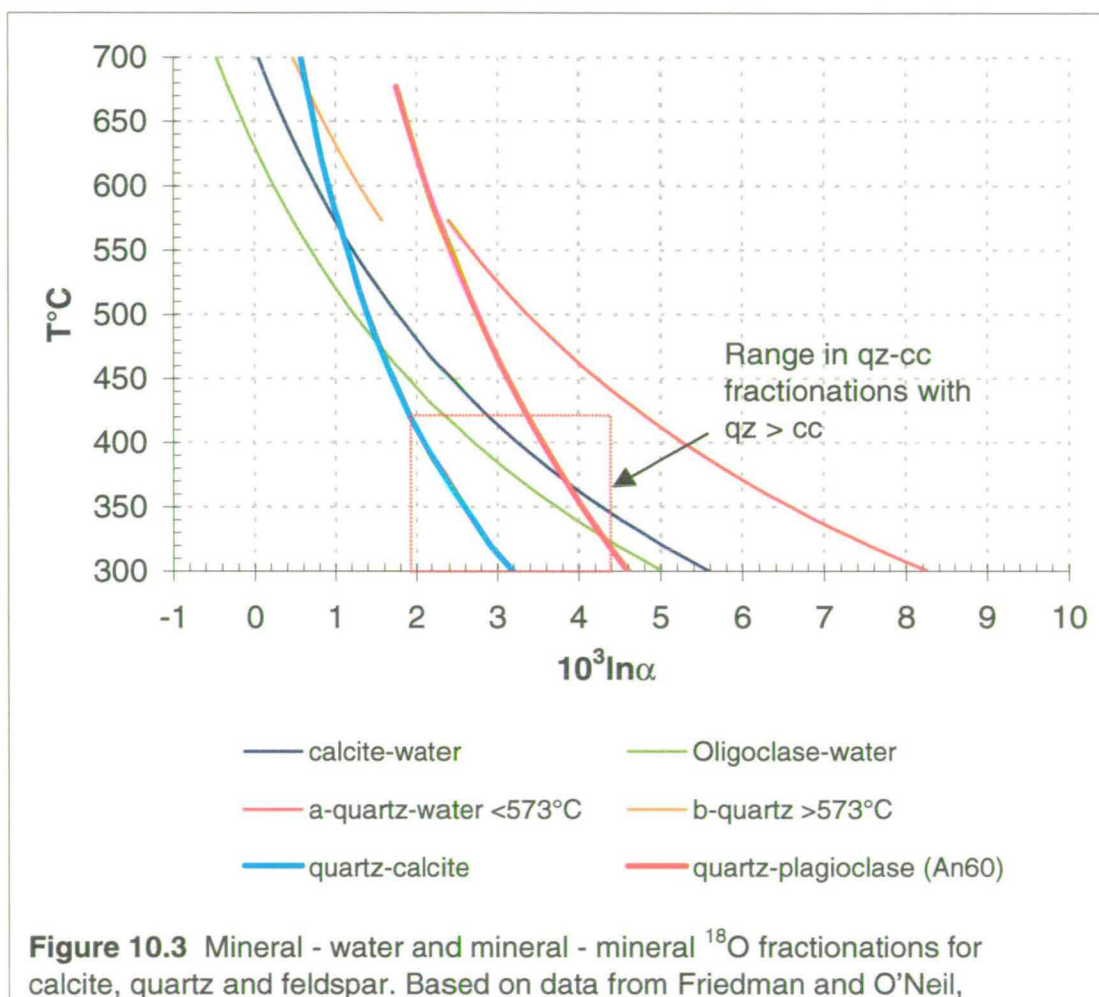
Table 10.3 Summary of features and $\delta^{18}\text{O}$ compositions of calcite, quartz and feldspar in the samples LWQ1/28 and LWQ1/30

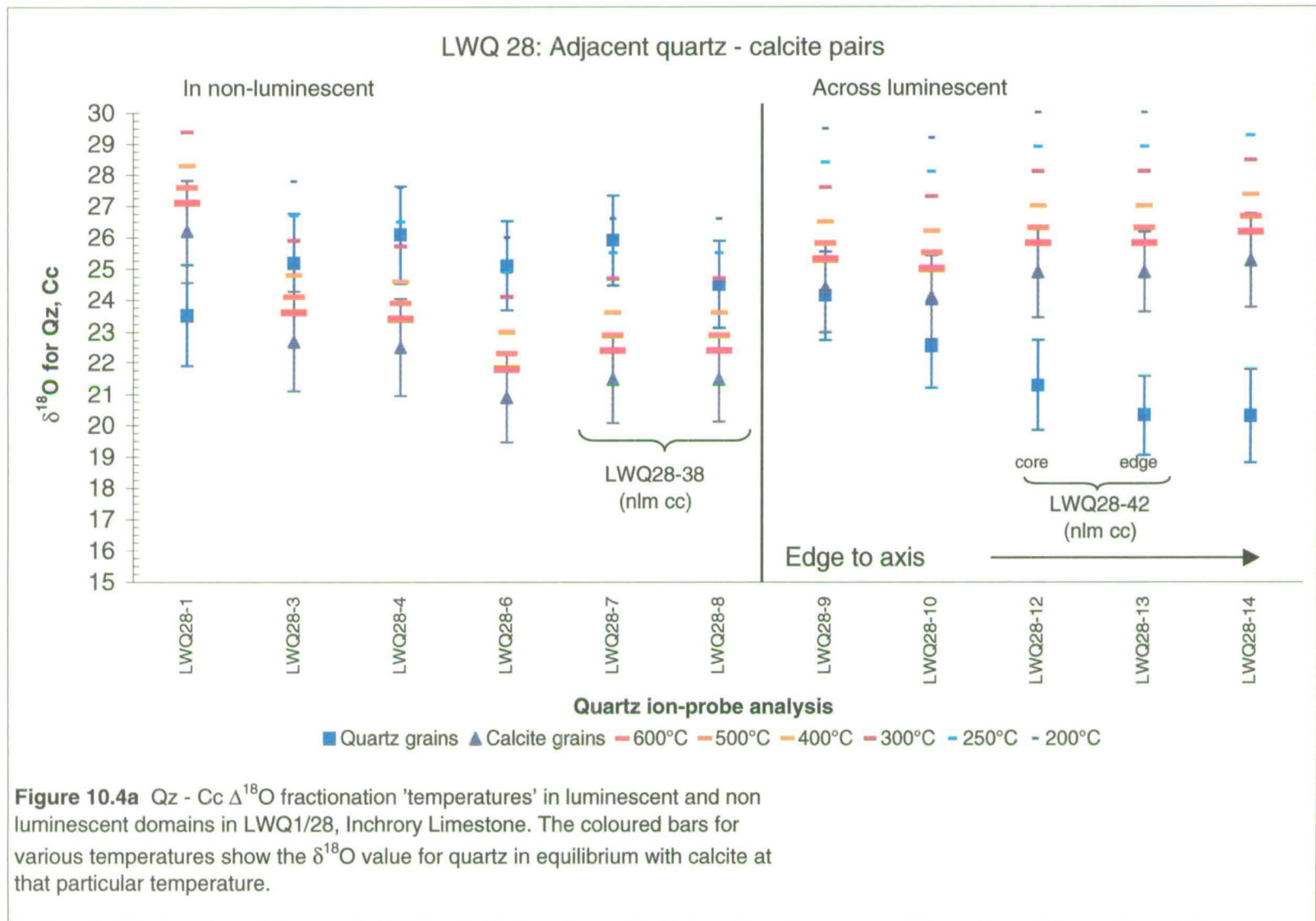
10.4.1 Are quartz and calcite in oxygen isotope equilibrium?

The two samples (LWQ1/28, LWQ1/30) contain only calcite, quartz and feldspar; oligoclase is altered to albite in the halos of microveins (Chapter 9). The equilibrium fractionation of ^{18}O into these three minerals should be in the order quartz > calcite > feldspar (see Figure 10.3). O'Neil (1986) cites three criteria for the presence of isotopic equilibrium (here $\delta^{18}\text{O}$) between minerals:

- lack of isotopic reversals (i.e. fractionations should follow the above order, with quartz being the most ^{18}O – rich phase,
- lack of unusually large fractionations,
- concordancy of isotope fractionation temperatures between the n-1 phases in the rock.

With regard to calcite and quartz $\delta^{18}\text{O}$ fractionation, both samples fail all the criteria. Although domains in the samples locally have $\delta^{18}\text{O}_{\text{qz}} > \delta^{18}\text{O}_{\text{cc}}$ (e.g. Domain A in LWQ1/28; Figures 9.13, 9.26), the fractionations are large and the isotope fractionation temperatures indicated are low and inconsistent (Figure 10.4). They do not indicate equilibration at peak metamorphic conditions (500 – 600°C). The presence of $\delta^{18}\text{O}_{\text{qz}} > \delta^{18}\text{O}_{\text{cc}}$ fractionations suggests that calcite and quartz may once have been in isotopic equilibrium, but have been strongly reset subsequently; they are not in equilibrium as would be anticipated by a conventional view of isotope fractionation. Indeed, within domains showing ‘correct’ quartz – calcite fractionations, there are also reversals, where calcite grains immediately adjacent to quartz veins are heavier in $\delta^{18}\text{O}$ (e.g. see calcite analysis 37 and quartz analysis 1 in Figure 9.26). Possible mechanisms to account for resetting of the oxygen isotope





fractionation between adjacent calcite and quartz grains are slow cooling (e.g. Eiler et al., 1992) and/or interaction with an infiltrating fluid of low $\delta^{18}\text{O}$. The possible mechanisms will be discussed further below.

Matters are more complex within the halos of altered feldspar on either side of the microvein networks of bright yellow luminescent calcite (Figures 9.27, 9.28). In LWQ1/28, quartz $\delta^{18}\text{O}$ values are consistently less than those of calcite cores, but are about the same as rim values. Quartz $\delta^{18}\text{O}$ values also decline towards the microvein (Figure 9.27b and Figure 10.4a), where they are the same, within error, as the calcite $\delta^{18}\text{O}$ values. This decline in quartz values is counter-intuitive: the microvein and altered feldspar are clear evidence for fluid infiltration (see also discussion in Chapter 9) and one would expect the calcite to show extensive alteration rather than quartz, because of the faster diffusion rate of oxygen in calcite relative to quartz.

In LWQ1/30, the opposite situation is observed: calcite $\delta^{18}\text{O}$ values are lower than those of nearby quartz grains (Figure 10.4b). Both quartz and calcite $\delta^{18}\text{O}$ values appear to increase towards the microvein axis, but both are lower within the axis itself.

The oxygen isotope disequilibrium both within and between phases within the halos is clear, and consistent with the petrographical evidence for fluid infiltration. How can the observed differences in oxygen isotope behaviour in the quartz and calcite in these two samples be resolved, if at all? I discuss a possible solution in the next section.

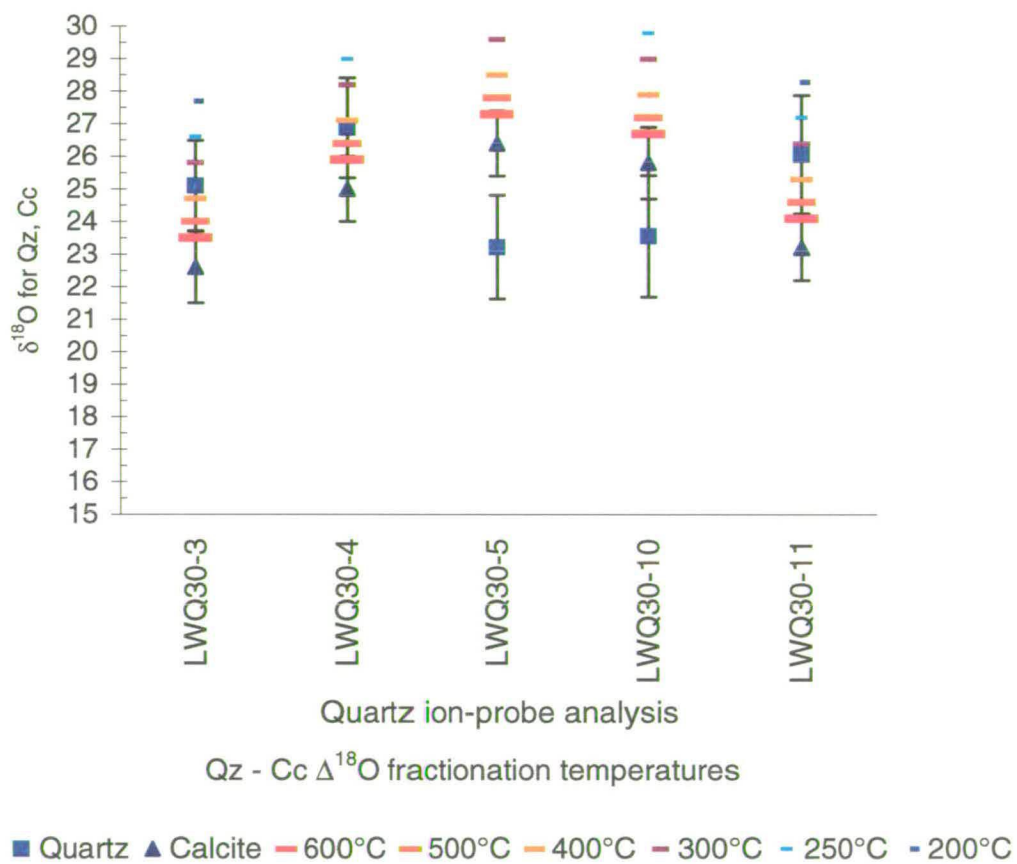


Figure 10.4b Qz - Cc $\Delta^{18}\text{O}$ fractionation 'temperatures' in the altered feldspar domain in LWQ1/30, Inchroty Limestone. Coloured bars as for Figure 10.4a

10.4.2 The influence of grain-size and modal mineralogy on oxygen isotope fractionation in LWQ1/28 and 1/30

There are three important features which differ markedly between the two samples, as summarised in Table 10.3:

- **mode:** calcite is much more abundant in LWQ1/28, but only slightly more abundant than the siliciclastic phases in LWQ1/30, where both feldspar and quartz are much more abundant.
- **grain-size:** calcite is much coarser grained overall in LWQ1/28, where it is also generally much more than twice the size of siliciclastic grains; in LWQ1/30 calcite is the same size or only slightly larger than the quartz and feldspar.
- the half-width of the halo in LWQ1/28 is $\sim \frac{2}{3}$ that of the halo in LWQ1/30.

These differences are important and probably hold the key to understanding the oxygen isotope fractionation characteristics of these samples. I believe the rocks have exchanged oxygen with an infiltrating fluid phase by a combination of reaction and diffusion.

The role of feldspar

In both samples, the feldspar is very heavily altered to albite within the halos, relict oligoclase being preserved in the cores and in irregular patches. This alteration is probably due to interaction with a sodic fluid, since there is local whole-scale alteration to albite, rather than just the development of peristerite exsolution patches. The alteration of the feldspar and the fracture-like nature of the microvein indicate

infiltration facilitated by hydrofracture (note also the veins lie oblique to the calcite elongation directions in LWQ1/28 and 1/30).

Exchange of oxygen isotopes between fluid and feldspar would thus have been facilitated dominantly by reaction involving Na and Ca exchange between fluid and feldspar. Because of this exchange reaction, the feldspar, rather than calcite or quartz, would have been the dominant buffer of $\delta^{18}\text{O}$ in the fluid phase – note that this exchange would have locally involved some 20 – 35% of the rock in the two samples (Table 10.3). If that was so, and if we assume that feldspar was in metamorphic equilibrium with quartz and calcite prior to infiltration, then, noting the likely relative quartz – feldspar $\delta^{18}\text{O}$ fractionation (approximately 2 – 2.5 ‰ at 550 – 600°C; see Figure 10.3), it would have buffered the (*unknown*) $\delta^{18}\text{O}$ of the fluid towards higher values, since it would have had $\delta^{18}\text{O}$ values of ~ 24 ‰, given peak quartz $\delta^{18}\text{O}$ values of ~ 27 ‰. Unfortunately, insufficient time was available to obtain feldspar $\delta^{18}\text{O}$ analyses with which to test this hypothesis.

Is this consistent with indications of a lower fluid $\delta^{18}\text{O}$ in LWQ1/30 (≤ 15.7 ‰) compared to that in LWQ1/28 (≤ 20.7 ‰), as estimated from SIMS analyses of luminescent calcite in the axis of the altered feldspar domains? The axis- to boundary-width of the altered domain in LWQ1/30 is about 1.5 times the width of that in LWQ1/28. This suggests that the infiltration was more extensive or longer lasting in the former sample, involving a greater flux of fluid and exceeding the local buffer capacity of the feldspar, so that the fluid maintained a more ^{18}O -depleted composition. Indeed, the abundance of feldspar may have rendered the rock more permeable because of its reactivity with the fluid.

Oxygen isotope exchange in calcite and quartz – grain-size and diffusion controls

Feldspar very readily exchanges $\delta^{18}\text{O}$ with fluids (e.g. Forester and Taylor (1977).

This may occur by rapid diffusion, or, as seems more likely in this case, by exchange during reaction with the fluid. Thus, the buffering of the fluid $\delta^{18}\text{O}$ by feldspar may have been sufficient to reduce the effects the fluid had on the quartz and calcite.

However, the calcite and quartz have clearly interacted variably and locally with a fluid of lower $\delta^{18}\text{O}$. In the case of these two minerals, any oxygen isotope exchange with the rock must have taken place by infiltration along micro-fractures, twin planes and grain-boundaries and then by diffusion; there is no alteration in quartz and calcite grain-shape or major petrographical characteristics within the altered feldspar domains, other than the luminescence picking out fluid pathways in the calcite. Exchange facilitated by solution-reprecipitation was very limited in extent and, therefore, this was not a significant mechanism for isotope exchange.

As a limiting case, the different calcite – quartz oxygen isotope fractionations across the altered feldspar domains in the LWQ samples may be considered to reflect the relative diffusivity of oxygen in calcite and quartz, which is a function of grain-size, as well as temperature.

Oxygen diffusion in quartz in the *presence of water* is at least an order of magnitude slower than that in calcite at metamorphic temperatures of 550 – 600°C (Farver, 1994; Farver and Yund, 1991) (Figure 10.5). Thus the extent of isotopic resetting by diffusion in either quartz and calcite is a function of the grain-size as well as time an temperature and time. The grain-size effect can be modelled semi-quantitatively by considering the relative diffusion distances in quartz and calcite with varying temperature.

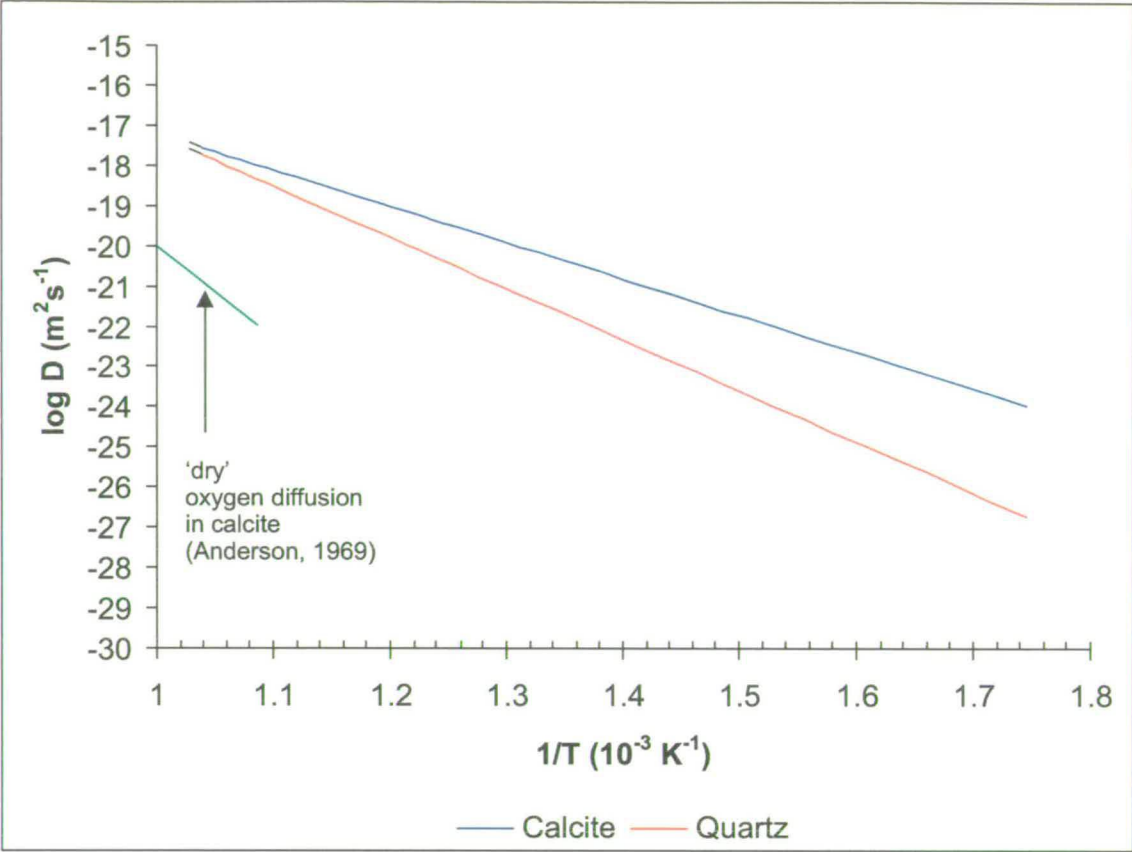


Figure 10.5 Arrhenius plot of oxygen diffusion in calcite and quartz in the presence of water. Calcite data from Farver, 1994 and quartz data from Farver and Yund 1991. The diffusion of oxygen in calcite under dry conditions is shown for comparison..

Two equations of the form (10.3) for calcite and quartz can be combined and rearranged to give an expression for the diffusion distance in calcite relative to a diffusion distance in quartz, here defined as half the grain diameter, and temperature:

$$x_{cc} = (D_{cc}^T / D_{qz}^T)^{1/2} \bullet x_{qz} \quad (10.4)$$

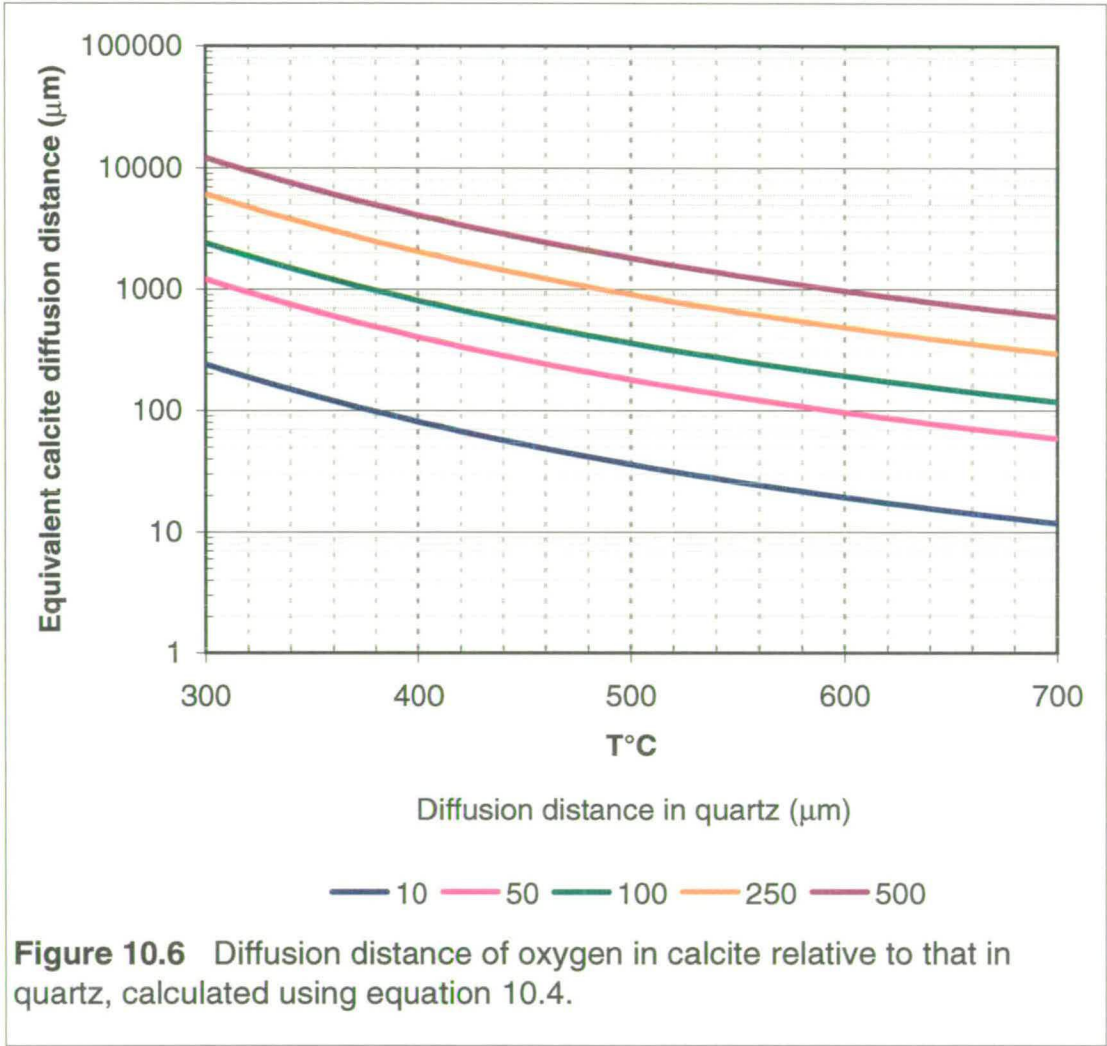
where:

$D_{cc, qz}^T$ are the diffusivities of oxygen in calcite and quartz at the same temperature, and

x_{qz} is the diffusion distance in quartz.

(Note: all the assumptions required in use of equation 10.1 apply here also, including the assumption that, at the grain boundary, quartz, calcite and fluid maintain equilibrium). The results are shown in Figure 10.6, where x_{cc} is plotted against temperature. This plot can be used semi-quantitatively to understand the features of calcite – quartz oxygen isotope fractionation across the altered feldspar domains in the LWQ samples.

In LWQ1/28, the quartz grain size is approximately 100 μm , so that the effective diffusion distance is 50 μm . Figure 10.6 shows that, at 600°C, for a diffusion distance of 50 μm in quartz, the diffusion distance in calcite is ~100 μm ; this increases to 200 μm at 500°C. Given that the diameter of calcite grains in LWQ1/28 is at least 3 time larger than that of quartz, the results indicate that even though quartz and calcite rim $\delta^{18}\text{O}$ compositions may be reset, calcite cores will remain unaffected in this sample where diffusion occurred at high temperatures. Quartz grains are thus reset to lower values in the altered feldspar domain, while calcite cores retain their high values and the rims are reset (Figure 9.26b), in accordance with the predictions of the diffusion model.



In LWQ1/30, the oxygen isotope data across the altered feldspar domain are ambiguous, particularly because of the decline in quartz and calcite $\delta^{18}\text{O}$ values towards the margins of the domain. However, calcite is only a little larger than the quartz in this sample, but is generally more ^{18}O depleted than the latter. Also, the larger quartz grains *generally* preserve higher $\delta^{18}\text{O}$ values. This is *consistent* with the interpretation that the calcite grain-size is too small to ‘protect’ the cores from diffusional exchange with the fluid. If the fluid which reset $^{18}\text{O}/^{16}\text{O}$ in the calcite and quartz is the same fluid which altered the feldspar, then the reason(s) for the occurrence of lower $\delta^{18}\text{O}$ values in quartz and calcite grains towards the margins of the altered feldspar domains is/are unclear. The inconsistency in the data *may* be due to variations in grain boundary geometry relative to analytical sites. The sites may appear to be in the grain cores, but may be near to grain boundaries parallel to the plane of the section, because of the orientation of the section; the SIMS pits may, therefore, be sampling diffusionally exchanged grain margins.

Time-scale of fluid infiltration in the LWQ samples

It is possible to get at least a first-order estimate of the time-scale of fluid infiltration in these two limestones using a temperature – log time plot for both quartz and calcite, contoured by characteristic diffusion distance. This I have done using the same approach used for the Torulian Limestone sample, as discussed in section 10.2.2. I have plotted the characteristic diffusion distances for oxygen in calcite and quartz in Figure 10.7. For the likely diffusion distances in quartz and calcite estimated for LWQ1/28 (50 and 100 μm at 600°C, and 50 and ~200 μm at 500°C, respectively) the time-scales are of the order of $10^2 - 10^4$ years. The textural evidence

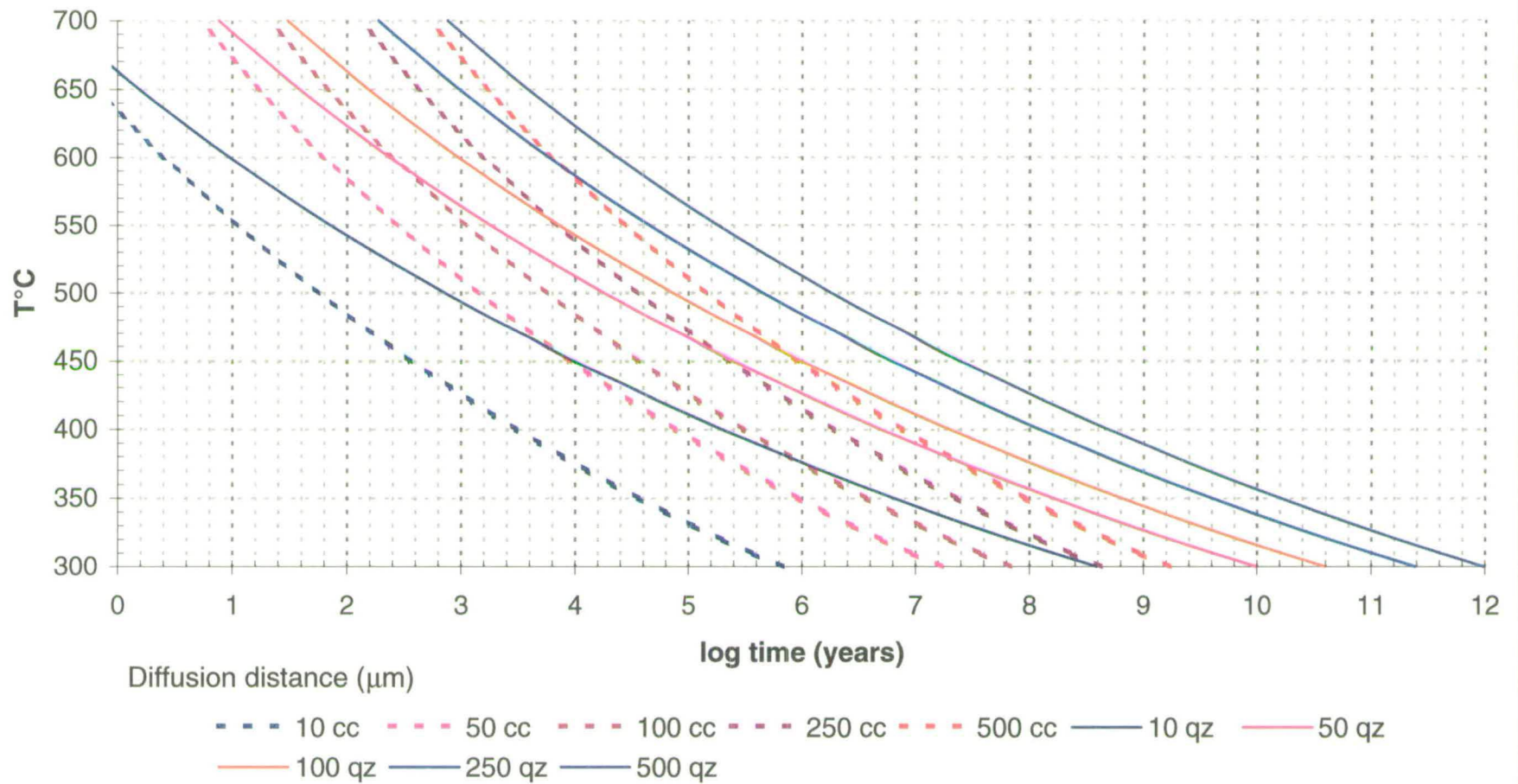


Figure 10.7 Relative time-scales for oxygen diffusion in calcite and quartz, contoured for characteristic diffusion distances

suggests that cracking, accompanied by feldspar reaction, facilitated infiltration over domain widths of ~ 1.5 mm, suggesting shorter, rather than longer time-scales. As with the evidence for the Torulian Limestone, I suggest that the time-scale for infiltration was unlikely to have been much greater than 10^3 years, and to have occurred at high temperatures. Although there may have been some diffusional resetting, I do not believe its effects to be significant because of the preservation of heterogeneities on a small scale which can be attributed largely to fluid infiltration at high temperatures. By analogy with the interpretation of the results from CT53, I suggest that the fluid escaped quickly and that the rocks cooled under anhydrous conditions, preventing significant diffusional re-equilibration.

Discussion

Isotope exchange and fractionation in multi-phase rocks is complicated by a number of factors, including resetting on cooling (Eiler et al., 1992). Eiler et al. (1992) show that fractionation of isotopes between phases in a multi-phase system during slow cooling is strongly a function of the mineral modes, their relative diffusivities and other factors, including temperature, grain shape and the isotropy, or otherwise, of diffusion in particular minerals. However, these factors *must* be important in general isotope diffusion processes and models similar to the fast grain-boundary model of Eiler et al. (*op. cit.*), which takes into account relative diffusivities and mass-balance, could be used to elucidate the isotopic evolution of rock such as these relatively simple limestones, particularly during fluid-rock interaction. The development of such modelling is beyond the scope of this thesis, but would represent a useful advance in aiming to understand the *integrated* behaviour of isotopes in a rock during

fluid – rock interaction. An important consideration is the mass balance constraint and this is considered to have been significant in controlling the nature of isotopic fractionation in these samples, particularly the role played by the feldspar in buffering the fluid phase.

10.4.3 Summary

- Samples LWQ1/28 and 1/30 have suffered minor fluid infiltration along transient micro-vein networks which resulted in the alteration of feldspar from oligoclase to albite.
- Although there is evidence to suggest that calcite and quartz approached oxygen isotope equilibrium during prograde metamorphism, the rocks are generally in a state of isotopic disequilibrium.
- Complex factors controlled the fractionation of oxygen isotopes between calcite and quartz in the limestone samples, including modal mineralogy and grain-size.
- Estimation of relative diffusion distances in calcite and quartz indicate that time scales were too short for oxygen diffusion to reset completely the larger calcite grains in LWQ1/28 and were probably 10^3 years or less at temperatures in excess of 500°C; this is consistent with the infiltration time scale estimates calculated for the Torulian Limestone.
- The abundance of feldspar is suggested to have been important in controlling fluid-rock interaction processes.

10.5 Conclusions

- Quantitative and semi-quantitative analysis of the stable isotope data in the samples of the Inchrory and Torulian limestones provide good evidence for fluid infiltration at high temperatures and for the infiltration being short-lived.
- In both rocks there is a general state of isotopic disequilibrium in which locally high ($\sim 25\%$), primary or near primary $\delta^{18}\text{O}$ values have been reset to metamorphic values (17% or less) by interaction with low $\delta^{18}\text{O}$ metamorphic fluids.
- Infiltration was facilitated by hydrofracture, solution-reprecipitation and diffusion in the Torulian Limestone. In the Inchrory Limestone, infiltration was facilitated initially by hydrofracture, but was also likely to have been facilitated by interaction with feldspar.
- In both rocks, estimates of infiltration time-scales ($10^2 - 10^4$ years) are short relative to the likely duration of the metamorphic event(s) to which they are likely to be related. As in other studies, this is consistent with non-pervasive fluid infiltration of limestones by transient permeability, largely created by hydrofracturing mechanisms.
- Fluid-rock interaction in the Torulian Limestone was much more extensive than that in the Inchrory Limestone.

Chapter 11

Summary, conclusions and suggestions for further work

11.1 Summary and conclusions

I have determined the strontium, carbon and oxygen isotope compositions of metamorphosed Dalradian limestones and dolostones and undertaken detailed petrological and microchemical work on these and calc-silicate rocks, with three broad aims:

- to determine the extent to which metamorphic fluid-rock interaction has modified original sedimentary/diagenetic chemical signatures in Dalradian metamorphosed limestones and dolostones,
- to elucidate the nature of any such original signatures with regard to the pre-metamorphic history of the carbonate rocks, and
- to elucidate and quantify the mechanisms and time-scales of fluid-rock interaction during metamorphism.

The thesis is divided into three distinct areas of work:

- Description of the lithological and petrological characteristics of metamorphosed Dalradian limestones, dolostones and calc-silicate rocks, and elucidation of fluid-rock interaction and fluid composition by the use of T-X_{CO₂} sections

- Determination of the $^{87}\text{Sr}/^{86}\text{Sr}$, $\delta^{13}\text{C}$ and $\delta^{18}\text{O}$ compositions of bulk-carbonate in the limestones and dolostones, their state of preservation and their implications for the age of the Dalradian and its wider correlation with other Neoproterozoic carbonate rock-bearing successions
- Determination of calcite and quartz $\delta^{18}\text{O}$ and calcite trace elements at the grain-scale in two limestones to elucidate the state of isotope equilibration and the characterisation and quantification of fluid-rock interaction during metamorphism.

I introduced the first part with an outline of the lithostratigraphy of Dalradian metamorphosed carbonate rocks, highlighting the importance of limestones near the base of the Grampian Group and those at the top of the Argyll Group, dated at 595 Ma. In Chapters 3 and 4, I described and discussed the petrology of the limestones, dolostones and calc-silicate rocks. The rocks are lithologically and petrologically diverse. Primary carbonate grains are locally preserved in limestones from the Southwest Scottish Highlands and Islay, where metamorphic grades only locally exceeded greenschist facies. Limestones from the Northeast Grampian Highlands of Scotland are thoroughly re-crystallised, with metamorphic textures, although dolostones associated with tillites at the base of the Islay Subgroup retain chemical zoning texture considered to result from dolomitisation. The petrology of the calc-silicate rocks from the Pitlurg Calcareous Flag Formation reveals complex phase relationships indicative of internal buffering, with no evidence of extensive infiltration by hydrous metamorphic fluid during metamorphism.

Part two of the thesis considers the whole-rock, bulk-carbonate strontium, carbon and oxygen isotope compositions of the limestones and dolostones. Grampian and Appin Group limestones are characterised by low $^{87}\text{Sr}/^{86}\text{Sr}$ values (0.7064 – 0.7075), commonly high $\delta^{13}\text{C}$ up to to $\sim 8\text{‰}$, and a wide range in $\delta^{18}\text{O}$ from (~ 6 to $\sim 25\text{‰}$). Low $^{87}\text{Sr}/^{86}\text{Sr}$ values are retained in Grampian Group Limestone samples, even in some limestones where both $\delta^{18}\text{O}$ and $\delta^{13}\text{C}$ are considerably depleted. $^{87}\text{Sr}/^{86}\text{Sr}$ in the Tayvallich, Boyne, Torr Head and Dungiven limestones from the top of the Argyll Group is considerably more radiogenic, with values in excess of 0.7080. However, the primary or near-primary $\delta^{13}\text{C}$ values are commonly $\sim 5 - 7\text{‰}$, again despite wide-ranging $\delta^{18}\text{O}$ values. The Leny Limestone is characterised by the most radiogenic $^{87}\text{Sr}/^{86}\text{Sr}$ (0.711 – 0.712) strongly negative $\delta^{13}\text{C}$ ($\sim -4\text{‰}$) and $\delta^{18}\text{O}$ values of $\sim 17\text{‰}$.

The data indicate very variable degrees of modification of primary isotope and trace element compositions by a variety of mechanisms due both to diagenesis and metamorphic fluid-rock interaction. For example, the Torulian Limestone at Bridge of Avon underwent extensive exchange during infiltration at amphibolite facies. Co-variation between $\delta^{13}\text{C}$ and $\delta^{18}\text{O}$ in the Tayvallich Limestone at Port an Sgadain can be interpreted as resulting from hydrothermally-driven fluid-rock interaction. Very low $\delta^{13}\text{C}$ in the Leny Limestone can be attributed to exchange with C from very abundant graphite in the limestones and adjacent mudrocks.

When compared with $^{87}\text{Sr}/^{86}\text{Sr}$ data from other, unmetamorphosed Neoproterozoic carbonate rock sequences for which estimates of age are available, the carbonate $^{87}\text{Sr}/^{86}\text{Sr}$ data for Dalradian limestones indicate strongly that the Dalradian is

younger than ~ 800 Ma. This age limit has particular relevance for the Dalradian because of the current debate concerning the status of a Neoproterozoic metamorphic event dated at $\sim 800 - 850$ Ma in the gneissose rocks in the Central Highlands of Scotland and its putative effects on Appin and Grampian Group rocks. The strontium data corroborate recently emerging lithostratigraphical evidence for a major, probably orogenic, unconformity at the base of the Grampian Group.

Appin and Grampian Group limestones are separated from uppermost Argyll Group limestones by the Varangan Port Askaig Tillite (~ 600 Ma). The shift from relatively low $^{87}\text{Sr}/^{86}\text{Sr}$ values in Appin and Grampian Group limestones to higher values in the limestones at the top of the Argyll Group is consistent with shifts in $^{87}\text{Sr}/^{86}\text{Sr}$ observed elsewhere in the world between carbonate rocks either side of Varangan/Marinoan tillite sequences.

Part three of the thesis presents and discusses detailed work on the variations in calcite $\delta^{18}\text{O}$ and $\delta^{13}\text{C}$ in outcrop-scale profiles, and on variations in $\delta^{18}\text{O}$ in calcite and quartz on the grainscale.

In an outcrop of the Torulian Limestone near Tomintoul, North East Grampian Highlands, there is a systematic increase in bulk-carbonate $\delta^{18}\text{O}$ from values of $\sim 11 - 14$ ‰ near the lower boundary of the limestone with underlying schistose pelite, to peak values of ~ 22 ‰ in the upper part of the limestone. $\delta^{18}\text{O}$ then decline slightly in the top boundary layer of the limestone where it is bounded by more pelite. The asymmetric profile is very similar to other outcrop-scale $\delta^{18}\text{O}$ profiles recorded in metamorphosed

limestones in other studies and which have been used to constrain metamorphic fluid fluxes using modelling based on chromatographic theory.

The profile is attributed to metamorphic fluid flow focussed in the underlying pelite. Fluid flow in the pelite was predominantly layer-parallel, but a significant cross-strike component of flow drove infiltration into the limestone from the structurally and stratigraphically lower boundary.

In contrast, in the Inchrory Limestone, also sampled near Tomintoul, a high resolution profile from the boundary of an amphibolite pod ~0.5 m into the limestone revealed no significant variation in bulk carbonate $\delta^{18}\text{O}$ or $\delta^{13}\text{C}$ with distance from the amphibolite. There is no evidence of isotopic exchange between the limestone and the amphibolite, nor any evidence of modification in $\delta^{18}\text{O}$, despite the partitioning of deformation some 10 to 12 cm into the limestone.

Cathodoluminescence imaging of samples from the Torulian and Inchrory Limestones reveal very different states of chemical equilibrium. CL images of the former reveal very extensive alteration and disequilibrium due to metamorphic fluid infiltration consistent with the strong modification of observed in bulk carbonate $\delta^{18}\text{O}$. The CL images of the Inchrory Limestone reveal limestone with generally good metamorphic textural equilibration and low luminescence, consistent with the lack of evidence from the bulk carbonate $\delta^{18}\text{O}$ data for metamorphic fluid infiltration. However, the CL imaging also reveals significant evidence for fluid infiltration along microfractures which have millimetre-scale haloes of albitised oligoclase feldspar.

Investigation of the spatial variations of $\delta^{18}\text{O}$ at the grain-scale in the two limestones reveals that both are in a state of considerable isotopic disequilibrium. This is

not surprising for the Torulian Limestone, but is so for the Inchrory Limestone, given the latter's apparent textural equilibrium in the CL images and the lack of variation in $\delta^{18}\text{O}$ on the outcrop scale. The scale of isotopic variation in *both* limestones is about 12 – 13 ‰.

In the Torulian Limestone, metamorphic fluid infiltration has resulted in the development of $\delta^{18}\text{O}$ diffusion gradients in calcite grains. Modelling of these gradients by fitting the profile data to the diffusion equation provides estimates of Dt which are significant at the 95 % level (as measured by χ^2). The Dt values give estimates of time for fluid infiltration on the order of 10^3 years at temperatures of $\sim 550^\circ\text{C}$.

In the Inchrory Limestone, both calcite and quartz show considerable disequilibrium in $\delta^{18}\text{O}$. Quartz-calcite oxygen isotope fractionations are large and commonly reversed. Variations in quartz and calcite $\delta^{18}\text{O}$ across the altered feldspar domains with axial micro-fractures filled with luminescent calcite, are different in the two limestones in which these domains are observed. The differences can be rationalised in terms of variation in modal abundance of oligoclase feldspar and its buffering effect on $\delta^{18}\text{O}$ of the fluid phase, in terms of absolute and relative variations in quartz and calcite grain-size between the two samples and the relationship between grain-size and diffusion distances in quartz and calcite. By considering the relative grain-size of quartz and feldspar in the two samples in terms of oxygen diffusivity in calcite and quartz in the presence of water, it is possible to obtain broad estimates of the likely time-scales of fluid infiltration at peak metamorphic temperatures. These range from 10^2 years at 600°C to 10^4 years at 500°C . Infiltration in these rocks was achieved by micro-cracking

resulting from hydrofracture. The time-scale estimates are consistent with theoretical estimates of the duration of micro-cracking on the order of 10^2 years.

My main conclusions are:

- metamorphism generally has had limited effect on the primary $^{87}\text{Sr}/^{86}\text{Sr}$ and $\delta^{13}\text{C}$ signatures in Dalradian limestones, especially in the absence of metamorphic fluid infiltration.
- Dalradian limestones are not well equilibrated isotopically, despite metamorphism at amphibolite facies.
- Where infiltration has occurred, it is possible to elucidate fluid-rock interaction mechanisms and to quantify likely time-scales for metamorphic fluid infiltration.
- With careful petrographic and analytical work, it is possible to determine pre-metamorphic isotope signatures in metamorphosed limestones and to use the isotopic data to help elucidate their pre-metamorphic geochemical evolution
- Knowledge of the degree and scale of equilibrium is crucially important in any interpretation of isotopes or, indeed, phase relations and is a recurring theme in this thesis (Chapters 4, 9, 10)
- Diagenesis is likely to be the most important agent for extensive modification of isotope and trace element compositions in limestones and dolostones; modifications arising from metamorphic fluid-rock interaction will be generally much limited, although they are important locally (from a geographical point of view).

- Dalradian limestones commonly preserve primary or near-primary $^{87}\text{Sr}/^{86}\text{Sr}$ and $\delta^{13}\text{C}$ values. The strontium isotope data are particularly significant as they constrain the age of the Dalradian to be younger than 800 Ma.

11.2 Suggestions for further work

Strontium isotopes

I have shown that the limestones are poorly equilibrated with respect to oxygen isotopes on the grain-scale. It would be very interesting to determine whether this heterogeneity extended to strontium isotopes. It is reasonable to anticipate this, because diffusion rates for Sr in calcite will be orders of magnitude slower than for oxygen. The carbonate $^{87}\text{Sr}/^{86}\text{Sr}$ data are based on bulk carbonate powders. They are, therefore, averages, and show considerable variation relative to the analytical precision possible in determinations of $^{87}\text{Sr}/^{86}\text{Sr}$ in carbonates. At present, grain-scale analysis of $^{87}\text{Sr}/^{86}\text{Sr}$ is not possible by in-situ techniques, such as SIMS, although new developments in laser ablation technology allied to mass spectrometry may make this possible soon. Knowledge of the grain-scale variation would allow determination of the true range in $^{87}\text{Sr}/^{86}\text{Sr}$ in a similar fashion to the oxygen isotope data.

U-Pb and Pb-Pb dating of the limestones

The secular $^{87}\text{Sr}/^{86}\text{Sr}$ 'seawater' curve for the Neoproterozoic shows important shifts in $^{87}\text{Sr}/^{86}\text{Sr}$ at key times in Neoproterozoic history. However, the ages of the data used to constrain the curve are not well constrained, particularly in the Riphean. I suggest that Pb-Pb and/or U-Pb dating of suitable limestone samples (cf. Jahn and Cuvellier, 1994;

Zachariah, 1999) which can be shown to retain low $^{87}\text{Sr}/^{86}\text{Sr}$ and high $\delta^{18}\text{O}$ may have potential for constraining the curve more precisely and help date the age of Dalradian sedimentation more precisely.

The variation in $^{87}\text{Sr}/^{86}\text{Sr}$ across the Port Askaig Tillite

The variation in $^{87}\text{Sr}/^{86}\text{Sr}$ across the Port Askaig Tillite and other Varangan and Marinoan tillites is well established. Further work on Islay may help constrain the rate of this change still further. I have not examined the Lossit Limestone in this study. This lies with local unconformity upon the Ballygrant Formation in North Islay, but beneath the Port Askaig Tillite. Furthermore, although much of the Bonahaven Formation is dolomitised, there are one or two small domains within which calcitic limestones with radial oolites are preserved. $^{87}\text{Sr}/^{86}\text{Sr}$ data on these and other potential targets on Islay could be of considerable value in extending our knowledge of variations in $^{87}\text{Sr}/^{86}\text{Sr}$ at around 600 Ma.

Modelling of modal abundance and grain-size controls on oxygen isotope exchange in metamorphic rocks

The variations in $\delta^{18}\text{O}$ revealed in the Inchrory Limestone within the altered domains are interpreted in terms of a combination of fluid isotope buffering by reaction exchange, modal abundance and relative grain-size controls on diffusion distances. The mineralogy of the limestone is simple and the isotope exchange and diffusion characteristics of the quartz, calcite and feldspar are well known. This suggests that it might be possible to formulate a generalised quantitative model for quantifying fluid-rock interaction more

rigorously in these limestones by combining mass balance, reaction exchange and diffusion constraints, possibly in a similar manner to the fast grain boundary model of Eiler et al., (1992).

References

- Anderson, T. F., 1969, Self-diffusion of carbon and oxygen in calcite by isotope exchange with carbon dioxide: *Journal of Geophysical Research*, v. 74, p. 3919-3932.
- Anderton, R., 1985, Sedimentation and tectonics in the Scottish Dalradian: *Scottish Journal of Geology*, v. 21, p. 407-436.
- Anderton, R., 1988, Dalradian slides and basin development: a radical interpretation of stratigraphy and structure in the SW and Central Highlands of Scotland: *Journal of the Geological Society, London*, v. 145, p. 669-678.
- Anderton, R., and D. R. Bowes, 1983, Precambrian and Palaeozoic rocks of the Inner Hebrides: *Proceedings of the Royal Society of Edinburgh*, v. 83B, p. 31-45.
- Anovitz, L. M., and E. J. Essene, 1987, Phase Equilibria in the System CaCO_3 - MgCO_3 - FeCO_3 : *Journal of Petrology*, v. 28, p. 389-414.
- Arita, Y., and H. Wada, 1990, Stable isotopic evidence for migration of metamorphic fluids along grain boundaries of marbles: *Geochemical J.*, v. 24, p. 173-186.
- Ashcroft, W. A., B. C. Kneller, A. G. Leslie, and M. Munro, 1984, Major shear zones and autochthonous Dalradian in the north-east Scottish Caledonides: *Nature*, v. 310, p. 760-762.
- Asmerom, Y., S. B. Jacobsen, A. H. Knoll, N. J. Butterfield, and K. Swett, 1991, Strontium isotope variations of Neoproterozoic seawater: Implications for crustal evolution: *Geochimica et Cosmochimica Acta*, v. 55, p. 2883-2894.
- Atkinson, B. K., 1984, Subcritical crack growth in geological materials: *Journal of Geophysical Research*, v. 89, p. 4077-4114.
- Baker, A. J., 1985, Pressures and temperatures of metamorphism in the eastern Dalradian: *Journal of the Geological Society, London*, v. 142, p. 137-148.
- Baker, J., 1990, Petrological and isotopic constraints on metamorphism and metamorphic fluid flow on Naxos, Greece: PhD thesis, University of Cambridge, Cambridge, 293 p.

- Baker, J., and A. Matthews, 1995, The stable isotope evolution of a metamorphic complex, Naxos, Greece: *Contributions to Mineralogy and Petrology*, v. 120, p. 391-403.
- Baker, J., and M. Spiegelman, 1995, Modelling an infiltration-driven geochemical front: *Earth and Planetary Science Letters*, v. 136, p. 87-96.
- Baker, J., M. J. Bickle, I. S. Buick, T. J. B. Holland, and A. Matthews, 1989, Isotopic and petrological evidence for the infiltration of water-rich fluids during the Miocene M2 metamorphism on Naxos, Greece: *Geochimica et Cosmochimica Acta*, v. 53, p. 2037-2050.
- Baker, J., T. J. B. Holland, and R. Powell, 1991, Isograds in internally buffered systems without solid solutions: principles and examples: *Contributions to Mineralogy and Petrology*, v. 108, p. 170-182.
- Banner, J. L., and G. N. Hanson, 1990, Calculation of simultaneous isotopic and trace element variations during water-rock interaction with applications to carbonate diagenesis: *Geochimica et Cosmochimica Acta*, v. 54, p. 3123-3137.
- Bartley, J. K., M. Pope, A. H. Knoll, M. A. Semikhatov, and P. Y. Petrov, 1998, A Vendian - Cambrian boundary succession from the Northwestern margin of the Siberian Platform: stratigraphy, palaeontology, chemostratigraphy and correlation: *Geological Magazine*, v. 135, p. 473-494.
- Bathurst, R. G. C., 1975, Carbonate Sediments and their diagenesis: *Developments in Sedimentology*, v. 12: Amsterdam, Elsevier, 620 p.
- Beddoe-Stephens, B., 1990, Pressures and temperatures of Dalradian metamorphism and the andalusite-kyanite transformation in the northeast Grampians: *Scottish Journal of Geology*, v. 26, p. 3-14.
- Bentley, M. R., 1988, The Colonsay Group, *in* J. A. Winchester, ed., *Later Proterozoic stratigraphy of the Northern Atlantic regions*, Glasgow and London, Blackie, p. 119-130.
- Bentley, M. R., A. J. Maltman, and W. R. Fitches, 1988, Colonsay and Islay: a suspect terrane within the Scottish Caledonides: *Geology*, v. 16, p. 26-28.
- Benus, A. P., 1988, Sedimentological context of a deep-water Ediacaran fauna (Mistaken Point Formation, Avalon Zone, Eastern Newfoundland), *in* E.

- Landing, G. Narbonne, and P. Myrow, eds., Trace Fossils, Small Shelly Fossils, and the Precambrian-Cambrian boundary:: New York State Museum Bulletin, The University of the State of New York, The State Education Department, Albany, New York, p. 8-9.
- Bertrand, S. J., and P. A. Mossine, 1983, Platform-to-basin facies evolution; the carbonates of late Proterozoic (Vendian) Gourma (West Africa): *Journal of Sedimentary Petrology*, v. 53, p. 275-293.
- Bickle, M. J., and J. Baker, 1990, Advective-diffusive transport of isotopic fronts: an example from Naxos, Greece: *Earth and Planetary Science Letters*, v. 97, p. 78-93.
- Bickle, M. J., and H. J. Chapman, 1990, Strontium and oxygen isotope decoupling in the Hercynian Trois Seigneurs Massif, Pyrenees: evidence for fluid circulation in a brittle regime: *Contributions to Mineralogy and Petrology*, v. 104.
- Bickle, M. J., and D. MacKenzie, 1987, The transport of heat and matter by fluids during metamorphism: *Contributions to Mineralogy and Petrology*, v. 95, p. 384-392.
- Bickle, M. J., H. J. Chapman, S. M. Wickham, and M. T. Peters, 1995, Strontium and oxygen isotope profiles across marble-silicate contacts, Lizzies Basin, East Humboldt Range, Nevada: constraints on metamorphic permeability and fluid flow: *Contributions to Mineralogy and Petrology*, v. 121, p. 400-413.
- Bickle, M. J., H. J. Chapman, J. M. Ferry, D. Rumble III, and A. E. Fallick, 1997, Fluid Flow and Diffusion in the Waterville Limestone, South-Central Maine: Constraints from Strontium, Oxygen and Carbon Isotope Profiles: *Journal of Petrology*, v. 38, p. 1489-1512.
- Blundy, J. D., and T. J. B. Holland, 1990, Calcic amphibole equilibria and a new amphibole-plagioclase geothermometer: *Contributions to Mineralogy and Petrology*, v. 111, p. 208-224.
- Bowen, N. L., 1940, Progressive metamorphism of siliceous limestone and dolomite: *Journal of Geology*, v. 48, p. 225-274.

- Brasier, M. D., and D. McIlroy, 1998, *Neonereites uniserialis* from c. 600 Ma year old rocks in western Scotland and the emergence of animals: *Journal of the Geological Society, London*, v. 155, p. 5-12.
- Brasier, M. D., M. M. Anderson, and R. M. Corfield, 1992, Oxygen and carbon isotope stratigraphy of early Cambrian carbonates in southeastern Newfoundland and England: *Geological Magazine*, v. 129, p. 265-279.
- Brasier, M. D., G. Shields, V. N. Kuleshov, and E. A. Zhegallo, 1996, Integrated chemo- and biostratigraphic calibration of early animal evolution: Neoproterozoic - early Cambrian of southwest Mongolia: *Geological Magazine*, v. 133, p. 445-485.
- Brennan, J., 1991, Development and Maintenance of Metamorphic Permeability: Implications for Fluid Transport, *in* D. M. Kerrick, ed., *Contact Metamorphism: Reviews in Mineralogy*, Washington, DC, Mineralogical Society of America, p. 291-319.
- Burke, W. H., R. E. Denison, E. A. Hetherington, R. B. Koepnick, H. F. Nelson, and J. B. Otto, 1982, Variation of seawater $^{87}\text{Sr}/^{86}\text{Sr}$ throughout Phanerozoic time: *Geology*, v. 10, p. 516-519.
- Burns, S. J., U. Haudenschild, and A. Matter, 1994, The strontium isotopic composition of carbonates from the late Precambrian (~560-540 Ma) Huqf Group of Oman: *Chemical Geology (Isotope Geoscience Section)*, v. 111, p. 269-282.
- Castelli, D., J. A. D. Connolly, and G. Franceschi, 1997, VertexView: an interactive program to analyze and plot petrological phase diagrams: *Computers and Geosciences*.
- Cole, C. M., 1997, Mechanisms and timing of metamorphic fluid flow in the Scottish Dalradian: PhD thesis, University of Edinburgh, Edinburgh, 380 p.
- Cole, C., and C. M. Graham, 1994, Stable isotope and textural evidence on the mechanisms of metamorphic fluid infiltration within a zone of structurally-focussed high fluid flux (extended abstract): V M Goldschmidt Conference, Edinburgh, p. 187-188.

- Connolly, J. A. D., 1990, Multivariable Phase Diagrams: An Algorithm based on Generalised Thermodynamics: *American Journal of Science*, v. 290, p. 666-718.
- Connolly, J. A. D., and V. Trommsdorff, 1994, Petrogenetic grids for metacarbonate rocks: pressure-temperature phase-diagram projection for mixed volatile systems: *Contributions to Mineralogy and Petrology*, v. 108, p. 93-105.
- Cowie, J. W., A. W. A. Rushton, and C. J. Stubblefield, 1972, A correlation of Cambrian rocks in the British Isles: *Special Reports of the Geological Society of London*, v. 2.
- Crank, J., 1975, *The mathematics of diffusion*: Oxford, Clarendon Press.
- Cunningham-Craig, E. H., W. B. Wright, and E. B. Bailey, 1911, *The geology of Colonsay and Oronsay, with part of the Ross of Mull*: Memoir of the Geological Survey of Scotland.
- Dalziel, I. W. D., L. H. Dalla Salda, and L. M. Gahagan, 1994, Paleozoic Laurentia-Gondwana interaction and the origin of the Appalachian-Andean mountain system: *Bulletin of the Geological Society of America*, v. 106, p. 243-252.
- Dalziel, I. W. D., and L. H. Dalla Salda, 1996, *Discussion on Ordovician palaeogeography of Siberia and adjacent continents; reply* by Torsvik, T. H., Tait, J., Moralev, V. W., McKerrow, W. S., Sturt, A. & Roberts, D.: *Journal of the Geological Society, London*, v. 153, p. 329-330.
- Deer, W. A., R. A. Howie, and J. Zussman, 1966, *An Introduction to the Rock Forming Minerals*: London, Longman, 528pp p.
- Dempster, T. J., 1983, *Studies of orogenic evolution in the Scottish Dalradian*: PhD thesis, University of Edinburgh.
- Dempster, T. J., 1984, Localised uplift in the Scottish Dalradian: *Nature*, v. 307, p. 156-159.
- Dempster, T. J., 1985, Uplift patterns and orogenic evolution in the Scottish Dalradian: *Journal of the Geological Society, London*, v. 142, p. 111-128.
- Dempster, T. J., and B. Harte, 1986, Polymetamorphism in the Dalradian of the Central Scottish Highlands: *Geological Magazine*, v. 123, p. 95-104.
- Denison, R. E., R. B. Koepnick, A. Fletcher, M. W. Howell, and W. S. Callaway, 1994, Criteria for the retention of original seawater $^{87}\text{Sr}/^{86}\text{Sr}$ in ancient shelf

- limestones: *Chemical Geology (Isotope Geoscience Section)*, v. 112, p. 131-143.
- Derry, L. A., L. S. Keto, S. B. Jacobsen, A. H. Knoll, and K. Swett, 1989, Sr isotopic variations in Upper Proterozoic carbonates from Svalbard and East Greenland: *Geochimica et Cosmochimica Acta*, v. 53, p. 2331-2339.
- Derry, L. A., A. J. Kaufman, and S. B. Jacobsen, 1992, Sedimentary cycling and environmental change in the Late Proterozoic: Evidence from stable and radiogenic isotopes: *Geochimica et Cosmochimica Acta*, v. 56, p. 1317-1329.
- Deynoux, M., and R. Trompette, 1976, Late Precambrian mixite: glacial and/or non-glacial? Dealing especially with the mixite of West Africa: *American Journal of Science*, v. 276, p. 117-125.
- Dutrow, B., and D. Norton, 1995, Evolution of fluid pressure and fracture propagation during contact metamorphism: *Journal of Metamorphic Geology*, v. 13, p. 677-686.
- Eiler, J. M., J. W. Valley, and L. P. Baumgartner, 1993, A new look at stable isotope thermometry: *Geochimica et Cosmochimica Acta*, v. 57, p. 2571-2583.
- Eiler, J. M., L. P. Baumgartner, and J. W. Valley, 1992, Intercrystalline stable isotope diffusion: a fast grain boundary model: *Contributions to Mineralogy and Petrology*, v. 112, p. 543-557.
- Eiler, J. M., J. W. Valley, C. M. Graham, and L. P. Baumgartner, 1995a, The oxygen isotope anatomy of a slowly cooled metamorphic rock: *American Mineralogist*, v. 80, p. 757-764.
- Elderfield, H., 1986, Strontium isotope stratigraphy: *Palaeogeography, Palaeoclimatology, Palaeoecology*, v. 57, p. 71-90.
- Elderfield, H., and J. M. Gieskes, 1982, Sr isotopes in interstitial waters of marine sediments from Deep Sea Drilling Project cores: *Nature*, v. 300, p. 493-497.
- Elsenhimer, D., and Valley, J. W., 1993, Submillimetre scale zonation of $\delta^{18}\text{O}$ in quartz and feldspar, Isle of Skye, Scotland: *Geochimica et Cosmochimica Acta* 57: 3669-3676.
- Eyles, C. H., and Eyles, N., 1983, Glaciomarine model for upper Precambrian diamictites of the Port Askaig Formation, Scotland: *Geology*, v. 11, p. 692-696.

- Fairchild, I. J., 1978, Sedimentation and post-depositional history of the Bonahaven Formation of Islay: Ph.D thesis, University of Nottingham.
- Fairchild, I. J., 1980a, Sedimentation and origin of a Late Precambrian 'dolomite' from Scotland: *Journal of Sedimentary Petrology*, v. 50, p. 423-446.
- Fairchild, I. J., 1980b, Stages in a Precambrian dolomitization, Scotland: cementing versus replacement textures: *Sedimentology*, v. 27, p. 631-650.
- Fairchild, I. J., 1985, Petrography and carbonate chemistry of some Dalradian dolomitic metasediments: preservation of diagenetic textures: *Journal of the Geological Society, London*, v. 142, p. 167-185.
- Fairchild, I. J., and M. J. Hambrey, 1995, Vendian basin evolution in East Greenland and NE Svalbard: *Precambrian Research*, v. 73, p. 217-233.
- Fairchild, I. J., and B. Spiro, 1987, Petrological and isotopic implications of some contrasting Late Precambrian carbonates, NE Spitsbergen: *Sedimentology*, v. 34, p. 973-989.
- Fairchild, I. J., J. D. Marshall, and J. Bertrand-Sarfati, 1990, Stratigraphic shifts in carbon isotopes from Proterozoic stromatolitic carbonates (Mauritania): influence of primary mineralogy and diagenesis: *American Journal of Science*, v. 290A, p. 46-79.
- Farver, J. R., 1994, Oxygen self-diffusion in calcite: Dependence on temperature and water fugacity: *Earth and Planetary Science Letters*, v. 121, p. 575-587.
- Farver, J. R., and R. A. Yund, 1991, Oxygen diffusion in quartz: Dependence on temperature and water fugacity: *Chemical Geology*, v. 90, p. 55-70.
- Fein, J. B., C. M. Graham, M. B. Holness, and A. E. Fallick, 1994, Controls on the Mechanisms of Fluid Infiltration during Regional Metamorphism: An Isotopic and Textural Study of Retrograde Dalradian Rocks of the SW Scottish Highlands: *Journal of Metamorphic Geology*, v. 12, p. 249-260.
- Ferry, J. M., 1983, Application of the Reaction Progress Variable in Metamorphic Petrology: *Journal of Petrology*, v. 24, p. 343-376.
- Ferry, J. M., 1984, A Biotite Isograd in South-Central Maine, USA: Mineral Reactions, Fluid Transfer, and Heat Transfer: *Journal of Petrology*, v. 24, p. 871-893.

- Ferry, J. M., 1986, Reaction Progress: A Monitor of Fluid-Rock Interaction during Metamorphic and Hydrothermal Events, *in* J. V. Walther, and B. J. Wood, eds., *Fluid-Rock Interactions during Metamorphism: Advances in Physical Geochemistry*, New York, Berlin, Heidelberg, Tokyo, Springer-Verlag, p. 61-88.
- Ferry, J. M., 1989, Contact metamorphism of roof pendants at Hope Valley, Alpine County, California, USA: *Contributions to Mineralogy and Petrology*, v. 101, p. 402-417.
- Ferry, J. M., 1992, Regional Metamorphism of the Waits River Formation, Eastern Vermont: Delineation of a new type of giant metamorphic hydrothermal system: *Journal of Petrology*, v. 33, p. 45-94.
- Fettes, D. J., C. M. Graham, B. Harte, and J. A. Plant, 1986, Lineaments and basement domains; an alternative view of Dalradian evolution: *Journal of the Geological Society, London*, v. 143, p. 453-464.
- Fitches, W. R., and A. J. Maltman, 1984, Tectonic development and stratigraphy at the western margin of the Caledonides: Islay and Colonsay: *Transactions of the Royal Society of Edinburgh, Earth Sciences*, v. 75, p. 365-382.
- Fitches, W. R., R. J. Muir, A. J. Maltman, and M. R. Bentley, 1990, Is the Colonsay-west Islay block of SW Scotland an allochthonous terrane? Evidence from Dalradian tillite clasts: *Journal of the Geological Society, London*, v. 147, p. 417-420.
- Forester, R. W., and H. P. Taylor, 1977, $^{18}\text{O}/^{16}\text{O}$, D/H and $^{13}\text{C}/^{12}\text{C}$ studies of the Tertiary Igneous Complex of Skye, Scotland: *American Journal of Science*, v. 277, p. 136-177.
- Friedman, I., and J. R. O'Neil, 1977, Chapter KK: Compilation of Stable Isotope Fractionation Factors of Geochemical Interest, *in* M. Fleischer, ed., *Data of Geochemistry: Geological Survey Professional Paper 440-KK*, Washington, United States Geological Survey.
- Friedrich, A. M., S. A. Bowring, M. W. Martin, and K. V. Hodges, 1999, Short-lived continental magmatic arc at Connemara, western Irish Caledonides: Implications for the age of the Grampian Orogeny: *Geology*, v. 27, p. 27-30.

- Gao, G., 1990, Geochemical and isotopic constraints on the diagenetic history of a massive stratal, late Cambrian (Royer) dolomite, Lower Arbuckle Group, Slick Hills, SW Oklahoma, USA: *Geochimica et Cosmochimica Acta*, v. 54, p. 1979-1989.
- Garde, A. A., 1979, Strontium geochemistry and carbon and oxygen isotopic compositions of Lower Proterozoic dolomite and calcite marbles from the Marmorilik Formation, West Greenland: *Precambrian Research*, v. 8, p. 183-199.
- Gerdes, M. L., and J. W. Valley, 1994, Fluid flow and mass transport at the Valentine wollastonite deposit, Adirondack Mountains, New York State: *Journal of Metamorphic Geology*, v. 12, p. 589-608.
- Gorokhov, I. M., M. A. Semikhatov, A. V. Baskakov, E. P. Kutyavin, N. N. Mel'nikov, A. V. Sochava, and T. L. Turchenko, 1995, Sr Isotopic Composition in Riphean, Vendian, and Lower Cambrian Carbonates from Siberia: *Stratigraphy and Geological Correlation*, v. 3, p. 1-28.
- Graham, C. M., 1986, The role of the Cruachan Lineament during Dalradian evolution: *Journal of the Geological Society, London*, v. 132, p. 257-270.
- Graham, C. M., and J. W. Valley, 1996, Ion microprobe analysis of oxygen isotope ratios in quartz from Skye granite: healed microcracks, fluid flow and hydrothermal exchange: *Contributions to Mineralogy and Petrology*, v. 124, p. 225-234.
- Graham, C. M., K. M. Greig, S. M. F. Sheppard, and B. Turi, 1983, Genesis and mobility of the H₂O-CO₂ fluid phase during regional greenschist and epidote amphibolite facies metamorphism: a petrological and stable isotope study in the Scottish Dalradian: *Journal of the Geological Society, London*, v. 140, p. 577-599.
- Graham, C. M., A. D. L. Skelton, M. Bickle, and C. Cole, 1997, Lithological, structural and deformation controls on fluid flow during regional metamorphism, *in* M. B. Holness, ed., *Deformation-enhanced Fluid Transport in the Earth's Crust and Mantle: Mineralogical Society Series*, London, Chapman and Hall, p. 196-226.

- Graham, C. M., J. W. Valley, J. M. Eiler, and H. Wada, 1998, Timescales and mechanisms of fluid infiltration in a marble: an ion microprobe study: *Contributions to Mineralogy and Petrology*, v. 132, p. 371-389.
- Greig, K. M., 1984, Metamorphosed carbonates and fluid behaviour in the Dalradian of SW Argyll, Scotland: PhD thesis, University of Edinburgh, Edinburgh.
- Greenwood, H. J., 1967, Mineral equilibria in the system MgO - SiO₂ - H₂O - CO₂, *in* P. H. Abelson, ed., *Researches in geochemistry*, New York, Wiley, p. 542-567.
- Grotzinger, J. P., Saylor, B. Z., Pelechaty, S. M., and S. A. Bowring, 1996, Calibrating the terminal Proterozoic time scale (Abstract): *International Geological Congress*, p. 47.
- Hall, A. J., 1982, Gypsum as a precursor to pyrrhotite in metamorphic rocks: *Mineralium Deposita*, v. 17, p. 401-409.
- Halliday, A. N., C. M. Graham, M. Aftalion, and P. Dymoke, 1989, The depositional age of the Dalradian Supergroup,: U-Pb and Sm-Nd isotopic studies of the Tayvallich Volcanics, Scotland: *Journal of the Geological Society*, London, v. 146, p. 3-6.
- Hambrey, M. J., 1983, Correlation of Late Proterozoic tillites in the North Atlantic region and Europe: *Geological Magazine*, v. 120, p. 209-232.
- Hambrey, M. J., I. J. Fairchild, B. W. Glover, A. D. Stewart, J. E. Treagus, and J. A. Winchester, 1991, *The Late Precambrian Geology of the Scottish Highlands and Islands*: London, The Geologists Association.
- Harris, A. L., D. J. Fettes, and N. J. Soper, 1998, Age of the Grampian event: a Discussion of "New Evidence that the Lower Cambrian Leny Limestone at Callander, Perthshire, belongs to the Dalradian Supergroup, and a reassessment of the 'exotic' status of the Highland Border Complex": *Geological Magazine*, v. 135, p. 575-579.
- Harris, A. L., P. J. Haselock, M. J. Kennedy, and J. R. Mendum, 1994, The Dalradian Supergroup in Scotland, Shetland and Ireland, *in* W. Gibbons, and A. L. Harris, eds., *A revised correlation of Precambrian rock in the British Isles*: *Geological Society of London Special Report*, p. 33-53.

- Harte, B., 1988, Lower Palaeozoic metamorphism in the Moine-Dalradian belt of the British Isles, *in* A. L. Harris, and D. J. Fettes, eds., *The Caledonian - Appalachian Orogen: Geological Society Special Publication No. 38*, The Geological Society of London, p. 123-134.
- Harte, B., J. E. Booth, T. J. Dempster, D. J. Fettes, J. R. Mendum, and D. Watts, 1984, Aspects of the post-depositional evolution of Dalradian Highland Boundary rocks in the Southern Highlands of Scotland: *Transactions of the Royal Society of Edinburgh: Earth Sciences*, v. 75, p. 151-163.
- Harte, B., and N. F. C. Hudson, 1979, Pelite facies series and the temperatures and pressures of Dalradian metamorphism in E Scotland, *in* A. L. Harris, ed., *The Caledonides of the British Isles - reviewed: Special Publication of the Geological Society of London*, The Geological Society of London, p. 323-337.
- Hays, R. S., and B. Evans, 1988, Intergranular Distribution of Pore Fluid and the Nature of High-Angle Grain Boundaries in Limestone and Marble: *Journal of Geophysical Research*, v. 93, p. 8959-8974.
- Hickman, A. H., and A. E. Wright, 1983, Geochemistry and chemostratigraphical correlation of slates, marbles and quartzites of the Appin Group, Argyll: *Transactions of the Royal Society of Edinburgh, Earth Sciences*, v. 73, p. 251-278.
- Hickman, S. H., and B. Evans, 1987, Diffusional crack healing in calcite: the influence of crack geometry on healing rate: *Physics and Chemistry of Materials*, v. 15, p. 91-102.
- Highton, A. J., E. K. Hyslop, and S. R. Noble, 1999, U-Pb zircon geochronology of migmatisation in the northern Central Highlands: evidence for pre-Caledonian (Neoproterozoic) tectonometamorphism in the Grampian block, Scotland: *Journal of the Geological Society, London*.
- Hinxman, L. W., and E. M. Anderson, 1915, *The geology of Mid-Strathspey and Strathdearn, including the country between Kingussie and Grantown: Memoir of the Geological Survey, Scotland, Sheet 74 (Scotland)*.
- Hoefs, J., 1987, *Stable Isotope Geochemistry: Minerals and Rocks*, v. 9, Springer-Verlag, 241 p.

- Hoffman, P. F., D. P. Hawkins, C. E. Isachsen, and S. A. Bowring, 1996, Precise U-Pb zircon ages for early Damaran magmatism in the Summas Mountains and Welwitschia Inlier, Northern Damara belt, Namibia: *Communications of the Geological Society of Namibia*, v. 11, p. 47-52.
- Hoffman, P. F., A. J. Kaufman, and G. P. Halverson, 1998a, Comings and goings of global glaciations on a Neoproterozoic tropical platform in Namibia: *GSA Today*, v. 8, p. 1-9.
- Hoffman, P. F., A. J. Kaufman, G. P. Halverson, and D. P. Schrag, 1998b, A Neoproterozoic Snowball Earth: *Science*, v. 281, p. 1342-1346.
- Holland, T. J. B., and J. D. Blundy, 1994, Non-ideal interactions in calcic amphiboles and their bearing on amphibole-plagioclase thermometry: *Contributions to Mineralogy and Petrology*, v. 116, p. 433-447.
- Holland, T. J. B., and R. Powell, 1990, An enlarged and updated internally consistent thermodynamic dataset with uncertainties and correlations: the system K_2O - Na_2O - CaO - MgO - MnO - FeO - Fe_2O_3 - Al_2O_3 - TiO_2 - SiO_2 - C - H_2 - O_2 : *Journal of Metamorphic Geology*, v. 8, p. 89-124.
- Holland, T. J. B., and R. Powell, 1991, A compensated-Redlich-Kwong (CORK) equation for volumes and fugacities of CO_2 and H_2O in the range 1 bar to 50 bars and 100° - $1600^\circ C$: *Contributions to Mineralogy and Petrology*, v. 109, p. 265-273.
- Holness, M. B., and C. M. Graham, 1991, Equilibrium dihedral angles in the system H_2O - CO_2 - $NaCl$ -Calcite, and implications for fluid flow during metamorphism: *Contributions to Mineralogy and Petrology*, v. 108, p. 368-383.
- Holness, M. B., and C. M. Graham, 1995, P-T-X effects on equilibrium carbonate- H_2O - CO_2 - $NaCl$ dihedral angles: constraints on carbonate permeability and the role of deformation during fluid infiltration: *Contributions to Mineralogy and Petrology*, v. 119, p. 301-313.
- Hoschek, G., 1980, Phase Relations of a Simplified Marly Rock System With Application to the Western Tauern (Austria): *Contributions to Mineralogy and Petrology*, v. 73, p. 53-68.

- Hudson, N. F. C., 1985, Conditions of Dalradian metamorphism in the Buchan area, NE Scotland: *Journal of the Geological Society, London*, v. 142, p. 63-76.
- Iyer, S. S., M. Babinski, H. R. Krouse, and F. Chemale Jr, 1995, Highly ^{13}C -enriched carbonate and organic matter in the Neoproterozoic sediments of the Bambui Group, Brazil: *Precambrian Research*, v. 73, p. 271-282.
- Jaeger, J. C., and N. G. W. Cook, 1979, *Fundamentals of rock mechanics*: London, Chapman and Hall.
- Jahn, B. -m., and Cuvellier, H, 1994, *Chemical Geology (Isotope Geoscience Section)*, v. 115, p. 125-151
- Jenkins, D. M., 1994, Experimental reversal of the aluminium content in tremolitic amphiboles in the system $\text{H}_2\text{O}-\text{CaO}-\text{MgO}-\text{Al}_2\text{O}_3-\text{SiO}_2$: *American Journal of Science*, v. 294, p. 593-620.
- Karhu, J. A., and H. D. Holland, 1996, Carbon isotopes and the rise of atmospheric oxygen: *Geology*, v. 24, p. 867-870.
- Kaufman, A. J., J. M. Hayes, A. H. Knoll, and G. J. B. Germs, 1991, Isotopic compositions of carbonates and organic carbon from upper Proterozoic successions in Namibia: stratigraphic variation and the effects of diagenesis and metamorphism: *Precambrian Research*, v. 49, p. 301-327.
- Kaufman, A. J., S. B. Jacobsen, and A. H. Knoll, 1993, The Vendian record of Sr and C isotopic variations in seawater: implications for tectonics and paleoclimate: *Earth and Planetary Science Letters*, v. 120, p. 409-430.
- Kaufman, A. J., and A. H. Knoll, 1995, Neoproterozoic variations in the C-isotopic composition of seawater: stratigraphic and biogeochemical implications: *Precambrian Research*, v. 73, p. 27-49.
- Kaye, C. A., and Zartman, R. F., 1980, A late Proterozoic Z to Cambrian age for the stratified rocks of the Boston Basin, Massachusetts, USA, *in* Wones, D. R., editor, *The Caledonides in the USA, Proceedings: Memoir of the Department of Geological Sciences, Virginia Polytechnic Institute*, p. 257.
- Kennedy, M. J., 1996, Stratigraphy, sedimentology, and isotopic geochemistry of Australian Neoproterozoic postglacial cap dolostones: deglaciation, $\delta^{13}\text{C}$ excursions, and carbonate precipitation: *Journal of Sedimentary Research*, v. 66, p. 1050-1064.

- Kennedy, M. J., B. Runnegar, A. R. Prave, K.-H. Hoffmann, and M. A. Arthur, 1998, Two or Four Neoproterozoic Glaciations?: *Geology*, v. 26, p. 1059-1063.
- Kimura, H., R. Matsumoto, Y. Kakuwa, B. Hamdi, and H. Zibaseresht, 1997, The Vendian-Cambrian $\delta^{13}\text{C}$ record, North Iran: evidence for overturning of the ocean before the Cambrian Explosion: *Earth and Planetary Science Letters*, v. 147, p. E1-E7.
- Kirschvink, J. L., 1992, Late Proterozoic low-latitude global glaciation: The Snowball Earth, *in* J. W. Schopf, and C. Klein, eds., *The Proterozoic Biosphere*, Cambridge, Cambridge University Press, p. 51-52.
- Kitchen, N. E., and J. W. Valley, 1995, Carbon isotope thermometry in marbles of the Adirondack Mountains, New York: *Journal of Metamorphic Geology*, v. 13.
- Kneller, B. C., and A. G. Leslie, 1984, Amphibolite facies metamorphism in shear zones in the Buchan area of NE Scotland: *Journal of Metamorphic Geology*, v. 2, p. 83-94.
- Knipe, R. J., 1989, Deformation mechanisms - recognition from natural tectonites: *Journal of Structural Geology*, v. 11, p. 127-146.
- Knipe, R. J., and A. M. McCaig, 1994, Microstructural and microchemical consequences of fluid flow in deforming rocks, *in* J. Parnell, ed., *Geofluids: origin, migration and evolution of fluids in sedimentary basins: Special Publication 78*, Geological Society of London, p. 99-111.
- Knoll, A. H., and M. R. Walter, 1992, Latest Proterozoic stratigraphy and Earth history: *Nature*, v. 356, p. 673-678.
- Knoll, A. H., J. M. Hayes, A. J. Kaufman, K. Swett, and I. B. Lambert, 1986, Secular variation in carbon isotope ratios from Upper Proterozoic successions of Svalbard and East Greenland: *Nature*, v. 321, p. 832-838.
- Krogh, T. E., D. F. Strong, S. J. O'Brien, and V. S. Papezik, 1988, Precise U-Pb zircon dates from the Avalon Terrane in Newfoundland: *Canadian Journal of Earth Sciences*, v. 25, p. 442-453.
- Kuznetsov, A. B., I. M. Gorokhov, M. A. Semikhatov, N. N. Mel'nikov, and V. I. Kozlov, 1997, Strontium isotopic composition in the limestones of the Inzer Formation, Upper Riphean Type Section, Southern Urals: *Transactions*

- (Doklady) of the Russian Academy of Sciences (Earth Science Section), v. 353, p. 319-324.
- Lewis, S., 1999, Metamorphic fluid flow and stable isotope modification in marble: an example from Naxos, Greece: PhD thesis, University of Edinburgh, Edinburgh, 350 p.
- Lewis, S., M. Holness, and C. M. Graham, 1998, Ion microprobe study of marble from Naxos, Greece: Grain-scale fluid pathways and stable isotope equilibration during metamorphism: *Geology*, v. 26, p. 935-938.
- Lindsay, N. G., P. J. Haselock, and A. L. Harris, 1989, The extent of Grampian orogenic activity in the Scottish Highlands: *Journal of the Geological Society*, London, v. 146, p. 733-735.
- Mackenzie, F. T., and J. D. Piggott, 1981, Tectonic controls of Phanerozoic sedimentary rock cycling: *Journal of the Geological Society*, London, v. 138, p. 183-196.
- Marshall, J. D., 1992, Climatic and oceanographic isotopic signals from the carbonate rock record and their preservation: *Geological Magazine*, v. 129, p. 143-160.
- McCaig, A. M., 1997, The geochemistry of volatile fluid flow in shear zones, *in* M. B. Holness, ed., *Deformation-enhanced Fluid Transport in the Earth's Crust and Mantle: Mineralogical Society Series*, London, Chapman and Hall, p. 227-266.
- McCrea, J. M., 1950, On the isotope chemistry of carbonates and a paleotemperature scale: *Journal of Chemical Physics*, v. 18, p. 849-857.
- Melezhik, V. A., and A. E. Fallick, 1996, A widespread positive $\delta^{13}\text{C}_{\text{carb}}$ at around 2.33 - 2.06 Ga on the Fennoscandian Shield: a paradox?: *Terra Nova*, v. 8, p. 141-157.
- Melezhik, V. A., A. E. Fallick, V. V. Makarikhin, and V. V. Lybutsov, 1997, Links between Palaeoproterozoic palaeogeography and rise and decline of stromatolites: Fennoscandian Shield: *Precambrian Research*, v. 82, p. 311-348.

- Mendum, J. R., 1987, Dalradian of the Collieston Coast Section, *in* N. H. Trewin, B. C. Kneller, and C. Gillen, eds., *Excursion guide to the geology of the Aberdeen area*, Edinburgh, Scottish Academic Press, p. 161-172.
- Meert, J. G., and R. Van der Voo, 1994, The Neoproterozoic (1000-540Ma) glacial intervals: No more snowball earth?: *Earth and Planetary Science Letters*, v. 123, p. 1-13.
- Migeon, H. N., Schumacher, M., and Slodzian, G., 1990, Analysis of insulating specimens with the Cameca ims-4f: *Surface Interface Analysis*, v. 16, p. 9-13.
- Misi, A., and J. Veizer, 1998, Neoproterozoic carbonate sequences of the Una Group, Irece Basin, Brazil: chemostratigraphy, age and correlations: *Precambrian Research*, v. 89, p. 87-100.
- Molyneux, S. G., 1998, An upper Dalradian microfossil reassessed: *Journal of the Geological Society, London*, v. 155, p. 741-743.
- Moore, E. M., 1991, Southwest U.S. - East Antarctica (SWEAT) connection: A hypothesis: *Geology*, v. 19, p. 425-428.
- Muir, R. J., A. J. Fitches, and A. J. Maltman, 1992, Rhinns Complex: A missing link in the Proterozoic basement of the North Atlantic region: *Geology*, v. 20, p. 1043-1046.
- Muir, R. J., W. R. Fitches, A. J. Maltman, and M. R. Bentley, 1994, Precambrian rocks of the southern Inner Hebrides - Malin Sea region: Colonsay, west Islay, Inishtrahull and Iona, *in* W. Gibbons, and A. L. Harris, eds., *A revised correlation of Precambrian rocks in the British Isles: Special Report of the Geological Society, London*, The Geological Society of London.
- Muir, R. J., T. R. Ireland, M. R. Bentley, W. R. Fitches, and A. J. Maltman, 1997, A Caledonian age for the Kiloran Bay appinite intrusion on Colonsay, Inner Hebrides: *Scottish Journal of Geology*, v. 33, p. 75-83.
- Myrow, P. M., and A. J. Kaufman, 1999, A newly discovered cap carbonate above Varanger-age glacial deposits in Newfoundland, Canada: *Journal of Sedimentary Petrology*, v. 69, p. 784-793.
- Nakashima, Y., 1995, Transport model of buoyant metamorphic flow by hydrofracturing in leaky rock: *Journal of Metamorphic Geology*, v. 13.

- Narbonne, G. M., and J. D. Aitken, 1995, Neoproterozoic of the Mackenzie Mountains, northwestern Canada: *Precambrian Research*, v. 73, p. 101-121.
- Narbonne, G. M., A. J. Kaufman, and A. H. Knoll, 1994, Integrated chemostratigraphy and biostratigraphy of the Windermere Supergroup, northwestern Canada: Implications for Neoproterozoic correlations and the early evolution of animals: *Bulletin of the Geological Society of America*, v. 106, p. 1281-1292.
- Niyashima, T., 1989, Kinetics of hydrofracturing and metamorphic veining: *Geology*, v. 17, p. 1068-1071.
- Noble, S. R., E. K. Hyslop, and A. J. Highton, 1996, High precision U-Pb monazite geochronology of the c. 806 Ma Grampian Slide and the implications for the evolution of the Central Highlands: *Journal of the Geological Society*, London, v. 153, p. 511-514.
- Odling, N. E., 1997, Fluid flow in fractured rocks at shallow levels in the Earth's crust: an overview, *in* M. B. Holness, ed., *Deformation-enhanced Fluid Transport in the Earth's Crust and Mantle: Mineralogical Society Series*, London, Chapman and Hall, p. 289-320.
- O'Neil, J. R., 1986, Theoretical and experimental aspects of isotopic fractionation, *in* J. W. Valley, H. P. Taylor Jr, and J. R. O'Neil, eds., *Stable Isotopes in High Temperature Geological Processes: Reviews in Mineralogy*, Mineralogical Society of America, p. 1-36.
- Palmer, M. R., and J. M. Edmond, 1989, The strontium budget of the modern ocean: *Earth and Planetary Science Letters*, v. 92, p. 11-26.
- Palmer, M. R., and H. Elderfield, 1985, Sr isotopic composition of seawater over the past 75Myr: *Nature*, v. 314, p. 526-528.
- Phillips, E. R., A. J. Highton, E. K. Hyslop, and M. Smith, 1999, The timing and P-T conditions of regional metamorphism in the Central Highlands, Scotland: *Journal of the Geological Society*, London, v. in press.
- Piasecki, M. A. J., and S. Temperley, 1988, Central Highland Division, *in* J. A. Winchester, ed., *Later Proterozoic Stratigraphy of the Northern Atlantic Regions*, Glasgow, Blackie, p. 46-53.

- Piasecki, M. A. J., and O. Van Breeman, 1979, The 'Central Highland Granulites': cover-basement tectonics in the Moine, *in* A. L. Harris, C. H. Holland, and B. E. Leake, eds., *The Caledonides of the British Isles - Reviewed: Special Publication*, Geological Society of London, p. 139-144.
- Powell, R., and T. J. B. Holland, 1985, An internally consistent thermodynamic dataset with uncertainties and correlations: 1. Methods and a worked example: *Journal of Metamorphic Geology*, v. 3, p. 327-342.
- Prave, A. R., 1999, Two diamictites, two cap carbonates, two $\delta^{13}\text{C}$ excursions, two rifts: The Neoproterozoic Kingston Peak Formation, Death Valley, California: *Geology*, v. 27, p. 339-342.
- Pringle, I. R., 1973, Rb-Sr age determinations on shales associated with the Varanger ice age: *Geological Magazine*, v. 109, p. 465-472.
- Pringle, J., 1940, The discovery of Cambrian trilobites in the Highland Border rocks near Callander, Perthshire (Scotland), *British Association for the Advancement of Science*.
- Robertson, S., and M. Smith, 1999, The significance of the Geal Charn - Ossian Steep Belt in basin development and inversion in the Central Scottish Highlands: *Journal of the Geological Society*, London.
- Rock, N. M. S., 1985, Value of chemostratigraphical correlation in metamorphic terrains; an illustration from the Colonsay Limestone, Inner Hebrides, Scotland: *Transactions of the Royal Society of Edinburgh, Earth Sciences*, v. 76, p. 515-517.
- Rogers, G., T. J. Dempster, B. J. Bluck, and P. W. G. Tanner, 1989, A high precision U-Pb age for the Ben Vuirich granite: implications for the evolution of the Scottish Dalradian Supergroup: *Journal of the Geological Society*, London, v. 146, p. 789-798.
- Rogers, G., B. A. Paterson, T. J. Dempster, and S. D. Redwood, 1994, U-Pb geochronology of the 'Newer' Gabbros, NE Grampians (abstract): *Caledonian Terrane Relationships in Britain*, p. 8.
- Rosenbaum, J., and S. M. F. Sheppard, 1986, An isotopic study of siderites, dolomites and ankerites at high temperature: *Geochimica et Cosmochimica Acta*, v. 50, p. 1147-1150.

- Rowe, K. J., and E. H. Rutter, 1990, Palaeostress estimation using calcite twinning: experimental calibration and application to nature: *Journal of Structural Geology*, v. 12, p. 1-17.
- Rye, R. O., R. D. Schuiling, D. M. Rye, and J. B. H. Jansen, 1976, Carbon, hydrogen and oxygen studies of the original metamorphic complex at Naxos, Greece: *Geochimica et Cosmochimica Acta*, v. 40, p. 1031-1049.
- Robertson, S., 1994, Timing of Barrovian metamorphism and 'Older Granite' emplacement in relation to Dalradian deformation: *Journal of the Geological Society, London*, v. 151, p. 5-8.
- Saylor, B. Z., A. J. Kaufman, J. P. Grotzinger, and F. Urban, 1998, A composite reference section for Terminal Proterozoic strata of Southern Namibia: *Journal of Sedimentary Research*, v. 68, p. 1223-1235.
- Schmidt, P. W., G. E. Williams, and B. J. J. Embleton, 1991, Low palaeolatitude of Late Proterozoic glaciation: Early timing of remanence in hematite of the Elatina Formation, South Australia: *Earth and Planetary Science Letters*, v. 105, p. 355-367.
- Sholkovitz, E. R., and D. Copeland, 1981, The coagulation, solubility and adsorption properties of Fe, Mn, Cu, Ni, Cd, Co and humic acids in river water: *Geochimica et Cosmochimica Acta*, v. 45, p. 181-189.
- Skelton, A. D., 1993, Petrological, Geochemical and Field Studies of Fluid Infiltration during Regional Metamorphism of the Dalradian of the SW Scottish Highlands: Ph.D thesis, University of Edinburgh.
- Skelton, A. D. L., C. M. Graham, and M. J. Bickle, 1995, Lithological and Structural Controls of Regional 3-D Fluid Flow patterns during Greenschist Facies Metamorphism of the Dalradian of the SW Scottish Highlands: *Journal of Petrology*.
- Sleep, N. H., 1971, Thermal effects of the formation of Atlantic continental margins by continental break-up: *Geophysical Journal of the Royal Astronomical Society*, v. 4, p. 325-350.
- Smalley, P. C., C. N. Maile, M. L. Coleman, and J. E. Rouse, 1992, LASSIE (Laser ablation sampler for stable isotope extraction) applied to carbonate minerals: *Chemical Geology (Isotope Geoscience Section)*, v. 101, p. 43-52.

- Smelik, E. A., M. W. Nyman, and D. R. Veblen, 1991, Pervasive exsolution within the calcic amphibole series: TEM evidence for a miscibility gap between actinolite and hornblende in natural samples: *American Mineralogist*, v. 76, p. 1184-1204.
- Smith, M., S. Robertson, and K. E. Rollin, 1999, Rift basin architecture and stratigraphical implications for basement-cover relationships in the Neoproterozoic Grampian Group of the Scottish Caledonides: *Journal of the Geological Society, London*.
- Soper, J., 1994, Neoproterozoic sedimentation on the northeast margin of Laurentia and the opening of Iapetus: *Geological Magazine*, v. 131, p. 291-299.
- Soper, N. J., and R. Anderton, 1984, Did the Dalradian slides originate as extensional faults: *Nature*, v. 307, p. 357-360.
- Soper, N. J., and R. W. England, 1995, Vendian and Riphean rifting in NW Scotland: *Journal of the Geological Society, London*, v. 152, p. 11-14.
- Spencer, A. M., 1971, Late Precambrian glaciation in Scotland: *Memoir of the Geological Society, London*, v. 6, 98pp
- Stephenson, D., and D. Gould, 1995, *The Grampian Highlands: British Regional Geology*: London, Her Majesty's Stationary Office, 261 p.
- Stewart, A. D., 1962, On the Torridonian sediments of Colonsay and their relationship to the main outcrop in north-west Scotland: *Liverpool and Manchester Geological Journal*, v. 3, p. 121-155.
- Stoker, M. S., Howe, J. A., and Stoker, S. J., 1999, Late Vendian-?Cambrian glacially influenced deep-water sedimentation, Macduff Slate Formation (Dalradian), NE Scotland: *Journal of the Geological Society, London*, v. 156, p. 55-62.
- Sullivan, M. D., R. S. Haszeldine, and A. E. Fallick, 1990, Linear coupling of carbon and strontium isotopes in Rotliegend Sandstone, North Sea: Evidence for cross-formational fluid flow: *Geology*, v. 18, p. 1215-1218.
- Swart, P. K., 1990, Calibration of the ion microprobe for the quantitative determination of strontium, iron, manganese, and magnesium in carbonate minerals. *Analytical Chemistry*, v. 62, p.722-728.
- Tucker, M. E., 1986, Carbon isotope excursions in Precambrian/Cambrian boundary

- beds, Morocco: *Nature*, v. 319, p. 48-50.
- Tanner, P. W. G., 1995, New evidence that the Lower Cambrian Leny Limestone at Callender, Perthshire, belongs to the Dalradian Supergroup, and a reassessment of the 'exotic' status of the Highland Border Complex: *Geological Magazine*, v. 132, p. 473-483.
- Tanner, P. W. G., 1996, Significance of the early fabric in the contact metamorphic aureole of the 590 Ma Ben Vuirich Granite, Perthshire, Scotland: *Geological Magazine*, v. 133, p. 683-695.
- Thomas, C. W., 1989, Application of geochemistry to the stratigraphic correlation of Appin and Argyll Group carbonate rocks from the Dalradian of northeast Scotland: *Journal of the Geological Society*, v. 146, p. 631-647.
- Thomas, C. W., and J. Aitchison, 1998, Application of logratios to the statistical analysis of the geochemistry of metamorphosed limestones from the Northeast and Central Highlands of Scotland: the case for Appin Group correlations: British Geological Survey Technical Report WA/98/03.
- Torsvik, T. H., and A. Trench, 1991, The Ordovician history of the Iapetus ocean in Britain: New palaeomagnetic constraints: *Journal of the Geological Society*, London, v. 148, p. 423-425.
- Tucker, M. E., and V. P. Wright, 1990, *Carbonate Sedimentology*: Oxford, Blackwell Scientific Publications, 482 p.
- Upton, P. S., 1986, A structural cross-section of the Moine and Dalradian rocks of the Braemar area: British Geological Survey Report, v. 17, No. 1, p. 1-19.
- Valley, J. W., 1986, Stable isotope geochemistry of metamorphic rocks, *in* J. W. Valley, H. P. Taylor, and J. R. O'Neil, eds., *Stable Isotopes in High Temperature Geological Processes: Reviews in Mineralogy*, p. 445-489.
- Valley, J. W., and C. M. Graham, 1996, Ion microprobe analysis of oxygen isotope ratios in quartz from Skye granite: healed microcracks, fluid flow, and hydrothermal exchange: *Contributions to Mineralogy and Petrology*, v. 124, p. 225-234.
- Valley, J. W., Eiler, J. M., Graham, C. M., Gibson, E. K., Romanek, C. S. and Stolper, E. M., 1997, Low-temperature carbonate concretions in the Martian

- meteorite ALH84001: evidence from stable isotopes and mineralogy: *Science*, v. 275, p. 1633-1638.
- Valley, J. W., C. M. Graham, B. Harte, B. Eiler, and P. D. Kinny, 1998, Ion microprobe analysis of oxygen, carbon and hydrogen isotope ratios, *in* M. A. McKibben, and W. C. Shanks, eds., *Microanalytical Techniques to Understanding Mineralizing Processes: Reviews in Economic Geology*, Society of Economic Geologists, p. 73-98.
- Veizer, J., 1989, Strontium isotopes in seawater through time: *Annual Review of Earth and Planetary Science*, v. 17, p. 141-167.
- Veizer, J., 1992, Depositional and Diagenetic History of Limestones: Stable and Radiogenic Isotopes, *in* N. Clauer, and S. Chaudhuri, eds., *Isotopic Signatures and Sedimentary Records*, Berlin, Springer-Verlag, p. 13-48.
- Veizer, J., and W. Compston, 1976, $^{87}\text{Sr}/^{86}\text{Sr}$ in Precambrian carbonates as an index of crustal evolution: *Geochimica et Cosmochimica Acta*, v. 40, p. 905-914.
- Veizer, J., W. Compston, N. Clauer, and M. Schidlowski, 1983, $^{87}\text{Sr}/^{86}\text{Sr}$ in Late Proterozoic carbonates: evidence for a "mantle" event at ~900 Ma ago: *Geochimica et Cosmochimica Acta*, v. 47.
- Wada, H., 1988, Microscale isotopic zoning in calcite and graphite crystals in marble: *Nature*, v. 331, p. 61-63.
- Walls, R. A., P. C. Ragland, and E. L. Crisp, 1977, Experimental and natural early diagenetic mobility of Sr and Mg in biogenic carbonates: *Geochimica et Cosmochimica Acta*, v. 41, p. 1731-1737.
- Williams, G. E., 1979, Sedimentology, stable isotope geochemistry, and palaeoenvironment of dolostones capping late Precambrian glacial sequences in Australia: *Journal of the Geological Society of Australia*, v. 26.
- Wilkinson, B. H., R. M. Owen, and A. R. Carroll, 1985, Submarine hydrothermal weathering, global eustasy and carbonate polymorphism in Phanerozoic marine oolites: *Journal of Sedimentary Petrology*, v. 55, p. 171-183.
- Winchester, J. A., and B. W. Glover, 1988, The Grampian Group, Scotland, *in* J. A. Winchester, ed., *Proterozoic stratigraphy of the Northern Atlantic regions*, Glasgow and London, Blackie, p. 146-161.

Appendix A

A.1 Sampling details

A.2 Details of lithostratigraphical units used to constrain

Neoproterozoic seawater $^{87}\text{Sr}/^{86}\text{Sr}$

A.3 Mini-core sampling of the Inchrory Limestone

A.1 Details of sampling for isotope analyses

Whole-rock sampling and sample preparation

Apart from those samples obtained from sample profiles in the Torulian and Inchrory Limestones (see below), all the samples used for bulk carbonate isotope determinations are whole-rock samples, most of which were collected for whole-rock geochemical characterisation of the limestones as described by Thomas (1989). The samples were collected from the freshest parts of outcrops and the samples themselves consisted of fresh material, free of surface weathering and veining. Any such material was removed in the field. In the laboratory, samples were cleaned and checked again before being jaw-crushed and splits removed for grinding. Agate mills were used for powder preparation and these were acid-cleaned between samples to remove probable mechanical graphite-carbonate admixture which adhered to the insides of the tema; the usual cleaning procedure with fine quartz sand was inefficient at completely removing this material. Aliquots of Tema powder ($<150\text{ }\mu\text{m}$) from this stage were used as sample material for isotope analysis.

Carbon and Oxygen isotope analysis of bulk carbonate

The mini-core samples of the Inchrory Limestone in Limeworks Quarry, Tomintoul, were obtained using methods and equipment detailed in below at A.3. Micro-drilling of powders from hand-specimens of Torulian Limestone collected from the River Avon Torulian Limestone profile, was effected using a hardened and pointed steel bit in a dentist's drill.

A.2 Details of lithostratigraphical units used to constrain Neoproterozoic seawater $^{87}\text{Sr}/^{86}\text{Sr}$

This section summarises the geology of the lithostratigraphical units for which $^{87}\text{Sr}/^{86}\text{Sr}$ data are available and for which samples have been assigned relative ages. These data have been used to construct a Neoproterozoic seawater $^{87}\text{Sr}/^{86}\text{Sr}$ and $\delta^{13}\text{C}$ curves discussed in Chapters 6 and 7 and are summarised in Table 6.5

Canada

Victoria Island, Canadian Arctic Archipelago, Northern Territories

Lithostratigraphy Neoproterozoic rocks assigned to the Shaler Group have been described by Asmerom et al. (1991). The group is comprised of ~ 4 km of clastic and carbonate rocks. The lowermost Glenelg Formation consists of 600 m of basal shallow marine shales and sandstones are overlain by a further 600 m of dolostones and limestones. The carbonate rocks are succeeded by ~ 1400 m of deltaic siliciclastic rocks capped by distinctive stromatolitic carbonates. In the overlying ~ 1 km thick Reynolds Point Formation, basal deltaic and shallow marine siliciclastic rocks give way to sub- to intertidal marine limestones and dolostones which include

oolites and stromatolites. The Minto Inlet Formation consists of about 200 m of evaporites and dolostones, indicating deposition in an arid environment. A return to tidal to platform marine conditions is recorded by carbonate rocks of the uppermost Wynniatt Formation (400 – 900 m), comprised of ‘micrites, oolitic and intraclastic grainstones, oncolites and stromatolites’ (Asmerom et al., op. cit., page 2884.). Carbonate rocks, red beds and evaporites of the Kilian Formation cap the Shaler succession and are correlated, at least in their upper part, with the Coates Lake Group. The Shaler Group itself is correlated with the Mackenzie Mountain Supergroup (e.g. Narbonne and Aitken (1995). Samples used to determine $^{87}\text{Sr}/^{86}\text{Sr}$ were taken from the Reynolds Point, Minto Inlet and Wynniatt formations. Note that no tillite sequences have been recorded in this succession.

Age constraints The rocks lie unconformably on lavas dated at 1.2 Ga and correlation with the Mackenzie Mountain Supergroup constrains the age of the Shaler Group to be $\leq \sim 880$ Ma but older than ~ 790 Ma, based on a radiometric age of 776 ± 24 Ma determined for dolerite sills which cut the succession. Estimated ages for individual samples are based on the empirical subsidence rate equation developed by Sleep (1971).

Windermere Supergroup

Lithostratigraphy The Windermere Supergroup (Kaufman et al., 1993; Narbonne and Aitken, 1995; Narbonne et al., 1994) is located in the Mackenzie Mountains, western Northwest Territories, Canada. It consists of basal rift deposits, including volcanoclastic conglomerates and sandstones, which pass up into sulphate evaporites,

followed by carbonate rocks deposited in a progressively deepening marine environment. These rocks are assigned to the Coates Lake Group, mentioned above as a correlative of the Kilian Formation. The succeeding Sayunei Formation contains deep water mudstones to debris-flow conglomerates, whilst the overlying Shezal Formation contains tillites with largely intrabasinal clasts. These two groups are collectively referred to as the 'Rapitan Glacials' (Narbonne and Aitken, 1995). These glacial deposits have been correlated with other tillites assigned to the Sturtian glaciation (e.g. Young (1992), currently constrained to be younger than 746 ± 2 Ma (Hoffman et al., 1996). Above the Rapitan Glacials, the rocks are subdivided into three 'grand cycles', comprising siliciclastic rocks passing up into carbonate sequences. The close of the lowest grand cycle is marked by the Ice Brook Formation which, appropriately enough, contains diamictites, some of which are of glacial origin, with largely intrabasinal clasts of the underlying carbonate Keele Formation. The glacial deposits have a dolostone cap, the Tepee Dolostone, a feature this succession shares with other Neoproterozoic tillites, including the Marinoan tillites of South Africa (Deynoux and Trompette, 1976) and Australia (Williams, 1979).

Age constraints The Ice Brook tillites are considered to be equivalents of the Varanger Tillites of Norway. Kaufman et al. (1993) use a lower bounding age of 598 Ma, based on extrapolation from the Polarisbreen Group (see below). The rocks above the tillite sequences contain Ediacaran fauna, considered by Kaufman et al op. cit. to lie between 560 – 580 Ma. The top of the Windermere Group is marked by a karstic disconformity and is overlain by rocks which contain Cambrian trilobites; based on this, the upper age limit is the Cambrian – Precambrian boundary at 540 Ma. Age estimates for samples upon which $^{87}\text{Sr}/^{86}\text{Sr}$ determinations have been made

are based on interpolation between bounding ages using Sleep's subsidence rate equation.

Southern Africa

Namibia

Lithostratigraphy The Nama and Witvlei Groups of Namibia comprise a thick, mixed siliciclastic and carbonate succession deposited on a shallow marine platform (e.g. Saylor et al., 1998, and references therein). No tillites occur within this succession. However, an unconformity inferred to occur between lacustrine and marine deposits in the lower part of the Witvlei Group is considered by Kaufman et al. (1991) to be coeval with glaciation elsewhere in Namibia on the basis of $\delta^{13}\text{C}$ data.

Age constraints The base of the Nama Group is dated at 592 Ma, based on the presence of Ediacaran fauna and Sleep's subsidence rate equation, whilst the top is considered, on similar grounds to be no younger than 552 Ma. The underlying Witvlei Group is considered to straddle the 'Varanger' time interval (c. 600 Ma). The subsidence rate equation is used to estimate the ages of individual samples drawn from the Namibian successions.

Svalbard and Greenland

Northeast Svalbard and East Greenland

Lithostratigraphy The two principal lithostratigraphical units in Svalbard are the Akademikerbreen and Polarisbreen Groups. The Akademikerbreen Group consists of

some 2 km of limestones and dolostones, including stromatolites, oolites and pisolites, deposited in peri- to sub-tidal, shallow marine conditions. The succeeding Polarisbreen Group was deposited after an apparent hiatus on the Akademikerbreen Group. This group consists of about 1 km of siliciclastic and carbonate lithologies and includes two tillite horizons (e.g. Fairchild and Hambrey, 1995, page 220, Table 1). The lowermost of these occurs in the E2 Member of the Elbobreen Formation, one member up from the base of the group. The overlying Wilsonbreen Formation constitutes the upper tillite sequence and has abundant extrabasinal clasts, chiefly of granite gneiss, as well as intrabasinal dolostone. The clasts in this tillite are almost exclusively of intrabasinal carbonate rocks, although some schists, gneiss and volcanic clasts occur near the top. Note the correspondence in clast assemblages between these Svalbard tillites and the upper and lower Port Askaig tillites (Chapter 2, Section 2.3.3.1). The equivalent tillites in East Greenland are the (lower) Ulvesø and (upper) Storeelv units. The former lies at the base of the 'Tillite' Group and overlies the Andreeland Group. These two groups are approximately equivalent to the Polarisbreen and Akademikerbreen Groups.

Age constraints The Polarisbreen Group is unconformably overlain by the Oslobreen Group which contains Cambrian fossils (Derry et al., 1989). The absence of Ediacaran fauna and acritarchs considered to be very latest Vendian, indicate that the Polarisbreen Group was deposited before 580 Ma (Kaufman et al., 1993). The Varangan tillites in North Norway (Mortensnes, Smålfjord), correlated with the Wilsonbreen and Elbobreen tillites of Svalbard, are separated by the Nyborg Formation, from which shales have been dated by whole-rock Rb-Sr at 654 ± 23 Ma

(recalculated by Fairchild and Hambrey (1995) from original work by Pringle (1973). Derry et al. (1989) estimated the ages of their sub-tillite Polarisbreen samples to be between 654 and 695 Ma, based on extrapolation of calculated ages of samples within the underlying Akademikerbreen Group. Kennedy et al. (1998) also discuss the possible age of the lower tillite sequence in the North Atlantic region, suggesting a Sturtian correlation. They quote as evidence for this the above Rb-Sr age and the presence of a microfossil (*Balinella faviolata*) which, although regarded as a Vendian index fossil is known to occur in Riphean rocks (references in Kennedy et al., 1998). In contrast, Kaufman et al. (1993) assumed a 610 Ma age for the base of the Polarisbreen Group, based on the 610 Ma age assigned to the base of the Vendian (Knoll and Walter, 1992). Their subsidence rate derived sample ages indicated that the end of the Varangan ice age was about 598 Ma. Note the consistency of this estimate with the 595 ± 4 Ma age for the Tayvallich lavas (Halliday et al., 1989). The Akademikerbreen group was estimated by Derry et al. (1989) to be between 800 and 700 Ma in age, based on acritarchs and stromatolites considered to be of Riphean age; their calculated ages have been retained for the purposes of constructing the seawater $^{87}\text{Sr}/^{86}\text{Sr}$ curve in Figure 8.2. In all probability, the group is much younger than this. Although stratigraphical continuity into the Polarisbreen Group is apparently marked by a hiatus, Derry et al. (1989) maintain there is no obvious disconformity which could be considered to represent c. 90 Ma. It seems reasonable to conclude, therefore, that the top of the Akademikerbreen Group is little older than 610 Ma and the base no more than c. 700 Ma.

Oman

Lithostratigraphy Burns et al. (1994) present data for the latest Precambrian Huqf Group of Oman. This group is comprised of two siliciclastic and two carbonate units, capped by an evaporite. The carbonate rocks include a range of dolostones and dolostones which commonly preserve ooids, pisoids and cryptalgal laminations. Although the units are extensively dolomitised, Sr contents low and Sr/Mn ratios $\ll 1$, the authors conclude from several lines of evidence that the $^{87}\text{Sr}/^{86}\text{Sr}$ ratios of the carbonate rocks can be interpreted broadly as 'initial'.

Age constraints The age of the Huqf Group is reasonably well-constrained radiometrically. Acid-igneous extrusive rocks upon which the carbonates are deposited, are dated at 556 ± 10 Ma (Burns et al., 1994), indicating that the Huqf Group is no more than c. 560 Ma old. The age of their uppermost sample is estimated at c. 540 Ma, based, once again, on empirical subsidence rate calculations.

Russia

Riphean to early Cambrian carbonate rocks from Siberia

Lithostratigraphy Gorokhov et al. (1995) present $^{87}\text{Sr}/^{86}\text{Sr}$ data for carbonate rocks from three cratonic 'uplifts' in northern Siberia. The Olenek uplift contains Riphean through to Lower Cambrian (Tommotian) carbonate rocks. Very gently dipping Riphean carbonate rocks lie unconformably on metamorphosed basement with granites. The Riphean rocks are overlain transgressively by Vendian strata containing Ediacaran fossils in middle sections and a small shelly fauna in the upper parts. Vendian rocks are succeeded by rocks with fossil assemblages characteristic of the

Tommotian. The Turukhansk ‘uplift’, some 750 km west of the Olenek ‘uplift’ contains Riphean carbonates deposited on the margins of the Siberian Platform. These are overlain unconformably by Vendian rocks which grade upward into fossiliferous Cambrian carbonate rocks. The Ura ‘uplift’, c. 500 km south of the Olenek ‘uplift’, includes carbonate rocks which are disposed in folds which propagate onto the Siberian Platform from a fold belt to the east. Little detail is given of the carbonate rock lithologies and no mention is made of the presence or otherwise of tillites, although the base of the Vendian in the Ura ‘uplift’ is marked by sandstones and shales and lithologies described as ‘gravelstones’.

Age constraints Age estimates are based on a number of radiometric dates and interpolation between using Sleep’s subsidence equation, and palaeontological data. Resulting estimated ages for formations range from c. 1480 Ma at the base of the Riphean rocks in the Olenek ‘uplift’, to 530 Ma in lowest Cambrian rocks in the Ura ‘uplift’. The accuracy of the ages is difficult to assess, particularly for the older Riphean rocks, as several of the radiometric ages quoted are Rb-Sr or K-Ar ages on glauconites. The apparent absence of basal Vendian (‘Varangan’) tillite lithologies also renders correlation of these sequences with the other Neoproterozoic carbonate sequences discussed here very difficult. Thus, the age data for these Siberian carbonate rocks are accepted at face value for the purposes of this study.

Upper Riphean Inzer Formation, Southern Urals, Russia

Lithostratigraphy The Inzer Formation from the Upper Riphean of the Southern Urals is dominated by calcitic limestones (Kuznetsov et al., 1997). Limestones from

a section near the town of Min'yar (~57° 30'E 55°N) are described as well-bedded and micritic commonly with thin siliciclastic partings. Limestones from a section near Kulmas, 100 km SW of Min'yar, are characterised by stylolites and are cut by fissures filled with late calcite. Limestones near the top of both sections contain stromatolites and clastic lithologies.

Age constraints Pb-Pb and Rb-Sr data indicate that the base of the succession is 836 ±27 Ma in age. Higher parts of the succession have been dated by K-Ar methods on glauconite (Kuznetsov et al., 1997, and references therein), yielding an age of 791 Ma for the uppermost member. The overlying Min'yar Formation is dated at 740 – 710 Ma. Ages of individual samples have been calculated assuming a linear relationship between sediment thickness and time and interpolation between the radiometric dates. As with the Siberian sections discussed above, ages are clearly not precise, but are taken at face value.

A.3 High-resolution (1cm) core sampling in the field for geochemical profiling studies, using a cordless powerdrill: A short report

I outline here the minicoring technique and equipment I used for the high resolution sample profile in Limeworks Quarry, near Tomintoul (Chapter 9).

Introduction

A number of modern petrological research studies have used numerous, accurately-located samples to provide detailed information on geochemical and

petrological profiles across lithological units and discontinuities (ie across 'fronts') (Bickle and Baker, 1990; Skelton, 1993). The emphasis on accurate location is important because the data are used in numerical models which fit equations describing isotope and reaction front behaviour to real data, allowing modelling of the physico-chemical controls on the profiles and thereby elucidating such things as fluid infiltration mechanisms.

The resolution with which samples can be obtained controls the precision of geochemical and petrological profiles and elucidates the degree to which noise affects the data. To date, the maximum resolution obtainable at outcrop level is about 25mm, using the petrol-engined coring device available in the Department. This resolution may be too coarse to provide enough control over the form of a profile, particularly close to boundary layers, where the shape of a profile may change very rapidly. A further problem with the current sampling equipment is its weight and bulk and the requirement for pressurised water cooling and irrigation.

Effectively, the equipment requires two people to operate it, it needs to be used near a water supply and requires two-stroke fuel to be carried as well. This equipment is not easy to use above waist height and is not readily portable. Furthermore, the large core holes are obtrusive, particularly because the equipment is not easy to use in discrete parts of outcrops. The visual damage is less easily disguised than with hammered sampling, the effects of which can at least be made to look natural, and is rather longer-lasting.

In planning the detailed sampling of metacarbonate rocks for isotope analysis, it was considered necessary to improve the resolution of the sampling and to use much more portable and less obtrusive equipment. Suitable coring drills were

purchased from Abrasive Technology, Inc., USA. The obvious solution to the problem of portability was to use a cordless power drill, assuming that such a device would be powerful enough and battery power sufficient to drill at least a few holes. Experiments indicated that a 12v cordless drill would be adequate, and one of these, together with four batteries, was hired from an Edinburgh hire shop.

Equipment

The following items made up the light-weight, portable coring 'kit':

No	Description	Supplier/manufacturer	Cost
2	10mm (3/8") diamond-tipped core drill	Abrasive Technology	£34 net
1	12v cordless power drill (£30 hire includes 4 NiCad batteries + charger)	Makita	
1	300ml water bottle with fine swan-necked nozzle		
1	200 x 2mm wire 'prodger' for core removal (from old coat-hanger!)		

Coring drills

The coring drills consist of a 45mm long, diamond-tipped barrel, with an outside diameter of 10mm and an inside diameter of 7.5mm, on a 19mm long shank with a 6mm outside diameter. The diamond tipping is 5mm long and consists of industrial diamonds set in phosphor-bronze. The shank is hollow, with a 3mm hole drilled through to the core barrel. The drills are intended for use in a lapidary workshop and are designed to be used with a drill-press at speeds of 1000-2000rpm, using water as a coolant and lubricant. Furthermore, they are designed more for cutting through holes, rather than coring blind into outcrops. Trials at the outcrop using a cordless

power drill showed that the coring drills could be used handheld successfully as long as the slower (340rpm) chuck speed was selected. The higher chuck speed of 1100rpm tended to result in fragmented core, with poor recovery, but was useful for starting holes accurately. Despite the rather modest claims made for the coring drills, they have proved to be eminently suitable for use in the field. With practise, it was possible to collect 2.5-3.5cm long, 7.5mm diameter cores, giving sufficient material for thin sections and isotope analysis.

Power drill and batteries

The 12v cordless drill used for this work has two chuck speeds (340 & 1100 rpm), forward and reverse and a progressive switch, allowing very slow speeds to be selected. The chuck was a simple hand-operated, twist and lock device which held the coring drill sufficiently tightly. The batteries are 12v rechargeable NiCads, weighing an estimated 500g each. These clip into the base of the drill and help to balance the power drill in the hand. Because of the very steep discharge characteristics of NiCads towards the end of their charge, they are able to perform useful work for nearly the whole of the charge capacity. However, once performance begins to decline, it does so very rapidly. One battery was capable of drilling about 4 holes, depending upon the depth

Water

Water is absolutely essential if the coring drills are to run without being damaged and if good core is to be obtained. Experience showed that c. 200-250ml of water was sufficient for most holes; what appears to matter most is not the amount of water, but

the way it is used. Cutting efficiency is much improved if the hole is flushed out frequently and the drill head washed off at the same time, rather than simply dribbling water on to the drill barrel proud of the hole. A squeeze laboratory water bottle with a fine nozzle is ideal, allowing a hole to be flushed with water at pressure.

In use

Holes can be drilled with a minimum spacing of 1cm; the resolution is therefore 1cm, with the effective sample being ~ 7 mm in diameter. Water was applied once the hole was begun and the slower speed selected. Harder rocks (amphibolite) proved just as quick to drill as soft ones (metallimestone); the drill mud from the latter tended to clog the drill head more readily, thereby slowing progress. Once broken, core was easily extracted by slowly withdrawing the core drill.

The time taken to drill a hole varied, but total drilling time is roughly 5-8 minutes. Forty-six holes were drilled over two days from one profile. This included all the setting up, sample description, preparation, etc. Battery charge lasts for about four holes.

Discussion

The equipment described above permits core sampling of profiles at a resolution of 1cm and is perfectly effective in obtaining satisfactory amounts of sample material. There is sufficient for isotopic analysis and for the preparation of a thin section and/or probe slide.

The only real problem with the equipment is battery charge life. Each battery was sufficient for only three to five holes, depending upon the depth of the hole and

the nature of the rock; this is equivalent to about 15-20 minutes of continuous drilling. If charging facilities are not available locally (eg a friendly garage), then it is necessary to consider carrying at least 6-8 batteries to complete a day's work. The batteries are small and relatively light, so that carrying sufficient batteries is not a problem. The cost of hiring extra batteries is not be exorbitant. At least two battery chargers will be required to recharge batteries in the evening, since the high capacity batteries take about 1 hour to charge from flat.

The drill and four batteries cost £28-90 to hire for three days. The drills cost about £34 net from the USA; freight was a considerable £29 and there was a hefty £24 import duty to pay on delivery. The total cost was about £87, of which some £53 was tax and shipping.

Conclusions

- 1) The drills worked well, showing little in the way of wear of the diamond tipping. With practise, they provided good, clean sample material.
- 2) The cordless drill was perfectly capable of powering the drills.
- 3) Although battery charge life is a significant limitation, the small size and relatively light weight of the batteries means that sufficient could be carried to allow a full day's work in remote ground. The discharge characteristics of NiCad batteries means that useful work can be done with them over most of their charge capacity.
- 4) Five to six litres of water should be sufficient for a day's work.
- 5) Sample resolution of 1cm is achievable with this system; sample length averaged about 30mm with ~ 7.5 mm diameter.

6) The equipment described provides a viable alternative to the petrol-powered drill. It is portable and permits discreet, high-resolution sampling of profiles in the field.

Appendix B

Strontium isotope analysis

Sample preparation, Sr separation and isotope analysis

Strontium isotope ratios analytical procedures are described below, with special reference to the ammonium acetate leaching procedure described by Gorokhov et al. (1995).

Reagents

Distilled water: Ultrapure (resistance: 18.2 MΩ) from a Milli-Q+ water purification system

Ammonium Acetate (NH₄OAc): 1M stock solution made up using 99% grade NH₄OAc in distilled water

Acetic acid (HOAc): 1M, Aristar grade

Hydrochloric acid (HCl): Various stocks made from 12M, Romil Ultrapure double distilled conc, diluted with Milli-Q water

Hydrofluoric acid (HF): Conc (40% v/v) Suprapure, with blank values of <200pg for silicates and ~5pg for carbonates

Nitric acid (HNO₃): 4M, sub-boil distilled in teflon

Phosphoric acid (H₃PO₄): 1M, Ultrex grade (Baker)

Rb spike: 99.13% ⁸⁷Rb at 0.024 μmols/gm

Cation exchange equipment

Columns: Quartz glass, with sintered glass frit, height ~14.5 cm, diameter ~1.2 cm.

Cation exchange resin: Bio-rad analytical grade, AG 50W-X8, 200-400 mesh, hydrogen form; resin bed height ~ 11.5cm and volume ~12ml.

Sample preparation

Saville[®] screw-top teflon pots + caps were cleared of static by covering the pot bases with aluminium foil and spraying with an antistatic gun and weighed to 5 decimal places. About 100 milligrams of *c.* 150 µm grade powdered sample were weighed into the pots and the weights recorded. The samples were removed to the clean laboratory for chemical preparation.

Pilot study

Gorokhov et al. (1985) used an ammonium acetate washing technique to remove surface bound, radiogenic, $^{87}\text{Sr}/^{86}\text{Sr}$ which could bias $^{87}\text{Sr}/^{86}\text{Sr}$ in the carbonate. However, it is unclear whether they used 1M or 1N (0.15M) NH_4OAc for their leaching work. Three separate sample preparation experiments were undertaken to establish the method that gives the lowest $^{87}\text{Sr}/^{86}\text{Sr}$ values for the calcite fraction alone and to determine the optimum concentration of NH_4OAc .

Experiment 1

Sample: Tayvallich samples T1, T2

Samples were leached in 2.5ml of 1M NH_4OAc to remove surface bound Sr, then leached successively in 2.5 ml 0.1M HOAc and 2.5 ml 1M HOAc for 2 hours at

room temperature, dissolving calcite. The remaining non-silicate component was dissolved in HF.

Experiment 2

Sample Tayvallich sample T1

Samples were leached in 2.5ml of 1M NH₄OAc then leached in 2.5 M HCl for 2 hours at room temperature.

Experiment 3

Sample: Tayvallich samples T1, T2

Samples were leached in 2.5ml of 0.15 M (1N) NH₄OAc then leached in 1 M HOAc for 2 hours at room temperature.

Reagent blanks were prepared for all three experiments

Leaching procedure details

During the NH₄OAc/HOAc leaching procedure, leachates and solids were transferred quantitatively to centrifuge tubes and centrifuged at 3000rpm for 2 minutes. The first leachate was retained for ⁸⁷Sr/⁸⁶Sr analysis. The sample was washed in distilled water twice and centrifuged between each wash to remove NH₄OAc. The first of the washings was added to the NH₄OAc leachate, the second was discarded. The residue was transferred back to the teflon pot with a little distilled water. Note that some particulate matter (s.g. < 1) adhering to the sides of the centrifuge tubes was not transferred. This material is probably graphite. The residue was then leached in 1M CH₃COOH for 2 hours. The resulting leachate was separated

from residue non-soluble in HOAc by centrifuging, spiked with Rb and evaporated to incipient dryness on a hot plate at *c.* 57°C.

Separation of Sr and Rb

Empty sample beakers were cleaned with a small volume of 6M HCl and heated on a hotplate for 30 mins. Once cool, the acid was discarded and the beakers rinsed with distilled water.

Sr and Rb were separated into cleaned beakers in 2.5 N HCl using Bio-Rad AG50W X8 200-400 mesh cation exchange resin. Total procedure blanks for Rb and Sr were less than 0.5 ng.

⁸⁷Sr/⁸⁶Sr analysis

Dried Sr samples were dissolved in 1μl 1N H₃PO₄ and loaded onto single Ta filaments. Rb samples were loaded onto triple Ta filaments. Sr samples were analysed on either a VG 54E single collector thermal ionisation mass spectrometer or a VG Sector 54-30 multiple collector mass spectrometer. On the VG 54E instrument ion beams were managed to give a total intensity of 1.5V (1.5 x 10⁻¹¹A). On the Sector 54-30, ⁸⁸Sr intensity was maintained at 1V (1 x 10⁻¹¹A) ± 10%. On both instruments, the ⁸⁷Sr/⁸⁶Sr ratio was corrected for mass fractionation using ⁸⁶Sr/⁸⁸Sr = 0.1194 and an exponential law. On the VG 54E up to 6 sets of 25 ratios were collected and the mean and standard error computed until an internal precision better than ± 0.00004 (2 SE) was achieved. Repeat analysis of Sr standard NBS 987 gave ⁸⁷Sr/⁸⁶Sr = 0.71024 ± 3 (1 SD, n = 20). The VG Sector 54-30 mass spectrometer

was operated in the peak-jumping mode with data collected as 15 blocks of 10 ratios. For this instrument NBS987 gave 0.710243 ± 10 (1 SD, $n = 88$).

Rb samples were analysed on either a VG MM30 or a VG54E single collector mass spectrometer. 3 sets of 10 ratios are collected and the mean and standard error computed.

Rb and Sr and isotope ratios are adjusted for mass fractionation and spike contribution and concentrations calculated using adaptations of the standard algorithms of Krough & Hurley (1968; J. Geophys. Res 73, 7107-7125).

Appendix C

Oxygen and carbon isotope analysis

C.1 SIMS analysis by ion microprobe

C.2 Conventional carbon and oxygen isotope analysis

C.3 LASSIE carbon and oxygen analysis

C.1 – Ion Probe Secondary Ion Mass Spectrometry

I outline briefly the principles of SIMS analysis used in this study. More technical details are given by Valley et al., (1998).

The ion microprobe, University of Edinburgh

All SIMS analyses presented in this thesis were made using the Cameca ims-4f ion microprobe facility in the Department of Geology and Geophysics at the University of Edinburgh. The instrument is controlled by a Charles Evans and Associates computer system

The ion microprobe facilitates analysis of isotopes and trace elements at the grain-scale. Material is sputtered from the sample surface by a primary high energy beam of ions. Secondary ions in the sputtered material are collected using a mass spectrometer and an ion detection system.

There are two primary ion beam sources: a duoplasmatron and a caesium source. Ions generated at the primary source are passed to the sample via the primary column which controls the shape, size and position of the beam and its intensity. The secondary ions generated from the sample by the primary beam are removed by the

extraction lens and transferred to the mass spectrometer by a second electrostatic lens. Charge neutralisation to prevent charge build up on the insulating sample surface during analysis is achieved using a normal incidence electron flood gun (Migeon, et al., 1990).

Because the secondary ions have wide ranging energies, they are filtered to separate them from unwanted molecular species present at low energy levels. Only a small proportion of the energy range of the secondary ions is allowed to pass through the energy slit. This filtered beam is then passed through a magnetic field (the mass analyser) which deflects this secondary beam according to the mass/charge ratio of the ions. This permits mass resolution of the secondary ion beam. The secondary ions are then passed to the detector. The magnitude of the secondary ion beam is measured using an electron multiplier in which the secondary ions trigger a pulse of secondary electrons. This pulse is amplified and, if above a certain threshold, is passed to the counting circuit.

$\delta^{18}\text{O}$ analysis

Operating conditions

Primary beam: Cs^+ ions generated from the primary gun at 10 kV, defocussed to ~ 25 – 30 microns in diameter.

Charge neutralisation: Normal incidence electron flood-gun. Electrons are emitted from a tungsten filament held at –4150 V and deflected and shaped by coils and lenses to arrive at the sample surface, also at –4150 V, with zero energy. The electron cloud is held just above the sample surface to facilitate charge compensation.

Electron multiplier: ETP AF 133H

Count times: 80 cycles of 8 seconds on ^{18}O and 1 second on ^{16}O , giving a total of 640 seconds counting ^{18}O and 80 seconds counting ^{16}O . This counting regime is designed to give 10^6 counts on ^{18}O in order to achieve $\sim 1\%$ precision.

Standards:

Calcite: University of Wisconsin Calcite (UWC): $\delta^{18}\text{O} = 23.28 \pm 0.06\%$ (Valley, et al., 1997)

Quartz: Bogola Quartz (BOG): $\delta^{18}\text{O} = 12.3 \pm 0.3\%$ (Elsenhimer and Valley, 1993)

Data processing

Count rate (CR) = total number of counts / counting time

The count rate is corrected for dead-time:

$\text{CR} = \text{CR} / (1 - \text{CR}\tau)$, where τ is the dead time correction

The isotope ratio is calculated from:

$$^{18}\text{O}/^{16}\text{O} = \text{CR}(^{18}\text{O}) / \text{CR}(^{16}\text{O})$$

The mean and standard deviation of $^{18}\text{O}/^{16}\text{O}$ for all the counting cycles is then calculated. Values lying $\pm 3\sigma$ from the mean are rejected and the mean is recalculated on the remaining analyses.

This procedure gives the average $^{18}\text{O}/^{16}\text{O}$ for the sample: R_{sam}

Instrumental drift is corrected for by regressing the analysed value of the standards against analysis number using linear least squares. This allows $^{18}\text{O}/^{16}\text{O}$ of the standard to be calculated for the time of the equivalent sample analysis.

The corrected value of the standard $^{18}\text{O}/^{16}\text{O}$ analysis at the time of each individual sample analysis is then used to calculate $\delta^{18}\text{O}$ in the sample via:

$$\delta^{18}\text{O}_{\text{sam}} (\text{‰}) = (R_{\text{sam}} / R_{\text{std}}) \times (\delta^{18}\text{O}_{\text{std}} + 1000) - 1000$$

Calculation of error on the $\delta^{18}\text{O}$ values

I followed the methodology of Fitzsimons and Harte (in press) in which they formulate an expression which propagates error on the sample and standards through to the $\delta^{18}\text{O}$ value. The errors quoted in the listing of analyses below are calculated on this basis. Errors on $\delta^{18}\text{O}$ in calcite are typically $\sim \pm 1 \text{ ‰}$. On quartz $\delta^{18}\text{O}$ analyses they are typically $\pm 1.5 \text{ ‰}$.

SIMS Trace element analysis

Elements/mass analysed:

^{26}Mg , ^{30}Si , ^{44}Ca , ^{54}Fe , ^{55}Mn , ^{88}Sr , mass 131, ^{138}Ba

Operating conditions

Primary beam:

Duoplasmatron, yielding a beam of negative ^{16}O ions, filtered to yield an isotopically pure beam; charge neutralisation is not required.

Accelerating voltage: 4.5 kV

Beam diameter: 20 microns

Counting conditions:

20 count cycles, counting each mass counted for two seconds.

Standard:

Norman Cross Calcite (NCC) (Swart, 1990)

Data processing:

The concentration of the element in the sample in ppm is given by

$$\text{Conc}_{\text{sam}}(x) = [\text{CPS}_{\text{sam}}(x) / \text{IY}_{\text{sam}}(\text{Ca})] \times 1 / \text{RIY}_{\text{std}}(x)$$

where:

x is the element of interest

$\text{CPS}_{\text{sam}}(x)$ is counts per seconds of x in the sample

$\text{IY}_{\text{sam}}(\text{Ca})$ is the ion yield of Ca in the sample

$\text{RIY}_{\text{std}}(x)$ is the relative ion yield of x in the standard.

The relative ion yield of x in the sample is assumed to be the same as that in the standard.

Errors:

In ion probe trace element analysis, the errors on the analyses are based directly on the errors on the counting statistics:

$$\% \text{ error } (1\sigma) = \sqrt{N} / N \times 100$$

where N is the total number of counts over the counting period.

C.2 Conventional carbon and oxygen isotope analysis

Method

Conventional stable isotope analysis was carried out at the Scottish Universities Research and Reactor Centre (SURRC), East Kilbride.

Bulk carbonate analyses of $\delta^{18}\text{O}$ and $\delta^{13}\text{C}$ were determined on powders of whole-rock samples, micro-drilled powders from hand-specimens and powdered fragments of mini-core. CO_2 was extracted under vacuum from 10 – 15 mg powder from each sample by reaction with 5 cm^3 of concentrated phosphoric acid (H_3PO_4) at 25°C (McCrea, 1950; Rosenbaum and Sheppard, 1986). Samples were left to react for 24 hours. After extraction, the CO_2 was purified and then analysed in a VG Isogas SIRA 10 mass spectrometer.

C.3 Laser ablation stable isotope analyses

Reconnaissance isotope analyses of $\delta^{13}\text{C}$ and $\delta^{18}\text{O}$ were obtained on samples of the Torulian and Inchroty Limestones from the sample profiles by lasers ablation isotope analysis using the LASSIE (Laser Ablation System for Stable Isotope Extraction) system at SURRC, East Kilbride (Smalley et al., 1992)

At SURRC the LASSIE laser system is been adapted to use a 10.6 μm wavelength CO_2 laser and a Leitz Metallux petrographic microscope with motorised XYZ stage. Carbonate minerals decompose thermally beneath the laser beam to produce CO_2 gas which is frozen into the mass-spectrometer for analysis. From replicate analyses of carbonate mineral standards, analytical precisions of $\pm 1\text{‰}$ for both $\delta^{13}\text{C}$ and $\delta^{18}\text{O}$ are obtained.

To optimise analytical reproducibility operating condition of the laser system, such as laser beam incidence angle and laser power must vary as little as possible.

Variations in operating conditions and variations in sample texture and chemistry, can affect the laser-induced fractionation factors $\Delta^{13}\text{C}$ and $\Delta^{18}\text{O}$ (the difference between laser-derived isotope values and true isotope values) which result from the production during thermal decomposition of carbonate minerals of some CO, C and O as well as CO₂. The use of analytical standards similar in nature to the sample unknowns being analysed, in combination with conventional analysis cross-checks, are employed to monitor fractionation factor stability. These laser fractionation factors are then used to correct the carbon and oxygen isotopic values of the sample gas measured in the mass spectrometer.

Appendix D

SIMS $\delta^{18}\text{O}$ and trace element results

The $\delta^{18}\text{O}$ and trace element data are presented in the following tables D.1, D.2. Only the compiled corrected data are given.

Errors on $\delta^{18}\text{O}$ include error on the measurement of the standard (see Appendix C)

Errors on the trace elements are not listed but are typically as follows, based directly on the error on the counting statistics:

Mg: $\pm 0.25 \%$

Si: $\pm 24 \%$

Fe: $\pm 0.51 \%$

Mn: $\pm 0.19 \%$

Sr: $\pm 0.15 \%$

Ba: $\pm 4.2 \%$

SIMS Project: IMP/119/1097

Calcite $\delta^{18}\text{O}$ analyses, Torulian Limestone sample CT53, Inchrory Limestone samples LWQ1/28, 1/30

Final compiled results

Analysis	Result	(+/-)	Comments	Profile	Distance
17/6/98					
B:LWQ28-1.DAT	22.5	1.20			
B:LWQ28-2.DAT	20.9	1.28			
B:LWQ28-3.DAT	20.3	1.17			
B:LWQ28-4.DAT	21.4	1.27			
B:LWQ28-5.DAT	22.8	1.19		28/1	322.0
B:LWQ28-6.DAT	21.3	1.36		28/1	48.4
B:LWQ28-7.DAT	20.5	1.33			
B:LWQ28-8.DAT	27.0	1.38			
B:LWQ28-9.DAT	22.7	1.47		28/1	380.0
B:LWQ28-10.DAT	20.4	1.45		28/1	147.0
Max:	27.0	1.5	Mean precision:	1.31	Median: 1.30
Min:	20.3	1.2	Standard deviation:	0.11	n: 10
18/6/98					
B:LWQ28-11.DAT	25.7	1.09		28/1	230.0
B:LWQ28-12.DAT	25.6	0.95			
B:LWQ28-13.DAT	26.9	0.98			
B:LWQ28-14.DAT	21.5	0.88			
B:LWQ28-15.DAT	24.0	0.96			
B:LWQ28-16.DAT	24.2	1.07			
B:LWQ28-17.DAT	24.4	1.04			
B:LWQ28-18.DAT	22.8	0.96			
B:LWQ28-19.DAT	24.3	1.05			
B:LWQ28-20.DAT	24.1	1.00			
B:LWQ28-21.DAT	23.1	0.83			
B:LWQ28-22.DAT	24.8	1.11			
B:LWQ28-23.DAT	21.9	0.90			
B:LWQ28-24.DAT	20.8	1.09			
B:LWQ28-25.DAT	22.4	0.98			
B:LWQ28-26.DAT	22.0	0.96			
B:LWQ28-27.DAT	18.4	0.85			

Table D.1 SIMS oxygen isotope results

Analysis	Result	(+/-)	Comments	Profile	Distance
B:LWQ28-28.DAT	22.4	0.97			
B:LWQ28-29.DAT	22.5	1.01			
B:LWQ28-30.DAT	22.7	0.86			
B:LWQ28-31.DAT	22.8	1.06			
B:LWQ28-32.DAT	23.6	1.98	Aborted analysis		
B:LWQ28-33.DAT	20.7	1.07			
B:LWQ28-34.DAT	25.3	0.97			
B:LWQ28-35.DAT	23.7	0.98			
Max:	26.9	2.0	Mean precision:	1.02	Median: 0.98
Min:	18.4	0.8	Standard deviation:	0.21	n: 25
19/6/98			Mean Standard:	23.3	Standard deviation: 1.1
B:CT53-1.DAT	16.2	1.0			
B:CT53-2.DAT	17.5	0.9			
B:CT53-3.DAT	17.0	1.0			
B:CT53-4.DAT	16.5	1.0			
B:CT53-5.DAT	13.3	1.0			
B:CT53-6.DAT	22.3	0.9			
B:CT53-7.DAT	20.7	1.1			
B:CT53-8.DAT	18.5	0.9			
B:CT53-9.DAT	18.7	0.8			
B:CT53-10.DAT	21.2	0.9			
B:CT53-11.DAT	18.6	0.9			
B:CT53-12.DAT	19.6	1.0			
B:CT53-13.DAT	15.3	1.1			
B:CT53-14.DAT	15.0	0.9			
B:CT53-15.DAT	15.3	0.9			
B:CT53-16.DAT	10.8	1.0			
B:CT53-18.DAT	14.4	1.0			
B:CT53-19.DAT	14.6	1.0			
Max:	22.3	1.1	Mean precision:	0.96	Median: 0.96
Min:	10.8	0.8	Standard deviation:	0.06	n: 18
22/6/98			Mean Standard:	23.3	Standard deviation: 0.9
B:LWQ25-1.DAT	23.7	1.3			
B:LWQ25-2.DAT	22.5	1.0			
B:LWQ25-3.DAT	22.4	1.0			
B:LWQ25-4.DAT	23.1	1.0			
B:LWQ25-5.DAT	22.4	1.0			

Table D.1 SIMS oxygen isotope results

Analysis	Result	(+/-)	Comments	Profile	Distance
B:LWQ25-6.DAT	22.9	1.2			
B:LWQ25-7.DAT	23.7	1.0			
B:LWQ25-8.DAT	24.3	1.0			
B:LWQ25-9.DAT	23.9	1.0			
B:LWQ25-10.DAT	25.0	1.0			
B:LWQ25-11.DAT	27.2	1.3			
B:LWQ25-12.DAT	26.1	1.2			
Max:	27.2	1.3		Mean precision:	1.09
Min:	22.4	1.0		Standard deviation:	0.11
				Median:	1.04
				n:	12
				Mean Standard:	23.3
				Standard deviation:	1.7
23/6/98					
B:CT53-20.DAT	19.1	1.0		CT53/b	786.0
B:CT53-21.DAT	13.6	1.1		CT53/b	63.0
B:CT53-22.DAT	17.2	1.0		CT53/b	227.0
B:CT53-23.DAT	15.8	1.1		CT53/b	169.0
B:CT53-24.DAT	16.5	1.0		CT53/b	1110.0
B:CT53-25.DAT	16.3	1.1		CT53/b	416.0
B:CT53-26.DAT	16.5	1.0		CT53/b	126.0
B:CT53-27.DAT	15.5	1.1		CT53/b	711.0
B:CT53-28.DAT	19.4	1.0		CT53/b	331.0
B:CT53-29.DAT	18.1	0.9	Origin of profile CT53/b	CT53/b	0.0
B:CT53-30.DAT	17.8	0.9		CT53/b	892.0
B:CT53-31.DAT	17.2	1.1		CT53/b	526.0
B:CT53-32.DAT	16.4	0.9		CT53/b	617.0
B:CT53-33.DAT	16.6	0.9	Adjacent to profile CT53/b	CT53/b	
B:CT53-34.DAT	17.3	1.0	Adjacent to profile CT53/b	CT53/b	
B:CT53-35.DAT	15.5	1.0		CT53/a	1880.0
B:CT53-36.DAT	10.3	0.9		CT53/a	1130.0
B:CT53-37.DAT	15.2	1.1		CT53/a	1390.0
B:CT53-38.DAT	10.2	0.9		CT53/a	1300.0
B:CT53-39.DAT	17.5	1.1		CT53/a	1340.0
B:CT53-40.DAT	16.3	1.0		CT53/a	1700.0
B:CT53-41.DAT	17.9	1.0		CT53/a	1620.0
B:CT53-42.DAT	10.1	0.8		CT53/a	948.0
B:CT53-43.DAT	11.9	1.1		CT53/a	872.0
B:CT53-44.DAT	16.9	1.1		CT53/a	742.0
B:CT53-45.DAT	15.6	1.2	Origin of profile CT53/a	CT53/a	0.0
B:CT53-46.DAT	15.6	0.9		CT53/a	800.0

Table D.1 SIMS oxygen isotope results

Analysis	Result	(+/-)	Comments	Profile	Distance
B:CT53-47.DAT	15.0	1.0		CT53/a	593.0
B:CT53-48.DAT	17.7	1.1		CT53/a	387.0
B:CT53-49.DAT	13.8	1.1		CT53/a	186.0
Max:	19.4	1.2		Mean precision:	1.01
Min:	10.1	0.8		Standard deviation:	0.08
24/6/98					
B:CT53-56.DAT	17.3	0.9		CT53/c	2150.0
B:CT53-58.DAT	16.6	1.2		CT53/c	1340.0
B:CT53-59.DAT	18.4	1.1		CT53/c	1660.0
B:CT53-60.DAT	19.0	1.0		CT53/c	1780.0
B:CT53-61.DAT	17.6	0.9		CT53/c	1720.0
B:CT53-62.DAT	18.2	1.0		CT53/c	1560.0
B:CT53-63.DAT	16.3	1.0	Origin of profile CT53/c	CT53/c	0.0
B:CT53-64.DAT	17.7	1.1		CT53/c	2040.0
B:CT53-65.DAT	14.8	0.9		CT53/c	1100.0
B:CT53-66.DAT	13.8	1.0		CT53/c	387.0
B:CT53-67.DAT	18.3	1.1		CT53/c	203.0
B:CT53-68.DAT	13.0	1.0		CT53/c	1180.0
B:CT53-69.DAT	15.6	0.9		CT53/c	1260.0
B:CT53-70.DAT	12.4	0.9		CT53/c	1010.0
B:CT53-71.DAT	17.6	1.1		CT53/c	1450.0
B:CT53-73.DAT	11.2	1.0		CT53/c	826.0
B:CT53-74.DAT	14.3	1.1		CT53/c	679.0
B:CT53-75.DAT	13.1	1.1		CT53/c	297.0
Max:	19.0	1.2		Mean precision:	1.01
Min:	11.2	0.9		Standard deviation:	0.09
25/6/98					
B:CT53-76.DAT	10.5	1.3		CT53/c	1910.0
B:CT53-77.DAT	12.4	1.2		CT53/c	2510.0
B:CT53-78.DAT	16.4	1.0		CT53/c	2320.0
B:CT53-79.DAT	14.5	1.1		CT53/c	2580.0
B:CT53-80.DAT	9.3	1.2		CT53/c	2820.0
B:CT53-81.DAT	17.4	1.1			
B:CT53-82.DAT	13.0	1.0			
B:CT53-83.DAT	19.0	1.2			
B:CT53-84.DAT	20.7	1.0			
B:CT53-85.DAT	19.3	1.1			
B:CT53-86.DAT	18.6	1.1			
B:CT53-87.DAT	16.2	1.1			

Table D.1 SIMS oxygen isotope results

Quartz $\delta^{18}\text{O}$ analyses, Inchroly Limestone samples LWQ1/28, 1/30

Analysis	Result	(+/-)	Comments**
Date: 01/03/1999			
B:LWQ28-1.DAT	23.5	1.62	Adjacent LWQ28-37 calcite analysis
B:LWQ28-2.DAT	24.6	1.59	Other end of above quartz
B:LWQ28-3.DAT	25.2	1.59	Adjacent LWQ28-30 calcite analysis
B:LWQ28-4.DAT	26.1	1.49	Small quartz adjacent to analyses LWQ28-1 to 3
B:LWQ28-5.DAT	14.3	1.54	Carbonate, not quartz
B:LWQ28-6.DAT	25.1	1.43	Small quartz adjacent to LWQ28-2
B:LWQ28-7.DAT	25.9	1.43	Large quartz grain adjacent to LWQ28-38
B:LWQ28-8.DAT	24.5	1.37	Centre of above large quartz grain
B:LWQ28-9.DAT	24.1	1.43	Centre of small quartz grain adjacent to LWQ28-17
B:LWQ28-10.DAT	22.5	1.32	Centre of large quartz grain adjacent to LWQ28-20
B:LWQ28-11.DAT	23.1	1.28	Centre of quartz grain
B:LWQ28-12.DAT	21.3	1.44	Centre of quartz grain at edge of luminescent zone adjacent to LWQ28-42
B:LWQ28-13.DAT	20.3	1.27	Edge of quartz grain at edge of luminescent zone adjacent to LWQ28-42
B:LWQ28-14.DAT	20.3	1.50	Centre of small quartz grain in luminescent domain
B:LWQ28-15.DAT	21.1	1.47	Centre of small quartz grain in luminescent domain
B:LWQ28-16.DAT	22.4	1.50	Centre of small/medium quartz grain in luminescent domain
B:LWQ28-17.DAT	24.5	1.49	Centre of small quartz grain in texturally equilibrated area
B:LWQ30-1.DAT	21.8	1.35	Centre of small quartz grain adjacent to feldspar and in edge of calcite
B:LWQ30-2.DAT	22.5	1.44	Centre of small quartz grain isolated in calcite grains
B:LWQ30-3.DAT	25.1	1.39	Centre of small quartz grain adjacent to feldspar at edge of calcite plate with analysis LWQ30-5
B:LWQ30-4.DAT	26.9	1.53	Centre of small quartz grain in qtz-fsp cluster, N edge of luminescent domain adjacent LWQ30-13
B:LWQ30-5.DAT	23.2	1.59	Centre of larger quartz grain near LWQ30-11/12 and 14
B:LWQ30-6.DAT	27.6	1.52	Centre of quartz grain between LWQ30-11/12,13,14 and LWQ30-6, 8 and 9
B:LWQ30-7.DAT	19.6	1.79	Centre of quartz grain near LWQ30-6
B:LWQ30-8.DAT	23.2	1.87	Centre of small quartz grain at edge of altered feldspar halo
B:LWQ30-9.DAT	25.8	1.87	Centre of quartz grain SE of LWQ30-8
B:LWQ30-10.DAT	23.6	1.86	Centre of quartz grain adjacent to LWQ30-10
B:LWQ30-11.DAT	26.1	1.82	Centre of small quartz grain adjacent to LWQ30-2
Max:	27.6	1.9	Mean precision: 1.53
Min:	14.3	1.3	Standard deviation: 0.17
			Median: 1.50
			n: 28
			Mean Standard: 12.0
			Standard deviation: 1.5

Table D.1 SIMS oxygen isotope results

467

Analysis	Mg	Si	Fe	Mn	Sr	Ba	$\delta^{18}\text{O}$	error	Profile x	Sr/Mn
LWQ25-1	6054.0	2.1	11150.0	2468.0	2272.0	7.36	23.7	1.3		0.92
LWQ25-2	6073.0	1.9	11310.0	2464.0	2297.0	7.26	22.5	1.0		0.93
LWQ25-3	6058.0	3.2	11200.0	2513.0	2260.0	7.19	22.4	1.0		0.90
LWQ25-4	6167.0	2.9	11550.0	2484.0	2311.0	8.84	23.1	1.0		0.93
LWQ25-5	6900.0	58.7	12070.0	2621.0	2295.0	7.66	22.4	1.0		0.88
LWQ25-6	4624.0	219.5	9014.0	2537.0	2139.0	4.52	22.9	1.2		0.84
LWQ25-7	7900.0	1.6	13420.0	3026.0	2440.0	9.58	23.7	1.0		0.81
LWQ25-8	8792.0	3.0	13690.0	3177.0	2524.0	8.89	24.3	1.0		0.79
LWQ25-9	7223.0	99.2	10800.0	3303.0	2589.0	11.83	23.9	1.0		0.78
LWQ25-10	7422.0	5204.0	19830.0	3175.0	2089.0	7.14	25.0	1.0		0.66
LWQ25-11	9923.0	2.0	15130.0	3749.0	2661.0	9.18	27.2	1.3		0.71
LWQ25-12	8796.0	1.3	13730.0	3654.0	2470.0	8.13	26.1	1.2		0.68
LWQ28-1	2050.0	92540.0	7189.0	419.0	1280.0	5.22	22.5	1.20		3.05
LWQ28-9	3052.0	1471.0	6787.0	570.7	1951.0	7.20	22.7	1.47		3.42
LWQ28-5	3042.0	7.1	6809.0	571.9	1967.0	7.35	22.8	1.19		3.44
LWQ28-11	2989.0	3.4	6801.0	580.2	1968.0	7.15	25.7	1.09		3.39
LWQ28-10	3027.0	17.7	6849.0	588.6	1952.0	7.66	20.4	1.45		3.32
LWQ28-6	2943.0	20.7	6756.0	589.9	1855.0	6.55	21.3	1.36		3.14
LWQ28-8	3055.0	9.1	6753.0	585.2	1970.0	7.08	27.0	1.38		3.37
LWQ30-1	3877.0	8.8	7932.0	421.7	2047.0	6.87	22.4	1.1		4.85
LWQ30-3	2263.0	101.2	5150.0	360.2	1815.0	4.21	15.7	0.9		5.04
LWQ30-7	3956.0	6.2	7900.0	422.1	1978.0	5.86	27.0	1.1		4.69
LWQ30-13	3803.0	712.2	10570.0	418.3	1961.0	4.49	26.4	1.0		4.69
LWQ30-14	3594.0	39.3	8068.0	411.8	2040.0	4.82	25.0	1.0		4.95
CT53-35	5250.0	78.0	1293.0	67.0	909.5	13.91	15.5	1.0	1880.0	13.58
CT53-40	4069.0	89.4	2279.0	67.4	920.3	16.58	16.3	1.0	1700.0	13.65
CT53-41	3739.0	11.1	804.1	117.2	741.1	2.56	17.9	1.0	1620.0	6.32
CT53-37	1132.0	98.0	582.3	877.3	720.7	2.92	15.2	1.1	1390.0	0.82
CT53-38	20740.0	25100.0	10760.0	952.9	1205.0	3.38	10.2	0.9	1300.0	1.26
CT53-39	2594.0	42.1	1250.0	524.6	1215.0	5.54	17.5	1.1	1340.0	2.32
CT53-36	823.6	4.4	531.5	1299.0	432.5	0.19	10.3	0.9	1130.0	0.33

Table D.2 SIMS trace element analyses of calcite

Analysis	Mg	Si	Fe	Mn	Sr	Ba	$\delta^{18}\text{O}$	error	Profile x	Sr/Mn
CT53-42	596.5	8.0	402.7	1326.0	346.1	0.28	10.1	0.8	948.0	0.26
CT53-43	677.9	1223.0	369.5	1418.0	958.8	4.36	11.9	1.1	872.0	0.68
CT53-46A	25870.0	151600.0	5640.0	1036.0	768.9	31.37	15.6	0.9	800.0	0.74
CT53-46B	3045.0	84.4	1597.0	294.6	713.8	2.58	15.6	0.9	800.0	2.42
CT53-44	4152.0	34.9	1293.0	121.9	778.7	7.49	16.9	1.1	742.0	6.39
CT53-47	1611.0	17.4	649.1	312.8	926.5	4.55	15.0	1.0	593.0	2.96
CT53-48A	5071.0	40.5	1147.0	174.4	1280.0	49.33	17.7	1.1	387.0	7.34
CT53-48B	2073.0	27.4	886.5	312.5	875.5	8.43	17.7	1.1	387.0	2.80
CT53-49	1988.0	54.3	559.4	117.8	609.1	0.96	13.8	1.1	186.0	5.17
CT53-45A	3078.0	58.7	1523.0	80.8	1011.0	23.94	15.6	1.2	0.0	12.52
CT53-45B	12580.0	10.6	1591.0	115.8	849.2	2.47	15.6	1.2	0.0	7.33
CT53-86	1665.0	92.0	582.4	760.5	802.0	4.62	18.6	1.1		1.05
CT53-85	3758.0	29.6	774.1	109.4	1026.0	5.64	19.3	1.1		9.38

Values in ppm

Oxygen isotope data are from the adjacent analysis pit with the same corresponding sample number

Profile X is the position of the analysis along the grain scale profile; see Chapter 9

Table D.2 SIMS trace element analyses of calcite

Appendix E

Locality-specific details of geology, petrography and sampling procedures Torulian Limestone and Inchrory Limestone

In this Appendix, I discuss features of the geology and petrography of the Torulian and Inchrory limestones specific to the two localities from which detailed sample suites were obtained. This discussion sets the context for discussion of the O and C isotope and trace element data later in the chapter.

E1.1 Torulian Limestone in the River Avon, Bridge of Avon, Tomintoul

The Torulian Limestone is one of several white limestone units characteristic of successions lying immediately above the top of the Appin Quartzite throughout the Dalradian (Chapter 2). It is extremely pure, with chemical analyses showing that it verges on pure CaCO_3 (Table 4.2, Chapter 4; Thomas, 1989, bound in). It is of interest because limestones of this purity *should* be impervious to metamorphic fluid infiltration where undeformed (Holness and Graham, 1991; Holness and Graham, 1995). In theory, at least, this unit provides an ideal natural comparison to the experimental studies of fluid infiltration in pure calcitic matrices of Holness and Graham. However, work detailed below reveals that deformation has played a major role in the fluid-rock interaction history of this unit where sampled in the River Avon.

Torulian Limestone sample profile

The detailed stable isotope geochemistry of this limestone has been studied via hand-specimen size samples obtained from a profile across near-continuous bank-side exposure in the north-south course of the River Avon, immediately north of Bridge of Avon [NJ 150 201] and some 2.5 km northwest of Tomintoul (Figure 9.1), Northeast Grampian Highlands. The rocks in this area have undergone polyphase deformation during and following amphibolite facies metamorphism (Chapter 2). Sampling details are given in Appendix A. 14 samples through the limestone were selected for O and C isotope analysis. Most of the remaining samples, which included quartzites and semipelites, were sectioned and examined petrographically. Their location within the sampled profile is shown schematically with lithologies and lithostratigraphy in Figure 9.6, referred to in later discussion.

Lithostratigraphy and petrography

The bank-side outcrop contains a southward-younging succession from the Corriehabbie Quartzite (= Appin Quartzite) into thin, strongly schistose semipelite and white limestone of the Ailnack Phyllite and Limestone Formation (= Appin Phyllite and Limestone). All the units are assigned to the Ballachulish Subgroup, Appin Group. The white limestone is assigned to the Torulian Limestone Member and the overlying schistose and phyllitic semipelites are assigned to the Allte Dregnie Phyllite Member (Chapter 2).

The Corriehabbie Quartzite is a thin to locally thickly bedded quartzite with rare thin semipelite units towards its top; cross lamination observed in the lower part of the

measured section gives younging to the south, consistent with the lithostratigraphical succession. The quartzite is fine to medium grained, thoroughly crystalline and is generally white to creamy buff or pale grey in colour. Biotite altering to chlorite and white mica are present in variable amounts locally, as is minor, variably sericitised plagioclase feldspar. Disseminated sulphides are common. A thin semipelite at about within the quartzite contains rare garnet and staurolite. Biotite and white mica define an early penetrative fabric which is crenulated by a later fabric related to folding approximately normal to the bedding.

The quartzite is locally fractured due to faulting along the adjacent river bed (see also below). Fine drusy quartz coats open fracture walls in places and it is cut by white quartz veins locally. Where fractured, the rocks often discolours ochreous brown colour due principally to weathering of fine-grained sulphides.

Towards its top, the quartzite becomes more impure and micaceous. Between 26 and 27 m in the measured section, the quartzite is fractured and immediately overlain by schistose semipelite at the base of the Ailnack Phyllite and Limestone Formation at 27 m (Figure 9.6). Though there is a dislocation at this boundary, local lithostratigraphical control shows that there has not been significant displacement.

The semipelite at the base of the Ailnack Phyllite and Limestone is greenish-grey to dark brown, biotite-white-mica schist. The micas define a strong approximately bed-parallel penetrative fabric deformed by the later crenulation fabric which affects this section (see below). At its base, the semipelite contains a small amount of calcite

which becomes more abundant towards the top of the unit. This calcite is deformed by the later crenulation in that strings of calcite crystals appear folded round the crenulation micro-folds.

The Torulian Limestone comes in at 28.8 m. With the exception of two thin semipelite units at 29.2 – 29.4 m and 30.9 – 31.3 m, the limestone crops out continuously over about 6m until succeeded sharply by the Allt Dregnie Phyllite Member at 34.9 m. The limestone is pure white to very pale grey and coarsely crystalline. It is poorly bedded and massive, but lamination is picked out by strings of sulphide, which also occurs disseminated throughout the rock; sulphides are chiefly pyrite with a little pyrrhotite (reconnaissance $\delta^{34}\text{S}$ analyses of extracted sulphides from three limestone samples are presented in Appendix A.n).

The basal metasedimentary rocks of the overlying Allt Dregnie Member are schistose to phyllitic, calcareous semipelites. They carry strong penetrative to spaced early fabric(s) deformed by the oblique crenulation cleavage which, in these rocks, develops into minor chevron folding. Some small quartz veins are boundinaged and folded within the early fabric.

Structure

The section lies on the southern limb of a major kilometre-scale early (D_1 - D_2) periclinal fold (Figure 9.1). This has been deformed in the vicinity of the section by upright late orogenic, north-south aligned 100m-scale folds. Aligned approximately parallel to the late fold axial planes are two north-south trending steep faults which

disrupt the eastern part of the early fold structure. The eastern-most of these controls the course of the River Avon, immediately adjacent to the sampled section and is responsible for the local fracturing observed in the quartzites and grain-scale deformation observed in thin section (see below). This fault lies at the northern end of a complex curvilinear, north-trending fault system which extends from the eastern margin of the Cairngorm Granite intrusion. These faults probably belong to the family of N-S faults which occurs in the area. These faults are late structures, since they partly control and cut the Old Red Sandstone outliers in the Tomintoul area.

Bedding is generally highly oblique to line of the sampled section, so that the section is nominally across the strike and orientated north-south (Figure 9.1). The strike varies from 075° at the base of the section, swinging to 036° at $\sim 22.5\text{m}$ before increasing to near 090° near the top of the section. The dip is to the south or southeast at consistently moderate angles ($38\text{-}55^{\circ}$).

Two early cleavages are readily observed in the semipelitic lithologies. A penetrative cleavage recorded at about 36 m is orientated $032/50^{\circ}$ SE. Elsewhere, the main early cleavage is a spaced/crenulation fabric approximately parallel to bedding. These early fabrics are deformed by a crenulation cleavage which dips steeply east and which lies approximately axial planar to late minor neutral folds which plunge to the south. These minor folds are considered to be part of the late 100m scale folding

The section appears free of metre-scale folds affecting bedding *viz a vis* lithological repetition, although the 1 m thick limestone near the top of the section *may* be a repetition of the main limestone unit in a fold hinge. Pelitic laminae within the quartzite have a cleavage parallel to bedding. The base of the Ailnack Phyllite and Limestone Formation is marked by a dislocation containing a thin clay gouge.

The underlying quartzite is brecciated and the semipelite above the dislocation is strongly deformed and contains an isoclinal fold hinge; minor folds above this fold plunge at about 60E to 125E.

Fault deformation

Although brittle fracturing is manifest in the quartzites in the sampled section, grain-scale textural features in the quartzite and limestone described below show that there has also been some possible ductile deformation during movement of this fault and that the effects are more extensive than first realised.

Quartzite

The quartzite grain morphology shows that the rocks are in a generally strained state and there has been only partial recovery of any textural equilibrium it may once have had. Undulose extinction is ubiquitous, particularly in larger grains. Straight polygonal crystal boundaries are variably abundant and sutured boundaries are common. Quartz crystals vary from equant to elongate and the elongate crystals are parallel to the penetrative, bed-parallel fabric defined by the micas. This elongation thus appears early and syn-metamorphic. However, zones of cataclasis and protomylonitisation are common in a number of thin sections, forming anastomosing networks within which there is clear reduction in the crystal size (Figure E.1). The protomylonitic zones are near normal to the mica fabric and are considered a product of north-south ductile to brittle deformation along the fault in the River Avon. In places, the mica fabric is weakly crenulated parallel to the protomylonitic zones, suggesting a genetic link between protomylonite/cataclasis, the crenulation cleavage

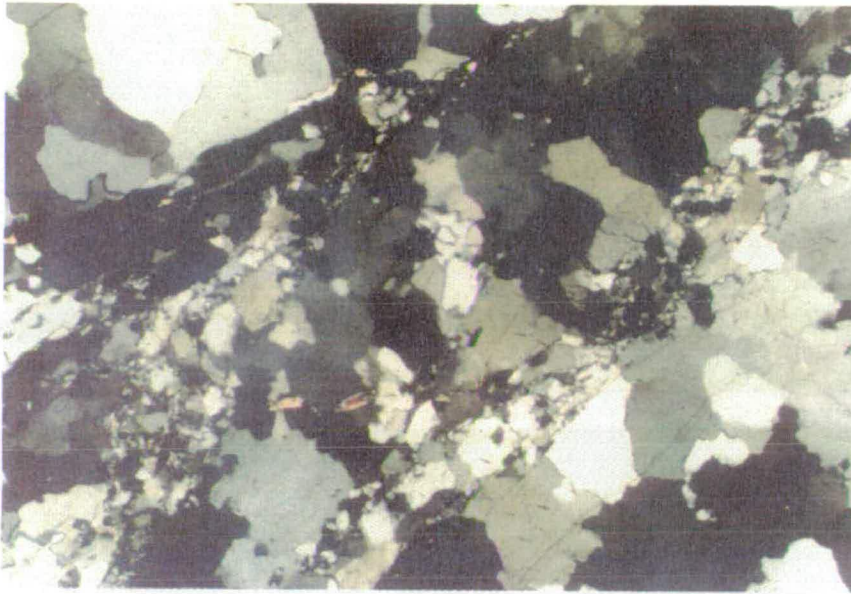


Figure E.1 Cataclasite textures in the Corriehabbie Quartzite, River Avon section, Bridge of Avon, near Tomintoul.

observed throughout the section and the larger late fold structures, to which the crenulation cleavage is parallel (Figure 9.1).

Torulian Limestone

Like the quartzite, the limestone shows considerable evidence of a strained state (e.g. Figure 3.23). Only in a few samples are equant polygonal triple-point textures well-developed and most calcite crystals have anhedral, sutured, ragged shape.

Protomylonitisation is seen at a very fine scale along grain boundaries in some samples. In many samples the calcite twin planes are very prominent, even under plane-polarised light, highlighting the strained state of the rocks. Some linear shear-bands contain recrystallised, fine-grained calcite and chlorite and calcite cleavage planes can be observed displaced across microfractures.

E1.2 Inchrory Limestone in Limeworks Quarry, Tomintoul

As noted in Chapter 2, a prominent feature of the Inchrory Limestone in the Northeast Grampian Highlands is the presence of pods of orthoamphibolite. These amphibolite pods are readily observed in Limeworks Quarry [NJ 155 194], about 1.5 km west of Tomintoul (Figures 9.1, 9.3). The presence of such metagneous material in the limestone is of interest because these two lithologies will have very different stable and Sr isotopic compositions and any significant interaction between them resulting from fluid infiltration would be apparent in changes in isotope and trace element chemistry. The boundary layers adjacent to the contact between the limestone and amphibolite thus provide the opportunity to determine the extent of

isotopic exchange between them and, thereby, elucidate the extent to which possible metamorphic fluid-rock interaction processes have affected the limestones.

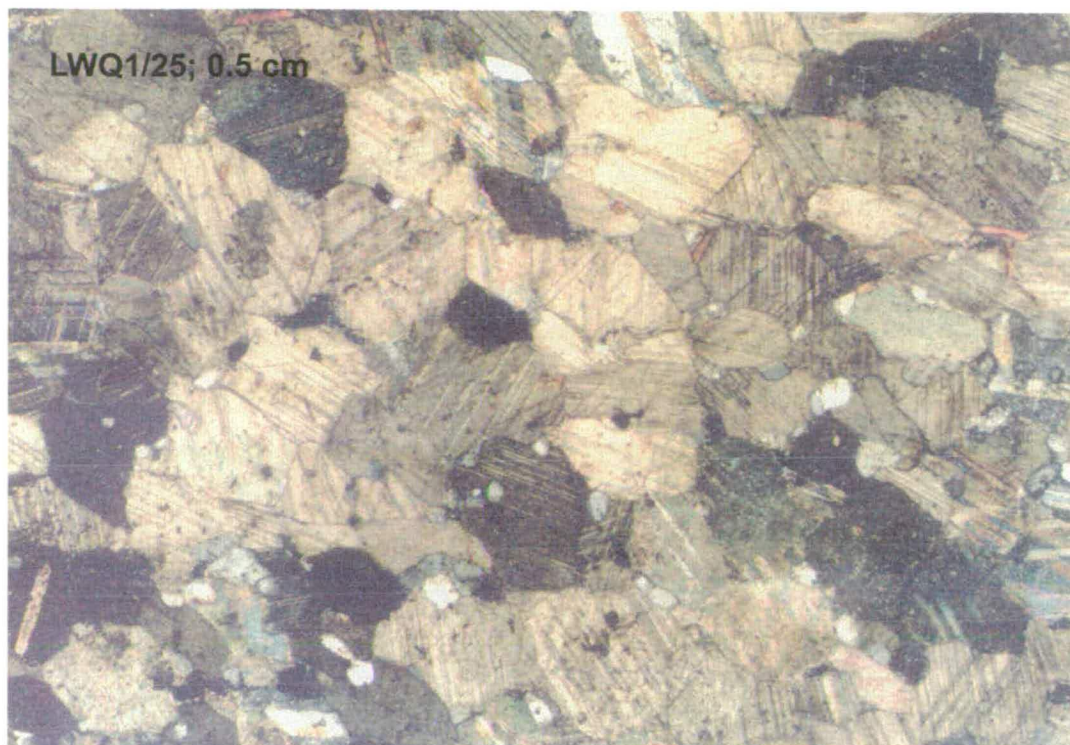
Limeworks Quarry sample profile

The north wall of Limeworks Quarry provides excellent exposure of contacts between limestone and amphibolite. One such contact (Figure 9.3) was sampled in detail using a high-resolution mini-coring technique, detailed in Appendix A.3. The profile was drilled from the centre of the amphibolite pod out into the limestone. The total profile length was 1 m, 0.43 m of which was drilled in the limestone. Forty-six samples of 7 mm diameter minicore were obtained, of which 22 were of limestone (LWQ1/25 – 46). Sampling spacing varied from ~1.25 cm at the amphibolite-limestone contact, to 5 cm in the outer part of the profile.

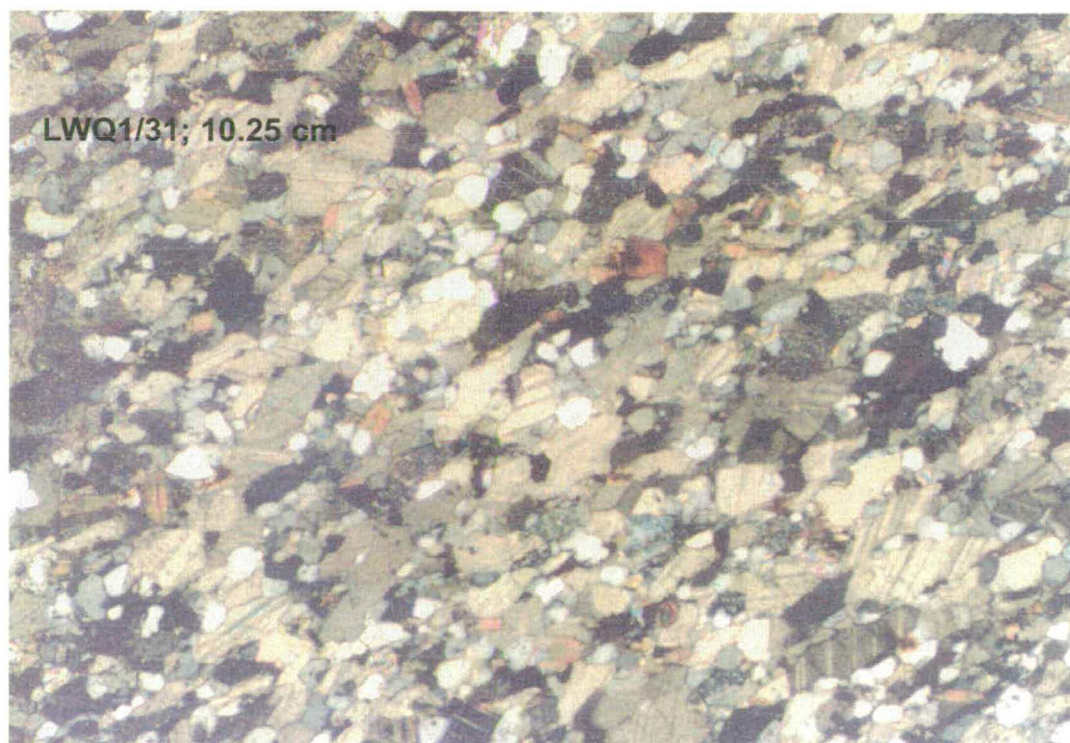
Lithologies

The limestone in the quarry is typical bluish-grey, medium grained Inchrory Limestone (Chapters 2, 4). Immediately adjacent to the amphibolite pods, the limestone develops a narrow pale grey to white rind. This rind is about 10 cm thick in the sampled profile and has a diffuse outer margin where it passes into more normal-looking grey limestone (Figure 9.3).

There is correlation between the textures in the limestone samples from the profile and distance from the amphibolite pod. Within the pale rind, the calcite crystals are equant to only weakly elongate. Samples with lesser amounts of plagioclase and quartz (e.g. LWQ1/25 in Figure E.2a) are more coarsely crystalline, but no more

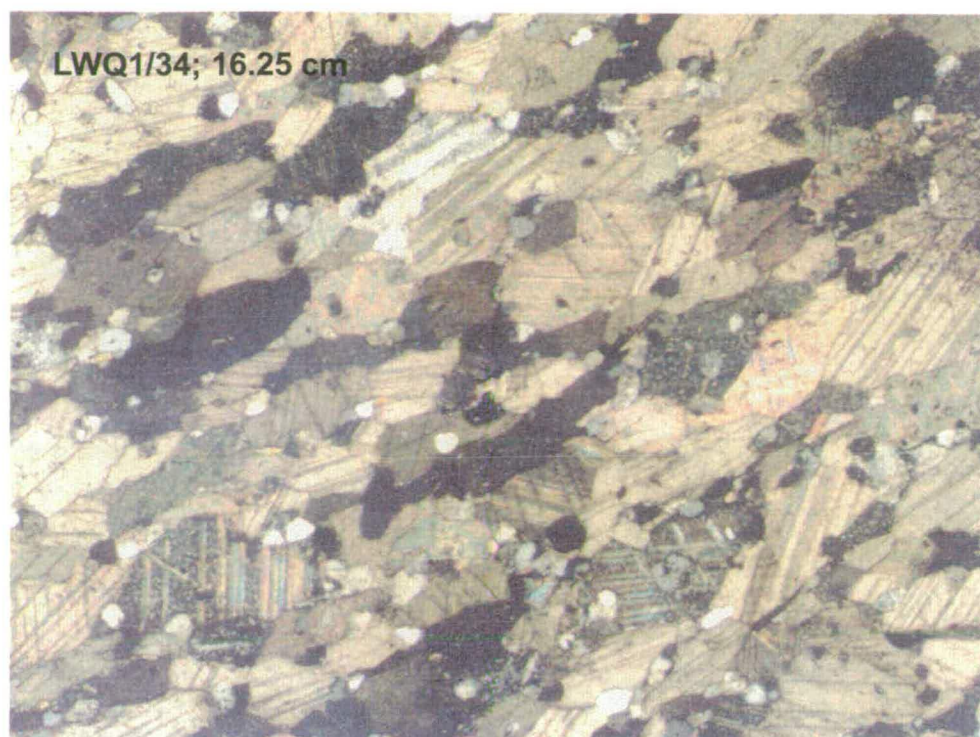


E.2a

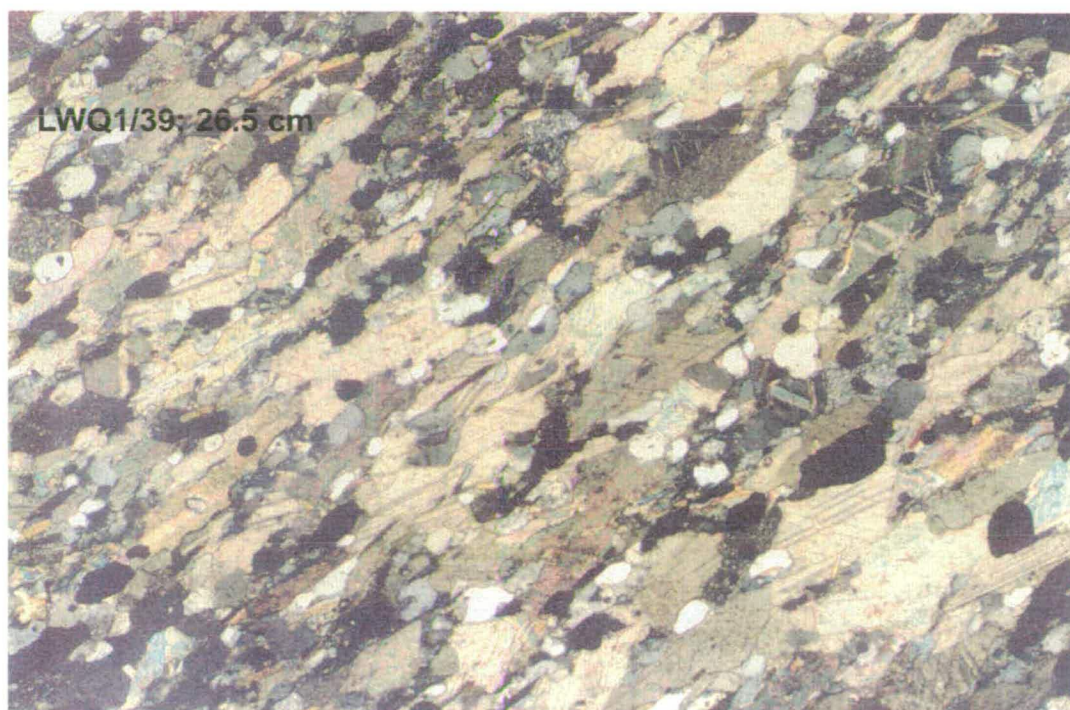


E.2b

Figure E.2a,b (c, d over page) Showing the increase in deformation in LWQ samples with distance from the amphibolite/limestone contact. Numbers given are sample number and distance from amphibolite - limestone contact in cms. Their location is also shown in Figure 9.3.



E.2c



E.2d

See previous page for caption

strongly or weakly deformed. Where the pale creamy grey limestone passes diffusely into the darker grey lithology (between 8.5 and 12.0 cm into the limestone), the calcite becomes markedly more elongate, both in silicate-poor and coarser- (and relatively more silicate-rich) and finer-grained types (e.g. compare LWQ1/31 and 1/34, Figure E.2b, c). This more deformed character persists throughout the remainder of the profile, locally becoming quite intense (e.g. LWQ1/39, Figure E.2d). Note that there is no clear correlation between the silicate content and the onset of more intense calcite elongation.

The amphibolite is dark greenish-grey and fine grained, appearing homogeneous in the field. Actinolite, subordinate blue-green hornblende and plagioclase dominate the mineralogy in the interior of the amphibolite pod. Although sparse in the interior, biotite becomes progressively more abundant towards the amphibolite margin, until it becomes the dominant ferromagnesian phase and actinolite develops as long bladed porphyroblasts. In the interior of the pod, biotite is commonly intimately associated with the amphibole, growing in anhedral plates amongst actinolite felts and clusters; the spatial and textural relationships, although commonly ambiguous, suggest that biotite is replacing actinolite. Small, but variable amounts of calcite occur throughout the amphibolite, sometimes spatially associated with small clusters of quartz crystals; like the biotite, it tends to become more abundant towards the margins of the pod. Ilmenite is replaced by scaly sphene which becomes more dispersed through the matrix towards the amphibolite rim. No good igneous textures are preserved, but neither are good deformation fabrics developed in the amphibolite margins – only very weak alignment of biotite and actinolite occur; the bladed actinolite

porphyroblasts are wrapped weakly by the incipient fabric where they lie oblique to it.

Structure

The dominant foliation in the Inchrory Limestone is a composite bedding/cleavage fabric which dips at moderate to shallow angles to the southeast (Figure 9.1). In places, the 'beds' contain metre-scale, tight to isoclinal early folds with limbs parallel to the bed margins. The crenulation cleavage which affects the nearby River Avon section is not observed in the samples obtained for the stable isotope work. The main fabric is penetrative, defined by elongate calcite and alignment of micas, and is parallel to the amphibolite pod margins.

Partition of deformation

It is quite clear from the textures in the limestone that deformation is partitioned into the outer parts of the profile, 10-12 cm away from the amphibolite/limestone boundary. This is counter to what might be expected, given that the limestone abuts amphibolite and that amphibolite pods *appear* to be dismembered and boudinaged parts of a more continuous igneous intrusion. One would anticipate that fabric intensity might increase towards the amphibolite, given the likely contrasting rheological properties of limestones and meta-igneous rocks. However, the lack of fabric in the margin of the limestone is consistent with the lack of even moderate fabric development in the amphibolite margins, indicating that the contact was not the focus of significant shearing. The evidence suggests that the amphibolite annealed the limestone over some 12 cm when it was intruded and that this annealed

margin has remained intact (this is supported by the oxygen isotope evidence from the SIMS study discussed below; see Section 9.6.6). The preservation of low-strain zones at the amphibolite-limestone contact raises questions as to whether the amphibolite pods do indeed represent a dismembered continuous intrusion, or whether their pod-like form was established when they were intruded. Whatever, the lack of significant deformation at the contact suggests that the role of this contact as a channel for fluid infiltration may well have been limited.

Application of geochemistry to the stratigraphic correlation of Appin and Argyll Group carbonate rocks from the Dalradian of northeast Scotland

C. W. THOMAS

British Geological Survey, Murchison House, West Mains Road, Edinburgh EH9 3LA, UK

Abstract: 240 samples from Appin and Argyll Group carbonate rock units of the Dalradian of northeast Scotland have been analysed for 10 major oxides and 14 to 19 trace elements in order to classify and correlate them using geochemistry. The carbonate rocks are chiefly limestones, with some dolostones. Rocks with $0.38 > \text{MgO}/\text{CaO} > 0.03$ are classed as dolomitic limestones; those with $\text{MgO}/\text{CaO} > 0.38$ are classed as dolostones. The data have approximately lognormal distributions at a high level of significance except for CaO, MgO and Sr. CaO and Sr have negatively skewed distributions. Median values for groups of sample analyses plotted on normalized multi-element variation diagrams and a nonlinear mapping (NLM) algorithm have been used to classify groups of samples. In the Appin Group, multi-element diagram patterns are distinctive for each unit, allowing correlations to be made. Though distinctive compositions do occur locally in Argyll Group carbonate rocks, correlation on a regional scale is not possible. The plot of NLM coordinates for suites of samples is consistent with the results from the spider diagrams; suites of Appin Group samples cluster closely whereas there is wide spread in samples from the Argyll Group. In several areas, most notably at Sandend Bay, the data have allowed reinterpretation of the stratigraphy. The data are consistent with other geological data in suggesting that crustal conditions were relatively stable during the deposition of the Appin Group, but not during the deposition of the Argyll Group.

The northeast of Scotland is currently the subject of a large scale study by the British Geological Survey (BGS), with the aim of improving the understanding of the stratigraphy and geological history of the Dalradian Supergroup in this region and of providing an updated 1:50,000 geological map base. Outcrop within this tract of metasedimentary and igneous rocks is very poor in many places, making stratigraphic correlation difficult. The problem is compounded by stratigraphic and structural complexity, and various geophysical and geochemical studies have been used to supplement traditional mapping programmes.

This paper documents a whole-rock geochemical study of carbonate rocks from the Appin and Argyll Groups of the Dalradian of northeast Scotland in which an attempt has been made to characterize and correlate major carbonate formations on geochemical grounds. A major aim has been to correlate the Banff coastal section with the succession inland, especially through the poorly exposed ground between Keith [NJ 343850] and the coast. Several previous studies (e.g. Hickman & Wright 1983; Lambert *et al.* 1981, 1982; Rock 1985, 1986; Rock & Waterhouse 1986) have shown that whole-rock geochemistry is potentially a useful correlative tool in areas of poor exposure and/or structural complexity. Although some previous studies have incorporated a range of lithologies, this study concentrates entirely on the carbonate metasediments, for the following reasons:

(i) The rocks of the northeast of Scotland are known to be deeply weathered in many places (Hall 1985). It was clear during sample collection that the carbonate rocks have suffered the least from weathering, whilst pelitic and semi-pelitic rocks are often heavily weathered. It was relatively easy to obtain fresh carbonate rock samples.

(ii) Exposure of carbonate rocks away from stream sections can be surprisingly good in places, providing better

sample coverage than would be possible for many of the siliciclastic rocks. Furthermore, the natural carbonate rock outcrop has been augmented by pits and quarries excavated for lime and building stone.

(iii) Carbonate rock formations occur at intervals throughout the Appin and Argyll Groups (e.g. Harris & Pitcher 1975). In the Appin Group, some of the larger formations are persistent laterally over several tens of kilometres, providing potential marker horizons.

Study area

Appin and Argyll Group rocks in northeast Scotland occur in a linear belt extending northeast from the northern margins of Cairngorm and the Glen Gairn Granite to the Banffshire coast between Spey Bay and Whitehills (Fig. 1). Although over 70 km long, this belt of metasediments is never more than 25–30 km wide. In general the amount of exposure decreases towards the coast, although the coast section itself is very well exposed. The metasediments comprise quartzites, pelites, semipelites and carbonate rocks. Most of the carbonate rocks are limestones, although some dolostones are present. The sediments were deposited on a continental margin in late Precambrian to Cambrian time (Harris & Pitcher 1975; Johnson 1983; Anderton 1982, 1985) and were deformed and metamorphosed to amphibolite facies during the Grampian Orogeny between 520 Ma and 490 Ma ago (Harte *et al.* 1984).

Carbonate rock lithologies

The carbonate rocks display wide variation in grain-size, colour and appearance at outcrop. Most samples are medium to dark grey; the purer of these often have an

reflect original sedimentary or diagenetic variations within the limestones. At outcrop, the carbonate rocks are often well bedded and massive; beds may exceed 2 m in thickness. The less pure varieties are more thinly bedded and flaggy.

Sampling

A total of 240 carbonate rock samples were collected from 64 localities (Fig. 1). The irregular distribution of samples is due mainly to the variation in the amount of exposure over the study area. The distance between samples within outcrops was approximately 10 to 15 m. In some instances, it was possible to collect samples along or across the strike. Samples were taken from single points on the outcrop and no attempt was made to take composite samples which might be considered to be 'representative' of the outcrop as a whole. Samples were cleaned of weathered crust in the field to leave about 3 kg for processing.

Sample preparation and analysis

Samples were split, crushed in a tungsten carbide jaw-crusher and then cone and quartered to leave about 100–150 g. This fraction was ground in a tungsten carbide or agate mill to leave a fine powder for analysis. It was necessary to use dilute (10%) HCl to clean the jaw-crusher and mill surfaces, as many of the darker carbonate rocks left a black residue containing finely divided carbonate dust on the active surfaces. Washing and milling with quartz sand was not effective in removing this deposit.

Samples were analysed for 10 major oxides and 19 (later 14) trace elements by XRF at Midland Earth Science Associates, Nottingham and at Nottingham University, using a Phillips PW1400 under automated control (Harvey & Atkin 1982). Loss on ignition was determined at 1000 °C.

Analysis of the early results showed that five of the 19 elements would be of little use in the study. The values of As, Cu, U, and Th fluctuated too widely or were frequently below detection limits whilst silica sand blanks showed that Co was affected significantly by contamination from the tungsten carbide surfaces. No other element or oxide showed any signs of being affected by contamination during processing.

Carbonate rock classification

Samples included in this study contain up to 21 wt% MgO and up to 46 wt% SiO₂, although only 22 samples contain more than 30 wt% SiO₂ (Fig. 2). No attempt has been made to define the carbonate rocks in terms of 'pure' and 'impure' varieties (cf. Rock 1986) since there is no distinct break in the frequency of SiO₂ values and the distribution of values, though skewed, is smooth (Fig. 3c). There is no evidence in these data to indicate that carbonate rocks with SiO₂ > 25 wt% are the products of metasomatic interactions with pelites, as was suggested by Rock (1986). This is discussed further below.

For the purposes of this study carbonate rocks have been classified according to the potential amount of dolomite in the rock, estimated from the MgO/CaO ratio (Fig. 2). Dolostones have a modal dolomite to calcite ratio in excess of 1 (e.g. Blatt *et al.* 1972) equivalent to MgO/CaO ≥ 0.38; thus carbonate rocks in this study with MgO/CaO ≥ 0.38 are classified as dolostones. This approach is justified as follows: The very strong correlation of CaO + MgO and Loss on Ignition (LOI) (Spearman Rank Correlation Coefficient = 0.993) and the LOI values themselves, indicate that the CaO and MgO are concentrated almost exclusively in the carbonate phase(s). A histogram of MgCO₃ values, calculated by considering the MgO, CaO and LOI values as analyses of pure carbonate alone, has a minimum in the 27.5–32.5 wt% MgCO₃ class interval (Fig. 3b). A pure carbonate rock at the limestone/dolostone boundary contains about 31 wt% MgCO₃, allowing for a maximum of about 4–5 wt% MgCO₃ in the calcite (C. W. Thomas—unpublished probe data; Bickle & Powell 1977). This value coincides with the minimum in the MgCO₃ histogram, indicating a simple link between chemistry and the dominant carbonate phase(s) and allowing classification via a familiar mineralogical scheme.

A similar approach can be used to distinguish dolomite-free and dolomite-bearing limestones. Experimental work in the system CaCO₃–MgCO₃ (e.g. Goldsmith

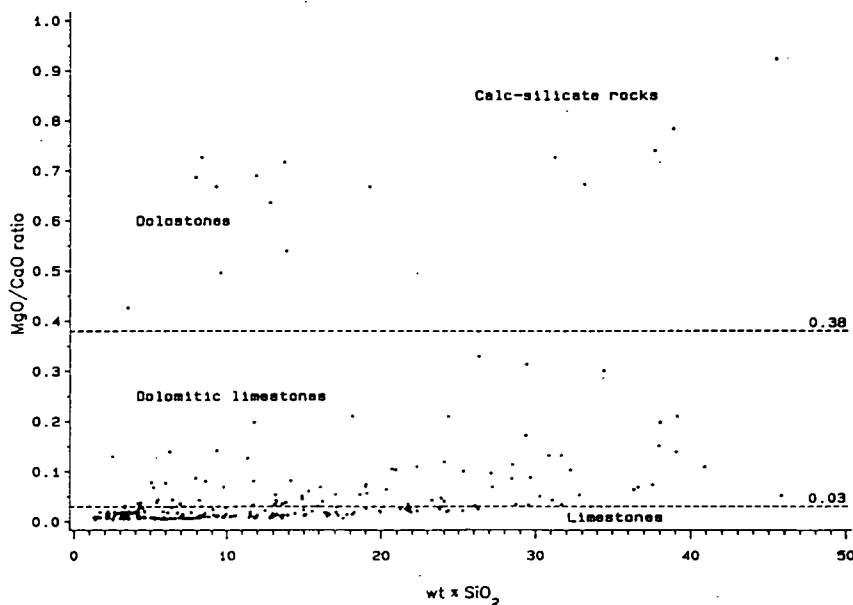


Fig. 2. Classification of all samples in the data set. Carbonate rocks with MgO/CaO > 0.38 are classed as dolostones. Those with 0.38 > MgO/CaO > 0.03 are classed as dolomitic limestones; the rest are classed as limestones. Limestones, dolostones and calc-silicate rocks are clearly differentiated. The calc-silicate rocks have markedly greater SiO₂/CaO ratios and much reduced Loss On Ignition values compared to the other samples in the data set.

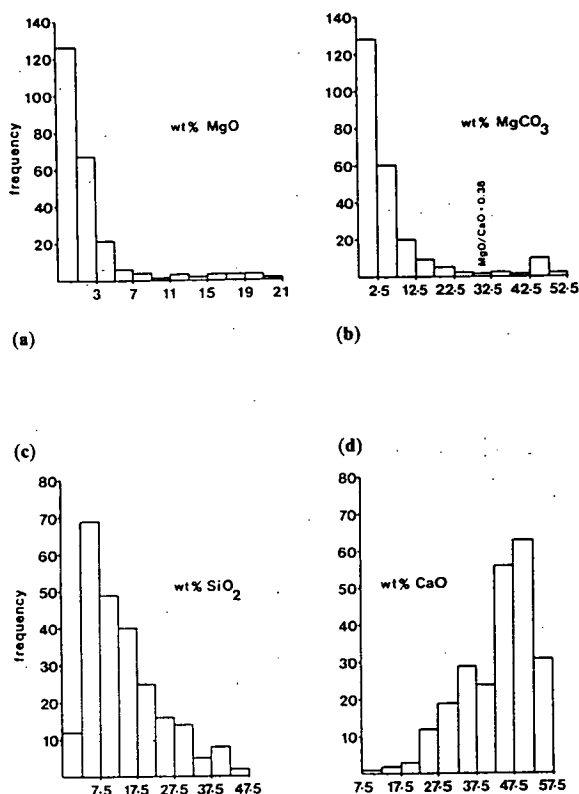


Fig. 3. Histograms of the major components of the carbonate rocks for the whole data-set; $n = 240$. (a) wt% MgO. (b) MgO recalculated as wt% MgCO_3 in a pure carbonate rock. The minimum in the class interval 27.5–32.5 wt% MgCO_3 coincides with the boundary between dolostones and limestones based on the modal mineralogy (Blatt *et al.* 1972). (c, d) Antipathetic distributions for wt% SiO_2 and wt% CaO, showing smooth positive and negative skewed characters respectively. The histogram for SiO_2 contrasts with that given by Rock (1986) and shows no marked minimum at 25 wt% SiO_2 . (Note: The histogram class intervals were calculated using the MINITAB (c) statistics package (Velleman & Hoaglin 1981). This computes conveniently rounded midpoints for class intervals rather than the class interval limits; it is for this reason that the lowest class interval does not start at zero. The upper limit of each class interval is shown).

1983) indicates that the calcite limb of the calcite–dolomite solvus lies between about 4 wt% MgCO_3 at 500 °C and about 6 wt% MgCO_3 at 600 °C. From this, the MgO/CaO ratio for a whole-rock analysis of a pure carbonate rock at about 500 °C will be about 0.03. Thus any carbonate rock with $\text{MgO}/\text{CaO} > 0.03$ will probably contain some dolomite, albeit in small and localized quantities (Stehli & Hower 1961). All rocks in this study with $0.03 > \text{MgO}/\text{CaO} > 0.38$ have been classed as dolomite-bearing limestones. Supporting evidence comes from the work of Leake *et al.* (1975) on Connemara marbles, where limestones with 3–5 wt% MgO were found to contain small concentrations of dolomite. In this study, 73 samples are identified as being potentially dolomite bearing.

Factors controlling the carbonate rock chemistry

The chemical data show that the carbonate rocks can be considered as mixtures of carbonate and siliciclastic material. With the exception of the five calc-silicate rock samples noted on Fig. 2, the rocks in this study appear to have been metamorphosed at amphibolite grade without significant changes in their post-diagenetic chemistry. Evidence to support this view is contained in bivariate plots of SiO_2 , Al_2O_3 , K_2O , Rb, V and Zr (Fig. 4). The

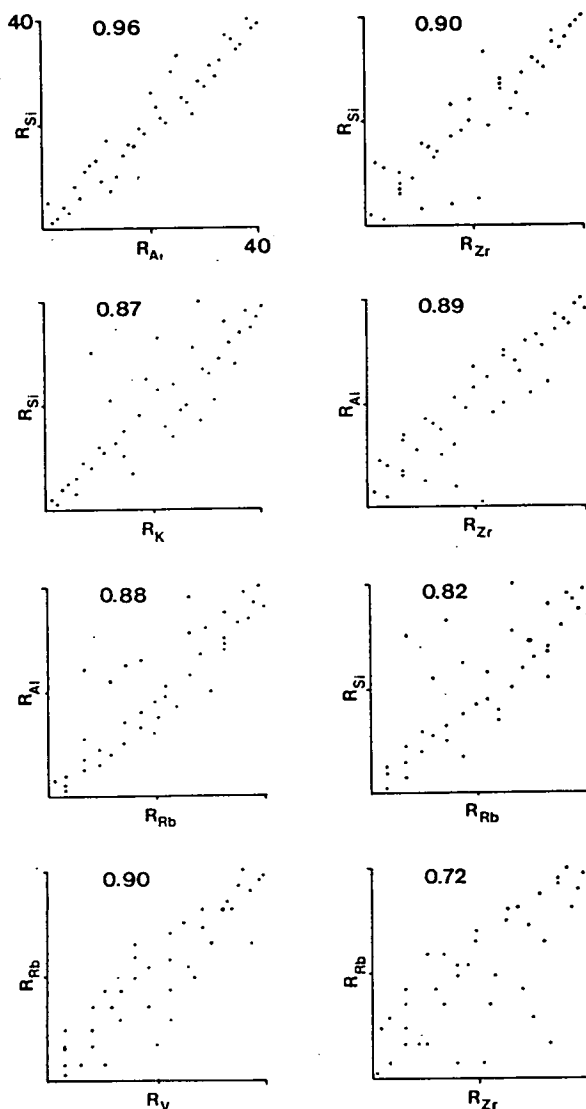


Fig. 4. Plots of selected oxides and trace elements for 40 samples of the Inchroy Limestone Formation (Blair Atholl Subgroup) from Glen Suie and Glen Fiddich. The data have been ranked (e.g. R_{Si} is the rank of a particular SiO_2 value) to be consistent with the Spearman Rank Correlation Coefficients, given at the top of each plot. The plots show that there has been little fractionation of components due to metamorphism or metasomatism with changing composition (cf. Leake *et al.* 1975, p. 247–248; Rock 1986).

correlations displayed in these plots of ranked data show that the proportions of these components are broadly the same across the whole range of compositions, although there is a little scatter in the plots with K_2O and Rb. If the rocks had been affected significantly by metamorphic or metasomatic processes with changing composition, wide scatter or inflections in the plots would be expected (cf. Leake *et al.* 1975). Hence the plots are more likely to relate to the original sedimentary and diagenetic compositions (this will be considered elsewhere). Furthermore, Ferry (1982, 1983) demonstrated that progressive alkali loss was the only likely change in carbonate rock chemistry during prograde metamorphism. Rock (1986) considered that decarbonation was unlikely to be significant, given that decarbonation reactions only significantly affect impure dolostones (Turner 1980); this is apparent in the five samples mentioned as exceptions above (Fig. 2). The variation in metamorphic grade over the sampled area is slight and isograds are approximately parallel to the strike (Fettes 1983). Thus any variation in the amount of decarbonation or alkali loss in the same formation is not likely to be significant.

The effects of mineralization may mask subtle variations in whole-rock chemistry. Russell *et al.* (1984) have shown that mineralization in the Dalradian is mainly syngenetic. Therefore, the products are an inherent part of the original chemistry, though they may be subject to later remobilization. However, mineralization is usually localized, for example at basin margin faults (Coats *et al.* 1980; Russell *et al.* 1984) and this could cause difficulties when interpreting whole-rock geochemical data within the context of

correlation on a regional scale. Evidence for mineralization from hand specimens and from the chemistry is sparse and is manifested as sulphides, which may be abundant in some samples. Samples from exposures near Tobar Fuar, Lecht [NJ 248108] have Mn concentrations ranging from 0.5 to 1.2 wt% MnO, more than 5 times higher than those in other limestones. These increased Mn levels are considered to reflect the low-grade cryptic Mn-mineralization found in phyllites near the Well of Lecht [NJ 234151] (Smith 1985).

Statistical properties of the data

Using the approach advocated by Tukey (1977), Exploratory Data Analysis (EDA) has been used to examine the character and statistical properties of the data, with particular reference to distribution shape and the identification of outliers.

Data from 40 samples of the Inchrory Limestone Formation (Appin Group; see Fig. 5), over which there is good mapping control in Glen Suie and Glen Fiddich, have been examined in some detail. It is assumed that the statistical properties of this group of data will reflect those of other groups in the data set.

With the exception of CaO and Sr, individual oxide and trace element distributions are positively skewed (Fig. 6). In these 40 samples, CaO has the same negatively skewed distribution as that for CaO for the whole data set (Fig. 3d); Sr also has a negatively skewed distribution (Fig. 6), since it is dominantly partitioned into the calcite. Chi-Square tests for goodness-of-fit (e.g. Conover 1980, p. 190) and Geary's A-statistic (Geary 1935; Lister 1982) show that the data do

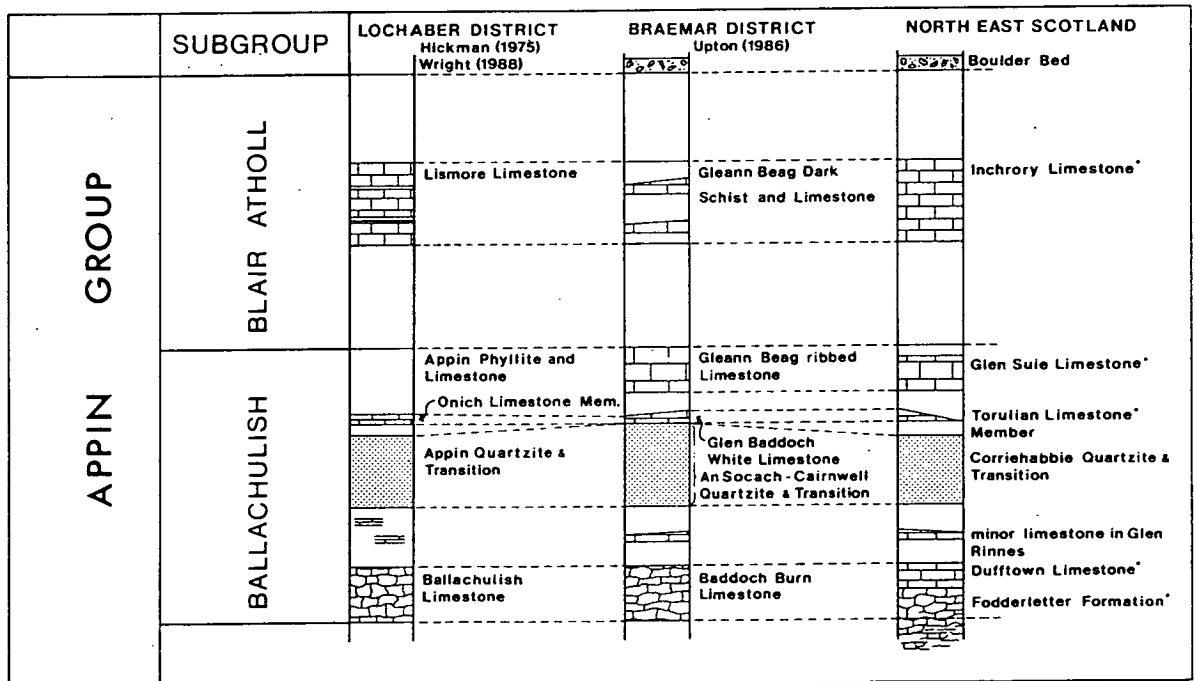


Fig. 5. Stratigraphic correlation of the major Appin Group carbonate rock units from the Dalradian of northeast of Scotland with those in the Braemar and Lochaber districts (Upton 1986; Hickman 1975; Wright 1988). The units are formations unless otherwise indicated. The Lochaber succession is included for comparison as the formation names within it are well-known. *, carbonate rock units analysed in this study. The Appin Quartzite and equivalents is included for reference. Stratigraphic names for NE Scotland are provisional.

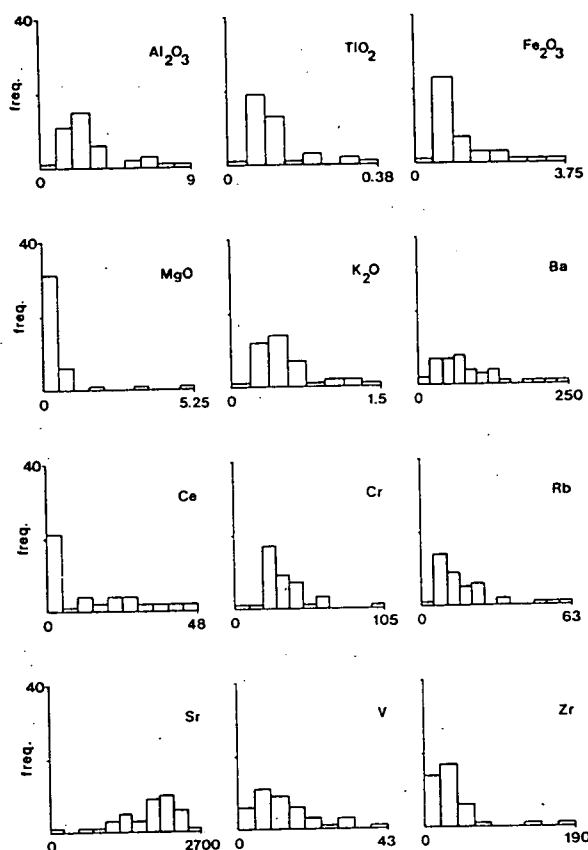


Fig. 6. Histograms of selected major oxide and trace element components for 40 samples from the Inchroy Limestone Formation (Blair Atholl Subgroup) in Glen Suie and Glen Fiddich, showing the skewed and non-Gaussian character of the distributions. This character mitigates against the use of standard parametric statistical summaries of the data and associated techniques. X-axis, class intervals; values are the upper limit of the last class in each case; Y-axis, frequency.

not have Gaussian distributions. However, many major oxides and trace elements have distributions which approximate to the lognormal distribution at the 95% significance level or better (Chi-Square test).

Outliers were identified using the EDA 'rule-of-thumb' of Velleman & Hoaglin (1981). Possible outliers lie beyond the inner fences (median $\pm 1.5 \times H$ -spread); probable outliers lie beyond the outer fences (median $\pm 3 \times H$ -spread; H -spread = Upper hinge - Lower hinge, see below). Outliers are ubiquitous in the data and are considered to be real data rather than rogue analyses; they reflect the extremes of composition which may be encountered.

It is now widely recognized that the mean and standard deviation are very poor estimators of location and scale for data with non-Gaussian distributions (e.g. Andrews *et al.* 1972). However, a range of robust and non-parametric estimators of location and scale are available (Andrews *et al.* 1972; Rock 1987) which allow data to be summarized in a way which is less susceptible to the effects of distribution

shape and outliers. Because of the variable size of the data sets, the median has been used to estimate location (see also Rock *et al.* 1987, p. 166). Hinges, which approximate to quartiles (Tukey 1977), were used as a measure of scale in the data where $n > 4$. Where $n = 3$ or 4 the extreme values have been used, giving the range. Hinge and extreme values for the data presented in Tables 1-4 and all analyses have been deposited with the Society library and the British Library at Boston Spa, W. Yorkshire, UK, as Supplementary Publication No. Sup 18055 (23 pp).

A common approach in dealing with non-Gaussian data is to transform the data (for example by standardization or by taking logarithms) thereby 'forcing' the data to approximate some distribution with known properties, such as symmetry. The approximate lognormal character of the data suggests that this might be justifiable. However, Link & Koch (1975) have shown that the application of lognormal estimation to data which are pseudo-lognormal, can introduce significant bias in the mean. Furthermore, Philip & Watson (1987, p. 580) point out that transformations should only be effected if they 'reflect some substantive law intrinsic to the formation of the data, i.e. the properties of interest must be invariant under the particular transformation' (see also Guttman 1985). For these reasons and because not all the data have lognormal-like distributions, log or other transformations have not been used.

Data analysis

In the following discussion, the sample groups referred to are groupings of samples from single or adjacent outcrops. Groupings of samples from several adjacent outcrops has only been done where there was good field evidence for the outcrops belonging to the same stratigraphic unit. Some 38 groups of samples have been constituted from the 64 sampled localities.

In spite of the plethora of techniques available for classifying and analysing multivariate data (e.g. Davis 1973; Mather 1976) and because of the statistical properties of the data described above, a deliberately straightforward graphical approach to data analysis has been adopted. Normalized multi-element variation diagrams similar in concept to REE diagrams allow presentation of the chemical characteristics in a pictorial manner. The diagrams have been constructed by normalizing median, hinge or extreme values for selected oxides and elements from groups of samples against medians for the whole data set (although, for clarity, only medians are presented in the figures). The normalizing values used to construct the multi-element diagrams are given in Table 5 (column 1). The patterns which emerge on these diagrams form the basis of the classification and correlations in the study. Checking the patterns against areas of known stratigraphy has shown consistently that the same patterns exist for groups of samples from the same formation. This has, with due regard to other geological information, permitted samples of unclear or unknown stratigraphic affinity to be correlated and classified.

The search for groupings in the data has also been investigated using nonlinear mapping (NLM) (Sammon 1969; Howarth 1973; Mather 1976). NLM is an ordination technique (Mather 1976, p. 329) which represents the distance relationships between objects in a space of reduced dimensionality; in this case, two. Any groupings in the data

can be determined from inspection of a two-dimensional plot of the coordinates calculated by the NLM algorithm, providing the distortion produced by the reduction in dimensionality is not too great. An advantage of NLM is that it overcomes the chief constraint of cluster analysis, namely the assumption that the samples 'on which the observations were recorded fall into one or more classes, which may be arranged hierarchically or in the form of non-overlapping clusters' (Mather 1976, p. 329). Furthermore, NLM does not require the data to conform to some specific data distribution, as does, for example, discriminant function analysis. The NLM plots add objective weight to the classification made on the basis of subjective examination of the normalized multi-element variation diagrams. Theoretical and computational details of NLM are given by Mather (1976).

Carbonate rock stratigraphy and chemistry

In the following discussion, stratigraphic names in the Appin Group refer to those in Fig. 5. For brevity, 'Formation' and 'Member' will be dropped from names in the following discussion, unless it is necessary to include them. Median values of analyses for each group of samples are presented in Tables 1-4. Summary statistics for each Appin Group carbonate rock formation or member are given in Table 5. Totals are not given in the tables, except where single analyses are quoted. This is because median values for individual major oxides and trace elements for a group of samples may come from any one of the samples within that group. Thus totals of the median values are meaningless in this context.

Appin Group

In the southwestern part of the study area, exposure is sufficiently good over a wide enough area to allow the establishment of a stratigraphic succession which can be assigned to the Appin Group with confidence. This provides a framework against which the geochemical data can be assessed, providing a basis for stratigraphic interpretation in less well-exposed areas.

Detailed discussion of the correlation of the Appin Group succession in northeast Scotland with Appin Group successions elsewhere in the Dalradian is outside the scope of this paper. However, recent mapping by BGS in the northeast has shown that the Appin Group here can be correlated with other Appin Group successions with some confidence (Fig. 5); some general comments will be made with regard to correlatives of the carbonate formations.

The Fodderletter Formation is a mixed sequence of carbonate and calc-silicate rocks and semipelites. The formation becomes more calc-silicate and carbonate-rich higher up in the succession and these rocks eventually pass up into the Dufftown Limestone or the Burn of Tervie Graphitic Schist (equivalent to Ballachulish Slate). In general the carbonate rocks from this formation are impure and MgO levels suggest that some may contain dolomite (Table 1). Though relatively abundant, trace element concentrations are rather variable.

In contrast, the overlying Dufftown Limestone is characterized by bluish grey limestones which are often quite coarsely crystalline. These are much purer than the underlying carbonate rocks (Table 2). The formation is

Table 1. Analyses of carbonate rocks from the Fodderletter Formation (1-5), Appin Group, northeast Scotland

	1	2	3	4	5
SiO ₂	29.34	37.63	19.00	13.58	20.52
TiO ₂	0.33	0.26	0.12	0.09	0.21
Al ₂ O ₃	8.05	6.20	3.20	2.09	5.06
Fe ₂ O _{3tot}	2.85	2.57	1.09	0.60	1.85
MnO	0.08	0.09	0.03	0.04	0.05
MgO	4.70	11.39	2.70	2.83	3.10
CaO	27.28	16.54	38.88	44.22	36.87
Na ₂ O	0.89	1.00	0.14	0.32	0.71
K ₂ O	1.73	1.65	0.56	0.50	1.15
P ₂ O ₅	0.07	0.10	0.06	0.06	0.06
L.O.I.	24.71	21.71	33.82	36.16	30.60
Totals	100.03				
MgO/CaO	0.17	0.69	0.07	0.06	0.08

Trace elements (ppm) in alphabetical order

Ba	331	387	bd	101	228
Ce	61	20	12	15	40
Cr	46	28	27	15	33
Ga	10	7	4	2	6
La	22	8	11	6	16
Nb	7	6	3	2	5
Ni	14	16	3	bd	9
Pb	10	15	15	5	11
Rb	65	54	36	19	45
Sr	429	220	1525	434	667
V	38	25	18	12	28
Y	19	17	12	5	13
Zn	45	33	64	6	20
Zr	104	140	48	68	78

Analysis 1 is for a single sample, the remainder are medians for groups of samples.

1 Bridge of Brown [NJ 12951990]; 2 Crathie Point [NJ 549674], *n* = 3; 3 southeastern side of Parkmore Quarry, Dufftown [NJ 334411], *n* = 3; 4, Burn of Tervie, south of Mains of Morinish [NJ 216298], *n* = 3; 5, 1 km south of Blairfindy Lodge Hotel [NJ 192275], *n* = 2; bd, below detection

discontinuous in places but very persistent along strike, developing into a limestone of considerable thickness in the Glen Rinnes-Dufftown area. MgO levels in this formation are lower than in the preceding formation and suggest that dolomite is a minor phase. However, 16.99% MgO in sample HY62 from Rinaitin Quarry, Glen Rinnes, shows that dolostones do occur in places. In general the limestones are pure with low levels of oxides other than CaO. With the exception of Sr, trace element concentrations are very low with values generally below 10 ppm. Sr values range from several hundred to over 2000 ppm, with most values lying in the 1000 to 1500 ppm range.

The upper, more calcareous part of the Fodderletter Formation and the Dufftown Limestone are considered to occupy the same stratigraphic position as the Ballachulish Limestone Formation. However, the position of the base of the Ballachulish Subgroup within the Fodderletter Formation is not yet clearly defined and remains rather arbitrary at present.

Table 2. Median analyses of groups of samples from the Dufftown Limestone Formation, Ballachulish Subgroup, Appin Group, northeast Scotland.

	1	2	3	4	5	6	7	8
SiO ₂	4.33	5.40	4.63	3.61	2.84	4.51	4.33	2.72
TiO ₂	0.03	0.01	0.04	0.02	0.03	0.01	0.03	0.02
Al ₂ O ₃	0.57	0.27	0.66	0.62	0.60	0.41	0.71	0.45
Fe ₂ O _{3tot}	0.24	0.21	0.26	0.18	0.29	0.22	0.40	0.13
MnO	0.03	0.01	0.01	0.04	0.03	0.01	0.05	0.01
MgO	0.85	1.91	1.03	0.94	1.01	1.04	1.63	1.27
CaO	52.42	49.85	51.86	52.41	52.71	52.21	50.91	53.07
Na ₂ O	0.12	0.28	0.23	0.05	0.18	0.16	0.07	0.09
K ₂ O	0.09	0.09	0.11	0.12	0.08	0.05	0.10	0.08
P ₂ O ₅	0.03	0.02	0.02	0.02	0.01	0.03	0.04	0.02
L.O.I	41.31	41.47	41.64	42.28	42.47	41.31	41.42	42.06
MgO/CaO	0.02	0.04	0.02	0.02	0.02	0.02	0.03	0.02
<i>Trace elements (ppm) in alphabetical order</i>								
Ba	11	30	44	19	16	bd	24	36
Ce	bd	bd	16	bd	bd	bd	4	4
Cr	14	9	12	6	12	11	9	3
Ga	bd	bd	2	bd	bd	bd	1	bd
La	bd	bd	bd	bd	2	2	4	bd
Nb	1	2	2	bd	bd	2	1	bd
Ni	bd	bd	bd	bd	bd	bd	bd	bd
Pb	8	7	7	5	7	7	7	3
Rb	7	5	12	7	6	4	7	6
Sr	1217	1961	1584	1578	1640	1470	1515	2349
V	6	5	9	1	6	4	8	1
Y	4	bd	3	1	3	1	2	3
Zn	19	bd	bd	bd	2	4	5	bd
Zr	21	19	34	19	23	19	3	22

1 Parkmore Quarry, Dufftown, [NJ 334411], *n* = 5; 2, Rinaitin Quarry, Glen Rinnies, [NJ 262328], *n* = 3; 3, Blackhillock Quarry, Keith, [NJ 439482], *n* = 3; 4, 0.5–1 km east of Glenfiddich Lodge, Glen Fiddich, *n* = 4; 5, west side, Sandend Bay [NJ 555667], *n* = 2; 6, Braes of Abernethy, [NJ 098163], *n* = 2; 7, Alehousehillock Quarries, Glen of Coachford [NJ 459446], *n* = 4; 8, Alltachoileachan, Glenlivet, [NJ 24432898], *n* = 2.

The Torulian Limestone Member is a conspicuous but impersistent white limestone, occurring in a series of transitional sediments above the Corriehabbie Quartzite (equivalent to Appin Quartzite). They are well exposed in Glen Suie and Allt Dregnie [NJ 245260], forming the Allt Dregnie Formation. The limestone is developed only locally within this formation. If anything, it is purer than the Dufftown Limestone, with some analyses approaching pure CaCO₃ (e.g. Deer *et al.* 1966, p. 474). Trace element concentrations are very low, with several at levels below detection limit, although Sr ranges to values over 1000 ppm (Table 3, 1–2).

The Torulian Limestone has equivalents elsewhere in the Appin Group at this stratigraphic level, for example, the Onich Limestone Member in the Lochaber district (Wright 1988) and the Glen Baddoch White Limestone in the Braemar district (Upton 1986).

The transitional sediments of the Allt Dregnie Formation which contain the white limestone pass up into the Glen Suie Limestone Formation. This is a strongly banded, buff-grey, mixed siliciclastic-carbonate sequence, well exposed in Glen Suie and Glen Fiddich. Individual carbonate rock units up to 2 or 3 m in thickness are

developed towards the top. They are pale to medium grey, massive and crystalline and are mostly impure with variable moderate MgO levels and variable trace element concentrations (Table 3, 3–4). Unequivocal mapping control on these units is limited to the known occurrences in Glen Suie and Glen Fiddich, though similar sequences recognized elsewhere are correlated with them (J. R. Mendum, D. Stephenson, pers. comm., 1987).

The Glen Suie Limestone Formation is considered to be the stratigraphic equivalent of Upton's (1986) Gleann Beag ribbed Limestone, the Monzie Limestone of Smith & Harris (1976) and the Strath Fionan Limestone of Treagus & King (1978). The correlative in the Lochaber district is the Appin Phyllite and Limestone (e.g. Wright 1988).

The Inchroary Limestone Formation is the uppermost carbonate rock formation in the Appin Group recognized in the study area. It is a thick well-bedded, medium to dark grey, crystalline limestone with pelitic laminae, containing amphibolite pods and lenses in places. The limestone is MgO-poor and relatively impure with SiO₂ and other oxides present at levels in the upper parts of their range for the whole data set. Trace element concentrations are generally well above detection limit. Sr concentrations are similar to

Table 3. Median analyses of samples from the Torulian Limestone Member (Allt Dregnie Formation) (1–2), the Glen Suie Formation (3–4), and the Inchroy Limestone Formation (5–11).

	1	2	3*	4*	5	6	7	8	9	10	11
SiO ₂	2.24	4.19	14.13	22.31	9.21	21.91	13.62	13.53	11.55	8.18	6.34
TiO ₂	0.01	0.02	0.08	0.18	0.08	0.27	0.10	0.13	0.09	0.07	0.05
Al ₂ O ₃	0.39	0.47	1.91	4.60	1.94	6.77	3.08	3.23	2.34	2.09	1.09
Fe ₂ O _{3tot}	0.16	0.37	1.77	1.54	0.64	2.11	1.34	1.15	0.95	0.74	0.61
MnO	0.02	0.04	0.05	0.06	0.03	0.04	0.04	0.03	0.02	0.02	0.02
MgO	0.51	0.75	1.66	2.11	0.44	0.95	0.60	0.70	0.54	0.34	0.40
CaO	54.48	52.53	41.89	37.27	47.65	35.15	43.54	43.99	46.25	48.74	50.39
Na ₂ O	0.05	0.15	0.27	0.60	0.13	1.11	0.54	0.29	0.24	0.17	0.30
K ₂ O	0.02	0.09	0.16	0.82	0.38	1.38	0.45	0.82	0.42	0.40	0.20
P ₂ O ₅	0.01	0.01	0.02	0.05	0.05	0.11	0.06	0.10	0.07	0.06	0.05
L.O.I.	41.75	41.69	35.63	31.21	39.21	30.38	36.04	35.98	37.60	38.93	40.29
MgO/CaO	0.01	0.01	0.04	0.06	0.01	0.03	0.01	0.02	0.01	0.01	0.01

Trace elements (ppm) in alphabetical order

Ba	10	23	bd	163	6	205	74	114	81	55	12
Ce	bd	bd	14	34	bd	48	20	22	16	9	9
Cr	4	11	8	24	26	47	33	33	31	26	13
Ga	bd	bd	4	5	bd	8	3	5	3	2	1
La	bd	bd	7	12	bd	15	12	9	8	7	4
Nb	bd	2	3	5	2	6	3	4	2	2	2
Ni	bd	bd	bd	8	3	8	4	bd	bd	bd	1
Pb	4	10	5	9	5	12	8	11	9	9	7
Rb	4	7	8	26	16	44	19	31	19	18	11
Sr	1193	827	723	686	2040	1266	906	1509	1722	1815	2612
V	bd	5	8	20	10	34	14	16	12	7	8
Y	2	2	11	14	4	13	5	6	5	5	3
Zn	bd	12	9	11	bd	24	9	13	8	8	5
Zr	18	12	46	72	33	66	44	43	33	20	25

Torulian Limestone Member, Glen Suie Limestone Formation: Ballachulish Subgroup; Inchroy Limestone Formation: Blair Atholl Subgroup, Appin Group, north-east Scotland. The Glen Suie Limestone analyses are given for completeness only.

1, Glen Suie and Glen Fiddich, $n = 7$; 2, Tomintoul and Conglass area, $n = 11$; 3, Back Burn and Coldwell Howes, Glen Suie, [NJ 279259], $n = 5$; 4, Glen Fiddich, $n = 10$. 5, Glen Suie and Glen Fiddich, $n = 40$; 6, Conglass, [NJ 1622], $n = 5$; 7, Muckle Allt Venney, [NJ 380379], $n = 12$, 8, east side of Sandend Bay, [NJ 562662], $n = 4$; 9, Tomintoul area, $n = 27$; 10, Goukstone Quarry [NJ 49165615] and quarry 400 m east of Rosarie, [NJ 39134991], Keith area, $n = 5$; 11, Luib Quarry, [NJ 26900918] and quarry 300 m southwest of Cockbridge, [NJ 25120872], Corgarff area, $n = 4$;

*Not shown on normalized multi-element variation diagrams or NLM plot (Figs 7–9).

those for the Dufftown Limestone Formation, though perhaps slightly higher overall; values in many samples exceed 2000 ppm (Table 3).

Typical correlatives of the Inchroy Limestone elsewhere in the Dalradian include the Lismore Limestone (Hickman 1975), the Blair Atholl Dark Schist and Limestone Formation (Smith & Harris 1976) and Upton's (1986) Gleann Beag Dark Schist and Limestone Formation in the Braemar district.

The Dufftown and Inchroy Limestone Formations have distinctive compositions and are laterally persistent, and the chemistry of these limestones has been significant in clarifying several stratigraphic problems in the East Grampians. The same is true, to a slightly lesser extent, of the Fodderletter Formation. However, the two other carbonate rock units from the Appin Group have proved to be of less use in stratigraphic correlation using whole-rock chemistry. Although the Torulian Limestone has a distinctive lithology, it is developed only on a local scale,

whilst the limiting factor with regard to the Glen Suie Limestone Formation is its variable chemistry, due principally to the lithologically inhomogenous character of the rocks. For this reason, samples from the Glen Suie Limestone are not represented on Figs 7, 8 and 9, and are not discussed further with regard to stratigraphic correlation.

Argyll Group

Several carbonate rock units in successions assigned to the Argyll Group have been sampled from outcrops from the Lecht–Allargue area in the SW to the coast between the Portsoy area [NJ 590665] and Boyne Bay [NJ 620660]. Unlike most of those in the Appin Group, the carbonate rock units in the Argyll Group are developed only on a local scale. Correlations in the field are unclear and carbonate rock units cannot be traced over more than 1–2 km or so. Consequently, though samples have been taken from

Table 4. Analyses of samples from carbonate rock units assigned to the Argyll Group, northeast Scotland.

	1*	2†	3	4*	5	6	7*	8*	9*	10
SiO ₂	12.72	16.32	11.34	5.34	14.89	33.10	29.38	14.00	13.15	6.95
TiO ₂	0.12	0.11	0.15	0.03	0.02	0.09	0.13	0.14	0.09	0.06
Al ₂ O ₃	2.67	2.88	3.31	0.71	0.45	1.93	3.31	3.52	2.54	1.53
Fe ₂ O _{3tot}	1.84	1.08	1.26	2.59	0.49	1.20	1.56	2.04	0.86	0.72
MnO	0.14	0.03	0.09	0.86	0.10	0.29	0.04	0.28	0.07	0.08
MgO	10.75	0.77	8.02	3.38	2.02	17.62	10.31	2.22	1.00	3.83
CaO	33.92	43.35	38.12	46.37	44.47	26.20	32.84	42.32	44.67	46.73
Na ₂ O	0.48	0.39	0.24	0.09	0.05	0.23	0.27	0.00	0.31	0.01
K ₂ O	0.44	0.69	0.43	0.23	0.10	0.54	1.07	1.09	0.62	0.95
P ₂ O ₅	0.06	0.05	0.07	0.14	0.08	0.05	0.06	0.10	0.08	0.04
L.O.I	36.99	34.74	34.72	37.36	37.38	18.77	20.59	34.00	35.83	38.84
Totals						100.02	99.56			
MgO/CaO	0.31	0.02	0.21	0.07	0.05	0.67	0.31	0.05	0.02	0.08
<i>Trace elements (ppm) in alphabetical order</i>										
Ba	53	121	133	bd	42	781	959	1453	64	82
Ce	19	12	36	bd	bd	60	65	20	11	13
Cr	16	32	36	13	9	98	92	25	21	16
Ga	3	4	9	bd	bd	20	25	4	3	2
La	8	15	15	bd	bd	34	38	15	5	6
Nb	3	4	8	bd	1	21	18	5	2	3
Ni	7	bd	4	bd	bd	41	46	6	bd	bd
Pb	10	9	8	62	16	18	25	13	11	8
Rb	18	24	50	5	4	128	179	40	19	19
Sr	455	1748	216	213	245	115	134	843	1490	679
V	16	11	22	8	8	118	98	22	13	24
Y	12	5	16	4	3	27	30	11	6	2
Zn	29	11	53	8	8	112	108	30	5	2
Zr	51	40	138	15	12	274	184	44	53	26

6, 7 are analyses of single samples, the remainder are medians of two or more analyses. The limestone from Limehillock Quarry (2) is now considered to belong to the Inchroy Limestone Formation, Appin Group.

1, Muckle Fergie, Upper Glen Avon, [NJ 16551398], *n* = 2; 2, Limehillock Quarry, [NJ 51645202], *n* = 3; 3, The Brecks, Portsoy, [NJ 58676631] *n* = 3; 4, Tobar Fuar, near Lecht, [NJ 246108], *n* = 4; 5, Allargue area, Strathdon, *n* = 5; 6, Rosehall Croft, Portsoy, [NJ 59786643]; 7, Links Bay, Portsoy, [NJ 59536631]; 8, west of Castle Point, Portsoy, [NJ 579667], *n* = 2; 9, Baloch Quarry, Strathdon, [NJ 336175], *n* = 4; 10, 400 m north of Broadland Farm, Milton of Cairnborrow, Huntly, [NJ 480417], *n* = 4. *, shown on Fig. 7a; †, shown on Fig. 7c.

different stratigraphic levels in the Argyll Group, there is not the same stratigraphic control over these samples as for those from the Appin Group.

The coast section in the Portsoy-Boyne Bay area is described in detail by Read (1923, pp. 4–38). The succession is lithologically complex and the carbonate rocks are associated with schists and are intruded by a series of mafic rocks, including gabbros, anorthosites and serpentinites. The carbonate rocks are pale to medium grey or white, sometimes with a greenish tinge; calc-silicate bands are present in some samples. Inland, carbonate rock units assigned to the Argyll Group are more uniform in their appearance and comprise medium to dark grey limestones associated with black schists or phyllites.

The impersistent and discontinuous character of these carbonate rocks is reflected in their variable chemistry as indicated in Table 4. Samples from the coast are generally impure with SiO₂ often in excess of 15 wt%. MgO values

are higher than the median value for the whole data set and many of the samples are classed as dolomitic limestones or dolostones. Inland, samples from exposures near Tobar Fuar [NJ 246108] and the adjacent Allargue area are amongst the purest from the Argyll Group, with SiO₂ values less than 10 wt%. This is also true for samples from Broadlands Farm [NJ 480417] near Huntly. However, other groups of samples are less pure, with SiO₂ values similar to those for rocks from the coast. Trace element values are variable and Sr varies from as low as 79 ppm to nearly 2000 ppm. Several samples from the Portsoy area have elevated Ba values, ranging up to 1905 ppm (median value for the whole data set is 60 ppm) and elevated levels of other trace elements, including Ce, Cr, Ni and Pb, are common. Although Ba can be introduced during diagenesis (Fairchild 1985), the unusual trace element concentrations do not compare closely with anything sampled inland and may reflect contamination by hydrothermal fluids associated

Table 5. Median values for the whole data set ($n = 240$); highlighted values are those used in the construction of the multi-element diagrams. 2–6, Median and hinge values for Appin Group carbonate rock formations

	1			2			3			4			5			6		
	LH	MED	UH	LH	MED	UH	LH	MED	UH	LH	MED	UH	LH	MED	UH	LH	MED	UH
SiO ₂	11.53	16.55	19.02	29.50	3.07	4.12	5.40	2.24	3.87	6.75	13.19	18.70	30.04	7.39	11.79	18.20		
TiO ₂	0.08	0.10	0.13	0.25	0.02	0.02	0.03	0.01	0.02	0.03	0.10	0.17	0.25	0.06	0.09	0.16		
Al ₂ O ₃	1.98	2.59	3.37	6.13	0.40	0.59	0.66	0.30	0.44	0.85	2.94	4.24	5.64	1.61	2.34	3.99		
Fe ₂ O _{3tot}	0.94	0.87	1.13	2.39	0.15	0.24	0.31	0.22	0.34	0.70	1.21	1.65	1.98	0.55	0.85	1.38		
MnO	0.04	0.04	0.05	0.07	0.01	0.02	0.04	0.02	0.03	0.05	0.05	0.06	0.08	0.02	0.03	0.04		
MgO	0.92	2.45	2.90	4.35	0.85	1.01	1.38	0.50	0.74	1.46	1.40	1.95	3.57	0.37	0.50	0.83		
CaO	45.20	30.09	38.80	40.68	50.75	51.98	52.83	48.48	52.58	53.69	30.08	38.47	42.26	40.20	46.02	49.58		
Na ₂ O	0.23	0.17	0.39	0.87	0.07	0.11	0.17	0.06	0.13	0.24	0.25	0.44	1.21	0.11	0.24	0.53		
K ₂ O	0.38	0.50	0.66	1.63	0.08	0.09	0.12	0.02	0.05	0.13	0.17	0.62	0.97	0.31	0.45	0.71		
P ₂ O ₅	0.06	0.05	0.06	0.08	0.02	0.02	0.03	0.01	0.01	0.02	0.03	0.05	0.06	0.05	0.07	0.10		
L.O.I	37.55	26.30	33.46	34.92	41.31	41.77	42.40	40.61	41.72	42.02	25.40	32.61	35.85	33.07	37.60	39.90		
<i>Trace elements (ppm) in alphabetical order</i>																		
Ba	61	bd	17	36	bd	20	40	9	106	313	27	138	194	41	76	121		
Ce	13	bd	bd	8	bd	bd	9	13	18	29	13	26	41	bd	13	26		
Cr	23	7	9	13	4	8	11	16	26	33	12	22	27	22	29	41		
Ga	2	bd	bd	bd	bd	bd	bd	2	4	7	4	5	6	bd	3	5		
La	7	bd	bd	bd	bd	bd	9	7	11	13	7	11	15	bd	6	13		
Nb	2	bd	1	2	bd	1	2	2	4	6	3	4	5	2	3	4		
Ni	bd	bd	bd	bd	bd	bd	bd	1	4	13	2	7	10	bd	2	5		
Pb	9	6	7	8	5	8	11	6	11	15	6	7	10	6	8	10		
Rb	16	5	6	7	4	6	8	22	34	58	10	22	35	12	18	30		
Sr	1387	1340	1563	1871	755	907	1193	438	627	1040	613	700	747	1378	1815	2136		
V	12	2	5	7	bd	3	5	12	20	28	12	19	23	7	12	19		
Y	5	2	2	3	bd	2	8	6	12	16	8	12	16	3	5	9		
Zn	9	bd	bd	8	bd	5	15	12	28	55	2	11	19	bd	7	14		
Zr	36	18	21	29	12	15	21	45	68	103	39	55	114	27	37	55		

Median for the whole data set, $n = 240$; Fodderletter Formation, $n = 12$; 3, Duftown Limestone Formation, $n = 25$; 4, Torulian Limestone Member, $n = 18$; 5, Glen Suie Limestone Formation, $n = 16$; 6, Inchroy Limestone Formation, $n = 99$.

with the introduction of the serpentinites, anorthosites and basic rocks which occur in the Portsoy area or by syngedimentary mineralization (Russell *et al.* 1984).

Appin Group normalized variation diagrams

Medians for groups of samples from the Fodderletter Formation, Duftown Limestone, Torulian Limestone Member and the Inchroy Limestone are displayed in Fig. 7. The Glen Suie Limestone is excluded for the reasons given above. The patterns are consistent and distinctive for each of the carbonate rock units displayed. The shape of the pattern from SiO₂ to CaO is often characteristic. The broadly similar patterns for the Duftown Limestone and the Torulian Limestone reflect the low levels of siliciclastic material contained in these rocks.

The relatively high MgO values in the Fodderletter Formation present as a strong peak (Fig. 7a). Patterns overall are moderately to strongly inflected, but the inflections remain the same, even in patterns with greater amplitude, highlighting more extreme compositions. The Duftown Limestone has a strong positive Fe₂O₃–MgO inflection, whilst in the Inchroy Limestone the pattern for these oxides is curved, with a negative inflection to MgO. From K₂O, the pattern for groups of samples from the Duftown and Torulian Limestones rise steadily towards Zr;

normalized values are below unity. Inflections are usually only weak to moderate, except for that over Rb–Sr (Fig. 7b, c). With the exception of the less pure groups of samples, patterns from K₂O are relatively flat for the Inchroy Limestone, with only minor inflections; values are slightly below or above unity (Fig. 7d).

Argyll Group normalized variation diagrams

No normalized variation diagram patterns which are consistent on a regional scale, can be discerned for samples from carbonate rock units assigned to the Argyll Group (Fig. 8). In general the patterns have stronger inflections than those for Appin Group carbonate rocks and they have greater amplitude, especially for samples from the coast. This lack of consistent patterns has precluded correlation of Argyll Group carbonate rocks on chemical grounds, although there are similarities between patterns for samples from Limehillock Quarry [NJ 51645202] and Baloch Quarry [NJ 336175] (see below). The variation in the patterns suggests that even if carbonate rock units were coeval in formation in different areas during Argyll Group times, environmental controls were such that they did not develop similar compositions. These data are consistent with other data which indicate restricted basin formation in Argyll Group times. This will be pursued further in the discussion.

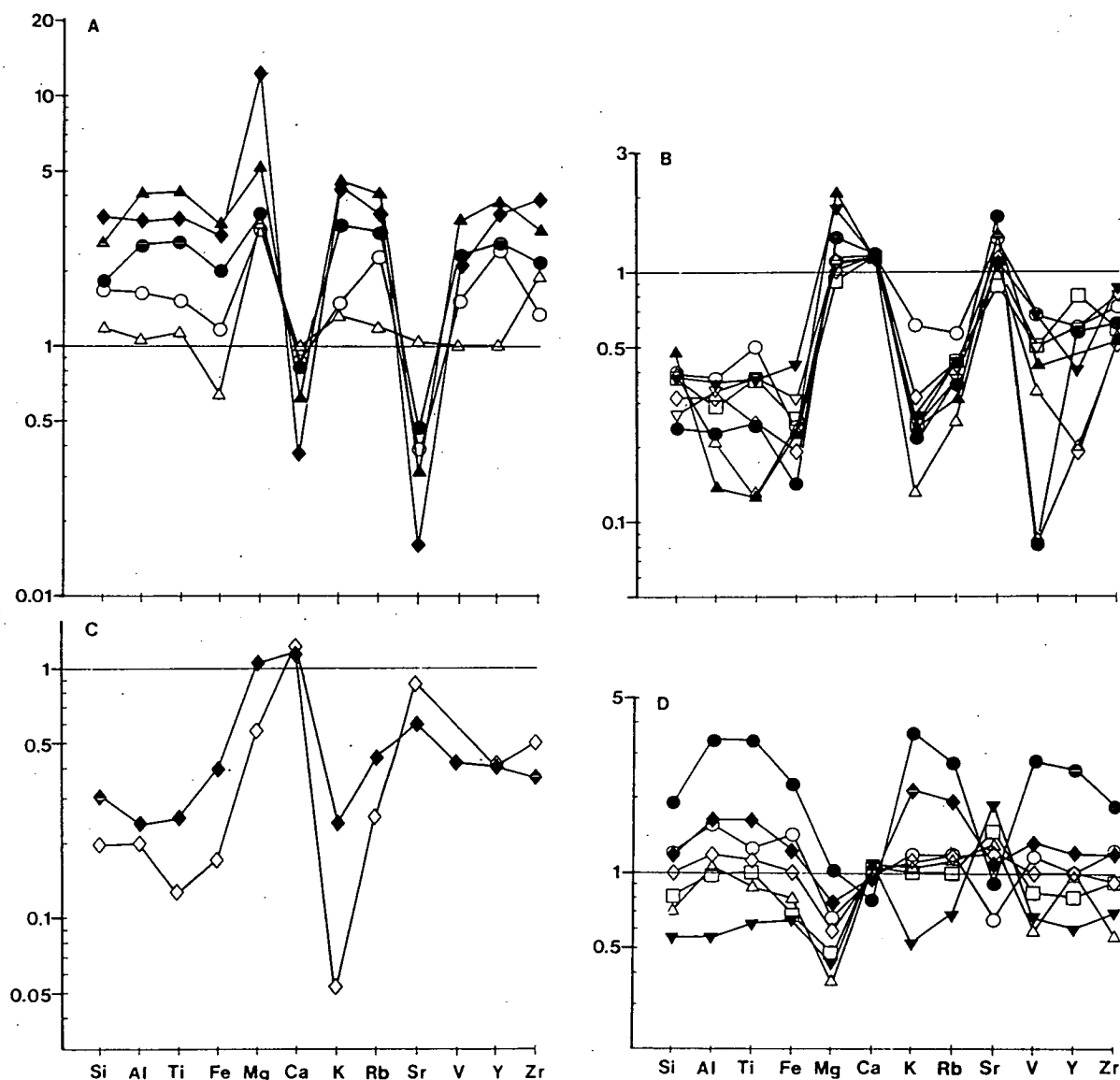


Fig. 7. Normalized multi-element variation patterns for Appin Group carbonate rock units. The values used for normalizing are given in column 1 of Table 5. The traces are of medians for groups of samples. Grid references and the number of samples are given in Tables 1–3. (A) Fodderletter Formation. ◆, Garron Point 'Group'; ▲, Bridge of Brown, Glen Brown; ●, Blairfindy, Glen Livet; △, Burn of Tervie, Glen Livet; ○, Parkmore Quarry, Dufftown. (B) Dufftown Limestone Formation. ▲, Rinaitin Quarry, Glen Rinnes; ○ Blackhillock Quarry, Keith; □, Parkmore Quarry, Dufftown; ▽, Sandend Bay; ◇, The Dune, Glen Fiddich; ●, Alltachoileachan, Glen Livet; △, Braes of Abernethy; ▽, Alehousehillock, Glen of Coachford. (C) Torulian Limestone Member. ◆, Tomintoul area; ◇, Glen Suie and Glen Fiddich. (D) Inchroary Limestone Formation. ●, Conglass, Glen Conglass; ◆, Sandend Bay; ○, Muckle Allt Venney; ◇, Tomintoul area; △, Goukstone and Rosarie Quarries near Keith; ▽, Corgarff, Strathdon; □, Glen Suie and Glen Fiddich.

Nonlinear mapping results

Median values of SiO_2 , TiO_2 , Al_2O_3 , Fe_2O_3 , MgO , CaO , K_2O and P_2O_5 for each group of samples were processed using the NLM algorithm discussed earlier. Sets of results were obtained for different starting configurations of coordinates in two-dimensional space. These configurations

were either the two variables with the greatest variance (SiO_2 , CaO) or scores on the first two Principal Components. Plots of the resulting coordinates are in close agreement, although those based on principal component scores give better separation, particularly when the unweighted variance-covariance matrix was used to calculate the principal components (Fig. 9). The agreement in the

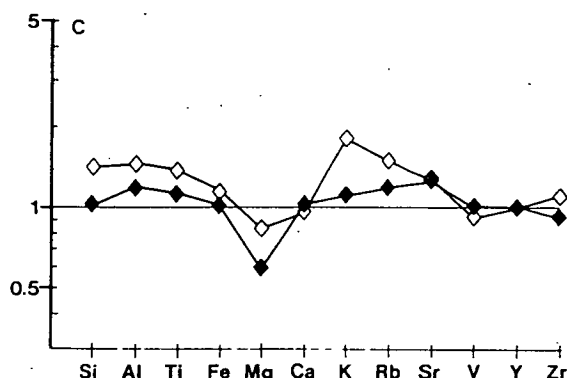
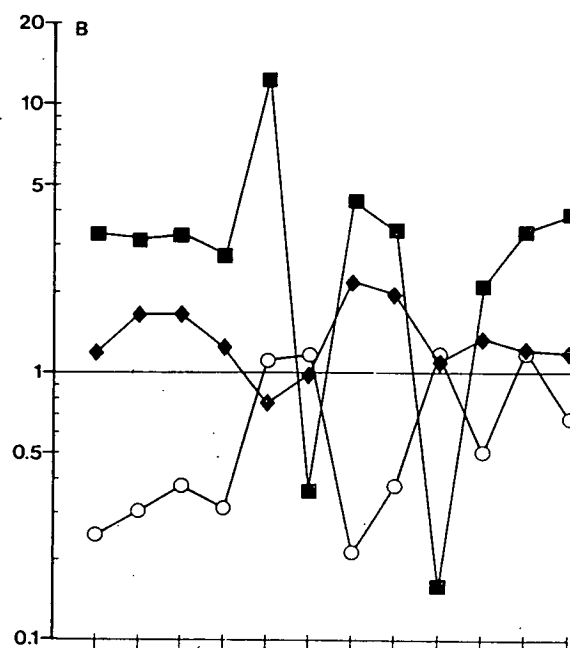
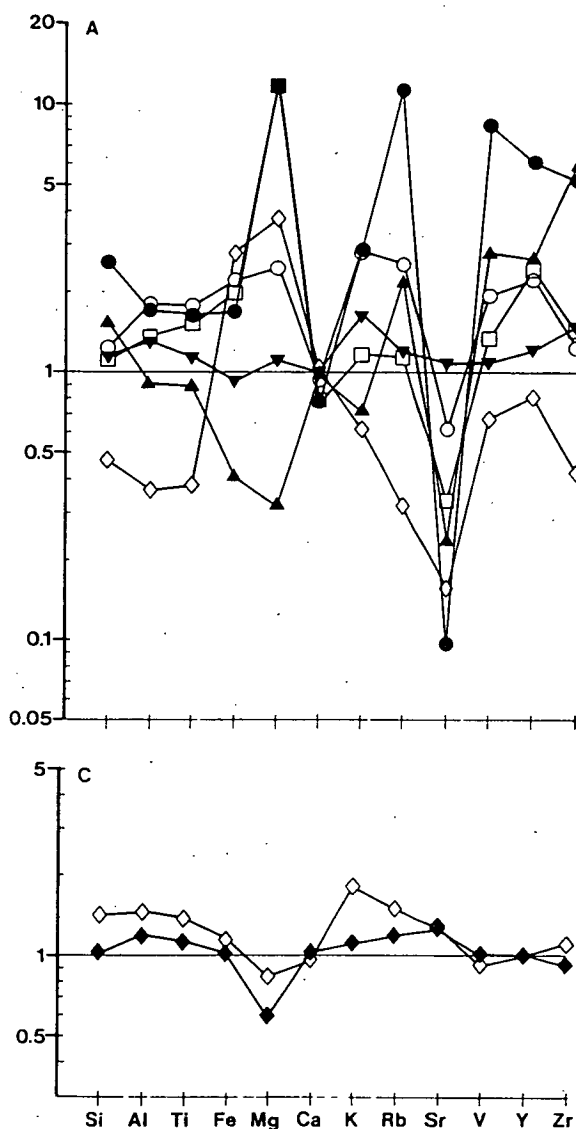


Fig. 8. Normalized multi-element variation patterns for six selected Argyll Group rocks and examples of groups correlated by use of the variation diagram. Traces are for medians for groups of samples. Grid references and numbers of samples are given in Table 4. The values used for normalizing are given in column 1 of Table 5. (A) Argyll Group rocks. ●, Links Bay, Portsoy; ○, Castle Point, Portsoy; △, Old Hythe Bay, Portsoy; ▼, Baloch Quarry, Strathdon; □, Muckle Fergie, Upper Glen Avon; ◇, Tobar Fuar, near Lecht. (B) Contrasting multi-element-diagram patterns for carbonate formations in the Sandend Bay area (cf. Fig. 7a, b, d). ■, Garron Point 'Group'; ○, west side of Sandend Bay; ◆, east side of Sandend Bay. (C) Comparison between multi-element-diagrams for Limehillock Quarry samples (◇) and the median of all Inchroary Limestone Formation sample groups (◆).

results indicates that the global rather than a local minimum in the mapping error has been located (Mather 1976, p. 340). The plots show that the classifications made on the (subjective) examination of the normalized multi-element diagrams are supported by (more objective) numerical analysis. The NLM results demonstrate further the contrasting behaviour of Appin and Argyll Group carbonate rock units.

The tight grouping of samples from the Dufftown Limestone and Torulian Limestone highlights the similarities in chemistry between these carbonate rocks. The groups of samples from the Inchroary Limestone Formation form an elongate cluster. Groups of samples from the Fodderletter Formation plot in similar fashion, but removed to the left somewhat. With one exception, groups of Appin

Group samples plot in variably elongate clusters. In contrast the Argyll Group sample groups plot much more widely, confirming the conclusions drawn from the multi-element diagrams that Argyll Group samples cannot be correlated on chemical grounds. The NLM plot also separates carbonate rocks classed as dolostones, dolomite-bearing limestones and dolostones into separate areas on the plot.

Correlations based on the whole-rock chemistry

Previously, carbonate rocks on either side of Sandend Bay have been incorporated into the Sandend 'Group' (e.g. Read 1955) and assigned to the Blair Atholl Subgroup (Harris & Pitcher 1975). Rock (1986) maintained the grouping in his overview of Dalradian carbonate rock

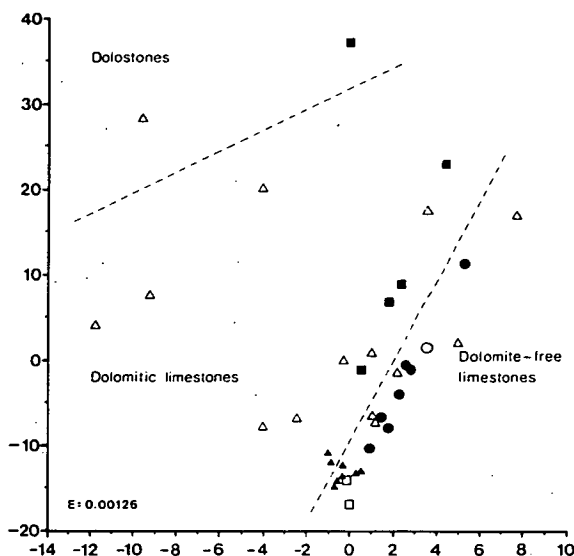


Fig. 9. Plot of Nonlinear mapping coordinates (dimensionless) of median values for groups of samples from Appin and Argyll Group carbonate rocks. Final mapping error, $E = 0.00126$. ■, Fodderletter Formation; ▲, Duftown Limestone Formation; □, Torulian Limestone Member; ●, Inchroary Limestone Formation; ○, Limehillock Quarry samples; △, Argyll Group rocks. Note the contrast in behaviour for groups of rocks from the Appin and Argyll Groups. The plot separates rocks defined as being dolostones, dolomitic limestones and limestones on the basis of the MgO/CaO ratio.

chemistry and stratigraphy but considered that the rocks in Sandend Bay were probably part of the Ballachulish Subgroup. However, a close examination of the chemistry and the field appearance of carbonate rocks on the west and east sides of the bay shows that they are distinctly different (Table 2, 5; Table 3, 8). Those on the west side of the bay are pure, with low siliciclastic oxide and trace element values and relatively high MgO contents. In contrast, those on the east side of the bay are more impure with reduced CaO values and increased trace element contents.

Multi-element diagram patterns reflect these differences (Fig. 8b). The patterns for samples on the west side of the bay match those for limestones from the Duftown Limestone Formation (Ballachulish Subgroup) (Fig. 7b, d). Conversely, patterns for samples from the east side of the bay are very similar to those for limestones from the Inchroary Limestone Formation (Blair Atholl Subgroup). On the NLM plot (Fig. 9) the two groups of samples are widely separated and lie with other groups of samples with which they would be associated by the multi-element diagrams (note filled triangles and circles). It is apparent therefore, that the Sandend 'Group' includes limestones from the lower part of the Ballachulish Subgroup up to at least the middle part of the Blair Atholl Subgroup. Furthermore, although they have greater amplitude, multi-element diagram patterns for samples from the Garron Point 'Group' (situated just to the west of Sandend [NJ 555663] and stratigraphically below the Sandend 'Group') correlate these rocks with others from the Fodderletter Formation, supporting the above correlations (Fig. 5, Fig. 7a).

Rocks are not exposed in the middle of Sandend Bay (Read 1923) and the Corriehabbie Quartzite (equivalent to Appin Quartzite) is conspicuous by its absence. Strong facies changes are known in the Ballachulish Subgroup (Harris & Pitcher 1975, p. 59) and Litherland (1980) demonstrated that the Appin Quartzite is restricted to thin pods and lenses in part of the Loch Creran area. Furthermore, detailed mapping by BGS has shown that considerable facies variations occur in Appin Group rocks in the Duftown-Keith area. Thus it is quite possible that the Corriehabbie Quartzite and other Ballachulish and lowermost Blair Atholl Subgroup rocks are only thinly developed or absent or faulted out in the Sandend Bay area.

In the Keith area major outcrops of limestone can be correlated by the whole-rock chemistry. Samples from quarries at Goukstone [NJ 49165615] and Rosarie [NJ 39134991] have multi-element diagram patterns which match those from the Inchroary Limestone Formation, with the characteristic negative MgO inflection (Fig. 7d). Samples from Blackhillock Quarry [NJ 439482] and Alehousehillock [NJ 459446] have patterns which match those from the Duftown Limestone Formation (Fig. 7b).

A thick, well-bedded sequence of limestones is well exposed in Parkmore Quarry [NJ 334411]. Eight samples were collected across the strike over about 70 m. The data show that there are two chemically distinct limestones here (Table 1, 3; Table 2, 1); three samples collected from the northwest end of the section in the quarry have multi-element diagram patterns similar to those from the Fodderletter Formation (Fig. 7a). The other five samples match the other Duftown Limestone patterns very closely (Fig. 7b). The marked change in composition occurs over a few metres, indicating a rapid change in sedimentary conditions. These similarities are reflected in the NLM plot (Fig. 9); the median of the five purer samples plot with other groups of samples from the Duftown Limestone Formation (filled triangles) whilst the median of the three less pure samples plot reasonably close to other Fodderletter Formation sample group medians (filled squares). As the rocks dip to the north-west and the carbonate rock chemistry implies that the Fodderletter Formation overlies the Duftown Limestone Formation, it is clear that the succession here is inverted.

Limestones exposed in Limehillock Quarry [NJ 51645202] have been placed in the Portsoy 'Group' (Read 1923). However, recent mapping in the area has cast some doubt on this interpretation of the stratigraphy and associated structure (J. R. Mendum, D. Stephenson, pers. comm. 1987). The chemistry of samples from this locality suggests strongly that the limestones belong to the Inchroary Limestone Formation (Blair Atholl Subgroup). The multi-element diagram pattern compares very closely to that for samples from the east side of Sandend Bay (Figs 7d, 8c) and the NLM plot confirms this similarity (Fig. 9; open circle). The only ambiguity here is due to some similarity between Limehillock Quarry samples and those from Baloch Quarry, Strathdon. There are broadly similar multi-element diagrams for each group of samples, and both plot with limestones from the Inchroary Limestone Formation on the NLM plot. However, the limestones in Baloch Quarry lie above a tillite horizon at the base of the Middle Dalradian (J. R. Mendum, pers. comm. 1987) and so lie in the Argyll Group whereas no tillite lithologies have been found below the Limehillock Quarry limestones. The geochemical and

mapping data indicate that Blair Atholl Subgroup rocks crop out in this area and not Portsoy 'Group' rocks as indicated by Read (1923).

Discussion

Whole-rock geochemistry in combination with regional mapping has proved a very useful guide to correlation in areas of poor exposure in the Appin and Argyll Groups of northeast Scotland. Where mapping information is ambiguous, whole-rock geochemistry has provided evidence which has clarified correlations or lent weight to a particular interpretation. It has also shed light on old problems or classifications, as in the correlation of the Sandend 'Group' with the inland succession, leading to a re-interpretation of the stratigraphy. However, for correlations based on geochemical criteria to be accepted with confidence in areas of poor exposure, some mapping control is necessary to show that there is some kind of consistency in the composition of samples from the mapped unit of interest. Furthermore, even limited mapping information in areas of poor exposure helps to constrain the interpretation based on the geochemistry.

It is improbable that the same chemical conditions and component compositions will exist at different stratigraphic levels, even in limestones formed in similar environments. In general, this work bears this out, although there are exceptions. For example, the white Torulian Limestone and the grey Dufftown Limestone have distinctly similar compositions. Fortunately, these units are readily distinguished in the field by their different colours and lithological associations. In addition the unit of interest must be sufficiently well developed over a wide enough area for it to be potentially useful as a geochemical marker.

Intuitively, for a distinctive carbonate rock composition to be developed over a large area, crustal conditions must have been relatively stable. Such conditions are considered to have prevailed elsewhere in the Dalradian during Appin Group times but not during Argyll Group times (Anderton 1982, 1985). The geochemical data in this study suggest that such conditions also prevailed during the deposition of the Appin and Argyll Group rocks in the northeast of Scotland. The variation in carbonate rock composition is controlled chiefly by the amount and composition of the siliciclastic material. To maintain compositions recognizable on a regional scale in the major Appin Group carbonate rock units, the siliciclastic material must have been derived from an extensive common source within or adjacent to the study area. Furthermore, the persistent compositions indicate that isolated or restricted basins were absent or only weakly developed, thereby implying relative crustal stability (although mapping in the area between Dufftown and Keith indicates that conditions differed in some aspects to those in the southwest of the study area).

During Argyll Group times, the lack of extensive carbonate rock formations and the variation in chemistry suggests that crustal conditions were much less stable. Corroborative evidence for this comes from the presence of basic and ultrabasic lavas, the former commonly with pillow structures, at Ardwell Bridge [NJ 378308] (D. J. Fettes, pers. comm. 1985) and in the Glass area (D. Stephenson, pers. comm. 1986). Green amphibolitic tuffaceous horizons have also been recognized in Islay Subgroup rocks from the Ladder Hills (author's mapping; J. R. Mendum,

pers. comm. 1986) suggesting episodic volcanism. Syn-sedimentary mineralization in isolated basins in Argyll Group rocks is further evidence of crustal instability during Argyll Group times, since mineralizing fluids are considered to have debouched from faults at basin margins (Coats *et al.* 1980; Russell *et al.* 1984).

The data sets represent extremely small sub-sets of the total population, so that outlying values due to natural variations may affect significantly any attempt to characterize a stratigraphic unit using statistical parameters. It is necessary, therefore, to use methods which can lessen the influence of such outliers on numerical summaries of the data. In such circumstances, the use of non-parametric statistics based on ranks and the median is preferable to statistics based on the mean and standard deviation. Furthermore, the non-Gaussian character of the data, the variable size of data sets, the preclusion of a statistically rigorous sampling programme and the statistical problems associated with closed data sets (Chayes 1971) mean that non-parametric and graphical techniques represent a more valid approach than certain complex multivariate techniques, the use of which carries assumptions about the data distributions.

An important part of the initial analysis lay in the application of EDA methods to investigate the character of the data. This influenced strongly the choice of subsequent techniques, particularly when non-Gaussian behaviour was revealed. Furthermore, it was thought important that two techniques of classifying the data should be used, since corroboration between results would provide more weight to the classification and subsequent correlations.

The work presented in this paper was very much concerned with investigating the relationship between chemistry and stratigraphy in Appin and Argyll Group carbonate rocks of northeast Scotland. Thus detailed comparisons with geochemical data from equivalent rock formations in other areas of the Dalradian have not been made. Furthermore, because the mean and standard deviation have been used in other studies, any conclusions drawn by comparing means with the medians in this study would have to be treated with great caution. However, bearing in mind the difference between the mean and median as measures of location, it is interesting to make some qualitative comparisons between data presented here and data presented by Hickman & Wright (1983) for Appin Group carbonate rocks.

Perhaps the most striking difference is the lack of compositions equivalent to the Dufftown Limestone in the rocks sampled by Hickman & Wright from the Ballachulish Limestone, although they both occupy broadly the same stratigraphic position. Their data (Hickman & Wright 1983; Table 5, 1-3) show that the Ballachulish Limestone, as sampled, is much more impure than the Dufftown Limestone (Table 2); both SiO_2 and MgO are several times higher, whilst Sr is much less than half that present in the Dufftown Limestone. Their data for the Ballachulish Limestone have much more in common with data presented for the Fodderletter Formation (Table 1). It is apparent, therefore, that the very pure facies represented by the Dufftown Limestone is not present as a major unit, if at all, in Hickman & Wright's study area. However, Litherland (1980) showed that the Ballachulish Limestone was subject to wide thickness and facies variations in the Loch Creran area, so the above contrasts between the two areas are

hardly surprising, given a strike separation of several hundred kilometres.

There are also some moderate differences between the Inchroary Limestone and its stratigraphic equivalent, the Lismore Limestone. The analyses of the Lismore Limestone (Hickman & Wright 1983; Table 5, 4–8) show it to be less siliceous but consistently more MgO-rich than the Inchroary Limestone. Whilst Ce, Ba, Sr and Zn values are much the same, Cr, Rb, Y and Zr are rather higher in the Inchroary Limestone, suggesting subtle variations in the composition of the source for the siliciclastic material.

The Appin Limestone analyses presented by Hickman & Wright (1983: Table 5, 9–12) show wide variation both in major and trace element composition. The same is true of the equivalent Glen Suie Formation in this study and the lack of constrained or systematically variable compositions in these two formations precludes direct correlation using geochemical data.

Conclusions

Whole-rock geochemical data have been used with success in correlating formations within Appin Group carbonate rocks of northeast Scotland. Although chemically distinct carbonate rocks exist locally in the Argyll Group, they do not exist on a regional scale and correlations cannot be made on the basis of their chemistry. This suggests that environmental conditions were relatively uniform over a wide area in Appin Group times but not during Argyll Group times. The geochemical data presented here support other data which show a deterioration in crustal stability in Argyll Group times.

From the geochemical data, the coastal section at Sandend Bay is now correlated with the Appin Group succession inland with some confidence. Both Ballachulish and Blair Atholl Subgroup rocks are present in the bay, and it is suggested that the term Sandend 'Group' for these rocks is now redundant.

The carbonate rocks can be considered as mixtures of siliciclastic and carbonate components, even in very silica-rich compositions. Furthermore, with the exception of samples with $\text{SiO}_2 > 30 \text{ wt\%}$ and $\text{MgO} > 10 \text{ wt\%}$, the chemistry of the carbonate rocks has not been affected by post-diagenetic processes. Rocks with SiO_2 in excess of 25 wt% are not necessarily the products of metasomatic interactions. Since MgO and CaO are concentrated in the carbonate phases and correlate very strongly with LOI, the carbonate rocks can be classified as limestone, dolomitic limestone or dolostone on the basis of the MgO/CaO ratio.

Most of the data have distributions which approximate to the log-normal distribution; exceptions are CaO, MgO and Sr. This has required that non-parametric statistics be used to summarize and analyse the data. Normalized multi-element variation diagrams and the nonlinear mapping algorithm have been successful in classifying the carbonate rocks, permitting correlations to be made. The results from the two techniques are consistent and provide weight to subsequent interpretations.

The author wishes to thank the following for their help with various aspects of this work. Discussions with J. R. Mendum and D. Stephenson and other colleagues helped considerably with interpretation of the data and with reviews of the initial drafts. N. M. S. Rock provided guidance on data analysis in the early

stages; P. M. Mather is thanked for suggesting the nonlinear mapping algorithm and for a copy of his NLM programme. M. J. Brown is thanked for supervising sample preparation and B. P. Atkin and P. K. Harvey are thanked for the analyses. A. Grout and J. R. Mendum collected some of the samples. I. J. Fairchild and A. E. Wright are thanked for their careful and constructive comments. This paper is published with the permission of the Director, British Geological Survey, NERC.

References

- ANDERTON, R. 1982. Dalradian deposition and the late Precambrian-Cambrian history of the N Atlantic region: a review of the early evolution of the Iapetus Ocean. *Journal of the Geological Society, London*, **139**, 421–431.
- 1985. Sedimentation and tectonics in the Scottish Dalradian. *Scottish Journal of Geology*, **21**, 407–36.
- ANDREWS, R. W., BICKEL, P. J., HAMPFEL, F. R., HUBER, P. J., ROGERS, W. H. & TUKEY, J. W. 1972. *Robust Estimates of Location*. Princeton University Press, Princeton, New Jersey.
- BICKLE, M. J. & POWELL, R. 1977. Calcite-Dolomite geothermometry for iron-bearing carbonates. *Contributions to Mineralogy and Petrology*, **59**, 281–292.
- BLATT, H., MIDDLETON, G. & MURRAY, R. 1972. *Origin of Sedimentary Rocks*. Prentice-Hall, Inc., Englewood Cliffs, New Jersey.
- CHAYES, F. 1971. *Ratio Correlation*. University of Chicago Press, Chicago.
- COATS, J. S., SMITH, C. G., FORTEY, N. J., GALLAGHER, M. J., MAY, F. & MCCOURT, W. J. 1980. Strata-bound mineralisation in Dalradian schist near Aberfeldy, Scotland. *Transactions of the Institution of Mining and Metallurgy, Section B, Earth Science*, **89**, B110–B122.
- CONOVER, W. J. 1980. *Practical Nonparametric Statistics*. John Wiley and Sons, Inc., New York.
- DAVIS, J. C. 1973. *Statistics and Data Analysis in Geology*. John Wiley and Sons, Inc., New York.
- DEER, W. A., HOWIE, R. A. & ZUSSMAN, J. 1966. *An Introduction to the Rock Forming Minerals*. Longman, London.
- FAIRCHILD, I. J. 1985. Petrography and carbonate chemistry of some Dalradian dolomitic metasediments: preservation of diagenetic textures. *Journal of the Geological Society, London*, **142**, 167–185.
- FERRY, J. M. 1982. A comparative geochemical study of the pelitic schists and metamorphosed carbonate rocks from south-central Maine. *Contributions to Mineralogy and Petrology*, **80**, 59–72.
- 1983. Mineral reactions and element migration during metamorphism of calcareous sediments from the Vassalboro Formation, south-central Maine. *American Mineralogist*, **68**, 334–354.
- FETTES, D. J. 1983. Metamorphism in the British Caledonides. In: SCHENK, P. E. (ed.) *Regional trends in the Geology of the Appalachian-Caledonian-Hercynian-Mauritanide Orogen*. NATO ASI Series, Series C, Mathematical and Physical Sciences, **116**, 205–219.
- GEARY, R. C. 1935. The ratio of the mean deviation to the standard deviation as a test of normality. *Biometrika*, **27**, 310–322.
- GOLDSMITH, J. R. 1983. Phase relations of rhombohedral carbonates. In: REEDER, R. J. (ed.) *Carbonates: Mineralogy and Chemistry*. Mineralogical Society of America Reviews in Mineralogy, **11**, 49–76.
- GUTTMAN, L. 1985. The illogic of statistical inference for cumulative science. *Applied Stochastic Models and Data Analysis*, **1**, 3–10.
- HALL, A. M. 1985. Cenozoic weathering covers in Buchan, Scotland, and their significance. *Nature*, **315**, 392–95.
- HARRIS, A. L. & PITCHER, W. S. 1975. The Dalradian Supergroup. In: HARRIS, A. L., SHACKLETON, R. M., WATSON, J., DOWNIE, A., DOWNIE, C., HARLAND, W. B. & MOORBATH, S. (eds) *A correlation of Precambrian rocks of the British Isles*. Special Report of the Geological Society, London, **6**, 52–75.
- HARTE, B., BOOTH, J. E., DEMPSTER, T. J., FETTES, D. J., MENDUM, J. R. & WATTS, D. 1984. Aspects of the post-depositional evolution of Dalradian and Highland Border Complex rocks in the Southern Highlands of Scotland. *Transactions of the Royal Society of Edinburgh: Earth Sciences*, **75**, 151–163.
- HARVEY, P. K. & ATKIN, B. P. 1982. Automated X-ray fluorescence analysis. In: Sampling and analysis for the minerals industry. *Institution of Mining and Metallurgy*.
- HICKMAN, A. H. 1975. The stratigraphy of late Precambrian metasediments between Glenroy and Lismore. *Scottish Journal of Geology*, **11**, 191–212.
- & WRIGHT, A. E. 1983. Geochemistry and chemostratigraphical correlation of slates, marbles and quartzites of the Appin Group, Argyll.

- Scotland. *Transactions of the Royal Society of Edinburgh: Earth Sciences*, 73, 251-278.
- HOWARTH, R. J. 1973. Preliminary Assessment of a Nonlinear Mapping Algorithm in a geological context. *Mathematical Geology*, 5, 39-57.
- JOHNSON, M. R. W. 1983. Dalradian. In: CRAIG, G. Y. (ed.) *Geology of Scotland*. Scottish Academic Press, Edinburgh. 77-104.
- LAMBERT, R. ST., J., WINCHESTER, J. A. & HOLLAND, J. G. 1981. Comparative geochemistry of pelites from the Moine and Appin Group (Dalradian) of Scotland. *Geological Magazine*, 118, 477-490.
- , HOLLAND, J. G. & WINCHESTER, J. A. 1982. A Geochemical comparison of the Dalradian Leven Schists and the Grampian Division Monadhliath Schists of Scotland. *Journal of the Geological Society, London*, 139, 71-84.
- LEAKE, B. E., TANNER, P. W. G. & SENIOR, A. 1975. The Composition and Origin of the Connemara Dolomitic marbles and Ophicalcites, Ireland. *Journal of Petrology*, 16, 237-277.
- LINK, G. S. & KOCH, R. F. 1975. Some consequences of applying Lognormal Theory to Pseudolognormal Distributions. *Mathematical Geology*, 7, 117-128.
- LISTER, B. 1982. Evaluation of analytical data: A practical guide for geologists. *Geostandards Newsletter*, 6, 175-205.
- LITHERLAND, M. 1980. The stratigraphy of the Dalradian rocks of Loch Creran, Argyll. *Scottish Journal of Geology*, 16, 105-123.
- MATHER, P. M. 1976. *Computational Methods of Multivariate Analysis in Physical Geography*. John Wiley and Sons, Inc., London.
- PHILIP, G. M. & WATSON, D. F. 1987. Probabilism in Geological Data Analysis. *Geological Magazine*, 124, 577-583.
- READ, H. H. 1923. The Geology of the Country round Banff, Huntly and Turriff. *Memoir of the Geological Survey of Great Britain, Sheets* 86, 96.
- 1955. The Banff Nappe: an interpretation of the structure of the Dalradian rocks in north-east Scotland. *Proceedings of the Geologists' Association*, 66, 1-29.
- ROCK, N. M. S. 1985. Value of chemostratigraphical correlation in metamorphic terrains; an illustration from the Colonsay Limestone, Inner Hebrides, Scotland. *Transactions of the Royal Society of Edinburgh, Earth Sciences*, 76, 515-517.
- 1986. Chemistry of the Dalradian (Vendian-Cambrian) metalimestones, British Isles. *Chemical Geology*, 56, 289-311.
- 1987. Robust: An interactive FORTRAN-77 package for exploratory data analysis, robust and nonparametric location and scale estimates, data transformations, normality tests and outlier assessment. *Computers and Geosciences*, 13, 463-494.
- & WATERHOUSE, K. 1986. Value of chemostratigraphical correlation in metamorphic terrains: an illustration from the Shinness and Armadale marbles, Sutherland, Scotland. *Proceedings of the Geologists' Association*, 97, 347-355.
- , WEBB, J. A., McNAUGHTON, N. J. & BELL, G. D. 1987. Nonparametric estimation of averages and errors for small data-sets in isotope geoscience: a proposal. *Chemical Geology*, 66, 163-177.
- RUSSELL, M. J., HALL, A. J., WILLAN, R. C. R., ALLISON, I., ANDERTON, R. & BOWES, G. E. 1984. On the origin of the Aberfeldy celsian + baryte + base metal deposits, Scotland. In: JONES, M. J. (ed.) *Prospecting in Areas of Glaciated terrain*. 1984. Institution of Mining and Metallurgy, 159-170.
- SAMMON, J. W., JR. 1969. A nonlinear mapping algorithm for data structure analysis. *Institute of Electrical Electronics Engineers Transactions on Computers*, C-18, 401-409.
- SMITH, C. G. 1985. Recent investigations of manganese mineralisation in the Scottish Highlands. *Transactions of the Institution of Mining and Metallurgy, Section B, Earth Science*, 95, 159-162.
- SMITH, R. A. & HARRIS, A. L. 1976. The Ballachulish rocks of the Blair Atholl district. *Scottish Journal of Geology*, 12, 153-158.
- STEHLI, F. G. & HOWER, J. 1961. Mineralogy and diagenesis of carbonate sediments. *Journal of Sedimentary Petrology*, 31, 358-371.
- TREAGUS, J. E. & KING, G. 1987. A complete Dalradian succession in the Schiehallion district, Scotland. *Scottish Journal of Geology*, 14, 157-166.
- TUKEY, J. W. 1977. *Exploratory Data Analysis*. Addison-Wesley, Reading, Massachusetts.
- TURNER, F. J. 1980. *Metamorphic Petrology*. McGraw-Hill, New York, NY.
- UPTON, P. S. 1986. A structural cross-section of the Moine and Dalradian rocks of the Braemar area. *Report of the British Geological Survey*, 17, 9-19.
- VELLEMAN, P. F. & HOAGLIN, D. C. 1981 *Applications, Basics, and Computing of Exploratory Data Analysis*. Duxbury Press, Boston, Massachusetts.
- WRIGHT, A. E. 1988. The Appin Group. In: WINCHESTER, J. A. (ed.) *Late Proterozoic Stratigraphy of The Northern Atlantic Regions*. Blackie, Glasgow, London. 177-199.

Figure 9.8 CL image of CT 53,
showing the location of SIMS
profiles A to D x40

